Eric P. Holowka · Sujata K. Bhatia

Drug Delivery

Materials Design and Clinical Perspective

Foreword by
Enrico G. Bellomo

Springer

Drug Delivery

Eric P. Holowka • Sujata K. Bhatia

Drug Delivery

Materials Design and Clinical Perspective

Foreword by Enrico G. Bellomo

Springer

Eric P. Holowka
DuPont Central Research and Development
Wilmington, USA

Sujata K. Bhatia
School of Engineering and Applied Science
Harvard University
Cambridge, MA, USA

ISBN 978-1-4939-1997-0 ISBN 978-1-4939-1998-7 (eBook)
DOI 10.1007/978-1-4939-1998-7
Springer New York Heidelberg Dordrecht London

Library of Congress Control Number: 2014952080

Printed on acid-free paper

Springer is part of Springer Science+Business Media (www.springer.com)

About the Authors

Eric P. Holowka is a Senior Research Investigator with DuPont Central Research & Development and holds appointments as Visiting Assistant Professor in both the Materials Science & Engineering Department at Drexel University and the Chemistry Department at Haverford College. Since 2007, he has led different research discovery and/or implementation efforts within Central Research involving the application of drug delivery methodologies to a broad range of technology areas encompassing regenerative medicine, energy storage, food science, agriculture, and nutrition, which has led to the publication of over 16 patents. He earned his bachelor's degree in chemistry with a minor in Polymer, Colloidal, and Surface Science at Carnegie Mellon University, while concurrently studying at the Center for Macromolecular Engineering under the guidance of Krzysztof Matyjaszewski as a Howard Hughes undergraduate research fellow. He then attended the University of California Santa Barbara (UCSB), where he earned his Ph.D in Materials Science & Engineering as a California NanoSystems Institute Fellow under Timothy Deming for his work on the design and implementation of self-assembled polypeptide copolymers for use in targeted drug delivery and tissue engineering. Prior to joining DuPont, he worked in research and development, intellectual property, and in-vitro trials at University of California Los Angeles' (UCLA) Department of Biomedical Engineering and in immunology, biochemistry, and cell biology at Cornell University's Department of Chemistry and Chemical Biology. The drug delivery technologies that Dr. Holowka developed in his time at UCSB and UCLA have been featured in Chemical & Engineering News (Technology Concentrates 2006), cited over 500 times in scientific journals and textbooks, and licensed to several biotechnology and drug delivery companies as part of their core technology platforms. He has been invited to speak at a number of universities for his work on "Rational Biomaterial Design for use in Intracellular Drug Delivery". In 2010, he published a textbook, "*Copolypeptide Vesicles: Size Control for Intracellular Drug Delivery*," which discusses core technologies behind the design and implementations of peptide-based drug delivery systems from the synthetic chemistry and materials science perspective.

Sujata K. Bhatia is a faculty member in Biomedical Engineering at Harvard University, and serves as the Assistant Director for Undergraduate Studies in Biomedical Engineering at Harvard. She is also an Associate of the Harvard Kenned School of Government, and a faculty member in the Harvard Kennedy School Executive Education program on Innovation for Economic Development. She earned three bachelor's degrees, in biology, biochemistry, and chemical engineering, and a master's degree in chemical engineering at the University of Delaware. She then attended the University of Pennsylvania School of Medicine, where she earned her M.D. and Ph.D in bioengineering. Prior to joining Harvard, she worked in research and development, intellectual property, and clinical trials at DuPont. From 2003 to 2008, she worked to develop tissue adhesives for closure of wounds. In 2009, she spent a year on technology licensing for cancer drug discovery. In 2010 and 2011, she led clinical trials of omega-3 fatty acids for heart health. She was an invited participant in the 2005 U.S. Frontiers of Engineering and 2006 Japan-U.S. Frontiers of Engineering symposia, and a co-organizer of the 2007 Japan-U.S. Frontiers of Engineering symposium. In 2010, she published a textbook, "Biomaterials for Clinical Applications," which discusses opportunities for both biomaterials scientists and physicians to alleviate diseases worldwide. In 2011, she published another book, "Engineering Biomaterials for Regenerative Medicine." In 2013, Sujata was awarded the Capers and Marion McDonald Award for Excellence in Mentoring and Advising, the highest award in the Harvard School of Engineering and Applied Sciences for excellence in advising. She was also awarded the Star Family Prize for Excellence in Advising, a distinguished award from Harvard University for exemplary intellectual and personal guidance of undergraduate students. In 2013, she was selected by the U.S. National Academy of Engineering for Frontiers of Engineering Education, a recognition for the most innovative engineering educators in the nation. In 2014, she was voted by the Harvard College Class of 2014 as a Harvard Yearbook Favorite Professor.

Foreword

Embarking upon the journey of teaching the design principles of drug delivery systems and their clinical application is a daunting task. Many current offerings in this area typically either fail to address the complexity of the physiology where they seek to operate, while highlighting innovative system designs, or choose outdated systems to address complex physiological problems. What remains absent is an approach both targeted at multidisciplinary design solutions rooted in biology, engineering, chemistry, and physics validated with an applied knowledge in clinical research and application.

In order for this approach to be effective, the authors have to be as uniquely diverse and experienced as the material they are about to cover. For the material design sections, Eric Holowka is astutely equipped for the challenge. In a young career, Holowka has been able to successfully extend his scientific interests into areas of polymer science (B.S. Carnegie Mellon University), immunology (Cornell University), materials science and engineering (Ph.D. University of California Santa Barbara), biomedical engineering (University of California Los Angeles), and nanotechnology (California NanoSystems Institute). Holowka has published a book, *Copolypeptide Vesicles: Size Control for Intracellular Drug Delivery*, and holds patents in diverse areas of technology application, which include drug delivery, food science, nutrition, agriculture, energy storage, and nanotechnology. He currently holds a position in DuPont Central Research & Development, with Visiting Assistant Professor appointments in the Materials Science & Engineering Department at Drexel University and the Chemistry Department at Haverford College. On the clinical perspective side, Sujata Bhatia assumed a strongly diverse counterpoint. In her short career, Bhatia has earned three B.S. degrees, in biology, biochemistry, and chemical engineering, an M.S. degree in chemical engineering (University of Delaware), a Ph.D. in bioengineering, and an M.D. (University of Pennsylvania). Bhatia has published two books in the field of biomedical engineering, *Biomaterials for Clinical Applications* and *Engineering Biomaterials for Regenerative Medicine*. She currently holds the position of Assistant Director of Undergraduate Studies in Biomedical Engineering at Harvard University.

Authors with such a broad technical range of applied knowledge are uniquely capable of distilling complex principles associated with structure, function, and application for the reader. These principles are not abandoned with the reader, but instead are reinforced with thoughtful examples and problem sets within each chapter. Taken as a whole, in addition to serving as a resource for undergraduates, graduate students, and medical students with an interest in biomedical science, this text stands as a solid resource for physicians and surgeons who desire novel therapeutic approaches, patient advocacy groups and educated patient populations, and industry executives desiring to learn about biomaterials. This text holds a unique perspective for young scientists, engineers, and physicians to effectively understand the field of drug delivery from multiple perspectives. I am confident that with Eric and Sujata as your guides, prepare to be not only edified, but also entertained. You are in very capable hands.

Los Angeles, CA, USA

Enrico G. Bellomo, Ph.D.
Biomolecular Research & Development
NantPharma, LLC

Acknowledgments

The authors would like to thank Dr. Enrico G. Bellomo and Professor Philip J. Costanzo, who graciously gave their time to read and comment on the technical text and problem sets within this manuscript. Their suggestions for improvements and corrections proved a valuable resource. We would also like to thank the students from the Chemistry Department at Haverford College and the Biomedical Engineering Department at Harvard University for their input into various topic areas and current research trends. We are especially indebted to Jennifer and Alex, who always offered their unwavering love and support while we weathered the long nights of researching, writing, and editing. To all these wonderful individuals, we offer our humblest gratitude.

Contents

Reference Equations

Area of a sphere:	$A = \pi r^2$
Surface area of a cylinder:	$\mathrm{SA} = 2\pi r^2 + 2\pi rh$
Surface area of a sphere:	$\mathrm{SA} = 4\pi r^2$
Volume of a sphere:	$V = (4/3)\pi r^3$
Volume of a cylinder:	$V = \pi r^2 h$
Force:	$F = P/A$
Element charge (proton):	$e = 1.602 \times 10^{-19}$ C
Element charge (electron):	$e = -1.602 \times 10^{-19}$ C
Permittivity of free space:	$\varepsilon = 8.854 \times 10^{-12}$ F/m
Beer–Lambert law:	$A = \varepsilon cl$

Constants

Boltzmann's constant:		1.38×10^{-23} m^2 kg/s^2 K
Planck's constant:		6.626×10^{-34} m^2 kg/s
Avogadro's number	N_A	$6.022 \times 1{,}023$ molecules/mol
Gas constant	R	8.315 J/mol K
Velocity of light (vacuum)	c	2.998×10^8 m/s
Bohr magneton	μ_B	9.274×10^{-24} A m^2 (J/T)

Unit Conversions

Calorie (cal):	6.35 cal = 14 °C
Pascal (Pa):	kg/ms^2
Watt (W):	$kg\ m^2/s^3$
Dyne (dyn):	$10^{-5}\ kg\ m/s^2$
Oersted (Oe):	$1{,}000\ (4\pi)^{-1}\ A/m$

Chapter 1
Introduction

1.1 The Pharmaceutical World to the Material Scientist

Drug systems come in all shapes and sizes [1]. When we cough or sneeze, have a headache, or become diagnosed with a disease, drug therapies provide us with a treatment that is based on a conditional relationship with a patient and rooted in technology. We say "conditional" since for every system where drugs are delivered within the human body, compromises are made between technology and physiology. Many are well aware of the defensive hurdles that a drug must overcome in order to reach its intended target. Our immune system creates a sophisticated communication network based on the signal recognition of only a few small molecules. Still, there are other means by which our bodies challenge the introduction of foreign materials within its borders. Properties such as charge, pH, concentration, temperature, and light all play a significant role in this signaling cascade within our bodies [2]. At the root, the drug designer tries to address as many of these confounding properties as possible, searching for an effective chemical structure capable of treatment within an acceptable dosage window, but still there are compromises. With each new drug introduced into the pharmaceutical market, there are a host of side effects that can deter potential patients from the drug's use [3]. Even to arrive at a drug target is a challenge within pharmaceuticals, where a majority of the initial drug candidates are weeded out en route to a final offering. The clinical success rate of these drugs can vary from 20 % for cardiovascular treatments to as low as 5 % for oncology, with a majority of the failure rates occurring in Phase 2 (50–70 %) of clinical trials [4].

This may seem like a bleak glimpse into the world of pharmaceutical drug development, but it was meant to highlight an opportunity. The opportunity is what material scientists see as a challenge in the rational or functional design of a drug delivery system. For each biological, physical, or chemical barrier, there is a system that can be designed from first principles to address it. These first principles serve as "knobs" that the engineer can use to tune his or her system to behave in a predictable way

E.P. Holowka, S.K. Bhatia, *Drug Delivery: Materials Design and Clinical Perspective*, DOI 10.1007/978-1-4939-1998-7_1

within the body. This behavior serves to limit the interaction of the system within the body until the drug reaches a target tissue site [5]. The engineer is challenged to form a system composed of materials modified at these different knobs to create a pathway for a drug through the human body that is minimally perturbed.

If we were to document the modes of interaction between physiology and foreign systems in their entirety, we could spend an entire text focusing on describing those interactions alone. We will instead begin with what scientists and engineers would refer to as the **rate-limiting steps** [6] in the prevention of drug propagation within the human body. These rate-limiting steps, or **rate-limiting properties**, will guide the engineer to different classes of drug delivery technology, which we will discuss throughout the remainder of this text, such as controlled-release systems, thin films, self-emulsifying or targeted systems, hydrogels, and smart responsive systems, which can provide a platform for the future design and optimization of drug delivery systems that can avoid interaction with critical physiological environments. Within each chapter, there is an initial section entitled "Engineering Concepts" that reviews the relevant fundamental principles that guide the design of the drug delivery system. A following section on "Material Design" discusses the rational design of materials that can exploit the engineering concepts for use in physiological systems. A third section on "Implementation" discusses current approaches in the literature that have demonstrated effective drug delivery in controlled environments. Finally, each chapter contains a fourth section on "Clinical Applications" that describes the validity of materials approaches from a clinical perspective; these sections review the safety and efficacy of drug delivery systems for specific, compelling medical applications. The book thereby bridges materials science with clinical medicine and provides the reader with a bench-to-bedside view of novel drug delivery systems.

1.2 The Engineering Concepts of Materials in Drug Delivery

The evaluation of drug delivery methods traditionally depends on a mechanistic understanding of the materials that govern the critical physiological properties of the desired drug. The identification of these properties comes from the combined efforts of medical researchers and medicinal chemists that design target molecules with robust characteristics to allow for passage within human physiology with a degree of predictability in terms of their efficacy. Drug delivery systems become of increasing importance when drug dosages begin to increase to levels approaching the limits of their effective windows as side effects become less predictable. The efficacy is dependent on the targeted delivery and sustainability of drug performance prior to reaching the desired target. The human body harbors a number of mechanisms to prevent facile targeting of drug molecules. These mechanisms are typically thought of as active and passive immune responses leveraged by the body

Fig. 1.1 Diagram of different representative drug delivery systems with respect to their targeted area of the body

to ward off foreign molecules or pathogens. In addition to the immune defenses, the body also elicits physical constraints for drug therapies. Tight membrane gaps and porosities within the skin, mouth, and eye prevent the passing of drug cargos to their intended destinations. Natural filtration systems within the liver [7], reduced pH in the stomach [8], and agents within the bloodstream with electrostatic charges [9] all convolute the physiological landscape where the drug delivery system must act (Fig. 1.1).

If we look from the perspective of the drug, we see that a number of factors influence movement within physiological systems as well. These factors can impact how the drug travels through the bloodstream (i.e., diffusion and shear), interacts with

barrier membranes (i.e., surface area and self-assembly), targets specific tissue domains (i.e., binding kinetics and degradation), and interacts with cellular environments (i.e., receptor-mediated endocytosis) [10]. In the "Engineering Concepts" section within each chapter, we discuss the specific addressable challenges that these factors present to the naked drug.

1.3 The Rational Design and Controlled Material Properties for Drug Delivery

The understanding of our ability to tune these knobs provides the engineer with fundamental building blocks to design drug delivery systems that can exist harmoniously within the body instead of predatorily. If the engineer strays too much from the design of bioinert or biocompatible systems, she runs the risk of emboldening a system that introduces more problems than the ones it proposes to solve.

The section on "Material Design" discusses the rational design of materials that can exploit the engineering concepts for use in physiological systems. We group these materials into three domains, which include *controlled-release systems, thin films*, and *self-emulsifying materials*. Within each domain we discuss the material from the perspective of structural (i.e., size, shape, porosity, surface area), compositional (i.e., elasticity, morphology), and chemical (i.e., surface functionality, targeting groups) design. The section on "Implementation" moves the discussion of system design forward by looking at current approaches in the literature that have demonstrated effective drug delivery in controlled environments. In the final technical chapter on "Smart Materials," we begin to layer in dynamic systems that are capable of responding to stimuli commonly encountered within specific regions of the body. The engineer can begin to design these systems based on the exploitation of the energetic transitions found within specific materials. These energetic transitions allow stimuli such as temperature, charge, magnetism, light, and sound to influence the opening (i.e., destabilization, swelling) of delivery systems to release drug cargo at an intended location.

This text presents a unique perspective gleaned from both engineering and medicine. The engineering aspect is focused on the design of systems that exploit the knobs by which the drug molecules are governed within human physiology. The knobs allow for the design and creation of advanced biomaterial systems for use in medical applications. The truest form of evaluation is for the system to be handed over to the actual medical doctor for whom these systems would seek to benefit the most. It is for this reason that the second portion, the "clinical perspective," is included as both a counterpoint and true validation (Fig. 1.2) of the application of the drug delivery materials in question. It is from this counterpoint that we can gain insight into the design and successful implementation of drug delivery systems for future applications.

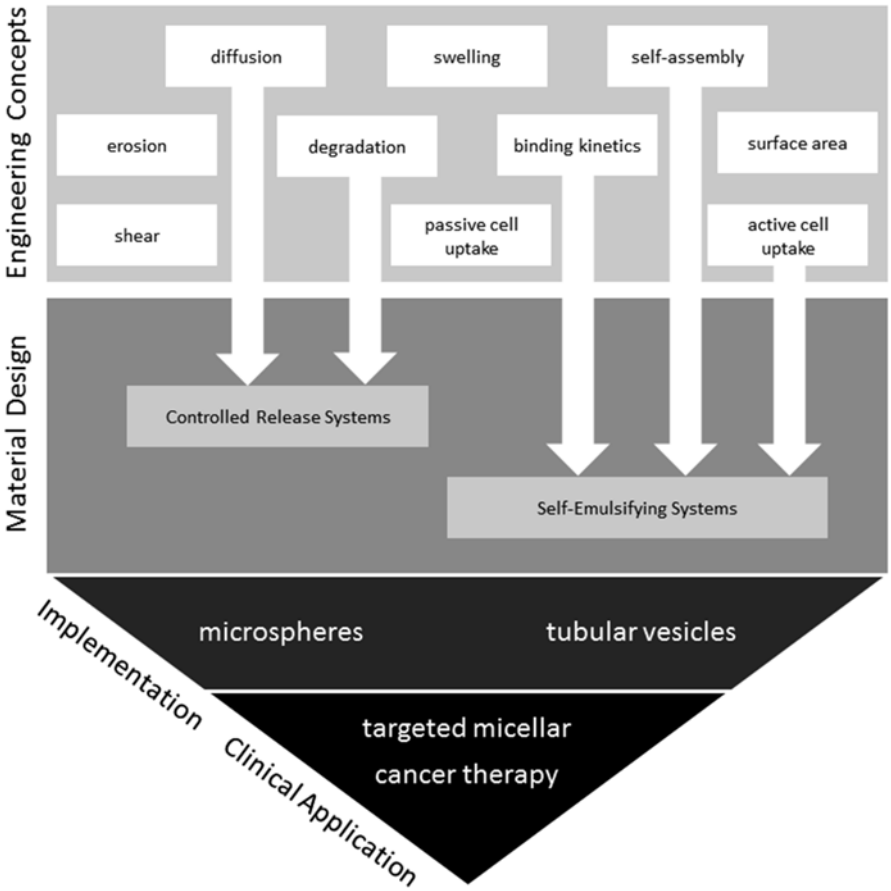

Fig. 1.2 Diagram of the design rationale of drug delivery systems from engineering concepts to clinical application

References

1. Daum, N., Tscheka, C., Neumeyer, A., & Schneider, M. (2012). Novel approaches for drug delivery systems in nanomedicine: Effects of particle design and shape. *Wiley Interdisciplinary Reviews. Nanomedicine and Nanobiotechnology, 4*(1), 52–65.
2. Beaulieu, J.-M., & Gainetdinov, R. R. (2011). The physiology, signaling, and pharmacology of dopamine receptors. *Pharmacological Reviews, 63*(1), 182–217.
3. Young, S. D., & Oppenheimer, D. M. (2006). Different methods of presenting risk information and their influence on medication compliance intentions: Results of three studies. *Clinical Therapeutics, 28*(1), 129–139.
4. Kola, I., & Landis, J. (2004). Can the pharmaceutical industry reduce attrition rates? *Nature Reviews. Drug Discovery, 3*(8), 711–715.
5. Anderson, J. M. (2001). Biological responses to materials. *Annual Review of Materials Research, 31*(1), 81–110.

6. Moddaresi, M., Brown, M. B., Zhao, Y., Tamburic, S., & Jones, S. A. (2010). The role of vehicle-nanoparticle interactions in topical drug delivery. *International Journal of Pharmaceutics, 400*(1–2), 176–182.
7. Vienken, J., & Christmann, H. (2006). How can liver toxins be removed? Filtration and adsorption with the Prometheus system. *Therapeutic Apheresis and Dialysis: Official Peer-Reviewed Journal of the International Society for Apheresis, the Japanese Society for Apheresis, the Japanese Society for Dialysis Therapy, 10*(2), 125–131.
8. Philip, A. K., & Philip, B. (2010). Colon targeted drug delivery systems: A review on primary and novel approaches. *Oman Medical Journal, 25*(2), 79–87.
9. Sahota, T. S., Latham, R. J., Linford, R. G., & Taylor, P. M. (1999). Physical characterization of polymer electrolytes as novel iontophoretic drug delivery devices. *Drug Development and Industrial Pharmacy, 25*(3), 307–313.
10. Bareford, L. M., & Swaan, P. W. (2007). Endocytic mechanisms for targeted drug delivery. *Advanced Drug Delivery Reviews, 59*(8), 748–758.

Chapter 2
Controlled-Release Systems

2.1 Engineering Concepts

2.1.1 Diffusion and Degradation

Why is there interest in the drug community in investing research time into the controlled drug release approach? Currently, the FDA estimates that approximately $150 million is invested over a 10-year period in the design and implementation of new drug offerings [1]. These drug offerings typically have a narrow therapeutic index (i.e., the difference between toxic and therapeutic levels). Additionally, there is patient-related physiological fatigue from multiple injections, infection, and hemorrhages, while the danger from systemic toxicity limits the potency of the drug [2]. Each of these pratfalls indicates a narrow window of utility for which the drug is permitted. A drug company cannot simply flood the body with a large excess of drug in order to ensure some small percentage reaches its intended target. Think of it as throwing 100 darts simultaneously at a dartboard. You will be statistically likely to hit a bull's-eye, but you are also more likely to damage the wall as well! A controlled-release profile can allow for targeting of the delivery, improve the availability of the drugs (i.e., short half-lives), and can serve multiple functions within the system (i.e., release systems can be adjuvants as well). So referring back to the dartboard analogy, imagine the thrower tossing the darts individually, 1 through 100, while progressively moving closer to the target. Now, statistically, his or her chances of a bull's-eye will increase sans the wall damage!

Drug release systems can be separated into two distinct classes: **sustained release** and **controlled release**. *Sustained-release* systems are traditionally a mix of agents that affect the net rate of dissolution of the drug molecule. *Controlled-release* systems are comprised of a drug molecule (i.e., active agent) and a bioinert or biocompatible polymer. Polymeric systems are discussed in more detail in Sect. 2.2. The system also contains a functionality that can be free or tethered to the polymer chain, which allows for tailoring the release kinetics of the system or cell targeting.

E.P. Holowka, S.K. Bhatia, *Drug Delivery: Materials Design and Clinical Perspective*, DOI 10.1007/978-1-4939-1998-7_2

Since there are inherent benefits for a controlled delivery approach, the next question to ask is

What is the desired location in the human physiology to which this treatment is going to be applied?

Controlled systems can be applied to a person through oral [3], ocular [4], parenteral [5], and sublingual [6] sites. Each site presents a series of challenges from both an engineering design and a medical treatment perspective, which we will evaluate throughout the remainder of Chap. 2.

2.1.2 Diffusion-Controlled Systems

The process of drug release from an aqueous stimulus has several distinct advantages in terms of the timing of the control and response of the system. The speed at which water can swell the matrix of a crosslinked system is significantly more rapid than the degradation or dissolution rates described in the erosion section previously discussed. The term "diffusion" refers to the actions of the drug molecules upon exposure to stimuli affecting its external environment. The rate-limiting step of diffusion drug release systems is the diffusion through typically a water-insoluble barrier. Diffusion drug delivery systems are typically either **matrix-based** or **reservoir** diffusion systems. In matrix-based systems, the drug is combined with a polymer to form a composite matrix where water permeation leads to either swelling or osmotically controlled systems [7]. Since the matrix is composed of both polymer and drug molecules, the swelling effect is seen as a uniform volume expansion of the bulk polymeric material, causing the opening of pores throughout the matrix structure. This is conceptually not unlike a sponge that uniformly swells with water. In order for effective diffusion of drug molecules to occur, the pore size of the swelled matrix must greatly exceed the size of the hydrophilic drug molecule or hydrophobic drug particle. In reservoir systems, the drug solution is encapsulated within a polymer droplet, creating a permeable barrier between the drug solution environment and the surrounding environment [8]. Since the reservoir is composed of a permeable polymer barrier coating, the swelling effect is seen as a nonuniform volume expansion, where the barrier coating allows for water permeability and swells, while the internal components can diffuse out of the system. This is conceptually not unlike a dialysis bag, which allows free diffusion of water and size-selective permeability of its internal constituents. In order for effective diffusion of drug molecules to occur, the pore size of the swelled barrier must greatly exceed the size of the hydrophilic drug molecule or hydrophobic drug particle.

If we are designing a controlled-release drug delivery system to specifically exploit a diffusion-controlled mechanism, the next question we could ask is

What factors can we manipulate in order to allow for control over the swelling or permeability of the barriers utilized in matrix or reservoir systems?

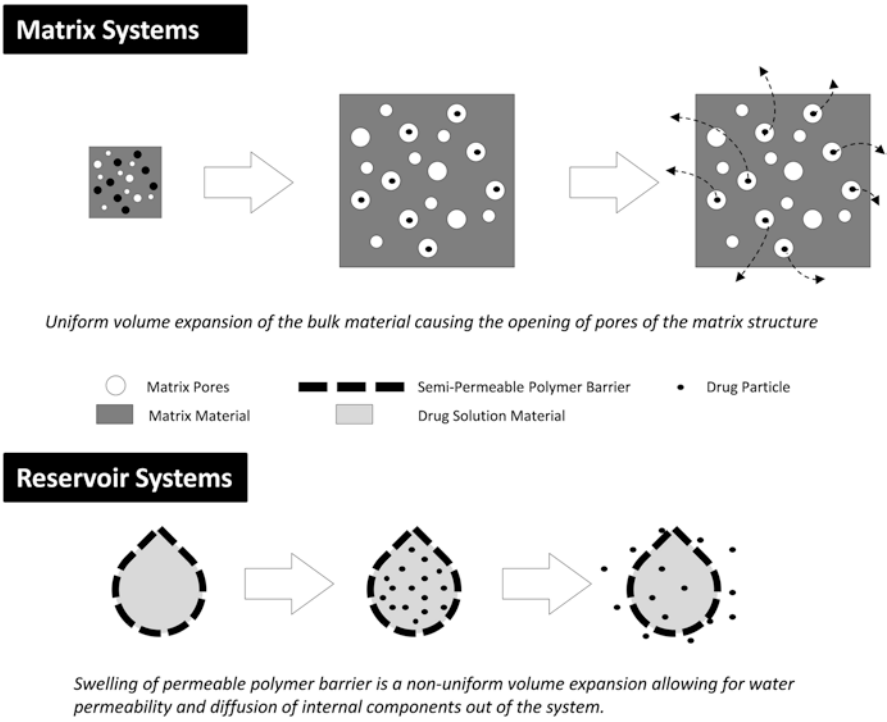

Fig. 2.1 Diagram of basic controlled-release systems for drug delivery

For the most part, the answer to this question lies in the chemistry of the polymer(s) used as either the matrix or permeable barrier. In matrix systems, the crosslinking of either a covalent or secondary bonding between, or within, polymer chains is used to stabilize the physical integrity while the system passively takes up water. In reservoir systems, crosslinking is also typically utilized with similar bonding as in matrix systems; however, the volumetric limitations of the swelling behavior are distinctly different. We engage in this discussion again in Sect. 2.2, where we look at the polymer characteristics and functionalities that contribute to the distinction between these two systems (Fig. 2.1).

2.1.3 Degradation-Controlled Systems

The primary modes of erosion-based drug delivery are through the release of the drug, typically from a bulk phase, which consists of a drug composite. Therefore, the rate-limiting step of degradation-controlled release systems is dissolution.

Table 2.1 Common erosion effects encountered by biomedical materials

Erosion effects	
Adhesion	Physical interaction with another surface via friction causing displacement
Abrasion	Loss of material due to hard materials (i.e., particles) that are pressed against the surface
Fatigue	Surface is weakened by cyclical application of load
Fretting	Surface is weakened by cyclical rubbing
Cavitation	Physical interaction with another physical state
Corrosion	Wear created by chemical reactions with surface functionalities

The composite can consist of a polymer of a tailored degradation or deformation rate. The degradation or dissolution effects are measured as the erosion of the material over time in response to its immediate physiological environment. The erosion can occur through a number of mechanisms related to either the surface or the bulk of the material. Erosion on the surface causes displacement of surface features or regularity due to several common effects (Table 2.1).

The deformation rate is measured from a matrix swelling effect in response to the adsorption or flux of physiological, typically aqueous fluids within the body [9]. In these matrix, or monolith, systems, the drug is homogeneously dispersed throughout a matrix. The changes to the bulk phase can be segregated into two distinct categories: **bulk erosion** and **surface erosion** [10]. In the case of bulk erosion, the material degrades or deforms uniformly throughout the bulk of the material. As the deformation proceeds, the volume of the material remains constant while the mass of the material reduces, resulting in a decrease in the density of the degrading material. In the case of surface erosion, the material degrades from the outer surface inward uniformly only at the interface between the bulk of the material and the surrounding environment. As the deformation proceeds, the volume of the material decreases linearly with mass, which results in the density of the material remaining constant (Fig. 2.2).

This is a critical distinction between the two approaches that distinguishes their responses to physical stress and dictates their application. Materials that *retain volume but reduce density* become porous and brittle over time, with weaker mechanical integrity. This effect can occur with swelling or dissolution, covalent bond rupture, and secondary bond dissociation within the system [11]. Materials with brittle and porous structures resemble weak ceramics that can crumble or crack in response to shear, compression, or tensile pressure [12]. Materials where *density is constant* have a more predictable response to physical external stresses. If volume is lost, however, the function of the material may be compromised (i.e., see embolics [13]).

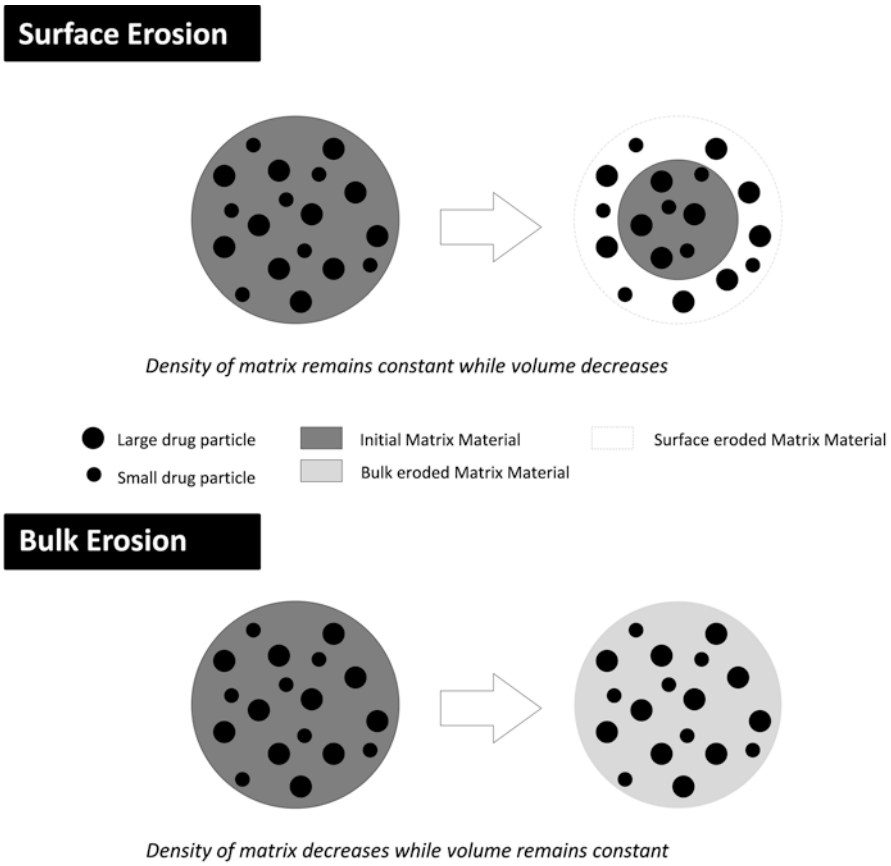

Fig. 2.2 Diagram of erosion mechanisms found in matrix systems

2.2 Material Design

2.2.1 Networked and Porous Structures

Given the different physiological environments possible for a controlled delivery approach, the next questions we can ask are

How can we predict when it is appropriate to select a bulk or surface erosion system?
How can we design a system to minimize or maximize its response to physical stimuli?

The simple answer is that it depends on two major characteristics: (1) the pharmacokinetics of the desired drug and (2) the function of the material construct being introduced into the physiological environment.

2.2.1.1 Pharmacokinetics

A majority of drugs in their base state display a first-order release, often referred to as "burst release," followed by a steady decrease in drug concentration in the physiological environment [14]. The pharmacokinetics of this initial approach shows a series of peaks and troughs over time. These peaks and troughs represent multiple extreme minima and maxima and are the most nonideal in terms of limiting the potentially toxic overdosages of drug molecules. The ideal pharmacokinetic response curve is represented by a zero-order kinetic response over time [15], where the drug has a steady state of delivery over a fixed time. The drug molecule system with a zero-order response allows for the delivery of a consistent amount of drug over time in a kinetically controlled system according to Eq. (2.1):

$$\frac{\delta m}{\delta t} = \frac{DS}{Vh}\left(C_s - C_t\right), \tag{2.1}$$

where δm is the rate of dissolution, D is the diffusion coefficient of the compound, S is the surface area of the drug product, C_s is the concentration of the solid in the diffusion layer that surrounds the solid, C_t is the concentration of the solid in the bulk dissolution medium, V is the volume of the dissolution media, and h is the thickness of the diffusing film adjacent to the surface being dissolved. The release can also be analyzed using the Higuchi model [15] as a way of determining the dissolution of a drug from a matrix. The Higuchi model for the amount of drug released over time (Q_t) can be written in the form

$$Q_t = k_H t^{1/2}, \tag{2.2}$$

where k_H is the Higuchi model release rate constant and t is time. Similarly, the Korsemeyer–Peppas [15] equation can be used to determine the mechanism of drug release; it is written in the form

$$\left(\frac{M_t}{M_\infty}\right) = Kt^n, \tag{2.3}$$

where M_t is the amount of drug released at time t, M_∞ is the total amount of drug present, K is the kinetic constant, and n is the diffusion exponent. This model allows for the mode of kinetics to be determined by the diffusion exponent value (n). Values of $n = 0.5$ indicate Fickian diffusion, or drug release that is diffusion-controlled, as in the Higuchi model. If the diffusion exponent is in the range of $0.5 < n < 1$, it indicates anomalous diffusion, or drug release that is both diffusion-controlled and erosion-controlled. If $n = 1$, it indicates case II transport, or drug release that is zero-order, where the release rate is constant and controlled by polymer relaxation. Finally, when $n > 1$, it indicates super case II transport, or drug release that is erosion-controlled.

The kinetic plot shown in Fig. 2.3 indicates a zero-order cumulative release of drug over time. This contrasts the sustained-release kinetic profile, which appears *first-order* in nature. The *first-order* release kinetics show a significantly slower, and consequently more variable, release rate over time (Fig. 2.3).

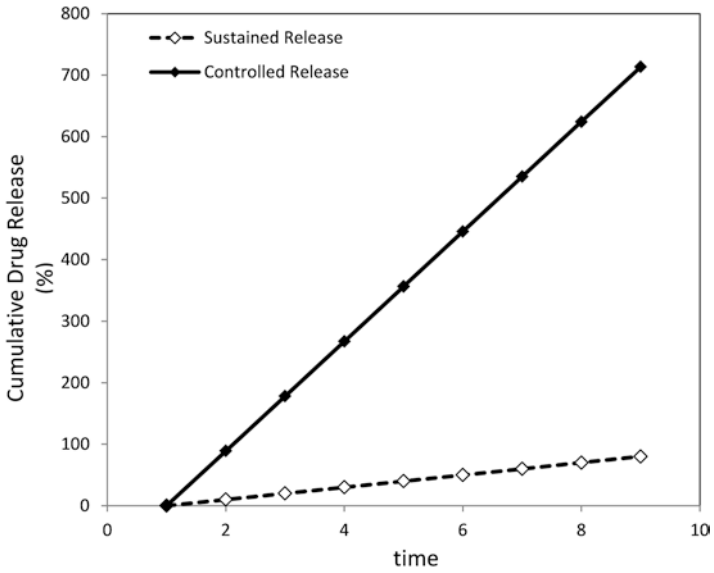

Fig. 2.3 Plot comparing zero-order and Fickian release kinetics (controlled release translates to zero-order release kinetics, while sustained release translates to first-order release kinetics)

The selection of the mode of release, zero- or first-order, relates to both the time required within the physiological system to reach the intended target and the desired dosage of drug to be delivered when it arrives.

2.2.1.2 Polymeric Materials

In order to effectively design a system to exploit the appropriate release kinetics, we need to discuss a basic grounding in polymer science. Polymers are commonly used as matrix or composite materials for controlled-release systems [16]. Polymers consist of a long chain of repetitive monomer segments, or mers, that are covalently bonded to one another. One does not have to look far to see examples of polymers in daily life. From plastic bottles (polyethylene) [17] to windows (polymethylmethacrylate) [18] to Blu-ray discs (polycarbonate) [19] to proteins (polyamide) [20], we see examples of polymeric materials, and it is critical to understand their benefits and limitations for applications in biological systems. In fact, our own DNA [21], to a material scientist, is considered an elaborate high-molecular-weight polymer chain!

The common structural nomenclature for polymer molecules is shown in Fig. 2.4; the bracketed area represents the repeat unit, or the repeated chemical domain, and the value *n* represents the **degree of polymerization** (**DP**), or the number of repeated domains, of the polymer molecule. The theoretical molecular weight of a polymer can be calculated by multiplying the molecular weight of the repeating unit by the value *n,* or the DP.

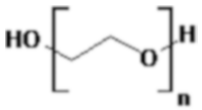

Fig. 2.4 Standard polymer structural nomenclature

Typically, polymers are described in terms of their **molecular weights** [22]. The molecular weight of a polymer is a unique property to this species of molecule since its physical properties of interest for our discussion include viscosity [23], degradation [24], and stimuli-responsiveness [25]. The glass transition temperature [26] (T_g) can be derived from this value.

Sample Problem 2a
In the case of two polymer molecules of polyethylene glycol with molecular weights of 1,000 Da and 20,000 Da dissolved in water, which polymer would you expect to have the higher viscosity?

We would expect that the polymer with the molecular weight of 20,000 Da would have a higher viscosity than the one with the molecular weight of 1,000 Da. Therefore, all domains being of equal functionality and concentrations, the higher molecular weight means the higher the viscosity. This, in fact, holds true.

While this reasoning appears to be fairly implicit, these properties become sufficiently more complicated, however, when looking at characteristics such as biodegradation, which will be addressed in examples throughout this text.

The molecular weights of polymer molecules differ relative to the method of their creation. For biologically created or synthesized polymers, such as proteins and DNA, the polymers have perfectly uniform chain length, molecular weight, and DP. This is somewhat of a relief since this specificity is tied to their physiological function, and the slightest imperfection of even one monomer unit may lead to significant repercussions in nature [27]. In synthetic systems, however, polymer chains are not all the same DP, but instead are a distribution of chain lengths. This is due to a number of factors that are tied to the organic chemistry of the monomer reactions. As a synthetic reaction proceeds, a few factors can predominate in the creation of a polymer. Generally, as the reaction propagates, the viscosity will increase, while the number of reactive monomers will simultaneously decrease since they are being consumed to form the polymer. As the reaction moves to a higher viscosity, the mobility of molecules in the system slows while the number of monomers that remain significantly decreases (Fig. 2.5).

This leads to a distribution of molecular weights and a percentage of the reaction that remains incomplete. The broadening and narrowing of this distribution can be tied to the synthetic method used to make the desired polymer molecule.

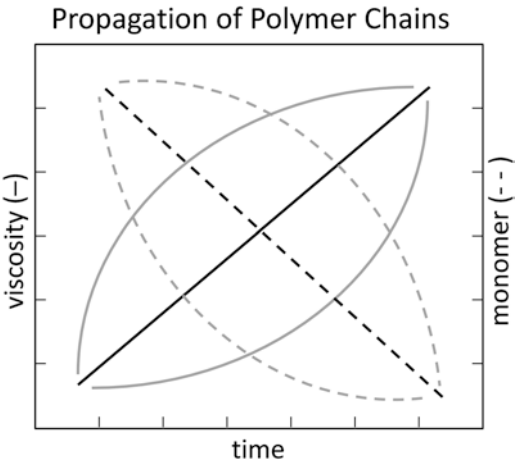

Fig. 2.5 Diagram of viscosity behavior with propagation of polymerization

Traditionally, molecular weights are described in terms of their number average molecular weight (M_n) [Eq. (2.4)], their weight average molecular weight (M_w) [Eq. (2.5)], and their molecular weight distribution or polydispersity index (M_w/M_n or PDI or MWD) [Eq. (2.6)] [28]:

$$\sum M_n = \sum \left(n_i M_i \right), \tag{2.4}$$

$$\sum M_w = \sum \left(w_i M_i \right), \tag{2.5}$$

$$\text{MWD} = \text{PDI} = \frac{M_w}{M_n}. \tag{2.6}$$

In the case of the molecular weight distribution, the M_w and M_n represent statistical overestimates and underestimates, respectively, of the actual molecular weight. The M_n is a summation of the number of molecular weights at each discrete chain length.

Sample Problem 2b
If a polyethylene glycol polymerization has five polymer chains with molecular weight 1,000 Da, three with 15,000 Da, and two with 50,000 Da, what would be the number average molecular weight?

The M_n would be $(5 \times 1{,}000) + (3 \times 15{,}000) + (2 \times 50{,}000)$ all divided by the total n, which in this case would be 10. Therefore, M_n for this example would be 15,000 Da.

The M_w is a summation of the weight fraction of molecules of each respective molecular weight.

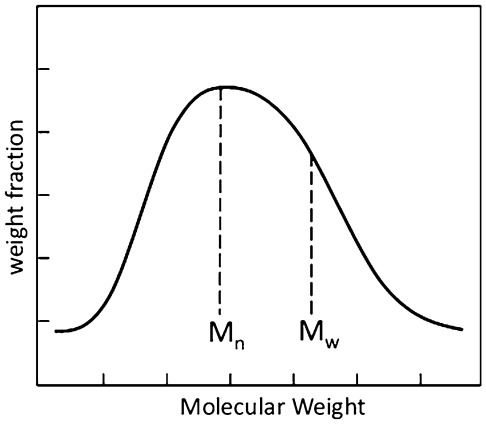

Fig. 2.6 Diagram of the molecular weight distribution as described in terms of M_n and M_w

Sample Problem 2c
If the same polyethylene glycol polymerization has five polymer chains with molecular weight 1,000 Da, three with 15,000 Da, and two with 50,000 Da, what would be the weight average molecular weight?

The M_w would be $(5 \times 1{,}000^2) + (3 \times 15{,}000^2) + (2 \times 50{,}000^2)$ all divided by the total weight fraction, which in this case would be $(5 \times 1{,}000) + (3 \times 15{,}000) + (2 \times 50{,}000)$ or 150,000. Therefore, M_w for this example would be 37,867 Da.

The molecular weight distribution (PDI) is a ratio of the weight average (M_w) and number average (M_n) molecular weights (Fig. 2.6).

Sample Problem 2d
For the same polyethylene glycol polymerization with an M_w of 37,867 Da and M_n of 15,000 Da, what would be the molecular weight distribution?

The molecular weight distribution would be M_w/M_n. Therefore, M_w/M_n for this example would be 2.52.

There are three PDI ranges that define the molecular weight uniformity [29] of a polymer molecule. The first range consists of perfect uniformity of molecular weights, which is defined as when M_n is equal to every individual M_i. The second range consists of polymers with a PDI of 1.0–1.5. These polymers are statistically uniform, contain highly predictable properties, and typically are run to a high degree of conversion of monomer to polymer. The third range consists of polymers with

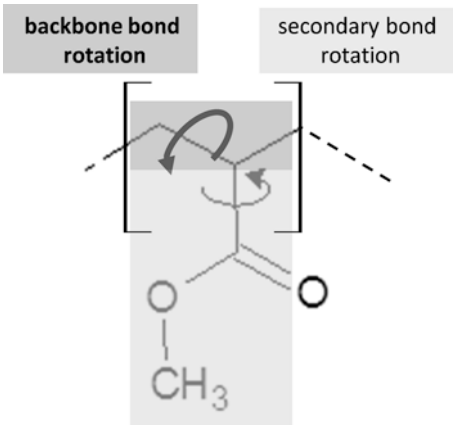

Fig. 2.7 Diagram of rotational modes of common polymers

PDI > 2.0. These polymers are statistically disperse and typically consist of a number of competing side reactions that can act to complicate their use in biological applications by introducing an undesirable chemistry to the human physiology unless otherwise addressed. Current examples of controlled-release systems use polymers that fall in the second or third range, whereby special attention is required to mitigate undesirable side effects.

We have discussed that the molecular weight can influence the properties of the matrix or surface used in a controlled-release system by the method of synthesis, the magnitude of the M_n or DP, and the values of the molecular weight distribution. The molecular weight is also integrated with the glass transition temperature (T_g) as well. The T_g is described as the temperature above which an amorphous polymer behaves like a viscous fluid or rubber and below which it behaves like a glass or brittle solid. The molecular weight can act either to shift the value of the T_g or to increase the rate at which the transition effects occur. If we look closer at T_g on the molecular level, it is also described by Adams and Gibbs [30] to be the temperature below which polymer backbone rotation slows or ceases while secondary molecular bond rotation remains (Fig. 2.7).

The Adams and Gibbs [30] definition provides a perspective on the effects that T_g can have on the matrix of controlled-release systems. Until this point, we have discussed controlled-release systems (matrix or reservoir) releasing via either surface or bulk erosion. In selecting your polymeric material for either of these systems, it is important to verify that the T_g of that polymer is amenable to the properties (i.e., density, volume, porosity) of that system [31]. We can ask, for example, what is occurring in this system with respect to its volume and density characteristics? For a matrix system with a bulk erosion release mechanism, the density is decreasing while the volume remains constant. Since it is a matrix system, there needs to be a base level of physical integrity to sustain the shape and function, and this needs to be maintained while the density of the system is decreasing. For this reason, the

design requires a polymer with a $T_g > 37$ °C, and likely in a stable temperature regime >60 °C.

This example accounts for more rigid systems. Special care should be taken as $T_g > 100$ °C since those polymers tend to be more brittle. What is occurring in systems that swell, with respect to their volume and density characteristics? For a reservoir system with a nonuniform volume expansion release mechanism, the volume is increasing with no net material loss other than the release of your drug. This system requires that the polymeric material be elastic in response to the volume expansion or swelling behavior. For this reason, the design requires a polymer with $T_g < 37$ °C, and likely in a stable temperature regime 0 °C $< T_g <$ 37 °C.

This example accounts for more elastic systems. Special care should be taken as $T_g < 0$ °C since those polymers tend to have a higher degree of viscous flow.

As T_g is shifted between higher and lower levels, the view of these systems in terms of molecular motions aids in determining the upper and lower thresholds of each temperature regime. For systems requiring elasticity for swelling, the lower T_g limit is established. While the T_g in this case can refer to the temperature at which the secondary molecular motion starts or stops, a low T_g (i.e., <0 °C) under physiological temperatures could lead to mobility of polymer chains past one another, or viscous flow. Viscous flow acts to destabilize an elastic network and subsequently change the release characteristics. For applications in physiological systems, the general rule of thumb is the operational temperature range of interest is 37 °C (±37 °C).

2.2.1.3 Biodegradation

Up to this point, the discussion has been abstract in its description of the chemical functionalities that are appropriate for the design of controlled-release systems. While the basic physical principles of polymer chains and structures have been discussed, the specific functionalities provide information regarding response to physiologically relevant stimuli. The degradation or, more specifically, biodegradation can govern a number of the major characteristics discussed thus far. Biodegradable polymers are composed from a pool of several common bonding types [32] (Table 2.2).

The mode of degradation behavior of polymeric materials can be separated into the following categories: oxidative, chemical, radiation, biological, and stress-induced [33]. For the purposes of biodegradation, we will limit our discussion to chemical and biological modes since the other modes do not represent a reasonable level of occurrence in drug delivery applications. The chemical mode is often the hydrolysis of a labile covalent linkage in either the backbone of the polymer or the pendant (i.e., side group) functionality. For example, if a polyamide undergoes hydrolysis, the peptide bond is cleaved to give amino acid products (Fig. 2.8).

Often this level of chemical hydrolysis can occur in different organs of the body, such as the stomach, where levels of (H^+) ions are high (i.e., pH 2) [34]. Chemical hydrolysis can also occur outside the body, where a diagnostic test may be exposed to aqueous conditions. The biological mode [35] is commonly referred to as the

Table 2.2 Examples of common degradable polymers used in controlled-release applications

Polymer	Degradable bond	Biodegradation	Examples
Polyanhydride	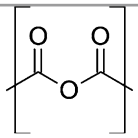	Hydrolysis	Poly(sebacic anhydride), poly(adipic anhydride)
Polyorthoester	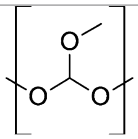	Hydrolysis	Dioxolane-based diketene acetals
Polyurethane	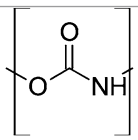	Hydrolysis- or enzymatic-mediated degradation	Chronoflex®, Pellethane™, Bionate®
Polyamide	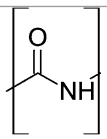	Hydrolysis- or enzymatic-mediated degradation	Poly(hexamethylene adipamide), poly(peptide)
Polyester	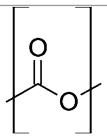	Hydrolysis- or enzyme-mediated degradation	Poly(lactide), poly(caprolactone)
Polycarbonate	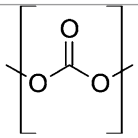	Hydrolysis- or enzymatic-mediated degradation	Lexan®, Apec®

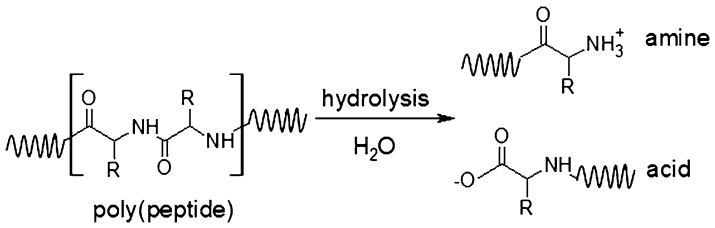

Fig. 2.8 Scheme of the general mechanism for the chemical hydrolysis of a polypeptide

enzymatic-mediated degradation mode, where an enzyme acts to activate a peptide bond, typically in a select location within the peptide sequence, for bond cleavage reactions. The enzymatic route [36] relies on a peptide being of a specific, stereochemical, geometry (i.e., tertiary structure) to fit into a catalytically active site on the enzyme. Once occupying this site, the peptide is activated for hydrolysis typically by a nucleophilic attack followed by a regeneration of the active enzymatic

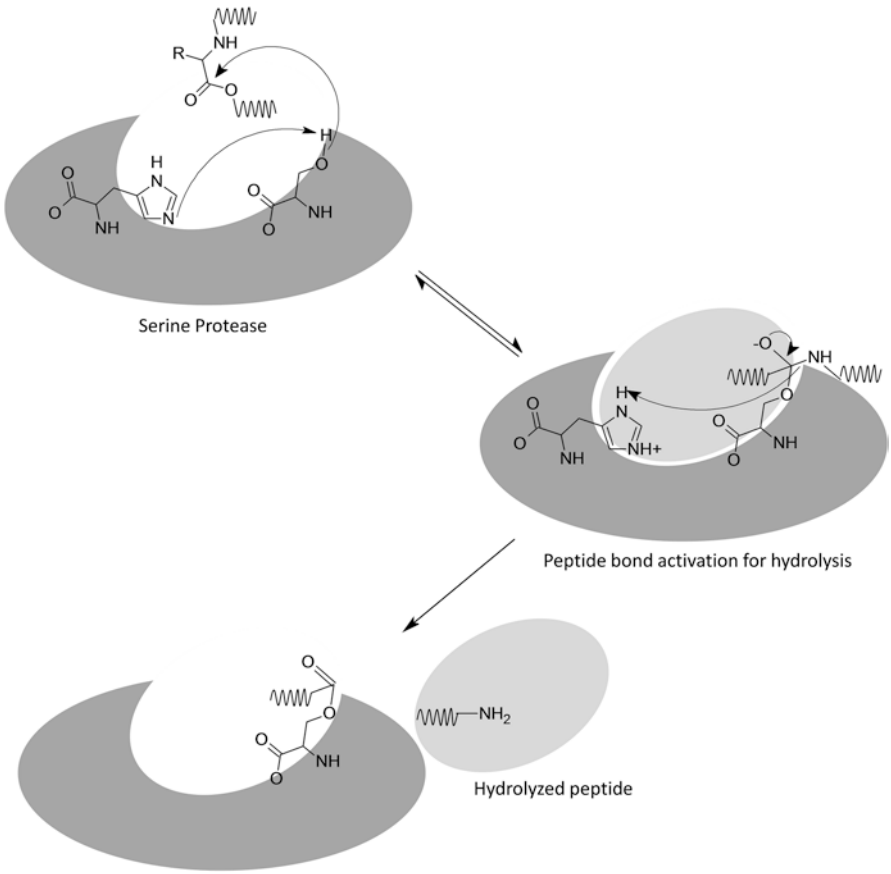

Fig. 2.9 Scheme of the general mechanism for the enzymatic hydrolysis of a polypeptide

site. For example, the case of serine protease enzyme acts to hydrolyze a peptide bond by nucleophilic attack of the peptide carboxylate by a serine residue that is stabilized by proton transfer between the histidine and serine residues of the catalytic binding domain. The rearrangement of electron density of the bound state leads to the release part of the cleaved peptide chain, leaving the remaining portion bound to the serine residue, which then is released, leaving the regenerated catalytic domain (Fig. 2.9).

What is commonly seen, however, is a combination of the chemical hydrolysis mode with the enzymatic-mediated degradation mode [37]. Some polymers, such as polyorthoesters, are in a majority of cases chemically hydrolyzed, while polyamides are degraded through both routes described here.

To frame this in our discussion thus far, we know that the erosion or degradation mode of the polymeric material can dictate whether the system hollows bulk or surface release kinetics and whether it would function as a matrix or reservoir

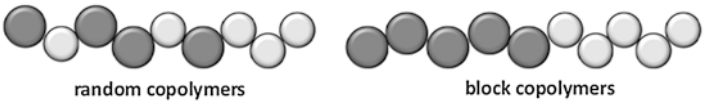

Fig. 2.10 Diagram of the random and block domain morphologies

system. The selection of the appropriate biodegradable material must follow the appropriate, predictable, rate of degradation. In the discussions regarding the mode of biodegradation, it is important to distinguish both the dominant mode of degradation and whether a desirable mode is present in the area of physiological release. What would you expect the degradation mode and T_g to be for a flexible poly(lactic-co-glycolic acid) polymer molecule? A matrix system comprised of poly(lactic-co-glycolic acid) (PLGA) typically takes on a bulk degradation whereby the rate of hydration into the matrix is greater than the rate at which the PLGA polymer is solubilized. This hydration also causes a polymer relaxation, shifting the T_g to a lower value, which increases the degradation rate.

In addition to the mode of biodegradation, the release kinetics are affected by the composition and molecular weight of the polymeric species used. Up to this point, we have assumed that our molecular weights of biodegradable species remain unchanged and our polymeric systems were homogeneous in nature. In fact, a majority of biodegradable systems for drug delivery are copolymers composed of two or more domains of degradable bond types. We will go into copolymers in more detail in the remaining chapters of this book. As a cursory view for this discussion, however, imagine copolymers as two or more functional monomers , which in our case are degradable bond types, grouped within a single polymer in one of two ways: either randomly distributed throughout the polymer chain (i.e., random copolymer) or grouped into discrete homogeneous domains next to another different homogeneous domain (Fig. 2.10) within the same polymer chain (i.e., block copolymer).

Looking closer at polymer composition, we can see that the weight fractions of different biodegradable groups and their molecular weights can influence both the rate of biodegradation (or erosion) and the percentage of the total material degraded [38]. For the purposes of this initial discussion, we will assume that all fabricated biodegradable species are in the same geometric conformation (i.e., tablet, disc) with the same dimensions. The erosion rate profiles of all species follow the same pattern. Initially, there is an induction period, which is dimensionless, or no change in rate of erosion based on the dimensions of the material. There is then a peak in erosion rate, followed by a sharp decrease. Both the timing of the peak and the duration of peak time prior to the decrease will stratify materials based on dimension and geometry. For example, in the case of drug discs, the thickness is approximately directly proportional to the time of the peak rate before reaching the decrease. For thicker discs, one would expect a longer erosion at the peak rate. For thinner discs, the erosion at the peak rate would be expected to be shorter. This is true for either bulk erosion or surface erosion cases (Fig. 2.11).

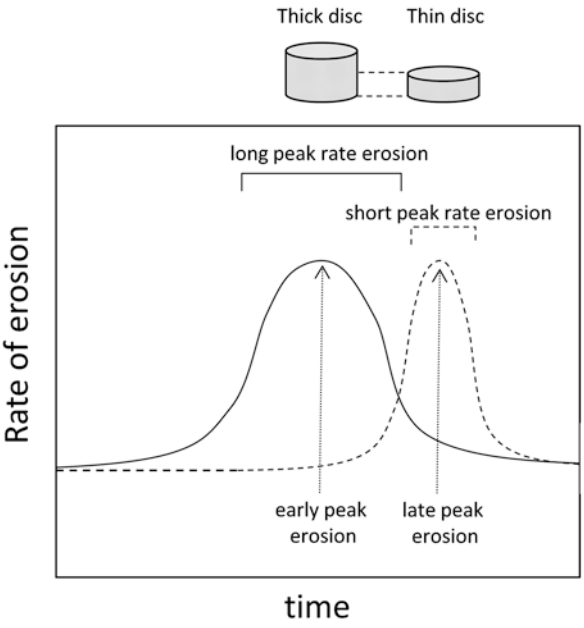

Fig. 2.11 Plot of the changes in the rate of erosion with changes to geometric shape

What if we now move into systems composed of two distinct erosion regimes? This could include a copolymer system, with each domain composed of a polymer with its own distinct erosion regime, or mixture of two polymer systems with different erosion regimes. This approach is commonly used to fabricate systems with multiple release phases. For example, in a layered system that undergoes surface erosion, the outer layer could dissolve at a faster rate than the inner surface. This method could be used to provide the delivery of a two-component system in a time-controlled method, predicted through the use of surface erosion properties.

For systems with a mixture of materials with two distinct erosion regimes, the amount of eroded material over time will show different degradation kinetics with each component. Both the kinetic differences and the positioning of the biodegradable polymer within the system help to dictate the overall shape and threshold of the kinetic curve. For example, in the case of a surface release system with multiple layers, if the outer layer is rapidly degradable relative to the inner layer, the percentage of eroded polymer will begin at a higher rate and will plateau over time. The inner layer would show a more gradual degradation over time due to unimpeded, slow degradation kinetics (Fig. 2.12).

Another way of looking at the system is by observing the weight fractions of each biodegradable domain of either the copolymer or polymer mixture. This will provide information regarding the change in the weight fraction of biodegradable species with the movement of the *erosion zone*, or mode of erosion, through the system [39]. In systems that are spherical or disclike in geometry, this would

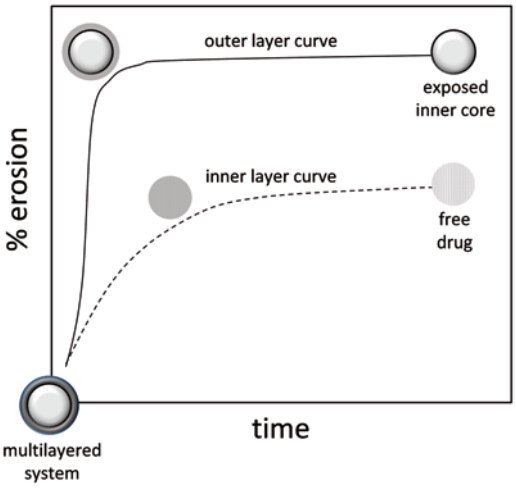

Fig. 2.12 Plot of the percent erosion with changes to the layering of a core-shell material

translate into the movement of the erosion zone uniformly from the outside surface toward the core. Let's look at a specific system comprised of a block copolymer with a polymer domain A, which is an 80:20 weight fraction of polymer functionality A to polymer functionality B, and polymer domain B, which is an 50:50 weight fraction of polymer functionality A to polymer functionality B. What would the system look like as it degrades? We would expect that the outer zone shows a rapid decrease in initial polymer domain A content relative to polymer domain B, whereas the inner zone retains the initial composition for a longer time. Therefore, polymer domain A is degraded from the erosion zone as it moves from outside to inside the system. The shell would then be polymer domain B material.

We have seen the changes to erosion and degradation due primarily to composition. One can infer that molecular weight would then act to change the rate of degradation (Fig. 2.13). A simple way of thinking about this would be cutting spaghetti. It would take less time to cut a plate of short spaghetti into small pieces than it would a plate of long spaghetti. As we move through subsequent chapters of this text, we will revisit erosion and degradation and highlight the effects of shape (Chap. 3), chemical functionality (Chap. 7), and morphology (Chap. 4).

2.2.1.4 Crosslinked-Networked Systems

The perspective of controlled-release materials becomes more complete when we look at crosslinked systems. **Crosslinked**, or **networked**, systems are comprised of any structure that is joined in a three-dimensional lattice of polymeric materials by covalent or secondary bonds. The premise of this approach is to induce the formation of a lattice surrounding drug molecules, in essence encapsulating them in a

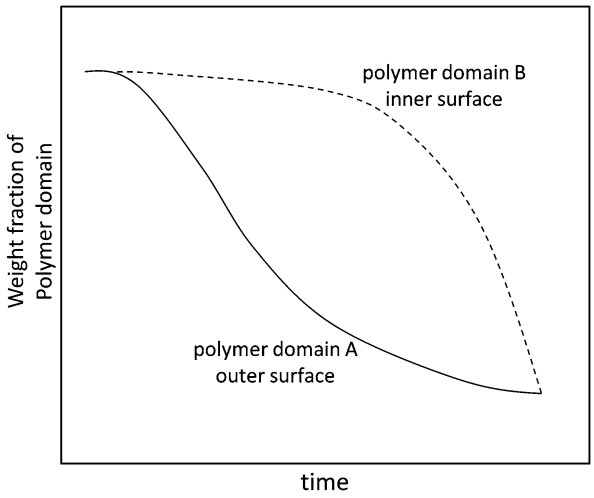

Fig. 2.13 Plot of the weight loss of a multilayered material due to degradation with time

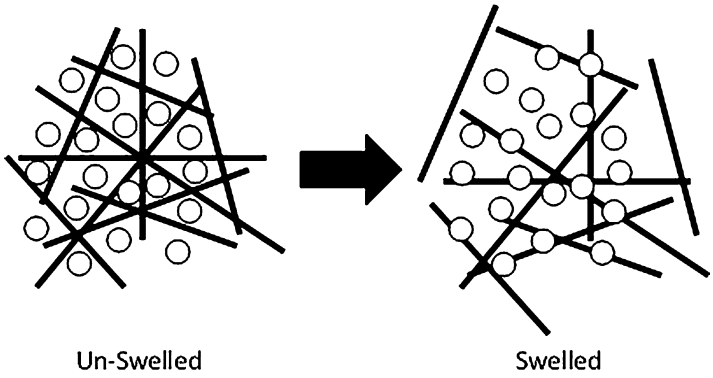

Fig. 2.14 Diagram of crosslinked systems in swelled and unswelled states

matrix [40]. The properties of the lattice typically are similar to those of the matrix systems discussed earlier in this chapter, whereby degradation or swelling drives drug release (Fig. 2.14).

In crosslinked systems, the key design characteristics are (1) crosslink density, (2) type of bonding, (3) molecular weight, (4) rigidity, and (5) T_g [41]. The **crosslink density** dictates the size of the drug species being encapsulated, or vice versa, and relates to the amount of drug that can be released at any given time. It also provides an indication of the structural integrity of the system. Materials with high crosslink densities tend to be stronger materials due to their having a higher number of points to dissipate stresses to the system. Think of it as denser scaffolding on a building. The higher crosslink density also allows for the tighter hold over smaller drug species. In order for release to occur via a crosslink density mechanism, the

crosslink point must be either reversible, as in secondary bonding, or responsive, as in degradation or another stimulus. The **type of bonding** at crosslink points dictates the energy, type, or magnitude, required for the collapse of the system. The collapse of the system induces release of drug species [42]. The system can be designed to have covalent, secondary, or labile bonds that are responsive to swelling, temperature, concentration, light, or sound, among others. The **molecular weight** [43] of constituent polymers can indicate the degree of swelling, when coupled with the crosslink density, or the rate of degradation. The values for M_n, M_w, and PDI are important for determining the extent of control the polymer molecular weight has on these behaviors. The **rigidity** [43], or *structural rigidity of the polymer chain,* ties into the functionality of the polymer and the degrees of bond rotation. As a general rule, the higher the number of bond rotations within the polymer structure, the greater the chain flexibility. The chain flexibility is correlated to the rate and threshold of swelling of the system. The more flexible the system, the higher the swelling, assuming the molecular weight is constant among compared species of polymer. The T_g [43] of constituent polymers also has implications relative to the rigidity of the polymer molecules. Higher bond rotations typically correlate with lower T_g materials since more energy—in this case, temperature—must be removed from the polymer system in order to allow for the slowing of the more numerous bond rotations. While the rigidity provides information regarding the swelling and release kinetics, the T_g provides information regarding the structural integrity of the swelled and unswelled species. In order to fabricate a successful controlled-release system, the designer wants to have either a stable structure upon release or a collapsed one. For a matrix system whose release is based on polymer swelling, one would want the swelled system to have some structural or mechanical integrity. This would lead to a balance between the rigidity of the polymer system and the T_g. For a matrix system whose release is based on biodegradable bulk erosion, the structural integrity is not a required property, and the selection of the polymer system is less restricted (Fig. 2.15).

2.2.1.5 Drug–Polymer Conjugates

To this point in our discussion, we have identified a number of design properties to exploit degradation, erosion, system shape, and release of encapsulated drug cargo. There are a number of drug delivery systems that can take advantage of any single property or combination of these properties [44]. Another approach works on the general premise that drug molecules can be made more physically durable, chemically stable, soluble, and amenable to processing by conjugating the drug to a polymer molecule. These conjugate systems can consist of the following isolated or combined design elements from our previous discussion in this chapter: molecular weight, polydispersity, biodegradation, swelling, crosslinking, chemical functionality, composition, and release kinetics [44] (Fig. 2.16).

The **chemical functionality** is perhaps the most critical point to address related to conjugate systems. The polymer is chosen, in part, to deliver a conjugated molecule

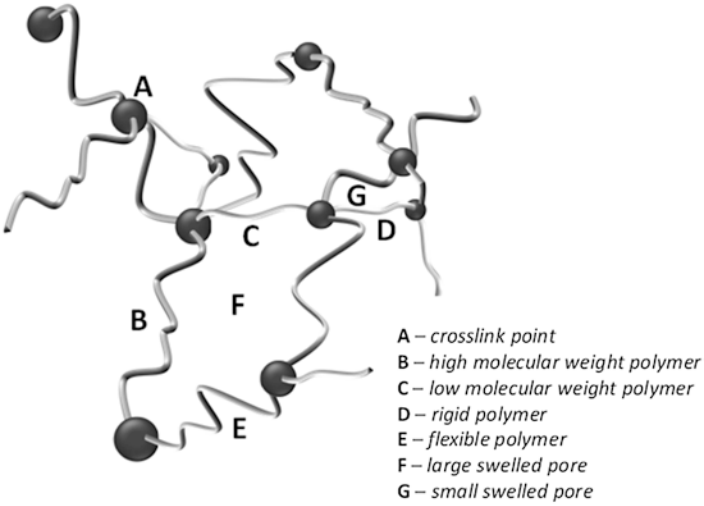

Fig. 2.15 Diagram of the components of crosslinked systems

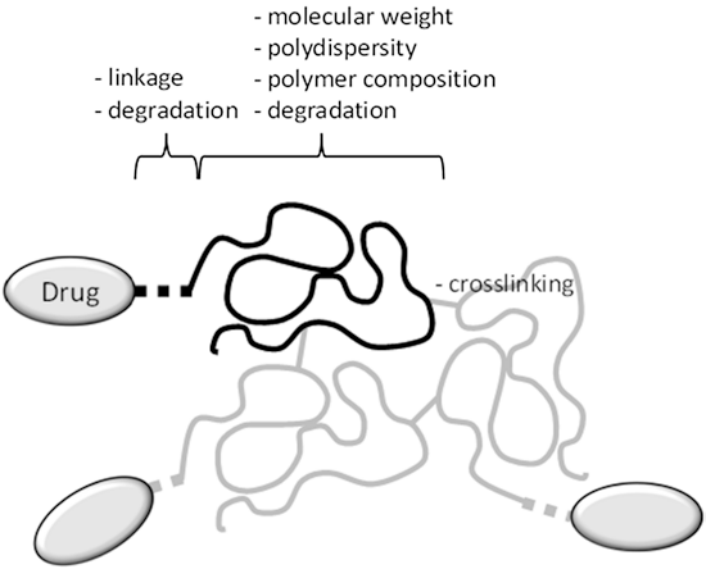

Fig. 2.16 Diagram of the components of drug–polymer conjugate systems

with more favorable aqueous solubility [45]. Care must be taken not to chemically degrade the drug molecule or protein molecule. Typically, the list of polymer candidates consists of the biodegradable polymer systems discussed in this chapter with the addition of PEG as a bioinert polymer. Each candidate is appropriate for the purposes of imparting favorable solubility to the system. In addition to functionality,

the **molecular weight** and polydispersity become relevant as well. The rate or threshold solubility is dictated by molecular weight [46]. The higher the molecular weight of a water-soluble species, or any species for that matter, the longer it takes for that molecule to solvate. Think of it from another perspective. In order for a polymer to be soluble in water, it must hydrogen-bond with water; therefore, the polymer chain must be entirely accessible to water molecules in the system. The larger the molecular weight, the slower the mobility of the polymer chain and the more *sterically* shielded the hydrogen bonding groups on the polymer chain to water. This is, for the most part, a time-dependent phenomenon whereby the polymer chain will eventually become fully solvated provided enough time has elapsed. The **polydispersity** simply allows for insight into the predictability of the behavior. We learned previously that a larger PDI indicates a broader distribution (PDI > 2) of molecular weights within the system. If the system being designed requires specific control over viscosity or degradation, then one would benefit from a narrower PDI (PDI 1.0–1.5).

The **biodegradation** encompasses two regimes of the design: the backbone polymer and the linkage. The backbone polymer may or may not be desired to be a degradable species. In this case, the degradation of the polymer system would lead to a marked reduction in the localized viscosity, potential change in the solubility of the system, and exposure of the drug to its immediate environment [47]. Care must also be taken that biodegradation conditions do not compromise the drug function themselves or yield degradation products that compromise drug function. The linkage could be one of the degradable functional groups discussed earlier in the *Biodegradation* section in this chapter, or it could be a stimuli-responsive group triggered by temperature [48], light [49], sound [50], magnetic field [51], or electric current [51]. The stimuli-responsive linkages are discussed in greater detail in Sect. 7.2.1. The linkages typically occupy either the end groups of the polymer chain or the side chain (i.e., pendant) groups.

The design of a conjugate system can break into two general classes: particle systems or **crosslink** systems. It should be noted that there are a number of examples for systems comprising both properties (i.e., hydrogel particles); however, for simplicity, we'll start with these two classes here. *Particle systems* are those described earlier in this chapter referring to erodible or degradable matrix systems driven by bulk or surface erosion. *Crosslinked systems* refer to matrix systems whose release is dependent on **swelling** and changes to void volume with the addition of water [52]. Drug–polymer conjugate particle systems typically form 2–5-nm species that can be aggregated to form larger agglomerated microspheres for drug delivery applications [53] (Fig. 2.17). Drug–polymer conjugate crosslinked species can form gelled microsphere or fabricated surfaces for implantation (i.e., embolics).

The mode of **release kinetics** (i.e., zero-order or first-order) will depend on the degradation mode and rate, the swelling rate and absorption threshold (i.e., the maximum amount of water it can hold), crosslink density, polymer molecular weight, and polymer composition [54]. The polymer **composition** refers to the ratio of one polymer functionality to another different polymer functionality expressed in the same polymer molecule. Not only the ratio matters. The positioning within the polymer chain can influence the *self-asse*mbly of the polymer system in aqueous

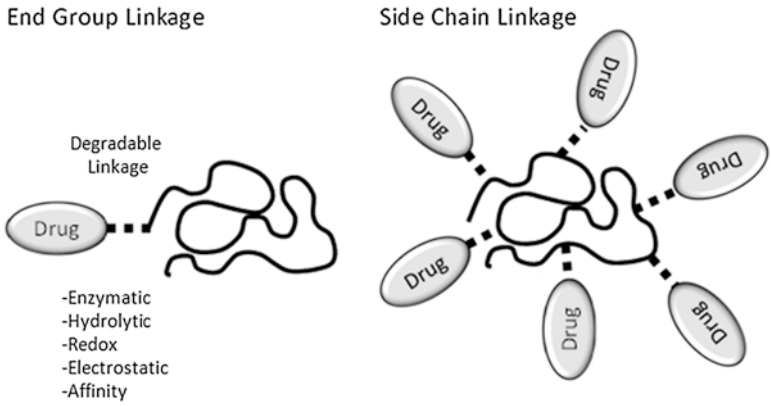

Fig. 2.17 Diagram of design strategies for drug–polymer conjugate systems

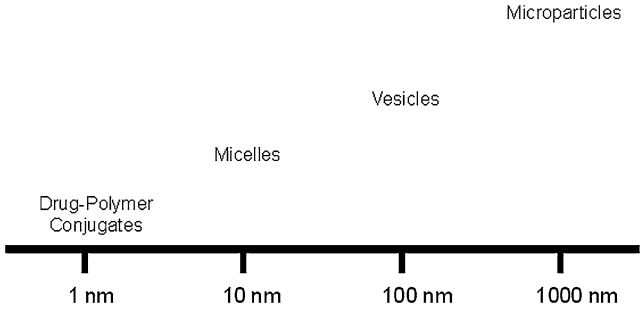

Fig. 2.18 Relationship between size and drug delivery system

environments. Self-assembly is discussed in more detail in Chap. 4. For the purposes of our discussions in this section, the polymer composition is strictly for the determination of degradation and release kinetics.

The drug–polymer conjugate process has a number of advantages over conventional controlled-release methods for several reasons. The size of these conjugate systems falls in the 1–5-nm regime [55], which is significantly smaller than traditional nanoparticles (Chap. 5), micelles (Chap. 4), vesicles (Chap. 4), and microparticles (Chap. 2). The size advantage is strictly application-dependent. The enhanced permeability and retention effect [56] (EPR), which is discussed in more detail in Chap. 4, imparts a size restriction for circulation through physiological systems to be possible. The smaller size regime for the conjugate materials allows for a number of biological modes of evacuation to be circumvented (Fig. 2.18).

Generally, conjugation of a polymer chain to a desired drug molecule or protein allows for adjustment of the dissolution or degradation of the drug complex. Polymer–drug conjugates, or as we will see later in Chap. 5 as **nanocarriers**, function as a drug molecule coupled to a polymer via some degradable or labile linkage [57]. This conjugate system can be fabricated in a number of ways to form

controlled-release materials with perhaps the widest range of applications currently known [58].

In each of our sections, we will deconstruct several critical characteristics of each of the approaches and show examples of the design criteria associated with each. It is important to keep in mind that the rational design of each of these methods relies on a substantially longer list of specific criteria; however, the approach taken here will ground the reader in the major fundamental properties governing the behavior we are seeing.

2.3 Implementation

2.3.1 Microspheres, Drug–Polymer Conjugates, and Biodegradable Particles

Traditionally, when one is approached with the task of identifying a controlled-release system, the term "gel caps" often arises. This may, in part, be due to the volume of sales, or the media attention in the late 1990s associated with "fast-acting" over-the-counter pain relief [59]. This typical example can be a good foundation to begin the discussion of fabricating a controlled drug release system. Gel capsules traditionally fall into one of two categories: single-piece [60] and two-piece [61] systems. Both are formed from aqueous solutions of gelling agents such as polysaccharides, gelatin, starch, xanthan gum, or a form of cellulose. The single-piece systems are formed when a drop of drug solution is sealed within a drop of the gelling agent, essentially creating a balloonlike structure where the gelatin functions as the barrier network between the drug environment and the surrounding physiological environment. This is an example of a **reservoir system,** which was described earlier in this chapter. The two-piece systems are formed by forming a film layer of gelling agent in the cavities from metal pins. The resulting cavities are blanketed with gelling agent, which looks similar to a hollow bullet casing. Two halves of casing are then filled with drug powder and compressed together to form the capsule (Fig. 2.19).

Based on the fabrication on the macroscale, we can see the influence on the constitution of the drug (i.e., liquid, powder) and its stability. What if we now move from this macroscopic view of the drug delivery to one where we can apply the fundamentals we have talked about in Sects. 2.1 and 2.2 to enhance the efficiency of drug release and delivery?

2.3.1.1 Microspheres

The term **microsphere** refers to spherical particles, typically consisting of polymeric or ceramic materials, in the size regime of 1–1,000 μm in diameter [62]. A more in-depth discussion involving nanoparticles, in the size regime <200 nm,

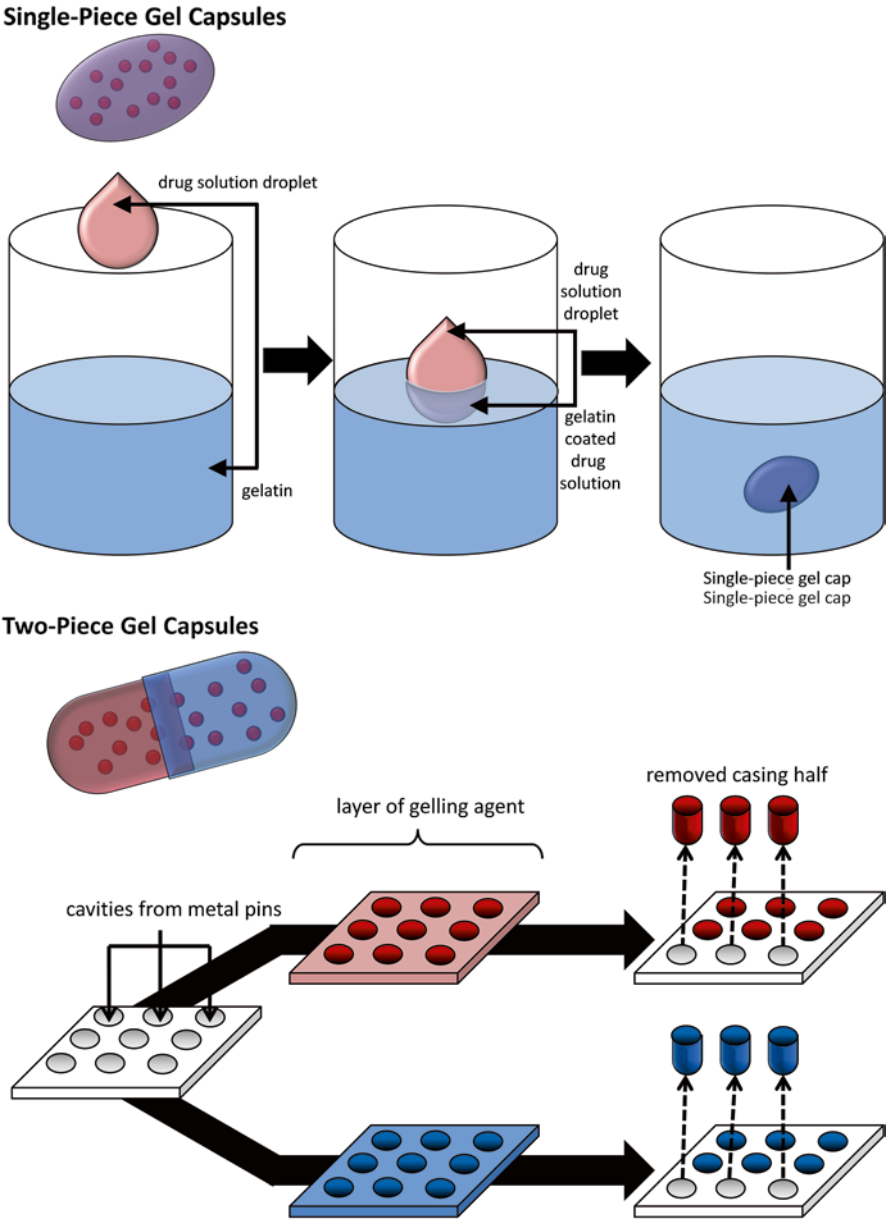

Fig. 2.19 Diagram of the common commercial controlled-release systems

appears in Chap. 5. A microcapsule is similar to a microsphere in that the size regimes are the same; however, the latter is hollow, whereas the former is not necessarily. So a microcapsule is always a microsphere, but a microsphere is not necessarily a microcapsule. The size regime can dictate the location and function of the material. In cases where the particle size is small enough (i.e., 1 μm), they are

capable of flow within a physiological system. In cases where the particle size is larger (i.e., 1,000 μm), they are typically stationary. To the designer, the size will tie into the function, where for small particles with flow, the controlled release of systemic drugs may be the goal, and for large particles that are too large for systemic flow, they are implanted at the site of infection. The fabrication of the correct particle size looks not unlike the two gel case examples discussed earlier. The advantages of the microsphere approach are increased active circulation, improved drug delivery, reduced side effects and toxicity, and injectability. There are a number of methods to successfully fabricate microspheres for drug delivery applications. A few of the more relevant methods at they pertain to drug delivery are the emulsion method [63], phase separation coacervation [64], spray drying [65], air suspension [66], solvent extraction [67], and particle replication in nonwetting templates PRINT® method(s) [68].

The selection of the drug and polymeric material(s) is of the utmost importance. The polymer must have controlled-release properties, water solubility, stability, low toxicity, drug shielding, long systemic circulation, and biocompatibility. The particle size of the fabrication process is also of critical importance and must tie into the function of the material.

The **emulsion method** [63] consists of single- or double-emulsion techniques. The single-emulsion technique involves solubilizing or dispersing a polymeric component within the aqueous phase of a mixture followed by the addition of an oil phase composed of the drug. Upon addition of the two components, the system is rapidly stirred and crosslinking of either the polymeric component or the oil phase by means of heat or covalent linkages occurs. The double-emulsion technique involves multiple emulsions within one another. The case of a water-in-oil-in-water (w/o/w) emulsion allows for the drug to be contained in either the aqueous phase, oil phase, or both. This is achieved by dispersing an aqueous drug solution in an organic hydrophobic continuous phase containing a soluble polymer, which also may contain drug constituents. The polymer in the hydrophobic phase will encapsulate the drug in the aqueous phase, which is an inverse of what occurs in the single-emulsion case. The solution is then exposed to homogenization to break up the emulsified particulates, followed by the addition of an aqueous polymer solution to stabilize the emulsion particulates formed. The final step involves the evaporation of the organic phase, yielding the last phase of a w/o/w emulsion.

The **phase separation coacervation** [64] method typically involves aqueous drugs but can involve hydrophobic drugs, to form a **reservoir** delivery system. This method involves two phases: a polymer-rich organic phase and an aqueous (or in the hydrophobic case simply) drug phase. The drug phase is added continuously to the organic phase, causing the polymer to be steadily exposed to an unfavorable solvent environment and form a coacervate with the aqueous drug particles (or drug particles) under high stirring to aid in the control of the particle size. The phase separation causing the formation of the coacervate can be accelerated or stabilized using salt, pH, or incompatible polymer.

The **spray-drying** [65] method involves the drying and stabilization of atomized polymer particles of drug molecules. This is achieved by dissolving the drug and polymer in a volatile organic solvent such as tetrahydrofuran, acetone, or methylene

chloride. The solution is homogenized in the event that it is not fully soluble. The polymer–drug solution is then flowed through an orifice that is attenuated through an atomization tip. This process can also be done using the process of electrospinning. In the electrospinning application of this process, the polymer–drug solution would be attenuated through a charged tip, and nitrogen flow coupled with a voltage differential relative to a grounded collection plate leads to the formation of sprayed microparticles.

The **air suspension** [66] method involves the drying and suspension of drug particles in an air stream. The suspended particles are then spray-coated with a rapidly drying polymer solution. Because the particles are consistently cycling through the system, the process allows for sequential coating or layered coating. While solid particles are typically used in this process, liquid particles and emulsions are also possible.

The **solvent extraction** [67] method involves the quenching of particle formation by the extraction of the organic miscible solvent in an aqueous phase. The organic phase is composed of polymer and is chosen to be miscible in water. The drug particles are added to the organic phase, which is then extracted using an aqueous solution. The size of the precipitated microspheres can be controlled by the temperature of the water, the solubility of the polymer, and the ratio of the polymer to water and organic phases.

The **PRINT®** [68] method was developed by DeSimone et al. and involves the top-down fabrication of microparticles of differing size, shape, strength, and surface functionality to drive a variety of applications, which include drug delivery. The process involves several steps borrowed from the electronics, materials, and chemical industries. The process begins by creating a master template using common lithographic etching techniques used in the semiconductor industry. A liquid fluoropolymer is then poured into the master template and set by the photocrosslinking process. Once the material is solidified after the crosslinking process, it is removed from the master template, resulting in the precise mold that is used for the remainder of the process. A liquid solution of drug and polymeric material is then poured into the template, pressed by a roller to ensure complete template filling without bleedover, and allowed to set. The solidified material is then transferred to a harvesting film that allows for facile removal of cast materials (Fig. 2.20).

Currently, at the time of drafting this text, PRINT® materials are not typically referred to as microspheres, due in part to their size (1–3 μm) being on the low end of the size regime commonly used and their ever-changing shape as a driver for their fabrication method. Instead, they are referred to somewhat anomalously as **microparticles**, given the lack of reference to shape. It is becoming ever more accepted within the biomaterials community, however, that shape can be a factor contributing to the enhanced cellular internalization and intracellular trafficking of drug molecules.

The specified internalization of microparticles as large as 3 μm was recently demonstrated in nonphagocytotic HeLa cells by nonspecific endocytosis. The microparticles were poly(ethylene glycol)- (PEG) based hydrogels fabricated using the PRINT® system with fluorescent probes as intracellular markers. The microparticles

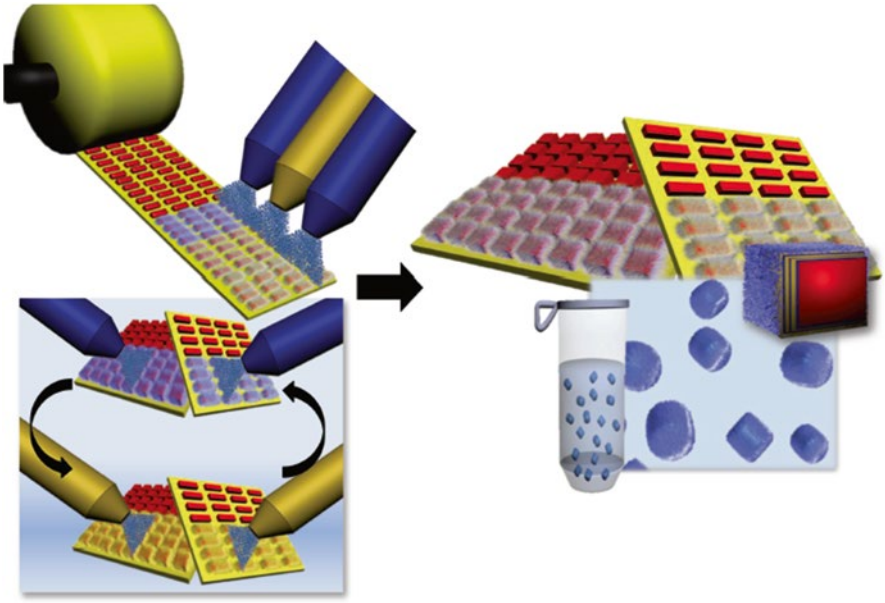

Fig. 2.20 Spray-LbL on PRINT nanoparticles. PRINT particles were fabricated and stored as particle arrays on the harvesting layer. Arrays were subsequently crosslinked under vapor-phase glutaraldehyde/concentrated acid conditions, followed by spray-LbL application (sequential deposition of polycation/wash/polyanion/wash comprising one bilayer). Functionalized particles were harvested by sonication of the arrays in water and purified by filtration and ultracentrifugation [68]

were cubic, cylindrical, and rod-like in shape and fabricated to different sizes and aspect ratios. It is a widely held belief that the upper size threshold for nonspecific internalization of particles is in the 150-nm size regime. Therefore, the particles fabricated using the PRINT® process highlight the additional importance of shape in addition to size to dictate preferential internalized drug delivery materials. There was also a benefit within the shape itself, where rodlike particles with a high aspect ratio appeared to internalize more than their cylindrical analogs (Fig. 2.21).

It would be appropriate to take what we have learned to this point in terms of controlled-release materials and apply those learnings to the microspheres developed using the PRINT® system. These PRINT® microparticles are designed as a **matrix** system. The drugs are to be loaded via the absorption of molecules with water within the PEG-based hydrogel matrix. Similar to how a sponge absorbs water, these hydrogels form in situ with drug molecules. The hydrogel system allows for a **bulk erosion** mechanism in the sense that the swelling of the matrix causes a net decrease in the density of the system since the volume is increasing with decreasing mass. Note that this is *not* bulk erosion in the classical sense since the volume does not remain constant with mass loss. This is in part due to the fact that the system is not undergoing any true erosion but rather a structural fluctuation that is reversible. In other words, one can oscillate the swelling and deswelling of

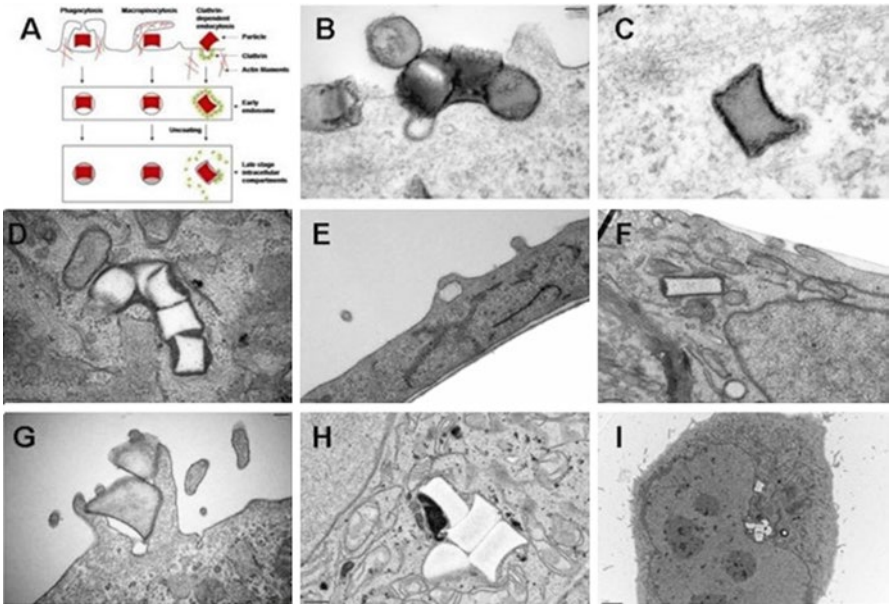

Fig. 2.21 Transmission electron microscopy images of HeLa cells at 37 °C (incubation times in parentheses). (**a**) Illustration depicting the major pathways of cellular internalization used by PRINT particles. (**b**–**d**) With 200-nm (AR-1) cylindrical particles (AR-1) (**b** and **c**, 15 min; **d**, 4 h). (**e** and **f**) With 150-nm (AR-3) cylindrical particles (**e** and **f**, 1 h). (**g**–**i**) With 1-**μ**m (AR-1) cylindrical particles (**g**, 1 h; **h** and **i**, 4 h) [68]

the hydrogel as a mode of releasing drug as opposed to a true bulk erosion system where once the system erodes, the behavior is exhausted. Perhaps the more accurate indicator of the drug delivery within the hydrogel system described here is the zero-order release kinetics. The zero-order or *burst release* kinetics is dependent on the swelling of the hydrogel system and not the concentration of drug or environment (i.e., first-order) to induce the release of drug molecules. This allows for release upon hydration, the rate of which is dependent on crosslinking. The crosslinking within these hydrogels depends primarily on the crosslink density and the molecular weight of the PEG molecules. As an aside, to refer back to our discussion earlier in this section, the type of bonding in this case is covalent to form the crosslinks, the rigidity is considerably low due to the high number of bond rotations possible for PEG polymers, and the T_g is low since PEG is a highly flexible polymer with no functional side groups. The crosslink density dictates the pore size or void space within the hydrogel matrix. As the number of introduced crosslink points increases, the size of the voids decreases. This is, of course, only if the molecular weight is held constant. The molecular weight adds to what we will refer to as the *threshold void space*. This is the maximum void space permitted in the system and is achieved upon full hydration of the PEG polymer chains in water. Therefore, one has the ability to tune the hydrogel system by adjusting the molecular weight and crosslink density to dictate the size of polymer release possible. We discuss hydrogels in more

detail in Chap. 6. The crosslinks in the hydrogel system are covalent in nature, leaving few chemical reaction possibilities in physiological systems. This is somewhat of a relief since, for the most part, these systems are meant to be stable in physiological environments. Finally, these hydrogels are PEG-based, so they are bioinert but not biodegradable. This poses a challenge from the application standpoint since the goal of use is the internalization of the system within a cell, which exposes it to an unknown physiological circulation time. We discuss the advantages of using a biodegradable polymeric material later in this section.

2.3.1.2 Drug–Polymer Conjugates

Earlier in this chapter , we outlined the major criteria for the design of a drug–polymer conjugate system for drug delivery as it relates to its chemical functionality, physical properties, and physical behavior. We can now begin to look at examples of conjugate systems in contact with living cells and tissue.

In cancer therapies, there is often treatment that involves the delivery of two drug components that need to interact in order to become functional [69]. Two such drugs are all-trans-retanoic acid (RA), a metabolite of vitamin A, and cisplatin(IV)-prodrug [Cis(IV)], a less toxic form of cisplatin that is an extremely effective solid tumor treatment. In combination, RA acts as a sensitizer to Cis(IV), acting to enhance its sensitivity concomitantly. Currently, the variability in the release kinetics, physiological sequestering, and transport inhibition across membranes has led to unpredictable efficaciousness of both drugs. Higher-potency combinations have led to serious side effects. One strategy adopted by Wang et al. [70] has been the use of a block copolymer [MPEG-b-p(LA-co-DHP)] composed of methylated-polyethylene glycol (MPEG) with a biodegradable copolymer of lactic acid (LA-co-DHP) as grafting agents for RA and Cis(IV). The design involves forming a reversible covalent linkage between the RA and the MPEG-b-p(LA-co-DHP) in one pot and forming a reversible covalent linkage between the Cis(IV) and the MPEG-b-p(LA-co-DHP) in a separate pot. The MPEG-b-p(LA-co-DHP) is what is known as an amphiphilic copolymer—which is discussed in more detail in Chap. 4—which self-assembles into large micelles (<200 nm) in water (Fig. 2.22).

The mixture of respective RA and Cis(IV) MPEG-b-p(LA-co-DHP) copolymers in water leads to the formation of a composite micelle of both drug forms within the same *micellar particle*. The premise of this approach is to introduce these micellar particles into the proximity of cancer cells, which will internalize these particles due to the *EPR effect* since their size is 100–200 nm. It should be noted that materials falling within the nanoscale size regime require a series of analytical methods to verify the size and size distribution. This is addressed in more detail in Chaps. 4 and 5. The endocytosis of the micellar particles compartmentalizes them into intracellular lysosomes, which have a lower pH (5) than in the extracellular environment (pH 7.4). The lower pH leads to hydrolysis of the biodegradable lactic acid segments of the MPEG-b-p(LA-co-DHP) copolymers. We know that both the molecular weight and composition of that lactic acid copolymer segment influence the rate

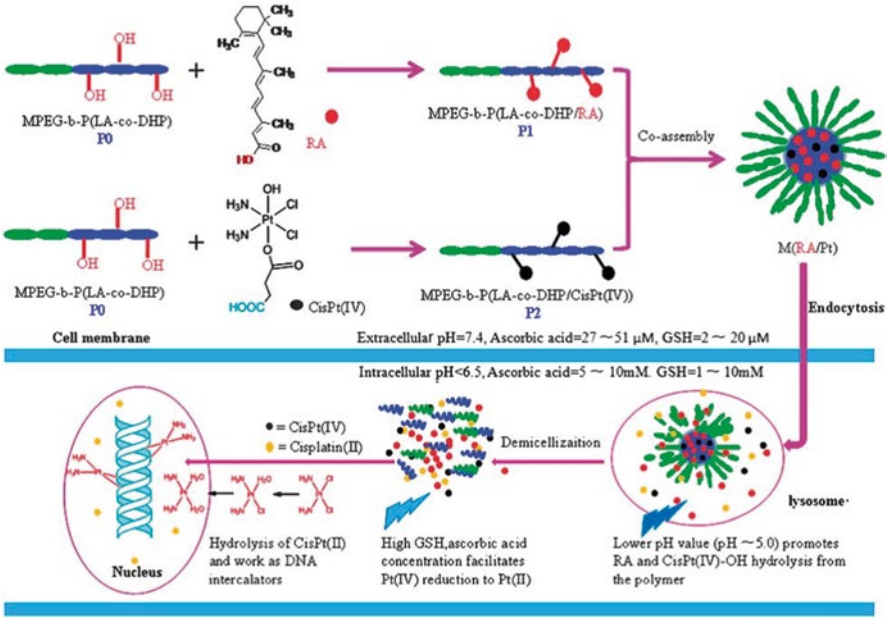

Fig. 2.22 Preparation of M(RA/Pt) micelles and possible mechanism of their action [70]

of hydrolysis within the cell. As an added degree of complexity, as the lactic acid segment degrades, the micelle begins to break down, or *demicellization* occurs. The demicellization exposes the Cis(IV) to the intracellular environment, which has a high concentration of reducing agents such as ascorbic acid to convert the Pt(IV) to Pt(II). The Pt(II) can then be further sensitized by RA. The hydrolyzed Pt(II) acts as a good DNA intercalator, which functions as an effective antitumor drug (Fig. 2.23).

One area of focus in relation to our discussion regarding design is associated with the release kinetics of the two drugs. In the case of Fig. 2.23b we can see that the rate of release of Pt appears to follow a burst release kinetics, whereas the RA follows a first-order release. In addition, the peak release of Pt is approximately five times greater than that of RA. In order to ensure effective hydrolysis of a two-component system within the cell, these components need to be closer in terms of both their peak release as well as their release kinetics. Despite the irregularity of the release kinetics, this drug–polymer conjugate approach does prove to be effective in terms of both the internalization of micellar particles and trafficking of Pt to the nuclei. Additionally, the cytotoxicity (i.e., cell toxicity) experiments using this approach show no significant cell death. This micellar particle drug–polymer conjugate approach highlights several important concepts related to the design of an effective controlled-release system. There is a definitive advantage in terms of cellular toxicity in the use of biodegradable materials for cellular internalization. The conjugation of drugs to a polymer system allows for the experimenter to expose it to a broad series of environmental conditions without the risk of drug decomposition or inactivity. There is an additional layer to this conjugation in that the system

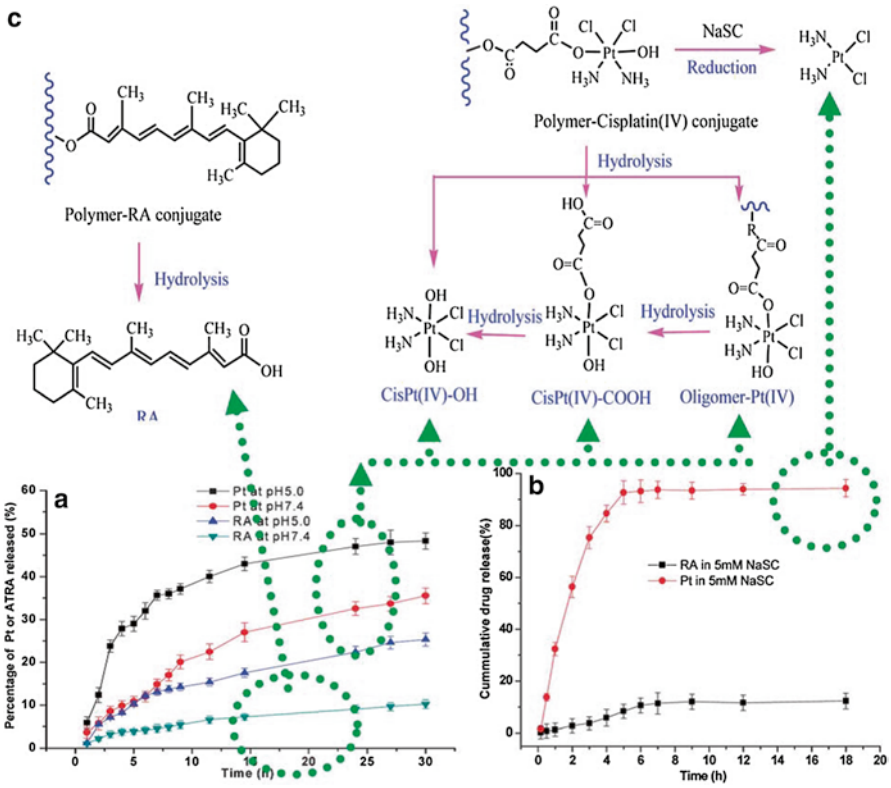

Fig. 2.23 Synthesis of MPEG-b-P(LA-co-DHP/RA) conjugate P1 and MPEG-b-P(LA-co-DHP/CisPt(IV)) conjugate P2 [70]

is also self-assembled into a higher-order micellar structure, further shielding the drug and allowing for multidrug delivery within the same system without significant risk of cross contamination or premature sensitization of the Cis(IV) by the RA. We look more closely at the advantages of using a biodegradable system in the remainder of this chapter (Fig. 2.24).

2.3.1.3 Biodegradable Particles

To finish our discussion of controlled-release systems, we will step back a bit from the biology and look more carefully at the implication of the biodegradation system on release kinetics. Throughout this chapter we have discussed a number of functional domains that have potential for use as biodegradable templates for the fabrication of controlled-release systems. One particular copolymer, poly(lactic-co-glycolic acid) (PLGA), has been the most widely studied in this area for use as matrix material for controlled-release systems [71]. Poly(lactic-co-glycolic acid) has the advantage of being highly tunable in terms of its degradation. The ratio of

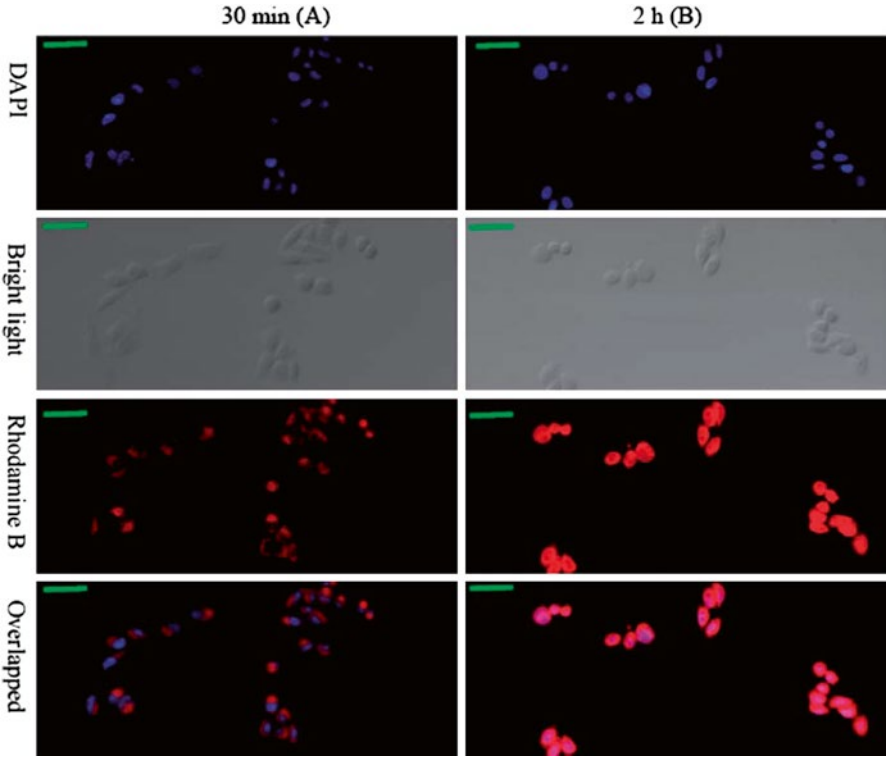

Fig. 2.24 Preparation of M(RA/Pt) micelles and possible mechanism of their action [70]

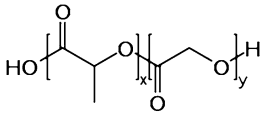

Fig. 2.25 Structure of poly(lactic-co-glycolic acid) (PLGA)

glycolic acid (GA)—the more rapidly degradable functionality—to lactic acid (LA)—the slower to degrade—in the copolymer composition as well as molecular weight allow the experimenter to adjust the biodegradation profile from a matter of days to a matter of months. The degradation of PLGA is a combination of surface diffusion, bulk diffusion, and erosion (Fig. 2.25).

Furthermore, the synthesis of this copolymer via *ring-opening polymerization* has several facile routes with chemistry allowing for amenable coupling reactions with other desired materials such as drug molecules, proteins, nanoparticles, and surfaces (Fig. 2.26).

In an early study into biodegradable nanospheres, Niwa et al. [71] explored the differences between compositions of PLGA fabricated into nanospheres using a spontaneous emulsification process. In the study, indomethacin and 5-fluorouracil

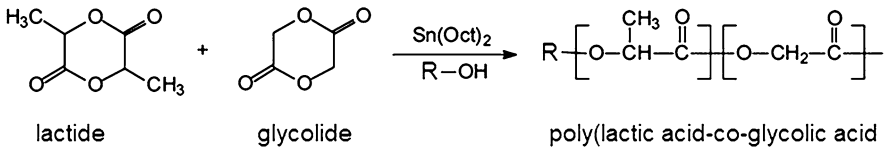

Fig. 2.26 Synthetic polymerization to form poly(lactic-co-glycolic acid) (PLGA) [71]

were used as the hydrophobic drugs in need of stabilization within biodegradable nanospheres for drug delivery. The fabrication of the nanosphere structure is a fairly representative method that we'll discuss in more detail in Chaps. 4 and 5. The process involves dissolving or dispersing the drug and PLGA in a common volatile (i.e., low-vapor-pressure) organic solvent such as acetone or methylene chloride, followed by homogenization. An emulsifying agent is then added to the solvent and the entire system is stirred and exposed to atmosphere for the volatile organic solvent to evaporate. During evaporation, the emulsifying agents stabilize PLGA particles that form around the drug molecule precipitate and allow for the stabilization of significantly smaller-sized species than possible without emulsifiers present.

If we now look more closely at these PLGA nanospheres, we can see the effect of the composition and molecular weight of LA and GA on the release kinetics of the system. Let's look first at the release of indomethacin. It is evident that the increase in the molecular weight of the biodegradable species contributes to the reduction of the indomethacin released. Upon a closer review, it is also evident that the mode of release appears to differ with changes to the molecular weight from 12,279 to 127,598 Da, which correlates with a change from burst release kinetics to first-order kinetics, respectively. This is not entirely surprising if we revisit our previous conversation regarding polymer molecular weight and degradation. The spaghetti analogy suggested that the degradation rate would occur more rapidly in the lower-molecular-weight system. The other point that has not been mentioned thus far is related to a high-molecular-weight polymer phenomenon known as physical entanglements. If we move back to spaghetti as an analogy, we know that often, unbroken spaghetti becomes entangled when you pick it up with a fork, prompting cutting. This entanglement occurs when long pieces of spaghetti form button hooks (i.e., entanglements) with one another or with groups of other pieces. Similarly with polymers, the button hooking of polymer chains occurs in all molecular weight systems. The probability of this effect increases dramatically with molecular weights >30,000, where systems begin to appear similar to a chemically networked or crosslinked matrix. In polymers, this phenomenon also manifests itself by exhibiting a rubberlike or networked behavior that is dependent on the flexibility of the polymer chains (Fig. 2.27).

It should be noted that the PDI of these PLGA polymers fell in the somewhat anomalous 1.5–1.9 range, which we know from our previous discussion in this chapter is somewhere between a statistically uniform and statistically broad distribution of molecular weights. The composition of PLGA in terms of its ratio of LA to GA functional components contributes to the degradation profile as well. Zhou et al. identified

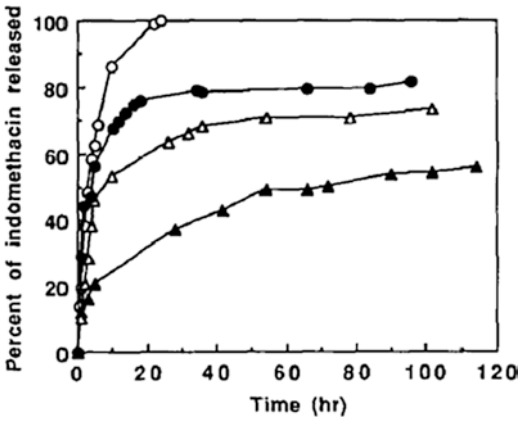

Fig. 2.27 Release profiles of indomethacin from PLGA nanospheres in phosphate buffer (0.1 M, pH 7.4). *Key*: (*open circle*) solution; nanospheres with (*filled circle*) PLGA (85-15)-12 279; (*open triangle*) PLGA (85-15)-66 671; (*filled triangle*) PLGA (85-15)-127 598 [71]

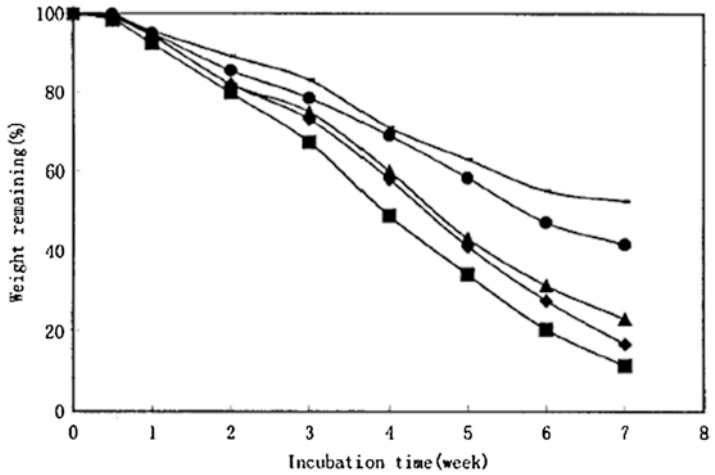

Fig. 2.28 Weight remaining percentage of (*hyphen*) PLA, (*filled circle*) PLGA (85/15), (*filled triangle*) PLGA (75/25), (*filled diamond*) PLGA (65/35), and (*filled square*) PLGA (50/50) containing microspheres has incubated in PBS at 37 °C. Each point represents the mean of three individual samples of microspheres [71]

the effects of changes to the LA/GA ratio on low-molecular-weight PLGA species. The lower-molecular-weight species of PLGA have been identified for their utility in applications such as biodegradable linkers and surface treatments as well as in matrix-based controlled-release systems. If we observe the effects of an increased GA composition on the percentage of polymer weight reduction, it is evident that they are indirectly proportional. The decrease in polymer weight with incubation time appears to show a differently shaped curve with each incremental increase in [GA] (Fig. 2.28).

If we look at the degradation profile more closely, there appears to be a sharper dropoff in remaining polymer weight as the GA content >15 %. If we think of this from a chemical perspective, there are critical compositions, depending on respective molecular weights, that allow for more rapid degradation of PLGA. These compositions are dependent on [GA] within the PLGA polymer, which introduces a higher degree of chain flexibility due to decreased sterics in the molecule. Therefore, it is highly predictable to know the degradation kinetics of PLGA provided we know the molecular weight, composition [LA], and composition [GA].

2.3.2 Summary

The release of drug species within a physiological environment is critical to its therapeutic function. In Sect. 2.1, we discussed the fundamentals and building blocks for the design of basic controlled-release drug delivery systems. The concepts of diffusion and degradation have provided a grounding in the governing physics and chemistry behind delivering drug molecule systems. In Sect. 2.2, we focused on networked and porous systems ranging from biodegradable matrices, hydrogel particles, conjugated materials, and solid microparticles/nanoparticles and discussed their pharmacokinetic behavior with material modification. Finally, in Sect. 2.3, we discussed nearly commercial systems capable of fine control over the shape and composition of their controlled-release materials. The remaining chapters of this book will expand a number of these fundamentals into other systems designed to exploit physiological behavior to deliver a desired drug molecule(s) to an intended target cell or tissue (Table 2.3).

2.4 Clinical Applications

2.4.1 Translational Pathways for Novel Drug Delivery Systems

As shown in the first three sections of this chapter, drug delivery systems present a novel opportunity for the controlled and targeted release of essential therapeutics. Drug delivery systems are increasingly being recognized as a beneficial means for lessening the global disease burden. For instance, a controlled-release system for antibiotics can dramatically simplify the treatment of infectious diseases such as tuberculosis while also lessening the risk of drug-resistant bacterial infections. A controlled-release system for insulin can raise the efficacy of diabetes treatment while also lowering the rate of complications from the disease. The emerging generation of drug delivery systems can enable healthcare that is both more effective and more affordable.

Table 2.3 Common scientific disciplines tied to critical fundamentals in controlled-release drug delivery systems

Fundamental	Disciplines
Degradation (i.e., chemical hydrolysis)	• Chemistry • Materials engineering • Chemical engineering
Biodegradation (i.e., enzymatic degradation)	• Biochemistry • Protein chemistry • Enzymatics • Chemistry
Material fabrication	• Chemistry • Electrical and computer engineering • Materials engineering
Diffusion	• Chemistry • Chemical engineering • Materials engineering • Physics
Erosion (i.e., abrasion, fatigue, cavitation, fatigue)	• Physics • Chemistry • Materials engineering
Pharmacokinetics	• Medicine • Pharmaceutical engineering • Biology
Polymer composition	• Chemistry • Materials engineering
Crosslinking	• Materials engineering • Chemistry

2.4.1.1 Product Development Considerations

Because drug delivery systems incorporate new biomaterials that can modify the pharmacokinetics of therapeutics, the safety and efficacy of such systems must be proven and not assumed. Modern polymeric biomaterials must meet stringent performance requirements and overcome difficult practical challenges. A number of technical factors must be considered in the selection and development of new biomaterials. First, biomaterials must demonstrate sufficient physical and mechanical properties to survive the physiological environment. Second, novel biomaterials must meet biocompatibility specifications. The biomaterial must be biocompatible to the target site, performing in its desired application without causing adverse effect. Both the biomaterial construct and any residuals or degradation products must be noncytotoxic, nonhemolytic, and noninflammatory; undesirable responses such as irritation and sensitization must be avoided. The biomaterial must not interfere with wound healing or induce fibrosis or a foreign body response; it is also necessary that the material does not act as a hospitable environment for bacteria, so that it does not propagate an infection.

If the drug delivery vehicle is degradable, the degradation products must be easily excreted by the kidneys. The molecular weight cutoff for kidney elimination of native globular proteins is considered to be 70,000, which is close to the molecular weight of serum albumin [72]. Hydrophilic polymers utilized in biomaterials may have a higher molecular volume than compact globular proteins; because of the larger effective size of polymers, the molecular weight cutoff for kidney excretion of polymers may be even more stringent. An additional consideration is that polymers with higher molecular weights exhibit longer retention times in the blood.

Finally, drug delivery systems must satisfy commercial requirements and clinical needs. The ideal biomaterial for medical usage should be readily delivered through a user-friendly device. The system should demonstrate adequate shelf stability, and an optimal system should be storable at room temperature, requiring minimal advance preparation time. Production of the biomaterial must be scalable to allow cost-effective manufacture; this quality is particularly critical for global health, as low- and middle-income countries carry 80 % of the worldwide disease burden. The reality is that biomaterials will be most needed in low-resource settings, where staffing and facilities are severely limited. Drug delivery systems that are low-cost and easy to use will have the largest impact on public health.

Throughout the development process, new polymeric biomaterials must be assessed to ensure their suitability for medical applications; the characterization should include mechanical properties, physical/chemical properties, biological properties, shelf stability, and usability. A listing of recommended tests for biomaterials is presented in Table 2.4. The precise properties required of each biomaterial are determined to a large extent by the clinical target. Clinician input is an essential component of the design process, so that surgeon needs and patient needs can be translated into technical specifications. The clinical target should continually guide and inspire the creation of a drug delivery system. Both developing and developed nations are battling poverty and ill health; the situation demands innovative drug delivery solutions.

2.4.1.2 Regulatory Considerations

Regulatory approval is absolutely essential to the translation of novel systems from bench to bedside. Since drug delivery systems are often combinations of drugs with polymeric biomaterials, it is important for drug delivery scientists to understand U.S. Food and Drug Administration (FDA) Standards and Regulations for testing, manufacturing, approval, and marketing of medical devices containing biopolymers.

The first issue that the drug delivery scientist must appreciate is that the FDA does not actually grant blanket approval for individual biopolymers. Rather, the FDA grants approval for complete medical devices for specific clinical indications. In order to correctly specify the approval status of a device containing a biopolymer, the clinical indications of the device must be stated. So, for instance, it would be inaccurate to state, “Alginate is an FDA-approved biopolymer.” It would also be

Table 2.4 Methods for characterization of polymeric biomaterials

Mechanical characterization	Biological characterization
Mechanical strength	Sterility properties
• Tensile strength	• Bioburden
• Shear strength	• Bacterial endotoxin assay
• Impact strength	Tissue compatibility
• Cohesive and adhesive strength	• Cytotoxicity
Physical/chemical characterization	• Cellular inflammation
Curing and reaction properties	• Cell and protein attachment
• Extent of reaction	• Tissue irritation
• Residual starting materials	• Tissue implantation response
• Heat of reaction	• Wound healing
Degradation properties	Hemolysis testing
• Degradation rate	Systemic effects
• Degradation products	• Pyrogenicity
Swelling determination	• Sensitization
Drug release properties	Toxicokinetic evaluation
• Drug delivery rate	• Metabolic fate
• Drug bioactivity	Antimicrobial effects
Device characterization	Encapsulated live cell viability
Accelerated shelf stability test	Clinical characterization
Physical integrity	Ease of use
Device functionality	Patient and clinician acceptance
Device preparation time	Clinical efficacy
	Cost-effectiveness

inaccurate to state, "Calcium alginate wound dressings are FDA-approved." It would be most accurate to state

> Silverlon® calcium alginate wound dressings, which consist of a sterile, non-woven pad composed of a High M (mannuronic acid) alginate and a silver nylon contact layer, are FDA-approved for the following clinical indications: management of moderately to heavily exudating partial and full thickness wounds, including first- and second-degree burns, skin graft and donor sites, chronic wounds such as pressure ulcers, dermal ulcers, vascular ulcers, diabetic ulcers, traumatic and surgical wounds.

The FDA explicitly forbids manufacturers from marketing medical devices for any uses other than approved indications. Therefore, biopolymer scientists must be conscientious about endorsing approved clinical uses of medical devices containing biopolymers, and may not promote off-label uses.

2.4.1.3 FDA Definition of a Medical Device

The U.S. Food and Drug Administration defines a medical device as "an instrument, apparatus, implement, machine, contrivance, implant, in vitro reagent, or other similar or related article, including a component part, or accessory which is

- Recognized in the official National Formulary, or the United States Pharmacopoeia, or any supplement to them,
- Intended for use in the diagnosis of disease or other conditions, or in the cure, mitigation, treatment, or prevention of disease, in man or other animals, or
- Intended to affect the structure or any function of the body of man or other animals, and which does not achieve any of its primary intended purposes through chemical action within or on the body of man or other animals and which is not dependent upon being metabolized for the achievement of any of its primary intended purposes." [73]

Medical devices are regulated through the FDA's Center for Devices and Radiological Health (CDRH). The FDA regulates a broad range of medical devices, including complicated, high-risk medical devices, such as artificial hearts, and relatively simple, low-risk devices, including tongue depressors, as well as devices that fall somewhere in between, for instance, sutures. The FDA has the authority to regulate medical devices before and after they reach the marketplace [74].

2.4.1.4 Medical Device Classifications

Medical devices are classified into Class I, II, and III depending on the intended use and indications of the device as well as the amount of control that the device requires to ensure safety and effectiveness. The classification procedures are described in the Code of Federal Regulations, Title 21, part 860 (usually known as 21 CFR 860) [75]. Regulatory control increases from Class I to Class III. The device classification regulation defines the regulatory requirements for a general device type.

Class I devices are deemed to be low-risk and are therefore subject to the fewest regulatory controls. Class I devices typically have limited, external contact with the human body and are not life-sustaining devices. Class I devices will have almost no role in preventing impairment to human health. For example, dental floss is classified as a Class I device. Other devices that are simple in design such as tongue depressors, elastic bandages, handheld dental instruments, and examination gloves would be classified as Class I devices. Medical devices classified as Class I are subject to "general controls." This means that Class I devices must follow general FDA policy, which includes registering the medical device, proper branding and labeling, and proper manufacturing techniques. In addition, the FDA must be notified prior to marketing the device.

Class II devices are higher-risk devices than Class I devices and require greater regulatory controls to provide reasonable assurance of the device's safety and effectiveness. Class II devices have more contact with the human body than Class I devices, yet Class II devices are still not life-sustaining devices. Most medical devices fall into the Class II medical devices category; this category includes X-ray machines, powered wheelchairs, infusion pumps, and surgical and acupuncture needles. Medical devices classified as Class II are subject to "general controls" plus "special controls." This means that Class II devices must satisfy all requirements for

Class I devices as well as special labeling, mandatory performance standards, and postmarketing surveillance.

Class III devices are generally the highest-risk devices and are therefore subject to the highest level of regulatory control. Class III devices must usually be approved by the FDA before they are marketed. Class III medical devices are typically life-sustaining devices that maintain intimate contact with the human body; a malfunction of such a device would be life-threatening. Class III medical devices include implanted pacemakers, HIV diagnostic tests, heart valves, and implanted cerebral simulators. Medical devices classified as Class III are subject to "general controls" plus "premarket approval." This means that Class III devices must satisfy all requirements for Class I and Class II devices and, in addition, Class III devices must be premarket-approved by the FDA. Premarket approval necessitates a scientific review of the medical device prior to marketing.

The FDA maintains an online searchable database of classifications for all currently approved medical devices at http://www.accessdata.fda.gov/scripts/cdrh/cfdocs/cfPCD/classification.cfm.

2.4.1.5 FDA Regulatory Approval Process for Medical Devices

The approval pathway for a medical device depends on the device classification. The approval pathways for various device classifications are summarized in the following table.

Device class	Description	Approval path	Example
Class I	Safest devices	Preapproved	Walking cane, toothbrush
Class II	Some risk if misused	Premarket notification (510K)	Blood glucose tester
Class III	Misuse could result in severe injury or death	Premarket approval (PMA)	Heart valve

Class I devices are preapproved; the applicant must provide a notification to the FDA prior to marketing, but there is typically no requirement for a regulatory application.

Class II devices typically require the applicant to file a 510 K premarket notification to the FDA. A 510 K is a premarket submission made to the FDA to demonstrate that the device to be marketed is at least as safe and effective, that is, "substantially equivalent," to a legally marketed device [76]. The advantage of a 510 K application is that it does not require a clinical trial of the new medical device. For example, suppose you have manufactured a new surgical suture made of a novel silk biopolymer; you could file a 510 K application for the surgical suture and argue that your new suture is "substantially equivalent" to existing silk sutures. The FDA maintains an online searchable database of all submitted 510 K applications at http://www.accessdata.fda.gov/scripts/cdrh/cfdocs/cfPMN/pmn.cfm.

A device is substantially equivalent if, in comparison to a predicate, it

- has the same intended use as the predicate, **and**
- has the same technological characteristics as the predicate, **or**
- has the same intended use as the predicate, **and**
- has different technological characteristics and the information submitted to FDA,
  - does not raise new questions of safety and effectiveness, **and**
  - demonstrates that the device is at least as safe and effective as the legally marketed device.

A claim of substantial equivalence does not mean the new and predicate devices must be identical. Substantial equivalence is established with respect to intended use, design, energy used or delivered, materials, chemical composition, manufacturing process, performance, safety, effectiveness, labeling, biocompatibility, standards, and other characteristics, as applicable. A device may not be marketed in the United States until the submitter receives a letter declaring the device substantially equivalent [77].

Class III devices will always require the applicant to file a premarket approval (PMA) application to the FDA. A PMA is the most stringent type of device marketing application required by the FDA. The applicant must receive FDA approval of its PMA application prior to marketing the device. Premarket approval is based on a determination by the FDA that the PMA contains sufficient valid scientific evidence to assure that the device is safe and effective for its intended use(s). An approved PMA is, in effect, a private license granting the applicant (or owner) permission to market the device [78]. The PMA application will always require the applicant to conduct a clinical trial. The FDA maintains an online searchable database of all submitted PMA applications at http://www.accessdata.fda.gov/scripts/cdrh/cfdocs/cfPMA/pma.cfm.

2.4.1.6 Good Manufacturing Practices

Regardless of classification, all medical devices must be manufactured according to good manufacturing practices (GMPs). Good manufacturing practice ensures that products are consistently produced and controlled to the quality standards appropriate to their intended use and as required by the marketing authorization. Good marketing practice is primarily concerned with pharmaceuticals, biotech products, medical devices, and some foods. Good manufacturing practice regulations address issues including recordkeeping, personnel qualifications, sanitation, cleanliness, equipment verification, process validation, and complaint handling.

Good manufacturing practice regulations are issued by the FDA and are laid out in Section 21 of the Code of Federal Regulations, Part 820, for medical devices. These regulations are enforced via inspections of manufacturing facilities; failure to comply with GMP requirements can result in regulatory actions against manufacturers and can even jeopardize FDA approval of a new device. Chemical professionals

must recognize that GMP regulations are continually evolving to meet the demands of new technologies; for this reason, GMP is often denoted as cGMP, meaning current good manufacturing practice. Also, keep in mind that GMP regulations represent the minimum requirements for a compliant process; many companies choose to exceed these standards.

To allow manufacturers the maximum flexibility in equipment selection and process design, the FDA does not maintain a list of approved cGMP manufacturing equipment. Instead, the cGMP standards require that equipment be appropriately designed for its intended use and that equipment be designed for thorough cleaning and maintenance. The equipment surfaces in contact with the starting materials, in-process materials, or products must be nonreactive, nonadditive, and nonabsorptive.

Good manufacturing practice also requires documentation of any changes to the fermentation process or equipment; this is known as change control. Change-control procedures apply to changes in operating conditions, standard operating procedures, manufacturing facilities, raw materials, production equipment, technical specifications, software, and quality assurance protocols [79]. A rule of thumb is that change control applies to any change that affects one of the five inputs of a process (also known as the five Ms): man, material, method, machine, and Mother Nature. The goal of change-control procedures is to limit risk by assessing the impacts of any process changes. Whenever engineers introduce a process alteration, the change must be documented and reported, and the adverse impacts on the safety, quality, efficacy, potency, and purity of the product must be evaluated and appropriately mitigated.

2.4.1.7 Good Clinical Practices

For Class III devices requiring clinical trials, these clinical trials must be conducted according to good clinical practices (GCPs). Good clinical practice is a standard for the design, conduct, performance, monitoring, auditing, recording, analyses, and reporting of clinical trials. The objective of GCP is "to provide a unified standard for the European Union (EU), Japan, and the United States to facilitate the mutual acceptance of clinical data by the regulatory authorities in these jurisdictions" [80]. Good clinical practice provides assurance that the data and reported results are credible and accurate and that the rights, integrity, and confidentiality of trial subjects are protected.

A quality clinical trial research site must

- protect the welfare and rights of all trial participants,
- assure that the research data generated are valid and can be used to draw reliable conclusions about study outcomes, ensuring benefits to current and future patients,
- comply with the International Conference on Harmonization (ICH) Good Clinical Practice (GCP) guidelines (http://ichgcp.net).

The main elements of GCP are

- the subject's rights, welfare, and confidentiality,
- data validity, integrity, and credibility.

Patient safety and data credibility are important not only for GCP, but also for regulatory authorities as their requirements for clinical investigations on human therapeutic products.

Compliance with GCP also provides public assurance that patients' rights are respected and that the clinical trial data are credible.

The foundation of GCP is the Declaration of Helsinki. The World Medical Association developed the Declaration of Helsinki as a statement of principles to provide guidance to physicians and other participants in medical research involving human subjects. Medical research involving human subjects includes research on identifiable human material or identifiable data. Good clinical practice should be considered applicable to any investigation where human subjects are participants.

In medical research on human subjects, considerations related to the well-being of the human subject should take precedence over the interests of science and society. Every medical research project involving human subjects should be preceded by careful assessment of predictable risks and burdens in comparison with foreseeable benefits to the subject or to others. The design of all studies should be publicly available. Physicians should abstain from engaging in research projects involving human subjects unless they are confident that the risks involved have been adequately assessed and can be satisfactorily managed. Physicians should cease any investigation if the risks are found to outweigh the potential benefits or if there is conclusive proof of positive and beneficial results. Medical research is only justified if there is a reasonable likelihood that the populations in which the research is carried out stand to benefit from the results of the research.

The subjects must be volunteers and informed participants in the research project. In any research on human beings, each potential subject must be adequately informed of the aims, methods, sources of funding, any possible conflicts of interest, institutional affiliations of the researcher, the anticipated benefits and potential risks of the study and the discomfort it may entail. The subject should be informed of the right to abstain from participation in the study or to withdraw consent to participate at any time without reprisal.

To summarize, clinical trials conducted according to GCP must satisfy 13 core principles:

1. Clinical trials should be conducted in accordance with the ethical principles that have their origin in the Declaration of Helsinki and that are consistent with GCP and the applicable regulatory requirement(s).
2. Before a trial is initiated, foreseeable risks and inconveniences should be weighed against the anticipated benefit for the individual trial subject and society. A trial should be initiated and continued only if the anticipated benefits justify the risks.

3. The rights, safety, and well-being of the trial subjects are the most important considerations and should prevail over interests of science and society.
4. The available nonclinical and clinical information on an investigational product should be adequate to support the proposed clinical trial.
5. Clinical trials should be scientifically sound and described in a clear, detailed protocol.
6. A trial should be conducted in compliance with the protocol that has received prior institutional review board (IRB)/independent ethics committee (IEC) approval/favorable opinion.
7. The medical care given to, and medical decisions made on behalf of, subjects should always be the responsibility of a qualified physician or, when appropriate, of a qualified dentist.
8. Each individual involved in conducting a trial should be qualified by education, training, and experience to perform his or her respective task(s).
9. Freely given informed consent should be obtained from every subject prior to clinical trial participation.
10. All clinical trial information should be recorded, handled, and stored in a way that allows its accurate reporting, interpretation, and verification.
11. The confidentiality of records that could identify subjects should be protected, respecting the privacy and confidentiality rules in accordance with the applicable regulatory requirement(s).
12. Investigational products should be manufactured, handled, and stored in accordance with applicable GMP. They should be used in accordance with the approved protocol.
13. Systems with procedures that assure the quality of every aspect of the trial should be implemented.

Good clinical practice is an international scientific and ethical standard; it is absolutely crucial for clinical trials of all medical devices containing biopolymers.

2.4.1.8 FDA Advisory Panels

The FDA's advisory committees provide independent, expert advice to the agency on a range of complex scientific, technical, and policy issues. This includes questions related to the development and evaluation of products regulated by the FDA. The agency currently has 48 technical and scientific advisory committees and panels. Although advisory committees provide recommendations to the agency, the FDA makes the final decisions.

An FDA advisory committee is utilized to conduct public hearings on matters of importance that come before the FDA, to review the issues involved, and to provide advice and recommendations to the commissioner. The commissioner has sole discretion concerning action to be taken and policy to be expressed on any matter considered by an advisory committee. An advisory committee may be a standing advisory committee or an ad hoc advisory committee. An advisory committee may

be a policy advisory committee or a technical advisory committee. A policy advisory committee advises on broad and general matters. A technical advisory committee advises on specific technical or scientific issues, which may relate to regulatory decisions before the FDA.

For specific products, advisory committees consider the available evidence and provide scientific and medical advice on safety, effectiveness, and appropriate use. Committees might also advise the agency on broader regulatory and scientific issues. An advisory committee lends credibility to the product review process and provides a forum for public discussion of certain controversial issues. The process helps air issues that do not have simple answers.

An advisory committee must meet the following standards:

1. Its purpose is clearly defined.
2. Its membership is balanced fairly in terms of the points of view represented in light of the functions to be performed. Although proportional representation is not required, advisory committee members are selected without regard to race, color, national origin, religion, age, or sex.
3. It is constituted and utilizes procedures designed to ensure that its advice and recommendations are the result of the advisory committee's independent judgment.
4. Its staff is adequate. The commissioner designates an executive secretary and alternate for every advisory committee, who are employees of the FDA. The executive secretary is responsible for all staff support unless other agency employees are designated for this function.
5. Whenever feasible, or required by statute, it includes representatives of the public interest.

The FDA will consider the following questions in deciding whether to convene an advisory committee:

1. Is the matter of such significant public interest that it would be highly beneficial to obtain the advice of an advisory committee as part of the agency's regulatory decision-making process?
2. Is the matter at issue so controversial that it would be highly beneficial to obtain the advice of an advisory committee as part of the agency's regulatory decision-making process?
3. Is there a special type of expertise that an advisory committee could provide that is needed for the agency to fully consider a matter?

If one or more of these factors is met, the matter is referred to an advisory committee.

The FDA will convene an advisory committee in the following scenarios [81]:

- The FDA is evaluating a first-of-a-kind, first-in-class medical product for human use.
- The FDA is evaluating a first-in-class antimicrobial for use in food-producing animals.

- The FDA is evaluating a medical product for a significant new indication.
- The FDA is evaluating a novel product or use of new technology.
- The FDA is evaluating a medical product that involves a significant diagnostic, therapeutic, or preventative advance.
- The FDA's assessment of the risk–benefit ratio of a product or class of products is likely to be controversial or it appears that the risks and benefits are of similar magnitude, especially where the products may have a narrow therapeutic effect.
- The FDA has significant safety concerns about a class of products. This scenario includes such concerns in pre- or postmarket situations (e.g., significant safety concerns relating to the premarket review of a medical product regulated by the FDA, or significant safety concerns relating to the postmarket review of such a medical product, including significant concerns about adverse event reports or other data that signal a potential safety issue).
- The FDA has significant questions or concerns about the use of a product in certain subpopulations (e.g., pediatric dosing or a newly discovered contraindication).
- The FDA has significant questions or concerns about a study, including a clinical trial, postmarket assessment, or product development protocol (PDP). The questions or concerns may relate to any aspect of such a study, including human subject protection, novel endpoints or surrogates, the study's design, or its results.
- FDA personnel have a significant difference of scientific opinion on a complex matter, for example, on the interpretation of data or judgments about the risk–benefit ratio of a regulated product.
- The FDA has questions or concerns involving the intersection of several scientific disciplines.
- The FDA is seeking outside expertise on scientific techniques or research.
- The FDA is evaluating whether to switch a product class from one regulatory status to another (e.g., switching a class of drug products from prescription to over-the-counter status.)
- The FDA has significant questions or concerns regarding the development or implementation of a regulatory policy or guidance document.
- The FDA wants independent, outside evaluation of the quality, relevance, or productivity of an agency communication program or research program.

Committee membership typically includes ethnic, gender, and geographic diversity. Members have recognized expertise and judgment in a specific field. Typical members include

- physician-scientists,
- statisticians,
- epidemiologists,
- pharmacologists,
- nutritionists,
- nurses,
- experts in animal (preclinical) studies.

Every meeting of an FDA advisory panel is comprised of an open public hearing followed by closed deliberations, with the committee ultimately delivering a recommendation to the FDA. Such panels can play a crucial role in determining the fate of a novel medical device.

2.4.1.9 FDA GRAS List

Biopolymers may be used not only in medical devices, but also as food additives. It is therefore worthwhile for biopolymer scientists to understand the FDA's Generally Recognized as Safe (GRAS) list. Under sections 201(s) and 409 of the Federal Food, Drug, and Cosmetic Act, any substance that is intentionally added to food is a food additive and is subject to premarket review and approval by the FDA, unless the substance is designated GRAS. A GRAS designation means that the substance is generally recognized, among qualified experts, as having been adequately shown to be safe under the conditions of its intended use [82]. A substance with a GRAS designation can be added to foods without premarket review and approval by the FDA. Moreover, a substance with a GRAS designation is likely to be viewed favorably when incorporated into a medical device.

Under sections 201(s) and 409 of the Federal Food, Drug, and Cosmetic Act, and the FDA's implementing regulations in 21 CFR 170.3 and 21 CFR 170.30, the use of a food substance may be GRAS either through scientific procedures or, for a substance used in food before 1958, through experience based on common use in food.

- Under 21 CFR 170.30(b), general recognition of safety through scientific procedures requires the same quantity and quality of scientific evidence as is required to obtain approval of the substance as a food additive and ordinarily is based upon published studies, which may be corroborated by unpublished studies and other data and information.
- Under 21 CFR 170.30(c) and 170.3(f), general recognition of safety through experience based on common use in foods requires a substantial history of consumption for food use by a significant number of consumers.

Biopolymers currently listed on the FDA GRAS list include alginate, starch, agar, carrageenan, cellulose, cornsilk, carob bean gum, dextran, dextrins, guar gum, methylcellulose, and pectin.

2.4.2 Summary

Regulatory approval of drug delivery systems is essential for translation into clinical applications. This section has described FDA regulations and standards for medical device classification and approval, as well as the requirements of GMPs and GCPs for the production and evaluation of novel medical devices. This section has also described the important roles of FDA Advisory Panels and the FDA GRAS listings.

With these considerations in mind, the drug delivery scientist can clearly understand the high bar that must be met by medical devices incorporating polymeric biomaterials.

2.5 Problems

2.1 An oncologist has decided to use SIR-Spheres as a targeted release anticancer treatment for a patient with liver tumors. SIR-Spheres are microspheres, typically 10 μm in diameter, which are delivered through a catheter tube in the hepatic artery. The oncologist wants to test the microspheres ahead of time in vitro to verify the pharmacokinetic profile prior to use as a therapy. If the doctor recorded the following data, answer the subsequent questions:

(i) Do the SIR-Spheres follow a first-order or zero-order release profile? Surface area of sphere $= S = 4\pi r^2$

t	C	C_s	C_t	k	S	dm/dt
Time (h)	Total concentration (ng/ml)	Surface concentration (ng/ml)	Solution concentration (ng/ml)	Diffusion rate constant (/h)	Surface area (μm^2)	Release rate
1	10	10	0	120	314.2	377,040
2	6	6	4	120	314.2	75,408
3	4	4	6	120	314.2	−75,408
4	3	3	7	120	314.2	−150,816
5	2	2	8	120	314.2	−226,224
6	1	1	9	120	314.2	−301,632
7	0.4	0.4	9.6	120	314.2	−346,877

(ii) Are these spheres good candidates as cancer therapies? Why?

(iii) What if the particle shape for SIR-Spheres were actually cylindrical? How would that affect the pharmacokinetic profile?

2.2 Draw *one example* for the chemical reaction for each of the following:

(i) Chemical degradation of a polypeptide

(ii) Enzymatic degradation of a polypeptide

2.3 A pharmaceutical company has developed a drug that requires delivery via the circulatory system. In order to improve the effective dosage range, the R&D department requires the development of a biodegradable polymer with a viscosity similar to that of human blood (i.e., 3–4 cP), which for this polymer corresponds to an $M_n < 1{,}000$ Da (PDI < 2) at a concentration of 0.1 % (w/v) in water. The research chemist has decided to mix the following different molecular weights in order to reach the desired target. From the following data, please answer the following questions:

(i) What are the M_n, M_w, and PDI of the resulting mixed-polymer system?
(ii) Is this mixture going to achieve the effective target?
(iii) How could the research chemist adjust the polymer mixture to achieve the desired target viscosity?

n	M_w
Polymers	Molecular weight (Da)
2	20,000
4	1,000
1	5,000
1	2,000
4	6,000

2.4 A biomaterials scientist is trying to design a system that has a high-amplitude burst release pharmacokinetic drug release profile. In order to fabricate a relevant system, several factors are necessary. Look at the following polymer structures and answer the following questions:

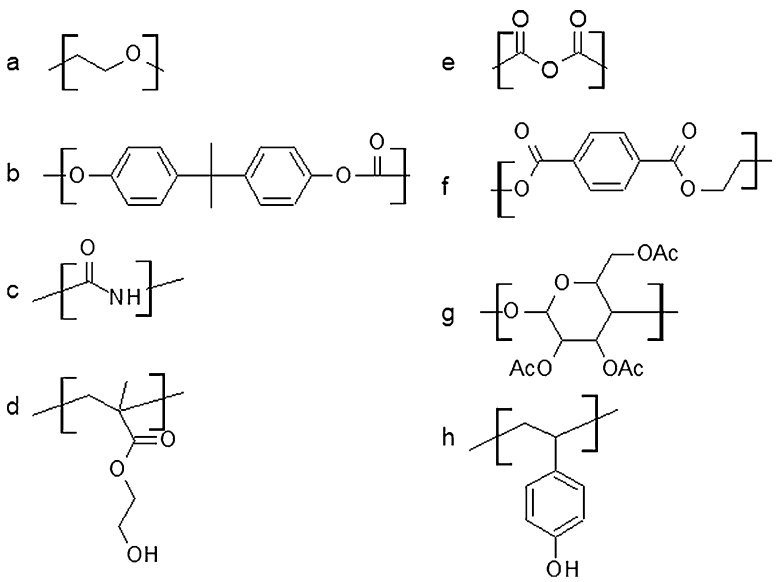

(i) What do the structural characteristics of a crosslinked material typically contribute to high burst release behavior?
(ii) Which of the polymers above exhibit these characteristics from (i)? Why?
(iii) From the components above, how might a biomaterials scientist change the pharmacokinetic release profile for a crosslinked system from a burst release to Fickian release kinetics?

2.5 The drug molecule *rosuvastatin calcium* is marketed by Astra Zeneca as Crestor® as a lipid-lowering agent for patients with high cholesterol. Oral

cardiovascular treatments typically require a specific residence time in order to increase the efficacy of the drug. One method we have discussed involves the formation of a prodrug system. From your knowledge of prodrug drug delivery systems, answer the following questions:

(i) We will learn in later chapters that polymers with a high persistence length have been shown to have desirable circulation lifetimes due to their behavior in flowable environments, such as tubes or blood vessels. Using this logic, what polymer structure from Problem 2.4 could be used to enhance the flow of a prodrug system? Why?
(ii) How would increasing the molecular weight affect the circulation lifetime of the prodrug system from (i)?
(iii) Which of the following design strategies would offer the most effective degradation (i.e., drug release) profile: End-Group Linkage or Side-Chain Linkage? Why?

2.6 A group has invented a novel drug release technology (listed below as Composition 1) and is comparing it to a currently marketed product. The group compared release of the drug metoprolol from the new composition with that from the existing marketed product (these data are from U.S. Patent Application US20090053310 A1). From your knowledge of controlled-release drug delivery systems, answer the following questions:

Time (hours)	Composition 1 % Cumulative Drug Release	A Marketed product % Cumulative Drug Release
0	0	0
1	15.5	11.87
2	21.2	14.34
4	33.2	25.43
6	42.3	35.50
8	53.7	45.75
12	65.4	64.46
16	76.6	77.44
20	84.9	91.5

(i) Prepare a plot of drug release versus time for each of these technologies (the new composition and the existing marketed product).
(ii) Then conduct an analysis to determine the mechanism of drug release from each of these technologies.
(iii) Calculate rate constants where necessary, and be sure to use correct units.

2.7 Alginic acid, also called algin or alginate, is a viscous gum that is abundant in the cell walls of brown algae. Alginate is biocompatible and forms gels when exposed to calcium ions, so it is under intense investigation as a drug delivery vehicle. Surita Bhatia's research group at the University of Massachusetts–Amherst has studied the release of glucose from various alginate formulations. The ability to tune glucose release could have applications for diabetes management.

(i) The following glucose release data were obtained for two different alginate formulations:

1% alginate, 0.1 M Ca

Time (min)	% glucose released
1	36.70
2	47.00
3	58.40
4	62.30
5	64.00
6	69.20
8	74.40
10	82.50
15	90.00
20	95.40
25	95.50
30	99.10

3% alginate, 0.1 M Ca

Time (min)	% glucose released
2	46.60
3	53.24
4	57.46
5	60.58
6	67.29
7	69.63
8	71.90
10	79.39
15	82.36
20	91.41
25	95.00
30	94.77
35	98.13

(ii) Based on your analysis, what is the effect of increasing the alginate concentration on the Higuchi rate constant? How does the alginate concentration affect the diffusivity of glucose out of alginate in this system?

(iii) The group also studied the effect of calcium ion concentration on glucose release. For example, the following data were obtained for a 1 % alginate, 1.0 M Ca system:

1% alginate, 1.0 M Ca

Time (min)	% glucose released
1	41.01
2	60.85
3	75.41
4	77.40
5	88.93
6	87.74
7	87.74
8	90.53
9	97.29

Conduct a Higuchi analysis for this formulation, and derive the Higuchi rate constant k_H.

(iv) Based on your analysis, what is the effect of increasing the Ca concentration on the Higuchi rate constant? How does the Ca concentration affect the diffusivity of glucose out of alginate in this system?

References

1. Office, C. B. (2006, October). *Congress of the United States Congressional Budget Office Study*.
2. Park, K. (1997). *Controlled drug delivery: Challenges and strategies* (p. 629). Washington, DC: American Chemical Society.
3. Singh, B. N., & Kim, K. H. (2000). Floating drug delivery systems: An approach to oral controlled drug delivery via gastric retention. *Journal of Controlled Release: Official Journal of the Controlled Release Society, 63*(3), 235–259.
4. Patel, U. L., Chotai, N. P., & Nagda, C. D. (2012). Design and evaluation of ocular drug delivery system for controlled delivery of gatifloxacin sesquehydrate: In vitro and in vivo evaluation. *Pharmaceutical Development and Technology, 17*(1), 15–22.
5. Packhaeuser, C., Schnieders, J., Oster, C., & Kissel, T. (2004). In situ forming parenteral drug delivery systems: An overview. *European Journal of Pharmaceutics and Biopharmaceutics, 58*(2), 445–455.
6. Vasir, J. K., Tambwekar, K., & Garg, S. (2003). Bioadhesive microspheres as a controlled drug delivery system. *International Journal of Pharmaceutics, 255*(1–2), 13–32.
7. Siepmann, J., Kranz, H., Bodmeier, R., & Peppas, N. A. (1999). HPMC-matrices for controlled drug delivery: A new model combining diffusion, swelling, and dissolution mechanisms and predicting the release kinetics. *Pharmaceutical Research, 16*(11), 1748–1756.
8. Stevenson, C. L., Santini, J. T., & Langer, R. (2012). Reservoir-based drug delivery systems utilizing microtechnology. *Advanced Drug Delivery Reviews, 64*(14), 1590–1602.
9. Grassi, M., & Grassi, G. (2005). Mathematical modelling and controlled drug delivery: Matrix systems. *Current Drug Delivery, 2*(1), 97–116.

10. Von Burkersroda, F., Schedl, L., & Göpferich, A. (2002). Why degradable polymers undergo surface erosion or bulk erosion. *Biomaterials, 23*(21), 4221–4231.
11. Colombo, P., Bettini, R., Santi, P., & Peppas, N. (2000). Swellable matrices for controlled drug delivery: Gel-layer behaviour, mechanisms and optimal performance. *Pharmaceutical Science & Technology Today, 3*(6), 198–204.
12. Ray, P., & Chakrabarti, B. K. (1985). The critical behaviour of fracture properties of dilute brittle solids near the percolation threshold. *Journal of Physics C: Solid State Physics, 18*(9), L185–L188.
13. Saralidze, K., Koole, L. H., & Knetsch, M. L. W. (2010). Polymeric microspheres for medical applications. *Materials, 3*(6), 3537–3564.
14. (a) Zur Mühlen, A., Schwarz, C., & Mehnert, W. (1998). Solid lipid nanoparticles (SLN) for controlled drug delivery—Drug release and release mechanism. *European Journal of Pharmaceutics and Biopharmaceutics: Official Journal of Arbeitsgemeinschaft für Pharmazeutische Verfahrenstechnik e.V, 45*(2), 149–155. (b) Huang, X., & Brazel, C. S. (2001). On the importance and mechanisms of burst release in matrix-controlled drug delivery systems. *Journal of Controlled Release: Official Journal of the Controlled Release Society, 73*(2–3), 121–136.
15. (a) Dash, S., Murthy, P. N., Nath, L., & Chowdhury, P. (2010). Kinetic modeling on drug release from controlled drug delivery systems. *Acta Poloniae Pharmaceutica, 67*(3), 217–223. (b) Higuchi, T. (1963). Mechanism of sustained-action medication. Theoretical analysis of rate of release of solid drugs dispersed in solid matrices. *Journal of Pharmaceutical Sciences, 52*(12), 1145–1149.
16. Reza, M. S., Quadir, M. A., & Haider, S. S. (2003). Comparative evaluation of plastic, hydrophobic and hydrophilic polymers as matrices for controlled-release drug delivery. *Journal of Pharmacy & Pharmaceutical Sciences, 6*(2), 282–291.
17. Soroka, W. (1999). *Fundamentals of packaging technology* (p. 589). Naperville, IL: Institute of Packaging Professionals.
18. Ashby, M. F. (2004). *Materials selection in mechanical design (Google eBook)* (p. 624). Oxford, UK: Butterworth-Heinemann.
19. Exclusive TDK durabis coating technology makes cartridge-free, ultra-durable Blu-ray discs a reality. Retrieved January 9, 2005, from http://phys.org/news2615.html.
20. Reynaud, E. (2010). Protein misfolding and degenerative diseases. *Nature Education, 3*(9), 28.
21. Campolongo, M. J., Tan, S. J., Xu, J., & Luo, D. (2010). DNA nanomedicine: Engineering DNA as a polymer for therapeutic and diagnostic applications. *Advanced Drug Delivery Reviews, 62*(6), 606–616.
22. Odian, G. (2004). *Principles of polymerization (Google eBook)* (p. 832). New York: Wiley.
23. Kumar, A., & Gupta, R. K. (2003). *Fundamentals of polymer engineering, revised and expanded (Google eBook)* (p. 712). Boca Raton, FL: CRC Press.
24. Leja, K., & Lewandowicz, G. (2010). Polymer biodegradation and biodegradable polymers: A review. *Polish Journal of Environmental Studies, 19*(2), 255–266.
25. Hoffman, A. S. (2013). Stimuli-responsive polymers: Biomedical applications and challenges for clinical translation. *Advanced Drug Delivery Reviews, 65*(1), 10–16.
26. Jadhav, N., Gaikwad, V., Nair, K., & Kadam, H. (2009). Glass transition temperature: Basics and application in pharmaceutical sector. *Asian Journal of Pharmaceutics, 3*(2), 82.
27. Hoeijmakers, J. H. (2001). Genome maintenance mechanisms for preventing cancer. *Nature, 411*(6835), 366–374.
28. Billmeyer, F. W. (2007). Characterization of molecular weight distributions in high polymers. *Journal of Polymer Science, Part C: Polymer Symposia, 8*(1), 161–178.
29. Chandra, M. (2006). Introduction to polymer science and chemistry: A problem solving approach (p. 304). Polymer Molecular Weights, Boca Raton, FL: CRC/Taylor & Francis.
30. Hodge, I. M. (1997). Adam–Gibbs formulation of enthalpy relaxation near the glass transition. *Journal of Research of the National Institute of Standards and Technology, 102*(2), 195.
31. Kaushal, A. M., Gupta, P., & Bansal, A. K. (2004). Amorphous drug delivery systems: Molecular aspects, design, and performance. *Critical Reviews in Therapeutic Drug Carrier Systems, 21*(3), 133–193.

32. Amass, W., Amass, A., & Tighe, B. (1998). A review of biodegradable polymers: Uses, current developments in the synthesis and characterization of biodegradable polyesters, blends of biodegradable polymers and recent advances in biodegradation studies. *Polymer International, 47*(2), 89–144.
33. Park, J., Ye, M., & Park, K. (2005). Biodegradable polymers for microencapsulation of drugs. *Molecules, 10*(1), 146–161.
34. Engineer, C., Parikh, J., & Raval, A. (2011). Review on hydrolytic degradation behavior of biodegradable polymers from controlled drug delivery system. *Trends in Biomaterials & Artificial Organs, 25*(2), 79–85.
35. Azevedo, H. S., & Reis, R. L. (2005). Understanding enzymatic degradation of biodegradable polymers and strategies to control their degradation rate. In: *Biodegradable systems in tissue engineering and regenerative medicine* (pp. 177–202). Boca Raton, FL: CRC Press.
36. (a) Jun, H.-W., Yuwono, V., Paramonov, S. E., & Hartgerink, J. D. (2005). Enzyme-mediated degradation of peptide-amphiphile nanofiber networks. *Advanced Materials, 17*(21), 2612–2617. (b) Kim, S., Kim, J.-H., Jeon, O., Kwon, I. C., & Park, K. (2009). Engineered polymers for advanced drug delivery. *European Journal of Pharmaceutics and Biopharmaceutics: Official Journal of Arbeitsgemeinschaft für Pharmazeutische Verfahrenstechnik e.V, 71*(3), 420–430.
37. Domb, A. J., Kost, J., & Wiseman, D. (1998). *Handbook of biodegradable polymers (Google eBook)* (p. 544). Boca Raton, FL: CRC Press.
38. Miller, R. A., Brady, J. M., & Cutright, D. E. (1977). Degradation rates of oral resorbable implants (polylactates and polyglycolates): Rate modification with changes in PLA/PGA copolymer ratios. *Journal of Biomedical Materials Research, 11*(5), 711–719.
39. Tamada, J. A., & Langer, R. (1993). Erosion kinetics of hydrolytically degradable polymers. *Proceedings of the National Academy of Sciences of the United States of America, 90*(2), 552–556.
40. (a) Peppas, N. A., & Hoffman, A. S. (2012). Hydrogels for biomedical applications. *Advanced Drug Delivery Reviews, 64*, 18–23. (b) Gander, B., Gurny, R., Doelker, E., & Peppas, N. A. (1989). Effect of polymeric network structure on drug release from cross-linked poly(vinyl alcohol) micromatrices. *Pharmaceutical Research, 6*(7), 578–584.
41. (a) Graessley, W. W. (1974). *The entanglement concept in polymer rheology* (p. 179). Berlin: Springer. (b) Peppas, N. A., Huang, Y., Torres-Lugo, M., Ward, J. H., & Zhang, J. (2000). Physicochemical foundations and structural design of hydrogels in medicine and biology. *Annual Review of Biomedical Engineering, 2*, 9–29.
42. Lee, P. I., & Kim, C.-J. (1991). Probing the mechanisms of drug release from hydrogels. *Journal of Controlled Release, 16*(1), 229–236.
43. Omelczuk, M. O., & McGinity, J. W. (1992). The influence of polymer glass transition temperature and molecular weight on drug release from tablets containing poly(DL-lactic acid). *Pharmaceutical Research, 9*(1), 26–32.
44. (a) Duncan, R. (1992). Drug-polymer conjugates: Potential for improved chemotherapy. *Anti-Cancer Drugs, 3*(3), 175–210. (b) Vicent, M. J., & Duncan, R. (2006). Polymer conjugates: Nanosized medicines for treating cancer. *Trends in Biotechnology, 24*(1), 39–47.
45. Wang, B., Yuan, H., Zhu, C., Yang, Q., Lv, F., Liu, L., et al. (2012). Polymer-drug conjugates for intracellar molecule-targeted photoinduced inactivation of protein and growth inhibition of cancer cells. *Scientific Reports, 2*, 766.
46. Godwin, A., Hartenstein, M., Müller, A. H. E., & Brocchini, S. (2001). Narrow molecular weight distribution precursors for polymer-drug conjugates. *Angewandte Chemie (International Ed. in English), 40*(3), 594–597.
47. Ulbrich, K., Pechar, M., Strohalm, J., Subr, V., & Ríhová, B. (1997). Synthesis of biodegradable polymers for controlled drug release. *Annals of the New York Academy of Sciences, 831*, 47–56.
48. Ward, M. A., & Georgiou, T. K. (2011). Thermoresponsive polymers for biomedical applications. *Polymers, 3*(4), 1215–1242.

49. (a) Jochum, F. D., & Theato, P. (2013). Temperature- and light-responsive smart polymer materials. *Chemical Society Reviews, 42*(17), 7468–7483. (b) Nicoletta, F. P., Cupelli, D., Formoso, P., De Filpo, G., Colella, V., & Gugliuzza, A. (2012). Light responsive polymer membranes: A review. *Membranes, 2*(4), 134–197.
50. Han, D., Tong, X., & Zhao, Y. (2012). Block copolymer micelles with a dual-stimuli-responsive core for fast or slow degradation. *Langmuir: The ACS Journal of Surfaces and Colloids, 28*(5), 2327–2331.
51. Bawa, P., Pillay, V., Choonara, Y. E., & du Toit, L. C. (2009). Stimuli-responsive polymers and their applications in drug delivery. *Biomedical Materials (Bristol, England), 4*(2), 022001.
52. Gupta, P., Vermani, K., & Garg, S. (2002). Hydrogels: From controlled release to pH-responsive drug delivery. *Drug Discovery Today, 7*(10), 569–579.
53. Van Vlerken, L. E., & Amiji, M. M. (2006). Multi-functional polymeric nanoparticles for tumour-targeted drug delivery. *Expert Opinion on Drug Delivery, 3*(2), 205–216.
54. Pillay, V., & Fassihi, R. (2000). A novel approach for constant rate delivery of highly soluble bioactives from a simple monolithic system. *Journal of Controlled Release: Official Journal of the Controlled Release Society, 67*(1), 67–78.
55. Canal, F., Sanchis, J., & Vicent, M. J. (2011). Polymer–drug conjugates as nano-sized medicines. *Current Opinion in Biotechnology, 22*(6), 894–900.
56. Greish, K. (2007). Enhanced permeability and retention of macromolecular drugs in solid tumors: A royal gate for targeted anticancer nanomedicines. *Journal of Drug Targeting, 15*(7–8), 457–464.
57. Saito, G., Swanson, J. A., & Lee, K.-D. (2003). Drug delivery strategy utilizing conjugation via reversible disulfide linkages: Role and site of cellular reducing activities. *Advanced Drug Delivery Reviews, 55*(2), 199–215.
58. Stella, V., Borchardt, R., Hageman, M., Oliyai, R., Maag, H., & Tilley, J. (Eds.). (2007). *Prodrugs: Challenges and rewards* (p. 1464). Berlin: Springer.
59. Lachman, L., Lieberman, H. A., & Kanig, J. L. (1986). *The theory and practice of industrial pharmacy* (p. 902). Philadelphia, PA: Lea & Febiger.
60. Rajput, M. S., & Agrawal, P. (2010). Microspheres in cancer therapy. *Indian Journal of Cancer, 47*(4), 458–468.
61. Brandau, T. (2002). Preparation of monodisperse controlled release microcapsules. *International Journal of Pharmaceutics, 242*(1–2), 179–184.
62. Sinha, V. R., Bansal, K., Kaushik, R., Kumria, R., & Trehan, A. (2004). Poly-ϵ-caprolactone microspheres and nanospheres: An overview. *International Journal of Pharmaceutics, 278*(1), 1–23.
63. Morita, T., Sakamura, Y., Horikiri, Y., Suzuki, T., & Yoshino, H. (2000). Protein encapsulation into biodegradable microspheres by a novel S/O/W emulsion method using poly(ethylene glycol) as a protein micronization adjuvant. *Journal of Controlled Release: Official Journal of the Controlled Release Society, 69*(3), 435–444.
64. Bayomi, M. A., al-Suwayeh, S. A., el-Helw, A. M., & Mesnad, A. F. (1998). Preparation of casein-chitosan microspheres containing diltiazem hydrochloride by an aqueous coacervation technique. *Pharmaceutica Acta Helvetiae, 73*(4), 187–192.
65. Mu, L., & Feng, S. S. (2001). Fabrication, characterization and in vitro release of paclitaxel (Taxol) loaded poly (lactic-co-glycolic acid) microspheres prepared by spray drying technique with lipid/cholesterol emulsifiers. *Journal of Controlled Release: Official Journal of the Controlled Release Society, 76*(3), 239–254.
66. Bodmeier, R., & McGinity, J. W. (1987). The preparation and evaluation of drug-containing poly(dl-lactide) microspheres formed by the solvent evaporation method. *Pharmaceutical Research, 4*(6), 465–471.
67. Yang, Y. Y., Chung, T. S., & Ng, N. P. (2001). Morphology, drug distribution, and in vitro release profiles of biodegradable polymeric microspheres containing protein fabricated by double-emulsion solvent extraction/evaporation method. *Biomaterials, 22*(3), 231–241.

68. (a) Morton, S. W., Herlihy, K. P., Shopsowitz, K. E., Deng, Z. J., Chu, K. S., Bowerman, C. J., et al. (2013). Scalable manufacture of built-to-order nanomedicine: Spray-assisted layer-by-layer functionalization of PRINT nanoparticles. *Advanced Materials (Deerfield Beach, FL), 25*(34), 4707–4713. (b) Gratton, S. E. A., Ropp, P. A., Pohlhaus, P. D., Luft, J. C., Madden, V. J., Napier, M. E., et al. (2008). The effect of particle design on cellular internalization pathways. *Proceedings of the National Academy of Sciences of the United States of America, 105*(33), 11613–11618 (Copyright (2008) National Academy of Sciences, U.S.A.).
69. Carter, P. (2001). Improving the efficacy of antibody-based cancer therapies. *Nature Reviews Cancer, 1*(2), 118–129.
70. Wang, R., Xiao, H., Song, H., Zhang, Y., Hu, X., Xie, Z., et al. (2012). Co-delivery of all-trans-retinoic-acid and cisplatin(iv) prodrug based on polymer–drug conjugates for enhanced efficacy and safety. *Journal of Materials Chemistry, 22*(48), 25453.
71. Niwa, T., Takeuchi, H., Hino, T., Kunou, N., & Kawashima, Y. (1993). Preparations of biodegradable nanospheres of water-soluble and -insoluble drugs with D, L-lactide/glycolide copolymer by a novel spontaneous emulsification solvent diffusion method, and the drug release behavior. *Journal of Controlled Release, 25*(1), 89–98.
72. Lote, C. J. (2000). *Principles of renal physiology*. New York: Springer.
73. U.S. Food and Drug Administration. Retrieved April, 2013, from http://www.fda.gov/AboutFDA/Transparency/Basics/ucm211822.htm
74. U.S. Food and Drug Administration. Retrieved April, 2013, from http://www.fda.gov/AboutFDA/Transparency/Basics/ucm194413.htm
75. Code of Federal Regulations–860 CFR 21. Retrieved April, 2013, from http://www.accessdata.fda.gov/scripts/cdrh/cfdocs/cfCFR/CFRSearch.cfm?CFRPart=860
76. U.S. Food and Drug Administration. Retrieved April, 2013, from http://www.accessdata.fda.gov/scripts/cdrh/cfdocs/cfCFR/CFRSearch.cfm?fr=807.92
77. U.S. Food and Drug Administration. Retrieved April, 2013, from http://www.fda.gov/medicaldevices/deviceregulationandguidance/howtomarketyourdevice/premarketsubmissions/premarketnotification510k/default.htm#se
78. U.S. Food and Drug Administration. Retrieved April, 2013, from http://www.fda.gov/MedicalDevices/DeviceRegulationandGuidance/HowtoMarketYourDevice/PremarketSubmissions/PremarketApprovalPMA/default.htm
79. Muchemu, D. N. (2007). *Change control for FDA regulated industries: A risk assessment approach*. Bloomington, IN: AuthorHouse.
80. International Conference on Harmonisation/Good Clinical Practices. Retrieved April, 2013, from http://ichgcp.net/
81. U.S. Food and Drug Administration. Retrieved April, 2013, from http://www.fda.gov/downloads/RegulatoryInformation/Guidances/UCM125651.pdf
82. U.S. Food and Drug Administration. Retrieved April, 2013, from http://www.fda.gov/Food/IngredientsPackagingLabeling/GRAS/ucm2006850.htm

Chapter 3
Thin-Film Materials

3.1 Engineering Concepts

3.1.1 Diffusion and Lateral Fabrication

Our initial discussions surrounding controlled-release systems focused on the fundamentals of composition, release, and diffusion [1]. Alterations to these three basic parameters led to distinct profiles that identified their potential areas of application, such as embolics [2] or gel caps [3]. We can recall from Chap. 1 that there are various routes we can either actively or passively enter the body. The general applications were restricted in our discussion in Chap. 2 to *oral drug delivery*, traditionally entering the bloodstream through hydrolysis in the stomach, or *implantation*, done at the site of treatment. Since drug delivery encompasses a broad spectrum of treatment methodologies, we can ask two basic questions:

Can we identify alternate routes of entry?
What other fundamentals can be exploited to gain entry and reach a target?

In some cases we can revisit oral drug delivery and probe the advantage of alternate routes of entry, such as *bucally* (i.e., cheek) [4] or *sublingually* (i.e., tongue) [5], over *enterically* (i.e., small intestine) [6]. The primary advantage of bucal and sublingual deliveries is that they avoid metabolism in the liver, known as **first-pass metabolism** [7], which can greatly reduce the drug quantity. The avoidance of the liver allows for a much more potent concentration of drug to be delivered systemically through the mucosal membranes. These pathways can be exploited using *thin-film materials*.

Interest in thin-film drug delivery approaches has gained momentum since they were developed and pioneered by Wyeth Laboratories as Zydis® [8] in the 1970s. Perhaps the most popular applications of this system are seen today in NicoDerm® [9] patches and Listerine PocketPaks® [10]. The approach represents a facile mode of application (i.e., a film) for an efficient dosage form of a specific drug. This has

E.P. Holowka, S.K. Bhatia, *Drug Delivery: Materials Design and Clinical Perspective*, DOI 10.1007/978-1-4939-1998-7_3

implications in the dosage window (i.e., concentration and timing) of specific drugs where side effects can become harmful or debilitating. The area of oral thin-film drugs alone encompasses greater than $2.6 billion today [11]. As one can imagine, the thin-film approach allows for a much less esoteric view of taking a medication. One may be more inclined to pull out a strip of Benadryl® [12] than one would be to take a pill. The pill form can carry with it the stigma of overmedication, but a film strip evokes the thought of convenience. Overlapping with existing drug delivery modes, however, is not the only advantage of a thin-film approach. Pediatric or geriatric patients can often take issue with a solid dosage form due to swallowing, sensitive stomach, throat fatigue, chewing, choking, or the time delay of an efficacious dose. In cases such as high blood pressure, transdermal drug delivery offers a distinct benefit of rapid efficacy and delivery of small drugs such as Clonidin® [13] through the skin. Conditions such as advanced macular degeneration (AMD) in the eye have been recently addressed with thin-film drug delivery technology to allow for the introduction of anti-VEGF proteins without the dangers of ocular injections.

The term **thin-film material** in drug delivery refers to any system consisting of a film geometry that promotes the release of a drug through *dissolution*, *swelling*, or *degradation*. Each of these three characteristics is influenced, respectively, by the **lateral fabrication** of the film, which provides information regarding the *quality*, *dispersion*, *flexibility*, *shear*, and *tensile strengths* of the material, which will be discussed later in this section.

We will extrapolate on these principles to discuss design characteristics of thin films for applications in transdermal and ocular drug delivery in Sect. 3.2 and examine current strategies in Sect. 3.3.

Thin-film materials extend the application base for controlled-release systems with a new set of challenges we will address from an engineering design and medical treatment perspective in this chapter.

3.1.2 Physiological Models for Thin-Film Applications

The properties of release and diffusion, as we have defined them in the traditional sense of controlled-release systems in Chap. 2, require a more in-depth look when designing a thin-film release system. The change in geometry, thickness, and surface area of thin-film systems allow for them to be leveraged in applications requiring a rapid dissolution and/or a fine control of release kinetics on a robust range of tissue surfaces. Common physiological models such as oral, transdermal, and ocular delivery each carry with them a series of challenges [14] that affect the release of a drug at a correct dosage form, dissolution, diffusion, and ultimate delivery within tissue systems. In this section, we look at three model systems for the mouth, the skin, and the eye, where the rate-limiting step of the delivery can change based on the physiological barriers that are encountered. We will decouple those barriers into their respective core engineering concepts. In the next section, we will build a system based on the concepts we have deconstructed (Fig. 3.1).

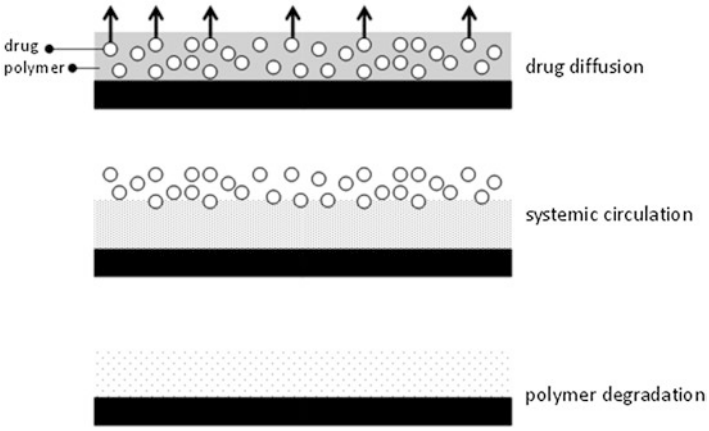

Fig. 3.1 Diagram of basic release modes from a thin film

3.1.2.1 Physiological Models: The Mouth

The mouth represents the simplest mode of effective delivery of drugs throughout multiple possible locations within the body. In Chap. 2, we deconstructed the typical controlled-release systems involved in oral drug delivery. The primary limitations of the systems described previously are that they rely on reaching the stomach or gastrointestinal tract in order to allow for the prolonged dissolution of drug matrices [15]. This can significantly delay the effective treatment of an ailment or disease and can cause a degree of fatigue associated with interaction with the tissue lining of the digestive tract. A substantial benefit exists with the ability to introduce oral drugs into the bloodstream by absorption through tissue in the mouth.

Transmucosal drug delivery in the mouth typically is focused on delivery of a thin film either *bucally,* to the cheek, or *sublingually*, to the tongue [16]. Each approach carries with it a different barrier system to drug delivery. They both generally function by suspending insoluble drug molecules (i.e., actives) in a controlled-release thin-film matrix, which adheres to the mucosal wall and releases into the bloodstream to avoid first-pass metabolism. We begin a more detailed discussion with the *sublingual delivery* approach. A significant degree of focus has been given to the introduction of drugs through the sublingual mucosae [17]. The tissue behaves similar to filter paper when in contact with aqueous content, whereby material is readily absorbed. This process resembles the traditional *diffusion* approach discussed in Chap. 2. Both *Fickian diffusion* and *capillary wicking* would drive the absorption of drugs into the sublingual tissue. If we recall, Fickian diffusion occurs in the direction of high concentration to low concentration. A more traditional way to think about Fickian diffusion is in terms of *osmotic potential* or *diffusion* [18]. Most forms of physiological absorption are governed by osmosis. Uptake into the circulatory system depends on the concentration difference of blood from the intracellular

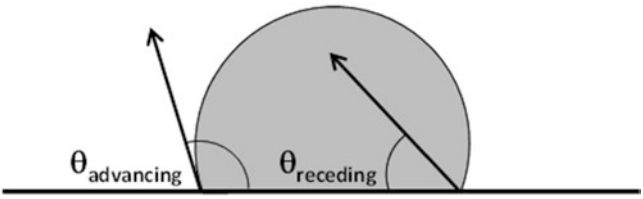

Fig. 3.2 Diagram of contact angle analysis

and extracellular volume. The concentration difference creates an osmotic pressure of blood plasma within the cell membranes. This pressure leads to a hydrostatic pressure originating from within the blood vessel [19].

Capillary wicking is the result of adhesion and absorption of water to the walls of a vessel and the cohesive hydrogen bonding between water molecules. This is a process similar to that of the solvent migration that occurs when you touch the surface of a puddle of water with a paper towel placed perpendicular to it. When the water comes in contact with the towel, it migrates up the towel to a degree based on the nature of the porous matrix of the towel. A similar effect is seen in the xylem of trees [20], where they work against gravity to absorb water through capillary channels in the center. With both of these properties working in concert, one can imagine a film with a high concentration of drug being placed on the tongue. Fickian diffusion would drive a percentage of that film to diffuse into the sublingual tissue. Another driving force would be the solvent migration created by a mixture of saliva and drug molecules. In this simplistic model, no barrier of entry into the bloodstream is discussed. We propose for this chapter that the rate-limiting steps to internalization into the bloodstream are related to the wetting of the thin film, which creates a Fickian diffusion gradient in the direction of the tissue, and the apparent flux created by the capillary wicking into the tissue itself.

Since capillary wicking, to a first approximation based on our current assumptions, is the rate-limiting step for *sublingual delivery* [21], the characteristic behavior we focus on is the way a drug solution droplet interacts with the surface tissue. The measure of solvent droplets on a surface is typically done using contact angle analysis. The primary measurement of interest in the contact angle is the *advancing angle* (θ_a), which is the maximum stable angle, and the *receding angle* (θ_r), which is the minimum stable angle (Fig. 3.2).

Both advancing and receding contact angles relate to the *hysteresis*. The *hysteresis* measures (3.1) the expansion or retraction of a droplet on a surface [22]:

$$H = \theta_a - \theta_r. \tag{3.1}$$

For a metastable droplet or surface, the hysteresis would show a number of different thermodynamically stable contact angles. For the purposes of this discussion, we will focus on the surface, in this case sublingual tissue, as the source of any potential hysteresis in the system. A surface can either be smooth, which typically refers to machine-polished surfaces, or rough, which has some form of irregular or regular

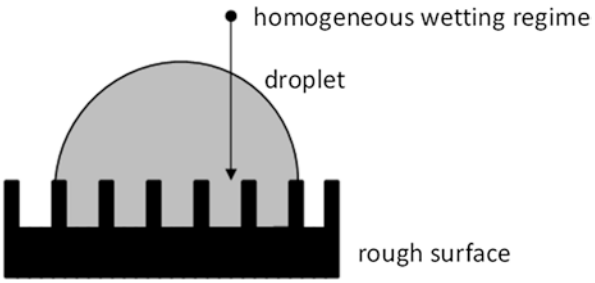

Fig. 3.3 Diagram of the Wenzel model of surface wetting

terrain. In the case of sublingual tissue, we would expect a rough surface. The wetting is a somewhat different characteristic. The surface roughness and regularity are factored into the *surface tension* felt by a droplet of drug solution. It is important to form a relevant comparison to a first approximation between the surface of the sublingual cells and the droplet of drug solution in order to predict the effect of capillary wicking.

Let's first look at the simplest case (3.2), an ideal homogeneously wetting tissue surface:

$$\cos\theta^* = r\cos\theta. \tag{3.2}$$

The **Wenzel model** [23] is the wetting approximation of a homogeneous regime on a rough surface, where $\theta*$ is the apparent contact angle at a stable equilibrium state, θ is the ideal contact angle, and r is the roughness ratio, or the ratio of true area to apparent area on the surface. If there is no hysteresis present, the model predicts the homogeneous wetting regime.

The measure of r in the Wenzel model (Fig. 3.3) accounts for the surface area of the interaction of the droplet in a homogeneous system. This would appear analogous to a physiological system where cells are not densely packed, creating a highly porous tissue layer, which allows for homogeneous wetting between the gaps in the tissue surface. This can occur in vitro when a cell culture is not permitted to grow to confluence, which is the regime where tight cell–cell packing occurs (Fig. 3.4). When we are dealing with in vivo systems, these highly porous tissue layers can be induced by an outside stimulus, acting to change the permeability. We discuss this induction in more detail in the Sects. 3.1.2.2 and 3.2.

The **Cassie–Baxter model** [24] (Fig. 3.5) approximates wetting on a heterogeneous surface [Eq. (3.3)]. Since there is likely some form of hysteresis on physiological tissue surfaces, this model appears to more accurately predict behavior in metastable systems, such as the mouth.

$$\cos\theta^* = r_f f\cos\theta_Y + f - 1, \tag{3.3}$$

where $\theta*$ is the apparent contact angle at a stable equilibrium state, θ is the ideal contact angle, r_f is the wet surface roughness ratio, and f is the fraction of the surface that is wetted by the droplet.

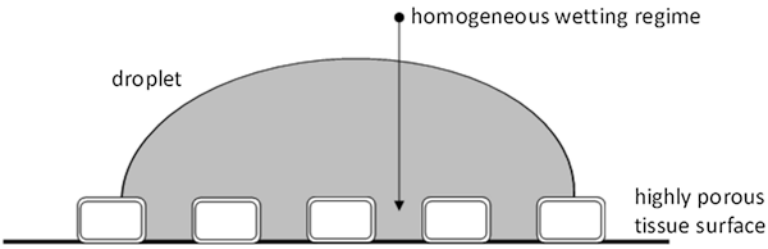

Fig. 3.4 Extrapolation of Wenzel model in terms of the tissue surface

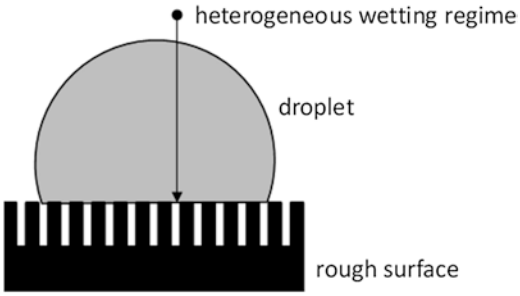

Fig. 3.5 Diagram of the Cassie–Baxter model for surface wetting

In this model, the wet surface roughness is different than the overall surface roughness. Since the droplet is not in contact with the entire substrate in this case, some diffusion limitations also exist. We can see that as the fraction of wetted surface approaches 1 ($f \longrightarrow 1$) and as the wet surface roughness ratio approaches the overall surface roughness ratio ($r_f = r$), the Cassie–Baxter model becomes the Wenzel model [24].

In the physiological realm (Fig. 3.6) of the sublingual tissue of the mouth, we fall somewhere between the Wenzel model and the Cassie–Baxter model in terms of capillary wicking. Since our assumption is that the route for drug internalization into the circulatory system occurs through the gaps in cell adjacencies within the sublingual tissue, the Wenzel model would be the ideal [25]. Therefore, in order to reach the ideal rate of drug uptake in this system, we would look to **maximize Fickian diffusion** of our drug solution, while inducing a response in the sublingual tissue to move $f \longrightarrow 1$ and $r_f = r$. We discuss strategies for this approach later in Sect. 3.2.

If we now move to the *buccal delivery approach*, we see that the tissue adopts a more challenging barrier of entry into the bloodstream [26]. The buccal barrier resembles that of skin, which we discuss in more detail in the following section. The absorption potential of the buccal mucosae, in the cheek, is dependent on several properties, including solution permeability, pH, and molecular weight of the drug to be transported. The solution permeability in this case refers to the potential for the solvent carrying the drug molecule to be permeable through the buccal tissue.

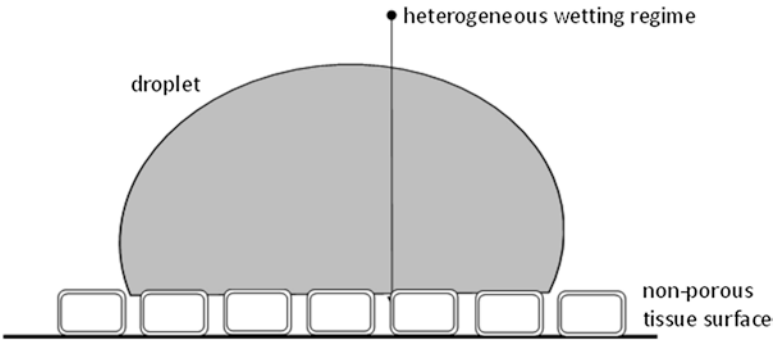

Fig. 3.6 Extrapolation of the Cassie–Baxter model in terms of the tissue surface

Similarly to sublingual, which was discussed earlier, and transdermal systems, which we discuss later in this section, the buccal systems require diffusion through gaps in cell adjacencies. This encompasses both diffusion and capillary wicking behaviors, as discussed in the *sublingual drug delivery case*. The pH involves the ionization of the buccal tissue as a way of "priming it" for more efficient drug absorption, which is partially driven by electrostatic interactions on the cell surfaces [27]. The introduction of pH is a form inducing drug uptake by a perturbation of the tissue surface. The molecular weight of the transported drug relates primarily to geometric size. In the oral epithelium (i.e., buccal tissue), typically small molecules are taken up by endocytosis. For the process of uptake into the bloodstream, it is necessary to penetrate multiple cells in depth. Therefore, in order for the drug to reach the bloodstream, it would need to traverse through multiple cells:

$$(\text{membrane} \longrightarrow \text{cytosol} \longrightarrow \text{membrane} \longrightarrow \text{membrane} \longrightarrow \text{cytosol} \longrightarrow \text{membrane, etc.}).$$

This approach is highly disfavored as a main route of entry. Another route with a higher, though hindered, efficiency of uptake is the route that the solvent takes, which is between the gaps of the cell adjacencies. This is where the molecular weight aspect becomes more critical [28]. The higher the molecular weight of the drug, typically the larger the size of the molecule. The larger the molecule, the harder it is to navigate between the gaps in the cell adjacencies. Even with the appropriate molecular weight, however, we are still bound by the restraints of capillary wicking, which was discussed in the *sublingual drug delivery case* (Fig. 3.7).

A further complication of the buccal case is that the consequence of the pH change not only induces a more porous tissue surface by vasodilation, but also stimulates the salivary glands to secrete saliva as a form of defense against the increasing acidity level. This creates more drug solvent, which leads to higher solvent migration due to Fickian diffusion.

In the case of buccal delivery, more than likely it is a combination of each of these factors that dictates the approach and behavior. A solvent is chosen, such as saliva, which has the appropriate level of permeability and pH to allow for the vasodilation, or widening of blood vessels, in the mucosal tissue, which permits a

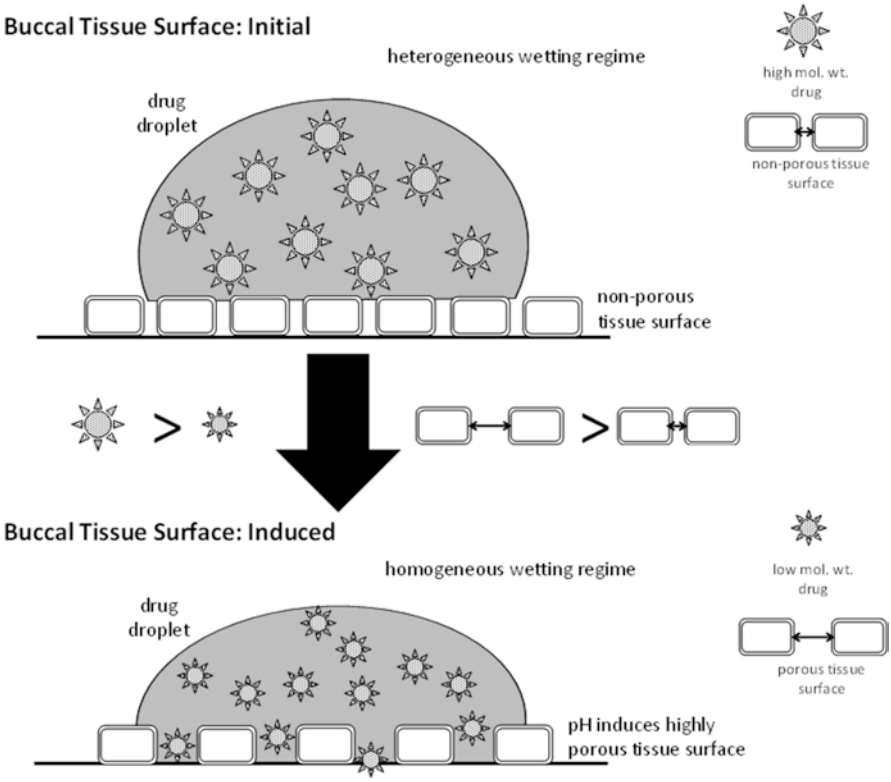

Fig. 3.7 Extrapolation of Wenzel and Cassie–Baxter models to drug delivery through tissue interfaces

robust range of drug molecular weights to be taken up into the circulatory system by absorption. We discuss examples of these combinations in more detail in Sect. 3.2.

3.1.2.2 Physiological Models: The Skin

The skin is an extremely desirable route for the delivery of pharmaceutical drugs. This is due primarily to the fact that skin is both readily accessible and the fact that it receives one third of all the blood circulating within the human body [29]. With this attraction, however, come challenges. Due to both of these benefits, the barrier of entry within skin is complex, excluding a number of drug candidates based on solubility and optimal dosage range. The structure of skin (Fig. 3.8) consists of an outer layer known as the epidermis that is 0.05–1.5 mm in thickness, followed by a dermis layer that is 0.3–3 mm in thickness, followed by a layer of subcutaneous tissue. The epidermis itself consists of five layers of varying thicknesses [29]. From innermost to outermost, they are *stratum basale*, *stratum spinosum*, *stratum granulosum*, *stratum licidum*, and *stratum corneum*. The innermost layer, the *stratum*

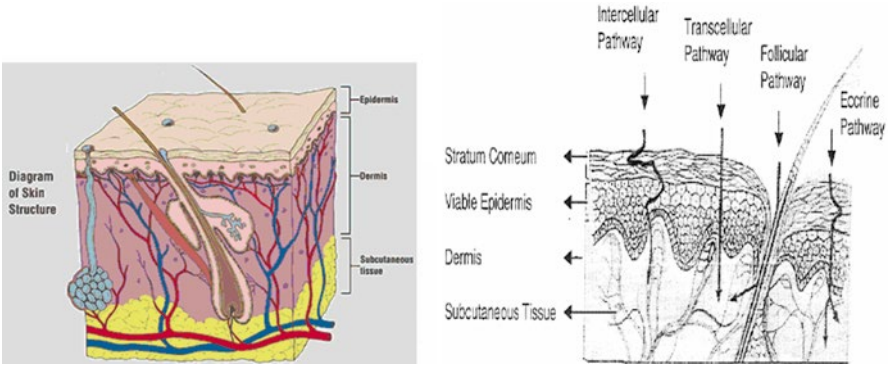

Fig. 3.8 Model of the stratum corneum [29]

basale, is constructed from columnar cells that act to constantly cycle replenished cells out to the other three inner layers known as the *viable epidermis*. The viable epidermis is referred to in this way due to the constant replenishment of skin cells. Once the cells die, they are cycled up to the *stratum corneum* to make up the outermost cell layer, where they remain for two weeks until they are shed. It is with the *stratum corneum* that we begin our discussion of transdermal drug delivery [29].

The *stratum corneum* is the most significant barrier to transdermal diffusion [29]. This is primarily due to its constituency of dead skin cells that are tightly packed together in a layer 12 μm (±3 μm) thick. If the outermost layer of the *stratum corneum* is composed of dead cells, the potential for active cellular transport across membranes within that layer is significantly limited. The tight cellular packing of 10 nm also presents a challenge for diffusion of drug molecules around the outermost cell layer.

Currently, the two main routes for transdermal drug delivery through the stratum corneum are known as the **transcellular pathway** and the **intracellular pathway**. In the transcellular pathway, the drug molecule travels through the cell membranes and intracellular domains themselves, traversing multiple cell layers [30]. This process would involve crossing dead skin cells (i.e., keratinocytes) by movement through the phospholipid bilayer, which is amphiphilic, the cytoplasm, which is hydrophilic, to the phospholipid bilayer once again and repeat this process through several cells of depth. This is the shortest distance in terms of depth through the skin. To help frame how difficult this journey would be, as an analogy try to imagine a passive barrier system consisting of stacked dialysis tubes. The drug molecule would have to permeate the semipermeable membrane of the tubing on one side, then diffuse through the interior of the bag, followed by diffusion out the other end and iterate through this process several times in series. The main requirements of this analogy are simplified to size and diffusion (Fig. 3.9).

Keep in mind that there are a number of confounding factors to this analogy. Diffusion through a dialysis membrane is *not* active transport, as is the case with a cell, but rather passive transport. In passive transport there needs to be a driving force to

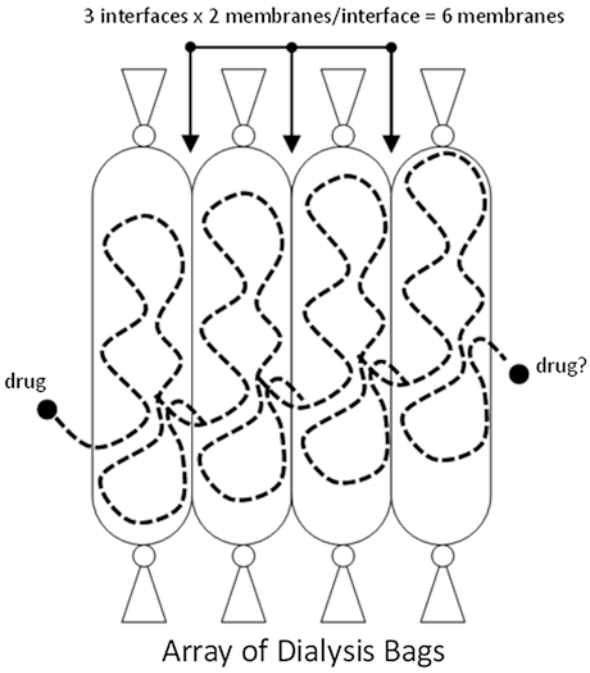

Fig. 3.9 Analogy of stacked dialysis membranes to multilayered cellular environment in the skin

push the molecules with the appropriate size through the semipermeable membrane in a timely manner rather than waiting extended times for Brownian, or random, molecular motions to occur. Typically, this is done using an osmotic pressure gradient between internal and external dialysis environments. In order to internalize a drug into a dialysis bag, one could fill the bag with water and place it in a beaker full of concentrated sucrose solution with the drug molecules. The sucrose will diffuse from a higher concentration to a lower concentration, or Fickian diffusion (3.4), into the dialysis bag:

$$\text{flux} = \frac{D\Delta C}{z}\left(\text{Fick's law}\right), \tag{3.4}$$

where C is the concentration, D is the diffusivity of the solvent through the solute, and z is the thickness of the film or membrane. The osmotic flow or stress will carry

Sample Problem 3a
What is the flux of a 5-μg/ml solution of the drug *clenbuterol*, a decongestant ($D = 2.14 \times 10^{11}$ cm^2/s), that can be expected through the stratum corneum of the skin?

Since we know the diffusivity ($D = 2.14 \times 10^{11}$ cm^2/s) and concentration (5 μg/ml) of the drug solution, all that remains is the thickness of the filter

membrane layer, or in this case the stratum corneum. We identified from the reading that the thickness of the stratum corneum is approximately 12 μm (0.0012 cm). Therefore, we can substitute the values into (3.4) as follows:

$$\text{flux} = \frac{D\Delta C}{z} = \frac{\left(2.14\times10^{11}\ \text{cm}^2/\text{s}\right)\left(5\ \mu\text{g}/\text{cm}^3\right)}{\left(0.0012\ \text{cm}\right)} = 8.92\times10^{14}\ \mu\text{g}/\text{s}.$$

Another way to look at this is if 1 ml of clenbuterol was applied to the skin, the flux indicates that it would take 0.056 ps to diffuse across a permeable membrane of that thickness. The key term to pay attention to is "permeable." As we know from earlier in this chapter , the stratum corneum has 10-nm pores that restrict diffusion in terms of the size of drug particles in solution. We will see later in this section the degree to which that restriction can occur.

with it the drug molecules that are within the appropriate size regime according to Eq. (3.4) to pass through the semipermeable membrane. In order for a drug to then diffuse out of the dialysis tubing, it would be required to have an induced osmotic stress in the opposite direction.

The dialysis analogy is dependent on the application of appropriate concentration gradients at the correct time to induce drug movement into and out of the system. So think of this as a form of energetic input: the energy it takes the experimenter to pump in one solution and remove another one to gain the intended movement. In cellular systems, conversely, endocytosis, or cell internalization, can be triggered by a number of stimuli depending on the cell type in question. These stimuli trigger an energetic cascade that begins with the binding of receptors leading to a signal relay event (i.e., receptor-mediated endocytosis) [31]. In cellular systems with less specific responses, the cell membrane can have a channel allowing for passive transport of drug molecules through the system based on general criteria such as size (i.e., protein channel). It can be inferred that should one encounter a drug system capable of delivering through the transcellular pathway, the amount of drug that arrives within the body would be a small percentage of that applied. The massive excess in dosages that are typically required to utilize this approach leads to inflammatory responses within the epidermal and subdermal layers [31]. We will not go into detail about the biology of these interactions; however, there are several reference texts that would appropriately address questions in this area.

The challenge of traversing multiple through-cell pathways highlights the limited likelihood of this approach to be feasible as a drug delivery route. In the **intracellular pathway**, however, the drug travels between the gaps in stratum corneum cells. This route is simplified in that it does not rely on the crossing of intracellular boundaries for delivery; however, the drug molecule is then required to traverse a route up to 20 times longer than that of the transcellular pathway. As an additional

complication, we recall that the gaps in the stratum corneum are approximately 10 nm in diameter, which severely limits molecular permeability [31].

If we return our attention to the topic of diffusion, the intracellular pathway can be seen as represented by a filter with an impediment in terms of both the pore size and tortuosity of the membrane material. The pressure (P), termed *bubble pressure*, felt by a film or membrane in terms of water adsorbed can be defined as

$$P = \frac{4k\cos\theta}{d}\sigma, \tag{3.5a}$$

where k is the shape correction factor, θ is the liquid–solid contact angle, d is the pore diameter, and σ is the surface tension.

The key variables we will focus our discussion on are θ, d, and σ in terms of the saturated volume. We can see that increasing the pore size (d) is inversely proportional to the bubble pressure through the membrane. This is intuitive since increases to the size of the holes in a barrier lead to a higher flux of material through that barrier. If the adsorbed thickness increases, filling more pores and reducing the effective pore diameter, one would expect that the back pressure felt at the surface would increase. The contact angle is inversely related to hydrophobicity, or the degree to which to surface is compatible with water. We can see that as the contact angle approaches 90° (i.e., hydrophobic), the cosine term approaches 0, which leads to a pressure term of 0. This would indicate that the surface is in a model consistent with Cassie–Baxter, where the applied droplet has minimal interaction with the porous surface. Therefore, we can see that the more an applied droplet can wet the surface [i.e., cos(0) = 1], the greater the bubble pressure due to the increased interaction with the porous surface.

The diffusional flow (DF) of a film or membrane in terms of porosity, relative pressure, and path length can be defined as

$$\mathrm{DF} = \frac{K\left(P_1 - P_2\right)Ap}{L\left(r\right)}, \tag{3.5b}$$

where K is the diffusivity, $P_1 - P_2$ (ΔP) is the pressure difference across the membrane, A is the membrane area, p is the membrane porosity, and $L(r)$ is the path length of the pores.

The key variables we will focus our discussion on are ΔP, p, and $L(r)$ in terms of the diffusional flow. We can see that increasing the porosity (p) has a direct influence on the diffusional flow. This is intuitive since increases to the porosity correspond to more holes in a barrier, which leads to a higher flux of material through that barrier. The path length of the pores [$L(r)$] carries more significant meaning. In terms of diffusional flow, we can see that $L(r)$ decreases the total amount, which is consistent with an increase in the volume of the total pore volume of the system. An increase in the path length leads to a greater internal volume to travel before reaching the other side of the filter. This correlation for $L(r)$ also has implications in terms of tortuosity.

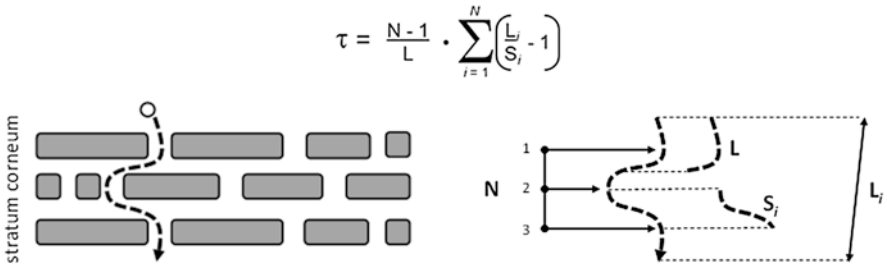

Fig. 3.10 Diagram of tortuosity as an analogy for movement of small molecules through the outer epidermis

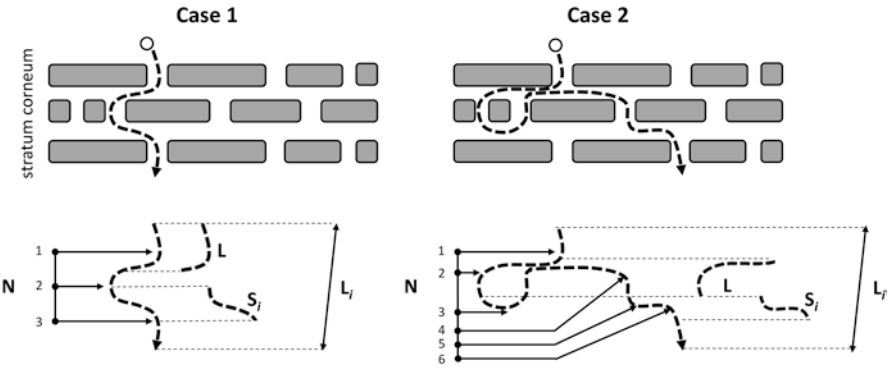

Fig. 3.11 Diagram of the component breakdown of tortuosity

The *tortuosity* of a film is described as the curved pathway of a molecule or particle in porous substrates or membranes, which can be defined as

$$\tau = \frac{N-1}{L}\sum_{i=1}^{N}\left(\frac{L_i}{S_i}-1\right), \tag{3.6}$$

where N is the number of curves, L is the curve length, S_i is the turn curve length of a segment, and L_i is the chord length of a segment, or the length between the two extremes [32].

We have broken down the tortuosity (Fig. 3.10) in terms of its substituents from Eq. (3.6). To put these variables in a more relatable context, imagine N is the number of peaks in the curve, L is the length of those peaks, S_i is the length of the inflection, and L_i is the length between the most extreme curvatures.

In the previous figure, a simplistic pathway was chosen in order to effectively illustrate the relationships within the tortuosity equation. One can imagine a more complicated route of a drug molecule through the stratum corneum, such as the one in Fig. 3.11.

For example, let's compare two cases with dramatically different routes through the simplified model of the stratum corneum. When the route is decoupled from the model and segmented accordingly, what trends emerge between the two cases in terms of molecular travel through the tissue membrane? The first trend would highlight the similarities between the two routes. Both the values for L and S_i appear to be approximately equivalent between the two cases. The number of peaks, or N, appears significantly larger for Case 2. Keep in mind that the circle turn in Case 2 is equivalent to two peaks in terms of N. The value for L_i is also larger for Case 2. Remember that L_i is the length of the route between the two extreme curvatures and *not* the end-to-end length. Generally, we can see in the following equation with the assumptions that the N and L_i for Case 2 > Case 1, so, therefore, Case 2 has a higher tortuosity than Case 1:

$$\frac{\text{Case 1}}{\text{Case 2}} = \frac{\dfrac{N-1}{L}\displaystyle\sum_{i=1}^{N}\left(\frac{L_i}{S_i}-1\right)}{\dfrac{N-1}{L}\displaystyle\sum_{i=1}^{N}\left(\frac{L_i}{S_i}-1\right)} \quad \text{Case 1} < \text{Case 2}.$$

Sample Problem 3b What is the pressure felt by a layer of the skin after the application of a solution of the drug *clenbuterol* that fully wets the stratum corneum, with a surface tension of 51 mN/m and a value of $k = 1$?

Since we know the surface tension ($\sigma = 51$ mN/m) and the shape correction factor ($k = 1$), all that remains is the pore diameter of the membrane and the contact angle of the deposited clenbuterol solution. We know from the reading that the pore diameter of the stratum corneum is 10 nm. We also know that the contact angle of a droplet that fully wets the surface is 0. Therefore, we can substitute the values into (3.5a) as follows:

$$P = \frac{4k\cos\theta}{d}\sigma = \frac{4(1)(\cos 0)}{\left(10\times10^{-9}\,\text{m}\right)}\left(51\ \text{mN/m}\right) = 2.04\times10^{7}\,\text{N/m}^2.$$

This calculation shows that the pressure felt due to the wetting of a membrane composed of the features of the stratum corneum with a clenbuterol solution would be in the range of millions of newtons per square meter. If we look at this in the context of our answer to Sample Problem 3a, we can see that the reasonable diffusion characteristics of the stratum corneum calculated in terms of flux are offset by the disfavorable wetting characteristics of the drug solution on the surface due to the pressure felt by the membrane. Modes of alleviating this pressure remain highly desirable in the selection of transmembrane drug delivery therapies. We will discuss the design of these therapies throughout this chapter.

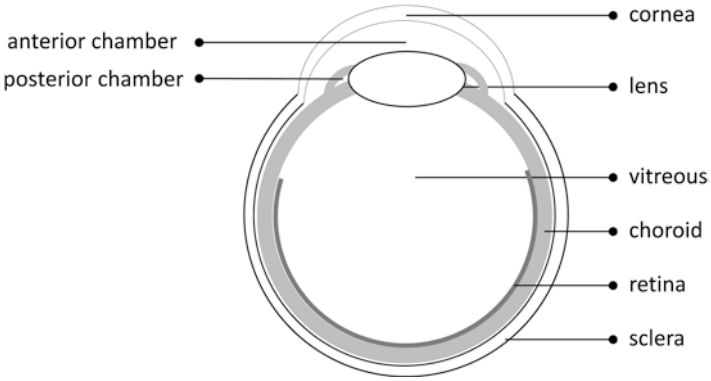

Fig. 3.12 Diagram of the human eye and its components

The primary impediment that we have discussed for the transdermal system has been simplified in this section to porosity and tortuosity. We will begin to build a system from these first principles and discuss strategies to increase porosity and reduce the tortuosity of the dermal system in Sect. 3.3.1.2. In Sects. 3.2 and 3.3, we will discuss the design strategies for using thin films to modify the interface between tissue and drug molecules to enhance delivery.

3.1.2.3 Physiological Models: The Eye

Ocular drug delivery is an extremely challenging route for the treatment of disease. Where oral and transdermal delivery techniques rely on ultimately reaching the circulatory system, ocular delivery typically treats localized disorders related to the eye or its immediate proximity. Similar to the skin, the eye consists of multiple tissue layers (Fig. 3.12), which can act as boundaries to entry. These boundaries, which limit uptake into the blood vessels of the eye, are the *cornea*, the *conjunctiva*, the *sclera*, the *choroid*, and the *retina*. In ocular systems, tears on the cornea act to rapidly wash away potential drug candidates from the surface at a rate of 1 μl/min on a total ocular surface volume of 10 μl [33]. This cyclical dilution on the surface of the eye limits the residence time of a dosage form. The *cornea* consists of a trilayer tissue film composed of the *epithelium*, *stroma*, and *endothelium*, each of which constrains the surrounding environment based on *size* or *polarity*. The *conjunctiva* is represented as both the white tissue of the eye (i.e., *bulbar*) and the inner side of the eyelid (i.e., *palpebral*). This membrane system is highly porous and represents a facile route of entry into the bloodstream. The *sclera* are the collagen-based fibers suspended in the *conjunctiva* of the eye. The permeability of the sclera is based on *molecular weight* and *size*. The *choroid* is a vascular tissue that aids in supplying blood to the retina. The *retina* is composed of a multi-layer of tissue with differing degrees of permeability. Drugs can be eliminated from the retina through

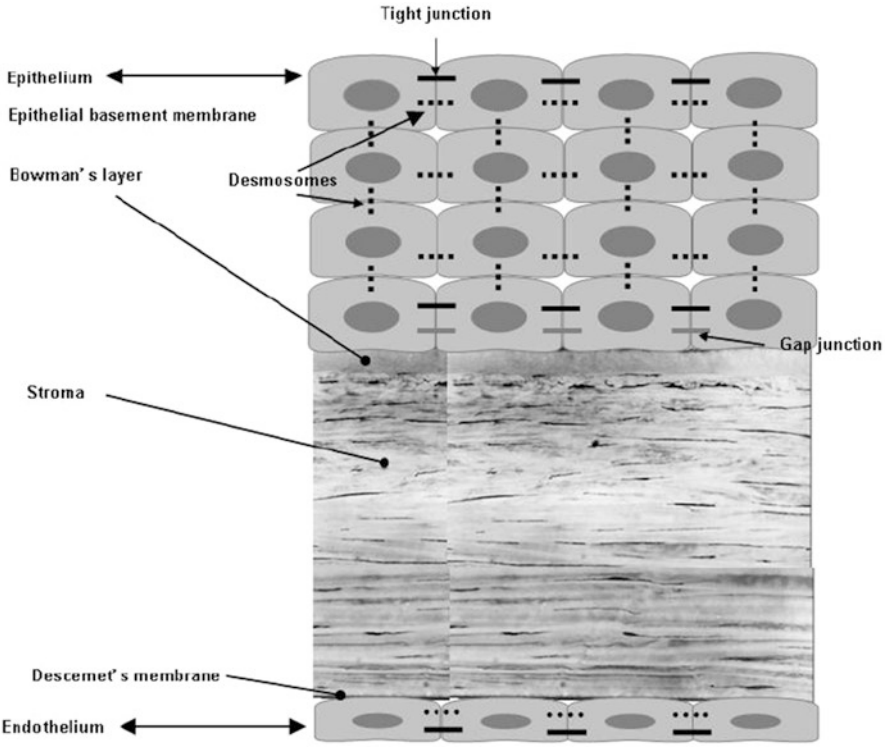

Fig. 3.13 Diagram of the different layers of the cornea [34]

either the anterior or posterior routes. The *anterior* route involves the indiscriminant diffusion laterally across the vitreous, or internal tissue, layers of the retina, for eventual evacuation. The *posterior* route involves the ultimate expulsion through the **internal limiting membrane** (**ILM**) [33], which selectively filters molecules based on *molecular weight* and *size*.

We will begin by simplifying the mode of drug uptake to one of diffusion/adsorption, molecular weight, and size. The focal point for this approach will be regions of the eye such as the *cornea*.

3.1.2.4 The Cornea

Perhaps the most challenging obstacle when attempting drug delivery into the ocular environment is the trilayer membrane of the cornea (Fig. 3.13). The *cornea* is composed of a trilayer filter system with varying degrees of porosity throughout the depth of the cellular layers. The epithelium consists of a series of cell layers connected in gap junctions by desmosomes. The porosity of these cell layers amounts

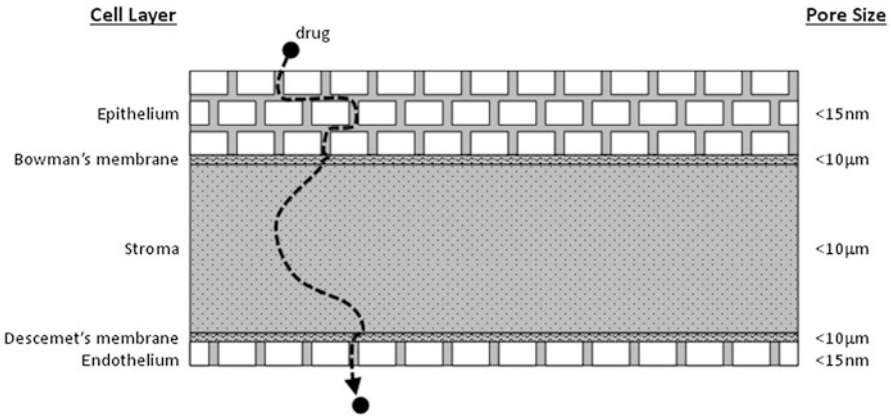

Fig. 3.14 Simplified diagram of a trilayer filter as an analogy for the multilayered film of the cornea in terms of tortuosity

to <15 nm [34]. At the base of the epidermis, Bowman's membrane acts as a less constrained filter layer approximately 15 μm thick and is composed of collagen fibers responsible for maintaining the elasticity and shape of the cornea. The stroma allows for more traditional diffusional constraints with small pores ranging in size from <10 μm. The base of the stroma consists of Descemet's membrane, which is similar to Bowman's membrane with the exception of the type (IV) of the collagen from which it is composed. The endothelium returns to a <15-nm pore size similar to that of the epithelium [34].

If we reassemble the corneal trilayer membrane as we did in the transmembrane section of this chapter, we can begin to see where the rate-limiting steps to drug delivery appear. To the engineer, the independent layers resemble commercially available filtration systems to a first approximation. The epithelium looks very similar to a *track etched membrane* [35] one would typically use for liposome formation, which we discuss in more detail in Sect. 4.2.2. This layer also resembles the epidermis in skin, where small pore sizes limit passage of unwanted molecules on the basis of size and tortuosity. The membranes, Bowman's and Descemet's, resemble what are known as *nonwoven membranes*. Nonwoven membranes consist of a random array of nanometer- to micron-diameter fibers, or collagen, which can act as a filter. Nonwovens tend to have the highest levels of porosity and highly variable tortuosity. The stroma functions similarly to a highly porous traditional filter membrane consisting of fibroblasts. The endothelium is similar to the epithelium in terms of its filtration based on particle size; however, tortuosity becomes less of a factor due to the reduction of cell layers in depth (Fig. 3.14).

When we take these factors into account, it appears that the rate-limiting membrane, based on size, would be the epithelium. Since we know this critical layer acts

as a barrier to drug uptake on the basis of size, what other factors contribute to drug uptake into the cornea?

We will start by operating based on a few assumptions. First, filters limit molecular passage based on size. Second, molecules need to be present long enough on the surface of a membrane to allow for diffusion through the membrane to occur. You want the *diffusion* to occur *through tissues* that are acting as filters. You want *adsorption* to occur *within tissues* that you want to deliver drugs. The aqueous phase on the surface of the cornea is essential for the promotion of drug delivery through a robust range of methods. There is an ideal range, however, which will correspond to the necessary residence time for a drug at the surface prior to uptake. This range can be improved upon by changing the *adsorption*, *molecular weight*, and *size* of the drug system. For adsorption, we can follow the van't Hoff [36] equation for enthalpy of the system:

$$\Delta H_{\text{ads}} = \Delta H_{\text{liq}} - RT \ln c, \tag{3.7}$$

where c is the equilibrium constant multiplied by the vapor pressure of the adsorbent, T is temperature, R is a constant, and ΔH_{ads} and ΔH_{liq} are the drug adsorption and drug liquid enthalpies, respectively. We can see provided that temperature remains relatively constant within the system, the primary indicator of the enthalpy of adsorption (ΔH_{ads}) is the enthalpy associated with the drug in the aqueous phase on the surface (ΔH_{liq}). The stability of this aqueous phase is then correlated with the chemical functionality of the drug molecule. Drug molecules can be hydrophilic, or water-loving, hydrophobic, or water-fearing, or amphiphilic, or stable in both water and oil. Drugs that are hydrophobic or amphiphilic form a condensate such as a micelle (Chap. 4) or colloidal aggregate (Chap. 5), which have surfaces that interact with the surrounding solvent. The chemical functionality of these surfaces can act to increase or decrease ΔH_{liq} based on their ability to effectively disperse the drug in solution. We will discuss this in more detail in Sect. 3.2, where we will begin to assemble systems to improve adhesion of drug systems on the surface of the eye.

The *molecular weight* and *size* of the drug in solution are the main recurring antagonists in the successful uptake of drugs in ocular systems. We will begin by stating that molecular weight and size are interrelated. If we are dealing with a polymer- or protein-based drug, this relationship is highly predictable for linear molecules (3.8) in terms of what is known as the **radius of gyration** (R_{g}) [37]:

$$R_{\text{g}} = (S^2)^{1/2}, \quad S^2 = \frac{\sum_0^n m_i s_i^2}{\sum_0^n m_i}, \tag{3.8}$$

where S is the size angular dependence and m_i is the distance to a polymer chain repeat unit from the center of mass. The radius of gyration predicts what we perceive as the size of the polymer molecule in an ideal solvent by measuring the size weight of a molecule by the mass distribution about its center of mass (c).

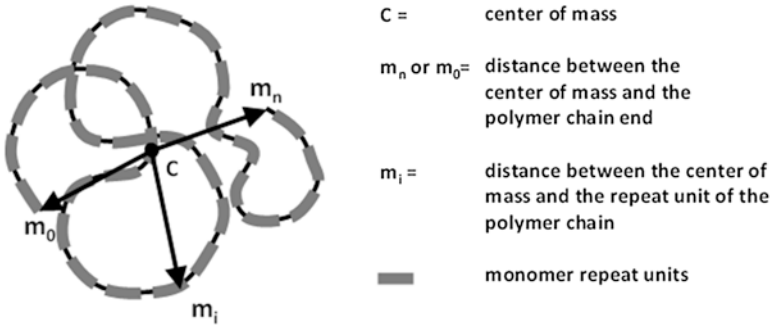

Fig. 3.15 Diagram of the radius of gyration (R_g) of a polymer molecule

We can see (Fig. 3.15) that the larger the molecular weight of the polymer chains, the larger the sample size for the values of m_i and the longer the distance between c and m_i. There are strategies to exploit this relationship by changing to a branched polymer topology, which would act to lower the *radius of gyration* and what is referred to as the *hydrodynamic radius*. We discuss this approach in more detail in Sect. 3.2.

If we look again at the diffusion of our drug systems, we can see that the particle size of our drugs can be related to diffusion by the Stokes–Einstein equation [38]:

$$D = \frac{k_B T}{6\pi r \eta}, \tag{3.9}$$

where k_B is Boltzmann's constant, T is temperature, r is the radius of the particle, and η is the viscosity. Here we can see that as the particle size decreases, the diffusion coefficient increases. If we substitute the Stokes–Einstein equation [Eq. (3.9)] into the adsorption enthalpy equation discussed earlier in this section, we can see the following relationship:

$$H_{ads} = H_{liq} - (6\pi KDr\eta)\ln c \qquad \text{where } K = \frac{R}{k_B}. \tag{3.10}$$

From (3.10), two critical points are brought to light. The particle size and the rate of diffusion are both inversely related to the enthalpy of adsorption. In other words, the larger the particle size or the larger the diffusion coefficient, the smaller the change in enthalpy of adsorption. This coincides with the logic used for membrane systems, whereby the larger an object on a surface, the more surface is required to adsorb in a stable manner. We can also see that the enthalpy of adsorption and the diffusion coefficient are competing phenomena [39]. In the case of drug delivery in ocular systems, an ideal range or balance exists between ΔH_{ads} and D to allow for diffusion of drugs through one membrane layer and adsorption of the same drug into another.

The cornea introduces another layer of complexity when we look at the polarity of the epithelium. The epithelium expresses permselectivity, where an ionic potential of approximately 20 mV exists. This flux (3.11) is created by the inward flow of sodium ions through the membrane:

$$J = Cu\left(\frac{\delta c}{\delta x}\right), \tag{3.11}$$

where C is the ion concentration in the solution, u is the ion mobility, and δc is the concentration difference over distance δx. This ionic flow and permeability can act to segregate surface species on the basis of charge. The ionic potential for negatively charged species reduces the potential for positively charged species from passing the epithelium due to electrostatic coupling or *salting out* of aqueous solution. Negative- or neutral-polarity drug species can be driven based on this potential, provided the size, molecular weight, and adsorption characteristics are consistent with the permeability requirements discussed earlier in this section. What happens, however, if the ionic potential of the epithelium is disturbed? A number of thin-film applications operate on the assumption of covering the surface of the cornea to enhance the adsorption and diffusion of drug species through the epithelium. It turns out that perturbation of the ionic potential of the surface destabilizes the epithelium and can lead to a reduction in the barrier to infection [40]. Therefore, it remains critical that the selection of thin-film drug delivery treatments remain harmonious with the biological environment in which they reside.

In addition to tears diluting and washing away drugs, the eyelid provides a source of shear upon opening and closing [41]. Up to this point, we have been referring to the limitations in the membrane itself for the uptake of drug dosage forms. We have not gone into detail regarding the film requirements for ocular therapies. We are beginning to see that control over the interfacial volume is critical from diffusion and adhesion perspectives. The inherent geometry of a thin film placed on the surface of the cornea can reduce the effect of tears and dilution on drug uptake. The next challenge in this approach would then be the act of blinking. The closing of the eyelid creates a shear stress on the surface of the eye [41]. This stress is not significant in terms of the shear stresses typically measured in rheology labs, or people's eyes would slowly be shaving their own surface. Ouch! The stress is large enough, however, to move a thin film floating on the water layer on the surface of the cornea. Think of contact lenses on your eye and how they can move from time to time when you blink. So how do we protect against perturbation of our thin film by our eyelids? This can be addressed in the preparation of the thin film itself. If we follow the model developed for contact lenses, the ideal ocular thin film that reduces movement on the cornea surface is one that allows for minimal apical contact with good uniform circulation of tear volume under its surface, good film curvature on the eye surface, and good gas permeability [42]. These characteristics are what we refer to as **lateral fabrication**, or simply **fabrication**, of thin films. We discuss strategies in lateral fabrication in greater detail in Sect. 3.2.

3.2 Material Design

3.2.1 Thin Films and Polymer Morphology

In the previous section, we looked at the critical driving forces for uptake into tissues commonly targeted using thin-film drug delivery systems. The oral, transdermal, and ocular membranes discriminated between molecules based on *diffusion* [43], *adsorption* [44], *polarity* [45], *size* [46], and *molecular weight* [46]. In this section, we will begin to piece together systems that will satisfy these requirements through the use of a thin-film–based approach. The first question to ask is

What is the benefit of a thin-film approach to drug delivery?

Perhaps more specifically, what is the benefit in oral, transdermal, and ocular systems? Thin-film systems will carry with them many, if not all, of the benefits of the controlled-release systems discussed in Chap. 2. One might even look at thin films as a subset of Chap. 2 overall. The primary difference is in the mode of application. Thin films are fabricated in a geometry that allows for one to force an interface of application. For example, when you place a thin film on the cornea of the eye, you are localizing the drug reaction at the surface of the cornea and not any other portion of the eye. This is a valuable technique since it allows for chemists to tailor surface chemical functionality and release profiles based on a specific *known* biological surface, rather than creating an overly robust system that must be amenable to multiple cell types within the body.

The first task will be to discuss the factors affecting the formation of a film. Then we will discuss methods for fabricating thin films. Finally, we will show systems that have applicable adhesion, polarity, and diffusion characteristics for drug delivery.

3.2.1.1 Film Formation

A number of physical stresses influence the formation of a film. In Sect. 3.1, we discussed the various requirements of drug delivery systems within three physiological domains: the mouth, the skin, and the eye. Each of these environments requires a different characteristic within the formation of a film to exploit effective surface delivery of drug dosage forms. The characteristics we will discuss relate to the *porosity* of the film, the *surface roughness* [47], and the *elasticity* [48]. The process of film formation is a mitigation of physical stresses felt by a polymer solution on a base surface or substrate. We can generalize the process to two stages. The initial stage involves the modal distribution of solution constituents on the edges of the solvent interface with the surface, due to nonuniform solvent evaporation [49]. The second stage involves the lateral tension felt by the solution relative to the surface,

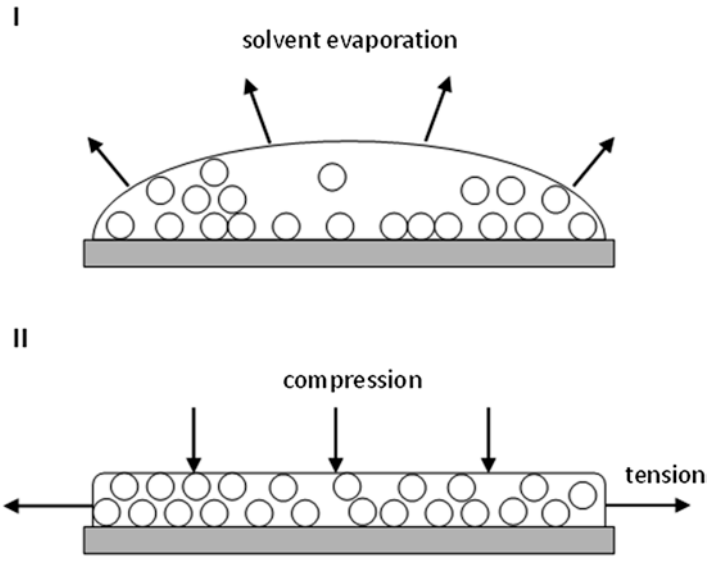

Fig. 3.16 Diagram of different forces involved with film formation

inducing a compression, which instigates the alignment of solution constituents into a film array [49] (Fig. 3.16).

This is, of course, the ideal situation leading to the formation of a perfectly uniform film. Films will almost always contain some degree of defect, such as a crack or a bump. Films consist of two basic components: the *particle phase* and the *matrix phase*. The particle is typically a colloidal molecule, such as a hydrophobic drug or polymer, which contributes to the hardness and toughness of the film. In the case of a polymer particle, the T_g can strongly influence film behavior [50]. If we recall, the T_g is the softening temperature of the polymer. Selection of a polymer operating at a temperature approaching its T_g would have implications on the packing of particles. The matrix phase is typically a polymer, latex emulsion, or surfactant that acts to stabilize the particle and add elasticity. The ratio of particle to its matrix phase is a common method to measure the change in the porosity of their materials in order to vary the opacity [51]. There are tradeoffs to this approach, however, where increases in porosity can lead to a loss of the elasticity of the film (Fig. 3.17).

The ratio of constituents is not the only factor needed to effectively predict film behavior. Interfacial surface tension can help to predict how the film forms and consequently how it will behave [52]. The stresses associated with the polymer components in the film can be either *polymer–air* ($\gamma_{poly\text{-}air}$) or *polymer–water* (γpoly-water) surface tension, which are related to what is known as *sintering*. **Sintering** is the act of bringing together a species of particulate (i.e., polymer or ceramic) to create a solid surface. The surface tension prevents deformation, while the base

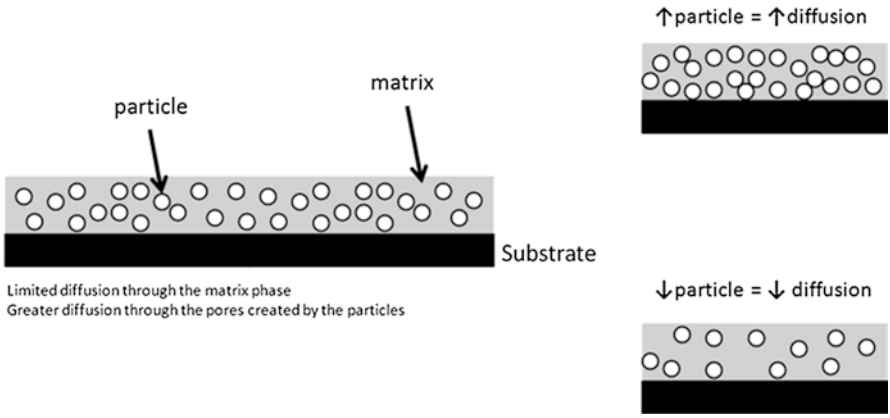

Fig. 3.17 Diagram of the different film components

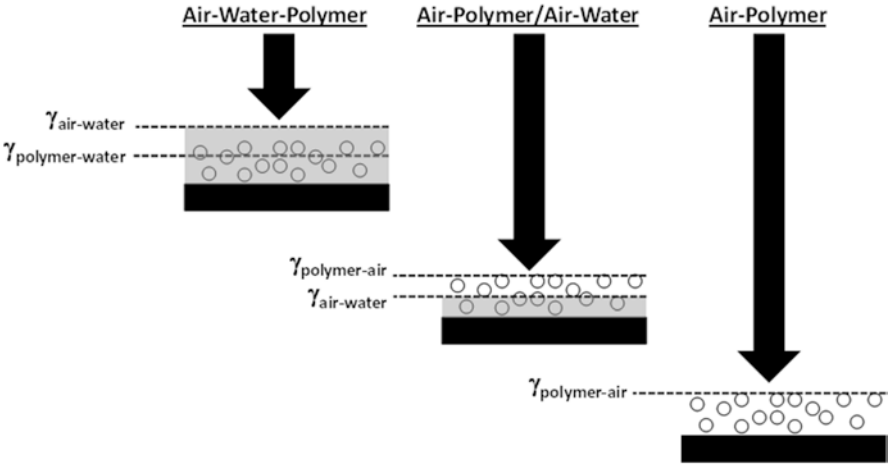

Fig. 3.18 Diagram of the different interfacial interactions between phases during film formation

substrate allows for uniformity to develop in the film. We are beginning to see where our characteristics of porosity (surface tension and sintering), surface roughness (sintering), and elasticity (sintering and chemical identity) can be tailored. It is evident that the interfacial surface tension is a significant driving force for film formation [52] (Fig. 3.18).

The surface tension felt at the air–water interface is known as *capillary deformation*. The time and temperature it takes for a solution to move from *air–water–polymer* to *air–polymer/air–water*, to *air–polymer* can dictate the *porosity* of the film. The interfaces between the phases are not the only factor in determining the film characteristics. The binding affinity of the polymer particles to either themselves or the substrate contributes as well. Films can form through three primary growth modes:

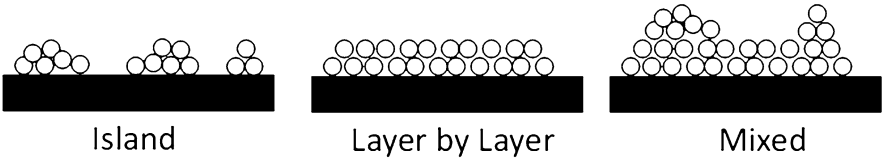

Fig. 3.19 Diagram of the radius of gyration (R_g) of a polymer molecule

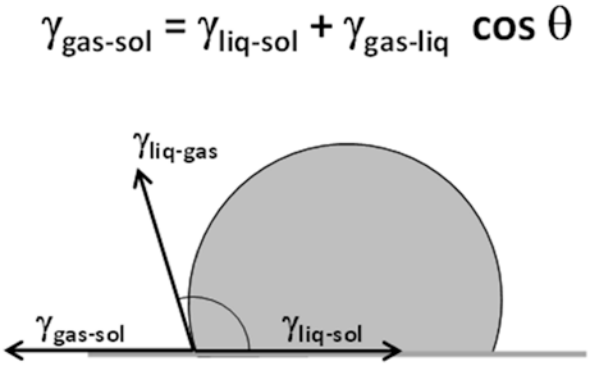

Fig. 3.20 Diagram of the interfacial effects between phases and contact angle using Young's equation

island, **layer by layer**, and **mixed** [53]. In island growth, the polymer particles have a higher binding affinity to themselves than to the substrate [54], leaving irregular pockets on the substrate surface after solvent evaporates. In layer-by-layer growth, the polymer particles have a higher affinity to the surface than to themselves, leaving a more uniform film. In mixed growth, the polymer particles initially have an affinity to the substrate and then develop islands upon reaching a high enough film build on the substrate (Fig. 3.19).

Each of these modes of film growth can be predicted based on their relative surface tensions in terms of Young's equation [55]:

$$\gamma_{\text{gas}-\text{sol}} = \gamma_{\text{liq}-\text{sol}} + \gamma_{\text{gas}-\text{liq}} \cos\theta. \tag{3.12}$$

Young's equation describes the relationship between the interfaces of the solid, liquid, and gas phases by the prediction of the contact angle of a drop on a substrate. From our earlier discussion of contact angle, we can recall the equation that appears in Fig. 3.20.

In Fig. 3.20, $\gamma_{\text{gas-sol}}$, $\gamma_{\text{liq-sol}}$, and $\gamma_{\text{gas-liq}}$ are the surface tensions at the interface between gas and solid, liquid and solid, and gas and liquid, respectively. The θ-term is the advancing contact angle of the droplet. A typical estimate used to distinguish between the three modes is that contact angles in the 0–90° range are

indicative of island growth, contact angles of 0° are indicative of layer-by-layer growth, and contact angles approaching 0° are indicative of mixed-growth film formation.

There is one remaining basic factor that can aid in the prediction of porosity, surface roughness, and elasticity, which is referred to as **Ostwald ripening** [56]. Ostwald ripening is the thermodynamically driven effect of smaller particles aggregating together with larger particles over time:

$$(R)^3 - (R)_0^3 = \frac{8\gamma c_\infty \upsilon^2 D}{9R_g T} t \tag{3.13}$$

where $\langle R \rangle$ is the average radius of all particles, c_∞ is the solubility of the particle, υ is the molar volume, R_g is the ideal gas constant, γ is the surface tension, and D is the diffusion coefficient. This effect is simply a surface area minimization over time. Larger particles have less overall surface area per mole than small particles, which makes them a more thermodynamically stable entity in solution since surface molecules are inherently less stable than bulk molecules. The larger the difference in particle size from R_0 to R, the larger the diffusion coefficient (D). We can see that particle size returns as a critical property in both film formation and enhanced diffusion and adhesion in drug delivery. This difference in stability is consistent with our discussion in Chap. 2 regarding bulk and surface erosion kinetics. *Ostwald ripening* is coupled with *sintering* to drive the formation of island growth modes.

For example, let's revisit the question at the beginning of this section. How can we modify the porosity, surface roughness, and elasticity of a film? We can begin by looking at porosity. If we desire a highly porous film, we would first identify the appropriate set of components. The particles would ideally be large in size to allow for the least close packing, accounting for a greater degree of unoccupied space. The matrix phase would have a relatively high interfacial surface tension with air that would allow for a θ of 0–90°, which coincides with the island film growth mode, while the solvent would have relatively low interfacial surface tension with the substrate. The ratio of the particles and matrix phase components would have to be high, in the range >10, relative to the desired porosity to allow for the desired level of diffusion through the film bulk.

This provides insight into the porosity selection process as an isolated property. The system becomes more complicated with the addition of compounding material properties. What happens when we apply the same criteria to the properties of surface roughness and elasticity? Here we begin to see the compromise in the factors between the three properties. The surface roughness is largely correlated with the mode of film growth. We can infer that the greatest change in the roughness of the film would occur when moving from a layer-by-layer mode to an island mode. In the case of high porosity, the system tends toward a more heterogeneous surface with selection of the matrix phase to allow for a θ of 0–90°; the island mode would be consistent. One could also decrease the interfacial surface tension of the substrate to achieve a similar effect. If we move in the other direction, toward film uniformity, the system is more complicated. Uniformity implies reduced particle

size, which generally decreases the interfacial surface tension that favors the layer-by-layer mode of formation at low ratios of particles to matrix phase.

While some adjustment is required to allow for an effective balance between porosity and surface roughness, this is made simpler by the fact that the roughness is a surface and not a bulk film property. Porosity is a bulk property, where changes to the bulk affect the entire material, whereas surface properties can impose a barrier to bulk properties but can ultimately be mitigated by adjustments to particle size, interfacial surface tension, and solvent. The elasticity, however, is tied to the bulk characteristics of the film in a manner similar to porosity. Therefore, elasticity presents a more complicated issue. High-porosity and high-elasticity films appear at first glance to be diametrically opposed properties. The answer is tied to what level of compromise is required to gain the desired performance range for both properties.

For example, if we return to a highly porous film, the particles would ideally be large to allow for the least close packing, accounting for a high degree of unoccupied space. The larger the particle size and the higher the frequency of the unoccupied spaces, the less polymer material is present. The island film growth mode also lends itself to a more porous and less elastic film. Lastly, high ratios of particles to matrix phase imply less polymeric materials present. The less polymer present, typically the less elastic the film.

In this section, we have discussed the methods for the formation of a film from a fundamental approach in terms of effects to the bulk volume (porosity), surface area (roughness), and bulk density (elasticity). Next, we will look at component options for general film formation and identify candidates for biological systems.

3.2.1.2 Films for Biomedical Applications

In the previous section, we discussed the primary components of thin films and the physical behavior of their formation. We can now begin to identify the components of a thin film in more detail. Thin films are typically composed of a drug molecule (i.e., particles), water-soluble polymer (i.e., matrix phase), *plasticizers*, and fillers (i.e., colorants). A plasticizer is an additive that can increase the fluidity of a material by lowering its T_g, effectively softening the polymer. For physiological applications, the breakdown of components falls somewhere close to <25 % drug, <50 % water-soluble polymer, <20 % plasticizer, and <5 % filler [57]. We discuss each of the components in more detail next.

3.2.1.3 Drug Molecules

Drugs can effectively function as the colloidal particles of the film. This is primarily true of hydrophobic drug molecules. In order to minimize interfacial free energy, hydrophobic molecules will aggregate, leading to phenomena such as Ostwald ripening, which was discussed earlier in this section. A critical component of film formation is the effective distribution of the drug particles throughout the matrix of

Table 3.1 Collection of the different components of a film for drug delivery

Component	Function in film	Function in drug delivery	Examples
Drug	Colloid or particles that can increase porosity and decrease elasticity of the film	• Antihistamine • NSAIDs • Antiulcer	• Salbutamol • Paracetamol • Omeprazole
Water-soluble polymer	Promote easier processability and functions as a malleable matrix	• Degrades into benign components • Remains inert within the circulation lifetime	• PLGA • PHEMA • PEG
Plasticizer	Improve flexibility, reduce brittle fracture, and reduce T_g of the polymer	• Improves polymer degradation profile • Inert small molecule	• Glycerol • Propylene glycol • Dibutyle phthalate
Filler	Surfactants, thickeners, dyes, or colorants to improve film appearance and dispersability in water	• Improves drug release and dispersion • Tailors the diffusion of the drug	• Sodium lauryl sulfate • Xanthan gum

the film. This returns our discussion to film fabrication, where there needs to be a balance of interfacial surface tension, particle size, molecular weight, and P to B ratio (Table 3.1).

3.2.1.4 Water-Soluble Polymer

The polymer component accounts for up to 50 % of the total mass of the thin film. What, then, are the choices that govern the selection of polymeric materials for these applications? For adequate film behavior, the polymer needs to be hydrophilic enough to allow for effective wetting, while retaining physical properties such as resistance to delamination, shear, and tensile strengths. In biological applications, the polymer should also be nontoxic, be noninflammatory, and have no leachable impurities. Natural examples can include materials such as maltodextrin and cellulose. In order for effective application in physiological systems, film fabrication is typically focused on hydrolytically degradable polymers. These polymers are mixed with drug molecules in the form of a matrix solution and deposited on a film casting substrate during the process of film formation. We will discuss a more detailed account of film-coating methods later in this section.

3.2.1.5 Plasticizer

The act of plasticization improves elasticity and reduces the brittleness of the fabricated film. The plasticizer does this by effectively lowering the T_g of the polymer matrix of the film. Remember, the T_g represents the temperature at which bulk

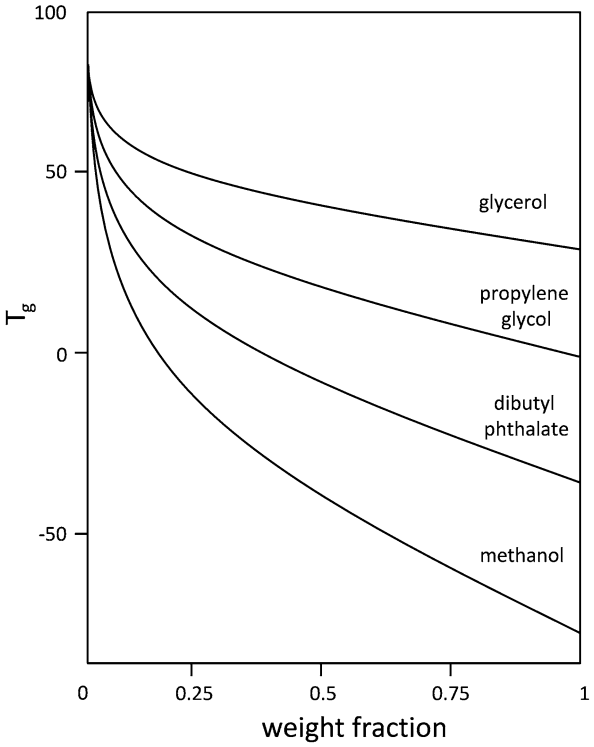

Fig. 3.21 Plot of the effect of differing amounts of plasticizer on the T_g of the base polymer system

polymer chain backbone motion ceases. The introduction of small molecules that are highly soluble in the bulk of the polymer matrix can reduce the cohesive forces between polymer chains or increase the entropy of the system by increasing the segmental motion of the polymer chains. This entropic increase requires a greater energetic reduction in the system in order to reach the T_g. A simple way to think of this is that more plasticizer means more mobility, which means the more you need to freeze the system to avoid mobility (Fig. 3.21).

3.2.1.6 Filler

The filler is comprised of a range of materials from surfactant to colorant to flavorant to thickeners. Additives such as flavorant and colorant are to enhance the aesthetic of the end-use thin-film product and are typically associated with oral drug delivery applications. These factors may appear trivial from a scientific

standpoint; however, entire business models for products can be based on achieving a specific color or taste. The thickeners serve as a film promoter by adding viscosity to the film component mixture. Achieving the correct viscosity range can lead to the effective drawing of the film. Thickeners are inert additives that allow for this viscosity tenability to be possible. Many fillers can come from natural products such as xanthan gum, which offer cheap alternatives to synthetic products. The surfactant serves to effectively stabilize the drug molecules evenly throughout the polymer matrix. Uniform dispersion of the drug molecules within the thin-film system is critical to achieve the desired release kinetics. Unwanted agglomeration of drug particles within the matrix will decrease the rate of diffusion and broaden the dosage windows in terms of both time and concentration. Surfactants disperse drug particles by stabilizing the interface of the hydrophobic drug particle with hydrophilic water molecules. One can look to either small molecule surfactants, such as sodium lauryl sulfate (SLS) [58], or polymeric amphiphiles [59], such as fatty acid ethoxylates (FAE) [60]. Small surfactants (SLS) typically stabilize drug particles more rapidly upon introduction, while polymers (FAE) typically take longer to establish a stable interface with the drug particle surface. With speed, however, small surfactants sacrifice long-term stability, whereby other molecules can easily displace the surfactant from the drug–surfactant interface (Table 3.2).

3.2.1.7 Film Fabrication Methods

While there are a number of approaches that exist for the successful formation of thin films, extreme temperatures and pressures for the respective extrusion processes can degrade or denature biocompatible materials. The approaches highlighted here prove to be robust toward biomaterial systems (Table 3.3).

An intriguing question is: Can we modify the deposition method to allow for the fabrication of multilayer films? Multilayer films have gone largely unmentioned in this text. They allow for the potential for multiple dosage forms to be available for tailoring of different release rates. Each method above allows for the fabrication of multilayer films, with semisoidal casting being the most effective of the methods mentioned. Multilayer film fabrication is also necessary in cases such as transdermal drug delivery, where different film phases allow for different levels of drug release and different levels of compatibility with the film–epidermal interface. We look in more detail at film applications in Sect. 3.3.

Table 3.2 Collection of biocompatible film formers used in drug delivery

Polymer	Repeat unit
Poly β-aminoesters	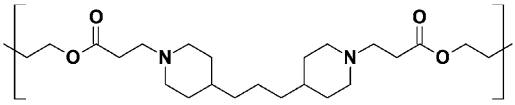
Poly L-lysine	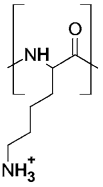
Poly L-glutamate	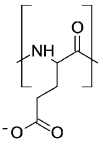
Hyaluronic acid	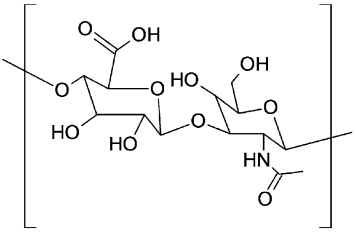
Poly hydroxyethyl methacrylate	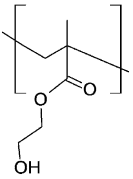
Poly methacrylic acid	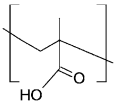
Poly ethylene glycol	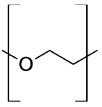
Alginic acid	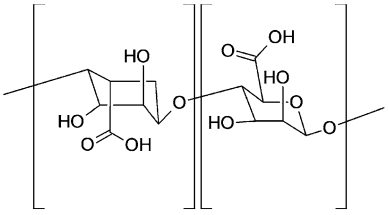

(continued)

Table 3.2 (continued)

Polymer	Repeat unit
Chitosan	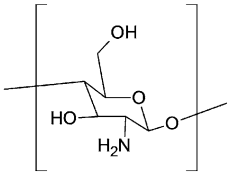
Poly lactic-co-glycolic acid	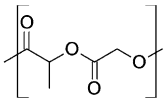

Table 3.3 Collection of the different thin-film processing methods and application fabrication techniques

Method	Components	Application technology
Solvent casting	• Drug • Water-soluble polymer • Plasticizer • Filler	Components dissolved and deposited into an evaporation plate
Dispersion extrusion	• Drug • Surfactant • Filler	Components mixed and die-cast to desired thin-film shape
Roll process	• Drug • Water-soluble polymer • Plasticizer • Filler	Components dissolved in a water–volatile solvent mix and deposited onto a carrier substrate, where evaporation takes place
Semisoidal casting	• Drug • Water-soluble polymer • Hydrocolloids • Plasticizer • Filler	Film components are dissolved in water to form a viscous solution, added to a concentrated drug solution, and run through a high-shear processor followed by homogenization, drying, and casting

3.3 Implementation

3.3.1 Oral, Transdermal, and Ocular Delivery

3.3.1.1 Oral Drug Delivery Films

We have discussed the advantages of applying a thin-film drug dosage form orally in terms of patient convenience, comfort, and efficacy. The importance becomes more critical in applications where the patient's decision of whether to move forward with a specific treatment method depends on one of these three criteria. In cancer patients, the emetic (i.e., vomiting) response to chemotherapy medication after a 24-h period

Table 3.4 Thin-film components for the delivery of dexamethasone as an oral drug delivery system

Component	Function in film	Function in drug delivery	Examples	Film composition (%)
Drug	Colloid or particles that can increase porosity and decrease elasticity of the film	• Antiemetic	• Dexamethasone	• 13.9
Water-soluble polymer	Promote easier processability and functions as a malleable matrix	• Disintegrant • Remains inert within the circulation lifetime	• L-HPC • PEG	• 15 • 1.3
Plasticizer	Improve flexibility, reduce brittle fracture, and reduce T_g of the polymer	• Improves polymer degradation profile	• Hypromellose	• 7.4
Filler	Surfactants, thickeners, dyes, or colorants to improve film appearance and dispersability in water	• Improves drug release and dispersion	• Polysorbate	• 5.4
		• Tailors the diffusion of the drug	• Microcrystalline cellulose	• 57

is a significant deterrent for a patient in the decision to move forward with an anticancer treatment regime. A number of drugs are currently used to mitigate this effect; however, the treatment window is relatively narrow to prevent the induction of an emetic response in the patient. In our discussion in Sect. 3.1, we recall that thin-film systems offer a more rapid, burst release, pharmacokinetic profile than typical pill-form controlled-release systems. The ideal pharmacokinetic system for oral delivery of antiemetic treatment would be a dispersed drug in liquid form. While ideal in the pharmacokinetic sense, this approach is not ideal in patients since the requirement of water can create concerns with emetic symptoms or difficulty swallowing. What is advantageous is a system that can be effectively dissolved with saliva to a form exhibiting a pharmacokinetic profile similar to that of a freely dispersed drug. The current development with respect to fast-dissolving thin films presents significant implications in the treatment of disease with narrow dosage windows.

The fabrication of rapid-release thin films was approached by Shimoda et al. for the delivery of dexamethasone through the oral mucosae to mitigate an emetic response in cancer patients prior to chemotherapy treatment [61]. The versatility of the film fabrication processes described allows for the use of natural polymers in conjunction with synthetic materials (Table 3.4). The introduction of natural materials, such as microcrystalline cellulose, provides a highly efficient lubricant and dispersant that is stable, safe, and physiologically inert.

These natural polymers can be used as substitutes for materials such as poly(lactic-co-glycolic acid) or poly(methacrylic acid). In the rapid-release cancer system being described here, the microcrystalline cellulose functions as the matrix material, where the raid dissolution of the matrix is necessary for the intended application.

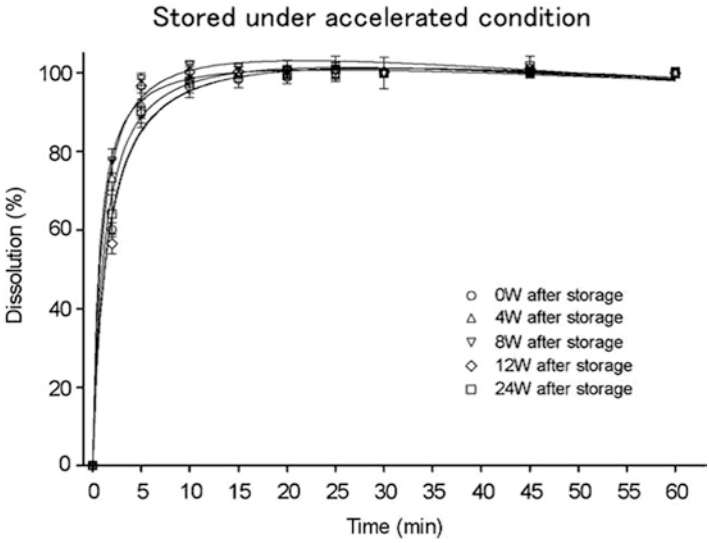

Fig. 3.22 Dissolution profile of dexamethasone-containing film stored for up to 24 weeks under accelerated conditions. Each film was wrapped in an aluminum package and stored at 25 °C with 50–60 % humidity (normal condition) or at 40 °C with 75 % humidity (accelerated condition). Each point represents the mean ± SD of six experiments. Data were statistically analyzed by Dunnett's test [61]

The hypromellose, or hydroxypropyl methyl cellulose, has similar solubility properties as the microcrystalline cellulose film bulk and functions to increase the flexibility of the system.

The polyethylene glycol (PEG) provides a route of water permeability within the film. While microcrystalline cellulose is a highly dispersible material, the rapid absorption of water by PEG allows for an additional driving force for the dissolution of the film matrix. Enhancing this dissolution further is the presence of L-HPC, or a low-substituted hydroxypropyl ether of cellulose. These components were used to prepare films using the solvent casting fabrication method described in Table 3.3.

In rapid-release thin films, a key concern is the premature release of drug or perturbation of the film under what is known as accelerated aging conditions. Accelerated aging, in this case, is referring to the exposure of the thin-film drug dosage form to high-relative humidity and elevated temperature for a period of time. This becomes critical since the response of rapid-release materials is dramatic and typically occurs in a narrow window with respect to external stimuli (i.e., moisture and temperature). The goal is to exploit the release characteristics in the desired environment (i.e., body) instead of in storage (Fig. 3.22). In observing the rate of dissolution with changing exposure to accelerated aging conditions, it appears there is virtually no effect of temperature shifts between room temperature to 40 °C and changes to relative humidity between 50 and 75 %. This supports the choice of microcrystalline cellulose and PEG and critical film component materials from an applied engineering standpoint.

We can then begin to look at the release response in a physiological system (i.e., rat) relative to the ideal level of dissolution (i.e., aqueous drug dispersion). Here we

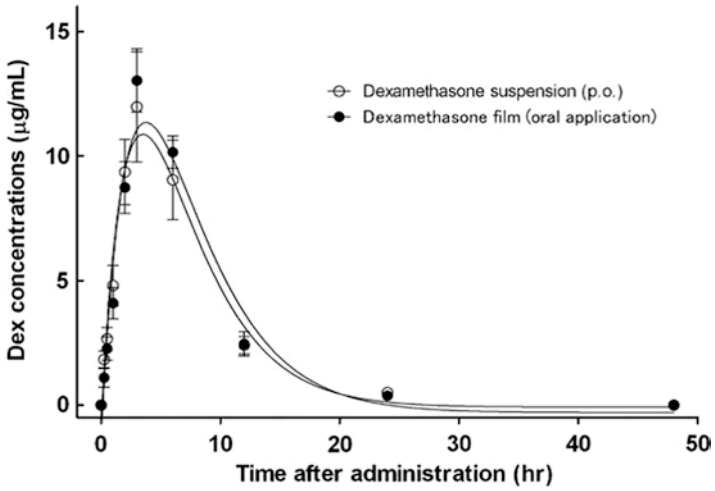

Fig. 3.23 Comparison of time course changes in plasma concentration of dexamethasone administered with oral film or suspension in rats. Rats were lightly anesthetized with ethyl ether and dexamethasone was administered orally with solution or ingested with oral film preparation at a dose of 5 mg. Each point represents the mean ± SD of 10 animals [61]

Table 3.5 Comparison of pharmacokinetic parameters of dexamethasone between oral film and oral suspension in rats [61]

	Oral film ($N=10$)	Solution ($N=10$)	P-values
T_{max} (h)	3.20 ± 1.03	3.40 ± 1.43	0.724
C_{max} (μg/ml)	13.33 ± 3.97	12.66 ± 6.61	0.785
$AUC_{(\infty)}$ (μg/ml/h)	98.01 ± 22.28	93.64 ± 37.75	0.756
ke (h^{-1})	0.42 ± 0.01	0.42 ± 0.02	0.713
$T_{1/2}$ (h)	1.65 ± 0.06	1.66 ± 0.07	0.696
Cl_{tot} (l/h)	0.05 ± 0.01	0.06 ± 0.02	0.410
Vd_{ss} (l)	0.37 ± 0.12	0.44 ± 0.20	0.344

T_{max} and C_{max} were determined from individual real values. Each value represents the mean ± SD

can see the rapid-release thin-film system overlap the aqueous drug suspension nearly identically. We can see that the dexamethasone can be applied in two different dosage forms (suspension and thin film) and achieve the same desired burst release kinetics (Fig. 3.23).

The use of rapid-release thin-film (Table 3.5) drug dosage forms to achieve high levels of release within a narrow target dosage window in a short period of time highlights the tunability of thin-film systems to mucosal uptake. In Sect. 3.1, we recall that a key limiting factor to drug uptake in the mouth was the improved drug diffusion through mucosal tissue by adjusting the characteristics of the interface between tissue and film. The desired interface was one that exhibited properties consistent with the **Wentzel model**, where the entirety of the film and tissue surfaces was wetted by water. This allows for maximum surface area present for drug

diffusion. The drug is in its most effective state when its particle size is reduced. We recall from earlier in Chap. 3 that this reduction allows for improved diffusion through the pores of the wetted tissue surface. We can see in the rapid-release films that the dexamethasone is effectively stabilized by polymer surfactants, polysorbate, which allows for the stabilization of smaller drug particle sizes in solution. This system successfully allowed for drug delivery based on the criteria discussed in Sect. 3.1. Next, we will discuss a more complex thin-film system based on a less robust physiological regime.

3.3.1.2 Transdermal Drug Delivery Films

In Sects. 3.1.1 and 3.1.2, the focus of thin-film composition was based on surface erosion or bulk erosion systems that act either by a reduction or retaining of film volume. Another form of bulk erosion release was discussed briefly in Chap. 2, referred to as swellable materials. These swellable materials, known as hydrogels, provide another method for drug delivery from a controlled-release system that is hydration-dependent. Hydrogels are discussed in more detail in Chap. 6. The basic behavior of a hydrogel is the uniform volume expansion of the polymer gel lattice in response to both hydrogen bonding to water and solvation of hydrophilic groups. The gel retains its shape and avoids full solvation due to a crosslinked component. The crosslinked component can be formed through covalent, electrostatic, Van der Waals, or hydrophobic interactions. It is an important distinction that in noncovalent crosslinked hydrogel systems, water acts as a plasticizer, effectively reducing the cohesive forces between polymer chains in the gel. At some critical dilution point, the energetic cost to retain the physical integrity of the hydrogel by means of noncovalent crosslinking will exceed the solvation energy, resulting in a solvated or dispersed system. This is an important point for thin-film fabrication, where an awareness is required to fabricate at crosslink concentrations above this dilution limit.

The investigation of biocompatible hydrogel crosslinking agents has allowed for the discovery of a number of robust hydrogel systems in terms of biodegradation, swelling, pharmacokinetics, stability, and controlled release. A unique system developed by Abbasi et al. [62] demonstrates the effective use of a gelatin-based crosslinking agent known as *genipin* for thin-film drug dosage forms. Genipin is a natural crosslinking agent for gelatin, proteins, collagen, and chitosan, with a low acute toxicity (LD_{50}). The film fabrication methods can vary for hydrogel-based thin-film materials due to the swelling and plasticization implications and film integrity concerns. This typically leads to a number of *lab-specific* fabrication methods found in the art. The genipin crosslinked gelatin system described in this example was fabricated using a *dip centrifugation* method. The hydrogel films contrast the typical films that we have discussed so far in this chapter, which consist of a drug, water-soluble polymer, plasticizer, and filler. The hydrogel systems appear at first glance to be composed of only drug and water-soluble polymer. Upon a closer review, the same elements are present in the hydrogel system. The water-soluble

polymer in this case is the pre-crosslinked gelatin. The plasticizer is water. The filler is the crosslinked gelatin and the genipin crosslinker (Table 3.6).

A common method for the assessment of adequate release characteristics in thin-film drug dosage forms is by comparative modeling. Using Fick's second law (3.14), one can model the expected and ideal release behavior of a drug from a surface. This model assumes uniform swelling in the axial direction:

$$\frac{\delta C_i}{\delta t} = \frac{\delta}{\delta z}\left(D_i \frac{\delta C_i}{\delta t} \right), \tag{3.14}$$

where C_i is the concentration of water in the system, t is time, z is the matrix thickness in one dimension, and D_i is the diffusion coefficient.

For hydrogel systems, the diffusion of drug molecules from the thin-film matrix is dependent on the rate of swelling of the gel structure. The more predictive the swelling behavior, the more robust the method and system for drug delivery applications. The present genipin–gelatin system shows an acceptable agreement between experimental and modeled swelling behavior (Fig. 3.24).

The pharmacokinetic behavior with respect to diffusion should be highly predictable. Deviations from ideal pharmacokinetic behavior, however, would manifest as a poor agreement between experimental swelling or release of drug and modeled behavior. Those deviations are suggestive of impedance present in the hydrogel matrix, which pushes the system to a pharmacokinetic response that is more difficult to predict.

In the case of drug release, we can see a similar agreement that was evident in the matrix swelling behavior, where there is clear agreement between experimental and modeled release kinetics (Fig. 3.25).

The genipin–gelatin system allows for facile fabrication of a thin film with efficient predictive capability in terms of swellability and drug release. Controlled interfacial drug release at a tissue–film interface is only part of the challenge of effectively delivering drugs transdermally. In Sect. 3.1, we discussed the importance of changing the *molecular weight* and *size* of the drug particle and increasing skin *porosity* as strategies to enhance skin permeability of drug dosage forms in transdermal systems. A common approach to decrease drug particle size is the introduction of vesicle or micellar systems. Vesicles and micelles are comprised of surfactant monolayers or bilayers, which act to stabilize a fixed volume containing a drug as the cargo. We discuss the design and application of vesicles and micelles as part of our discussion of *self-emulsifying drug delivery systems* in Chap. 4. One advantage of vesicles and micelles that applies to our current thin-film approach is the ability to stabilize drug particles of reduced size. We recall from Sect. 3.1 that the reduction in particle size allows for an increased probability of transdermal diffusion through the small pore sizes of the epidermis.

The fundamental vesicle system developed by *Verma et al.* [63] provides a clear example of the advantage of particle size reduction on transdermal drug uptake. The vesicle system being described is known as a liposome, which translates to a lipid vesicle. The lipid or surfactant system of interest was a mixture of stearic and

Table 3.6 Thin-film components for the delivery of DBSP as a transdermal drug delivery system

Component	Function in film	Function in drug delivery	Examples
Drug	Colloid or pigment particle that can increase porosity and decrease elasticity of the film	• Market drug	• DBSP
Water-soluble polymer	Promote easier processability and functions as a malleable matrix	• Remain inert within the circulation lifetime	• Pre-crosslinked gelatin
Plasticizer	Improve flexibility and reduce T_g of polymer	• Improves polymer flexibility	• Water
Filler	Matrix material	• Improves drug release and dispersion • Tailors the diffusion of drug	• Crosslinked gelatin • Genipin

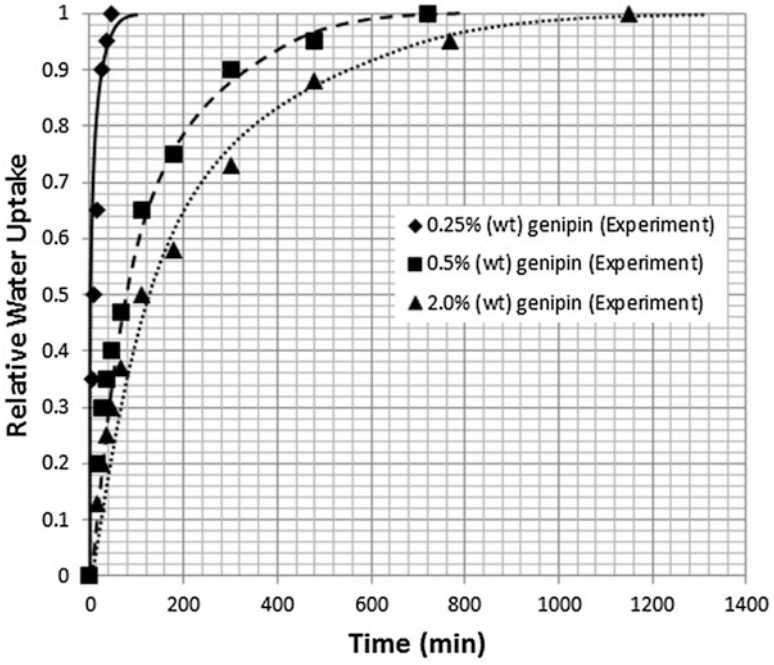

Fig. 3.24 Relative swelling behavior of genipin systems relative to modeled examples [*solid line* 0.25 % (wt) genipin from modeling; *dash-dotted line* 0.5 % (wt) genipin from modeling; *dotted line* 2.0 % (wt) genipin from modeling] (Adapted from Abbasi, A., Eslamian, M., Heyd, D. & Rousseau, D., *Pharmaceutical Development and Technology*, *13*(6), 549–557, 2008) [62]

palmitic acid that was encapsulated with a fluorescent drug marker DiI (1,1-dioctadecyl-3,3,3,3-tertramethylindocarbo-cyanine perchlorate). The liposome system was applied to the skin surface, and the fluorescence was measured as a function of skin depth (Fig. 3.26).

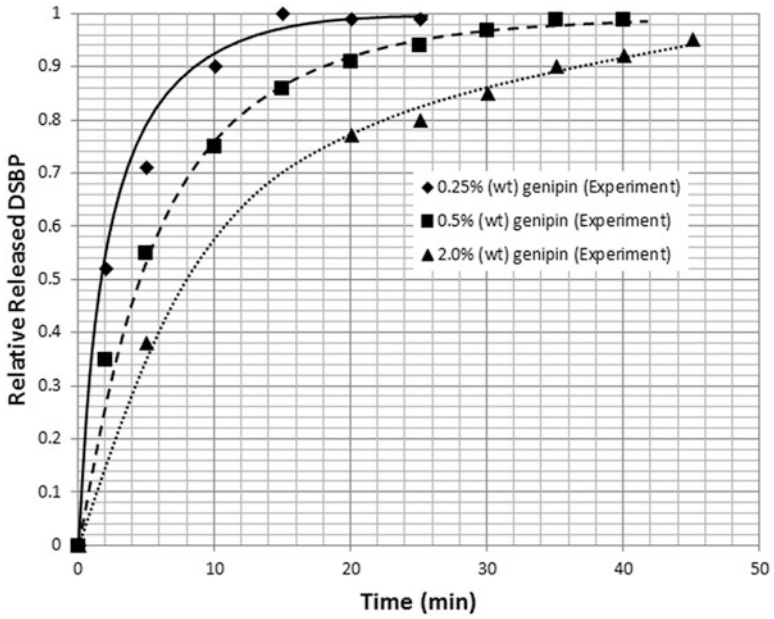

Fig. 3.25 Relative release behavior of genipin systems relative to modeled examples [*solid line* 0.25 % (wt) genipin from modeling; *dash-dotted line* 0.5 % (wt) genipin from modeling; *dotted line* 2.0 % (wt) genipin from modeling] (Adapted from Abbasi, A., Eslamian, M., Heyd, D. & Rousseau, D., *Pharmaceutical Development and Technology*, *13*(6), 549–557, 2008) [62]

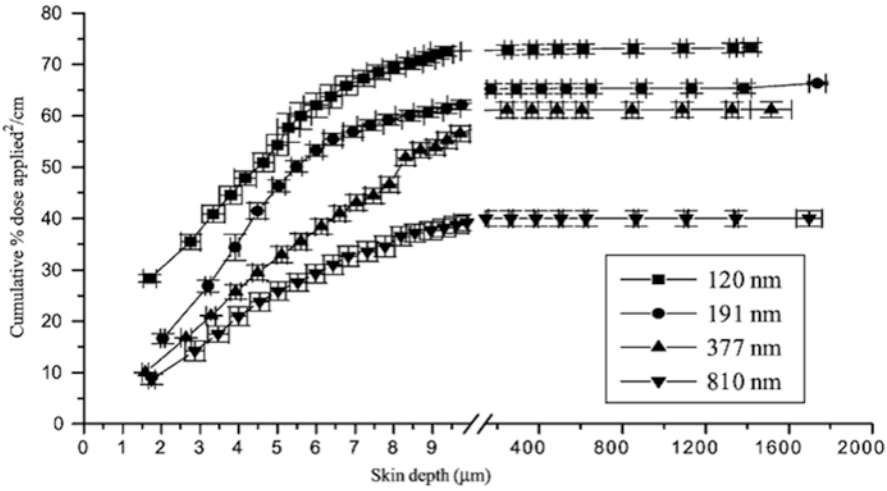

Fig. 3.26 Depth profile of CF liposomes across the human abdominal skin after 14 h of nonocclusive application (expressed as percent dose applied ± SE) $n = 3$ [63]

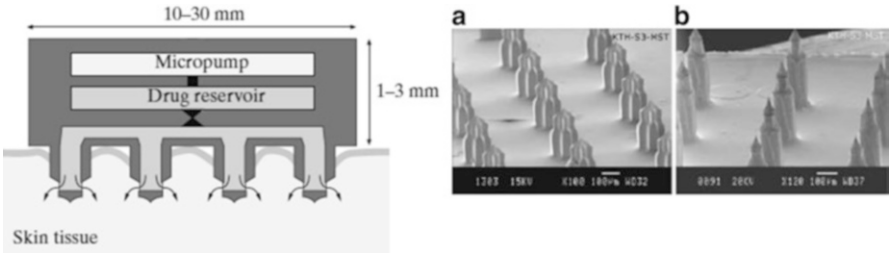

Fig. 3.27 Conceptual drawing of a microneedle-based drug delivery system. Gold membrane sealed side-open hollow microneedles. (*a*) 310-**μ**m-long cross-shaped microneedles; (*b*) 400-**μ**m-long circular-shaped microneedles [64]

We can clearly see that the reduction of particle size, from 810 to 120 nm, corresponds to an appreciable increase in uptake, twofold, of the DiI fluorescent marker. The initial slope is consistent with the filter analogy discussed in Sect. 3.1, where the pore size and tortuosity of the skin contribute to a low level of diffusion. The characteristics of skin uptake demonstrated with these results further indicate *zero-order* adsorption as the pharmacokinetic mechanism as the particle size increases. If we recall, *zero-order* kinetics offers less of an impedance to drug uptake the larger the ratio of pore size to particle size. It is when the particle size is at or above that of the pore size that Fickian diffusion becomes the dominant mechanism. If the pore size remains unchanged, the reduction in particle size translates to a shift in the diffusion mechanism from *zero order* to *Fickian*.

What if the transdermal pore size is altered as well?

There are a number of strategies that we discuss throughout this text for the alteration of epidermal pore size. They can be focused on ultrasound, electric current, physical separation, or chemical inflammation. Roxhed et al. [64] focus on the use of microneedles (Fig. 3.27) as a means of physically introducing temporary pores within the stratum corneum of the epidermal layer. The film in this case is actually an SiO_2 chip with channels etched using lithographic techniques (i.e., reactive-ion etching).

The outer surface of the needle is coated with a membrane film of gold, to allow for effective removal and biocompatibility. The microneedles can be induced to deliver drug by three mechanisms: *burst pressure, electrochemical*, and *insertion force*. It is clear that the introduction of any of these three mechanisms corresponds to the removal or rupture of the gold film on the tip surface. The gold film itself also appears to be a sufficient barrier to controlled drug release in the sealed versus the unsealed state (Fig. 3.28).

The most common trend that we have seen thus far in the art is that the goal of the thin film is a system for managing the tissue–drug interface. The critical properties of film behavior for this approach are to allow for an amenable interfacial surface with predictable release profiles of different molecular species, such as drugs and *penetration enhancers* (Chap. 4). We have seen that some strategies, such as

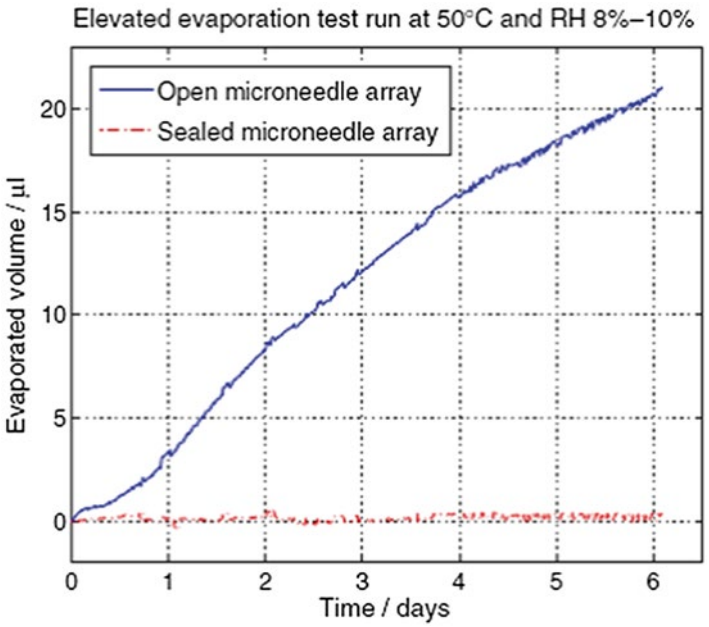

Fig. 3.28 Conceptual drawing of a microneedle-based drug delivery system [64]

microneedles, can be adopted to circumvent the pore size restriction of the stratum corneum by physically applied stress. In Chap. 4, we will discuss the second half of the delivery dilemma for transdermal therapy, where we will identify strategies to directly adjust the drug size and alter the tissue pore structure through chemically based approaches.

3.3.1.3 Ocular Drug Delivery Films

The discussion in Sect. 3.1 was focused on the use of *molecular weight, size,* and *radius of gyration* as a means of enhancing drug uptake within the corneal region of the eye. For ocular systems, as was true for transdermal systems, the thin film also functions to manage the interfacial interactions between tissue and drug, effectively shielding the interaction from external contaminants. This shielding is no more important than in ocular environments, where infections can lead to anything from fatigue to blindness. For this reason, drug-eluting thin-film materials have gained significant attention as a facile means to deliver drugs at the corneal surface. To this extent, Ciolino et al. [65] have designed a representative drug-eluting stent composed of poly(lactic-co-glycolic acid) (PLGA) coated with poly(hydroxyethyl methacrylate) (PHEMA) cured by ultraviolet light to use for a contact lens (Fig. 3.29).

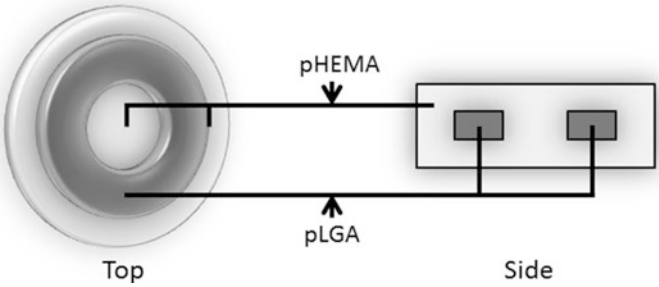

Fig. 3.29 Schematic of a prototype contact lens made of pHEMA hydrogel coating a PLGA film (in this case with ciproflaxin) with a 5-mm clear optical aperture (Adapted from Ciolino, J. B., Hoare, T. R., Iwata, N. G., et al., *Investigative Ophthalmology & Visual Science*, *50*(7), 3346–3352, 2009) [65]

Table 3.7 Thin-film components for the delivery of ciproflaxin as an ocular drug delivery system

Component	Function in film	Function in drug delivery	Examples
Drug	Colloid or pigment particle that can increase porosity and decrease elasticity of the film	• Marker or drug	• Ciproflaxin • Fluorescein
Water-soluble polymer	Promote easier processability and functions as a malleable matrix	• Remain inert within the circulation lifetime	• PHEMA
Plasticizer	Improve flexibility and reduce T_g of polymer	• Improves polymer flexibility	• Water
Filler	Matrix material	• Improves drug release and dispersion by degradation	• PLGA

The lens was loaded with fluorescein as a marker or ciproflaxin as the drug molecule for controlled-release studies. If we refer back to our account of film components, we can see that this model system follows our previous ones for oral and transdermal thin-film systems in terms of drug, water-soluble polymer, plasticizer, and filler. It is worth noting that as we have seen systems move from more traditional bulk or surface-release thin films to more soluble thin films, the complexity of these four components has decreased significantly. This can be partially attributed to the dual role of the matrix and the use of water as the plasticizing agent. The predominant message is that complex thin-film systems are not always necessary. Look to the physiological system and function to dictate the composition of your thin-film system (Table 3.7).

If we look at changes to the PHEMA and PLGA base components, we can see that there is a marked difference in pharmacokinetic response based on the combination of each component. The PLGA alone appears to show the typical Fickian release profile, while the application of a coating of PHEMA to PLGA indicates a trend

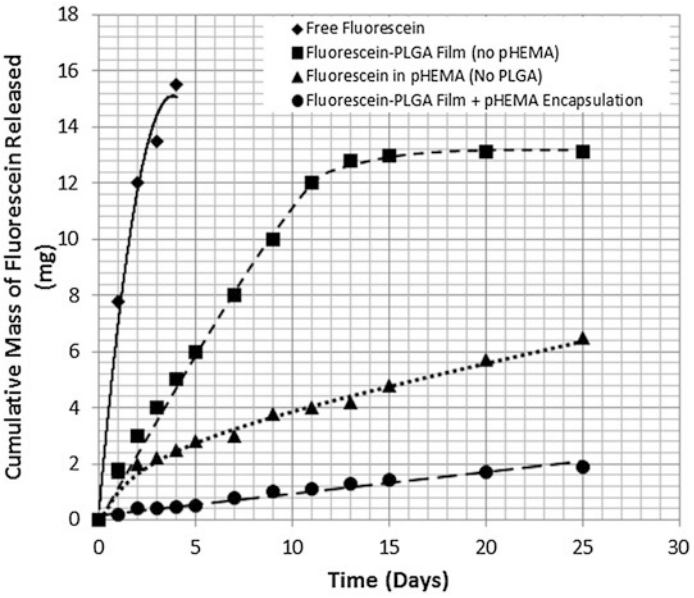

Fig. 3.30 Cumulative release (28 days) from free fluorescein powder, fluorescein-PLGA films, fluorescein coated with pHEMA and fluorescein-PLGA films coated with pHEMA. Data are the mean ± SD (Adapted from Ciolino, J. B., Hoare, T. R., Iwata, N. G., et al., *Investigative Ophthalmology & Visual Science*, *50*(7), 3346–3352, 2009) [65]

toward more zero-order release behavior. This is likely due to the increased water adsorption on the surface of the thin film in the presence of PHEMA, which changes the diffusion of water within the system due to swelling behavior. A base PLGA system is also more susceptible to both degradation and plasticization by the water molecules, which contributes to thin-film breakdown and drug release (Fig. 3.30).

While the combination of components shows significant effects on the pharmacokinetics, the characteristics of the polymer also become a factor as well. The PLGA matrix material releases based on hydrolytic degradation of the base polymer. We can see that an increase in molecular weight contributes to a slower degradation profile, which translates to a slower zero-order release profile (Fig. 3.31).

The drug-eluting contact lens model system demonstrates a thin film with a controlled tissue–drug interface composed of tunable components for a desired pharmacokinetic response. We recall that the strategy of alteration of the pore structure of the membrane in transdermal drug delivery is not acceptable in delicate systems such as the eye. In Sect. 3.1, we discussed the advantages of size, molecular weight, and radius of gyration as a means of altering diffusion through the constrained porosity of the corneal membranes. In Chaps. 4 and 7, we will discuss the design of multicomponent devices to enhance delivery response and efficiency.

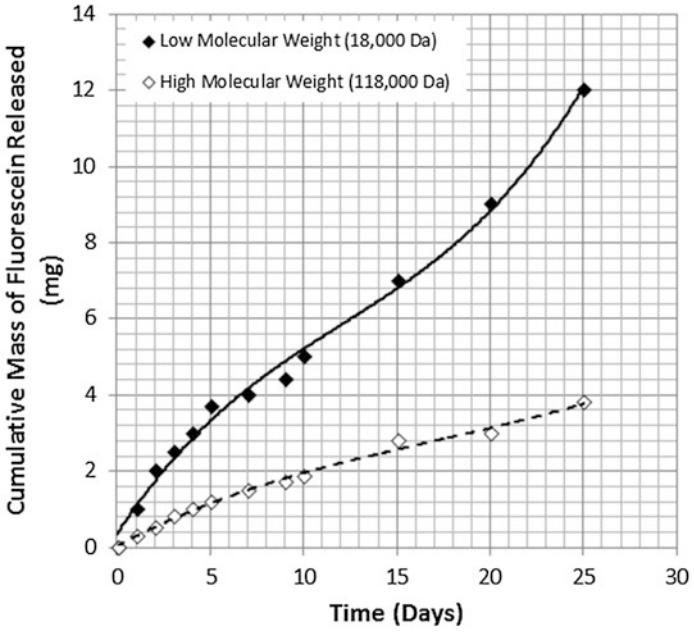

Fig. 3.31 Cumulative release of fluorescein from low- (18-kDa) and high- (118-kDa) molecular-mass PLGA films coated with pHEMA. Data are the mean ± SD (Adapted from Ciolino, J. B., Hoare, T. R., Iwata, N. G., et al., *Investigative Ophthalmology & Visual Science*, *50*(7), 3346–3352, 2009) [65]

3.3.2 Summary

The recent attention to thin-film systems for drug delivery indicates a shift in focus toward medications with a higher relative ease of application. In Sect. 3.1, we outlined three models of the *mouth*, the *skin*, and the *eye*. The focus on these models was to highlight the underlying physical characteristics of the tissue–media interfaces, where properties such as *diffusion*, *tortuosity*, and *porosity* draw effective comparisons with the engineering principles of modern filter technology. In Sect. 3.2, we began our discussion surrounding film components and growth modes in order to design a material with the desired drug release kinetics and tissue interaction. We then moved to film fabrication techniques to highlight advantages and functional limitations of the thin-film approach. We pinpointed our focus in Sect. 3.3 to current examples from the oral (i.e., rapid-release film), transdermal (i.e., microneedle patches), and ocular (i.e., hydrogel drug release contact lens) systems in early stages of clinical development. The further extension of the thin-film delivery mode allows for both a broader application of current drug therapies and the ability to control treatment to patients whose physiological modes are more difficult to access (Table 3.8).

Table 3.8 Common scientific disciplines tied to critical fundamentals in thin-film drug delivery systems

Fundamental	Disciplines
Porosity and tortuosity (i.e., membrane design)	• Chemistry • Materials engineering • Chemical engineering
Adhesion	• Biochemistry • Protein chemistry • Materials engineering • Chemistry
Film fabrication	• Chemistry • Materials engineering
Diffusion	• Chemistry • Chemical engineering • Materials engineering • Physics
Tensile mechanics and elasticity	• Polymer rheology • Polymer physics • Materials engineering
Pharmacokinetics	• Medicine • Pharmaceutical chemistry • Biology
Polymer composition	• Chemistry • Materials engineering
Colloidal stability	• Chemistry • Physics • Material engineering • Chemical engineering

3.4 Clinical Applications

3.4.1 Thin Films for Drug-Eluting Stents

This chapter discusses the design of thin films for drug delivery. Such films can be particularly useful for coating implantable devices, to create drug–device combinations. In this clinical applications section, we focus on applications of thin films in drug-eluting stents for coronary artery disease. A typical drug-eluting stent consists of a metallic mesh coated with a polymeric, drug-loaded thin film; the drug is embedded within the thin film and is released for a prolonged time at the implantation site in the coronary artery.

Coronary artery disease, also known as ischemic heart disease, is the leading killer of men and women worldwide. The condition represents the culmination of cholesterol accumulation, cellular capture, vascular injury, and inflammatory activation. A minimally invasive device for opening blocked coronary arteries, known as the

coronary stent, has been developed to avoid many of the complications of open bypass surgery. During a stenting procedure, the stent is mounted on a balloon catheter, which is inserted through the femoral (leg) artery. The stent balloon system is then guided from the femoral artery to the affected coronary artery, using X-ray/fluoroscopy for visualization. Once the device is properly located at the narrowed lesion in the coronary artery, the balloon and stent are expanded, compressing the atherosclerotic plaque and opening up the arterial lumen. The balloon is withdrawn, and the expanded stent is permanently set in place. The stent becomes embedded into the vessel wall, as vascular endothelial cells populate the stent surface in a process known as endothelialization. The stent subsequently maintains the blood vessel in an enlarged state and prevents the vessel from recoiling. Stenting essentially allows a patient with coronary artery lesions to undergo surgery via a small puncture in the leg, rather than a large open surgical wound on the chest. The widespread adoption of coronary stents has enabled shorter hospital stays, faster recovery times, and lower hospitalization costs.

Drug-eluting stents are devices that combine the mechanical properties of coronary stents with the functional properties of biomolecules such as pharmaceuticals, cytokines, and antibodies. The main motivation for bioactive stent development is to reduce complications associated with stent implantation. Bare metallic stents, while permitting targeted treatment for occluded coronary arteries, are associated with high rates of restenosis (i.e., re-narrowing of the coronary artery). Though the design of bare metallic stents has been continually upgraded, as many as 25 % of patients treated with bare-metal stents experience restenosis [66]. Restenosis is caused in part by the expanding balloon and stent, which leads to vascular wall injury and cellular overproliferation. More complex arterial lesions, such as long lesions, smaller-diameter lesions, vascular bifurcations, and ostial locations, are more prone to restenosis [67]; the complication may occur in 30–60 % of patients with complex lesions [68]. Restenosis has proven to be intractable to the systemic administration of drugs. The rationale for incorporating biological agents into stents is to optimize the tissue response to stent implantation, prevent restenosis, and thereby improve patient outcomes.

An ideal drug-eluting stent must fulfill both mechanical and biological specifications, and thin films enable stents to function in this desired capacity. First, the stent must have the ability to be crimped onto an angioplasty balloon catheter with a resulting diameter of approximately 1 mm; this is an absolute requirement for stent introduction into the body [69]. The stent must be flexible enough to deform, so that the stent on the balloon catheter can be inserted through the femoral artery and guided to the site of the coronary artery lesion. Once the balloon reaches the desired site, the stent must be deployed and retain its nominal diameter, typically between 2–4 mm. A stent must have enough radial strength to resist arterial spasm and maintain the artery in an open state; however, the strength must be finely tuned since exaggerated radial resistance will hinder the natural elasticity of the artery. In addition, an exceedingly rigid stent will encumber the deliverability of the device, since access to the artery usually goes through a tortuous vascular bed. In terms of biological properties, the bioactive stent must be compatible with the blood and its various constituents, as well as with the endothelium and other arterial wall cells.

Table 3.9 Comparison of drug-eluting stent structures and compositions

	Cypher® (μm)	Taxus® express (μm)	Xience™ V (μm)	Endeavor® (μm)
Stent thickness	140	132	81	91
Polymer thickness	14	16	7	6
Stent material	Stainless steel	Stainless steel	Cobalt-chromium	Cobalt-chromium
Chemical nature of polymer	PEVA and PEMA	Hydrocarbon-based elastormer	Biocompatible fluoropolymer	Hydrophilic phosphoryl-choline
Bioactive drug	Sirolimus	Paclitaxel	Everolimus	Zotarolimus

Fig. 3.32 The Cypher® drug-eluting stent (Food and Drug Administration)

The surface properties are critical, since the initial compatibility with the blood elements will depend entirely on the stent surface properties. The surface must also encourage rapid embedding in the endothelial lining of the artery, to avoid possible thrombosis due to prolonged blood contact. If the bioactive stent releases a therapeutic agent, it must deliver the agent in a consistent and predictable manner to avoid overdose. Both the mechanical and biological components of the bioactive stent must withstand sterilization conditions.

Drug-eluting stents are bioactive stents that release small-molecule therapeutics directly into the vessel lumen to forestall restenosis. A drug-eluting stent is created by coating a metallic stent with a drug-loaded polymer. The stent wires, or struts, are configured in a specific geometry to optimize local delivery of pharmacologic agents; strut configurations include the "slotted tube," which produces diamond-shaped cells upon expansion, or the corrugated tubular-like rings with bridging links. Once implanted, the stent releases a therapeutic amount of the drug over a short period of time (usually a few weeks). As discussed above, atherosclerotic plaque results from both lipid deposition and smooth muscle cell proliferation. Therefore, the pharmaceuticals utilized most commonly in drug-eluting stents are antiproliferative agents. Table 3.9 compares the materials of construction, technical specifications, and therapeutic agents for four leading drug-eluting stents. Such stents have been realized through advances in drug delivery, cell biology, and polymer science.

The first generation of drug-eluting stents includes sirolimus-eluting stents and paclitaxel-eluting stents. The Cypher® sirolimus-eluting stent (Johnson & Johnson/Cordis, Miami Lakes, Florida, USA) was the first drug-eluting stent to be made commercially available in 2003. This stent has been the most widely used drug-eluting stent in the world and is considered to be the standard of comparison for all drug-eluting stents [70] (Fig. 3.32). The Cypher® stent utilizes a stainless steel platform, coated with poly(ethylene co-vinyl acetate) and poly(*n*-butyl methacrylate).

The polymer releases sirolimus, an antiproliferative drug that inhibits the G1 phase of the cell cycle and halts cell replication. Most of the drug is delivered in approximately three weeks postimplantation of the stent [71]. Sirolimus-eluting stents have achieved yearly restenosis rates as low as 6.8–7.9 % [72]. The Cypher® stent is also associated with a significant reduction in both mortality and repeat revascularization procedures, compared to bare-metal stents [73].

The Taxus® paclitaxel-eluting stent (Boston Scientific, Natick, Massachusetts, USA) was also introduced commercially in 2003. As of 2009, nearly five million Taxus® drug-eluting stents had been implanted in patients worldwide [70]. This stent is made with a stainless steel platform, coated with the hydrocarbon-based elastomer poly(styrene-b-isobutylene-b-styrene). Embedded within the elastomer is the drug paclitaxel, an antiproliferative agent that stabilizes microtubules and blocks intracellular signaling, inhibiting smooth muscle cell migration and growth [74]. The elastomer-paclitaxel system is advantageous in that it is a diffusion-based controlled-release matrix, facilitating s slow and very specific delivery of the drug [71]. Paclitaxel-eluting stents exhibit restenosis rates of 10 % [70].

The second generation of drug-eluting stents includes everolimus-eluting stents and zotarolimus-eluting stents. This generation of devices incorporates flexible stent designs, more biocompatible polymers, and potent therapeutics; such biomaterials are now emerging in clinical use. The Xience™ V everolimus-eluting stent (Abbott Vascular, Markham, Ontario, Canada) employs a cobalt-chromium alloy within the stent. The alloy is stronger than stainless steel, allowing for very thin struts. The open cells and nonlinear structure make the Xience™ stent more flexible than previous stents. The stent is assembled onto a semicompliant balloon with short tapers that are designed to minimize vascular injury outside the stent area [70]. The polymer coating is a nonadhesive, durable, and biocompatible fluoropolymer composed of an outer layer of poly(*n*-butyl-methacrylate) and an inner layer of poly(vinylidene fluoride co-hexa-flu-oropropylene). The inner layer is a drug reservoir and contains everolimus, an antiproliferative agent that inhibits the G1 phase of the cell cycle; everolimus is distinguished from previous agents by its high potency and high lipophilicity. The Xience™ system releases approximately 80 % of the drug by the first month, and nearly all of it by 4 months postimplantation. The Endeavor® zotarolimus-eluting stent (Medtronic CardioVascular, Minneapolis, Minnesota, USA) uses a cobalt–chromium alloy stent coated with a phosphorylcholine-based polymer. The hydrophilic *polymer* is intended to be more biocompatible as phosphorylcholine is a naturally occurring phospholipid, and it delivers the drug zotarolimus, an analog of sirolimus. The release kinetics of zotarolimus enables nearly complete drug delivery within the first month after stent placement.

In general, drug-eluting stents have demonstrated an advantage over bare-metal stents with regard to restenosis rates; drug-releasing stents allow the coronary arteries to remain patent longer and reduce the necessity for repeat interventions. Drug-eluting bioactive stents are now estimated to reach 75 % of all stent procedures [70]; currently available coronary stents permit the treatment of complex cases with a wide safety margin and a high likelihood of optimal acute results. Drug-eluting stents improve the cost-effectiveness of treatment for coronary artery disease, given

the significantly fewer repeat revascularizations during the first year. These devices provide the means for a predictable interventional procedure, a function of both the mechanical properties of drug-eluting stents and their delivery systems [75], and this has been made possible by thin films.

3.5 Problems

3.1 A dermatologist would like to determine if a specific fentanyl skin patch would be a candidate treatment for her patient. The use of fentanyl drugs requires an effective transdermal penetration of 30 ml of drug to reach the subepidermal layers within 20 min of the application time. From your knowledge of skin physiology and drug delivery, answer the subsequent questions.

(i) What is the pressure difference generated by the skin layers by the topical application of fentanyl?
(ii) What would you expect the effective back pressure to be for the effective delivery of fentanyl that is complexed to a polymer in the form of a prodrug with a $\langle S^2 \rangle^{1/2}$ of 5 nm, assuming no biological events have occurred (i.e., facilitated translocation)?
(iii) Does the answer for (ii) seem possible? Why? What could be changed in order to allow for more effective transdermal fentanyl delivery?

3.2 An ophthalmology research assistant is trying to determine if a particular ocular drug will reach the endothelium of the eye as its target. He has estimates regarding the thickness and pore structure of several layers of ocular tissue and knows that the drug is capable of diffusing through the gap junctions within the epithelial layer. From your knowledge of the physiology of the eye and drug delivery, answer the following questions.

(i) What is the tortuosity of each tissue layer of the eye?
(ii) Which tissue layer of the eye would have the highest diffusion of drug?
(iii) Would this drug be capable of being effectively delivered to its target tissue? Why?
(iv) How would tortuosity change with decreasing particle size? Why?

Ocular tissue layer	N	L (μm)	S_i (μm)	L_i (μm)
Epithelium	7	10	35	500
Bowman's layer	1	7	1	12
Stroma	10	500	250	500
Descemet's membrane	1	5	1	10
Endothelium	2	2	10	80

3.3 A physician wishes to treat a metastasized tumor growth in a patient's hip bone and is exploring therapeutic options. She has narrowed her search to these choices: controlled-release embolic microspheres and transdermal multilayered films. From your knowledge of controlled-release materials for drug delivery, answer the subsequent questions.

(i) Which system would require a zero-order pharmacokinetic response to be effective? Why?
(ii) What is the rate-limiting step in terms of the diffusion of the drug molecule in each system?
(iii) What is the main barrier that needs to be overcome before using each system for the effective delivery of drugs?

3.4 A graduate student in biomedical engineering decides to explore the use of penetration enhancers in order to more effectively deliver a drug sublingually. The researcher decides to monitor the potential activity of the delivery mode using the contact angle and estimating the surface wetting of the drug solution on a membrane of sublingual tissue. From the data collected and your knowledge of oral drug delivery, answer the following questions.

(i) What model does the droplet appear to follow at the zero point of the experiment? Why?
(ii) What happens to the surface of the sublingual tissue throughout the course of the 20-min experiment?
(iii) Based on your answers to (i) and (ii), would you expect the sublingual surface to be more or less susceptible to the delivery of the drug at the zero point than after 20 min? Why?

Time (min)	θ * (°)	r_f	r	f
0	85	0.1	0.5	0.20
1	85	0.2	0.5	0.30
2	85	0.3	0.5	0.50
5	85	0.5	0.5	0.95
10	85	0.5	0.5	0.98
20	85	0.5	0.5	1.00

3.5 A cardiologist decides to use a new sirolimus-eluting coronary stent on the market for a patient that is similar to Cypher®, is composed of poly(ethylene-co-vinyl acetate), and substitutes poly(styrene-co-maleic anhydride) ($T_g = 110$ °C) in place of poly(*n*-butyl methacrylate) ($T_g = 15$ °C). From your knowledge of materials science and drug delivery, answer the following questions.

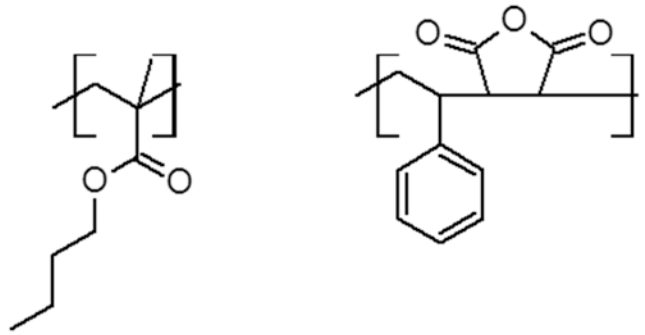

poly(n-butyl methacrylate) poly(styrene-co-maleic anhydride)

(i) Would you expect the substituted polymer to be more elastic or more brittle than the Cypher® drug-eluting stent? Why?
(ii) How would the drug release kinetics change with the substituted polymer? Why?
(iii) Can you think of one advantage to using the substituted polymer for the application of coronary stents?

References

1. (a) Wesselingh, J. A. (1993). Controlling diffusion. *Journal of Controlled Release, 24*(1), 47–60. (b) Lee, P. I. (1986). Initial concentration distribution as a mechanism for regulating drug release from diffusion controlled and surface erosion controlled matrix systems. *Journal of Controlled Release, 4*(1), 1–7.
2. Kerr, D. J. (1987). Microparticulate drug delivery systems as an adjunct to cancer treatment. *Cancer Drug Delivery, 4*(1), 55–61.
3. Stegemann, S., & Bornem, C. (2002). *Hard gelatin capsules today—And tomorrow* (pp. 2–24). Capsugel Library.
4. (a) Abrams, J. (1983). New nitrate delivery systems: Buccal nitroglycerin. *American Heart Journal, 105*(5), 848–854. (b) Sudhakar, Y., Kuotsu, K., & Bandyopadhyay, A. K. (2006). Buccal bioadhesive drug delivery—A promising option for orally less efficient drugs. *Journal of Controlled Release, 114*(1), 15–40.
5. Blumenthal, H. P., Fung, H. L., McNiff, E. F., & Yap, S. K. (1977). Plasma nitroglycerin levels after sublingual, oral and topical administration. *British Journal of Clinical Pharmacology, 4*(2), 241–242.
6. (a) Down, G. R. B. (1991). The etiology of pinhole and bubble defects in enteric and controlled-release film coatings. *Drug Development and Industrial Pharmacy, 17*(2), 309–315. (b) Wilding, I. R., Davis, S. S., Pozzi, F., Furlani, P., & Gazzaniga, A. (1994). Enteric coated timed release systems for colonic targeting. *International Journal of Pharmaceutics, 111*(1), 99–102.
7. Cohen, G. M., Bakke, O. M., & Davies, D. S. (1974). "First-pass" metabolism of paracetamol in rat liver. *The Journal of Pharmacy and Pharmacology, 26*(5), 348–351.
8. Seager, H. (1998). Drug-delivery products and the Zydis fast-dissolving dosage form. *The Journal of Pharmacy and Pharmacology, 50*(4), 375–382.

9. Gorsline, J., Okerholm, R. A., Rolf, C. N., Moos, C. D., & Hwang, S. S. (1992). Comparison of plasma nicotine concentrations after application of nicoderm (nicotine transdermal system) to different skin sites. *Journal of Clinical Pharmacology, 32*(6), 576–581.
10. Pham, C. L., Wood, A. J., Lambert, M. B., & Carpenter, W. (2005). Palatal erythema in patients using Listerine Cool Mint PocketPaks Oral Care Strips: Case reports. *Journal of Dentistry for Children (Chicago, Ill.), 72*(2), 52–55.
11. Oral Drug Delivery Market Report. Retrieved from http://www.contractpharma.com/issues/2012-06/view_features/oral-drug-delivery-market-report/
12. Evans, P. M., Lynch, G. L., & Labelle, P. (2012). Effects of oral administration of diphenhydramine on pupil diameter, intraocular pressure, tear production, tear film quality, conjunctival goblet cell density, and corneal sensitivity of clinically normal adult dogs. *American Journal of Veterinary Research, 73*(12), 1983–1986.
13. Sica, D. A., & Grubbs, R. (2005). Transdermal clonidine: Therapeutic considerations. *Journal of Clinical Hypertension (Greenwich, Conn.), 7*(9), 558–562.
14. (a) Kumar, S., Gupta, S. K., & Sharma, P. K. (2012). A review on recent trends in oral drug delivery-fast dissolving formulation technology. *Advances in Biological Research, 6*(1), 6–13. (b) Hanumanaik, M., Patil, U., Kumar, G., Patel, S. K., Singh, I., & Jadatkar, K. (2012). Design, evaluation, and recent trends in transdermal drug system: A review. *International Journal of Pharmaceutical Sciences and Research, 3*(8), 2393–2406. (c) Mohan Gandhi, B., & Shankar, P. D. S. (2012). Current trends and challenges faced in ocular drug delivery systems. *International Journal of Research Pharmacy and Chemistry, 2*(3), 801–808.
15. Sankar, V., Hearnden, V., Hull, K., Juras, D. V., Greenberg, M. S., Kerr, A. R., et al. (2011). Local drug delivery for oral mucosal diseases: Challenges and opportunities. *Oral Diseases, 17*(Suppl 1), 73–84.
16. Jyoti, A., Gurpreet, S., Seema, S., & Rana, A. C. (2011). Fast dissolving films: A novel approach to oral drug delivery. *International Research Journal of Pharmacy, 2*(12), 69–74.
17. (a) Chen, L. L., Chetty, D. J., & Chien, Y. W. (1999). A mechanistic analysis to characterize oramucosal permeation properties. *International Journal of Pharmaceutics, 184*(1), 63–72. (b) Sohi, H., Ahuja, A., Ahmad, F. J., & Khar, R. K. (2010). Critical evaluation of permeation enhancers for oral mucosal drug delivery. *Drug Development and Industrial Pharmacy, 36*(3), 254–282.
18. Philibert, J. (2006). One and a half century of diffusion: Fick, Einstein, before and beyond. *Diffusion Fundamentals, 4*, 1–19.
19. Schultz, S. G. (2001). Epithelial water absorption: Osmosis or cotransport? *Proceedings of the National Academy of Sciences of the United States of America, 98*(7), 3628–3630.
20. Zimmermann, U., Haase, A., Langbein, D., & Meinzer, F. (1993). Mechanisms of long-distance water transport in plants: A re-examination of some paradigms in the light of new evidence. *Philosophical Transactions of the Royal Society, B: Biological Sciences, 341*(1295), 19–31.
21. Wilding, I. (2000). Site-specific drug delivery in the gastrointestinal tract. *Critical Reviews in Therapeutic Drug Carrier Systems, 17*(6), 557–620.
22. Wenzel, R. N. (1936). Resistance of solid surfaces to wetting by water. *Industrial & Engineering Chemistry, 28*(8), 988–994.
23. Marmur, A. (2003). Wetting on hydrophobic rough surfaces: To be heterogeneous or not to be? *Langmuir, 19*(20), 8343–8348.
24. Whyman, G., Bormashenko, E., & Stein, T. (2008). The rigorous derivation of Young, Cassie–Baxter and Wenzel equations and the analysis of the contact angle hysteresis phenomenon. *Chemical Physics Letters, 450*(4), 355–359.
25. Yohe, S. T., Colson, Y. L., & Grinstaff, M. W. (2012). Superhydrophobic materials for tunable drug release: Using displacement of air to control delivery rates. *Journal of the American Chemical Society, 134*(4), 2016–2019.
26. Senel, S., & Hincal, A. A. (2001). Drug permeation enhancement via buccal route: Possibilities and limitations. *Journal of Controlled Release: Official Journal of the Controlled Release Society, 72*(1–3), 133–144.

27. Kokate, A., Li, X., & Jasti, B. (2008). Effect of drug lipophilicity and ionization on permeability across the buccal mucosa: A technical note. *AAPS PharmSciTech, 9*(2), 501–504.
28. (a) Rathbone, M. J., & Tucker, I. G. (1993). Mechanisms, barriers and pathways of oral mucosal drug permeation. *Advanced Drug Delivery Reviews, 12*(1), 41–60. (b) Damgé, C., Reis, C. P., & Maincent, P. (2008). Nanoparticle strategies for the oral delivery of insulin. *Expert Opinion on Drug Delivery, 5*(1), 45–68.
29. (a) Proksch, E., Brandner, J. M., & Jensen, J.-M. (2008). The skin: An indispensable barrier. *Experimental Dermatology, 17*(12), 1063–1072. (b) Krawczyk, W. S. (1971). A pattern of epidermal cell migration during wound healing. *The Journal of Cell Biology, 49*(2), 247–263.
30. (a) Sharma, N., Agarwal, G., Rana, A. C., & Bhat, Z. A. L. I. (2011). A review: Transdermal drug delivery system: A tool for novel drug delivery system. *International Journal of Drug Development & Research, 3*(3), 70–84. Retrieved from http://www.ijddr.in. Covered in Official Product of Elsevier, The Netherlands © 2010. (b) Keleb, E., Sharma, R. K., Mosa, E. B., & Aljahwi, A. Z. (2010). Transdermal drug delivery system—Design and evaluation. *International Journal of Advances in Pharmaceutical Sciences, 1*(3), 201–211. doi:10.5138/171.
31. Goldstein, J. L., Anderson, R. G. W., & Brown, M. S. (1979). Coated pits, coated vesicles, and receptor-mediated endocytosis. *Nature, 279*(5715), 679–685.
32. Epstein, N. (1989). On tortuosity and the tortuosity factor in flow and diffusion through porous media. *Chemical Engineering Science, 44*(3), 777–779.
33. Gaudana, R., Ananthula, H. K., Parenky, A., & Mitra, A. K. (2010). Ocular drug delivery. *The AAPS Journal, 12*(3), 348–360.
34. (a) Lu, L., Reinach, P. S., & Kao, W. (2001). Corneal epithelial wound healing. *Experimental Biology and Medicine, 226*(7), 653–664. (b) Dohlman, C. H. (1971). The function of the corneal epithelium in health and disease. The Jonas S. Friedenwald Memorial Lecture. *Investigative Ophthalmology, 10*(6), 383–407.
35. Ferain, E., & Legras, R. (1997). Characterisation of nanoporous particle track etched membrane. *Nuclear Instruments and Methods in Physics Research Section B: Beam Interactions with Materials and Atoms, 131*(1), 97–102.
36. Atkins, P. W. (1997). *Physical chemistry*. New York: Macmillan Higher Education.
37. Flory, P. J. (1953). *Principles of polymer chemistry* (p. 672). Ithaca, NY: Cornell University.
38. Miller, C. C. (1924). The Stokes–Einstein law for diffusion in solution. *Proceedings of the Royal Society A: Mathematical, Physical and Engineering Sciences, 106*(740), 724–749.
39. Qiu, H., Lv, L., Pan, B., Zhang, Q., Zhang, W., & Zhang, Q. (2009). Critical review in adsorption kinetic models. *Journal of Zhejiang University SCIENCE A, 10*(5), 716–724.
40. Chifflet, S., & Hernández, J. A. (2012). The plasma membrane potential and the organization of the actin cytoskeleton of epithelial cells. *International Journal of Cell Biology, 2012*, 121424.
41. Yamamoto, K., Ladage, P. M., Ren, D. H., Li, L., Petroll, W. M., Jester, J. V., et al. (2002). Effect of eyelid closure and overnight contact lens wear on viability of surface epithelial cells in rabbit cornea. *Cornea, 21*(1), 85–90.
42. (a) Brøndsted, H., & Kopeček, J. (1991). Hydrogels for site-specific oral drug delivery: Synthesis and characterization. *Biomaterials, 12*(6), 584–592. (b) Koppel, D. E., Sheetz, M. P., & Schindler, M. (1981). Matrix control of protein diffusion in biological membranes. *Proceedings of the National Academy of Sciences of the United States of America, 78*(6), 3576–3580.
43. (a) Dillman, W. J., & Miller, I. F. (1973). On the adsorption of serum proteins on polymer membrane surfaces. *Journal of Colloid and Interface Science, 44*(2), 221–241. (b) Peck, K. D., Hsu, J., Li, S. K., Ghanem, A. H., & Higuchi, W. I. (1998). Flux enhancement effects of ionic surfactants upon passive and electroosmotic transdermal transport. *Journal of Pharmaceutical Sciences, 87*(9), 1161–1169. (c) Barar, J., Javadzadeh, A. R., & Omidi, Y. (2008). Ocular novel drug delivery: Impacts of membranes and barriers. *Expert Opinion on Drug Delivery, 5*(5), 567–581.
44. Peck, K. D., Ghanem, A. H., & Higuchi, W. I. (1994). Hindered diffusion of polar molecules through and effective pore radii estimates of intact and ethanol treated human epidermal membrane. *Pharmaceutical Research, 11*(9), 1306–1314.

45. Barry, B. (2001). Novel mechanisms and devices to enable successful transdermal drug delivery. *European Journal of Pharmaceutical Sciences, 14*(2), 101–114.
46. Naik, A., Kalia, Y., & Guy, R. (2000). Transdermal drug delivery: Overcoming the skin's barrier function. *Pharmaceutical Science & Technology Today, 3*(9), 318–326.
47. Hu, G., Huang, J., Orkoulas, G., & Christofides, P. D. (2009). Investigation of film surface roughness and porosity dependence on lattice size in a porous thin film deposition process. *Physical Review. E, Statistical, Nonlinear, and Soft Matter Physics, 80*(4 Pt 1), 041122.
48. Vanstreels, K., Wu, C., Verdonck, P., & Baklanov, M. R. (2012). Intrinsic effect of porosity on mechanical and fracture properties of nanoporous ultralow-k dielectrics. *Applied Physics Letters, 101*(12), 123109.
49. Steward, P. A., Hearn, J., & Wilkinson, M. C. (2000). An overview of polymer latex film formation and properties. *Advances in Colloid and Interface Science, 86*(3), 195–267.
50. Miyazaki, T., Nishida, K., & Kanaya, T. (2004). Thermal expansion behavior of ultrathin polymer films supported on silicon substrate. *Physical Review E, 69*(6), 061803.
51. Asbeck, W. K., & Van Loo, M. (1949). Critical pigment volume relationships. *Industrial & Engineering Chemistry, 41*(7), 1470–1475.
52. Girifalco, L. A., & Good, R. J. (1957). A theory for the estimation of surface and interfacial energies. I. Derivation and application to interfacial tension. *The Journal of Physical Chemistry, 61*(7), 904–909.
53. Venables, J. (2000). *Introduction to surface and thin film processes* (p. 372). Cambridge: Cambridge University Press.
54. Young, T. (2007). An essay on the cohesion of fluids. *Philosophical Transactions of the Royal Society of London, 95*, 65–87.
55. Ostwald, W. (1897). Studies on the formation and transformation of solid bodies. *Chemie, 22*, 289–330.
56. Davis, F., & Higson, S. P. J. (2005). Structured thin films as functional components within biosensors. *Biosensors and Bioelectronics, 21*(1), 1–20.
57. Ash, M., & Ash, I. (2007). *Handbook of fillers, extenders, and diluents* (p. 503). Endicott, NY: Synapse Info Resources.
58. Mahato, R. I., & Narang, A. S. (2011). *Pharmaceutical dosage forms and drug delivery* (2nd ed., p. 512). Boca Raton, FL: CRC Press.
59. Qiu, L. Y., & Bae, Y. H. (2006). Polymer architecture and drug delivery. *Pharmaceutical Research, 23*(1), 1–30.
60. Pouton, C. W. (1997). Formulation of self-emulsifying drug delivery systems. *Advanced Drug Delivery Reviews, 25*(1), 47–58.
61. Shimoda, H., Taniguchi, K., Nishimura, M., Matsuura, K., Tsukioka, T., Yamashita, H., et al. (2009). Preparation of a fast dissolving oral thin film containing dexamethasone: A possible application to antiemesis during cancer chemotherapy. *European Journal of Pharmaceutics and Biopharmaceutics, 73*(3), 361–365.
62. Abbasi, A., Eslamian, M., Heyd, D., & Rousseau, D. (2008). Controlled release of DSBP from genipin-crosslinked gelatin thin films. *Pharmaceutical Development and Technology, 13*(6), 549–557.
63. Verma, D. D., Verma, S., Blume, G., & Fahr, A. (2003). Particle size of liposomes influences dermal delivery of substances into skin. *International Journal of Pharmaceutics, 258*(1–2), 141–151.
64. Roxhed, N., Griss, P., & Stemme, G. (2008). Membrane-sealed hollow microneedles and related administration schemes for transdermal drug delivery. *Biomedical Microdevices, 10*(2), 271–279.
65. Ciolino, J. B., Hoare, T. R., Iwata, N. G., Behlau, I., Dohlman, C. H., Langer, R., et al. (2009). A drug-eluting contact lens. *Investigative Ophthalmology & Visual Science, 50*(7), 3346–3352.
66. Zimmer, S., Jacobs, B., Levy, T., et al. (2002). *Med Tech 101: The medical device handbook*. New York: Deutsche Bank Securities.

67. Mercado, N., Boersma, E., Wijns, W., Gersh, B. J., Morillo, C. A., de Valk, V., et al. (2002). Clinical and quantitative coronary angiographic predictors of coronary restenosis: A comparative analysis from the balloon-to-stent era. *Journal of the American College of Cardiology, 38*, 645.
68. Fattori, R., & Piva, T. (2003). Drug eluting stents in vascular interventions. *Lancet, 361*, 247.
69. Sharkawi, T., Cornhill, F., Lafont, A., Sabaria, P., & Vert, M. (2007). Intravascular bioresorbable polymer stents: A potential alternative to current drug eluting metal stents. *Journal of Pharmaceutical Sciences, 96*, 2829.
70. Maluenda, G., Lemesle, G., & Waksman, R. (2009). A critical appraisal of the safety and efficacy of drug-eluting stents. *Clinical Pharmacology and Therapeutics, 85*, 474.
71. Acharya, G., & Park, K. (2006). Mechanisms of controlled drug release from drug-eluting stents. *Advanced Drug Delivery Reviews, 58*, 387.
72. Weisz, G., Leon, M. B., & Holmes, D. R., Jr. (2006). Two-year outcomes after sirolimus-eluting stent im-plantation: Results from the Sirolimus-Eluting Stent in de Novo Native Coronary Lesions (SIRIUS) trial. *Journal of the American College of Cardiology, 47*, 1350.
73. Groeneveld, P. W., Matta, M. A., Greenhut, A. P., & Yang, F. (2008). Drug-eluting compared with bare-metal coronary stents among elderly patients. *Journal of the American College of Cardiology, 51*, 2017.
74. Axel, D. I., Kunert, W., & Göggelmann, C. (1997). Paclitaxel inhibits arterial smooth muscle cell proliferation and migration in vitro and in vivo using local drug delivery. *Circulation, 96*, 636.
75. Lemos, P. A. (2007). Polymeric stents: Degradable but strong. *Catheterization and Cardiovascular Interventions, 70*, 524.

Chapter 4
Self-Microemulsifying Materials

4.1 Engineering Concepts

4.1.1 Self-Assembly

Up to this point in our discussions, we have looked at drug delivery systems at the mercy of their respective environments. In Chap. 2, we focused on the advantages of bulk and surface erosion. In Chap. 3, we addressed the control over fabricated shape in the form of a thin film with the effects and applications in delivery of drug dosage forms. These approaches largely focus on the viewpoint that the drug is housed in a system that is steadily or immediately affected by its external environment.

What if it were possible to effectively shield a drug as it traveled through a closed physiological system?

Would there be implications in the side effects of these drugs?

Would a wider range of drugs be usable for a given disease?

We know that even effective drugs deemed safe by federal agencies such as the FDA still possess a degree of perturbation within physiological environments [1]. The field of pharmacodynamics exists to test these effects and assess the short- and long-term implications with the administration of these drugs [2]. Within pharmacokinetics there is a state at which the drug dosage form is in its most stable conformation relative to its surrounding environment. The introduction of heat, dilution, chemical reactivity, electrostatics, erosion, biodegradation, hydrolysis, or precipitation all can contribute to the destabilization of a drug prior to reaching a target [1]. If the drug's nanoenvironment can be kept constant relative to a majority of these physiological instigating factors, perhaps a higher effective dosage of drug can reach an intended target tissue.

E.P. Holowka, S.K. Bhatia, *Drug Delivery: Materials Design and Clinical Perspective*, DOI 10.1007/978-1-4939-1998-7_4

We start our discussion with the assumption that a drug encapsulated within a vessel will not be exposed to detrimental conditions within physiological systems. Later in this chapter we will answer the broader question of whether a drug contained in a shielded nanoenvironment exhibits the behavior of a more desirable drug delivery system. The process begins by piecing together some common building blocks that form these hierarchical domains. The act of forming an ordered domain from a preexisting disordered system comprised of common building blocks is known as **self-assembly** [3]. The field of self-assembly comprises a range of materials with an amphiphilic structure, where the molecule exhibits both hydrophobic and hydrophilic behavior in aqueous solutions. Amphiphiles include polymers, small molecules, and biomolecules. Within each of these species, there are strong energetic forces acting to stabilize molecular organization, such as covalent, ionic, and/or metallic bonds. The organization of these species with other molecular species involves the energetic stabilization of *secondary interactions* such as Van der Waals forces, hydrogen bonds, π–π interactions, and/or capillary forces [3]. Generally, it is the reduction of the Gibbs free energy that leads to the stable formation of self-assembled species. For our discussions in this section, the focus lies on an overview of the thermodynamic, energetic, and geometric constraints involved in the self-assembly of commonly used materials in drug delivery. Please note that this section is not meant as a comprehensive assessment of the self-assembly of complex fluids or soft matter. For additional references, established comprehensive texts [4] exist to supplement our discussions.

4.1.2 Thermodynamics

The two most common soft matter systems used in drug delivery are micelles and vesicles [5]. We begin with the simpler micellar case from a thermodynamic perspective and follow with the vesicle case from the geometric and energetic perspective. For micellar systems, we are referring to the self-assembly of amphiphilic molecules in a head-to-tail monolayer orientation, whereby adjacent amphiphiles have their head groups uniformly occupying either the outer micellar or inner micellar (i.e., inverse micelle) surfaces (Fig. 4.1).

If we look at either of these assembly modes in terms of the chemical potentials of their identical individual domain components, we can see the following relationship [6]:

$$\mu = \mu_N = \mu_N^o + \frac{kT}{N}\log\left(\frac{X_N}{N}\right) \quad N = 1, 2, 3\ldots, \tag{4.1}$$

where μ_N is the mean chemical potential of the molecule in an assembly, $\mu_N{}^o$ is the mean interaction free energy per molecule, N is the assembly number, X_N is the concentration of molecules in an assembly of number N. For example, in Eq. (4.1),

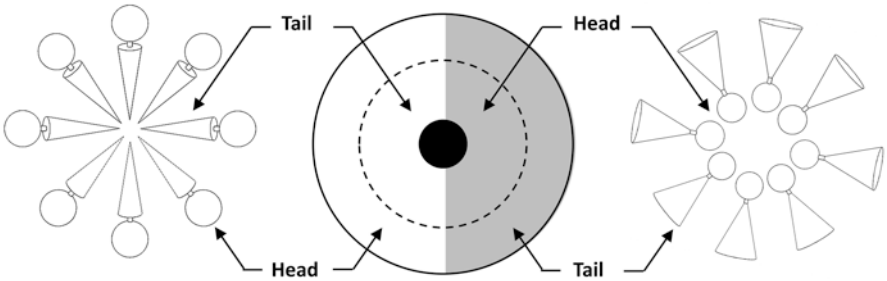

Fig. 4.1 Diagram of the micellar assembly (*left*) and inverse micellar assembly (*right*) by the organization of head-to-tail molecules

if $N=1$, you have monomers; if $N=2$, you have dimers; if $N=3$, you have trimers, and so on.

The onset of self-assembly occurs when the cohesion energies between molecules in assembled ($k_1X_1^N$) and dispersed [$k_N(X_N/N)$] states begins to differ. One way to observe this point mathematically is by assuming that each domain interacts with its respective environment equally, independent of its size (i.e., $\mu_N{}^o=\mu_2{}^o=\mu_3{}^o=\ldots=\mu_2{}^o$). If we operate based on this assumption, Eq. (4.1) can simplify to the following [6]:

$$X_N = NX_1^N. \tag{4.2}$$

The assembly of larger aggregates would occur at $\mu_N{}^o<\mu_1{}^o$, where the terms for $\mu_N{}^o$ and N can determine the size and dispersity of the assembled structures. But how does the thermodynamics of assembly differ, if at all, for different dimensional geometries such as rod (i.e., 1D), disc (i.e., 2D), and sphere (i.e., 3D)? We can account for the bond energy from domain to domain in terms of the simplest case, a 1D assembly, as $-\alpha kT$, where α correlates with the magnitude of the intramolecular interactions. The assembly number of a 1D system is simply N. If we move to a 2D system, the bond energy remains the same, while the assembly number is influenced by the geometry of a disc, which leaves $N^{1/2}$. If we move still further to a 3D system, the bond energy remains the same again, while the assembly number is influenced by the geometry of a sphere, which leaves $N^{1/3}$. We can begin to see that the dimensionality changes an isolated component of the base equation to a term, which we will refer to as p, which allows us to rewrite the chemical potential as the following relationship [6]:

$$\mu_N^o = \mu_\infty^o + \frac{\alpha kT}{N^p}. \tag{4.3}$$

The implication of Eq. (4.3) is that the geometry of the assembly itself is enough to influence the chemical potential of the respective domain components. We will revisit this idea from a different point of view later in this section.

Let's first refer to an earlier point, with a question. At what concentration do the cohesion energies of domains in the assembled and dispersed states begin to change? This concentration, known as the critical micelle concentration (CMC), can be written in terms of Eqs. (4.1) and (4.3) [6]:

$$X_1 \approx \exp\left[\frac{-\left(\mu_1^o - \mu_N^o\right)}{kT}\right]. \tag{4.4}$$

If we take into account Eqs. (4.2) and (4.4), we can see that the monomer state $X_1 < 1$, which implies that $X_1 \gg X_N$. This signifies that at concentrations above the CMC, additional amphiphiles will contribute to the cohesion of domains, leaving the monomer concentration relatively constant. Is there a difference in the magnitude of the CMC value with differing *types* of amphiphilic molecules? For example, this essentially simplifies to a difference in chemical potentials. We know that the chemical potential of a polymer is greater than that of a small molecule. Therefore, by Eq. (4.4), the CMC for a polymer would be much less than that of a small molecule. In other words, it would require a greater degree of energy to alleviate the cohesive interactions between polymer domains than it would for small molecules.

4.1.3 Geometric and Energetic

We now begin to move our discussion from the monolayer systems to those of bilayer self-assembled systems. Closed bilayer assemblies, known at vesicles, follow a majority of the thermodynamic constraints that were discussed in the micellar systems. In vesicles, however, the energetic behavior of self-assembly correlates more strongly with the geometric orientation of its components. Perhaps the simplest method of assembling common building blocks into hierarchical bilayer systems was discussed in 1976.* In this example, amphiphilic molecules were used as the building blocks to demonstrate the geometric constraint argument. As we recall, amphiphiles are molecules that contain both hydrophilic and hydrophobic domains. When placed in aqueous environments, these domains rearrange to minimize interfacial energy. This behavior leads to the formation of self-assembled species. Typically, the hydrophilic domain in these molecules is referred to as the *head* and the hydrophobic domain the *tail*. If we wish to form a spherical micellar assembly with radius R from N amphiphilic molecules, we require a certain area a to be occupied by the head groups of volume υ and tail groups of length l [7, 8]:

$$4\pi R^2 = Na, \tag{4.5}$$

$$\frac{4}{3}\pi R^3 = N\upsilon. \tag{4.6}$$

If we combine Eqs. (4.5) and (4.6), we arrive at Eq. (4.7), which gives the radius of the spherical assembly in terms of the volume of the amphiphilic head group relative to the area of the assembled species [7, 8]:

$$R = \frac{3\upsilon}{a}. \tag{4.7}$$

Let's assume that no void space exists in the center of the spherical micellar assembly; therefore, $l \geq R$. We can rewrite Eq. (4.7) in the form of Eq. (4.8) [7, 8]:

$$\ell \geq R = \frac{3\upsilon}{a} \Rightarrow \ell \geq \frac{3\upsilon}{a} \Rightarrow \frac{\ell}{3} \geq \frac{\upsilon}{a} \Rightarrow \frac{1}{3} \geq \frac{\upsilon}{a\ell}. \tag{4.8}$$

In Eq. (4.8), the final term υ/al is referred to as the packing parameter P for an assembled system, which in this case is spherical in geometry. This predicts that the system will assemble into a spherical geometry if the packing parameter $P \leq 1/3$.

While spherical micellar systems will occupy a majority of the discussion of Chap. 4, there is a continuing effort to leverage cylindrical and planar systems for drug delivery applications as well. How does a cylindrical and planar system compare with the spherical system in terms of packing parameters? The Na term is equal to $2\pi RL$, where L is the length of the cylinder and the $N\upsilon$ term is equal to $\pi R^2 L$. If we substitute as we did in Eq. (4.7), we can see that the formulas for sphere and cylinder are very similar [7, 8]:

$$R = \frac{2\upsilon}{a}. \tag{4.9}$$

If we now apply the same method we did for Eq. (4.8), we can see that cylindrical assemblies occupy a range of packing parameters, from $1/2 \geq P \geq 1/3$ [7, 8]:

$$\ell \geq R = \frac{2\upsilon}{a} \Rightarrow \ell \geq \frac{2\upsilon}{a} \Rightarrow \frac{\ell}{2} \geq \frac{\upsilon}{a} \Rightarrow \frac{1}{2} \geq \frac{\upsilon}{a\ell}. \tag{4.10}$$

Similarly, if the same methodology was applied for planar assemblies, the packing parameter P would be in the range $1 \geq P \geq 1/2$. The packing parameter calculations provide an accurate first approximation of the correlation between head-group size and self-assembly size by geometric shape. These estimates, however, do not take into account the volume of the tail group. In amphiphilic molecules such as lipids, polymers, and proteins, the tail group retains a certain volume that can dictate the possible curvature of the self-assembly.

The importance of curvature becomes more of a constraint in bilayer systems [9], such as vesicles, than in monolayer systems, such as micelles. Why is this? Vesicles represent a closed bilayer system, which essentially encapsulates an aqueous environment. The net result is a self-assembled system dispersed in an aqueous environment, which is simultaneously housing its own aqueous environment. An interesting

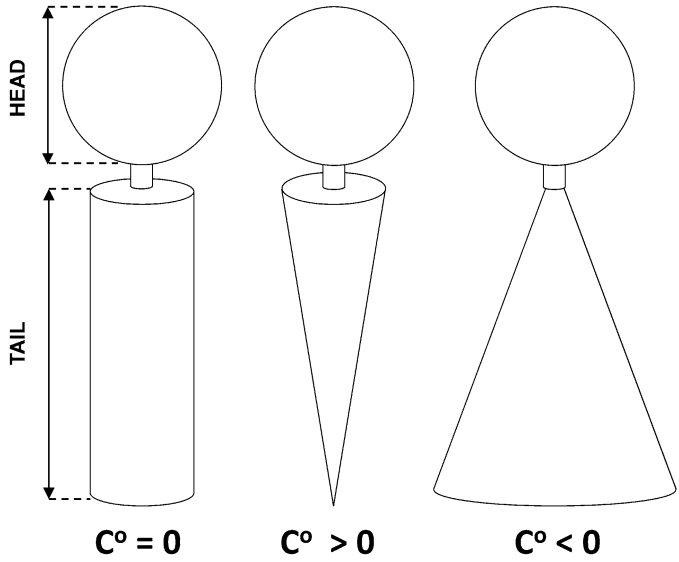

Fig. 4.2 Diagram of the geometry and expected curvature of head-to-tail molecular species in monolayer and bilayer assemblies

way of looking at this phenomenon is that the entire aqueous dispersion is a collection of compartmentalized water domains [4]. Within these compartmentalized domains lie individual modifiable environments, which can contain drug molecules (Figs. 4.2 and 4.3).

In vesicle systems it is easy to see that there is a large energetic cost associated with the stabilization of the curvature in a system with both interior and exterior aqueous phases [9]. We can see from the figure above that the geometric volume of the tail group can dictate positive, negative, or neutral curvature (C^{o}) in an assembled species. We can begin to see the effects of molecular curvature if we extrapolate the shapes in two dimensions. The zero curvature species ($C^{o}=0$) form sheets or planar assemblies and the negative ($C^{o}<0$) and positive ($C^{o}>0$) curvature species form round assemblies (spherical or cylindrical). If we draw a vector from tail group to head group, then in the $C^{o}<0$ and $C^{o}>0$ species, the sign indicates the direction of the tail–head vector. The vector direction tells us which chemical species occupies the core and shell of the assembly.

The discussion surrounding curvature brings to light a poignant question. What if the curvature C^{o} approaches zero? This can occur in several ways. In one, the tail group could be too large to effectively assemble in the hydrophobic domain. In another, the head group could be small relative to the size of the tail group. The self-assembly of bilayer systems occurs when the head-group area and tail-group area are nearly equivalent [4, 7]:

$$\frac{\upsilon}{a\ell} \approx 1.$$

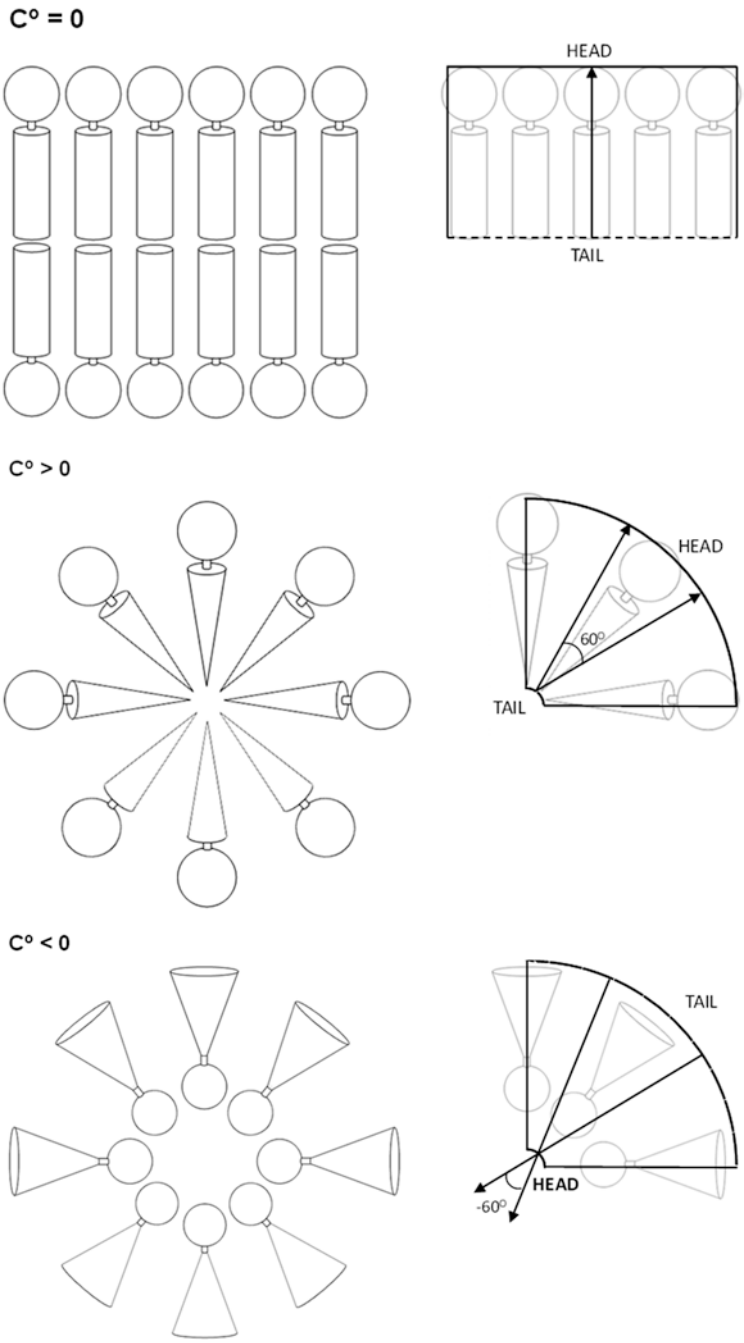

Fig. 4.3 Diagram of the expected curvature (positive, negative, and neutral) of head-to-tail molecular species in monolayer and bilayer assemblies

For this to occur, the volume of the tail group will roughly double in magnitude compared to its micellar counterpart. With the additional volume in the hydrophobic domain, is there any implication to the energetics of the self-assembled system?

The energies and forces involved in the self-assembly of closed bilayer systems are interrelated with the ability for molecular geometries to come together and stay together in different environments. Because this discussion is focused on an overview of influencing properties associated with self-assembly and the resulting behavior, a more comprehensive account of these behaviors and their respective energetics can be gained from reading widely accepted reference material focused on the field of soft matter [4]. We continue our discussion of energetics by focusing on the closed bilayer vesicle assemblies [9, 10], where the amphiphilic tail groups organize with lateral order and occupy the inner phase of the membrane, while the head groups are exposed to both the inner and outer vesicle environments. From this arrangement it is evident that the inner and outer membrane surfaces are subjected to different forces and energetic stresses [11]. The outer phase of the bilayer membrane is being stretched, while the inner phase is being compressed. This limits the ratio of amphiphilic molecules that can occupy the inner membrane relative to the outer membrane. At some location within the bilayer system, a neutral point exists where the stretching and compression forces balance each other and effectively cancel out the force vectors (Fig. 4.4).

The stretching and compressing forces can be represented in what is known as the bending energy (e_{bend}) per unit area, as shown in Eq. (4.11) [12]:

$$e_{\text{bend}} = \frac{E_{\text{bend}}}{L^2} = \frac{1}{24} Y \frac{h^3}{R^2}, \tag{4.11}$$

where Y is Young's modulus, h is the membrane thickness, and R is the radius of the assembled species. Perhaps the most striking correlation in Eq. (4.11) is between the membrane thickness term h and the bending energy term e_{bend}. As the membrane thickness increases, the bending energy increases exponentially (i.e., h^3). The importance of the thickness term to the energetics of bilayer systems highlights the influence of molecular design on self-assembled species.

Sample Problem 4a

What is the ratio in bending energies of the following two lipid systems with different hydrocarbon chain lengths?

- Palmitoyl-oleyl-*sn*-phosphatidylcholine (POPC)—15
- Dihexanoylphosphatidylcholine (DHPC)—5

We can compare the bending energies of two vesicle-forming phospholipid systems: palmitoyl-oleyl-sn-phosphatidylcholine (POPC) and dihexanoylphosphatidylcholine (DHPC). The POPC tail group is 15 hydrocarbons long, and the DHPC tail group is 5 hydrocarbons long. Therefore,

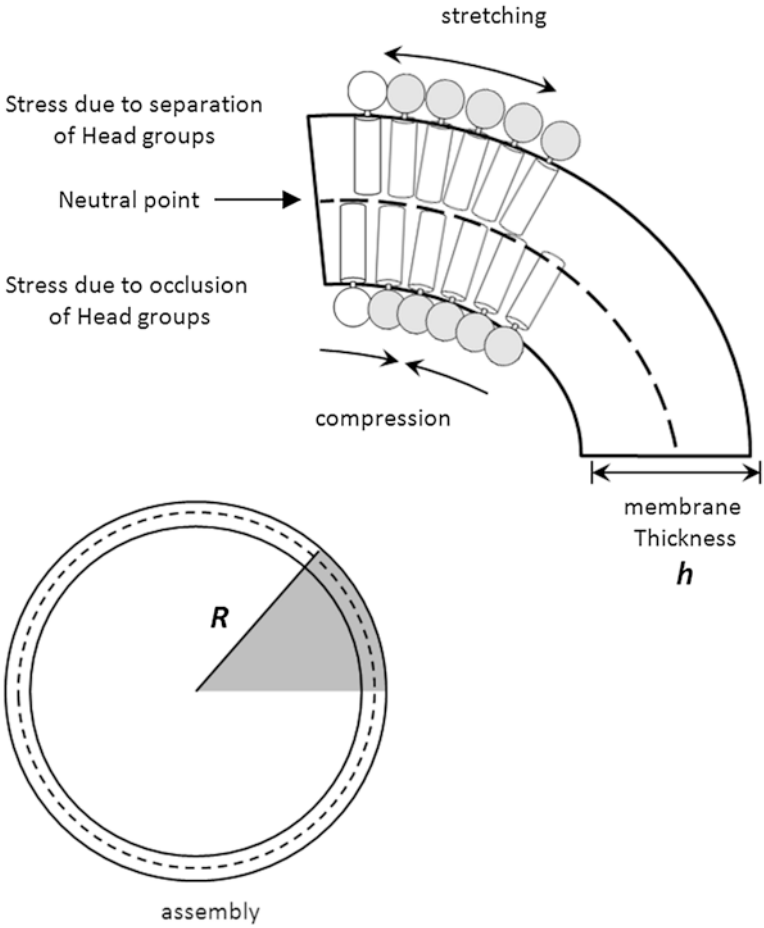

Fig. 4.4 Diagram of the physical stresses imposed on self-assembled bilayer species

assuming the radius of the curvature term is constant for both assembled species, the approximate membrane thickness ratio of POPC relative to DHPC is approximately 3:1:

$$\frac{E_{\text{bend POPC}}}{E_{\text{bend DHPC}}} \propto \frac{\left(h^3\right)_{\text{POPC}}}{\left(h^3\right)_{\text{DHPC}}} = \frac{\left(30^3\right)_{\text{POPC}}}{\left(10^3\right)_{\text{DHPC}}} = \frac{27}{1}.$$

The 3:1 difference in tail group length translates to a 27-fold increase in the bending energy of the resulting membrane!

The exponential influence of h on e_{bend} implies there is an effect of geometry and size on the energetics of the membrane. In our example, extended chain length

contributes significantly to the bending energy of the membrane. Can you think of any other factors that could impact bending energy? The rigidity (i.e., degree of saturation) or geometry of the tail group influences its length and therefore influences bending energy. The degree of hydrophobicity influences how freely extended the tail group will be in the interior of the membrane, which influences the tail length as well. Generally, it becomes evident that methods of adjusting the tail group domain through rigidity, orientation, sterics, or solvation will correspond to length and membrane energetic changes [13].

We can also see an effect of the bending energy on the size of the assembled species through the radius of curvature (R) term. If we rewrite Eq. (4.11) in the following form, it is apparent that the thickness of the membrane is directly proportional to the radius of curvature of the resulting assembly [12]:

$$R^2 = \frac{1}{24} Y \frac{h^3}{e_{\text{bend}}} \Rightarrow R \propto h.$$

Moreover, the radius of curvature corresponds to the size of the self-assembled species generated. The implication of this relationship is that the size of the self-assembled species is intimately connected to the thickness of its membrane.

Sample Problem 4b

What is the ratio in vesicle sizes of the two lipid systems from (4b) with different hydrocarbon chain lengths, assuming that you have reached the equilibrium bending energy?

Let's look once again at the two phospholipid systems of POPC and DHPC, where the tail groups are 15 hydrocarbons long and 5 hydrocarbons long, respectively. This time let's assume the radius of curvature term is variable for the assembled species. If we assume that we have reached an equilibrium bending energy, where the e_{bend} terms for POPC and DHPC are equal, then we can rewrite Eq. (4.7) *as the following ratio of the respective radii:*

$$\frac{R_{\text{POPC}}}{R_{\text{DHPC}}} = \frac{\left(\frac{1}{24} Y \frac{h^3}{e_{\text{bend}}}\right)_{\text{POPC}}}{\left(\frac{1}{24} Y \frac{h^3}{e_{\text{bend}}}\right)_{\text{DHPC}}} = \frac{\left[\left(h^3\right)^{\frac{1}{2}}\right]_{\text{POPC}}}{\left[\left(h^3\right)^{\frac{1}{2}}\right]_{\text{DHPC}}} = \frac{164.3}{31.6} \approx \frac{5}{1}.$$

*Therefore, for a lipid with a threefold greater tail length, we can expect a fivefold increase in the overall vesicle size under equilibrium conditions. It is important to note that this is bending energy and not bending elasticity. The radius term in the equation for bending elasticity cancels due to the surface area component of the equation in L^2 (*i.e., *L^2 is the surface area of a sphere $4\pi R^2$), leaving no dependence of bending elasticity on the radius of the vesicle.*

The discussion surrounding the bending energy is not excluded from our previous discussion related to the geometric shape and curvature. In relation to our example above, we can draw the analogy between the POPC lipid and a membrane system with curvature approaching $C^{o}=0$, while the DHPC lipid resembles a membrane system with a curvature $C^{o}>0$.

We can now begin to see how self-assembled systems can be designed from first principles. The material selection, whether it be macromolecular or small molecule, has a significant implication on the overall stability (e_{bend}), the size (R, h), the geometric shape (C^{o}), and the internal or external chemical functionalities of the self-assembled system [14]. Leveraging of these critical interrelationships within molecular design will be the focus of Sect. 4.2, where we will approach systems from both amphiphilic and polymeric domains.

4.1.4 Encapsulation

We have discussed some of the contributing characteristics for the bottom-up formation of self-assembled systems as a method of shielding a drug from its external physiological environment. What remains unanswered is the capacity of these systems to carry drug molecules as cargo. For example, typically for oral drug delivery systems involving the bloodstream, one requirement is a system no larger than 150 nm in size is used to pass through the filtration system in the human liver to arrive in the bloodstream [15]. If we were to form a vesicle of that size, what would the expected amount of aqueous drug molecules be as the encapsulant? Is it sufficient enough to illicit the intended physiological effect? The characteristic being described is referred to as the drug load (**DL**). We will assume for the purposes of our discussion in this section that, in the case of vesicle systems, the drug molecules are freely dissociated within the encapsulated environment and are not adhering to the vesicle bilayer surface [16].

$$\text{drug load} = \frac{W_D}{W_V} \times 100\%, \tag{4.12}$$

where W_D is the weight of the encapsulated drug molecule and W_V is the weight of the encapsulating vessel (i.e., micelle, vesicle, microsphere). Values for drug load will provide an indication of the relative ratio of encapsulated drug to that of the vessel on a per-weight basis, which is critical in determining whether an encapsulation method is effective, or if the vessel itself is relevant for a particular application [17]. If we look more closely at the weights of the components during each stage of the preparation of encapsulated drug systems, we see another metric for determining the encapsulation efficiency:

$$\text{encapsulation efficiency} = \frac{W_T - W_{DL}}{W_T} \times 100\%, \tag{4.13}$$

Table 4.1 Comparison of vesicle size to expected encapsulation efficiency (EE) and drug loading (DL) [18]

Vesicle size (nm)	Encapsulation efficiency (EE) (%)	Drug loading (DL) (%)
70	15	3.75
200	30	7.50
220	35	8.75
320	50	12.50

where W_T is the total weight of the drug and W_{DL} is the weight of the unencapsulated drug remaining in the water. The encapsulation efficiency (**EE**) allows us to know how much total drug is required, using a given method and self-assembled system, to achieve a prescribed level of encapsulation. The terms for EE and DL will vary depending on the system and the method of encapsulation. We will focus our discussion of these methods in more detail in Sect. 4.2. For the purposes of our current discussion, let's take an example from an existing preparation [18] method for comparative purposes (Table 4.1).

In the data above, it is clear that both EE and DL are directly proportional with respect to vesicle size. The utility of the data depends on the experimenter's goal. To determine the efficiency of the overall method, EE, should be the focus [19]. If one were trying to determine if the dosage was enough to engage the desired pharmacokinetic profile, then DL is the appropriate starting point. If we were to focus on the example of an oral drug with a desired delivery location within the circulatory system, then the appropriate vesicle size from the data above would be 70 nm, which would correspond to a 3.75 % DL. Therefore, if 100 mg of the system was ingested, only 3.75 mg of the mixture would include the actual drug molecule. How do we determine if this is an adequate amount?

We can begin to differentiate the dosage effectiveness by doing a cursory examination of the physiological, physicochemical, and biopharmaceutical properties to determine the absorption and metabolism of drug molecules. This will vary largely based on the mode of delivery, whether it is transdermal, oral, ocular, intravenous (IV), and so forth. For our discussion we will focus on oral drug delivery. We will not address the overall selection and determination of the likelihood of a drug's bioactivity. For this, we suggest a reading of Lipinski's Rule of 5 (RO5) [20] for purposes identifying the common traits associated with the interactions of drugs with oral physiological environments. In oral drug delivery systems, it is common to compare the drug pharmacokinetic profiles from both oral and IV routes [21]. The curves are notably different in character, with the oral route showing a Gaussian-like distribution with a peak at some time point and the IV route showing an exponential decrease with time (Fig. 4.5).

If we calculate the area under each curve, we will determine the total amount of drug delivered throughout the duration of the profile [21]. We can compare the ratio of the respective areas to that of their respective dosages to arrive at the **absolute bioavailability:**

$$\text{absolute bioavailability} = \frac{\text{AUC}_{\text{oral}}}{\text{AUC}_{\text{IV}}} \times \frac{\text{dose}_{\text{IV}}}{\text{dose}_{\text{oral}}}. \tag{4.14}$$

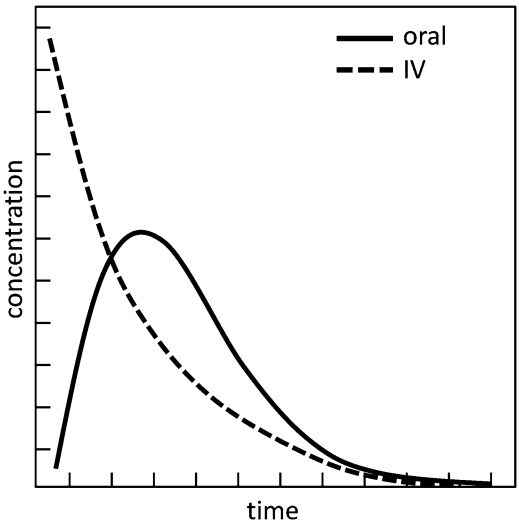

Fig. 4.5 Plot of the concentration of a drug in the body versus time for intravenous (IV) and oral application

Another method of assessing the area under the curve (AUC) is to assess the total area under the curve (AUC_t) and compare that with the area under the curve when it is extrapolated to infinite time ($AUC\infty$) [22]. From these three basic values (DL, EE, absolute bioavailability), combined with our knowledge of the physiological route the drug will encounter, we can determine the correct material selection and preparation method to allow for an effective dosage to be delivered to an intended target region.

Sample Problem 4c
What is the absolute bioavailability of the drug Risedronate®, which is used to treat osteoporosis, if we know that the ratio of AUC for oral and IV administration is 0.78 and that their dosages are 120 mg and 1 mg, respectively?

Let's look at the drug Risedronate®, with a ratio of AUC for oral and IV administration of 0.78 and at dosages of 120 mg and 1 mg, respectively. We can determine the absolute bioavailability as the following:

$$\text{absolute bioavailability} = \frac{\text{AUC}_{\text{oral}}}{\text{AUC}_{\text{IV}}} \times \frac{\text{oral}_{\text{IV}}}{\text{dose}_{\text{oral}}} = (0.78) \times \frac{(1\text{mg})}{(120\text{mg})} = 0.65\%.$$

The absolute bioavailability of 0.65 % assumes that roughly 0.65 mg of the original oral dosage is available for physiological absorption. If we look back at our example of an oral drug delivery system, would this be appropriate

for Risedronate® given its route and absolute bioavailability? In order to pass through the liver's filtration system, a 70-nm vesicle system would be appropriate, which correlates to a ratio of drug to vesicle of 3.75 %. In order to achieve a 120-mg dosage requirement, then 3.2 g of drug is required!

Based on our example, we can now answer our earlier question: How is a vesicle delivery system ultimately effective? The answer to this is through changing the absolute bioavailability of a drug by providing a shielded mode of interaction within a physiological system, which allows for a lower effective dosage depending on the delivery route [23]. Keep in mind that with each drug delivery route (transdermal, ocular, IV), there is a different series of equations to approximate the absolute bioavailability [24]. For the purposes of an introductory discussion of oral drug delivery systems, Eqs. (4.12)–(4.14) offer an adequate starting point for bridging our discussion to material design. In Chap. 5, we revisit this discussion and focus on active transport versus passive diffusion as a means of targeting the drug delivery of encapsulated systems.

4.2 Material Design

4.2.1 Soft Matter

The physical properties of the self-assembled encapsulating species discussed in Sect. 4.1 sought to provide an introductory glance at some of the critical requirements for a stable drug delivery system. The next step in the design of effective systems is the transition between physical requirement and chemical structure. For this discussion we will focus on the two basic systems of lipids and block copolymer amphiphiles [25].

4.2.2 Lipids

Polar or amphiphilic molecules offer distinct advantages in terms of the induction of controlled self-assembly for drug encapsulation [26]. Lipid molecules allow for a high level of control over the bending elasticity [27], geometric partitioning [27], and chemical functionality [28], which allows for a wide gradient of self-assembled structures such as micelles [29], tubular species [30], vesicles [31], and toroids [32] (Fig. 4.6).

In order to target a specific shape, geometric packing, and size, the lipid molecule requires the appropriate chemical functionality at its head group and tail group. There are three general criteria for the selection of the tail-group species.

The first criterion is the number of hydrocarbon tail groups (i.e., 1, 2), which relates directly to the curvature of the self-assembled species [33]. To put it quite

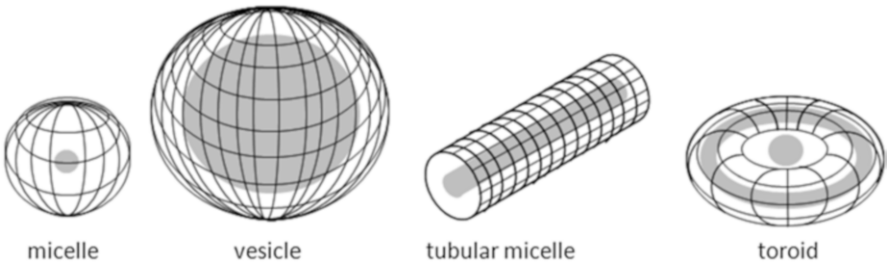

Fig. 4.6 Diagram of different self-assemblies from amphiphilic molecules

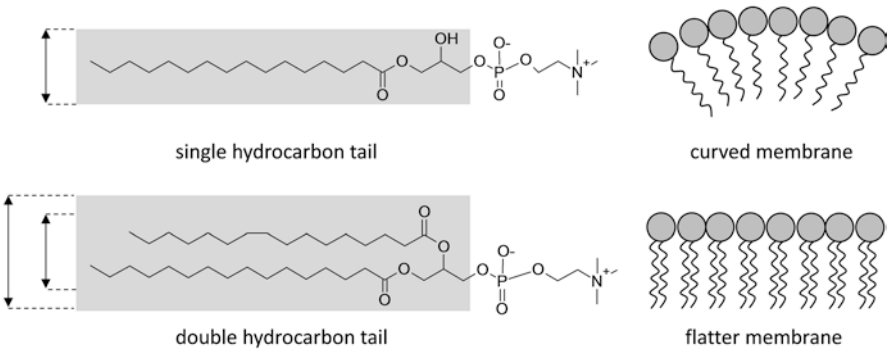

Fig. 4.7 Effect of the number of hydrocarbon tail groups on the curvature of the assembly

simply, if one were to have two lipid molecules differing only in the number of hydrocarbon tail groups, it would be expected that the favorable packing density would allow for a considerably smaller self-assembled structure in the case of one hydrocarbon tail versus two. It is a question of the difference in their respective free volumes (Fig. 4.7).

The second criterion is the degree of saturation within the hydrocarbon tail [34]. A fully saturated hydrocarbon tail group is one that has the maximum number of hydrogen atoms per carbon atom at each location within the chain. This allows for the highest number of bond rotations within the tail group, which results in a higher density of packing between adjacent tail groups in the monolayers and bilayers of self-assemblies. This is in part due to the high number of allowable conformations and the high speed at which the molecule can sample each, which increases the probability of a more densely packed arrangement. If the system is unsaturated, hydrogens are replaced with carbon–carbon double bonds (Fig. 4.8 and Table 4.2).

The π-orbitals of the double bond restrict the degree of bond rotations possible within the hydrocarbon tail group. This reduces the packing density since the hydrocarbon has fewer allowable rotational conformations [34]. The degree of packing has implications in both the size and stability of liposomes. The saturated cases are tightly packed but lack the membrane elasticity to permit small self-assemblies from forming, while the unsaturated cases often allow for nanoscale self-assembly but have compromised stability due to reduced packing density.

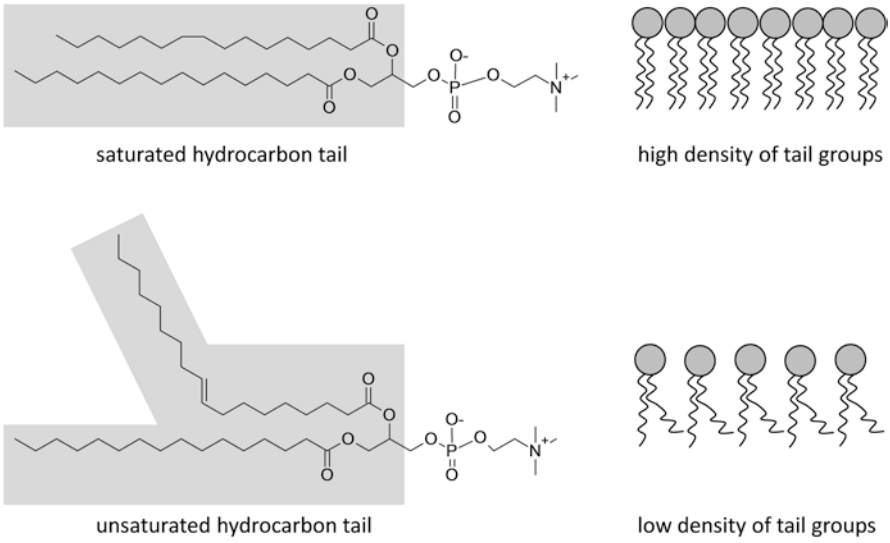

Fig. 4.8 Effect of the degree of saturation of the tail groups on the curvature of the assembly

The third criterion is the hydrocarbon chain length [35]. We discussed earlier in this chapter that the chain length has a direct correlation with the membrane thickness, which has a direct effect on the bending elasticity of the membrane. By combining elements of each of these criteria, one can design a molecular species that drives self-assembled structural characteristics [36] (Fig. 4.9).

Sample Problem 4d
What self-assembled structures would you expect from the following two lipid systems with different degrees of saturation and hydrocarbon tail lengths (unsaturation, hydrocarbon tail lengths)?

- Palmitoyl oleoyl phosphatidylcholine (POPC)—(0, 15-15)
- Dipalmitoyl phosphatidylcholine (DPPC)—(1, 17-15)

Let's compare two lipid systems with different degrees of saturation and hydrocarbon tail lengths. For POPC and DPPC, the degrees of unsaturation are 1 and 0 and the tail lengths are 15-15 and 17-15, respectively. Based on the saturation, one would expect a more elastic membrane for POPC due to the lower density of hydrocarbon packing. Similarly, the slightly longer lipid chains in the DPPC case would suggest that the thickness of the membrane is increasing, which results in a decreasing of its bending elasticity. By taking these two criteria into account, one could expect that the POPC vesicles would maintain more stable, smaller-sized species than the DPPC vesicles. This proves to be consistent since POPC vesicles are widely described as small unilamellar vesicles (SUV) [37], *while the DPPC vesicles are commonly grouped with giant unilamelar vesicles (GUV)* [38].

Table 4.2 Collection of common amphiphilic molecules used as self-assembled drug delivery systems

Lipid	Abbreviation	Chemical structure	Application
Palmitoyl oleoyl phosphatidylcholine	POPC	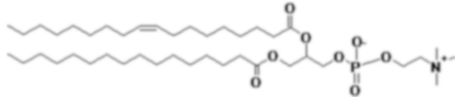	Transdermal Intravenous
Gangliosides	GM# (e.g., GM1)	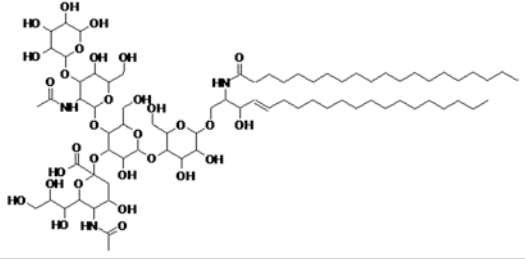	Oral Transdermal Ocular Respiratory
Phosphatidylinositol	PI	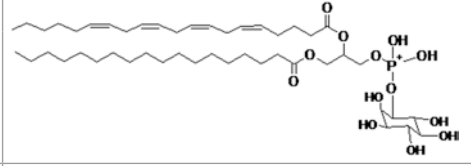	Oral Intravenous
Sulfogalactosylceramide	Sulphatide	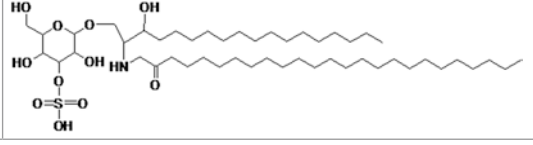	Intravenous

(continued)

Table 4.2 (continued)

Lipid	Abbreviation	Chemical structure	Application
Dipalmitoyl phosphatidylcholine	DPPC	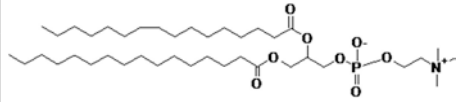	Transdermal Ocular Intravenous
Dipalmitoyl phosphatidylglycerol	DPPG	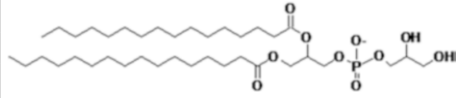	Transdermal Ocular Respiratory

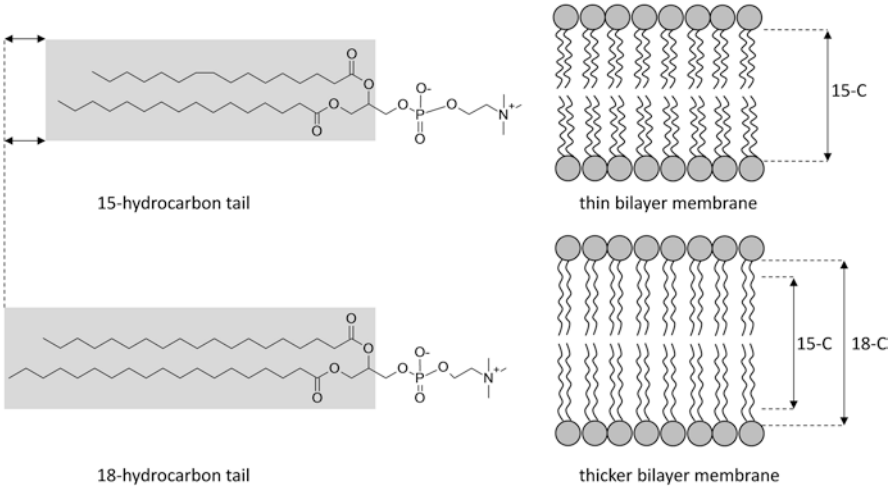

Fig. 4.9 Effect of the length of the tail groups on the curvature of the assembly

The head groups have different selection criteria that influence the shape and size of self-assembled species. In a majority of applications, the head group represents the surface of the self-assembled species (aside from inverse micellar structures) that is exposed to the physiological environment. For the purposes of our discussion in this section, we will focus on three criteria associated with the selection of head-group chemical species. The first criterion is tied to the electrostatic charge [39]. The head group does not simply identify an isolated point on the self-assembled surface but rather is a representative of a repeated surface domain. Therefore, when selecting a charged species, keep in mind that the charge will represent the entire charge of the surface that is interacting with its physiological environment. If one were to choose a cationic head group for an oral drug delivery application, the surface may be at risk of being eliminated from the body through the reticuloendothelial system (RES) [40], which we discuss in more detail in Chap. 5. Similarly, if an incorrect counterion is chosen for an anionic head group, a similar effect can be encountered. Electrostatic interactions with these surfaces can also destabilize the self-assembled order and lead to premature release and degradation of drug species [39]. It is for this reason that homogeneous lipid systems are rarely used commercially for liposomal drug delivery. Instead, typically, there is a mixture of lipid species, in either a cationic, anionic, or zwitterionic (i.e., both anionic and cationic) orientation. These lipids can also be mixed with sterols (i.e., cholesterol) in order to alter the bending elasticity by association with the hydrophobic assembled domain [41] (Fig. 4.10).

The second criterion is related to the presence of nonbilayer formers in the lipid mixture. This refers to a chemical functionality on the head group, which sterically hinders self-assembly of lipid systems into monolayer or bilayer membranes [42]. The primary reason that explains this behavior is the depolarization of the lipid head

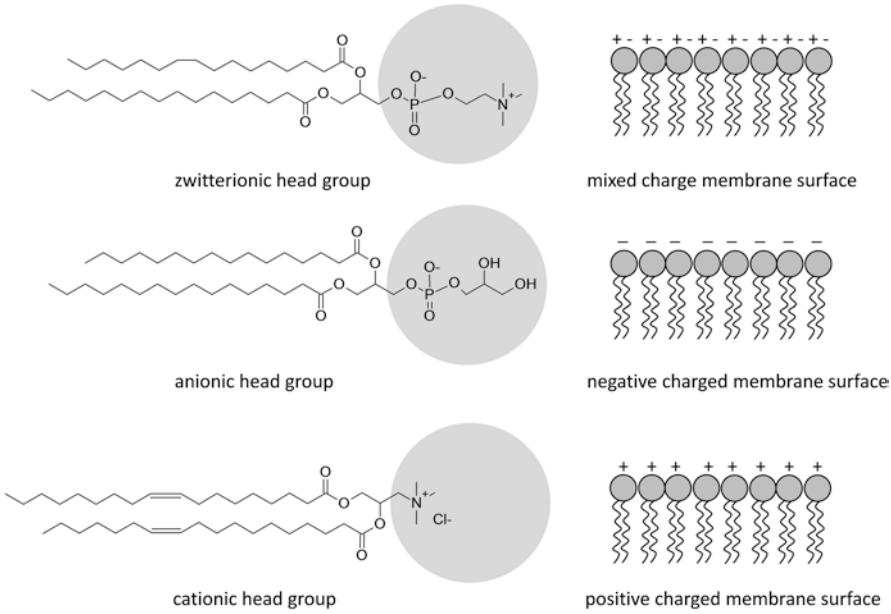

Fig. 4.10 Effect of the charge of the head groups on the physiological stability of the assembly

group, which renders the lipid to form a nonpolar species and disrupts bilayer formation. In the case of two zwitterionic lipids such as phosphatidylethanolamine (PE) and phosphatidylcholine (PC), the stabilizing cationic charge in the case of the ethanolamine is much greater since it is an amine instead of an imide from PC. This allows for a more stable electrostatic interaction between the two charges, which essentially forms a nonpolar head group (Fig. 4.11).

The third criterion is associated with physiological interaction. This refers to the selection of a head group for the sole purpose of interacting with a biological interface [43]. The general types of interactive head groups may include passive functionalities such as phosphates or carboxylates as well as targeted species such as inositol or a sialic acid derivative. We discuss active and passive targeting groups more extensively in Chap. 5. For example, let's compare two lipid systems with different electrostatic characteristics of their head groups. For dipalmitoyl phosphatidylglycerol (DPPG) and dipalmitoyl phosphatidylcholine (DPPC), the difference is a neutral charge to a single cationic charged species, respectively. The charged liposome DPPC tends to form more unstable vesicle species. This is in part due to the electrostatic repulsion felt between head groups on the lipid surface. Another observation is that DPPG systems tend to be more stable in physiological environments due, in part, to their lack of surface charge.

Typically, a functional liposomal system is comprised of a mixture of both charged and uncharged species in order to achieve the desired relative stability and biocompatibility [43].

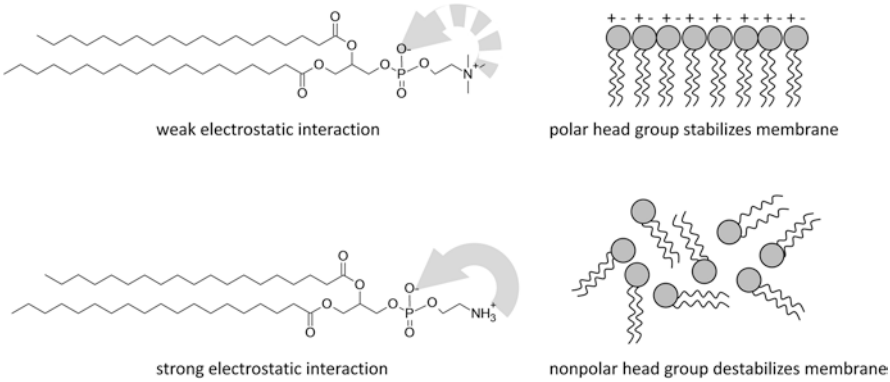

Fig. 4.11 Effect of shielding electrostatic interactions through sterics in the head groups on the physiological stability of the assembly

If we look more carefully at the aspect of bending elasticity, an important question arises. Thicker-membrane systems are known to form more rigid bilayer assemblies. Why is this the case? Longer hydrocarbon tail lengths stabilize the bilayer structure primarily through an increased density of hydrophobic packing [44]. Therefore, in order to fabricate smaller vesicle species by this logic, one would need to shorten the hydrocarbon tail length, leading to a less densely packed, destabilized bilayer. This can be mitigated to an extent with changes made to the lipid head group and the saturation of the tail groups; however, the inherent limitation remains to a large degree. In order to maintain stable submicron vesicle species, the environmental energetic factors (i.e., temperature) must be altered in order to trap the system in a kinetic state [45]. This is largely the reason why liposomal systems require storage in cool temperatures and only remain stable for a few months (Fig. 4.12).

If the elasticity or curvature is compromised with increases made to the hydrocarbon tail group, and stability is compromised with decreases made to the hydrocarbon tail group, how is a stable, nanoscale, vesicle species possible?

4.2.3 Polymer Block Amphiphiles

We can continue our discussion by approaching vesicle formation from amphiphilic polymeric materials. Polymer amphiphiles have several distinct advantages over lipids [46]. We will discuss three critical characteristics and their effects on both vesicle assembly and corresponding utility. The first characteristic focuses on the significantly longer length of the chemical domains comprising polymer amphiphiles [47]. The second characteristic is that they are typically far more malleable [48], which allows for a range of self-assembled structures. The third is that they can be readily synthesized [49] with a multitude of amphiphilic compositions (Fig. 4.13).

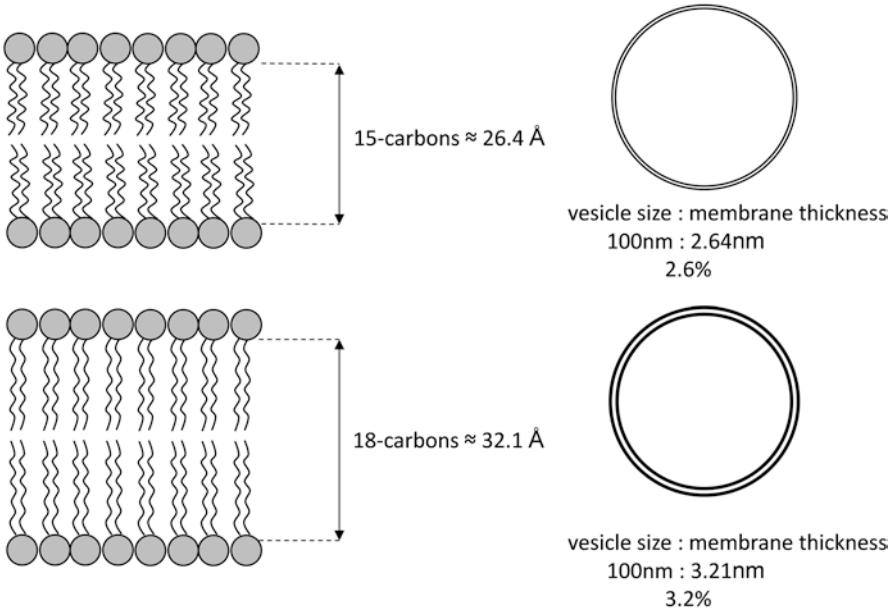

Fig. 4.12 Effect of the tail length on the ratio of vesicle size to bilayer thickness of the assembly

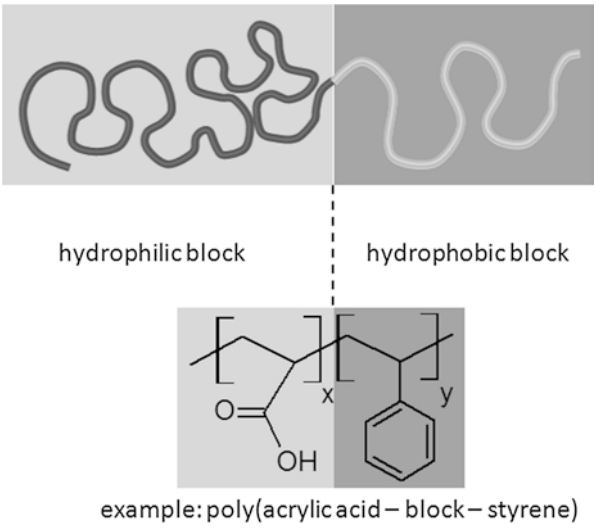

Fig. 4.13 Diagram of amphiphilic block copolymer species

Let's look more closely at the implications of each of these characteristics individually. The length of the chemical domain allows for control over the bilayer thickness, bending elasticity, curvature, and chemical functionality [47]. What is unique to polymeric materials is that the structural rigidity or elasticity of the block polymeric

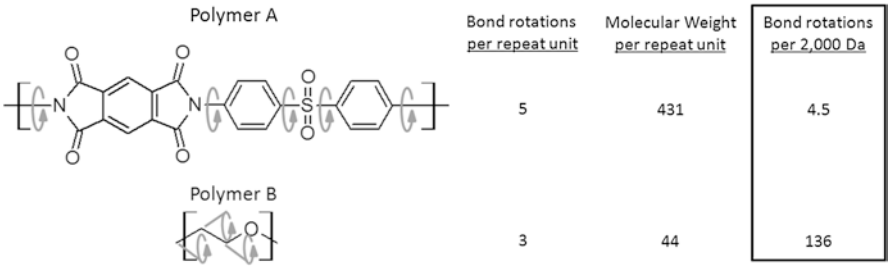

Fig. 4.14 Comparison of the flexibilities of two types of polymers by comparison of the number of bond rotations for a given molecular weight (i.e., 2,000 Da)

segments is tied directly to chemical functionality [50]. For example, polymers with a hydrocarbon-based backbone functionality will allow for a greater number of possible bond angle rotations for a given molecular weight (polymer B) than an aromatic or conjugated backbone polymer functionality (polymer A) (Fig. 4.14).

The bilayer thickness can be tied to the length, or molecular weight, of the polymer domains, which is analogous to our previous discussion of the influence of the hydrocarbon tail group length in lipid amphiphilic systems [51]. For rigid polymer systems, the length of the polymer chain will correlate almost directly to the membrane thickness. Therefore, one would expect a higher-molecular-weight, rigid polymer to have a thicker membrane with a lower degree of bending elasticity. What complicates the discussion in terms of polymeric materials is that in the case of elastic systems, the free mobility of the polymer chains results in what is known as **chain entanglement** upon reaching a critical molecular weight [52]. By "chain entanglement," we are referring to the molecular weight at which the motion of polymer chains is topologically restricted [52]. One can think of the analogy to a plate of spaghetti that has not been cut versus one that has been cut. One allows for a significantly more manageable fork full of food due to less entangled spaghetti than the other. The bilayer thickness, while considerably greater than that of lipid membranes, is more difficult to predict in cases where highly elastic polymers are used [53]. We could revisit our discussion from Chap. 2 regarding radius of gyration, which would allow for a physical estimation of the free volume of occupancy for a flexible polymer chain, as a guide for bilayer thickness. This difference in elastic chain-entangled polymer species and rigid species extends further to bending elasticity as well. Rigid systems can be estimated based on the lipid systems discussed earlier in this chapter, while elastic systems are more dependent on the degree of chain entanglement [52, 53].

We can predict the degree of mobility of a polymer chain based on the reptation model [54]. The reptation model predicts polymer mobility in a snakelike motion through the projection of a tube of length L, whereby polymer movement is restricted based on polymer chain length between points of entanglement. The tube itself will reform with the continued motion of the polymer chain past length L (Fig. 4.15).

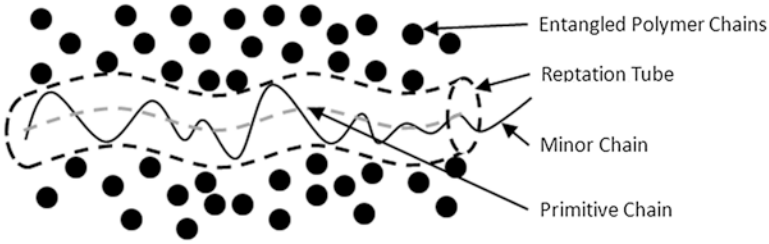

Fig. 4.15 Diagram of the reputation model for movement of a polymer chain in the bulk

The reptation model allows for the calculation of the relaxation time relative to the presence of chain entanglements for a polymer based on its molecular weight [55]:

$$t = \frac{l^2 n^3 \mu}{n_e kT}, \tag{4.15}$$

where l is the freely jointed chain length that is n **segments long**, μ is the coefficient of friction of the polymer chain, n_e is the length of the segments between each entanglement, k is Boltzmann's constant, and T is temperature. With the knowledge of relaxation time, we can gain insight into its effect on the bending elasticity of the bilayer membrane. Thinking qualitatively, we can imagine that membranes with fast relaxation times allow for a more elastic or rubbery membrane structure. This elasticity can translate to a higher bending elasticity as well. Polymers with slow relaxation times, then, would correspond to those with less elastic, more brittle, membranes that are more prone to rupture [56]. The point of rupture will depend on the degree of chain entanglement and cohesive forces within the membrane. Since this point of rupture reveals both the failure in cohesive energy and the bending elasticity, direct measures of these identifiers has been a critical tool in the design and evaluation of membrane-based assemblies.

In order to exploit the physical characteristics of effective vesicle formation, we first must assess the corresponding design features within the polymer structure. Amphiphilic systems first and foremost require compositional control [57] in order to synthesize the appropriate ratios of hydrophobic and hydrophilic regimes within the polymer structure. The lengths of the hydrophobic domains are correlated to the molecular weight and molecular weight distribution (PDI) of the polymer chain [57]. The rigidity and packing of the hydrophobic domains of the bilayer are correlated with the monomer functionality embedded within the polymer chain [58]. The compositional, molecular weight, and functional control of the polymer chain each come from the synthetic method employed in its creation.

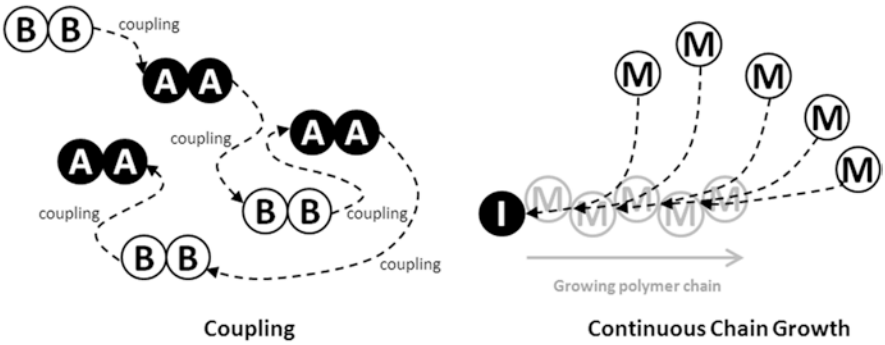

Fig. 4.16 Schematic of the mode of monomer addition for step-growth (i.e., coupling) and chain-growth polymerization methods

4.2.4 Synthesis of Amphiphilic Block Copolymers

Fine control over polymer chain length, polydispersity, composition, and topology are critical in the fabrication of stable vesicle systems [59]. The topology refers to the positioning of functional group domains within a polymer structure. Polymers typically adopt several types of topologies, such as random, block, graft, star, hyperbranched, dendrimeric, and gradient. Since our discussion is largely focused on block copolymers as the amphiphilic species, we will discuss the synthetic specificity needed to achieve the desired materials. Block copolymer species are typically synthesized by either the coupling of two distinct homopolymers at their respective end groups [60] or using a living polymerization of two monomer types added sequentially [61]. For the purposes of our discussion, we will look at the second method in more detail.

The main requirements of an effective block copolymer amphiphilic species are that there are polymerization of the desired functional monomers, predictable molecular weight of each block domain, and low polydispersity of the polymer [59]. The polymerization of the desired functional monomers is interdependent with the synthetic method chosen. Some methods that we will discuss do not allow for the polymerization of monomers with charged side chains, for example, acrylic acid (Fig. 4.16).

The predictability of the molecular weight through the ratio of monomer to initiator molecules (M:I) is critical for control over the domain length and solution behavior. Similarly, narrow polydispersities (PDI < 1.5) allow for the self-assembly of more predictable species to occur [62]. As polydispersity increases, a larger amount of low-molecular-weight material is present in the polymer melt, which can act to plasticize or soften the material. This softening will alter the expected self-assembly behavior of the material.

In order to focus our discussion in synthetic polymer chemistry, let's identify the chemical functionality of the biological materials being used and divide them into two distinct polymerization methods (Table 4.3).

Table 4.3 Common monomer types and polymerization methods used to form drug delivery materials

Monomer	Polymer	Polymerization method	Molecular weight (M_n)	Polydispersity (PDI)
ethylene glycol (EG) 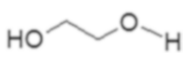	Polyethylene glycol (PEG) 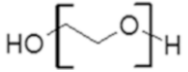	Condensation	<150,000	>2.0
hydroxyethylmethacrylate (HEMA) 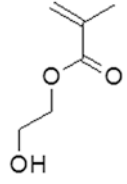	polyhydroxyethylmethacrylate p(HEMA) 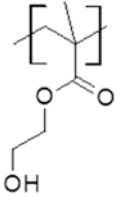	Living	<100,000	<1.2
N-carboxyanhydride (NCA) 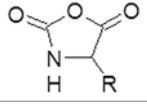	polypeptide 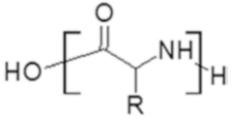	Living	<100,000	<1.3

4.2.5 Condensation Polymerization

When a bifunctional molecule bonds with other bifunctional molecules in a reaction, a condensation or step-growth polymerization has taken place [60]. Typically, these reactions involve two bifunctional monomers (A–A and B–B). If we put forth the stipulation that A–A can only react with BB, then the polymer structure would be comprised of sequences such as A–AB–BA–AB–BA–AB–BA–AB–BA–AB–BA–AB–BA–A. Some important questions become evident if we look at this method more carefully. First, what is the molecular weight of the final polymer if you have stoichiometric amounts (i.e., 1–1) of the A–A and B–B monomers? How many polymer chains will be present in this case? The answer is there would theoretically be only one polymer chain if the reaction were to run to complete (100 %) conversion of monomer to polymer and that the molecular weight would correspond to the weight of all the moles of monomers A–A and B–B added together. If only one polymer chain forms, then the polydispersity would be perfect.

4.2.5.1 Is this Outcome Possible?

The answer is no. This becomes clearer as we discuss the buildup of the molecular weight during the polymerization and the implications of the rate of this buildup. As we add A–A to B–B monomers in the system, we build up

monomer	+	monomer	= dimer
dimer	+	monomer	= trimer
dimer	+	dimer	= tetramer
dimer	+	trimer	= pentamer

This buildup yields low-molecular-weight polymers until approximately 90 % of the monomer is consumed, at which point we will assume that the statistical probability of two oligomers reacting is equivalent to that of a monomer reacting with another oligomer. When oligomers begin to react with one another, the molecular weight buildup increases exponentially (Fig. 4.17).

This plot informs us of a few key points regarding the molecular weight and the molecular weight distribution of the resulting polymeric materials. The rapid increase in molecular weight in the regime >90 % monomer conversion makes it difficult to pinpoint a specific polymer chain length [63]. This affects our ability to predict the true molecular weight of the polymer and effectively broadens the molecular weight distribution to a regime of PDI > 2.0. Since amphiphilic behavior is tightly controlled by the polymer chain lengths of the hydrophobic and hydrophilic domains, care must be taken to select a synthetic method that yields an appropriate level of control over chemical functionality and chain length distribution. A common method for more effectively predicting molecular weight in condensation systems involves the use of nonstoichiometric ratios of monomeric species.

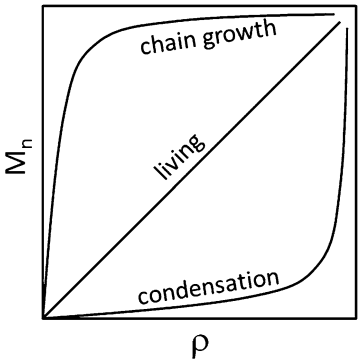

Fig. 4.17 Plot of the generation of molecular weight versus conversion using different polymerization methods

Sample Problem 4e
What is the degree of polymerization for a nonstoichiometric polymerization where the ratio of A–A to B–B is 0.9? 0.95?

Instead of a 1:1 ratio of A–A to B–B, we will try a 0.9:1 ratio. The effective prediction of nonstoichiometric condensation polymerizations can be generally predicted using the Carothers equation [64]:

$$X_n = \frac{1}{(1-p)}, \tag{4.16}$$

where p is the degree of conversion. In our example, p = 0.9, and the degree of polymerization (X_n) would therefore be 10. This means that 90 % conversion of monomers (remember 10 % will remain unreacted due to the stoichiometric imbalance) would yield only a 10-mer. Now, what if we move to 95 % conversion of monomer or a 0.95:1 ratio of A–A to B–B? The X_n would now be 20. If we move still further to 99 % conversion, the X_n would be 100. Similarly, if we move from 99.9 % to 99.99 % to 99.999 %, the conversions would be 1,000 to 10,000 to 100,000, respectively.

The Carothers equation clearly highlights a key point in the limitation of condensation polymerization as a method for synthesizing a highly controlled polymeric system in that even though nonstoichiometric ratios allow for a higher degree of polymer chain length control, the overall range of chain lengths is highly limited, and thereby the utility of the polymer as well.

For this reason, condensation polymerizations are typically used to form prepolymers or macromonomers [65], which are the basis for the addition of a second polymer domain. Condensation polymers have a few advantages over some of the

other prepared polymers we will discuss in this section. They are readily available and synthetically scalable. The chemistry and reaction variables are highly controllable and easy to translate from user to user. There is an extended base of knowledge dating back to the 1950s for many of the materials in question [60]. For applications in vesicle drug delivery, however, specific control over molecular weight, distribution, and composition supersedes those benefits and allows for the introduction of other, more powerful synthetic methods to control polymer topology.

4.2.6 Living Polymerizations

In the condensation polymerizations that we have discussed, the monomer and oligomer segments bond with one another through coupling reactions [60]. During this process, as the polymer chain is growing, the number of potential reaction sites is steadily reducing.

4.2.6.1 What if the Number of Reacting Sites Remained Constant?

In this proposed case, there would be a constant number of reaction sites that a monomer pool would steadily react to, growing polymer chains like grass, until they are fully consumed. Upon consumption, this reaction site would remain active if other monomers are added. Since the reactive chain end remains active, or "living," this method is known as a **living polymerization** [61]. Living polymerizations involve an initiating species, aptly referred to as an initiator, and a reactive monomer species. As the initiator reacts with the monomer species, an active group is generated at what is known as the propagating chain end. This active group can be a positive, negative, or radically charged species or a functionality with a high nucleophilicity. Since the active site remains reactive even after the consumption of monomer, this allows for the facile addition of another monomer. For example, to synthesize a copolymer of hydroxyethyl methacrylate (HEMA) and styrene (Sty), one would start with the polymerization of HEMA to form a poly(HEMA) with a reactive chain end and then add the Sty monomer to form a final amphiphilic copolymer of p(HEMA-block-Sty). In this particular case, the reaction could also be run in the reverse order, with the addition of Sty first, followed by HEMA.

Living polymerizations benefit from the ability for the continuous addition of monomers to active polymer chain ends due to the absence of two significant side reactions: termination and transfer [61, 63]. Termination is defined as the elimination of active chain ends through reactions such as coupling or disproportionation (Fig. 4.18).

Once a polymer chain is terminated, several things can occur [66]. If you eliminate the presence of active sites, then the ratio of unreacted monomer to active sites increases, which will yield higher than predicted molecular weights. This deviation of molecular weights from theoretical values also results in the broadening of the

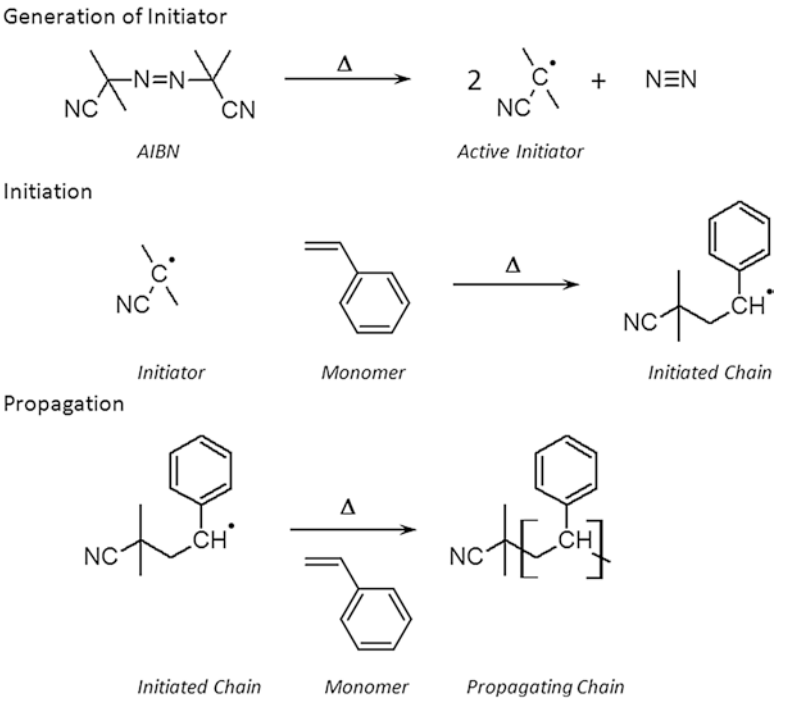

Fig. 4.18 Schematic of the reactions involved in chain polymerizations

molecular weight distribution (PDI). Transfer is defined as the exchange of active species with another molecule within the reaction mixture (i.e., solvent) [66]. The transfer of active species does not increase the number of active sites, but instead slows the reaction kinetics of the polymerization and lowers the molecular weight relative to the theoretical value. Alternate methods, known as controlled polymerizations, exist that control the rates of these two side reactions by reducing the rate kinetics of the interaction between the generation of active sites and the propagation of monomer molecules. This rate reduction is typically done using a capping species to allow for the polymer to lie in a dormant state for a period between monomer propagations [67]. The addition of capping species is simply a balance in reactions, whereby the reversible reactivity of the capping species is greater than that of the monomer addition. Therefore, in the absence of monomer, the polymer chain will appear dormant; however, upon addition of monomer, the chain will begin to propagate once again until the consumption of monomer is complete. Widely used vinyl monomer-based systems that exploit this behavior for controlled polymerizations include atom transfer radical polymerization (ATRP) [68], reversible addition-fragmentation chain transfer (RAFT) [69], and nitroxide-mediated polymerization (NMP) [70].

The key drawback of living polymerizations lies with the monomer selection pool, which falls largely within the regime of vinyl monomers or ring species. The stipulation can be generalized to molecules that are exoentropic, favoring bond

breaking upon the introduction of an instigating molecule, and have few possible side reactions. Chemists can think of this in terms of -ene or -yne species or cyclic molecules that contain a high degree of ring strain. We will look more closely at the resulting polymers from these systems later in this section.

Let's now revisit the critical criterion of lipid structure and its function in terms of vesicle formation and stability. We recall that the criterion for the selection of tail-group species was dependent on the free volume the tail groups occupy (i.e., one vs. two groups per lipid molecule) [33], the thickness of the bilayer (i.e., the hydrocarbon tail length) [34], and the bending elasticity or tail group rigidity (i.e., the degree of saturation of the tail group hydrocarbons) [35]. In terms of free volume, the hydrophobic domain of the polymer amphiphile is correlated to the radius of gyration (R_g) discussed in Chap. 3, whereby the molecular motion of the polymer chain is represented by a spherical volume signifying the potential chain movements in three-dimensional space. We can see that R_g is dependent on both the molecular weight of the polymer chain and the chemical functionality's solvation in its environment [71]. This provides us with two polymer properties that we can adjust. The analogy of hydrocarbon tail length in the case of polymers would simply be the molecular weight of the hydrophobic domain. The longer the domain, the higher the hydrophobic contribution to the overall membrane thickness [72]. As we mentioned earlier in this section, the rigidity of the polymer chain can increase the thickness as well while providing a method for reducing the bending elasticity of the vesicle membrane.

We can also recall the criterion for the selection of head-group species as dependent on charge [39], sterics [42], and physiological functionality [43]. Electrostatic charge can easily be introduced into the hydrophilic domain of a polymer molecule. It is worth noting, however, that the synthetic route to polymerization may require altering to accommodate a charged species. For example, if one wished to polymerize a polyacrylic acid block domain using ATRP, one would first have to polymerize tert-butyl acrylate and then deprotect the tert-butyl group in order to yield the acrylic acid. In the case of sterics, we can apply the same principle of radius of gyration that we discussed in the case of the tail group, whereby the molecular weight and chemical functionality play a role in determining the free volume occupied by the hydrophilic polymer domain [73].

The last principle we will revisit in our discussion of self-assembly is CMC. We discussed earlier in this chapter that the lipid vesicle stability was compromised by a combination of the relatively narrow bilayer thickness and poor cohesive properties of the hydrophobic domains relative to the physical stresses typically encountered in physiological environments. For reference [74], typical CMC values for lipid vesicles fall in the 10^{-2}–10^{-3}-mg/ml range, while values for polymer vesicles can reach as low as the 10^{-6}–10^{-8}-mg/ml range. From our discussion, we can propose that the balance among the bilayer thickness, curvature, and polymer entanglement provides key design criteria to create a bilayer with an adequate cohesive strength to maintain its self-assembled structure in the presence of physiological obstacles. In Sect. 4.3, we will discuss three systems that exploit these self-assembly design criteria and highlight the potential benefits and drawbacks of each (Table 4.4).

Table 4.4 Common amphiphilic block copolymer systems and their self-assemblies

Copolymer amphiphile	Structure	Self-assembly	Vesicle formation
Polyethylene oxide Polybutadiene	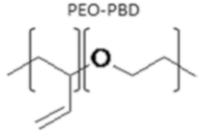	Vesicles	Aqueous
Polyacrylic acid polystyrene	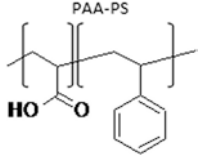	Vesicles	Cosolvent
Poly-(styrene-block-(isocyano-L-alanine-L-alanine)	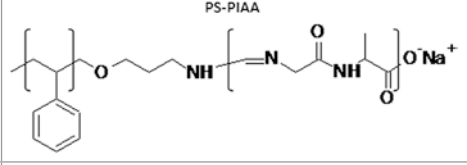	Vesicles and rods	Acidic
Poly(L-lysine-block-L-leucine)	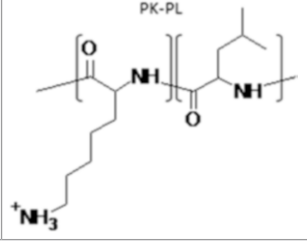	Vesicles	Cosolvent

Poly(oxyethylene-block-4-vinyl pyridine)	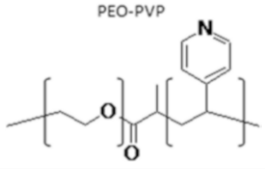	Vesicles Ellipsoid aggregates Vesicles	pH 1–3 pH 3–11 pH 11–14
Poly(oxyethylene-block-methyl phenyl silane	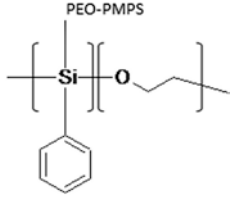	Vesicles	Aqueous
Poly(oxyethylene-block-propylene-block-oxyethylene)	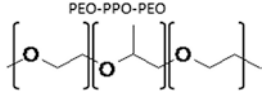	Vesicles	Aqueous
Poly(hydroxyethylmethacrylate-block-*n-butylmethacrylate*)	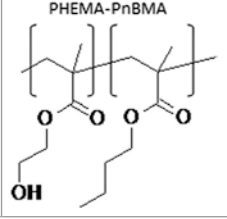	Vesicles	Cosolvent

4.3 Implementation

4.3.1 Micelles, Vesicles, and Membranes

4.3.1.1 Tubular or Wormlike Micelles

One common drug delivery system typically used to evade physiological detection is known as a stealth vesicle [75], which has a spherical geometry composed of an outer surface of PEG molecules. The PEG allows for an increased residence time within the body before expulsion or interaction with physiological molecules. While these spherical systems have shown great promise in the field of drug delivery, they are prone to interaction with cells both in the presence of flow and under static conditions. This limitation has led researchers to revisit biomimetic approaches such as the one taken by *filamentous viruses* using what is known as *tubular micelles*. The term **tubular, or wormlike, micelle** [76] refers to micellar aggregates with a persistence length greater than that of a typical spherical system. These assemblies resemble a range of materials from rigid fibers (i.e., matchsticks) to bendable cylinders (i.e., worms). For drug delivery systems, the critical advantage proposed for tubular systems is their behavior in response to flow. The route a drug takes in order to reach a target tissue typically involves flow through an elaborate network of vascular tubes. If cellular interaction is nonspecific under static or flow conditions, much of the drug introduced will become prematurely taken up by cells along their route. Tubular systems hold a proposed advantage over spherical systems in that they become elongated with flow, minimizing interactions between cells they encountered in the process. Upon gradually reaching a target region, the tubular micelle will begin to constrict its movement, resembling more of a spherical assembly and become taken up by the cell.

The Discher group [17] has identified such a block copolymer system composed of a PEG outer hydrophilic block and either a polyethylethylene (PEE) or polycaprolactone (PCL) biodegradable hydrophobic block, referred to as **filomicelles** (Fig. 4.19).

Copolymer compositions were chosen such that the molecular weights of the respective hydrophobic and hydrophilic domains were nearly equivalent. In the case of equivalent molecular weights, the solvated radius of gyration of the hydrophilic domain will be greater than that of the hydrophobic domain. Geometrically, this is known [2] to lead to the formation of cylindrical-shaped assemblies (i.e., tubes). The length of the tubes can be fabricated based on storage time and response to flow.

The Discher group began their assessment of self-assembled behavior by observing the circulation lifetime of filomicelle systems of different persistence lengths in rats and mice and compared them to a control spherical stealth vesicle system. The circulation times for these filomicellar species appear to persist through a 4-day period before reduction starts to occur, as opposed to the stealth polymersome systems, where reduction occurs instantly, followed by full consumption in 3 days. The effect of tube length was further evaluated by degradation of the tube length to 18,

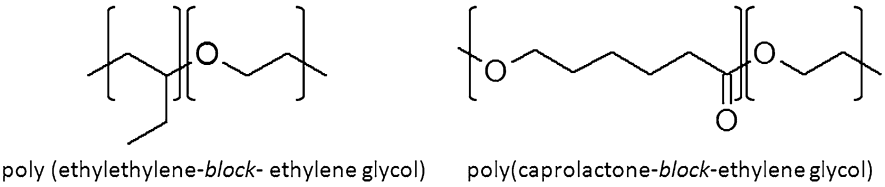

Fig. 4.19 Structures for tubular vesicle forming amphiphilic block copolymers [17]

8, 4, and 2 μm. As the tube length decreased, the circulation profile was shown to approach that of the spherical stealth vesicle species. Furthermore, filomicelles showed persistent circulation for up to 1 week compared with spherical systems that remain for 1–2 days (Fig. 4.20).

Based on the work of Geng et al. [17], it is clear that there is a reduction in filomicelle size with increasing residence time. Why? We discussed in Sect. 4.1 that two critical properties affecting stability in self-assembled species are molecular shape and rigidity. If we apply our discussion from Sect. 4.1 to this work, we encounter a system that maintains a high allowance for cross-sectional curvature of the tube species (d_o) and some degree of curvature allowance laterally through the tube length (L), as evidenced by the undulating shape (Fig. 1a [17]). In spherical systems, the cross-sectional curvature is the only relevant curvature of the self-assembled species. In tubular species, however, the lateral elongation provides an added curvature element that can destabilize the assembly. Simply upon observation, one could contend that the bending energy remains in a stable state cross-sectionally but falls closer to a metastable state laterally, contributing to the size reduction of the tubes with increasing circulation times. The rate at which this size reduction occurs appears correlated to the initial tube length, designated as L by the authors. This poses an interesting design question:

4.3.1.2 Are There Upstream Limitations in the Size of a Tubular Assembly, and if so, What Are They?

Should the circulation time be correlated to tube length, then both the target tissue and mode of application will be directly affected by the chosen length. It appears from the work on this specific system that the circulation time of increasing tube lengths approaching 8 μm begins to plateau, yielding a circulation range of 4.7 days. This is a broad enough circulation range to be relevant for applications involving a number of target organs such as the spleen, liver, kidney, brain, lungs, gastrointestinal tract, and colon. The authors evaluated two tube lengths in four target organs (liver, spleen, lung, kidney), which showed a few general trends. The longer tube lengths showed higher amounts within the tissue, and these amounts appeared more dramatic in the liver and spleen relative to baseline levels (Fig. 4.21).

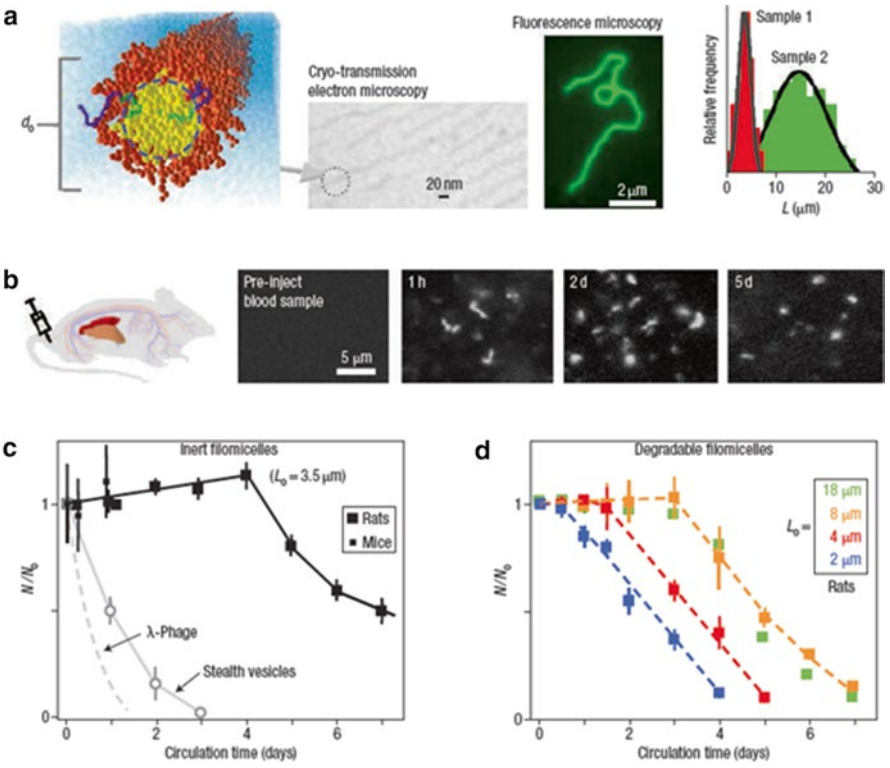

Fig. 4.20 Filomicelles and their persistent circulation. (**a**) Filomicelles are self-assembled from di-block copolymers: *Yellow/green* in cross section indicates hydrophobic polymer, orange/blue is hydrophilic, and aqua is water. Electron microscopy demonstrates the nanometer-scale diameter of the filomicelles, and fluorescence microscopy shows a single filomicelle. Distributions of filomicelle length are shown for two samples. (**b**) Injection of fluorescent filomicelles into rodents, followed by fluorescent imaging of blood samples showed that filomicelles circulated in vivo for up to 1 week. (**c**) Relative numbers of filomicelles in the circulation show that inert filomicelles (of OE70) persist when compared with stealth polymersomes12 and l-phage16. (**d**) Degradable filomicelles (of OCL3) also persist, and filomicelles with longer initial lengths (L_0) circulate longer up to a limiting length. The error bars in (**c**, **d**) show the standard deviation for four or more animals [17]

This system was further evaluated for the effect of tube length on the interaction of these materials with macrophages. Consistent with the persistent circulation behavior of the tubular systems in rats and mice, those systems showed an interaction with macrophages that was inversely correlated to the length of the tubular species (Fig. 4.22).

The application of this tubular micelle system to encapsulate and deliver the cancer treatment paclitaxel (TAX) was performed with different rates of drug as well as different tube lengths. In the 1-week incubation period, the short and long tube lengths showed an approximate 40–50 % reduction in tumor size relative to an equivalent dosage of the native drug. Perhaps even more remarkable, an increase in

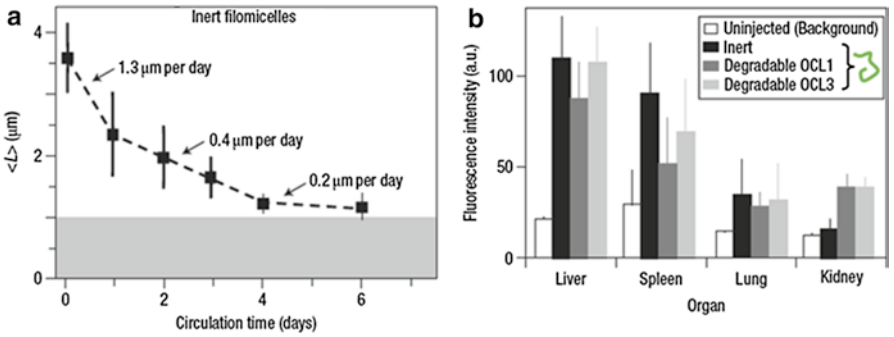

Fig. 4.21 Kinetics of filomicelle length reduction in vivo. (**a**) Inert filomicelles shorten, with the rate of shortening decreasing as they shorten. The *gray region* represents the optical limit of *L* measurements. (**b**) Degradable filomicelles (OCL3) shorten at a rate that depends on initial length. The *inset* plots the length-dependent shrinkage rate. All error bars show the standard deviation for three or more animals. (Adapted from Geng, Y., Dalhaimer, P., Cai, S., et al. *Nature Nanotechnology*, 2(4):249–255, 2004.) [17]

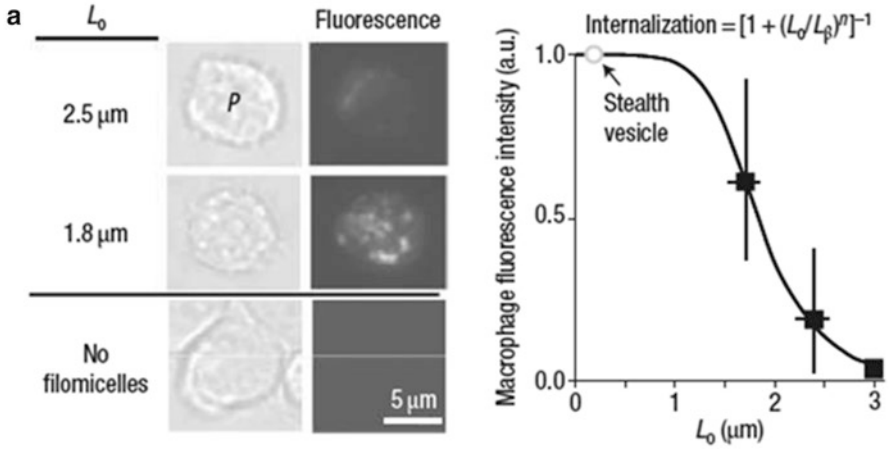

Fig. 4.22 In vitro interactions between filomicelles and phagocytes (P). Fluorescent filomicelles of varying contour length were incubated with activated macrophages for 24 h in static culture. The fluorescence intensity of cells is proportional to the phagocytosis of filomicelles and proves to be a strong function of L_0. The Hill exponent, $n = 6$, suggests strongly cooperative binding along the length of the cylinder to the cell surface. $L_b = 1.9$ mm. The error bars in the *right-hand* plot show the standard deviation [17]

dosage coupled with the long tube length reduced tumor to below the initial size. We can clearly see the implications of rationally designed geometries of self-assembled species and their effects on drug delivery.

The Discher lab [17] has designed a unique self-assembled species where the drug delivery vessel is uniquely positioned to be internalized by the cell in a

controlled mode under flow. This flow is largely encountered in the circulatory pathways of physiological systems. The control is designated by the copolymer compositions (i.e., ~1:1 of hydrophilic to hydrophobic molecular weights) necessary to fall within the geometric constraint of a tubular self-assembled system of a tailored tube length (2–8 μm). The tube length is itself tailored to achieve the desired delivery time before the length scale is reduced, allowing for cell internalization under a similar mode to a spherical stealth polymersome. We can envision extensions of this seminal work to include cell targeting (Chap. 5) and hybrid materials (Chap. 8) to enhance the potential application and efficiency of the tubular micelle system (Fig. 4.23).

4.3.2 Double Emulsions

Until this point we have discussed amphiphilic copolymer materials as a means of stabilizing aggregate or bilayer formation within an aqueous continuous phase. Generally, we now understand that the self-assembly behavior occurs as a means of minimizing the free energy of the system as a response of the hydrophobic and hydrophilic domains to their continuous aqueous environment [4]. An interesting extension of this behavior presents itself with significant implications in drug delivery.

4.3.2.1 What if We Introduce Amphiphilic Species to a Two-Phase System of Oil in Water?

The stabilization of a closed bilayer species containing two phases provides a mode of delivering both hydrophilic (i.e., in water) and hydrophobic (i.e., in oil) drug cargos simultaneously within one species. In order for this to occur, the amphiphilic species would have to be able to stabilize both a water–oil interface with a positive curvature ($C^o > 0$) and an oil–water interface with a negative curvature ($C^o < 0$) (Fig. 4.24).

Therefore, a single amphiphilic polymer system would have to be able to stabilize both a negative and positive curvature interface within the same assembly species.

4.3.2.2 How Is this Possible?

Let's start by looking more closely at the double-emulsion system, commonly referred to as the water–oil–water emulsion (w/o/w) [77]. As opposed to vesicle systems in a continuous aqueous phase, which are stabilized by an amphiphilic bilayer, the interfaces of the w/o/w emulsion system are stabilized by monolayers. This is because each polymer domain (hydrophilic or hydrophobic) can occupy a state with a freely extended chain while at the interface between water and oil

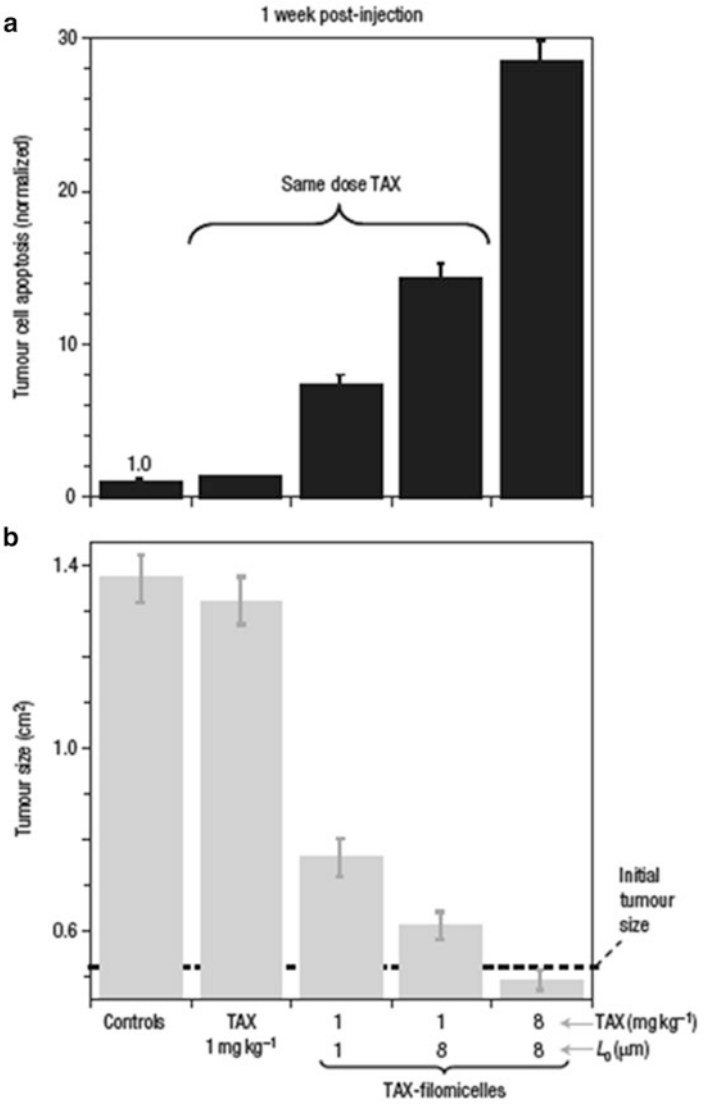

Fig. 4.23 Filomicelles mediate paclitaxel (TAX) delivery to rapidly growing tumor xenografts on nude mice. Tumor-bearing mice were injected with either saline or OCL3 filomicelles as controls, TAX as free drug in ethanol (1 mg/kg 21 is its maximum tolerated dose), or TAX loaded at two doses into the hydrophobic cores of filomicelles of two lengths. (**a**) Apoptosis was measured 1 week later by quantitative imaging of TUNEL-stained tumor sections and shows little effect of free drug but increasing cell death with increasing L_0 and increasing paclitaxel dose. (**b**) Tumor size decreases with increasing apoptosis, with tumor shrinkage clear for the longest filomicelles at the highest TAX dose. All data show the average from four mice. The error bars show the standard deviation [17]

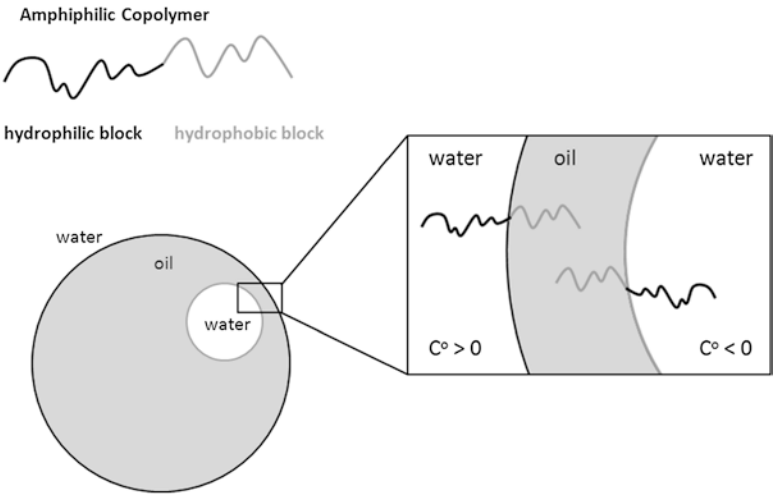

Fig. 4.24 Diagram of the oil–water and water–oil interfaces in double-emulsion systems

phases. In an only aqueous system, one polymer domain (i.e., hydrophobic) is in an unfavorable solvent; therefore, its domain remains in either a collapsed state (i.e., micelle) or self-assembles into a bilayer (i.e., vesicle) to form a boundary to the aqueous continuous phase.

If the w/o/w interfaces are therefore monolayers, then how do w/o/w monolayers maintain enough thickness to retain curvature and shape?

Much of this stabilization is tied to cohesion within the monolayer, which corresponds to molecular weight and chemical functionality [78]. We remember that higher-molecular-weight species allow for a higher degree of polymer chain entanglement [52–54]. When polymers are aligned in a monolayer, they maintain a proximity to one another, which permits entanglement of polymer chains should they be long enough. This proximity can also permit reactivity or associative forces such as hydrogen bonding or electrostatic charge coupling [79]. In this case, the term for bending energy (e_{bend}) could be applied to the thickness of the entangled or interacting polymer species within each phase of the interface. Since e_{bend} is directly proportional to the cube of the interfacial thickness, the degree of interaction or entanglement would increase the thickness component, therefore increasing the bending energy of the system.

It is important to note that there is a component that has largely been ignored to this point, and that is the molecular weight distribution of the copolymer species. A broad molecular weight distribution indicates that there is a disproportionate amount of low-molecular-weight species in solution with high-molecular-weight species. As self-assembly occurs, molecular weights could selectively partition between positive- and negative-curvature interfaces to yield a stable w/o/w emulsion.

This interaction, however, is disfavored for several reasons [80]. One reason is that this would have to occur during the initial self-assembly provided it is an extremely slow process [80], to allow for the amphiphilic copolymer to migrate in a solvated form to reach the interface. If too high a concentration of amphiphiles exists in any one region, the amphiphiles will self-assemble into aggregates or micelles to minimize their free energy in what they are perceiving is a homogeneous solvent. Once an aggregate forms, an energy source is typically required to break those aggregates to allow for reformation at a respective interface. Another reason is that, upon formation of a w/o/w emulsion, it is highly unlikely that low molecular weights would selectively rearrange from one interface to another due to the aggregation effect described in this section [80]. Double-emulsion systems present a number of challenges for stable self-assembly; however, researchers are beginning to develop design strategies to adopt these structures as viable drug delivery systems.

The Deming group [81] has identified a w/o/w double-emulsion system that is comprised of an amphiphilic copolymer system of poly(L-lysine-*block*-rac-leucine) [K_x(rac-L)$_y$], where the hydrophilic domain is a cationic lysine species and the hydrophobic domain is an uncharged leucine species. In this work, Hanson et al. [81] report the use of a handheld homogenizer with K_x(rac-L)$_y$ in the presence of silicon oil–water mixtures (Fig. 4.25).

Deming's group began their investigation with a system comprised of a K_x(L)$_y$ copolypeptide amphiphile under a series of compositions. This copolymer is known [82] to adopt a random coil for lysine and an α-helix for leucine in aqueous solution by circular dichroism (CD). The K_x(L)$_y$ copolypeptide system, when homogenized within a silicon oil–water mixture, yielded a stabilized dispersion of oil droplets ranging in size from 50–350 nm. The specific composition of copolypeptide used (i.e., $K_{60}L_{20}$) has been shown previously [83] to form stable nanoscale vesicles in aqueous media. It is important to note that polypeptide-based materials form intramolecular hydrogen bonds within their polymer backbones to allow for the formation of secondary structures, such as α-helices [84] and β-sheets [84]. The formation of these secondary structures adds a significant degree of rigidity to the hydrophobic domain of a self-assembled species. This rigidity is very different than traditional amphiphilic polymer systems, replacing random entanglement with sometimes highly ordered hydrogen bonding interactions. The authors sought to remove the rigidity of the α-helical domain while retaining the hydrogen bonding interactions by simply polymerizing a racemic mixture of the D- and L-handed leucine amino acids, resulting in a random coil. If we turn our attention to our previous discussion surrounding lipid amphiphiles, this would be a loose analogy to the differences encountered between saturated and unsaturated hydrocarbon tails. In both cases, the theoretical packing density changes, which has direct implications on the geometric packing parameter discussed in Sect. 4.1 [Eq. (4.5)]. As the K_x(rac-L)$_y$ copolypeptide was homogenized with the silicon oil–water mixture, a few trends emerged. Unlike the K_xL_y systems, which were unable to stabilize oil and water droplets, the K_x(rac-L)$_y$ system formed a stable w/o/w emulsion where the aqueous continuous phase was retained, yielding no phase inversion between water and oil (Fig. 4.26).

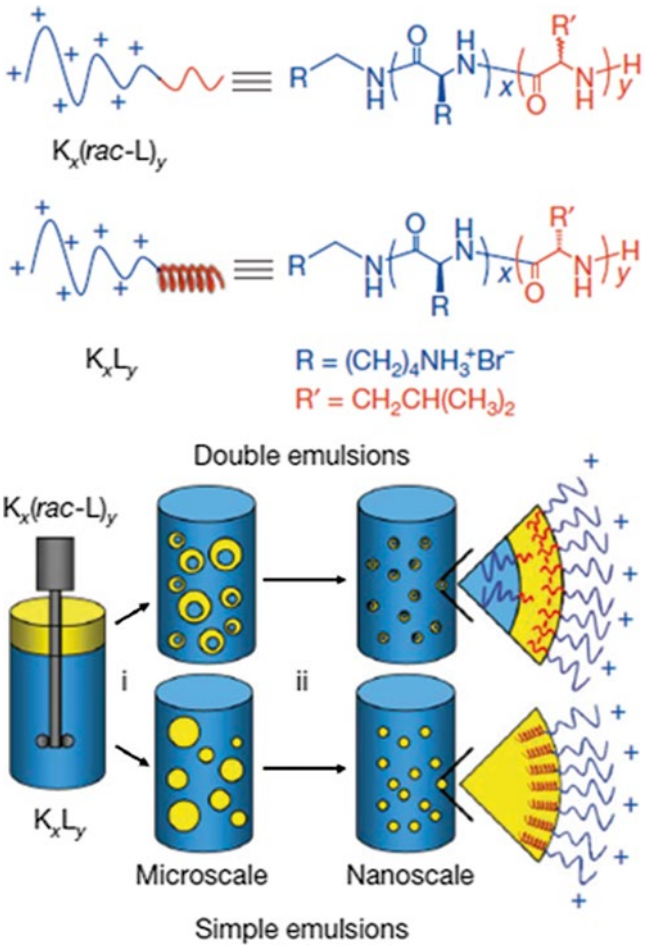

Fig. 4.25 Structures of block copolypeptide surfactants and emulsification procedure. (**a**) $K_x(rac\text{-}L)_y$. (**b**) K_xL_y. (c) Emulsification procedure used to generate both simple and double emulsions. Step (1), ultrasonic or handheld homogenization; step (2), microfluidic homogenization. *Yellow* represents the oil phase, *blue* the aqueous phase containing block copolypeptide surfactant [81]

The size of the droplets increased with decreasing hydrophobic content, signifying a correlation between composition and interfacial curvature. Also, as the concentration of $K_x(rac\text{-}L)_y$ copolypeptide and droplet size were shown to be inversely related, highlighting the need for the copolypeptide to stabilize the interfacial surface. In the absence of stabilizing copolypeptide, the surface area reduces, causing the increase in droplet size. These were able to stabilize a composition of $K_{40}(rac\text{-}L)_{20}$ w/o/w double emulsions in the size regime of 30–250 nm.

A simple centrifugation yielded a more homogeneous size range of 30–100 nm, a domain size previously unreached for w/o/w systems. Perhaps even more impressive,

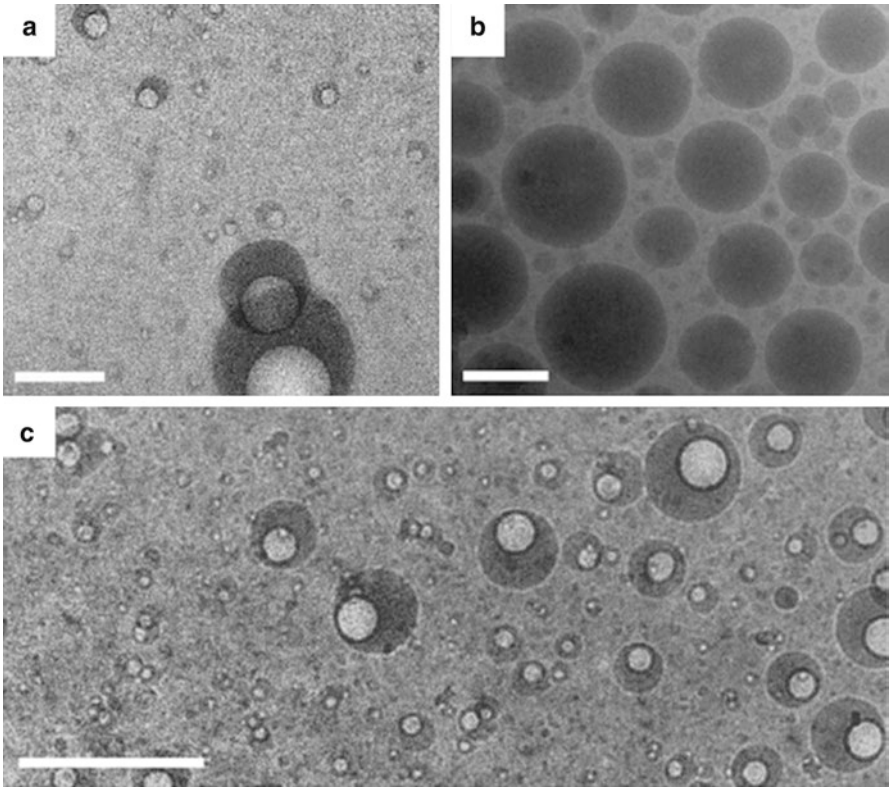

Fig. 4.26 Cryogenic transmission electron microscopy of copolypeptide-stabilized emulsions prepared using a microfluidic homogenizer. Vitrified water gives a light background and silicone oil appears dark and provides contrast. Emulsions prepared under the following conditions: number of passes $N=56$, homogenizer inlet air pressure $P=5{,}130$ psi, block copolypeptide concentration $C=51.0$ mM, and oil volume fraction $w=50.20$. (**a**) Image of a w/o/w double emulsion stabilized by $K_{40}(\text{rac-L})_{20}$. (**b**) Image of a single oil-in-water emulsion stabilized by $K_{60}L_{20}$. (**c**) Image of size-fractionated droplets isolated from a $K_{40}(\text{rac-L})_{20}$-stabilized double emulsion by low-speed centrifugation followed by ultracentrifugation. All scale bars, 200 nm [81]

the w/o/w emulsions in this size regime remained stable for 9 months without ripening or changing in size.

Finally, the Deming lab loaded the w/o/w droplets with fluorescent hydrophilic (i.e., pyrene) and hydrophobic (i.e., InGaP quantum dots) cargo to determine the feasibility as a drug delivery system. The $K_{40}(\text{rac-L})_{20}$ w/o/w double-emulsion system clearly indicates a compartmental partitioning of encapsulated species within both the water and oil phases (Fig. 4.27).

The Deming lab [81] has designed an elegant system that is feasible to fabricate on a large scale and demonstrates a high degree of control over self-assembly size, surface functionality, and encapsulation of cargo. The Deming lab also demonstrated

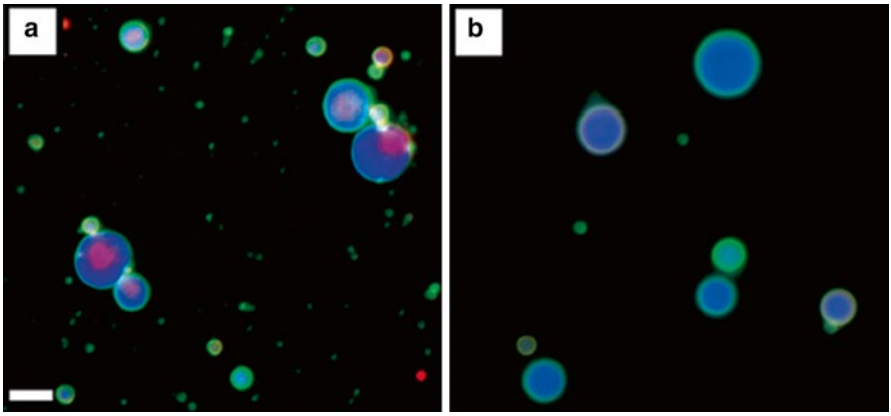

Fig. 4.27 Fluorescence micrographs of double emulsions containing polar and nonpolar cargos. Samples were prepared using an ultrasonic homogenizer (10 s at 35 % power) with $w = 50.2$ and $C = 50.1$ mM. The oil phase fluoresces blue because of entrapped pyrene (0.01 M), and the internal aqueous phase fluoresces red because of the encapsulation of InGaP quantum dots (2 mM). The polypeptides are labeled with fluorescein isothiocyanate (FITC) and therefore fluoresce green. Before imaging, the droplets were dialyzed against and subsequently diluted with pure water to remove red fluorescence from the external phase (see Supplementary Information). (**a**) Double emulsion stabilized by FITC-labeled K_{40}(rac-L)$_{10}$, loaded with both pyrene and quantum dots. (**b**) Single emulsion stabilized by FITC-labeled $K_{60}L_{20}$, loaded with both pyrene and quantum dots. Scale bars, 5 mm [81]

the versatility of the system by using a different polyelectrolyte peptide group for the water-soluble layer (i.e., guanidinium, glutamate). This system provides an effective foundation for the delivery of multicomponent treatments within a single delivery species. The natural extension of this work into the field of cancer therapeutics would be an exciting synergy between materials science and medicine.

We will look at another system of this type in Chap. 5, focused on the targeting of specific tissue types with self-assembled species. The versatility of the surface functionality of each system described in this section provides a useful starting point for the engineer in designing effective systems for use in physiological environments.

4.3.3 Summary

The encapsulation of drug species within self-emulsifying materials offers a foundation for the delivery for a broad range of drugs within a significant reduction in their interaction with physiological environments. In Sect. 4.1 of this chapter, we focused on a basic overview of the *thermodynamic*, *geometric*, and *energetic* elements critical to the self-assembly process. These elements helped to shape a

Table 4.5 Common scientific disciplines tied to critical fundamentals in self-emulsifying drug delivery systems

Fundamental	Disciplines
Membrane energetics	• Soft matter physics • Materials engineering • Chemistry
Tertiary-quaternary formation	• Biochemistry • Protein chemistry • Enzymatics • Chemistry
Thermodynamics of self-assembly	• Chemistry • Physics • Chemical engineering • Materials engineering
Polymer synthesis	• Chemistry • Materials engineering • Catalysis
Modeling of morphologies	• Chemical engineering • Materials engineering
Rupture and shear mechanics	• Polymer rheology • Polymer physics • Materials engineering
Dispersion stability	• Chemistry • Physics • Chemical engineering • Materials engineering
Cell internalization	• Cell biology • Molecular biology • Biophysics

picture of the forces involved in the stabilization and destabilization of *condensed phases* and *bilayers* commonly used in the encapsulation of drug species. In Sect. 4.2, we applied these self-assembly elements to *amphiphilic* systems (i.e., lipid and copolymer) in an effort to create a robust spectrum of self-assembled shapes for a range of drug delivery applications. Finally, in Sect. 4.3, we described two unique self-assembled systems currently in development for clinical use today. The first was a tubular micelle system, which exploits its aspect ratio in order to improve its interfacial interaction under vascular flow. The second was a peptide surfactant system capable of stabilizing two interfaces within the same nested self-assembled structure to allow for both hydrophilic and hydrophobic drug encapsulation. In the remaining chapters of this text, we will see methods for enhancing the delivery of these encapsulated species through the incorporation of targeting, stimuli-responsiveness, and hybridization (Table 4.5).

4.4 Clinical Applications

4.4.1 Self-Assembled Micelles for Cancer

This chapter has discussed self-assembling amphiphilic materials such as micelles for drug delivery. Such materials can be particularly powerful for the treatment of cancers. In this clinical applications section, we focus on clinical applications of self-assembled micelles for cancer treatment. In particular, polymeric micelles in the diameter range of 10–100 nm have the ability to solubilize hydrophobic chemotherapeutic molecules and carry the therapeutics specifically to solid tumors. Such nanoscale carriers take advantage of the "enhanced permeability and retention" effect. This effect is based on the unique pathophysiological characteristics of solid tumor tissues. Cancerous tumors are hypervascular with incomplete, leaky vascular tissue. In addition, tumors secrete vascular permeability factors that stimulate extravasation within cancer tissue. The enhanced permeability of the tumor vasculature allows bloodborne nanoscale drug carriers to penetrate into the tumor mass. Malignant tumors are characterized not only by increased permeability, but also by increased retention; tumors lack an effective lymphatic drainage system and cannot rapidly clear macromolecules from the tissues. As a result, nanosized polymeric micelles are retained within the tumor mass and release the chemotherapeutic drug. As micelles accumulate within the tumor mass, a high local concentration of chemotherapeutic drug is achieved. In contrast to tumor blood vessels, normal blood vessels are not leaky; micelles within the diameter range 10–100 nm cannot permeate normal vessel walls. Thus, micelles preferentially migrate to tumor tissue and accumulate within the target tissue, by virtue of the micelle size and the tumor architecture; this phenomenon is also known as "passive targeting" of cancerous tissue. Because nanosized micelles exploit the enhanced permeability and retention of tumors, they have several advantages compared to conventional chemotherapy. Advantages of nanotherapeutics for cancer therapy include improved antitumor efficacy, reduced toxicity to healthy tissues, reduced side effects, prolonged blood circulation times, and higher capacity to deliver a drug payload.

The properties of polymeric micelles are particular well suited for cancer therapy. Most anticancer drugs are inherently water-insoluble as a result of their lipophilic nature. When a lipophilic drug is encapsulated within the hydrophobic core of a micelle, there is a significant increase in the apparent solubility of the drug in aqueous environments. For example, the water solubility of the anticancer agent paclitaxel can be increased by several orders of magnitude, from 0.0015 to 2 mg/ml through micelle incorporation [85]. Micellar carriers therefore permit the clinical use of drugs that would otherwise be too hydrophobic or toxic. Further, micellar encapsulation does not require manipulation of the chemical structure of the therapeutic drug. The polymer core of the micelle also increases drug stability, by shielding the drug from enzymatic degradation and inactivation [86]. The critical micelle concentration (CMC, the concentration threshold of polymers at which micelles are formed) is very low for polymeric micelles, typically on the order of 10^{-6}–10^{-7} M;

polymeric micelles are stable constructs that do not readily dissociate in physiological environments [87].

Overall, polymeric micelles are uniquely well matched for cancer drug delivery applications, providing a natural carrier environment for anticancer drugs. Micellar carriers have been developed for at least three major chemotherapeutic drugs: doxorubicin, paclitaxel, and cisplatin. Doxorubicin is a hydrophobic anticancer agent and is currently an important part of treatment regimens for leukemia, breast cancer, bone cancer, lung cancer, and brain cancer. Two different polymer micelle formulations have been created for doxorubicin delivery. The first system utilizes Pluronic® copolymer, a tertiary copolymer of PEG and poly(propylene oxide) (PPO) oriented in a PEG–PPO–PEG configuration. During micelle formation, the hydrophobic PPO segments form the core, while the PEG segments form the corona. The doxorubicin-loaded Pluronic® micelles are also known as the SP1049C formulation [88]. The second system for doxorubicin encapsulation is constructed from a copolymer of PEG and doxorubicin-conjugated poly(aspartic acid). This system is also known as the NK911 formulation [89].

Table 4.6 compares the clinical pharmacokinetics of free doxorubicin to those of both micellar doxorubicin delivery systems. This comparison reveals several important advantages of micellar formulations. Free doxorubicin has an elimination phase half-life ($t_{1/2,}\beta$), or physiological excretion half-life, of 48 min. In contrast, both polymer micelle formulations roughly triple the half-life, to a range of 2.3–2.8 h. The drug clearance rates (C_L) further highlight important pharmacological differences. The clearance rate of free doxorubicin is 14.4 ± 5.6 ml/(min kg). Doxorubicin encapsulation within PEG-polyaspartate micelles reduces the clearance rate to 6.7 ± 1.1 ml/(min kg), almost half that of free doxorubicin. Pluronic® micelles have a less marked effect on the clearance rate, possibly due to the low stability of Pluronic® micelles [90]. Both micellar systems increase the maximum tolerated dose (MTD) of doxorubicin in patients. Taken together, these clinical data indicate the distinct benefits of micelle-delivered drugs over free chemotherapeutic drugs. Each of the doxorubicin-loaded micelle systems exhibit improved half-lives, slower clearance rates, higher maximum tolerated doses, and increased area under plasma concentration (AUC) values over nonencapsulated doxorubicin.

Paclitaxel is another potent anticancer drug that is utilized in treatment regimens for both non-small cell lung cancer and small cell lung cancer; it is also a useful agent for breast cancer, ovarian cancer, and head and neck cancers. However, paclitaxel is hydrophobic, with a very low water solubility (1.5 μg/ml), and the drug already requires administration with a surfactant called Cremophor® EL, which is a PEG-modified castor oil. Moreover, paclitaxel causes serious adverse effects, including neurotoxicity and neutropenia. There are no effective methods for preventing or reducing the nerve damage associated with paclitaxel, so that neurotoxicity constitutes a significant dose-limiting toxicity of the drug. In addition, paclitaxel is associated with severe hypersensitive reactions and anaphylaxis in 2–4 % of patients receiving the drug, even when patients are premedicated with antiallergic agents. These adverse reactions have been attributed to the mixture of Cremophor® EL surfactant and ethanol currently used for solubilizing paclitaxel.

Table 4.6 Comparison of clinical pharmacokinetics for free doxorubicin and micellar doxorubicin delivery systems

Formulation	Free doxorubicin[a]	SP1094C[b]	NK911[c]
Carrier	Doxorubicin-hydrochloride in 0.9 % NaCl	Pluronic® micelles, mixture of L61 and F127	PEG (5,000 MW)-pAsp (30 units) conjugated with doxorubicin
Diameter (nm)	–	22–27	40
Number of patients	8	26	23
$t_{1/2,}\alpha$ (min), distributional half-life	2.4 ± 0.9	6.0 ± 2.7	7.5 ± 0.7
$t_{1/2,}\beta$ (h), apparent elimination half-life	0.8 ± 1.1	2.4 ± 2.1	2.8 ± 0.3
$t_{1/2,}\gamma$ (h), apparent elimination half-life	25.8 ± 11.4	50.2 ± 29.2	64.2 ± 8.9
V_{ss} (l/kg), volume of distribution	24 ± 12	–	14.9 ± 3.6
C_L [ml/(min kg)], clearance rate	14.4 ± 5.6	12.6 ± 0.6	6.7 ± 1.1
MTD (mg/m^2), max. tolerated dose	50	70	67
AUC (μg h/ml), area under the plasma concentration curve	1.6 ± 1.1	1.8 ± 0.3	3.3 ± 0.4

Pharmacokinetic data are reported for a dose of 50 mg/m^2

(a) Mross K, Maessen P, van der Vijgh WJF, et al. Pharmacokinetics and metabolism of epidoxorubicin and doxorubicin in humans. *Journal of Clinical Oncology,* 6:517, 1988

(b) Danson S, Ferry D, Alakhov V, et al. Phase I dose escalation and pharmacokinetic study of pluronic polymer-bound doxorubicin (SP1049C) in patients with advanced cancer. *British Journal of Cancer,* 90:2085, 2004

(c) Matsumura Y, Hamaguchi T, Ura T, et al. Phase I clinical trial and pharmacokinetic evaluation of NK911, a micelle-encapsulated doxorubicin. *British Journal of Cancer,* 91:1775, 2004

To overcome the limitations of conventional paclitaxel, a polymeric micelle formulation known as Genexol®-PM (Samyang Pharmaceuticals, Korea) has been created for paclitaxel delivery. Genexol®-PM employs PEG-PLA copolymers for micelle formation [91]. Table 4.7 details the clinical pharmacokinetics of the traditional Cremophor®-EL formulation and the Genexol®-PM micelle system for paclitaxel delivery.

Both traditional paclitaxel and Genexol®-PM have similar half-lives and clearance rates. However, the Genexol®-PM micelle formulation demonstrated a marked improvement in patient morbidity in a Phase I clinical trial [91]. None of the patients in the trial exhibited hypersensitivity reactions, and a lower degree of neutropenia was observed for the Genexol®-PM formulation than for the conventional paclitaxel formulation. As a result, the micellar paclitaxel formulation achieved a considerable increase in the maximum tolerated dose, with an MTD of 390 mg/m^2, compared to 230 mg/m^2 for Cremophor® EL. Interestingly, in the Phase I clinical trial, one patient with non-small cell lung cancer experienced a 77 % decrease in the size of lung

Table 4.7 Comparison of clinical pharmacokinetics for traditional paclitaxel and micellar paclitaxel delivery systems

Formulation	Taxol®[a]	Genexol®-PM[b]
Carrier	Cremophor® EL PEG-modified castor oil	PEG-PLA micelles
Diameter (nm)	–	20–50
Number of patients	34	21
$t_{1/2,}\alpha$ (min), distributional half-life	21.8 ± 13.9	–
$t_{1/2,}\beta$ (h), apparent elimination half-life	8.9 ± 1.8	11.0 ± 1.9
C_L [ml/(min kg)], clearance rate	3.9 ± 1.1	4.8 ± 1.0
MTD (mg/m^2), max. tolerated dose	230	390
AUC (μg h/ml), area under the plasma concentration curve	25 ± 6.5	27.5 ± 8.2

Pharmacokinetic data are reported for a dose of 230 mg/m^2

(a) Wiernik PH, Schwartz EL, Strauman JJ, et al. Phase I clinical and pharmacokinetic study of taxol. *Cancer Research,* 47:2486, 1987

(b) Kim TY, Kim DW, Chung JY, et al. Phase I and pharmacokinetic study of Genexol-PM, a cremophor-free, polymeric micelle-formulated paclitaxel, in patients with advanced malignancies. *Clinical Cancer Research,* 10:3708, 2004

metastasis following Genexol®-PM administration; this patient had not shown a response to previous chemotherapy with a traditional paclitaxel formulation [91]. This raises the possibility that paclitaxel-loaded polymer micelles may succeed where conventional chemotherapeutics have failed. Another patient with refractory small cell lung cancer experienced an 84 % decrease in the size of the lung mass and mediastinal lymph nodes following Genexol®-PM administration. As of late 2009, Genexol®-PM had entered Phase III clinical trials for patients with advanced non-small cell lung cancers.

Cisplatin (*cis*-dichlorodiammineplatinum[II]: CDDP) is a key drug in the chemotherapy of various cancers, including lung, gastrointestinal, and genitourinary cancers. Regimens including cisplatin constitute the standard treatment for non-small cell lung cancer and small cell lung cancer, as well as gastric, testicular, and urothelial cancers. Despite the efficacy of cisplatin against malignant solid tumors, the chemotherapeutic must often be discontinued because of adverse effects, particularly neurotoxicity and nephrotoxicity. A micellar formulation of cisplatin has been constructed to enable more selective accumulation of cisplatin in solid tumors, while lessening its distribution in normal tissue. In this formulation, PEG constitutes the outer shell, and a coordinate complex of poly(glutamic acid) and cisplatin constitutes the inner core. These cisplatin-loaded micelles are also called the NC-6004 formulation [92]. The polymeric micelles are 20 nm in diameter, with a narrow size distribution. Cisplatin-loaded micelles show no dissociation upon dilution, and the critical micelle concentration (CMC) is less than 5×10^{-7} M, indicating remarkable stability compared with typical micelles from amphiphilic block copolymers.

The NC-6004 micelle delivery system for cisplatin has been evaluated in animal models [92]. Table 4.8 compares the in vivo pharmacokinetics of the traditional

Table 4.8 Comparison of in vivo pharmacokinetics for traditional cisplatin and micellar cisplatin delivery systems

Formulation	Cisplatin (CDDP)	NC-6004
Carrier	Aqueous solution	PEG-pGlu micelles
Diameter (nm)	–	20
AUC (μg h/ml), area under the plasma concentration curve	20.47 ± 2.25	1,325.90 ± 77.85
C_{max} (μg/ml), maximum plasma concentration	11.67 ± 0.57	89.90 ± 4.29
C_L [ml/(h kg)], clearance rate	70.67 ± 20.34	3.77 ± 0.21
MRT (h), mean residence time	46.57 ± 22.38	10.67 ± 0.15
V_{ss} (l/kg), volume of distribution	3.00 ± 0.61	0.04 ± 0.0023

Pharmacokinetic data are reported for a dose of 5 mg/kg
Uchino H, Matsumura Y, Negishi T, et al. Cisplatin-incorporating polymeric micelles (NC-6004) can reduce nephrotoxicity and neurotoxicity of cisplatin in rats. *British Journal of Cancer,* 93:678, 2005

cisplatin (CDDP) formulation and the NC-6004 cisplatin-loaded micelles. The PEG-poly(glutamic acid) micelles demonstrated a very long blood retention profile compared with CDDP. The AUC value for the polymer micelles was 65-fold higher than that of CDDP, and the polymer micelles achieved an eightfold higher maximum concentration (C_{max}) than CDDP. Within tumors, the C_{max} was 2.5-fold higher for the micelles than for CDDP, and the tumor AUC was 3.6-fold higher for the cisplatin-loaded micelles than for CDDP [92]. The polymer micelles achieved not only an improved pharmacokinetic profile, but also an improved toxicity profile for cisplatin. Notably, the cisplatin-loaded micelles induced significantly less neurotoxicity and nephrotoxicity in vivo than CDDP. Phase I clinical trials of the cisplatin-loaded NC-6004 micelles have been completed, and phase II clinical trials may soon be initiated.

Micellar delivery systems for doxorubicin, paclitaxel, and cisplatin demonstrate the therapeutic potential of polymer micelles for cancer chemotherapy. By delivering anticancer agents directly to cancerous tumors, micelles minimize the toxicity associated with traditional delivery systems and increase the maximum tolerated dose of chemotherapeutics. In addition, micelles enhance the pharmacokinetics of chemotherapeutic agents, allowing longer blood circulation times and slower clearance rates. These micellar carriers are typically "stealth" delivery vehicles, which are passively targeted toward the vasculature of malignant tumors. Further enhancements in therapeutic activity may be achieved by actively targeting micelles toward malignant cells; such actively targeted biomaterials are described in a subsequent chapter.

4.5 Problems

4.1 A graduate student in biomedical engineering would like to design a liposomal drug delivery system with a radius of exactly 50 nm. From your knowledge of self-assembled drug delivery systems, answer the following questions:

(i) What is the ideal hydrocarbon tail length of a lipid system in order to form a lipid vesicle of radius 50 nm assuming a Young's modulus of 1.2×10^7 Pa and a bending elasticity of $350 k_B T$ at 37 °C?
(ii) What would the bending elasticity be for a vesicle with twice the radius, assuming all other variables are held constant?
(iii) For which therapeutic application(s) would the system from (i) be a candidate?
(iv) Given your answer to (iii), would your answer to (ii) be a candidate as well for this/these therapeutic application(s)?

4.2 A medical research lab is interested in testing a biomedical engineering student's liposomal drug delivery system for use with their new developmental drug as a candidate for oral drug delivery at dosages from 100–200 mg and intravenous at dosages from 1–2 mg. From your knowledge of self-assembled drug delivery systems, answer the following questions:

(i) If we know that the ratio of the area under the curve for oral and intravenous administration is 0.6, determine the absolute bioavailability of the new developmental drug?

Vesicle size (nm)	Encapsulation efficiency (EE) (%)	Drug loading (DL) (%)
50	10	2.80
100	20	3.50
150	30	8.00
200	35	12.00
300	50	16.00
400	52	24.00

(ii) Given the data above, would this lipid vesicle system be a good candidate for the new developmental drug as an oral therapy? Why?
(iii) Would it be effective as an intravenous therapy? Explain.

4.3 A materials science researcher is trying to determine whether to use a lipid vesicle system (palmitoyl-oleoyl-phosphatidyl choline—POPC) or a polymer vesicle system [poly(ethylene glycol-block-propylene glycol)—p(EO-PO)] for a drug delivery screening of a new drug to treat Crohn's disease, which targets epithelial cells in the small intestine. The drug delivery system requires stability for several weeks during storage periods (4–20 °C) and 1 week at physiological temperature (37 °C). From your knowledge of self-assembled drug delivery systems, answer the following questions.

(i) What would you expect to be the relative ratio of CMCs between the lipid and polymer systems assuming the following:

- $(M_n)_{p(\text{EO–PO})} = 8{,}100$ Da and $(M_n)_{\text{POPC}} = 760$ Da
- $\mu_1^o = \dfrac{(M_n)_{\text{polymer}}}{(M_n)_{\text{lipid}}}$

(ii) Which vesicle system would allow for longer stability under dilute conditions? Why?
(iii) What are two characteristics in the structures of the lipid and polymer systems that contribute to the values in CMC calculated in (i)?
(iv) Which vesicle system would you use in the new drug screening? Why?

4.4 A research lab in biomedical engineering is looking to design a vesicle-based treatment method for the transdermal delivery of a new experimental drug. They are exploring both inverse micellar and vesicle self-assembled structures to determine the most suitable candidate system. Use the components in the table below and your knowledge of self-assembly to answer the following questions.

Lipid	Chemical Structure
DOPC	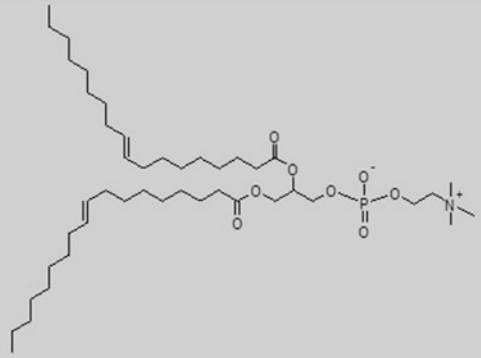
GM1	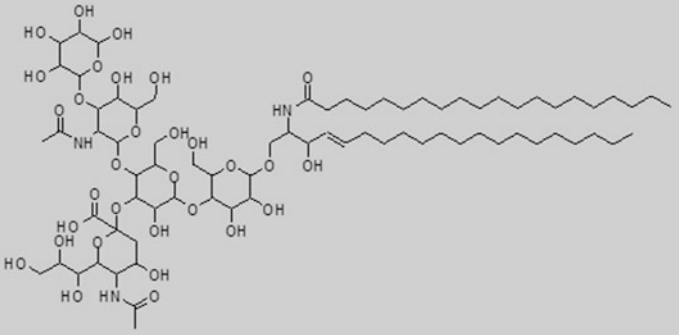
PC	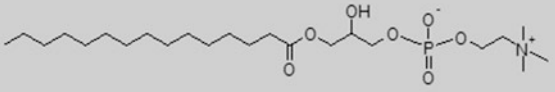
DPPC	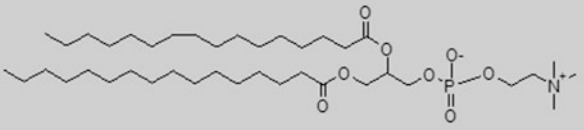

(i) Which lipid(s) would you expect to readily self-assemble into an inverse micellar system? Why?
(ii) Which lipid(s) would you expect to readily self-assemble into a vesicle system? Why?
(iii) What would you expect to be the challenges for the self-assembly of a GM1 vesicle system?
(iv) How could you design a vesicle system from the components in the table that would have the GM1 head groups on the surface?

4.5 Use the components in the table below and your knowledge of polymer science to answer the following questions.

Polymerization Component	Chemical Structure
hydroxyethyl methacrylate HEMA	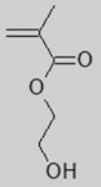
1,1'-methanediylbis(4-isocyanatobenzene) diisocyanate	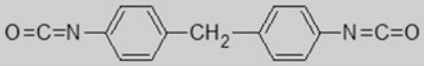
hexane-1,6-diol diols	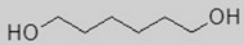
benzoyl peroxide BPO	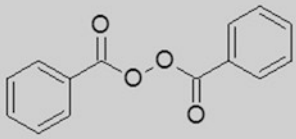

(i) Show an example of the polymerization reactions involved in a classic step-growth or condensation polymerization.
(ii) Show an example of the generation of initiator, initiation, and propagation in a classic chain-growth polymerization.
(iii) What could you do to terminate the polymerization in (i)?
(iv) What could you do to terminate the polymerization in (ii)?

4.6 Liposomes are drug delivery vehicles that mimic the lipid bilayer of the cell. In a typical liposome for drug delivery, a phospholipid bilayer surrounds an aqueous core that contains the drug of interest. If the pH and charge of the bilayer are adjusted appropriately, then a drug in the aqueous core can be released via diffusion through the lipid bilayer.

Liposome for Drug Delivery

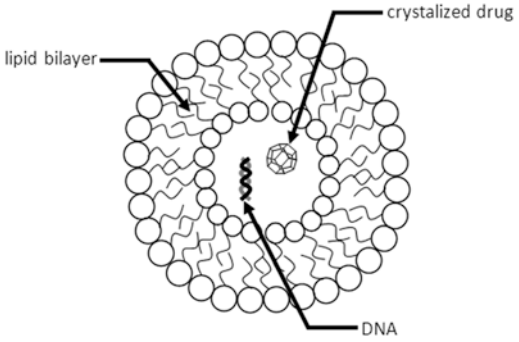

(i) Assuming that the drug is contained in the aqueous core and is released by diffusion through the lipid bilayer, what type of drug delivery kinetics might you expect? Assume that the lipid bilayer does not degrade.

(ii) A pharmacy research group in Europe has designed liposomes that encapsulate the chemotherapeutic drug 5-fluorouracil (Glavas-Dodov et al., *Bulletin of the Chemists and Technologists of Macedonia*, 23:13–18, 2004). The group synthesized liposomes with three different compositions in the aqueous phase:

- 1:100 mass ratio of drug/aqueous phase (formulation C1).
- 1:60 mass ratio of drug/aqueous phase (formulation C2).
- 1:40 mass ratio of drug/aqueous phase (formulation C3).

The researchers measured the release of 5-fluorouracil from each of these liposomal formulations. In each case, a plot of drug concentration versus time was approximately linear:

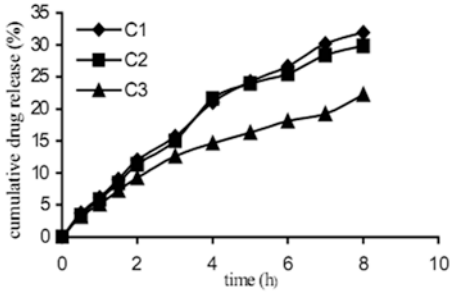

What does this indicate about the kinetics of drug release from the liposomes? Is your prediction for drug delivery kinetics from part (i) correct?

(iii) From the plot above, estimate the rate constant for drug release in each of the three formulations. Be sure to include the correct units!

(iv) What is the effect of aqueous phase composition (i.e., going from a 1:100 drug/water ratio to a 1:40 drug/water ratio) on the rate constant for drug release in this particular system?

References

1. Scannell, J. W., Blanckley, A., Boldon, H., & Warrington, B. (2012). Diagnosing the decline in pharmaceutical R&D efficiency. *Nature Reviews Drug Discovery, 11*(3), 191–200.
2. (a) Lin, J. H., & Lu, A. Y. H. (1997). Role of pharmacokinetics and metabolism in drug discovery and development. *Pharmacological Reviews, 49*(4), 403–449. (b) Estes, L. (1998). Review of pharmacokinetics and pharmacodynamics of antimicrobial agents. *Mayo Clinic Proceedings, 73*(11), 1114–1122.
3. Philp, D., & Stoddart, J. F. (1996). Self-assembly in natural and unnatural systems. *Angewandte Chemie, International Edition in English, 35*(11), 1154–1196.
4. Israelachvili, J. N. (2011). *Intermolecular and surface forces: Revised third edition (Google eBook)* (p. 704). Amsterdam: Academic Press.
5. (a) Israelachvili, J. N., Mitchell, D. J., & Ninham, B. W. (1976). Theory of self-assembly of hydrocarbon amphiphiles into micelles and bilayers. *Journal of the Chemical Society, Faraday Transactions, 2*(72), 1525. (b) Blanazs, A., Armes, S. P., & Ryan, A. J. (2009). Self-assembled block copolymer aggregates: From micelles to vesicles and their biological applications. *Macromolecular Rapid Communications, 30*(4–5), 267–77. (c) Israelachvili, J. (1987). Physical principles of surfactant self-association into micelles, bilayers, vesicles and microemulsion droplets. In K. L. Mittal & P. Bothorel (Eds.), *Surfactants in solution* (pp. 3–33). Boston, MA: Springer US. doi:10.1007/978-1-4613-1831-6.
6. Tanford, C. (1980). *The hydrophobic effect: Formation of micelles and biological membranes* (p. 233). New York: Wiley.
7. Gruen, D. W. (1985). A model for the chains in amphiphilic aggregates. 2. Thermodynamic and experimental comparisons for aggregates of different shape and size. *The Journal of Physical Chemistry, 89*(1), 153–163.
8. (a) Israelachvili, J. N., Marčelja, S., & Horn, R. G. (1980). Physical principles of membrane organization. *Quarterly Reviews of Biophysics, 13*(02), 121–200. (b) Israelachvili, J., & Ninham, B. (1977). Intermolecular forces—The long and short of it. *Journal of Colloid and Interface Science, 58*(1), 14–25.
9. Nagarajan, R., & Ruckenstein, E. (1977). Critical micelle concentration: A transition point for micellar size distribution. *Journal of Colloid and Interface Science, 60*(2), 221–231.
10. Israelachvili, J. N., Mitchell, D. J., & Ninham, B. W. (1977). Theory of self-assembly of lipid bilayers and vesicles. *Biochimica et Biophysica Acta, 470*(2), 185–201.
11. (a) Lipowsky, R., & Sackmann, E. (Eds.). (1995). *Structure and dynamics of membranes: I. From cells to vesicles/II. Generic and specific interactions (Google eBook).* (p. 1052). Amsterdam, The Netherlands: Elsevier. (b) Pautot, S., Frisken, B. J., & Weitz, D. A. (2003). Engineering asymmetric vesicles. *Proceedings of the National Academy of Sciences of the United States of America, 100*(19), 10718–10721.
12. (a) Fromherz, P. (1983). Lipid-vesicle structure: Size control by edge-active agents. *Chemical Physics Letters, 94*(3), 259–266. (b) Marsh, D. (2013). *Handbook of lipid bilayers* (2nd ed., p. 1174). Boca Raton, FL: CRC Press.
13. Leermakers, F. A. M., & Scheutjens, J. M. H. M. (1988). Statistical thermodynamics of association colloids. I. Lipid bilayer membranes. *The Journal of Chemical Physics, 89*(5), 3264.
14. Bates, F. S., & Fredrickson, G. H. (1990). Block copolymer thermodynamics: Theory and experiment. *Annual Review of Physical Chemistry, 41*, 525–557.
15. (a) Choi, H. S., Liu, W., Misra, P., Tanaka, E., Zimmer, J. P., Itty Ipe, B., et al. (2007). Renal clearance of quantum dots. *Nature Biotechnology, 25*(10), 1165–70. (b) Svenson, S., & Prud'homme, R. K. (Eds.). (2012). *Multifunctional nanoparticles for drug delivery applications: Imaging, targeting, and delivery* (p. 373). New York: Springer.
16. (a) Patel, K. (2008). *Design of diffusion controlled drug delivery systems* (p. 141). ProQuest. (b) Bakowsky, H., Richter, T., Kneuer, C., Hoekstra, D., Rothe, U., Bendas, G., et al. (2008). Adhesion characteristics and stability assessment of lectin-modified liposomes for site-specific drug delivery. *Biochimica et Biophysica Acta (BBA)—Biomembranes, 1778*(1), 242–249.

17. Geng, Y., Dalhaimer, P., Cai, S., Tsai, R., Tewari, M., Minko, T., et al. (2007). Shape effects of filaments versus spherical particles in flow and drug delivery. *Nature Nanotechnology, 2*(4), 249–255.
18. (a) Nagayasu, A., Uchiyama, K., & Kiwada, H. (1999). The size of liposomes: A factor which affects their targeting efficiency to tumors and therapeutic activity of liposomal antitumor drugs. *Advanced Drug Delivery Reviews, 40*(1), 75–87. (b) Chorny, M., Fishbein, I., Danenberg, H. D., & Golomb, G. (2002). Lipophilic drug loaded nanospheres prepared by nanoprecipitation: Effect of formulation variables on size, drug recovery and release kinetics. *Journal of Controlled Release: Official Journal of the Controlled Release Society, 83*(3), 389–400.
19. (a) Sun, B., & Chiu, D. T. (2005). Determination of the encapsulation efficiency of individual vesicles using single-vesicle photolysis and confocal single-molecule detection. *Analytical Chemistry, 77*(9), 2770–2776. (b) Lohse, B., Bolinger, P.-Y., & Stamou, D. (2008). Encapsulation efficiency measured on single small unilamellar vesicles. *Journal of the American Chemical Society, 130*(44), 14372–14373.
20. (a) Lipinski, C. A., Lombardo, F., Dominy, B. W., & Feeney, P. J. (2001). Experimental and computational approaches to estimate solubility and permeability in drug discovery and development settings1PII of original article: S0169–409X(96), 00423–1. *Advanced Drug Delivery Reviews, 46*(1), 3–26 (The article was originally published in Advanced Drug Delivery Reviews 23 (1997) 3). (b) Lipinski, C. A. (2004). Lead- and drug-like compounds: The rule-of-five revolution. *Drug Discovery Today: Technologies, 1*(4), 337–341.
21. (a) Lappin, G., Rowland, M., & Garner, R. C. (2006). The use of isotopes in the determination of absolute bioavailability of drugs in humans. *Expert Opinion on Drug Metabolism & Toxicology, 2*(3), 419–427. (b) Lappin, G., & Stevens, L. (2008). Biomedical accelerator mass spectrometry: Recent applications in metabolism and pharmacokinetics. *Expert Opinion on Drug Metabolism & Toxicology, 4*(8), 1021–1033.
22. Food and Drug Administration (2003, March). *Guidance for industry: Bioavailability and bioequivalence studies for orally administered drug products—General considerations* (pp. 1–23). Rockville, MD: US Department of Health and Human Services, FDA, Center for Drug Evaluation and Research.
23. Hinderling, P. H. (2003). Evaluation of a novel method to estimate absolute bioavailability of drugs from oral data. *Biopharmaceutics & Drug Disposition, 24*(1), 1–16.
24. Yuen, G. J., Morris, D. M., Mydlow, P. K., Haidar, S., Hall, S. T., & Hussey, E. K. (1995). Pharmacokinetics, absolute bioavailability, and absorption characteristics of lamivudine. *The Journal of Clinical Pharmacology, 35*(12), 1174–1180.
25. (a) El-Kattan, A., & Varma, M. (2012). Oral absorption, intestinal metabolism and human oral bioavailability. In J. Paxton (Ed.), *Topics on drug metabolism.* InTech. ISBN 978-953-51-0099-7. (b) Antonietti, M., & Förster, S. (2003). Vesicles and liposomes: A self-assembly principle beyond lipids. *Advanced Materials, 15*(16), 1323–1333. (c) Maggio, B. (1985). Geometric and thermodynamic restrictions for the self-assembly of glycosphingolipid-phospholipid systems. *Biochimica et Biophysica Acta (BBA)—Biomembranes, 815*(2), 245–258.
26. (a) Bergstrand, N. (2003). *Liposomes for drug delivery: From physico-chemical studies to applications* (Doctoral Dissertation), Uppsala University. (b) Allen, T. M. (1998). Liposomal drug formulations. Rationale for development and what we can expect for the future. *Drugs, 56*(5), 747–756.
27. Sekimura, T., & Hotani, H. (1990). Morphogenesis of liposomes and bending energy of lipid bilayer. *Mathematical and Computer Modelling, 14*, 690–693.
28. (a) Woodle, M. C. (1998). Controlling liposome blood clearance by surface-grafted polymers. *Advanced Drug Delivery Reviews, 32*(1), 139–152. (b) Jølck, R. I., Feldborg, L. N., Andersen, S., Moghimi, S. M., & Andresen, T. L. (2011). Engineering liposomes and nanoparticles for biological targeting. *Advances in Biochemical Engineering/Biotechnology, 125*, 251–280. (c) Lestini, B. J., Sagnella, S. M., Xu, Z., Shive, M. S., Richter, N. J., Jayaseharan, J., et al. (2002). Surface modification of liposomes for selective cell targeting in cardiovascular drug delivery. *Journal of Controlled Release, 78*(1), 235–247.

29. Brinker, C. J., Lu, Y., Sellinger, A., & Fan, H. (1999). Evaporation-induced self-assembly: Nanostructures made easy. *Advanced Materials, 11*(7), 579–585.
30. (a) Won, Y. (1999). Giant wormlike rubber micelles. *Science, 283*(5404), 960–963. (b) Spenley, N., Cates, M., & McLeish, T. (1993). Nonlinear rheology of wormlike micelles. *Physical Review Letters, 71*(6), 939–942. (c) Lin, Z., Cai, J. J., Scriven, L. E., & Davis, H. T. (1994). Spherical-to-wormlike micelle transition in CTAB solutions. *The Journal of Physical Chemistry, 98*(23), 5984–5993.
31. Brady, J. E., Evans, D. F., Kachar, B., & Ninham, B. W. (1984). Spontaneous vesicles. *Journal of the American Chemical Society, 106*(15), 4279–4280.
32. (a) Furukawa, K., Ebata, K., & Fujiki, M. (2000). One-dimensional silicon chain architecture: Molecular dot, rope, octopus, and toroid. *Advanced Materials, 12*(14), 1033–1036. (b) Lee, E., Jeong, Y.-H., Kim, J.-K., & Lee, M. (2007). Controlled self-assembly of asymmetric dumbbell-shaped Rod amphiphiles: transition from toroids to planar nets. *Macromolecules, 40*(23), 8355–8360. (c) Pochan, D. J., Chen, Z., Cui, H., Hales, K., Qi, K., & Wooley, K. L. (2004). Toroidal triblock copolymer assemblies. *Science (New York, NY), 306*(5693), 94–97.
33. Risselada, H. J., & Marrink, S. J. (2009). Curvature effects on lipid packing and dynamics in liposomes revealed by coarse grained molecular dynamics simulations. *Physical Chemistry Chemical Physics (PCCP), 11*(12), 2056–2067.
34. (a) Carnie, S., Israelachvili, J. N., & Pailthorpe, B. A. (1979). Lipid packing and transbilayer asymmetries of mixed lipid vesicles. *Biochimica et Biophysica Acta (BBA)—Biomembranes, 554*(2), 340–357. (b) Kaler, E. W., Herrington, K. L., Murthy, A. K., & Zasadzinski, J. A. N. (1992). Phase behavior and structures of mixtures of anionic and cationic surfactants. *The Journal of Physical Chemistry, 96*(16), 6698–6707.
35. (a) Rawicz, W., Olbrich, K. C., McIntosh, T., Needham, D., & Evans, E. (2000). Effect of chain length and unsaturation on elasticity of lipid bilayers. *Biophysical Journal, 79*(1), 328–39. (b) Balgavý, P., Dubničková, M., Kučerka, N., Kiselev, M. A., Yaradaikin, S. P., & Uhríková, D. (2001). Bilayer thickness and lipid interface area in unilamellar extruded 1,2-diacylphosphatidylcholine liposomes: A small-angle neutron scattering study. *Biochimica et Biophysica Acta (BBA)—Biomembranes, 1512*(1), 40–52.
36. Drummond, C. J., & Fong, C. (1999). Surfactant self-assembly objects as novel drug delivery vehicles. *Current Opinion in Colloid & Interface Science, 4*(6), 449–456.
37. Polozova, A., Li, X., Shangguan, T., Meers, P., Schuette, D. R., Ando, N., et al. (2005). Formation of homogeneous unilamellar liposomes from an interdigitated matrix. *Biochimica et Biophysica Acta (BBA)—Biomembranes, 1668*(1), 117–125.
38. Moscho, A., Orwar, O., Chiu, D. T., Modi, B. P., & Zare, R. N. (1996). Rapid preparation of giant unilamellar vesicles. *Proceedings of the National Academy of Sciences, 93*(21), 11443–11447.
39. (a) Scherer, J. R. (1989). Reply to "Hydrocarbon chain conformation in the HII phase.". *Biophysical Journal, 56*(5), 1047–1049. (b) Makino, K., Yamada, T., Kimura, M., Oka, T., Ohshima, H., & Kondo, T. (1991). Temperature- and ionic strength-induced conformational changes in the lipid head group region of liposomes as suggested by zeta potential data. *Biophysical Chemistry, 41*(2), 175–183.
40. Prokop, A. (Ed.). (2011). *Intracellular delivery: Fundamentals and applications* (p. 886). New York: Springer.
41. Kozlov, M. M., & Andelman, D. (1996). Theory and phenomenology of mixed amphiphilic aggregates. *Current Opinion in Colloid & Interface Science, 1*(3), 362–366.
42. Woodle, M. C., & Lasic, D. D. (1992). Sterically stabilized liposomes. *Biochimica et Biophysica Acta (BBA)—Reviews on Biomembranes, 1113*(2), 171–199.
43. Newton, A. C. (1993). Interaction of proteins with lipid headgroups: Lessons from protein kinase C. *Annual Review of Biophysics and Biomolecular Structure, 22*, 1–25.
44. Fattal, D. R., & Ben-Shaul, A. (1994). Mean-field calculations of chain packing and conformational statistics in lipid bilayers: Comparison with experiments and molecular dynamics studies. *Biophysical Journal, 67*(3), 985–995.

45. Malliaris, A., Le Moigne, J., Sturm, J., & Zana, R. (1985). Temperature dependence of the micelle aggregation number and rate of intramicellar excimer formation in aqueous surfactant solutions. *The Journal of Physical Chemistry, 89*(12), 2709–2713.
46. (a) Discher, B. M., Won, Y. Y., Ege, D. S., Lee, J. C., Bates, F. S., Discher, D. E., et al. (1999). Polymersomes: Tough vesicles made from diblock copolymers. *Science (New York, N.Y.), 284*(5417), 1143–6. (b) Leroux, J.-C., Burt, H., Amsden, B., Uludag, H., & Letchford, K. (2007). A review of the formation and classification of amphiphilic block copolymer nanoparticulate structures: Micelles, nanospheres, nanocapsules and polymersomes. *European Journal of Pharmaceutics and Biopharmaceutics, 65*(3), 259–269.
47. (a) Lin, J. J., Silas, J. A., Bermudez, H., Milam, V. T., Bates, F. S., & Hammer, D. A. (2004). The effect of polymer chain length and surface density on the adhesiveness of functionalized polymersomes. *Langmuir, 20*(13), 5493–5500. (b) Discher, D. E., & Ahmed, F. (2006). Polymersomes. *Annual Review of Biomedical Engineering, 8*, 323–341.
48. (a) Thiele, J., Abate, A. R., Shum, H. C., Bachtler, S., Förster, S., & Weitz, D. A. (2010). Fabrication of polymersomes using double-emulsion templates in glass-coated stamped microfluidic devices. *Small (Weinheim an der Bergstrasse, Germany), 6*(16), 1723–1727. (b) Cha, J. N., Birkedal, H., Euliss, L. E., Bartl, M. H., Wong, M. S., Deming, T. J., et al. (2003). Spontaneous formation of nanoparticle vesicles from homopolymer polyelectrolytes. *Journal of the American Chemical Society, 125*(27), 8285–8289.
49. (a) Levine, D. H., Ghoroghchian, P. P., Freudenberg, J., Zhang, G., Therien, M. J., Greene, M. I., et al. (2008). Polymersomes: A new multi-functional tool for cancer diagnosis and therapy. *Methods (San Diego, Calif.), 46*(1), 25–32. (b) Ahmed, F., & Discher, D. E. (2004). Self-porating polymersomes of PEG-PLA and PEG-PCL: Hydrolysis-triggered controlled release vesicles. *Journal of Controlled Release: Official Journal of the Controlled Release Society, 96*(1), 37–53. (c) Kukula, H., Schlaad, H., Antonietti, M., & Förster, S. (2002). The formation of polymer vesicles or "peptosomes" by polybutadiene-block-poly (L-glutamate)s in dilute aqueous solution. *Journal of the American Chemical Society, 124*(8), 1658–1663.
50. Bermúdez, H., Aranda-Espinoza, H., Hammer, D. A., & Discher, D. E. (2003). Pore stability and dynamics in polymer membranes. *Europhysics Letters, 64*(4), 550–556.
51. (a) Bermúdez, H., Hammer, D. A., & Discher, D. E. (2004). Effect of bilayer thickness on membrane bending rigidity. *Langmuir: The ACS Journal of Surfaces and Colloids, 20*(3), 540–543. (b) Bermudez, H., Brannan, A. K., Hammer, D. A., Bates, F. S., & Discher, D. E. (2002). Molecular weight dependence of polymersome membrane structure, elasticity, and stability. *Macromolecules, 35*(21), 8203–8208.
52. Discher, B. M., Bermudez, H., Hammer, D. A., Discher, D. E., Won, Y. Y., & Bates, F. S. (2002). Cross-linked polymersome membranes: Vesicles with broadly adjustable properties. *Journal of Physical Chemistry B, 106*, 2848–2854.
53. Srinivas, G., Discher, D. E., & Klein, M. L. (2004). Self-assembly and properties of diblock copolymers by coarse-grain molecular dynamics. *Nature Materials, 3*(9), 638–644.
54. (a) De Gennes, P. G. (1987). Reptation of a polymer chain in the presence of fixed obstacles. *The Journal of Chemical Physics* (American Institute of Physics), *55*(2), 572–571. (b) Rubinstein, M. (1987). Discretized model of entangled-polymer dynamics. *Physical Review Letters, 59*(17), 1946–1949.
55. (a) De Gennes, P. G. (1983). Entangled polymers. *Physics Today* (American Institute of Physics), *36*(6), 33–31. (b) Duhamel, J., Yekta, A., Winnik, M. A., Jao, T. C., Mishra, M. K., & Rubin, I. D. (1993). A blob model to study polymer chain dynamics in solution. *The Journal of Physical Chemistry, 97*(51), 13708–13712.
56. Coldren, B., van Zanten, R., Mackel, M. J., Zasadzinski, J. A., & Jung, H.-T. (2003). From vesicle size distributions to bilayer elasticity via cryo-transmission and freeze-fracture electron microscopy. *Langmuir, 19*(14), 5632–5639.
57. (a) Yamada, K., Yamaoka, K., Minoda, M., & Miyamoto, T. (1997). Controlled synthesis of amphiphilic block copolymers with pendant glucose residues by living cationic polymerization. *Journal of Polymer Science Part A: Polymer Chemistry, 35*(2), 255–261. (b) Stemmelen,

M., Travelet, C., Lapinte, V., Borsali, R., & Robin, J.-J. (2013). Synthesis and self-assembly of amphiphilic polymers based on polyoxazoline and vegetable oil derivatives. *Polymer Chemistry, 4*(5), 1445.
58. (a) Kuhl, T. L., Leckband, D. E., Lasic, D. D., & Israelachvili, J. N. (1994). Modulation of interaction forces between bilayers exposing short-chained ethylene oxide headgroups. *Biophysical Journal, 66*(5), 1479–88. (b) Werner, M., Sommer, J.-U., & Baulin, V. A. (2012). Homo-polymers with balanced hydrophobicity translocate through lipid bilayers and enhance local solvent permeability. *Soft Matter, 8*(46), 11714.
59. Nardin, C., Hirt, T., Leukel, J., & Meier, W. (2000). Polymerized ABA triblock copolymer vesicles. *Langmuir, 16*(3), 1035–1041.
60. Gupta, S., Tyagi, R., Parmar, V. S., Sharma, S. K., & Haag, R. (2012). Polyether based amphiphiles for delivery of active components. *Polymer, 53*(15), 3053–3078.
61. (a) Jankova, K., Chen, X., Kops, J., & Batsberg, W. (1998). Synthesis of amphiphilic PS- b -PEG- b -PS by atom transfer radical polymerization. *Macromolecules, 31*(2), 538–541. (b) Kanaoka, S., Omura, T., Sawamoto, M., & Higashimura, T. (1992). Star-shaped polymers by living cationic polymerization. 3. Synthesis of heteroarm amphiphilic star-shaped polymers of vinyl ethers with hydroxyl or carboxyl pendant groups. *Macromolecules, 25*(24), 6407–6413. (c) Delaittre, G., Dire, C., Rieger, J., Putaux, J.-L., & Charleux, B. (2009). Formation of polymer vesicles by simultaneous chain growth and self-assembly of amphiphilic block copolymers. *Chemical Communications (Cambridge, England), 20*, 2887–2889.
62. Jiang, Y., Chen, T., Ye, F., Liang, H., & Shi, A.-C. (2005). Effect of polydispersity on the formation of vesicles from amphiphilic diblock copolymers. *Macromolecules, 38*(15), 6710–6717.
63. Cowie, J. M. G. (1991). *Polymers: Chemistry and physics of modern materials* (2nd ed., p. 450). Boca Raton, FL: Taylor & Francis.
64. Carothers, W. H. (1936). Polymers and polyfunctionality. *Transactions of the Faraday Society, 32*, 39.
65. Jiang, G., & Ren, J. (2010). Synthesis of an amphiphilic multiarm star polymer as encapsulation and release carrier for guest molecules. *Designed Monomers and Polymers, 13*(3), 277–286.
66. (a) Baysal, B., & Tobolsky, A. V. (1952). Rates of initiation in vinyl polymerization. *Journal of Polymer Science, 8*(5), 529–541. (b) Mayo, F. R., Gregg, R. A., & Matheson, M. S. (1951). Chain transfer in the polymerization of styrene. VI. Chain transfer with styrene and benzoyl peroxide; the efficiency of initiation and the mechanism of chain termination 1. *Journal of the American Chemical Society, 73*(4), 1691–1700.
67. Otsu, T., Yoshida, M., & Tazaki, T. (1982). A model for living radical polymerization. *Die Makromolekulare Chemie. Rapid Communications, 3*(2), 133–140.
68. Wang, J.-S., & Matyjaszewski, K. (1995). Controlled/"living" radical polymerization. atom transfer radical polymerization in the presence of transition-metal complexes. *Journal of the American Chemical Society, 117*(20), 5614–5615.
69. Barner-Kowollik, C., Quinn, J. F., Morsley, D. R., & Davis, T. P. (2001). Modeling the reversible addition-fragmentation chain transfer process in cumyl dithiobenzoate-mediated styrene homopolymerizations: Assessing rate coefficients for the addition-fragmentation equilibrium. *Journal of Polymer Science Part A: Polymer Chemistry, 39*(9), 1353–1365.
70. (a) Georges, M. K., Veregin, R. P. N., Kazmaier, P. M., & Hamer, G. K. (1993). Narrow molecular weight resins by a free-radical polymerization process. *Macromolecules, 26*(11), 2987–2988. (b) Hawker, C. J. (1997). "Living" free radical polymerization: A unique technique for the preparation of controlled macromolecular architectures. *Accounts of Chemical Research, 30*(9), 373–382.
71. Tomasi, J., Mennucci, B., & Cammi, R. (2005). Quantum mechanical continuum solvation models. *Chemical Reviews, 105*(8), 2999–3093.
72. Bermudez, H., Brannan, A. K., Hammer, D. A., Bates, F. S., & Discher, D. E. (2002). Molecular weight dependence of polymersome membrane structure, elasticity, and stability. *Macromolecules, 35*(21), 8203–8208.

73. Xiang, T. X. (1993). A computer simulation of free-volume distributions and related structural properties in a model lipid bilayer. *Biophysical Journal, 65*(3), 1108–1120.
74. (a) Xu, J.-P., Ji, J., Chen, W.-D., & Shen, J.-C. (2005). Novel biomimetic polymersomes as polymer therapeutics for drug delivery. *Journal of Controlled Release, 107*(3), 502–512. (b) Soussan, E., Cassel, S., Blanzat, M., & Rico-Lattes, I. (2009). Drug delivery by soft matter: Matrix and vesicular carriers. *Angewandte Chemie, International Edition in English, 48*(2), 274–288.
75. Immordino, M. L., Dosio, F., & Cattel, L. (2006). Stealth liposomes: Review of the basic science, rationale, and clinical applications, existing and potential. *International Journal of Nanomedicine, 1*(3), 297–315.
76. Cates, M. E., & Candau, S. J. (1990). Statics and dynamics of worm-like surfactant micelles. *Journal of Physics. Condensed Matter, 2*(33), 6869–6892.
77. (a) Garti, N., & Aserin, A. (1996). Double emulsions stabilized by macromolecular surfactants. *Advances in Colloid and Interface Science, 65*, 37–69. (b) Sapei, L., Naqvi, M. A., & Rousseau, D. (2012). Stability and release properties of double emulsions for food applications. *Food Hydrocolloids, 27*(2), 316–323. (c) Pradhan, M., & Rousseau, D. (2012). A one-step process for oil-in-water-in-oil double emulsion formation using a single surfactant. *Journal of Colloid and Interface Science, 386*(1), 398–404.
78. Garti, N. (1997). Double emulsions—Scope, limitations and new achievements. *Colloids and Surfaces A: Physicochemical and Engineering Aspects, 123*, 233–246.
79. Pays, K., Giermanska-Kahn, J., Pouligny, B., Bibette, J., & Leal-Calderon, F. (2002). Double emulsions: How does release occur? *Journal of Controlled Release, 79*(1), 193–205.
80. Garti, N. (1997). Progress in stabilization and transport phenomena of double emulsions in food applications. *LWT—Food Science and Technology, 30*(3), 222–235.
81. Hanson, J. A., Chang, C. B., Graves, S. M., Li, Z., Mason, T. G., & Deming, T. J. (2008). Nanoscale double emulsions stabilized by single-component block copolypeptides. *Nature, 455*(7209), 85–88.
82. Su, J. Y., Hodges, R. S., & Kay, C. M. (1994). Effect of chain length on the formation and stability of synthetic alpha-helical coiled coils. *Biochemistry, 33*(51), 15501–15510.
83. Holowka, E. P., Pochan, D. J., & Deming, T. J. (2005). Charged polypeptide vesicles with controllable diameter. *Journal of the American Chemical Society, 127*(35), 12423–12428.
84. Voet, D., & Voet, J. G. (2011). *Biochemistry* (p. 1520). New York: Wiley.
85. Soga, O., van Nostrum, C. F., Fens, M., Rijcken, C. J., Schiffelers, R. M., Storm, G., et al. (2005). Thermosensitive and biodegradable polymeric micelles for paclitaxel delivery. *Journal of Controlled Release, 103*, 341.
86. Blanco, E., Kessinger, C. W., Sumer, B. D., & Gao, J. (2009). Multifunctional micellar nanomedicine for cancer therapy. *Experimental Biology and Medicine, 234*, 123.
87. Liu, J., Zeng, F., & Allen, C. (2007). In vivo fate of unimers and micelles of a poly(ethylene glycol)-block-poly(caprolactone) copolymer in mice following intravenous administration. *European Journal of Pharmaceutics and Biopharmaceutics, 65*, 309.
88. Danson, S., Ferry, D., Alakhov, V., et al. (2004). Phase I dose escalation and pharmacokinetic study of pluronic polymer-bound doxorubicin (SP1049C) in patients with advanced cancer. *British Journal of Cancer, 90*, 2085.
89. Matsumura, Y., Hamaguchi, T., Ura, T., et al. (2004). Phase I clinical trial and pharmacokinetic evaluation of NK911, a micelle-encapsulated doxorubicin. *British Journal of Cancer, 91*, 1775.
90. Sutton, D., Nasongkla, N., Blanco, E., & Gao, J. (2007). Functionalized micellar systems for cancer targeted drug delivery. *Pharmaceutical Research, 24*, 1029.
91. Kim, T. Y., Kim, D. W., Chung, J. Y., Shin, S. G., Kim, S. C., Heo, D. S., et al. (2004). Phase I and pharmacokinetic study of Genexol-PM, a cremophor-free, polymeric micelle-formulated paclitaxel, in patients with advanced malignancies. *Clinical Cancer Research, 10*, 3708.
92. Uchino, H., Matsumura, Y., Negishi, T., Koizumi, F., Hayashi, T., Honda, T., et al. (2005). Cisplatin-incorporating polymeric micelles (NC-6004) can reduce nephrotoxicity and neurotoxicity of cisplatin in rats. *British Journal of Cancer, 93*, 678.

Chapter 5
Targeted Materials

5.1 Engineering Concepts

5.1.1 Diffusion, Surface Area, and Binding Kinetics

The successful delivery of drug molecules to a desired tissue is contingent upon some degree of direct or indirect identification of that tissue by the drug dosage form. This can be approached from the perspective of engineering the material to be responsive to the environment either *at the interface* or *surrounding* the tissue. We discuss the first approach in this chapter and the second approach later in Chap. 7.

How can the engineer design a system to interact with a desired target tissue?

In order to enhance the effectiveness of this interaction, there are a number of physiological behaviors the engineer can exploit [1]. First-generation drug delivery systems drove the concept of water solubility and biocompatibility for functionalities expressed on the drug particle surface. The water-soluble groups allowed greater diffusion of particulates through physiological media [2]. As we discussed in Chap. 4, biocompatibility allows for the breakdown of drug particle species into components that are not harmful to the body. This limited focus, however, yielded systems that were unstable, expressed poor tissue targeting, and had short circulation lifetimes [2]. The poor circulation time was partially attributed to the presence of ionic surface charges, which led to the electrostatic complexation of opsonins on the particle surface. Designed to address the issues surrounding rapid clearance and targeting, second-generation drug delivery systems focused on the use of stealth surface coatings and the incorporation of receptor-targeting ligands [3]. The stealth surface, as was described in Chap. 4, was composed of a nonionic, water-soluble, polyethylene glycol (PEG) functionality, which allowed for an improved circulation lifetime at an appropriate molecular weight distribution of PEG. The strategy for cell targeting involved the incorporation of excess active targeting ligands on the particle surface for binding to tumor tissues [4]. While this approach appeared to be

E.P. Holowka, S.K. Bhatia, *Drug Delivery: Materials Design and Clinical Perspective*, DOI 10.1007/978-1-4939-1998-7_5

a sound strategy for utilizing the enhanced permeability and retention (EPR) effect seen in cancer cells, the excess expression of positive charges on the targeting ligands instead led to the adsorption of serum proteins, which triggered their evacuation by the mononuclear phagocyte system (MPS) found in the liver and spleen [4]. Currently, drug delivery systems are focused on the incorporation of stimuli-responsive materials that exhibit dynamic properties in response to cues associated with specific physiological environments [5]. We discuss these approaches and the material design associated with these cellular cues in Chap. 7.

We begin this section by identifying the key properties from the first and second generations of drug delivery systems that influence their material design, such as diffusion, surface area, and binding kinetics, discuss their implication on tissue delivery, and then layer in a few basic physiological elements while we design our biomaterial systems in Sect. 5.2.

5.1.2 Diffusion

We have addressed the principle of diffusion on several occasions throughout this text, all with a subtly different meaning. Here, *diffusion* refers to the *rate of diffusion* of the drug dosage form in physiological media. For this discussion we will focus on drug dosage forms encapsulated within nanoparticle, micellar, or vesicle systems and treat these systems in terms of their outer shell, or interacting surfaces.

If we imagine our system in terms of particles flowing through a tube and binding to a surface along the way, we can ask two important questions:

What is the flow rate felt by the drug particle?
What is the strength of the binding interaction to the surface?

We will address the first question in this section. The flow rate will vary depending on the physiological region the drug particle system is traversing and the viscosity of the biological medium [6]. The strength of the binding interaction, which will be discussed in a later section focused on **binding kinetics**, will vary depending on the specificity of the ligand-binding system chosen. The balance of these two interactions will provide the necessary information for the material design to determine the *ligand selection*, *ligand density*, *particle size*, and *particle shape* [7].

First, let's start with the common physiological fluid for drug delivery interactions: blood. Human blood is composed of five components [8] that contribute to its viscosity: *hematocrit*, *erythrocyte deformability*, *plasma viscosity*, *erythrocyte aggregation*, and *temperature*. The hematocrit is the concentration of red blood cells (RBC) present. Approximately 50% of changes in blood viscosity are accounted for by elevated levels of hematocrit [8]. The erythrocyte deformability refers to the elongated deformation of RBC to allow for laminar flow and the traversing of narrow, angular, capillary pathways. The plasma viscosity is what engineers would regard as a traditional measure of polymer solution viscosity. The plasma viscosity is affected by high-molecular-weight hydrated proteins. The erythrocyte aggregation is simply the clustering of RBCs in the blood plasma. The general temperature

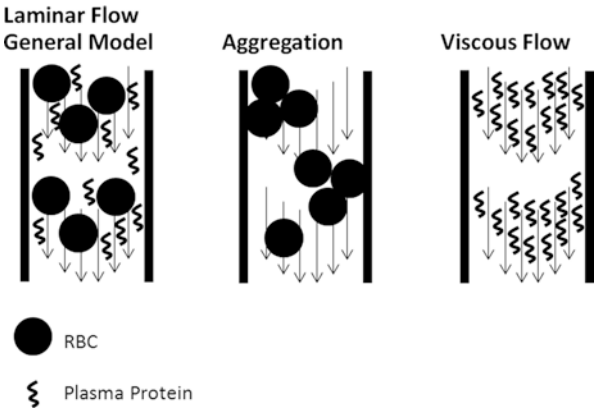

Fig. 5.1 Models of flow for viscous and aggregated colloid–polymer systems analogous to physiological blood flow

relationship is a 1 °C increase in physiological temperature correlates to a 2% decrease in viscosity [8]. If we look at these five contributing factors to blood viscosity from the perspective of the engineer, two assumptions can be made. The first assumption is that the presence of RBCs can be treated as irregular multimicron-sized (i.e., 6–8-μm) deformable colloids. Under ideal conditions, these colloids will occupy a range of viscosities. At specific concentration limits, these colloids will flocculate, or aggregate, into higher-order clusters. The second assumption we can make is that the viscosity of the blood plasma appears to follow the flow behavior of a concentrated polymer system [9]. If we take these two assumptions into account, we can create a model where the viscosity felt by a drug particle in the bloodstream will resemble that of a viscous polymer fluid traveling in a solid suspension of multimicron colloids (Fig. 5.1).

The introduction of solid colloids to a polymer solution increases viscous dissipation and melt viscosity [10]. If we view the RBC–plasma system as a suspension, then the viscosity will depend on the viscosity of the plasma proteins (i.e., polymer), the volume fraction of RBCs (i.e., colloids) in solution, and the interaction between the plasma proteins and the RBCs. We can see this more clearly by looking at the effect of the volume fraction of colloids on the viscosity of polymer solutions [11] (Fig. 5.2).

If the colloid concentration increases to a critical limit (ϕ_m), then flow becomes impossible [11]. We can safely assume as well that the viscosity behavior will resemble that of an exponential increase as the colloid concentration approaches the value for ϕ_m. If we analyze the two concentration extremes (i.e., dilute and concentrated), we can determine where human blood falls within this range. The viscosity of a dilute colloidal dispersion can be described in terms of Eq. (5.1) [12]:

$$\eta_{\text{relative}} = \frac{\eta_{\text{dispersion}}}{\eta_{\text{dispersing fluid}}} \sim 1 + [\eta]\phi^2 + \cdots, \tag{5.1}$$

where η_{relative} is the relative viscosity, $\eta_{\text{dispersion}}$ is the viscosity of the dispersion (i.e., RBC + plasma), $\eta_{\text{dispersing fluid}}$ is the viscosity of the dispersing fluid (i.e., plasma), and

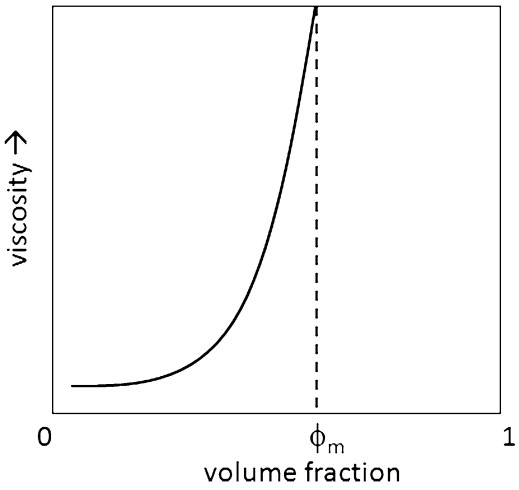

Fig. 5.2 Plot of volume fraction versus viscosity for colloidal systems

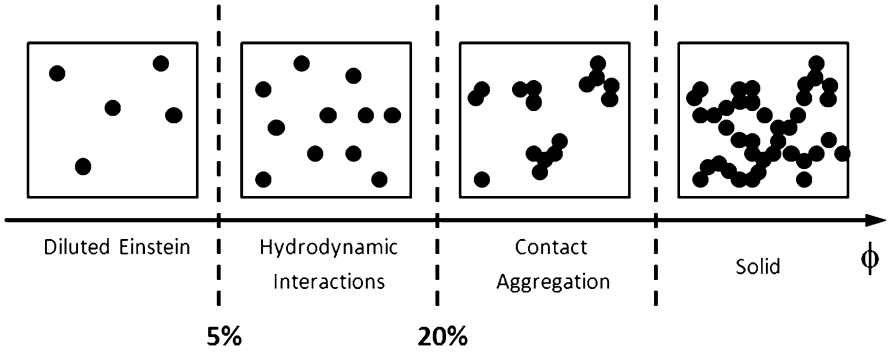

Fig. 5.3 Viscosity behavior as a function of colloidal concentration

[η] is the intrinsic viscosity. As the concentration progresses toward the critical limit, there are four general categories [11] that describe the viscosity behavior relative to the concentration of colloids (i.e., RBCs). The first is typically in the <5% colloids regime and is referred to as the *diluted Einstein* region. The second is in the 5–20% regime, associated with *hydrodynamic interactions*. The third is in the >20% regime associated with *contact aggregation*. The last region is associated with *solids* within the range of the critical limit. For each colloid–polymer mixture, the slope approaching the contact aggregation and solid region will vary (Fig. 5.3).

The viscosity at high colloid concentrations would correspond to the contact aggregation and solid regimes and can be described in terms of Eq. (5.2) [13]:

$$\eta_{\text{relative}} \sim K\left(1-\frac{\phi^*}{\phi_m}\right)^{-2}, \tag{5.2}$$

where K is a proportionality constant on the order of 1 and ϕ^* is the critical percolation value associated with the geometric shape of the particles in suspension. We can see that when the critical percolation value (ϕ^*) approaches the critical limit (ϕ_m), the value for $\eta_{relative}$ approaches ∞, to represent the movement from contact aggregation to solid [13]. If we now combine Eqs. (5.1) and (5.2), we can describe a general expression for the dispersion viscosity ranging from dilute to concentrated ($0 \leq \phi \leq \phi^*$) RBC content [13]:

$$\eta_{relative} \sim \left(1 - \frac{\phi^*}{\phi_m}\right)^{-2} \left[1 - 0.4\left(\frac{\phi}{\phi^*}\right) + 0.34\left(\frac{\phi}{\phi^*}\right)^2\right], \tag{5.3}$$

which is true for spherical colloids in a polymer solution. If we assume the diffusion of these spherical colloids is at an infinite dilution, viscosity can be related to diffusion in terms of the Stokes–Einstein equation [14]:

$$D = \frac{kT}{6\pi\eta R}, \tag{5.4}$$

where k is Boltzmann's constant, T is temperature, η is viscosity, and R is the particle radius. Here we can clearly see an inverse relationship between the solution viscosity and the diffusion of colloids in a dilute polymer solution.

In our model, however, the spherical colloids are deformable, like RBCs, and so we therefore must account for the influence of colloid shape. We can draw a loose analogy between RBCs and anisotropically shaped (i.e., ellipsoidal) rigid colloids [15]. Let's assume that the colloids are biaxially symmetric about their ellipsoidal geometry, which allows us to define these colloids in terms of aspect ratio, or $A_f = (c/a)$. If we extend this ratio to look at intrinsic viscosity, the work of Douglas and Garboczi [16, 20] demonstrates in Eq. (5.5) that

$$\eta_{relative} = \frac{1,012 + 2,904A_f - 1,855A_f^{1.5} + 1,604A_f^2 + 80.44A_f^3}{1,497A_f + A_f^2}, \tag{5.5}$$

where $A_f = 1$ for spheres, $A_f > 1$ for ellipsoids resembling fibers, and $A_f < 1$ for ellipsoids resembling platelets. Based on our current understanding of the shape changes in RBCs, we know that there is a shift between spherical and platelet-shaped cells based on their need to absorb oxygen in the blood [16]. This shape change would correspond to a range of aspect ratios from $0.001 < A_f < 1$. We can also see, based on our plot, that the intrinsic viscosity is decreasing as the shape changes from platelet to sphere (Fig. 5.4).

Now that we have evaluated the behavior of the RBCs in the blood mixture, let's shift to the protein or polymer component of the viscosity. In the case of blood plasma, it can be assumed based on the viscosity profile that the protein concentration is in the dilute solution regime [17]. If we are to generalize protein diffusion

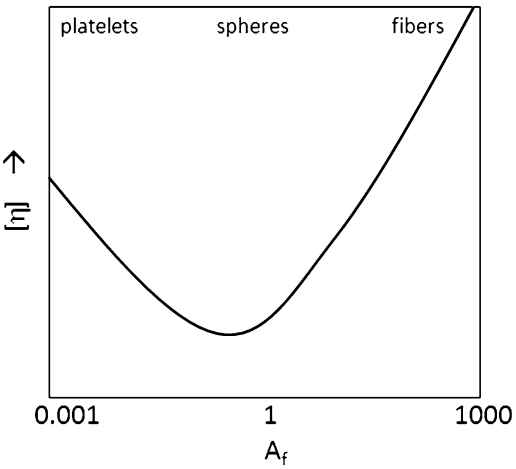

Fig. 5.4 Shape-change behavior of colloids as a function of aspect ratio

behavior in solution to that of polymers, we should determine the degree of solvation. If polymers are fully dissolved into an ideal solvent, it is known as a *theta solvent* (θ). Theta solvents allow for polymer chains to sample every possible geometric conformation into what is known as a *random walk* [18]. If the polymer chain is placed in nonideal solvent, then domains within the polymer chain will begin to condense upon themselves to minimize the free energy of disfavored interactions with the solvent. These solvents are known as *nontheta solvents*. We know that proteins typically adopt folded secondary (2°) and tertiary (3°) structures due to intramolecular hydrogen bonding at regular residue locations within the protein chain [19]. We can argue that this folded behavior resembles that of a polymer in a nontheta solvent. If we assume that blood plasma is a nontheta solvent, we can write the equation for the diffusion coefficient in terms of the mass concentration [20]:

$$D(\rho) = D(1 + k_D \rho + \cdots), \tag{5.6}$$

where ρ is the mass concentration of polymer, D is the diffusivity, and k_D can be written as

$$k_D = 2A_2M - k_s - b_1 - 2v_{20}, \tag{5.7}$$

where A_2 is the second virial coefficient, M is the polymer molecular weight, v_{20} is the partial specific volume of polymer at zero polymer concentration, k_s is a coefficient correlated to the concentration dependence of the friction coefficient, and b_1 is related to the partial specific volume of the pure solvent, which can be determined by density measurements. At first glance, Eqs. (5.6) and (5.7) appear to show a direct correlation between the polymer molecular weight (M) and the diffusion coefficient [D(ρ)]. It is important to realize, however, that molecular weight increase

and diffusion in these equations are *dependent* variables on k_s, b_1, and v_{20}. As the values for M increase, the values for k_s, b_1, and v_{20} simultaneously decrease [20]. The rate at which this decrease occurs indicates an inverse relationship between molecular weight and diffusion in Eqs. (5.6) and (5.7).

We have discussed that the diffusion of drug particles within a blood media is dependent on several key criteria. The drug particle *size* and *shape* will determine which system—either protein plasma or RBCs—could influence diffusion to a greater extent. The diffusion of drug particle systems can be dominated by the properties of the colloidal RBCs that can change shape, which affects the *laminar flow* and *viscosity* of the blood media. The diffusion of nanoparticle systems can be influenced by the *molecular weight* and *viscosity* of the plasma protein component of the blood media. The effective design of targeted drug delivery species must reflect an appropriate strategy to circulate within physiological media. This circulation time accounts for the greatest number of variables that can contribute to the loss of an effective therapeutic treatment. The use of PEG species in second-generation drug delivery approaches was a means of increasing circulation time by eliminating ionic interactions between the drug particle surface and plasma proteins, which increased drug particle diffusion while reducing viscosity.

5.1.3 Surface Area

The principle of surface area in our current discussion will focus on the area at the surface interface between the drug particle and tissue and the subsequent density of chemical binding functionalities that lie within that surface area. The first question that arises is

How do we define the surface interface between drug particle and tissue?

To answer this question with some degree of certainty, we must first define the hardness of the interacting materials. As we have done throughout this section, our assumption is that the drug particle system is a hard sphere. We can also extend our knowledge from Chap. 4 and draw the analogy between the cell membrane and that of an elastic surface [21]. Now we have a hard sphere interacting with an elastic surface [22], where

$$a = \sqrt{Rd}, \tag{5.8}$$

where a is the contact area (i.e., surface interface or contact area), R is the radius of the hard sphere (i.e., drug particle), and d is the depth of the elastic contact area.

The remaining variable is the force (F) associated with the movement of the sphere toward the elastic surface. We will discuss the force component and its association with the receptor–ligand binding in our discussion in the upcoming section on binding kinetics (Fig. 5.5). For the purposes of our current discussion, the

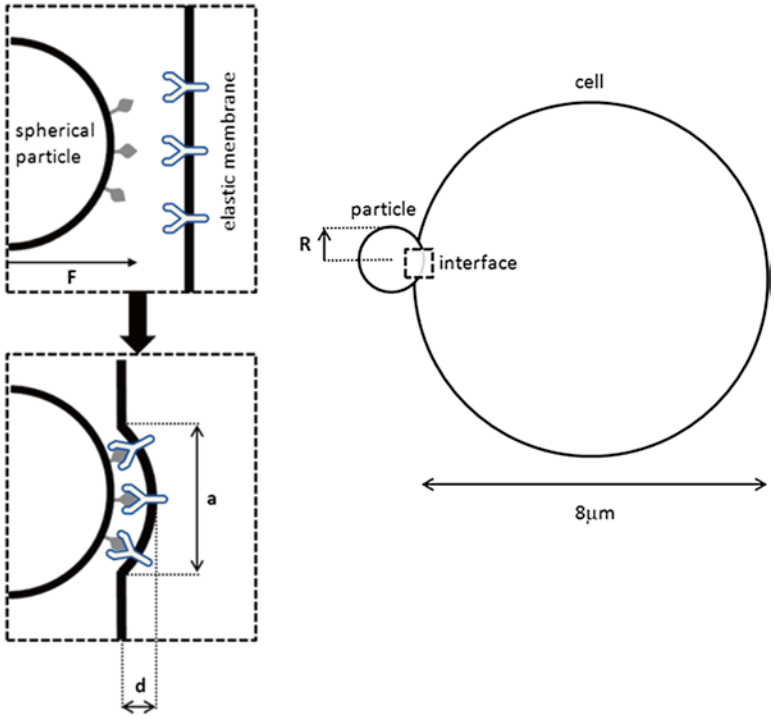

Fig. 5.5 Diagram for the interface between elastic cell membrane and spherical drug delivery particle

dependence of the interaction depth on force is correlated with the elastic modulus [23] of the surface (i.e., cell membrane), which can be written as

$$F = \frac{4}{3} E^* R^{\frac{1}{2}} d^{\frac{3}{2}}, \tag{5.9}$$

where E^* is the elastic modulus of the surface. We have some insight into the calculations of E^* from our discussion in Chap. 4 in the relation of bending elasticity and bending energy. We can now calculate the interacting surface area between a nanoparticle and a cell.

Sample Problem 5a
What is the contact area between a red blood cell and a 50-nm drug particle where the elastic modulus of the cell is 10^4 dyn/cm^2 under a propulsive force between receptor and ligand of 1.25 kcal/mol Å?

If we know the radius of a nanoparticle is 50 *nm, interacting with a RBC with an* E^* *of* 10^4 *dyn/cm*^{2} *under a propulsive force between receptor and*

ligand of 1.25 *kcal/mol Å, then we can combine Eqs.* (5.8) *and* (5.9) *and solve for a to give the following*:

$$a = \left(\frac{F}{\frac{4}{3} E R^{1/2}} \right)^{\frac{2}{3}} \sqrt{R}.$$

If we substitute our values for F, E, and R, we can calculate a contact area of* 31.7 nm^2.

From this example, we can see that several trends begin to emerge. The contact area is directly related to the drug particle radius and its propulsive force upon binding. In our example, we see that roughly 10% of the circumference of the nanoparticle is in contact with the cell. We can also see that the contact area is inversely related to the elastic modulus of the membrane.

In order to effectively design a drug delivery system for cellular internalization, we also need to estimate another value. Since we can calculate the contact area between drug particle and cell, we must also know the receptor density [24] that is contained within that area. If we have the density or concentration of cell receptors, we can more effectively approximate the desired ligand density to functionalize our drug particle surface [25].

Sample Problem 5b
What is the number of ligands at the contact interface between a rabbit corneal epithelial cell ($d = 10$ μm) and the drug particle from Sample Problem **5a** if we know that there is an average of 5,500 EGF receptors per cell?

Let's begin by looking at a system of rabbit corneal epithelium cells and calculate the EGF-receptor density on the cell surface assuming uniform coverage. We know that there are approximately 5,500 *EGF receptors on each cell. If we further assume that the cells are spherical in shape, then their diameter is* 10 μm ($r = 5$ μm). *Since the surface area of a sphere is* $4\pi r^2$, *then the surface area of a rabbit corneal epithelial cell would be on the order of* 314.16 μm^2. *So now we know that there are* 5,503 *EGF receptors per* 314.16 μm^2. *If our contact area was on the order of* 0.5 μm^2, *the number of ligands per contact area would equate to* 8.75 *receptors*.

We will see in the following section focused on binding kinetics how the number of receptors within the contact area can influence the strength of the net binding interaction and ability of the drug particle to reside on the cell membrane in the presence of flow [25].

In this section we have discussed a model for determining the surface area between a cell and drug particle by drawing an analogy to a hard sphere and elastic surface. From this approximation, we can estimate the contact surface area and subsequently use this number to determine the receptor density. We can use the receptor density to estimate the minimum ligand density on the drug particle necessary to facilitate a surface binding event.

5.1.4 Binding Kinetics

Since the rate of diffusion provides an indication of the movement of the drug dosage form in physiological media, and the surface area provides an indication of the density of the receptors at the interacting surface, in general terms, the design variable that remains is the binding strength at the interface of the tissue and dosage form (i.e., drug particle). This strength is typically viewed as a combination of three events: (1) the energetics associated with the binding of the drug particle to a chemical functionality on the cell surface [26]; (2) the energetics of release of the drug particle from the cell surface [27]; and (3) the energetics of cell internalization of the bound species [28]. We can see that each of these events can be set in competition with one another, which will dictate the effective dosage of a drug and the composition of the drug delivery system.

First, let's look more closely at the binding interaction. The system can be modeled after an affinity chromatography column [29], where a receptor-functionalized stationary phase binds free drug particle–ligand species. We can see that the equilibrium rate constant (K_{eq}) of the [drug particle–ligand] to [receptor] interaction (5.10) is equivalent to the association equilibrium rate constant (K_a) and the binding equilibrium rate constant (K_B) [30]:

$$K_{eq} = \frac{[\text{drug} - \text{particle} - \text{ligand}: \text{receptor}]}{[\text{drug} - \text{particle} - \text{ligand}][\text{receptor}]}. \tag{5.10}$$

If $K_{eq} = 1$, then the [drug particle–ligand] is equal to the [drug particle–ligand–receptor]. If $K_{eq} < 1$, then the unbound [drug particle–ligand] is greater than the bound [drug particle–ligand–receptor]. If $K_{eq} > 1$, then the bound [drug particle–ligand–receptor] is greater than the unbound [drug particle–ligand]. A rule of thumb is that if $K_{eq} > 1 \times 10^6$ M^{-1}, it will be in the effective range for targeted delivery. Remember, the greater the number, the greater the binding. Similarly, we can think of the interaction between targeting groups and their respective binding sites in terms of the equilibrium rate constants for the association (K_a) and dissociation (K_D). Here we can see that $K_{eq} = K_a/K_D$, where the dissociation effectively describes the affinity in terms of the necessary concentration of a ligand to achieve a predicted reaction with a specific target binding site. If we now reconfigure Eq. (5.10) in terms of K_D, we can see that the effective concentration range for targeted delivery would be $K_D < 1 \times 10^{-6}$ M, or micromolar quantities. In terms of dissociation, the smaller the number indicates a better binding. Currently, drugs have approached the

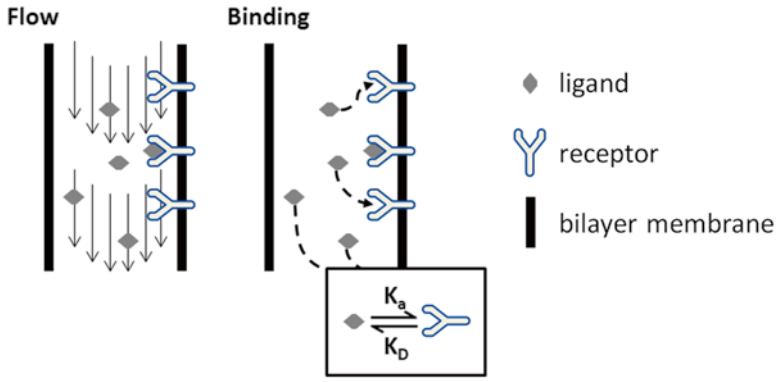

Fig. 5.6 Diagram of ligand–receptor surface binding versus particle flow in a tube

nanomolar range for an effective dosage [31], which indicates a significantly stronger binder, or reduction in the rate of dissociation for the binding site (Fig. 5.6).

In general, the greater the [drug particle–ligand], the greater the therapeutic effect, to a point [32]. The goal of a targeted system is to decrease the effective dosage. Another way to look at this is to increase the [drug particle–ligand] to within the optimal dosage range for the desired system. This will ensure having the most effective medicinal effect with relatively limited side effects.

If we look now in terms of rate constants, we can see a similar trend in behavior. The K_{eq} value can be equated to $K_{eq} = k_{bind}/k_{dissoc}$, where $K_D = 1/K_{eq}$. If we substitute our previous values of $K_{eq} > 1 \times 10^6\ M^{-1}$ and $K_D < 1 \times 10^{-6}$ M, we can estimate that the values typically seen for $k_{binding}$ and k_{dissoc} fall in the range of $>1 \times 10^7\ s^{-1}$, which indicates a rapid binding and dissociation interaction that occurs almost instantaneously upon exposure [33]. If this interaction is so rapid, what drives the effective binding and signal cascade behavior that is typically witnessed in eliciting a targeted cellular response? The answer to this question relates to the free energy of the system:)

$$\Delta G = \Delta H - T\Delta S, \tag{5.11}$$

where ΔG is the free energy of binding, ΔH is the enthalpy of binding, and ΔS is the entropy of binding. Let's look at each of these terms relative to their relative molecular motion in solution. The term for ΔH refers to the net energy resulting from the binding energy (E_b), dissociation energy (E_d), and molecular reorientation (i.e., free bond rotations or barrier to bond rotations) [34]. The term for ΔS refers to the net entropy or disorder of the species at a specific state [34]. It may appear that the binding of a ligand species would result in a less disordered state; however, remember that there may be multiple binding exchanges occurring in the process. If the molecule(s) the receptor releases is in a more disordered state than the ordering due to the binding of the ligand, then the net entropy is negative. This concept can become more apparent if we look back at our original model for flow and binding. If the entropy of the system during flow becomes higher due to ligand binding and the release of a small molecule resident, then the system shifts to a more favored

entropic state and the value for K_{eq} will be high, resulting in an increase in ΔG. In this way, the flow rate can dictate the local concentration of particle–drug–ligand that the tissue sees at any given time. For this reason, residence time becomes a critical influencing factor on targeting efficiency. If the circulation lifetime is increased, then the statistical probability of a ligand species finding a receptor surface increases.

These binding interactions are true for the internalization of small molecule ligands, but what about ligands bound on a particle surface? We recall from the discussion of **surface area** that the receptor–ligand density at the contact area of the interface between drug particle and tissue can augment the cellular response [35]. What about the retention time of the particle at the particle–tissue interface? As we discussed earlier in this section, if a particle is exposed to constant laminar flow, then the ligand source (i.e., particle) requires a stronger binding energy than that of the force felt due to flow [36]. Since particles are significantly larger than small molecules (i.e., >100-fold), then multiple binding sites between the particle–ligand and the tissue surface are required to allow for internalization while under constant flow. We can use the calculations for the drag force (F_D) of particles in solution in a pipe as a model for the force felt by a drug particle in the viscous circulatory system [37]:

$$F_D = 5\pi\eta V d, \tag{5.12}$$

where η is the viscosity of the polymer solution of blood plasma, V is the velocity of the particles in solution, and d is the diameter of the particles in solution. Since we know classically that the force of the particle [38] is

$$F = m\left(\frac{dv}{dt}\right), \tag{5.13}$$

where dv/dt is the change in velocity over time and m is the mass of the particle, then a simplified account of the net force felt by a particle due to flow and friction components would be $F_{net} = F - F_D$. From the ligand binding equations [39], we know

$$\Delta G = -F\Delta x, \tag{5.14}$$

where F is the force associated with ligand binding and Δx is the displacement. If we combine Eqs. (5.12)–(5.14), we can see that binding will occur when

$$n\left(F_{binding}\right) > \left(F_{net}\right)_{flow}, \tag{5.15}$$

where n denotes the number of ligands necessary to shift the $F_{binding}$ to a value greater than the F_{net} associated with the flow. We can relate this value for n back to our assessment of the receptor density at the drug particle–tissue interface to determine the density of ligands required for effective binding [40]. Keep in mind that this approach only accounts for the effective binding of particle ligands to a tissue surface. The influence of this binding on the cellular internalization has not been addressed to this point.

In this section , we determined several models for the events encountered during the process of cellular targeting by drug delivery systems (DDS) based on basic engineering principles. The movement of a drug particle DDS through the blood was described by the viscous flow of a colloidal polymer system. The contact area between the cell surface and DDS was described in terms of the interaction between a hard sphere and an elastic surface. The binding kinetics of ligands from the DDS and the cell surface receptors was described as a competition between the free energy of binding and the forces associated with particles flowing through a pipe. These analogies provided us with critical values, such as viscosity, particle size, shape, ligand density, and ligand selection, which will be critical in our discussion in Sect. 5.2, where we will begin to piece these principles together to form our targeted DDS.

5.2 Material Design

5.2.1 Size, Shape, Chemical Functionality, and Elasticity

In our previous discussions in Chap. 4, we learned several critical characteristics associated with the self-assembly of micellar and vesicle drug delivery species. The properties of bending elasticity, curvature, thickness, size, shape, composition, chemical functionality, and encapsulation efficiency were all critical to the function of the successful delivery of the drug dosage form. In this section, we begin to look at four of these characteristics under two basic modes of drug delivery known as *passive cellular uptake* and *active cellular uptake*.

5.2.2 Passive Cellular Uptake

The mode of *passive uptake* or *passive transport* refers to the internalization of a chemical or particulate species into a cell by movement across a membrane barrier driven by an increase in the entropy of the system [41]. Passive transport systems can operate by four different mechanisms, all requiring no cellular ATP or energy to function. These mechanisms, known as *simple diffusion* [42], *facilitated diffusion* [43], *filtration* [44], and *osmosis* [45], have varying degrees of applicability to self-assembled drug delivery species, as we discussed in Chap. 4.

Simple diffusion functions by the movement of a concentration gradient of a chemical species across the semipermeable cell membrane [42]. It is important to note that this is restricted to chemical species and not necessarily particulate matter. Once a threshold size is reached, it is no longer feasible to operate through simple diffusion by a passive system. Larger molecules are typically internalized through *facilitated diffusion*. Facilitated diffusion typically involves the formation of transmembrane channels, composed of lipids, proteins, and/or carbohydrates, to permit

the passive transport of larger molecules, such as glucose, through the membrane [43]. While this method allows for larger species to cross the cellular membrane barrier, the relative size remains small compared to a self-assembled drug delivery system as we have discussed them in this text. The *filtration* mechanism allows for a range of sizes to be transported across cellular membranes, which are dependent on the tissue type [44]. For example, kidney and intestinal cells will filter small (<10-nm) particulates, while liver or cancerous cells will permit 150–200-nm particles to pass though their membranes. Similar to simple diffusion, *osmosis* will permit the transport of water across membranes in a high to low concentration gradient. Of particular note in the case of osmosis, if a chemical or particulate species alters the effective water concentration gradient of the cell, membrane deformation and rupture can occur [45]. This is true for simple situations where salt or sugar gradients, for example, also exist between the intracellular and extracellular environment (Fig. 5.7).

For our discussion of targeted drug delivery, we find that the cases for simple diffusion and osmosis are inapplicable due to the size requirement necessary to facilitate the effect. Facilitated diffusion follows the same design principles that we will discuss in the upcoming section detailing active cellular uptake, and so we defer its discussion until then. This leaves the remainder of this section to focus on the *filtration mechanism*. If we model our cell membrane as a porous filter, then we can determine a correlation between an ideal particle size range and cell uptake. In filtration, the principle of membrane fouling refers to the critical buildup of material at one interface causing a significant increase in flow resistance. In the case of passive uptake via the filtration mechanism, we could define membrane fouling as the point at which cell internalization ceases to occur. From another perspective, membrane fouling can describe the critical particle size range required for passive cellular uptake to occur. We can express filter resistance in a circular shaped porous system [46] (i.e., transmembrane channels) as

$$R_{\text{circular}} = \left(\frac{24}{d^3 N} \right), \tag{5.16}$$

where d is the pore diameter and N is the number of pores. This relation provides the resistance of a membrane based on the flow of a uniform solvent system. If we begin to introduce a particulate species, we can see that the resistance can be expressed in terms of the pressure (ΔP) it generates under a constant flow [47]:

$$\Delta P = \mu R Q, \tag{5.17}$$

where μ is the coefficient of dynamic viscosity and Q is the flow rate, which can be described by Darcy's law [48]:

$$Q = \frac{a^3 \Delta P}{3\mu} \left[1 + \frac{8L}{3\pi a} \right]^{-1}, \tag{5.18}$$

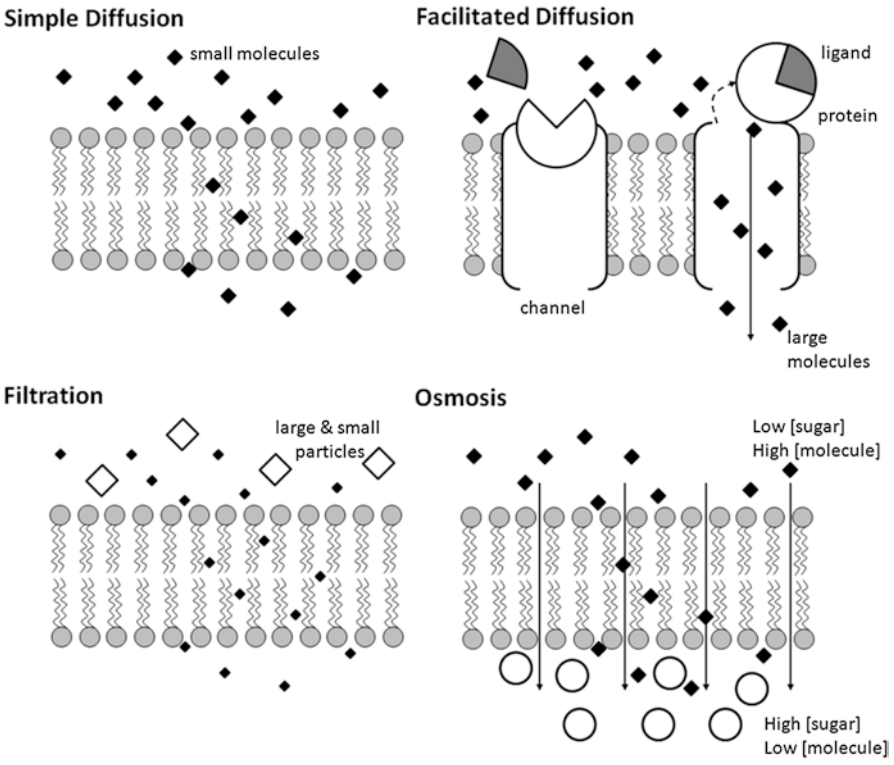

Fig. 5.7 Basic mechanisms for passive cellular uptake

where a is radius of the pores and L is the membrane thickness. The filtration time (t) of particles at constant flux (J_O) can be described [49] by

$$t^* = \frac{\pi x^2}{4S} NAJ_o t, \tag{5.19}$$

where x is the mean spherical particle size of the filtered material, S is the area of the filter pore, and A is the total filter area. If we combine Eqs. (5.16)–(5.19), we obtain an expression of the pressure felt by a filter of known pore size, membrane thickness, and particle size of the filtrant under constant flux:

$$\Delta P = \frac{6\pi\mu x^2 QAJ_o}{Sd^3}. \tag{5.20}$$

If we look more closely at Eq. (5.11), we can see that this expression can account for membrane fouling. If we plot the change in pressure over time as we change the particle size of the solution (Fig. 5.8), a fouling event would manifest as a sudden increase in the pressure over a short time duration [46]. Since we know the cell

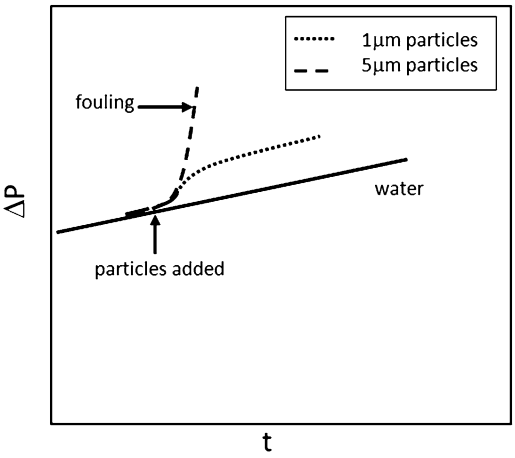

Fig. 5.8 Plot of the change in pressure with changes to particle size over time (fouling event shown at critical particle size over time)

membrane bilayer thickness (L), cell membrane pore size (a, d, and S), plasma viscosity (μ), area of the cell (A), flux of materials through the cell membrane (J_o), and the approximate number of pores, we can design a particle system in terms of size (x) in order to reduce the pressure felt by the membrane below the fouling threshold.

In this section, we modeled the filtration mechanism from a passive cellular uptake model based on the principle of fouling of a filtration membrane. This analogy provides a particle size threshold to aid in the design of DDS that can achieve cell internalization from a passive uptake model. In the next section, we will focus on the design elements from active targeting relationships in cells. The implications from our active targeting assumptions can be applied to the facilitated diffusion passive uptake mechanism that was described previously in this section.

5.2.3 Active Cellular Uptake

The mode of *active uptake* or *active transport* refers to the internalization of a chemical or particulate species into a cell by *movement through* or *movement with* a cell membrane [50]. Active transport systems can operate through a multitude of mechanisms. Our discussions will focus on *ion channels* [51], *receptor-mediated endocytosis* [52], and *macropinocytosis* [53]. We recall that in the case of passive transport, there was minimal interaction between chemical species or particulate and biological tissue. This allowed for the system to be described strictly in terms of the entropy of the cellular environment. In the case of active transport, we will see from our discussion that each mechanism relies on a different degree of interaction with the biological environment.

Ion channels function by using an associated stimulus as a means of creating an energetic driving force to move ions across their concentration gradient between the intracellular and extracellular environment, effectively pumping small molecules,

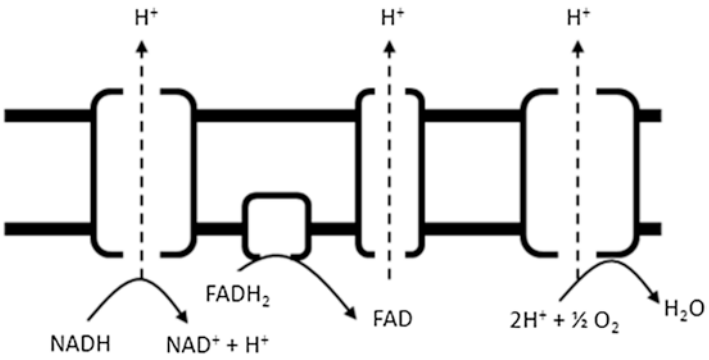

Fig. 5.9 Diagram of the electron transport chain of a basic ion channel

such as ions, in either direction. These stimuli act by providing energy (i.e., ATP → ADP) by redox reactions (i.e., NADH → NAD^+) or light ($h\nu$) to force ions to move through a membrane [51] (Fig. 5.9).

This mechanism is very similar to that of simple diffusion in the passive transport mode, where only small chemical species and not particulate matter are relevant to deliver using this mode. The more widely sought mechanism is that of internalization of the membrane to yield an intracellular vesicle. These interactions can be classified as *pinocytosis* [54] and *phagocytosis* [55]. In pinocytosis, the membrane forms concave pockets that imbibe localized extracellular fluid and its contents. Once internalized, these closed pockets will fuse with existing lysosomes and hydrolyze the internalized components (i.e., chemical species or particulate matter). In phagocytosis, the chemical species or particulate matter binds to a receptor species, which can be either specific or nonspecific, triggering a series on intracellular reactions to signal the bending and rearrangement of the cellular membrane to engulf the bound species. If we look at these two cases in more detail, we can begin to identify the critical response behaviors associated with an external stimulus, which in our case is a self-assembled drug delivery system.

5.2.4 Receptor-Mediated Endocytosis

The route of targeted cellular uptake that has attracted the most abundant attention has been that of receptor-mediated endocytosis (RME) [52]. We will begin our discussion of RME with a brief overview of the biological mechanism, followed by a discussion of the energetic implications of the interactions between targeted particles and cellular membranes, and briefly conclude with a perspective of more complicated bilayer drug delivery systems.

The process of RME involves five general steps, which account for the surface interaction of the drug dosage form, the mobilization of intracellular components, the readjustment of membrane elasticity at the particle–membrane interface, the internal budding of receptor-bound membrane, and the digestion and trafficking of receptor

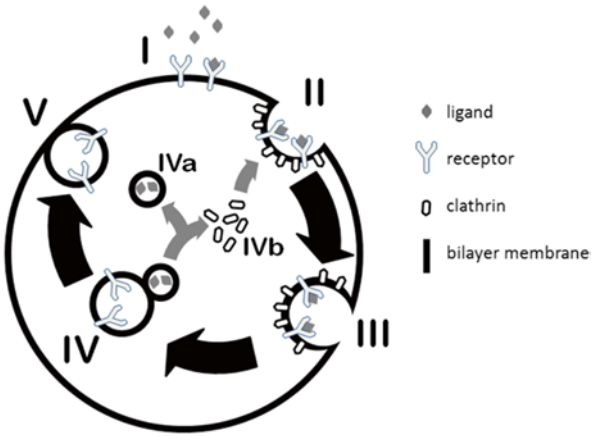

Fig. 5.10 Diagram of the cellular process of receptor-mediated endocytosis

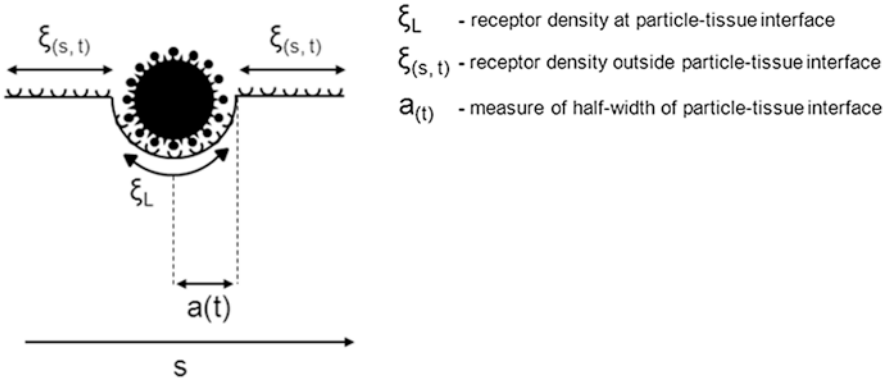

Fig. 5.11 Diagram of the receptor density at the particle–tissue interface

species back to the cell surface [56]. In the first stage (I), the targeting functionalities on the particle species (i.e., drug dosage form) bind to the receptor species on the cell surface. The binding event triggers stage 2 (II), which involves the mobilization of clathrin to the inner leaflet of the cell interface of the bound area. This clathrin mobilization triggers stage 3 (III), where the membrane increases its elasticity and begins the budding process. In stage 4 (IV), the membrane bud is fully internalized, forming an intracellular vesicle species, which digests the bound species, releasing it, along with the clathrin, into the intracellular matrix. The remaining intracellular vesicle is recycled to the cell surface in stage 5 (V) to complete the process. The entire process of RME occurs in a matter of minutes [57] when the cell is in the presence of excess ligand species. This timing will become more significant when we discuss the material design parameters for RME drug delivery systems (Fig. 5.10).

Since our universal goal for targeted drug delivery is the internalization of the drug dosage form (i.e., micelle, vesicle, or nanoparticle) within a cell, then we need

to better understand the energetics of the cellular membrane interactions for receptor-mediated endocytosis. For the purposes of our discussion, the self-assembled drug delivery system of a micelle, vesicle, or nanoparticle will be generalized to that of a solid sphere of varying size (i.e., 5.200 nm). The implications of membranous drug delivery systems are discussed later in this section. We can begin by separating the cellular system into the two events: *the binding event* to the cellular surface and the *uptake event* to internalize the dosage form. The binding event involves the surface area at the particle–tissue interface.

We will first make the global assumption that the total number of receptors in the membrane remains constant during the entire uptake event. Therefore, we can describe the distribution of receptors according to Gao et al. [58] as the following:

$$\frac{d}{dt}\left[\int_0^{a(t)} \xi_{\mathrm{L}}\, ds + \int_{a(t)}^{\infty} \xi_{(s,t)}\, ds\right] = 0, \tag{5.21}$$

where ξ_{L} is the receptor density that is within the particle–tissue interface, $\xi_{s,t}$ is the receptor density that is not within the particle–tissue interface, s is a measure of length, t is time, and $a(t)$ is a measure of half of the width of the particle–tissue interface.

The receptors themselves are not static. Therefore, a term for the lateral diffusion, or *diffusive flux*, of the receptors in the membrane can be described in terms of the following [59]:

$$j(s,t) = -D\frac{d}{ds}\xi_{(s,t)}, \tag{5.22}$$

where j is the flux and D is the diffusivity. The continuity condition for the interaction of a spherical particle with a flat cellular membrane can be written [59] as

$$\frac{d\xi}{dt} = -\frac{1}{s}\frac{d}{ds}(sj). \tag{5.23}$$

Similarly, from Eqs. (5.22) and (5.23), we can see that the density of receptors in any area can be described by [60]

$$\frac{d\xi(s,t)}{dt} = d\nabla^2\xi(s,t), \tag{5.24}$$

where $a(t) < s < \infty$. Since we can assume that diffusion is occurring at a nonsteady state, the conservation equation can therefore only be satisfied if the following is true:

$$a(t) = 2\alpha\sqrt{(Dt)}, \tag{5.25}$$

where α is referred to as the speed factor. Equation (5.25) should look familiar since it resembles the standard back-of-the-envelope calculation [61] relating the characteristic diffusion of a distance x [in this case $a(t)$] to time (t) and diffusion coefficient (D):

$$a(t) = 2\alpha\sqrt{(Dt)} \Rightarrow x \approx \sqrt{(Dt)}.$$

In Eqs. (5.21)–(5.25), we can see that the diffusion and binding of a targeted particulate species are dependent on the area of the particle–tissue interface (ξ_L), the diffusivity (D) and diffusive flux (j) of the receptors on the cell surface, and the receptor density in the remainder of the cell surface ($\xi_{s,t}$). If we look at this more carefully, we can see that the key material design parameter in terms of binding would be the term ξ_L and the *chemical functionality* of the receptor–ligand species.

If we turn our focus to the *uptake event*, we can use the elements of Eq. (5.25) with our knowledge from Chap. 4 to determine the amount of time it takes for the cellular membrane to envelop the particle species. From Chap. 4, we know that the effective curvature of a spherical particle is $2/R$, where R is the particle radius. If we substitute this into Eq. (5.25), we see that the membrane envelopment time (t_w) for receptor-mediated endocytosis can be described as [62]

$$t_w = \left(\frac{R}{\alpha\sqrt{D}}\right)^2. \tag{5.26}$$

From Eq. (5.26) we can see the effect of particle size on the time of membrane envelopment (t_w), where there is an exponentially longer timescale for uptake with increasing particle size.

Sample Problem 5c
How long would it take to envelop a spherical nanoparticle with a diameter of 5 nm relative to one with a diameter of 200 nm?

Let's take two self-assembled spherical drug delivery systems with diameters of 5 nm ($R = 2.5$ nm) and 200 nm ($R = 100$ nm). Since the membrane itself remains unchanged with each case, we can assume that the diffusivity (D) and speed factor (α) are relatively equivalent for both cases. Therefore, t_w is proportional to R^2. By the following ratio, we can see that a change in particle size from 5 to 200 nm would result in a 6,400× longer time to envelop the larger species!

$$\frac{t_{w(100\text{nm})}}{t_{w(2.5\text{nm})}} \propto \frac{R^2_{(100\text{nm})}}{R^2_{(2.5\text{nm})}} \approx 6,400$$

If we look at this effect more closely, we can see that there is an exponential relationship between self-assembly size and cellular envelopment time. Different drug delivery modes require uptake involving different tissues at different critical rates to ensure a therapeutic dosage of drug. We can see that a key material design parameter in terms of uptake would be size. It is worth noting that we have not discussed the implications of shape in this section. If one were to look at tubular shaped

delivery systems, Eq. (5.26) would change by a factor of $\pi/2$ to reflect the geometry of a cylindrically modeled system. In the systems described in this section, we made the initial assumption of hard particulate surface of 5.200 nm in diameter.

What if the particles were actually bilayers?

One could imagine several complicating factors to our current analysis. When two membrane systems of similar thickness and bending elasticity come in contact with one another, there is the propensity for a merger of membranous material. We will not go into deliberations of this behavior; however, there are several comprehensive texts in this area of study [63]. We can frame this behavior in terms of our discussions from Chap. 4. We know that bilayer systems can vary in the fluidity and rigidity, being measured in terms of bending elasticity, bending energy, thickness, curvature, packing, and CMC. We can imagine that the variation in the bending energy of two membranous vesicles could affect the interfacial contact area between vesicle and tissue in dramatically different ways.

Sample Problem 5d
What is the relative ratio of bending energy and Young's modulus between an elastic vesicle species and a cell? How would the ratio change with a rigid vesicle species?

Let's examine the interaction of two different vesicle species, one rigid and one elastic, where the Young's modulus for the elastic species is much greater than that of the rigid species. If we revisit the equation for bending energy from Chap. 4, we can compare the relative difference in energies of a cell and vesicle between rigid and elastic species:

$$\frac{\left(e_{\text{bend}}\right)_{\text{vesicle}}}{\left(e_{\text{bend}}\right)_{\text{cell}}} = \frac{\frac{1}{24}Y_{\text{vesicle}}}{\frac{1}{24}Y_{\text{cell}}} \times \frac{\frac{h_{\text{vesicle}}^3}{R_{\text{vesicle}}^2}}{\frac{h_{\text{cell}}^3}{R_{\text{cell}}^2}} = \frac{Y_{\text{vesicle}}\,R_{\text{cell}}^2}{Y_{\text{cell}}\,R_{\text{vesicle}}^2}.$$

Comparison of bending energy based only on size difference

$$\frac{\left(e_{\text{bend}}\right)_{\text{vesicle}}}{\left(e_{\text{bend}}\right)_{\text{cell}}} = \frac{Y_{\text{vesicle}}}{Y_{\text{cell}}} \times \frac{\left(100\text{nm}\right)_{\text{cell}}^2}{\left(10,000\text{nm}\right)_{\text{vesicle}}^2} = \frac{Y_{\text{vesicle}}}{\left(10,000\right)Y_{\text{cell}}}$$

$$Y_{\text{vesicle-rigid}} \ll Y_{\text{vesicle-elastic}}$$

We can see that based only on the size difference in the bilayer species, there is a 10,000-fold difference in the bending energy if you assume that the values for Young's modulus (Y) are similar between a vesicle and a cell. When the system becomes more rigid, Y decreases and the difference in bending energies becomes even greater. These values help to gauge the energetic cost to the cell for the merger of cell–vesicle membranes.

It is clear based on our cursory evaluation that the size, bending energy, and elasticity of the bilayer drug delivery species can greatly alter the energetics of the cell membrane. The beauty of physiological systems is that they are not controlled by a singular response, where in a cellular system, the mode of uptake may change in response to a change in the bending energy or elasticity offset described above, a ligand–receptor interaction, the mobilization of surface charges, or the size of an external assembly. The challenge in terms of material design is the fabrication of a system that can both effectively exploit a given spectrum of relevant physiological behaviors while remain robust in its response to the systemic physiological environment.

5.2.5 Macropinocytosis

The second route of targeted uptake that we will discuss, known as *macropinocytosis*, has gained significant attention within the last 10 years in the field of drug delivery [53]. The process of macropinocytosis involves the bulk internalization of a localized extracellular volume and its contents into cytoplasmic vesicles known as *macropinosomes* within a cell during a period of extensive membrane ruffling or reorganization. While the internalized components traditionally appear similar in terms of their membrane constituents with those of phagosomes, the fate of these components is largely misunderstood [64]. The process itself is actin-driven, independent of encapsulated material, but can be triggered by the activation of growth factor signaling pathways [65]. Unlike RME, these pathways are not tied to any specific markers or membrane topologies. It is understood that this process is exploited by antigens in order to perpetuate cellular internalization, while avoiding an immediate immune response [66]. Of particular interest in the field of drug delivery, macropinocytosis allows for a sufficient route for relatively large extracellular volumes (>200-nm diameter), with macromolecules to be internalized in a nonselective manner [66] (Fig. 5.12).

If we look more closely at what is currently accepted in terms of the mechanism for macropinocytosis, we can determine the design characteristics that can be used to exploit this mode of internalization for drug delivery. The process of macropinocytosis generally can be seen to have five stages [67]. In stage 1 (I), the activation of epidermal growth factors (EGFR) or platelet-derived growth factor (PDGFR) receptors (i.e., receptor tyrosine kinase) at the cell surface triggers mobilization and growth of actin. The actin filaments that are polymerized adjacent to the cell membrane cause a planar protuberance from the surface, referred to as membrane ruffling in stage 2 (II). The membranes within the ruffles then fuse back to the membrane, enveloping a localized volume of extracellular materials into what is known as a macropinosome in stage 3 (III). The remaining two stages (IV and V) can vary widely depending on the cell type within which the process is occurring. For example, in kidney cells, the macropinosomes appear to be targeted toward the late endosomal system (IV–IVb), while in fibroblast cells (i.e., NIH-3T3) they are rapidly recycled to the cell membrane (V), staying outside the endosomal pathway.

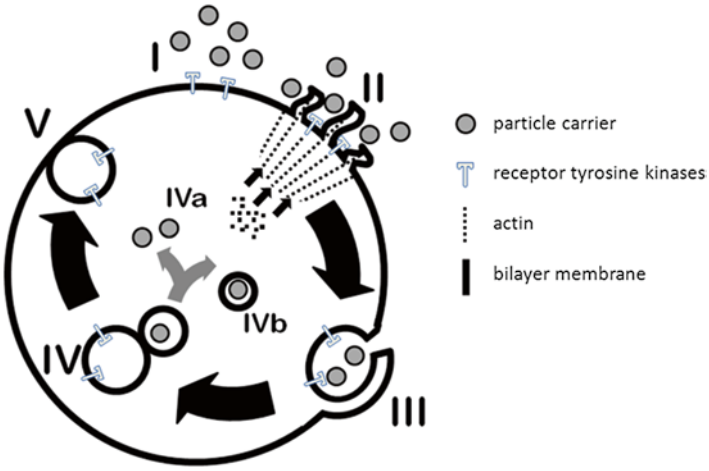

Fig. 5.12 Diagram of the cellular process of macropinocytosis

The process in its entirety lasts 40–45 min [68]. It is important to note that though it was not mentioned previously, both RME and macropinocytosis rely on the mobilization of actin to the cell membrane. The key difference is in the specificity of the interaction. While RME requires the coordination of a ligand to a receptor, which is concurrently associated to a component within the inner leaflet of the membrane (i.e., FC component), triggering an intracellular cascade leading to its internalization, macropinocytosis is nonspecific [65] and simply requires the mobilization of receptor tyrosine kinases to elicit a response.

We now know that unlike RME, the macropinocytosis route does not require targeted surface binding for the expressed purpose of internalizing drug cargo. The nonspecific chemical nature of the cellular interaction removes the requirement of precise chemical binding functionalities on the particle surface. In many respects, this allows for a much simpler delivery mode than that of RME. Since the process of macropinocytosis is essentially the imbibition [69] of a localized volume of the extracellular environment adjacent to the cell, one strategy used is to increase the localized concentration of particles at the cell surface through weak, nonspecific interactions such as electrostatics or hydrogen bonding. Chemical functionalities such as guanidinium, amine, carboxylic acid, and phosphate all fulfill the role of a source of nonspecific binding for these purposes. If we approach the design from this perspective, we can see that the primary function of the binding of particulate species is to remain localized to the cell surface under typical physiological conditions encountered within specific environments. Conditions such as shear flow [70] (I), membrane undulation forces [71] (II), and changing electrostatic potentials [72] (III) all create conflict modes that require factoring into the material design parameters. In the case of shear flow, the binding energy of the particulate species, as we calculated in Sect. 5.1, to the cell surface needs to be greater than that of the normal force felt due to the shear flow in the extracellular environment. Since cell membranes

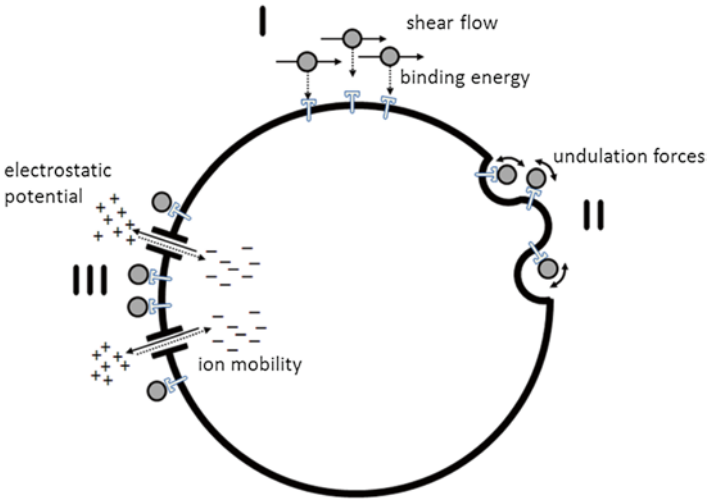

Fig. 5.13 Diagram of intracellular and extracellular forces that can effect macropinocytosis

have a fluid nature, the undulation forces represent the potential for a reduction in the number of contact points within the interface between the particulate and the cell membrane. Once again, the binding energy must be sufficient in the presence of a range of membrane undulations while experiencing external shear flow. In another layer of complexity, the binding must also be retained in the presence of localized ionic gradients (Fig. 5.13).

The presence of various ion channels within the cell membrane ensures an ever-changing distribution of ions in the area localized to the cell surface. While these criteria may appear to be insurmountable, keep in mind that the timing for the internalization of macropinosomes is 40–45 min. This short timescale leaves a wider range in terms of specifications than a timescale of, for example, one to two weeks.

We have discussed two routes for targeted systems to be internalized within a cell with receptor-mediated endocytosis and macropinocytosis from an engineering, biological, and chemical perspective. The discussion was largely focused on energetic compromises and confounding factors. When one looks at our approaches from a purely cell biological perspective, it is important to understand that these compromises and factors do not remain isolated and, in fact, will influence a variety of cellular responses. If we were to use larger particles of 500 nm on a noncancerous cell, the isolated response in terms of cell uptake would take a significantly long time. The actual cell response, however, would likely involve a different mechanism, such as the organization of *caveolin* instead of *clathrin*, and the mobilization of cholesterol to the particle–membrane interface to allow for a significantly greater degree of membrane fluidity.

From the material design perspective, this is an important point to frame your approach. The engineer can choose to design his system (Table 5.1) in a way that allows for it to move with an existing cellular uptake and delivery pathway, or she can choose to design and optimize her system in an isolated environment and

Table 5.1 Common targeting groups for use in drug delivery

Targeting group	Abbreviation	Chemical structure	Receptor	Route of uptake
Arginine (guanidinium)	R	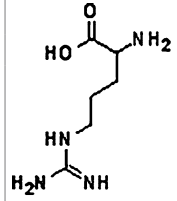	Phosphate Carboxylate Heparin sulfate	Macropinocytosis
Arginine–glysine–aspartate	RGD	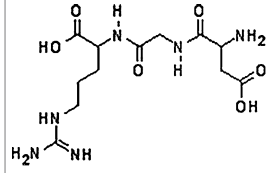	Integrin	Receptor-mediated endocytosis
Folic acid	Vitamin M Vitamin B_9 Pteroyl-l-glutamate	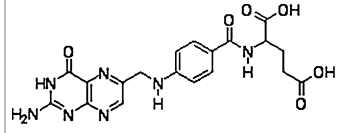	Folate receptor	Receptor-mediated endocytosis
Dinitrophenyl	DNP	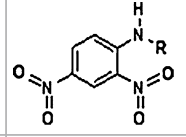	IgE	Receptor-mediated endocytosis
HIV–Tat sequence	$Tat_{(48–60)}$	H-GRKKRRQRRRPPQ-OH H-Gly-Arg-Lys-Lys-Arg-Arg-Gln-Arg-Arg-Arg-Pro-Pro-Gln-OH	Phosphate Heparin sulfate	Macropinocytosis
GM1-binding peptides	G## (i.e., G23)	HLNILSTLWKYRC H-His-Leu-Asn-IIe-Leu-Ser-Thr-Leu-Trp-Lys-Tyr-Arg-Cys-OH	GM1	Receptor-mediated endocytosis

navigate the compromises it brings to the different cellular uptake and delivery pathways as a result. This is an important distinction to make; an understanding of which pool of thought current scientific literature in the field of drug delivery falls is critical for the development of meaningful, functional, therapeutic systems.

5.3 Implementation

5.3.1 Nanoparticles and Vesicle-Targeted Drug Delivery

5.3.1.1 Vesicle-Targeted Drug Delivery

Up to this point in the chapter, we have discussed the design implications for both specific and nonspecific cell membrane targeting for drug delivery. A common method of implementing either strategy seen in the literature is the use of viruses as a model for targeted cell uptake [73]. In the viral model, the single virus is in a dormant state due to its uncharged surface, which disfavors flocculation and eventual surface interaction. The receptor targeting groups within the viral envelop bind with ligands on the cell surface and allow the virus to remain in close proximity to the cell membrane surface. It is after this docking event that the viral membrane can begin to fuse with the cell membrane and allow for subsequent pore formation and penetration.

One specific mechanism for viral cell uptake that has gained significant attention within the last decade has been the uptake of the trans-activating transcriptional activator (Tat) sequence within the HIV virus [74]. This sequence of 14 amino acids, approximately half of which are arginine, is believed to be responsible for driving the cell internalization mechanism for the HIV virus and, in doing so, has been co-opted by biomedical engineers [75] as a form of tag to cause cells to internalize numerous attached cargos (Fig. 5.14).

But what drives this internalization mechanism? Several theories have been actively explored to answer this question, some of which we will address in our current discussion. The first involves the charge neutralization of the guanidinium functionality on the six arginine amino acid components of the $Tat_{48–60}$ sequence [76]. The resonance positive charge from the guanidinium group is believed to form a bivalent complex with the resonance negative charge of a phosphate or carboxylate group on the cell surface. This change in polarity both alters the electrostatic potential in the proximity of the membrane surface as well as creates a driving force to reduce the free energy of the surface by shifting the nonpolar complex to the membrane interior. What occurs next is often debated. Some believe [77] that this driving force continues to a point where the complex reaches the interior of the membrane, causing decomplexation and release into the intracellular space (Fig. 5.15).

Tat_{48-60} H-CG**R**KK**RR**Q**RRR**PPQ-OH

C(Cys) G(Gly) **R(Arg)** K(Lys) Q(Gln) P(Pro)

Fig. 5.14 Sequence of amino acids comprising HIV-Tat_{48-60}

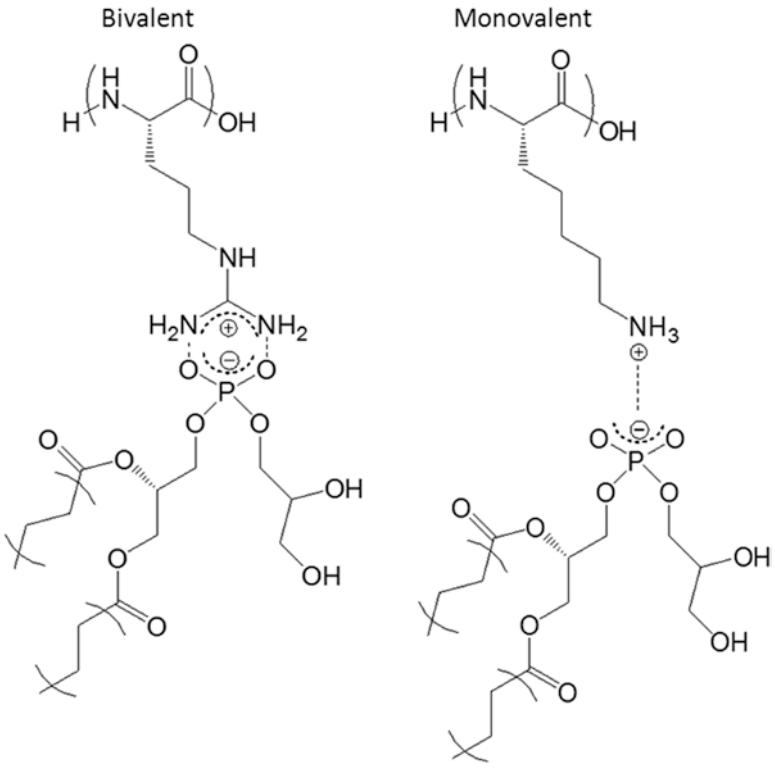

Fig. 5.15 Structure of bivalent and monovalent coupling of the guanidinium functionality of arginine to phosphate groups common to the cell membrane

This method can be used to rationalize the uptake of Tat–drug complexes, assuming the drug molecules are within a specific size regime (i.e., ~10 nm); however, it does little to explain the driving force behind the enhanced delivery that has been observed for significantly larger species (i.e., >100 nm) [78]. Another hypothesis is the binding of Tat sequences to the cell surface leads to an observed induced concavity, or negative Gaussian membrane curvature, of the cell membrane surface. The driving force from this membrane rearrangement is believed to be responsible for the internalization of larger Tat-bound cargos [79]. The mechanism for this behavior, however, is not well known. More recently, a proposed explanation for this cellular response by Mishra et al. [80] involved the formation of a multiplex species among the membrane, the actin cytoskeleton, and cell surface receptors formed by multidentate hydrogen-bonding interactions between lipid head-group domains (Fig. 5.16).

In this rationalization, the balance of arginine, lysine, and hydrophobic amino acid sequences facilitates an actin cytoskeletal rearrangement, resulting in higher translocation activity. The internalized vesicle species are encapsulated with actin species with no specific receptor–ligand systems present (Fig. 5.17).

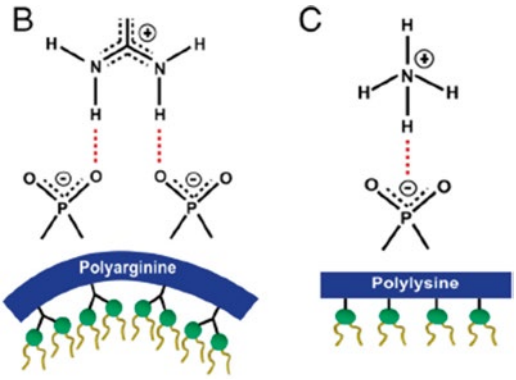

Fig. 5.16 Membrane activity of CPPs controlled by lipid crowding effects and amino acid content. (**b**) Multidentate coordination of arginine's guanidinium side chain induces positive curvature strain along the peptide. (**c**) Monodentate coordination of lysine's amino side chain does not induce positive curvature [80]

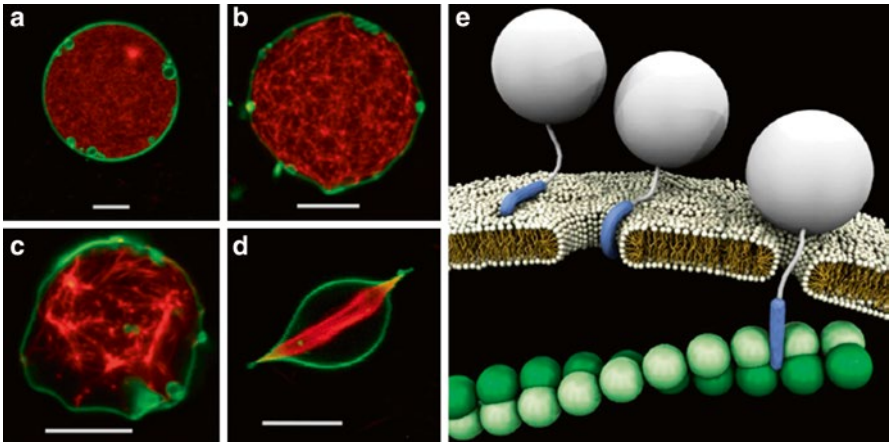

Fig. 5.17 TAT peptide can penetrate membranes and actively induce cytoskeletal actin response. (**a**) Confocal image of a GUV comprising 40/40/20 PE/PC/PS (labeled *green* with DiO) with 5% calcium ionophore (Calcimycin) and encapsulating 7 μM globular actin (G-actin). Exposure to 8 mM Mg2þ, diffusing into the GUV via the ionophores, induced polymerization into filamentous actin (F-actin, labeled *red* with rhodamine phallodin) network without any accompanying deformation of vesicle. (**b**, **c**) Exposure to approximately four μMTAT peptide-induced dimple instabilities on the membrane, and promoted growth of F-actin bundles encapsulated within the GUV. (**d**) In certain cases, the F-actin bundles distorted originally spherical vesicles to form sharp filopodium-like protusions, reminiscent of membrane ruffling and macropinocytosis. (**e**) Schematic showing a proposed autonomous pathway for TAT cellular transduction. TAT peptide can generate saddle-splay membrane curvature and enter through an induced pore, but large conjugated cargos cannot. The TAT peptide interacts strongly with cytoplasmic actin to promote cellular uptake of anchored cargo via endocytotic pathways. White scale bars are 10 μm [80]

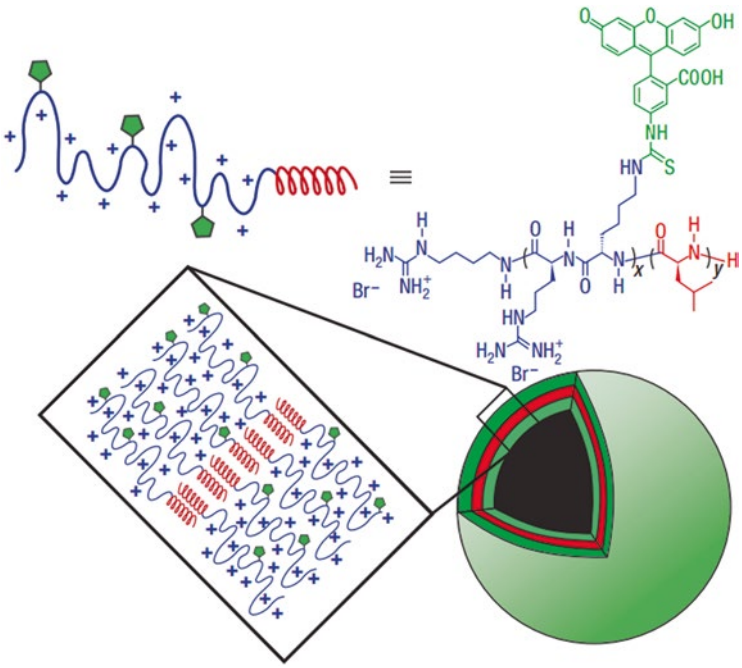

Fig. 5.18 Formation and properties of $R_{60}L_{20}$ vesicles. Schematic diagram of proposed self-assembly of $R_{60}L_{20}$ vesicles [81]

The induced cellular uptake of larger (>100-nm) Tat-based systems need not rely solely on Tat replicates and may additionally involve species rich in arginine residues. Holowka et al. [81] designed a block copolypeptide system comprised of leucine and arginine domains, which self-assemble to form vesicle species with outer and inner membrane surfaces of arginine with a controllable size down to 50 nm (Fig. 5.18).

The size adjustment was achieved simply by extrusion through track-etched membranes in a manner consistent with existing liposome preparation techniques [82] to form peptide vesicle species. The copolypeptides were synthesized using a transition metal–mediated ring-opening polymerization method from Timothy Deming [83] for use with *N*-carboxyanhydride monomers. This controlled polymerization allows for the fabrication of robust polymer architectures with fine control over polypeptide structure and composition. The hydrophilic portion of the polypeptide chain was tagged with an FITC molecule (i.e., green fluorescence), while the vesicle was loaded with a Texas Red-labeled Dextran (i.e., red fluorescence) as cargo. This labeling strategy allows for both the vesicle and the cargo to be monitored throughout the course of its cellular interaction in vitro (Fig. 5.19).

Holowka et al. evaluated the degree of internalization of the vesicle species (i.e., $R_{60}L_{20}$) after extrusion to a 100-nm diameter in both epithelial and endothelial cells.

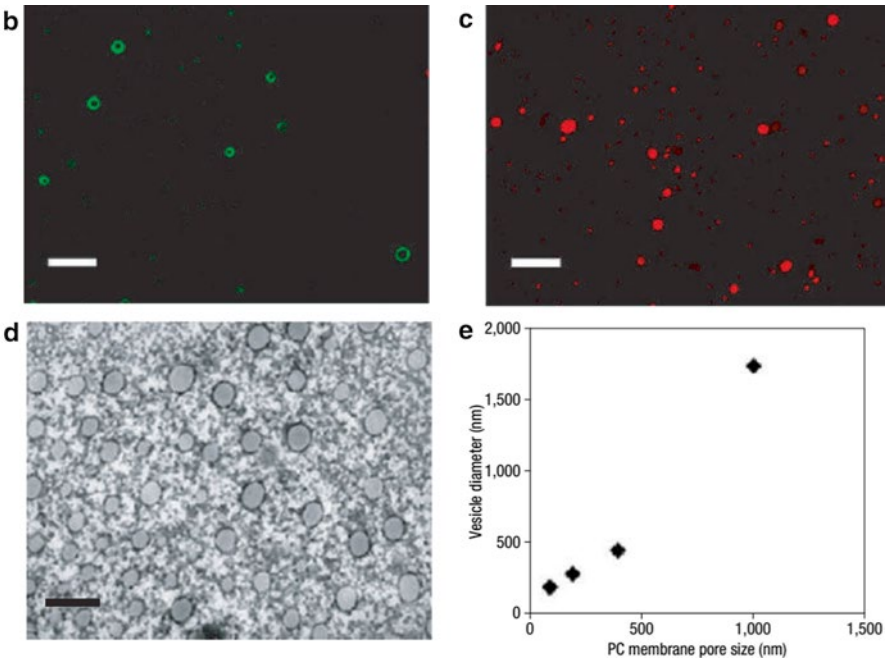

Fig. 5.19 Formation and properties of $R_{60}L_{20}$ vesicles. (**b**) LSCM image of 1.0-μm extruded vesicles (scale bar = 5 μm). (**c**) LSCM image of vesicles containing Texas Red–labeled dextran (total solution concentration = 1 μM). Scale bar = 5 μm. (**d**) Transmission electron micrograph of negatively stained vesicles that had been extruded through a 100-nm nucleopore polycarbonate (PC) membrane filter (scale bar = 200 nm). (**e**) Vesicle diameters determined using dynamic light scattering after extrusion through different PC membrane filters (100, 200, 400, and 1,000 nm) [81]

These arginine–leucine vesicles were compared to several controls, including the monovalent vesicle species of lysine–leucine (i.e., $K_{60}L_{20}$) and homopolymers of both arginine (i.e., R_{60}) and lysine (i.e., K_{60}). Time-lapsed cell culture revealed a distinct internalization behavior difference between the arginine–leucine system (a, c, e, f, g) and each of the other experimental controls (h). Though internalization of arginine vesicle systems was clearly demonstrated, the integrity of the internalized species of vesicle (i.e., green), cargo (i.e., red), and vesicle with encapsulated cargo (i.e., yellow) was difficult to determine. For drug delivery applications, it may be necessary to quantify the concentration of a drug that is effectively released from the vesicle complex within a specific intracellular location (Fig. 5.20).

Fig. 5.20 (continued) incubation with $R_{60}L_{20}$ vesicles (*green*) containing Texas Red–labeled dextran (*red*) at 37 °C without serum. (**e**–**g**) Three-dimensional LSCM reconstructions of T84 cells after incubation with $R_{60}L_{20}$ vesicles (*green*) containing Texas Red–labeled dextran (*red*) for 5 h at 37 °C without serum (**e**), at 37 °C with serum (**f**), and at 0 °C without serum. (**g**, **h**) LSCM image of T84 cells after incubation with fluorescein-isothiocyanate–labeled $K_{60}L_{20}$ vesicles (100 μM) for 5 h at 37 °C without serum [81]

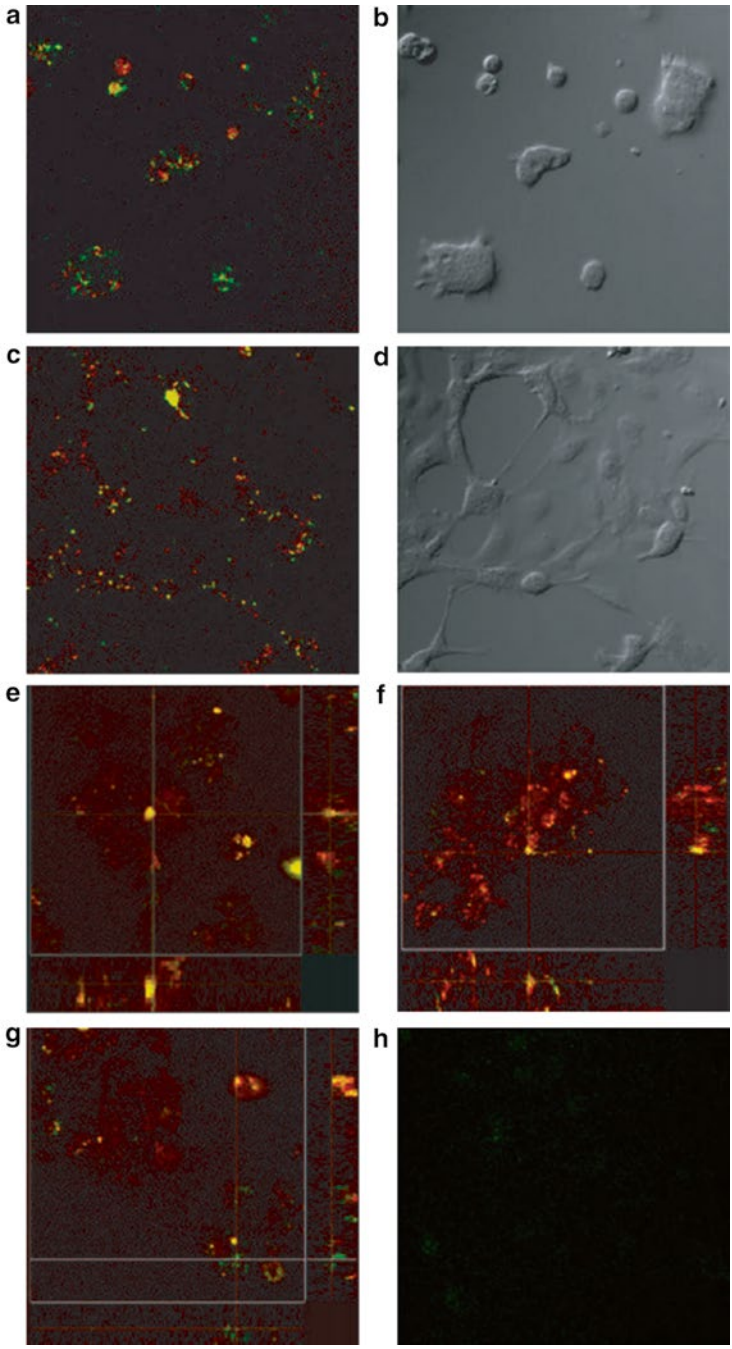

Fig. 5.20 Transport of polypeptide vesicles into cells in vitro. (**a**, **b**) LSCM (**a**) and differential interference contrast (DIC; **b**) images of T84 cells after 2.5 h incubation with $R_{60}L_{20}$ vesicles (*green*; 100 μM) containing Texas Red–labeled dextran (*red*; total solution concentration = 1 μM) at 37 °C without serum. (**c**, **d**) LSCM (**c**) and DIC (**d**) images of HULEC-5A cells after 2.5 h

Cell viability assays confirmed the dosage of these copolypeptide systems was safe within the concentrations designated by the experiments.

The use of nonspecific surface targeting domains allows for the design of biocompatible peptide-based drug delivery systems with enhanced cellular internalization profiles. As the specificity of these surface domains increases (i.e., arginine-rich to $Tat_{48–60}$), the mechanism for internalization becomes more easy to define. The advent of new systems that exploit existing macropinocytosis internalization pathways allows for a robust size range of drug delivery species to be effectively delivered to specific cell types.

5.3.2 Targeted Nanoparticle Systems

The use of nonspecific tissue targeting holds a distinct advantage for the delivery of drugs to an effected tissue domain, such as enflamed tissue in the intestine due to Crohn's disease. If, instead, the therapeutic approach involves delivery of a drug to a cell of a specific type, such as a cancer cell, then receptor-targeted drug delivery could provide some advantages. The use of specific targeting groups allows for a predictable binding event on the cell surface, internalization pathway, and ultimate consumption event within the cell, with a reduced propensity for cell toxicity.

Engineered nanoparticle design with surface ligands specific for cell types has been actively pursued within Robert Langer's Group at the Massachusetts Institute of Technology (MIT). In the work of Kolishetti et al. [84], a nanoparticle system was designed and fabricated from a blend of a platinum (IV)-prodrug conjugated system with polylactide [PLA-Pt(IV)], and poly(D,L-lactide-co-glycolide)-*block*-*poly*(ethylene glycol) (PLGA-*b*-PEG). The nanoparticle system was prepared by nanoprecipitation in microfluidic channels with cisplatin and docetaxel (Dtxl) to form a species ~100 nm in diameter. The nanoparticle surface was functionalized with an A10 aptamer targeting group specific for prostate antigen PSMA on affected cancer cells (Fig. 5.21).

The release kinetics of Pt(IV) and Dtxl was monitored for these nanoparticle systems in vitro using HPLC. As expected, the release profile of the conjugated Pt(IV) prodrug system was less than that of the free Dtxl drug within the nanoparticle blend. The Pt(IV) system showed a high release rate at the 75-h mark, which is consistent with the predicted degradation profile of the PLGA within the prodrug conjugate. The release kinetics displays the timed release of two component drugs within the time course of the experiment, which allows for a degree of tunability to the effective treatment of this form of prostate cancer cells (Fig. 5.22).

The authors then examined the biological effectiveness of the delivery of the Pt(IV) and Dxtl in terms of their IC_{50} cytotoxicity, which is the measure of the effectiveness of a chemical at inhibiting 50% of the biological or biochemical function of cells. Therefore, if we have a high IC_{50} value, we can infer that the drug system is not as effective in inhibiting biological function as a value less than it. We can see that several trends from the cytotoxicity data become apparent as we decouple the

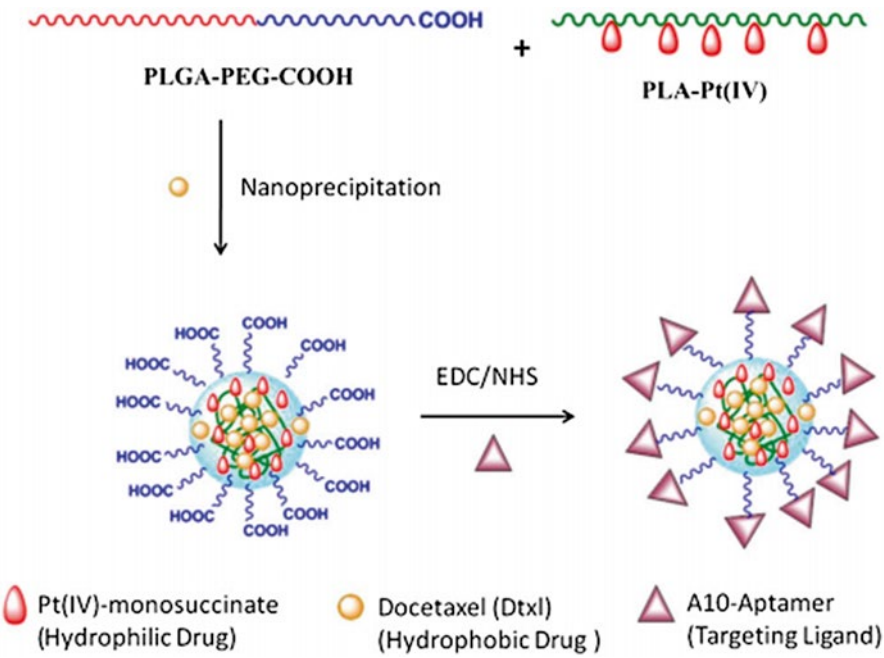

Fig. 5.21 Design and construction of NPs [84]

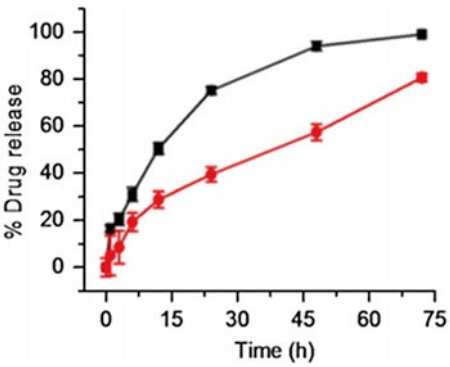

Fig. 5.22 In vitro release kinetics of encapsulated platinum (*circle*) and docetaxel (*square*) in PBS at 37 °C from NPs [84]

components of the nanoparticle system. First, the fabrication of the prodrug system of Pt(IV) within a nanoparticle indicates a performance improvement (i.e., IC_{50} of 5 vs. 106) in terms of the inhibition of cellular function. As the authors begin to add in the targeting aptamer, the IC_{50} level drops even further into the 0.95 regime. This trend is consistent with the Pt(IV) + Dxtl systems as well, where the values trend from 0.009 to 0.0036 as the system moves from nanoparticle to a targeted system [84].

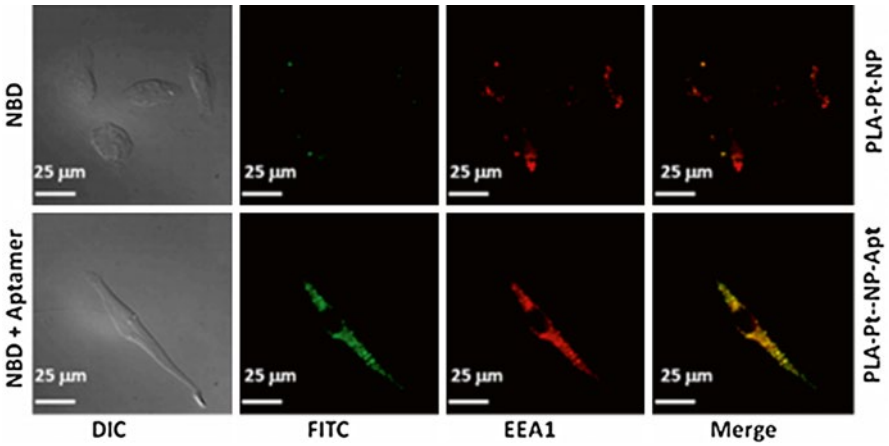

Fig. 5.23 Endocytosis of PSMA-targeted NPs in LNCaP cells. Green fluorescent 22-NBD-cholesterol was co-encapsulated in the PLGA-b-PEG nanoparticles and PSMA aptamers were conjugated to the surface of the particles. The early endosomes were visualized in red by using the early endosome marker EEA-1 [84]

If we now look at the effectiveness of the delivery in terms of the fluorescence imaging comparison between targeted and nontargeted systems, a clear advantage emerges. In this study, the authors clearly show the endocytosis of nanoparticle species with targeting groups as opposed to those with nontargeting groups (Fig. 5.23) through the colocalization of fluorescence species from the nanoparticle (i.e., FITC) with those of an endosomal cell marker (i.e., EEA1), which strongly suggests receptor-mediated endocytosis (RME) as a mode of cell internalization. The authors also showed an increase in the effective complexation of Pt(IV) with DNA when it is in the presence of Dtxl within the nanoparticle system (Fig. 5.24).

This targeted nanoparticle system provides a promising example of a rationally designed drug delivery system with components of controlled release (i.e., biodegradable PLGA and PLA), self-assembly (i.e., nanoparticle fabrication using nanoprecipitation within microfluidic channels), and cell-specific targeting (i.e., A10 aptamer for cancerous prostate cells). This approach also indicates potential benefits of noncovalently blended drug components within these nanoparticle systems to highlight the potential for multicomponent cancer therapies. In Chap. 7, we will discuss stimuli-responsive "Smart" drug delivery systems, which are not reliant upon a gradual pharmacokinetic release profile to deliver a drug and instead have a controlled burst release of the drug as the system reaches the desired environment or is induced by a targeted stimulus. These new systems will allow for a new generation of materials for drug delivery that can begin to modulate the dosage of delivery in vivo.

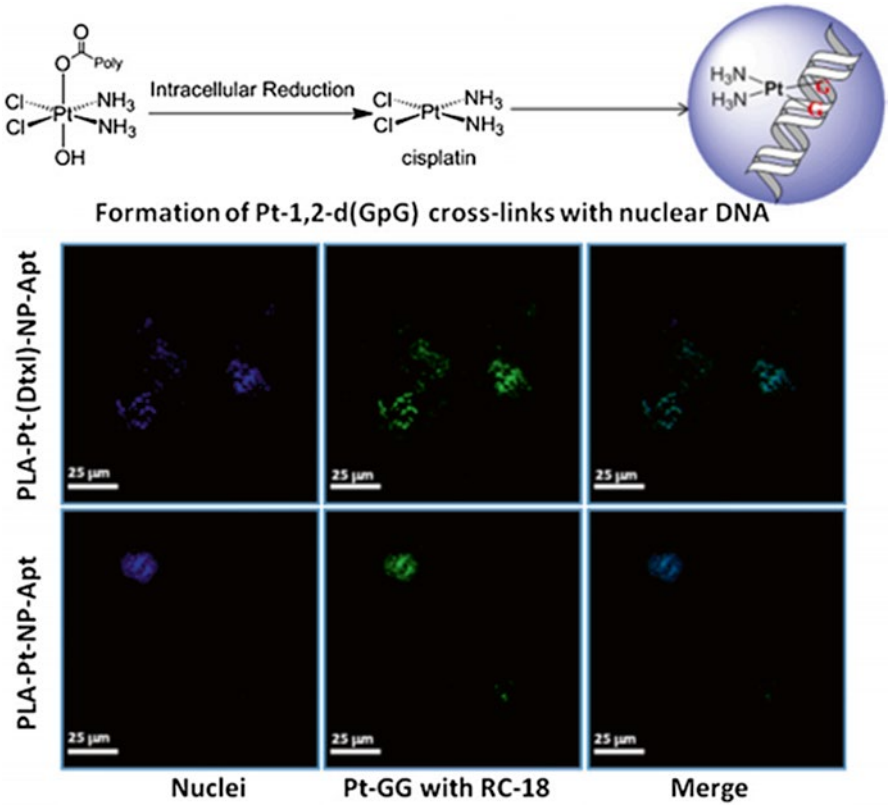

Fig. 5.24 Visualization of Pt-1,2,-d(GpG) intrastrand crosslinks in the nuclear DNA of LNCaP cells after treatment with PLA-Pt-NP-Apt and PLA-Pt-(Dxtl)-NP-Apt. Nuclei were stained with Hoeshst (*blue*) and Pt-1,2-d(GpG) in DNA were visualized using Mab R-C18 (*green*) [84]

5.3.3 Summary

The design and functionalization of drug delivery systems to enhance the efficiency of drug targeting has gained significant interest during the last 10 years. In Sect. 5.1, we discussed three primary factors that influence the effective binding of drug systems within a physiological environment: the *diffusion* of blood components in concert with drug molecules; the *surface area* and forces felt at the interface between the drug particle and the tissue; and the *binding kinetics* between the receptor and ligands in the presence of flow. These fundamental properties were extended in Sect. 5.2 to the design of drug delivery systems based on the criteria of *size*, *shape*, *chemical functionality*, and *elasticity*. We defined these criteria in terms of strategies to exploit *passive cellular uptake*, such as *facilitated diffusion* and *filtration*, or

Table 5.2 Common scientific disciplines tied to critical fundamentals in targeted drug delivery systems

Fundamental	Disciplines
Diffusion	• Chemistry • Chemical engineering • Materials engineering • Physics
Fluid mechanics	• Chemical engineering • Chemistry • Physics
Electrostatics	• Electrical engineering • Chemistry • Materials engineering • Biochemistry
Deformation	• Materials engineering • Mechanical engineering
Surface functionalization	• Chemistry • Biochemistry
Dispersion-colloidal stability	• Chemistry • Physics • Chemical engineering • Materials engineering
Cell trafficking	• Cell biology
Cell internalization	• Cell biology • Molecular biology • Biophysics

active cellular uptake, such as *RME* and *macropinocytosis,* to achieve successful delivery of drug dosage forms to cellular targets. Selected strategies were applied in Sect. 7.3 as enhanced binding and internalized arginine-based vesicle assemblies and highly specific targeted nanoparticle systems. These systems represent a still further manipulation of a material system to enhance the specificity of the physiological interaction to allow for effective drug delivery (Table 5.2).

5.4 Clinical Applications

5.4.1 Targeted Micelles for Cancer Therapy

This chapter has discussed targeted drug delivery vehicles for the treatment of specific cells and tissues. The previous chapter discussed self-assembled materials for drug delivery. In this clinical applications section, we will combine these two

Table 5.3 Ligand-functionalized micellar systems for active tumor targeting

Ligand type	Ligand	Polymer composition	Micelle size (nm)	Therapeutic drug
Small organic molecule[a]	Folic acid	PEG-PLGA	105	Doxorubicin
Small organic molecule[b]	Folic acid	PEG-PCL	50–130	Paclitaxel
Peptide[c]	cRGD peptide	PEG-PCL	20–40	Doxorubicin
Antibody[d]	Anticancer mAb 2C5	PEG-PE	20	Paclitaxel

[a]Yoo HS, Park TG, Folate receptor targeted biodegradable polymeric doxorubicin micelles. *J Control Release,* 96:273, 2004.
[b]Park EK, Lee SB, Lee YM, Preparation and characterization of methoxy poly(ethylene glycol)/poly(epsilon-caprolactone) amphiphilic block copolymeric nanospheres for tumor-specific folate-mediated targeting of anticancer drugs. *Biomaterials,* 26:1053, 2005.
[c]Nasongkla N, Shuai X, Ai H, et al., cRGD-functionalized polymer micelles for targeted doxorubicin delivery. *Angew Chem Int Ed Engl,* 43:6323, 2004.
[d]Torchilin VP, Lukyanov AN, Gao Z, et al., Immunomicelles: Targeted pharmaceutical carriers for poorly soluble drugs. *Proc Natl Acad Sci U S A,* 100:6039, 2003.

concepts and discuss targeted, self-assembled micelles for cancer treatment. We will also see that targeted micelles can often provide superior treatment options to non-targeted micelles, resulting in increased clinical efficacy.

Although nontargeted micelles can passively accumulate inside cancerous tumors with leaky vasculature, the majority of these nanoparticles are still cleared by the reticuloendothelial system, even if the micelles have "stealth" characteristics. This results in shorter micelle half-lives as well as unwanted micelle deposition in the liver and spleen [85]. While passively targeted micelles are a major advance for cancer treatment, and such systems are now having a positive impact on lung cancer patients, work is already underway to create actively targeted micelles for cancer chemotherapy. Actively targeted carriers are functionalized to allow specific interactions with tumor cells as well as specific control of drug release. These formulations can increase the exposure of tumor cells to chemotherapeutics, enabling greater antitumor efficacy.

A main strategy for creating functionalized polymer micelles is to introduce targeting ligands into the micellar structure. Such ligands selectively bind to surface receptors expressed by tumor cells. Targeting ligands are conjugated to the corona of the micelle and enable specific targeting and uptake of the micelle by tumor cells. Ligands for targeted binding of lung cancer cells may include small organic molecules, peptides, and antibodies. Table 5.3 provides an overview of ligand-functionalized micelle formulations that have been constructed.

Micelles bearing small organic molecules have been designed to target the receptor for folic acid. The folate receptor is a cell-proliferation protein that is overexpressed in lung cancer cells as well as in ovarian, breast, and brain cancer cells [86]. The receptor is a glycosyl-phosphatidyl-inositol-anchored glycoprotein that has high binding affinity to folic acid ($K_d = 10^{-10}$ M). The expression levels of the folate receptor in tumors have been reported to be 100–300 times higher than those

observed in normal tissue [87]. To enable binding to the folate receptor, functionalized micelles have incorporated the folic acid ligand. For instance, the folic acid ligand has been covalently conjugated, via its γ-carboxyl group, onto the hydrophilic corona of doxorubicin-loaded PEG–PLGA micelles [88]. In vitro, the doxorubicin-loaded folate micelles demonstrate greater cellular uptake and higher cytotoxicity than nontargeted micelles. In experimental in vivo tumor models, the doxorubicin-loaded targeted micelles achieved a marked improvement in antitumor efficacy and decreased the tumor growth rate by twice as much as nontargeted micelles [88]. Another folate-targeted micelle for chemotherapeutic delivery has been constructed using a unique conjugation strategy. In this system, folic acid is attached to the hydrophobic end of PEG–PCL block copolymers, and paclitaxel is then encapsulated in the micelle [89]. Although the folate molecule is conjugated to the hydrophobic portion of the micelle, the targeting ligand can be detected on the surface of the micelles via X-ray photoelectron spectroscopy. The folate-bearing paclitaxel-loaded micelles exhibited significant cytotoxicity toward cancer cells with folate receptor expression, while nontargeted micelles did not show significant toxicities in these cell lines [89]. These examples illustrate the potential of actively targeted micelles to enhance cancer chemotherapy, beyond the advances already made by traditional polymer micelles.

Micelles have also been functionalized with small, tightly binding peptides for cancer-targeted drug delivery. An advantage of this strategy is that ligand behavior can be optimized via adjustment of the peptide sequence or conformation. As a case in point, the cyclic RGD (cRGD) peptide has been integrated into micelle structures, to target the $\alpha_v\beta_3$ integrin receptor. This integrin is a cellular transmembrane protein, which is overexpressed on both tumor cells and sprouting tumor vasculature. The membrane receptor has been shown to greatly affect tumor growth, local invasiveness, and metastatic spread; overexpression of $\alpha_v\beta_3$ integrin correlates positively with tumor metastatic potential [90]. The receptor is highly expressed in angiogenic vessels but is not readily detectable in quiescent vessels. This makes $\alpha_v\beta_3$ integrin an appropriate target for treating tumors, which are in a constant state of new vasculature growth. In particular, $\alpha_v\beta_3$ integrin is an excellent target for antiangiogenic interventions. Cyclic(Arg-Gly-Asp-D-Phe-Lys), also known as cyclic RGD, peptides have been developed to provide specific binding to $\alpha_v\beta_3$ integrins [91].

Polymer micelles bearing cRGD peptides have been created to specifically bind tumor endothelial cells that overexpress $\alpha_v\beta_3$ integrin [92]. In these micellar constructs, micelles are formed from maleimide-terminated PEG-poly(ε-caprolactone) copolymer, with doxorubicin encapsulated inside the micelle core. The polymer is conjugated to cRGD after micelle formation. The uptake of cRGD-labeled micelles by tumor endothelial cells has been studied using flow cytometry: The degree of cellular uptake increased with increasing cRGD density on the micelle surface. With 5% cRGD occupancy on the micelle surface, the cRGD-labeled micelles achieved a threefold increase in cellular uptake compared to nontargeted micelles. With 76% cRGD occupancy on the micelle surface, the cRGD-labeled micelles demonstrated an impressive 30-fold increase in cellular uptake compared to nontargeted micelles

[92]. Peptide-labeled micelles can therefore be readily internalized by tumor cells, allowing direct exposure of tumor cells to chemotherapeutic drugs.

Cancer-specific monoclonal antibodies are another class of targeting ligands for micelles. Antibodies are large molecules (approximately 150 kDa) with a high affinity for their antigenic targets ($K_d = 0.1$ nM). An advantage of these ligands is that they can be customized to bind specifically to a wide variety of targets, such as cancer cell–specific antigens. Another advantage of antibodies is that few ligands are required to improve micelle behavior, due to the high binding affinity of antibodies for their targets; as few as 10 antibody ligands per micelle can enhance micelle efficacy. Since excessive levels of surface modification can lead to unintended nonspecific uptake of micelles, it is highly desirable to create targeted micelles with small levels of surface modifications. Micelles functionalized with antibodies have also been termed "immunomicelles" [93].

Antibody-linked immunomicelles have been developed to actively target lung cancer cells [93]. These micelles utilize PEG–PE copolymers, with the free PEG terminus activated with *p*-nitrophenylcarbonyl (pNP) to enable antibody conjugation. The cancer-targeting micelles are prepared from PEG–PE, with the addition of a small fraction of pNP–PEG–PE polymers. The PE residues form the micelle core, while the PEG forms the corona. The pNP groups allow for fast attachment of amino group–containing antibody ligands via the formation of a carbamate bond. The micelles are functionalized with anticancer monoclonal antibody 2C5, which targets the nucleosome of cancerous cells. The antibody-bearing micelles were assessed for their ability to bind nucleosome substrates: The 2C5 antibody retained its ability to bind substrates following conjugation to micelles [93]. The immunomicelles were also loaded with paclitaxel and evaluated in mouse models of lung cancer. Paclitaxel-loaded immunomicelles induced a fourfold increase in drug accumulation in the tumor at 2 h following administration compared to nontargeted micelles. The immunomicelles also demonstrated greater antitumor efficacy, inhibiting tumor growth to a greater extent than nontargeted micelles. Importantly, antibody conjugation to immunomicelles did not significantly change the blood clearance rate from that of nontargeted control micelles. Immunomicelles can thus effect improvements in chemotherapy of lung tumors, without adversely affecting pharmacokinetics.

Overall, micelles bearing small organic molecules, peptides, and antibodies have shown early success for actively targeting tumors. In all of these constructs, ligand presentation on the micelle surface is a critical design factor. Ligand presentation can make the difference between a successful and an unsuccessful therapeutic formulation: While some ligand-functionalized micelles have shown efficacy in binding tumor cells, other formulations have suffered from a lack of ligand binding to targets [94]. Problems with ligand binding have been attributed to the dynamic nature of the micellar PEG corona, which can assume conformations that bury the ligand within the hydrophilic chains. The polydispersity of PEG chains may also contribute to the problem, as ligands that attach to shorter PEG chains are shielded by longer PEG chains. Ligand optimization strategies have been explored, with the goal of optimizing the binding efficiency of actively targeted micelles to tumor cells

[85]. The focus of these efforts is to minimize the shielding effects of the PEG corona and maximize the chemical availability of the targeting ligand.

Two different ligand attachment methods have been evaluated and compared using the cRGD ligand and the PEG–PLA copolymer [85]. In the first case, the ligand was attached to the copolymer before micelle self-assembly. In the second case, the micelles were assembled from the copolymer first, and the ligand attached afterward; this method would ensure that the ligand was attached to chemically available sites on the micelle surface. The uptake of the two functionalized micelle preparations was compared in tumor cell lines, and the micelles prepared by the second method (i.e., ligand attachment to an already-formed micelle) demonstrated a marked increase in cellular uptake. This result suggests that ligand attachment to a formed micelle does indeed promote ligand availability. Although the two methods appear to be similar, they are different upon consideration of the polydisperse nature of the PEG corona. When ligands are attached to the copolymer before micelle formation, they are more likely to conjugate to shorter PEG chains within the population and suffer from shielding effects. This problem may be exacerbated by the higher chemical reactivity of shorter polymer chains. In contrast, the method of postmicelle ligand addition selects for ligands attaching to longer PEG chains, which aids in ligand presentation to targeted tumor cells. This analysis reveals the importance of synthetic strategy in the formulation of targeted biomaterials for drug delivery.

5.5 Problems

5.1 We have learned in this chapter that there are implications in solution properties to the change in the geometry of a self-assembly structure. This is apparent when comparing systems consisting of spherical versus tubular shapes, such as micelles, where there is a distinct difference in their respective aspect ratios (A_f). If a biomedical engineer is designing an oral drug delivery system where the target tissue is the small intestine, answer the following questions with your knowledge of *diffusion* in self-assembled systems.

(i) What are the relative viscosities of a spherical micelle ($A_f = 1$) and a tubular micelle ($A_f = 50$)?
(ii) Which geometry micelle would you expect to be a more effective drug delivery system for the oral application described? Why?
(iii) How would the percolation values differ for a spherical system relative to a fiber system?
(iv) If the concentration of both the spheres and tubes is 7 mg/ml, do you think the colloid concentration would be in an acceptable range for this application for each respective shape? Why?

5.2 The allergic response involves the aggregation of IgE receptor molecules within glycosphingolipid-cholesterol microdomains, known as lipid RAFTs, at the surface of mast cells to facilitate a process known as degranulation. If each

RAFT domain consists of an average surface area of 0.031 μm^2 relative and the mast cell is 20 μm in diameter with a cell membrane thickness of 5 nm and a Young's modulus of 1.2×10^7 Pa, answer the following questions with your knowledge of the interaction *surface area* between elastic and hard materials.

(i) Calculate the elastic modulus of the mast cell membrane assuming that E^* is approximately equal to the bending energy (e_{bend}) within a contact surface area of 0.01 μm^2.
(ii) A medical researcher would like to design a functionalized gold nanoparticle system to target a single RAFT domain on a mast cell. What would be the ideal particle radius if the pressure of the interaction between the nanoparticle and cell membrane is 1×10^{-10} Pa?
(iii) What would the ideal nanoparticle radius be if the surface area of the RAFT domain doubled?

5.3 A biomedical graduate student has designed a targeted vesicle system and is unsure of the possible mechanism of cellular internalization. If the vesicle system has a 50-nm diameter and is spherical in shape, answer the following questions with your knowledge of active and passive cellular delivery.

(i) Based on the properties of this vesicle system, what mode(s) of cellular delivery would be preferred? Why?
(ii) What is the vesicle size required to avoid lipid membrane fouling ($\Delta P = 8.75 \times 10^7$ ng/nm s^2) assuming the pore size is 60 nm in diameter, the dynamic viscosity is 1 with a constant flux of 50 nm/s, and the filter area is represented by the surface area of the cell of 20-μm diameter and 5-nm membrane thickness?
(iii) If you had to operate above the fouling limit, how would you increase the diffusive flux within the membrane?
(iv) How long would it take to envelop the particle when $D = 5 \times 10^5$ nm^2/s and $\alpha = 1$?

5.4 A research lab in biomedical engineering wishes to design a micellar oral drug delivery system that effectively targets the heart. If the micellar system is 20 nm in diameter and charge-neutral, answer the following questions with your knowledge of self-assembled and targeted systems.

(i) Discuss the sequence of physiological constraints in order as the oral drug passes from the mouth to the small intestine.
(ii) Would changing the diameter of the nanoparticle from 20 to 200 nm affect the constraints of the oral delivery system? Why?
(iii) Would changing the surface charge of the nanoparticle to one that is highly cationic affect the constraints of the oral delivery system? Why?

5.5 Use the components in the following table and your knowledge of *targeted* and *self-emulsifying drug delivery* to determine the desired route of internalization for a vesicle system based on the criteria and physical limitations discussed in this chapter.

(i)

Component	Structure	Information
phosphatidylenthanolamine PE	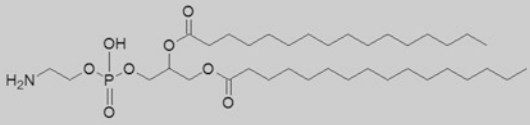	tail length 1.2nm C^{o}>1
arginylglycylaspartic acid RGD	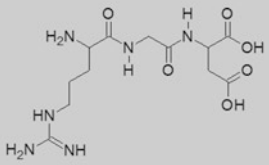	$K_{receptor}$ 1×10^{-8} M^{-1} K_{RGD} 3×10^{-8} M^{-1} Binding Density 10 ligands/ domain

Based on calculations of the *thickness*, *curvature*, and *size* of the self-assembled system, is it likely that it is internalized within the cell through an *active* or *passive* mechanism if the bending energy (e_{bend}) is 5×10^6 Pa/m^2 and Young's modulus is 1.2×10^7 Pa?

(ii) What is the likely kinetics of binding from your answer to (i) if the rate constant for the binding of RGD receptors to the cell is 1.35×10^{-9} M?

(iii) Do the characteristics of binding suggest that the binding force ($F_{binding} = 2 \times 10^{-10}$ N) of the micelle system with a mass of 1 ng to the target cell type is possible relative to opposing forces (i.e., drag force) if the velocity of the system is 50 mm/s in blood plasma with a viscosity of 4cP, with an acceleration of 5 mm/s^2? Why?

References

1. Muller, R. H., & Keck, C. M. (2004). Challenges and solutions for the delivery of biotech drugs—A review of drug nanocrystal technology and lipid nanoparticles. *Journal of Biotechnology, 113*(1), 151–170.
2. (a) Lincoff, A. M. (1998). Trials of platelet glycoprotein IIb/IIIa receptor antagonists during percutaneous coronary revascularization. *The American Journal of Cardiology, 82*(8), 36P–42P. (b) Chonn, A., & Cullis, P. R. (1995). Recent advances in liposomal drug–delivery systems. *Current Opinion in Biotechnology, 6*(6), 698–708.
3. (a) Harris, J. M., & Chess, R. B. (2003). Effect of pegylation on pharmaceuticals. *Nature Reviews Drug Discovery, 2*(3), 214–221. (b) Corsi, D. F., Prosperi, D. D., Wang, M., & Thanou, M. (2010). Targeting nanoparticles to cancer. *Pharmacological Research, 62*(2), 90–99.
4. Dainty, L. A., Risinger, J. I., Morrison, C., Chandramouli, G. V. R., Bidus, M. A., Zahn, C., et al. (2007). Overexpression of folate binding protein and mesothelin are associated with uterine serous carcinoma. *Gynecologic Oncology, 105*(3), 563–570.
5. Lopes, J., Santos, G., Barata, P., Oliveira, R., & Lopes, C. M. (2013). Physical and chemical stimuli-responsive drug delivery systems: Targeted delivery and main routes of administration. *Current Pharmaceutical Design, 19*(41), 7169–7184.
6. Leon Glass, P. H. (1991). *Theory of heart: Biomechanics, biophysics, and nonlinear dynamics of cardiac function*. New York: Springer.

7. Albanese, A., Tang, P. S., & Chan, W. C. W. (2012). The effect of nanoparticle size, shape, and surface chemistry on biological systems. *Annual Review of Biomedical Engineering, 14*, 1–16.
8. (a) Kensey, K. R., & Cho, Y. I. (2007). *The origin of atherosclerosis: What really initiates the inflammatory process* (p. 200). Summerville, WA: SegMedica. (b) Ernst, E., Resch, K. L., Matrai, A., & Paulsen, H. F. (1991). Hyperviscosity. An independent risk factor after a survived stroke. *Acta Medica Austriaca, 18*(Suppl 1), 32–36.
9. Sloop, G. D. (1996). A unifying theory of atherogenesis. *Medical Hypotheses, 47*(4), 321–325.
10. Van den Berg, A. M. J., de Laat, A. W. M., Smith, P. J., Perelaer, J., & Schubert, U. S. (2007). Geometric control of inkjet printed features using a gelating polymer. *Journal of Materials Chemistry, 17*(7), 677.
11. Harzallah, O., & Dupuis, D. (2003). Rheological properties of suspensions of TiO_2 particles in polymer solutions. 1. Shear viscosity. *Rheologica Acta, 42*(1–2), 10–19.
12. Wiese, G., & Healy, T. (1975). Coagulation and electrokinetic behavior of TiO_2 and Al_2O_3 colloidal dispersions. *Journal of Colloid and Interface Science, 51*(3), 427–433.
13. Heijman, S. G. J., & Stein, H. N. (1995). Electrostatic and sterical stabilization of TiO_2 dispersions. *Langmuir, 11*(2), 422–427.
14. Einstein, A. (1905). Über die von der molekularkinetischen Theorie der Wärme geforderte Bewegung von in ruhenden Flüssigkeiten suspendierten Teilchen. *Annalen der Physik, 322*(8), 549–560.
15. (a) Hochmuth, R. M., Mohandas, N., & Blackshear, P. L. (1973). Measurement of the elastic modulus for red cell membrane using a fluid mechanical technique. *Biophysical Journal, 13*(8), 747–762. (b) Kolhar, P., Anselmo, A. C., Gupta, V., Pant, K., Prabhakarpandian, B., Ruoslahti, E., & Mitragotri, S. (2013). Using shape effects to target antibody-coated nanoparticles to lung and brain endothelium. *Proceedings of the National Academy of Sciences of the United States of America, 110*(26), 10753–10758.
16. Prigogine, I., & Rice, S. A. (Eds.). (1995). *Advances in Chemical Physics* (Vol. 91). Hoboken, NJ: Wiley.
17. Kynch, G. J. (1954). The effective viscosity of suspensions. *British Journal of Applied Physics, 5*(S3), S5–S10.
18. Elias, H. (2003). *Theta solvents*. New York: Wiley (Wiley Database of Polymer Properties).
19. Pauling, L., Corey, R. B., & Branson, H. R. (1951). The structure of proteins; two hydrogen-bonded helical configurations of the polypeptide chain. *Proceedings of the National Academy of Sciences of the United States of America, 37*(4), 205–211.
20. Bicerano, J., Douglas, J. F., & Brune, D. A. (1999). Model for the viscosity of particle dispersions. *Journal of Macromolecular Science, Part C: Polymer, 39*(4), 561–642.
21. Helfrich, W. (1973). Elastic properties of lipid bilayers: Theory and possible experiments. *Zeitschrift für Naturforschung. Teil C: Biochemie, Biophysik, Biologie, Virologie, 28*(11), 693–703.
22. Johnson, K. L. (1987). *Contact mechanics* (p. 452). Cambridge, England: Cambridge University Press.
23. Popov, V. L. (2010). *Contact mechanics and friction: Physical principles and applications* (p. 378). Berlin, Germany: Springer (Google eBook).
24. Shadnia, H., Wright, J. S., & Anderson, J. M. (2009). Interaction force diagrams: New insight into ligand–receptor binding. *Journal of Computer-Aided Molecular Design, 23*(3), 185–194.
25. Elias, D. R., Poloukhtine, A., Popik, V., & Tsourkas, A. (2013). Effect of ligand density, receptor density, and nanoparticle size on cell targeting. *Nanomedicine: Nanotechnology, Biology and Medicine, 9*(2), 194–201.
26. Zhang, S., Li, J., Lykotrafitis, G., Bao, G., & Suresh, S. (2009). Size-dependent endocytosis of nanoparticles. *Advanced Materials (Deerfield Beach, Fla.), 21*, 419–424.
27. Davies, M., Brindley, A., Chen, X., Marlow, M., Doughty, S. W., Shrubb, I., & Roberts, C. J. (2005). Characterization of drug particle surface energetics and Young's modulus by atomic force microscopy and inverse gas chromatography. *Pharmaceutical Research, 22*(7), 1158–1166.

28. Rejman, J., Oberle, V., Zuhorn, I. S., & Hoekstra, D. (2004). Size-dependent internalization of particles via the pathways of clathrin- and caveolae-mediated endocytosis. *The Biochemical Journal, 377*(Pt 1), 159–169.
29. (a) Dunn, B. M., & Chaiken, I. M. (1974). Quantitative affinity chromatography. Determination of binding constants by elution with competitive inhibitors. *Proceedings of the National Academy of Sciences of the United States of America, 71*(6), 2382–2385. (b) Ruoslahti, E., & Pierschbacher, M. (1987). New perspectives in cell adhesion: RGD and integrins. *Science, 238*(4826), 491–497.
30. Lauffenburger, D. A., & Linderman, J. J. (1993). *Receptors: Models for binding, trafficking, and signaling* (p. 376). Oxford, England: Oxford University Press.
31. Wong, C. C., Cheng, K.-W., & Rigas, B. (2012). Preclinical predictors of anticancer drug efficacy: Critical assessment with emphasis on whether nanomolar potency should be required of candidate agents. *The Journal of Pharmacology and Experimental Therapeutics, 341*(3), 572–578.
32. Muzykantov, V., & Torchilin, V. (2002). *Biomedical aspects of drug targeting* (p. 506). Berlin, Germany: Springer (Google eBook).
33. Packeu, A., Wennerberg, M., Balendran, A., & Vauquelin, G. (2010). Estimation of the dissociation rate of unlabelled ligand-receptor complexes by a "two-step" competition binding approach. *British Journal of Pharmacology, 161*(6), 1311–1328.
34. Gilli, P., Ferretti, V., Gilli, G., & Borea, P. A. (1994). Enthalpy–entropy compensation in drug–receptor binding. *The Journal of Physical Chemistry, 98*(5), 1515–1518.
35. Donaruma, L. G. (1986). Surface and interfacial aspects of biomedical polymers. In J. D. Andrade (Ed.), *Surface chemistry and physics* (Vol. 1, p. 479). New York: Plenum. *Journal of Polymer Science Part C*: *Polymer Letters*, *24*(8), 427–428. (b) *Surfaces of Nanoparticles and Porous Materials* (*Google eBook*) (p. 812). 2002. CRC Press.
36. Aqvist, J., Medina, C., & Samuelsson, J. E. (1994). A new method for predicting binding affinity in computer-aided drug design. *Protein Engineering, 7*(3), 385–391.
37. (a) Nel, A. E., Mädler, L., Velegol, D., Xia, T., Hoek, E. M. V., Somasundaran, P., & Thompson, M. (2009). Understanding biophysicochemical interactions at the nano-bio interface. *Nature Materials, 8*(7), 543–557. (b) Batchelor, G. K. (2000). *An introduction to fluid dynamics*. Cambridge, England: Cambridge University Press.
38. Serway, R. A. (2012). Physics for scientists and engineers (Vol. 1, 9th ed., p. 784). New Delhi: Cengage Learning.
39. (a) Norde, W., & Haynes, C. A. (1995). In T. A. Horbett & J. L. Brash (Eds.), Proteins at interfaces II (Vol. 602, pp. 26–40). Washington, DC: American Chemical Society. (b) Yoon, J.-Y., Kim, J.-H., & Kim, W.-S. (1999). The relationship of interaction forces in the protein adsorption onto polymeric microspheres. *Colloids and Surfaces A: Physicochemical and Engineering Aspects, 153*(1), 413–419.
40. Lopez, J., Chew, S., Thompson, H., Malter, J., Insler, M., & Beuerman, R. (1992). EGF cell surface receptor quantitation on ocular cells by an immunocytochemical flow cytometry technique. *Investigative Ophthalmology & Visual Science, 33*(6), 2053–2062.
41. Heller, H. C., & Hillis, D. M. (2011). *Life: The science of biology* (p. 1266). New York: W.H. Freeman.
42. Mehrer, H. (2007). *Diffusion in solids: Fundamentals, methods, materials, diffusion-controlled processes* (p. 672). Berlin: Springer (Google eBook).
43. (a) Singh, S. K., Piscitelli, C. L., Yamashita, A., & Gouaux, E. (2008). A competitive inhibitor traps LeuT in an open-to-out conformation. *Science, 322*(5908), 1655–1661. (b) Rubinow, S. I., & Dembo, M. (1977). The facilitated diffusion of oxygen by hemoglobin and myoglobin. *Biophysical Journal, 18*(1), 29–42.
44. Prescott, D. M., & Zeuthen, E. (1953). Comparison of water diffusion and water filtration across cell surfaces. *Acta Physiologica Scandinavica, 28*(1), 77–94.
45. Haynie, D. T. (2001). *Biological thermodynamics* (pp. 130–136). Cambridge, England: Cambridge University Press.

46. Holdich, R., Kosvintsev, S., Cumming, I., & Zhdanov, S. (2006). Pore design and engineering for filters and membranes. *Philosophical Transactions. Series A, Mathematical, Physical, and Engineering Sciences, 364*(1838), 161–174.
47. (a) Kuiper, S., Brink, R., Nijdam, W., Krijnen, G. J. M., & Elwenspoek, M. C. (2002). Ceramic microsieves: Influence of perforation shape and distribution on flow resistance and membrane strength. *Journal of Membrane Science, 196*(2), 149–157. (b) Kuiper, S., van Rijn, C., Nijdam, W., Raspe, O., van Wolferen, H., Krijnen, G., & Elwenspoek, M. (2002). Filtration of lager beer with microsieves: Flux, permeate haze and in-line microscope observations. *Journal of Membrane Science, 196*(2), 159–170.
48. Dagan, Z., Weinbaum, S., & Pfeffer, R. (2006). General theory for the creeping motion of a finite sphere along the axis of a circular orifice. *Journal of Fluid Mechanics, 117*(1), 143.
49. Kosvintsev, S., Holdich, R. G., Cumming, I. W., & Starov, V. M. (2002). Modelling of dead-end microfiltration with pore blocking and cake formation. *Journal of Membrane Science, 208*(1), 181–192.
50. Alberts, B. (2002). *Molecular biology of the cell*. New York: Garland Science.
51. Camerino, D. C., Tricarico, D., & Desaphy, J.-F. (2007). Ion channel pharmacology. *Neurotherapeutics, 4*(2), 184–198.
52. Wileman, T., Harding, C., & Stahl, P. (1985). Receptor-mediated endocytosis. *The Biochemical Journal, 232*(1), 1–14.
53. Kerr, M. C., & Teasdale, R. D. (2009). Defining macropinocytosis. *Traffic, 10*(4), 364–371.
54. Campbell, N. A., & Reece, J. B. (2002). *Biology* (p. 1247). San Francisco: Benjamin-Cummings Publishing Company.
55. Parham, P. (2005). *The immune system, p. 246* (p. 18). New York: Garland Science.
56. Howe, C. L. (2005). Modeling the signaling endosome hypothesis: Why a drive to the nucleus is better than a (random) walk. *Theoretical Biology & Medical Modelling, 2*, 43.
57. Rappoport, J. Z. (2003). Real-time analysis of clathrin-mediated endocytosis during cell migration. *Journal of Cell Science, 116*(5), 847–855.
58. Gao, H., Shi, W., & Freund, L. B. (2005). Mechanics of receptor-mediated endocytosis. *Proceedings of the National Academy of Sciences of the United States of America, 102*(27), 9469–9474.
59. (a) Bredt, D. S., & Nicoll, R. A. (2003). AMPA receptor trafficking at excitatory synapses. *Neuron, 40*(2), 361–379. (b) Cottrell, J. R., Dubé, G. R., Egles, C., & Liu, G. (2000). Distribution, density, and clustering of functional glutamate receptors before and after synaptogenesis in hippocampal neurons. *Journal of Neurophysiology, 84*(3), 1573–1587. (c) Tzlil, S., Deserno, M., Gelbart, W. M., & Ben-Shaul, A. (2004). A statistical-thermodynamic model of viral budding. *Biophysical Journal, 86*(4), 2037–2048.
60. Shenoy, V. B., & Freund, L. B. (2005). Growth and shape stability of a biological membrane adhesion complex in the diffusion-mediated regime. *Proceedings of the National Academy of Sciences of the United States of America, 102*(9), 3213–3218.
61. Brogioli, D., & Vailati, A. (2001). Diffusive mass transfer by nonequilibrium fluctuations: Fick's law revisited. *Physical Review. E, Statistical, Nonlinear, and Soft Matter Physics, 63*(1 Pt 1), 012105.
62. Freund, L. B., & Lin, Y. (2004). The role of binder mobility in spontaneous adhesive contact and implications for cell adhesion. *Journal of the Mechanics and Physics of Solids, 52*(11), 2455–2472.
63. (a) Guseva, K. (2011). *Formation and cooperative behaviour of protein complexes on the cell membrane* (p. 92). Berlin: Springer. (b) Ohki, S. (1988). *Molecular mechanisms of membrane fusion* (p. 588). New York: Plenum Press.
64. (a) Racoosin, E. L., & Swanson, J. A. (1993). Macropinosome maturation and fusion with tubular lysosomes in macrophages. *The Journal of Cell Biology, 121*(5), 1011–1020. (b) Kerr, M. C., Lindsay, M. R., Luetterforst, R., Hamilton, N., Simpson, F., Parton, R. G., & Teasdale, R. D. (2006). Visualisation of macropinosome maturation by the recruitment of sorting nexins. *Journal of Cell Science, 119*(Pt 19), 3967–3980.

65. Schafer, D. A., D'Souza-Schorey, C., & Cooper, J. A. (2000). Actin assembly at membranes controlled by ARF6. *Traffic, 1*(11), 892–903.
66. (a) Hackstein, H., Taner, T., Logar, A. J., & Thomson, A. W. (2002). Rapamycin inhibits macropinocytosis and mannose receptor-mediated endocytosis by bone marrow-derived dendritic cells. *Blood, 100*(3), 1084–1087. (b) Hackstein, H., Steinschulte, C., Fiedel, S., Eisele, A., Rathke, V., Stadlbauer, T., et al. (2007). Sanglifehrin A blocks key dendritic cell functions in vivo and promotes long-term allograft survival together with low-dose CsA. *American Journal of Transplantation, 7*(4), 789–798. (c) Von Delwig, A., Hilkens, C. M. U., Altmann, D. M., Holmdahl, R., Isaacs, J. D., Harding, C. V., et al. (2006). Inhibition of macropinocytosis blocks antigen presentation of type II collagen in vitro and in vivo in HLA-DR1 transgenic mice. *Arthritis Research & Therapy, 8*(4), R93.
67. Yoshida, S., Hoppe, A. D., Araki, N., & Swanson, J. A. (2009). Sequential signaling in plasma-membrane domains during macropinosome formation in macrophages. *Journal of Cell Science, 122*(Pt 18), 3250–3261.
68. (a) West, M. A., Wallin, R. P. A., Matthews, S. P., Svensson, H. G., Zaru, R., Ljunggren, H.-G., et al. (2004). Enhanced dendritic cell antigen capture via toll-like receptor-induced actin remodeling. *Science, 305*(5687), 1153–1157. (b) Sallusto, F., Cella, M., Danieli, C., & Lanzavecchia, A. (1995). Dendritic cells use macropinocytosis and the mannose receptor to concentrate macromolecules in the major histocompatibility complex class II compartment: Downregulation by cytokines and bacterial products. *The Journal of Experimental Medicine, 182*(2), 389–400.
69. Joukov, V., Pajusola, K., Kaipainen, A., Chilov, D., Lahtinen, I., Kukk, E., et al. (1996). A novel vascular endothelial growth factor, VEGF-C, is a ligand for the Flt4 (VEGFR-3) and KDR (VEGFR-2) receptor tyrosine kinases. *The EMBO Journal, 15*(2), 290–298.
70. Park, J., Fan, Z., & Deng, C. X. (2011). Effects of shear stress cultivation on cell membrane disruption and intracellular calcium concentration in sonoporation of endothelial cells. *Journal of Biomechanics, 44*(1), 164–169.
71. Gov, N. (2004). Membrane undulations driven by force fluctuations of active proteins. *Physical Review Letters, 93*(26 Pt 1), 268104.
72. Lindström, F., Williamson, P. T. F., & Gröbner, G. (2005). Molecular insight into the electrostatic membrane surface potential by 14n/31p MAS NMR spectroscopy: Nociceptin-lipid association. *Journal of the American Chemical Society, 127*(18), 6610–6616.
73. Isaacs, L., Ma, Y., Nolte, R. J. M., & Cornelissen, J. J. L. M. (2012). Virus-based nanocarriers for drug delivery. *Advanced Drug Delivery Reviews, 64*(9), 811–825.
74. Wender, P. A., Galliher, W. C., Goun, E. A., Jones, L. R., & Pillow, T. H. (2008). The design of guanidinium-rich transporters and their internalization mechanisms. *Advanced Drug Delivery Reviews, 60*(4–5), 452–472.
75. Wadia, J. S., & Dowdy, S. F. (2005). Transmembrane delivery of protein and peptide drugs by TAT-mediated transduction in the treatment of cancer. *Advanced Drug Delivery Reviews, 57*(4), 579–596.
76. Wender, P. A., Mitchell, D. J., Pattabiraman, K., Pelkey, E. T., Steinman, L., & Rothbard, J. B. (2000). The design, synthesis, and evaluation of molecules that enable or enhance cellular uptake: Peptoid molecular transporters. *Proceedings of the National Academy of Sciences of the United States of America, 97*(24), 13003–13008.
77. (a) Futaki, S. (2005). Membrane-permeable arginine-rich peptides and the translocation mechanisms. *Advanced Drug Delivery Reviews, 57*(4), 547–558. (b) Mitchell, D. J., Kim, D. T., Steinman, L., Fathman, C. G., & Rothbard, J. B. (2000). Polyarginine enters cells more efficiently than other polycationic homopolymers. *The Journal of Peptide Research, 56*(5), 318–325.
78. (a) Tseng, Y.-L., Liu, J.-J., & Hong, R.-L. (2002). Translocation of liposomes into cancer cells by cell-penetrating peptides penetratin and tat: A kinetic and efficacy study. *Molecular Pharmacology, 62*(4), 864–872. (b) Torchilin, V. P., Rammohan, R., Weissig, V., & Levchenko, T. S. (2001). TAT peptide on the surface of liposomes affords their efficient intracellular delivery even at low temperature and in the presence of metabolic inhibitors. *Proceedings of the National Academy of Sciences of the United States of America, 98*(15), 8786–8791.

79. Mishra, A., Gordon, V. D., Yang, L., Coridan, R., & Wong, G. C. L. (2008). HIV TAT forms pores in membranes by inducing saddle-splay curvature: Potential role of bidentate hydrogen bonding. *Angewandte Chemie (International Ed. in English), 47*(16), 2986–2989.
80. Mishra, A., Lai, G. H., Schmidt, N. W., Sun, V. Z., Rodriguez, A. R., Tong, R., & Wong, G. C. L. (2011). Translocation of HIV TAT peptide and analogues induced by multiplexed membrane and cytoskeletal interactions. *Proceedings of the National Academy of Sciences of the United States of America, 108*(41), 16883–16888.
81. Holowka, E. P., Sun, V. Z., Kamei, D. T., & Deming, T. J. (2007). Polyarginine segments in block copolypeptides drive both vesicular assembly and intracellular delivery. *Nature Materials, 6*(1), 52–57.
82. Berger, N., Sachse, A., Bender, J., Schubert, R., & Brandl, M. (2001). Filter extrusion of liposomes using different devices: Comparison of liposome size, encapsulation efficiency, and process characteristics. *International Journal of Pharmaceutics, 223*(1–2), 55–68.
83. Deming, T. J. (1997). Facile synthesis of block copolypeptides of defined architecture. *Nature, 390*(6658), 386–389.
84. Kolishetti, N., Dhar, S., Valencia, P. M., Lin, L. Q., Karnik, R., Lippard, S. J., et al. (2010). Engineering of self-assembled nanoparticle platform for precisely controlled combination drug therapy. *Proceedings of the National Academy of Sciences of the United States of America, 107*(42), 17939–17944.
85. Sutton, D., Nasongkla, N., Blanco, E., et al. (2007). Functionalized micellar systems for cancer targeted drug delivery. *Pharmaceutical Research, 24*, 1029.
86. Goren, D., Horowitz, A. T., Tzemach, D., et al. (2000). Nuclear delivery of doxorubicin via folate-targeted liposomes with bypass of multidrug-resistance efflux pump. *Clinical Cancer Research, 6*, 1949.
87. Ross, J. F., Chaudhuri, P. K., Ratnam, M., et al. (1994). Differential regulation of folate receptor isoforms in normal and malignant tissues in vivo and in established cell lines. Physiologic and clinical implications. *Cancer, 73*, 2432.
88. Yoo, H. S., & Park, T. G. (2004). Folate receptor targeted biodegradable polymeric doxorubicin mi-celles. *Journal of Controlled Release, 96*, 273.
89. Park, E. K., Lee, S. B., & Lee, Y. M. (2005). Preparation and characterization of methoxy poly(ethylene glycol)/poly(epsilon-caprolactone) amphiphilic block copolymeric nanospheres for tumor-specific folate-mediated targeting of anticancer drugs. *Biomaterials, 26*, 1053.
90. Tucker, G. C. (2003). Alpha V integrin inhibitors and cancer therapy. *Current Opinion in Investigational Drugs, 4*, 722.
91. Kessler, H., Diefenbach, B., Finsinger, D., et al. (1995). Design of superactive and selective integrin receptor antagonists containing the RGD sequence. *Letters in Peptide Science, 2*, 155.
92. Nasongkla, N., Shuai, X., Ai, H., et al. (2004). cRGD-functionalized polymer micelles for targeted doxorubicin delivery. *Angewandte Chemie International Edition in English, 43*, 6323.
93. Torchilin, V. P., Lukyanov, A. N., Gao, Z., et al. (2003). Immunomicelles: Targeted pharmaceutical carriers for poorly soluble drugs. *Proceedings of the National Academy of Sciences of the United States of America, 100*, 6039.
94. Kunath, K., Merdan, T., Hegener, O., et al. (2003). Integrin targeting using RGD-PEI conjugates for in vitro gene transfer. *The Journal of Gene Medicine, 5*, 588.

Chapter 6
Hydrogel Materials

6.1 Engineering Concepts

6.1.1 Diffusion, Swelling, and Shear Recovery

In Chap. 2, we discussed the fundamental behavior behind the release of drug molecules from matrix species in response to degradation (i.e., chemical or enzymatic), erosion (i.e., surface or bulk), and swelling (i.e., crosslinks). In the case of swellable systems, we limited our focus only to the adjustment of swelling characteristics based on changing the crosslink density, polymer molecular weight between crosslinks, and hydrophilicity. These underlying features provide information regarding the pharmacokinetics of the system; however, they provide little indication of the physical requirements for actual therapeutic applications. For example, what if a swellable system reached a point within the human body where the matrix could not sustain its own structural integrity? What would be the consequences of the system breaking apart? Could we see premature drug release [1], an inflammatory response [2], or perhaps worse, the occlusion of an artery [3]? When we use swellable systems in physiological environments, care must be taken to understand the properties, both chemical and physical, to which it will be exposed throughout its life cycle within the body.

In this chapter, we will discuss aqueous swellable systems classified as *hydrogels* [4], and their applications as implantable [5] and injectable [6] systems. Hydrogels are a species of crosslinked, hydrophilic, polymer molecules that absorb large amounts of water ($\leq$99 %) to form a three-dimensional network. There is a broad application base for hydrogel materials, ranging from tissue engineering scaffolds [7] to breast implants [8] to contact lenses [9] (discussed in Chap. 2, Sect. 2.3). For the purposes of our current discussion, we will focus on *implantable biosensors* for diabetes treatment [10] and *injectable hydrogels* for cartilage repair [11]. We begin

E.P. Holowka, S.K. Bhatia, *Drug Delivery: Materials Design and Clinical Perspective*, DOI 10.1007/978-1-4939-1998-7_6

our discussion in Sect. 6.1, by focusing on the fundamentals behind the release kinetics (i.e., diffusion and swelling) and structural integrity (i.e., rheology, shear recovery) of hydrogel materials.

6.1.1.1 Diffusion

We recall from our earlier discussion in Chap. 2 that the release of molecules from a matrix system falls in either a *Fickian*, high concentration to low concentration, or *zero-order*, independent of concentration, mode. If we are to imagine our system as one that entraps a drug within the void space between crosslink domains, we can assume that the expansion of this space with the ingress of water would create a rapid release of drug molecules in accordance with Fickian kinetics. This kinetic behavior, often termed "burst release," involves a downhill release of drug from a previously contained matrix environment. We can think of this as a somewhat troubling approach given our discussion in Chap. 2 surrounding the selection of the most effective dosage window for a given system. How can we control the release of a drug at a set concentration range with such a rapid release of encapsulated material? To answer this question, we must first understand the modes of swelling typically encountered with hydrogel materials.

Traditionally, we think of swelling in hydrogel systems as being driven by the hydrogen bonding of water to solvate the polymer chains between the crosslink points within the network [12]. This hydrogen bonding propagates through the aqueous phase to create a hydrogen-bonded network of water molecules that fills the void space between polymer domains. Due to water's unique hydrogen-bonding characteristics, it offers some degree of physical integrity to support the gel structure in the swelled state through its occupancy of the void space within the gel network (Fig. 6.1).

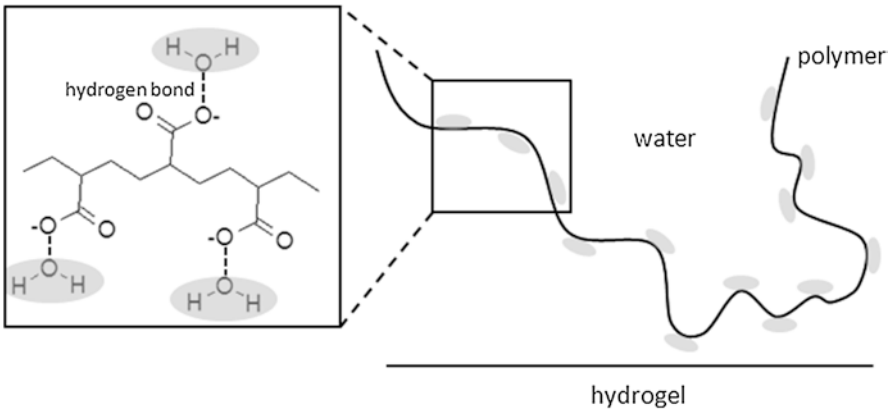

Fig. 6.1 Diagram of the hydrogen bonding of hydrogel networks

Since the aqueous phase is what ultimately drives the expansion of the void space within the gel network, the mode of swelling can be described in terms of how water sees the hydrogen-bonding groups on the polymer domains between crosslink points. These domains can be broadly classified as *ionic* and *nonionic* water-soluble groups.

In the case of ionic hydrogels, the pH or pK_a will determine whether you have a charged species or a charge-neutral species [13]. The charged species allows for hydrogen bonding to occur between water molecules and the charged functionality, creating a solvated polymer chain. When the charged species is neutralized through protonation (i.e., $–CO–O^- \rightarrow –CO–OH$) or deprotonation (i.e., $–NH_3^+ \rightarrow –NH_2$), the polymer chain will favor a more collapsed state to minimize its interface with water. It is important to keep in mind that in the case of ionic hydrogels, the charged polymers between the crosslink points are polyelectrolytes and follow the same rules that we discuss in Chap. 7 for pH-responsive materials. In general, for the purposes of our current discussion, polyelectrolytes are rigid polymer molecules due to the electrostatic repulsions felt between pendant moieties on each repeat group, limiting the energetically allowable bond rotations along the polymer chain [14]. The rigidity should be taken into account when designing a hydrogel material structure to determine the elasticity of the system both before and after the swelling behavior occurs. In the case of nonionic hydrogels, the hydrogen bonding of the polymer chains between crosslink points is not influenced by changes to pH. Instead, in materials such as PEG, there is a thermoresponsive component to the polymer's behavior in the presence of water [15]. As we discuss in more detail in Chap. 7, the nonionic polymer chain can undergo a *lower critical solution temperature* (LCST), where it changes from a freely extended chain to one in a collapsed state with increases to temperature through a critical point (Fig. 6.2).

If we look more closely at the functional species in the ionic and nonionic systems, it becomes apparent that there are additional forces that contribute to the

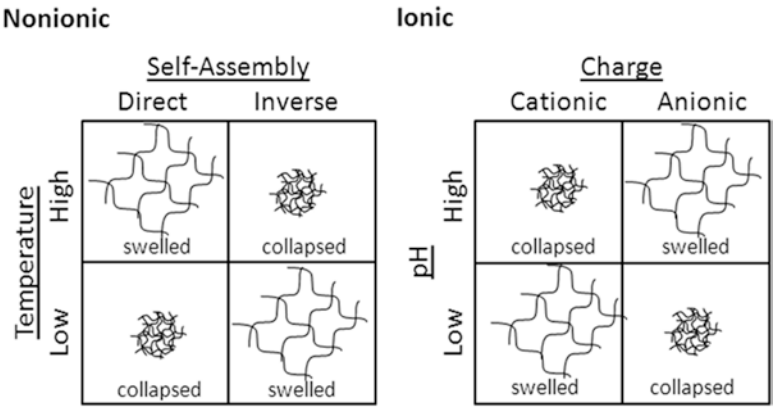

Fig. 6.2 Comparisons between ionic (i.e., pH) and nonionic (i.e., temperature) hydrogel systems

swelling of the hydrogel network in the ionic case compared to the nonionic case [16]. In the nonionic case, we can see that the free energy of the swelled system follows

$$\Delta G = \Delta G_{\text{mix}} + \Delta G_{\text{el}}, \tag{6.1}$$

where ΔG_{mix} is the free energy of mixing and ΔG_{el} is the elastic-retroactive free energy of the gel. We can rewrite this equation in terms of chemical potential by taking the derivative of Eq. (6.1) to the form [16]

$$\mu_1 - \mu_1^o = \left(\Delta\mu_1\right)_{\text{mix}} + \left(\Delta\mu_1\right)_{\text{el}} = 0, \tag{6.2}$$

where $\mu_1{}^o$and μ_1 and are the chemical potentials for the pure swelling agent and the swelling agent mixed with the polymer, and $(\Delta\mu_1)_{\text{mix}}$ and $(\Delta\mu_1)_{\text{el}}$ are the changes to the chemical entropy in terms of mixing and the elastic-retroactive behavior of the gel, respectively. If we shift our focus to the ionic system, we can see that there is an additional free-energy component to Eq. (6.1), termed the ionic free energy [16]:

$$\Delta G = \Delta G_{\text{mix}} + \Delta G_{\text{el}} + \Delta G_{\text{ion}}. \tag{6.3}$$

Similar to the nonionic case, the derivative of the free energy, in this case, yields a relationship with respect to the chemical potential [16] of the system

$$\mu_1 - \mu_1^o = \left(\Delta\mu_1\right)_{\text{mix}} + \left(\Delta\mu_1\right)_{\text{el}} + \left(\Delta\mu_1\right)_{\text{ion}} = 0. \tag{6.4}$$

If we look more carefully at the ionic contribution to the chemical potential, we can see that there is a factor of the degree of ionization that contributes to the chemical potential and swelling behavior. The ionic component of the chemical potential in physiological systems can be seen as one with a high relative concentration of counterion species in the surrounding media. This assumption [17] leads to the following form of $(\Delta\mu_1)_{\text{ion}}$:

$$\left(\Delta\mu_1^*\right)_{\text{ion}} - \left(\Delta\mu_1\right)_{\text{ion}} = V_1 RT\left(\frac{i^2 c_2}{4I}\right), \tag{6.5}$$

where V_1 is the molar volume of the solvent, i is the degree of ionization, c_2 is the concentration of the ionizable polymer, and I is the ionic strength of the swelling environment.

By taking into account Eqs. (6.2), (6.4), and (6.5), we can see that the additional charged component of ionic hydrogel systems is directly affected by the degree of the ionization of the polymer chain and the concentration of the ionizable polymer to a high degree (i.e., exponential). This behavior can be further influenced by the ionic strength that the system sees in its immediate external physiological environment. We can think of ionic hydrogel systems from a drug delivery application

standpoint as a system that is directly influenced by any charge felt by its surrounding physiological environment such as electrolytes, proteins, opsonins, sugars, and even tissue. As a general rule of thumb, the greater the number of charges in the surrounding environment, the lesser the chemical potential of the hydrogel species [18]. If we now factor the chemical potential into the diffusion equation according to Fick's first law, we can see that the flux is represented as

$$J = \frac{Dc}{6RT}\left(\frac{\delta\mu}{\delta x}\right), \tag{6.6}$$

where D is the diffusion coefficient, c is the concentration, R is the universal gas constant, T is the temperature, μ is the chemical potential, and x is the distance the molecule travels. As we would expect, the relationship for flux in Eq. (6.6) shows a correlation with the chemical potential of the system. Therefore, we can make the assumption, generally speaking, that changes made to positively affect the chemical potential of a hydrogel system would lead to an increase in the flux of materials (i.e., drug) from the same system. By the same token, from Eq. (6.5) we can see that changes to the degree of the ionization of the polymer chain and the concentration of the ionizable polymer will lead to changes to the flux of material or drug from the hydrogel matrix.

6.1.1.2 Swelling

If we understand that the degree of ionization, or lack thereof, in the hydrogel material influences the diffusion, chemical potential, and free energy of the system, then to what extent can we predict the degree of swelling of a hydrogel system? We begin the discussion by narrowing our focus to strictly nonionic hydrogel systems. This is done primarily because the nonionic hydrogel systems offer the least potential for deleterious electrostatic interactions with physiological media. In 1942, Flory and Rehner [19] predicted that the entropy of swelling is a function of characteristic events, consisting of the dilution of a number of polymer chains, the crosslinking of groups of chains, and the conversion of these groups to a network by the introduction of crosslink points. Using these assumptions, Flory [19] could approximate the molecular weight of the polymers between crosslinks (M_c), which would then allow for an estimation of the degree of physical swelling of the gelled system:

$$\frac{1}{M_c} = -\frac{\left(\frac{\upsilon}{V_1}\right)\left[\ln\left(1-\upsilon_{2m}\right)+\upsilon_{2m}+\chi_1\upsilon_{2m}^2\right]}{\left[\upsilon_{2m}^{1/3}-\frac{\upsilon_{2m}}{2}\right]}, \tag{6.7}$$

where υ is the specific volume of the polymer, υ_{2m} is the volume fraction of the polymer in the swollen or *mixed state*, and χ_1 is the Flory polymer–solvent interaction parameter. It is important to remember that the relationship in Eq. (6.7) is for

systems that have been crosslinked prior to exposure to an aqueous environment. For the purposes of our discussion in Sect. 6.2, this swelling would become most relevant in the design of implantable hydrogel materials. If we desire systems to form their crosslinks while in an aqueous environment, we can refer to the relationship derived by Peppas and Merrill [20]:

$$\frac{1}{M_c} = -\frac{\left(\frac{\upsilon}{V_1}\right)\left[\ln\left(1-\upsilon_{2m}\right)+\upsilon_{2m}+\chi_1\upsilon_{2m}^2\right]}{\upsilon_{2r}\left[\left(\frac{\upsilon_{2m}}{\upsilon_{2r}}\right)^{1/3}-\left(\frac{\upsilon_{2m}}{2\upsilon_{2r}}\right)\right]}, \tag{6.8}$$

where υ_{2r} is the volume fraction of the polymer in the *relaxed state*. The equation described by Peppas and Merrill [20] accounts for both the swelled and compressed states, which we will find to be relevant to our discussion in Sect. 6.2 regarding injectable hydrogels for drug release systems. In both relationships shown in Eqs. (6.7) and (6.8), we can clearly see that the molecular weight of the polymers between crosslink points is correlated with the volume fraction of the polymer in the swollen state. Therefore, not surprisingly, as the molecular weight between crosslinks increases, so does the degree to which the hydrogel can swell volumetrically.

6.1.1.3 Shear Recovery

To this point we have discussed the relationships at the basis for diffusion and swelling of hydrogel materials. In our design of effective hydrogel drug delivery systems, we will also need to understand the physical requirements tied to their potential therapeutic applications [21]. For this discussion we will focus on two systems, , *implantable hydrogels* and *injectable hydrogels*; we detail these systems further in Sect. 6.2. In the case of implantable hydrogel materials, the system must either retain its physical integrity upon swelling by avoiding common forms of erosion or degrade at a controlled rate upon swelling, yielding bioinert or biocompatible components within the body [22] (Fig. 6.3).

The degree of swelling [Eqs. (6.7) and (6.8)] can be adjusted to allow for the release of a desired dosage of drug, while the swelling occurs to a volume consistent with that of its surrounding physiological constraints [23] (i.e., the diameter of a blood vessel), which we discussed in Chap. 2. In the case of injectable hydrogel materials, the system must endure *shear thinning* and be capable of resetting its gel matrix structure upon removal of the shear force. Shear thinning is when a fluid becomes less viscous with the application of a shear force. The shear-thinning behavior functions to allow for the hydrogel system to be injectable [24] [Eq. (6.9)] based on the effective viscosity (μ_{eff}):

$$\mu_{\text{eff}} = K\left(\frac{\delta u}{\delta y}\right)^{n-1}, \tag{6.9}$$

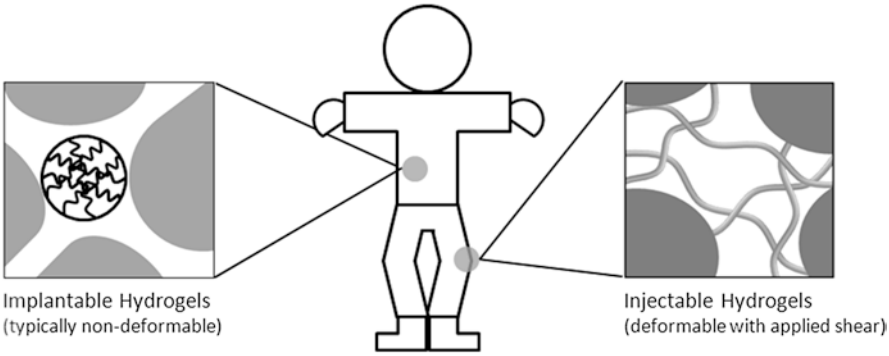

Fig. 6.3 Diagram of implantable and injectable hydrogel systems for drug delivery

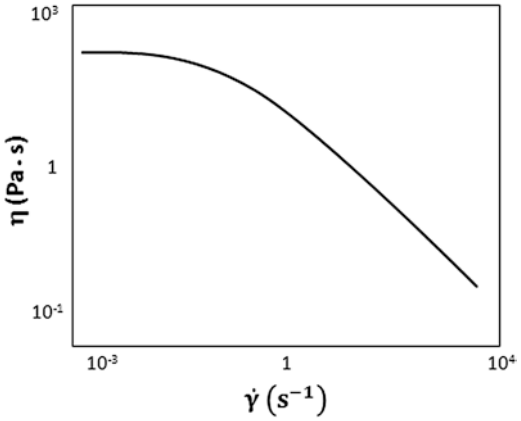

Fig. 6.4 Plot of the viscosity behavior of a shear-thinning fluid with changing shear rate (γ)

where K is the flow consistency index, $\delta u/\delta y$ is the shear rate, and n is the flow behavior index. If the value for $n < 1$, then the fluid is designated as a *pseudoplastic* ($n = 1$ for a Newtonian fluid), which is typically used for injectable drug delivery applications. A simple way to visualize this effect is if we measure the dependence of the viscosity of a shear-thinning system on the shear rate (Fig. 6.4). In this case, the viscosity decreases with increasing shear rates (γ), as we would expect for a system intended to be injected through a syringe. If we shift our perspective now from the fluid state to that of the networked structure, we can gain even more insight into its behavior.

The rate at which the gel returns to its native networked structure is known as the *gel restoration kinetics* [25], which is measured in terms of the *storage* (G') and *loss modulus* (G''):

$$G^* = G' + iG''. \tag{6.10}$$

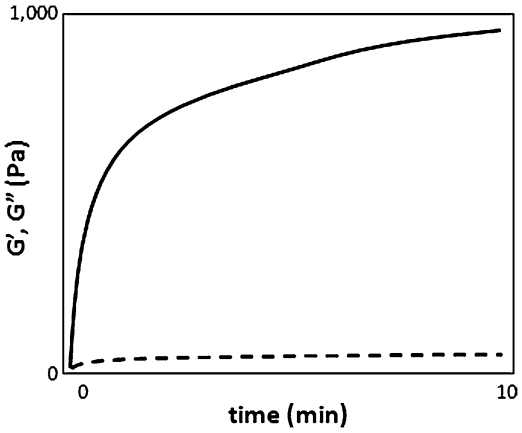

Fig. 6.5 Plot of the storage (G') and loss (G'') modulus behaviors of an injectable hydrogel system (typical shear rates = 10/s, 100/s, and 1,000/s)

For a hydrogel system to be deemed relevant for injectable applications, the storage modulus (G') values must return to their restored values as a function of time under constant stress. It is also expected that the storage modulus will be greater than that of the loss modulus (G'') through the course of the experiment (Fig. 6.5). It is important to note that a number of morphological changes are occurring within the gel structure of the material during this time, a majority of which are beyond the scope of our discussion. For a more comprehensive account of the rheological behavior of hydrogel scaffolds, there are a number of reliable texts to explore. For the purposes of our discussion, we will focus on the self-assembly behavior of the hydrogel restoration, which will lead us to Sect. 6.2.

6.2 Material Design

6.2.1 Self-Assembly and Crosslinking

The design of hydrogel systems for drug delivery applications follows the same structural property principles that we have introduced throughout this text. We know, for instance, that polymers can run the gamut from rigid and brittle materials to ones having flexible and elastic responses to applied stress [26]. Each polymer type has advantages from holding its shape as a scaffold (i.e., rigid) to remaining malleable to fit in a variety of orifices (i.e., elastic) within the body. If we continue in our discussion of implantable and injectable hydrogel materials, we can begin to look at the effects of stress on the self-assembled structure(s). The self-assembly behavior provides important information regarding the types of chemical functionalities, molecular weights, and compositional morphologies that are ideal [27] for the formation of the desired responsive hydrogel drug delivery systems.

6.2.1.1 Implantable Systems

As we discussed in Chap. 2, hydrogels can form based on several driving forces: chemical crosslinking [28], aggregated domains [29], electrostatics [30], or ligand–receptor interactions [31], to name but a few. Each of these driving forces has its own polymers with ideal properties. We can start by trying to identify the material properties based on a set of conditional requirements for the intended application. In the case of implantable materials, the desired goal is controlled release of drug material from a swellable, microscale gel that does not place undue strain on the surrounding tissue. From Chap. 2, we understand the controlled-release requirements of the hydrogel material, and from Sect. 6.1, we understand the swelling behavior as a function of the crosslink density. What follows from a functional perspective is to design a system that does not place undue strain on the physical environment and remains in a microscale-size regime for implantation. Since each region of the body has its own constraint limits, we will provide a foundation for the development of materials based on the properties defined within this section.

The topic of strain to the physiological system ties back to the self-assembled structure and the degree of elasticity of the swelled system. For implantable systems, the crosslinking that ties the network structure together can be formed from chemical or physical crosslinking (Fig. 6.6).

There are advantages and disadvantages to both crosslinks. Chemical crosslinks [32] provide a greater degree of stability under dilute conditions; however, each chemical crosslink represents an added point of rigidity to the overall system. Physical crosslinks [33] can be tuned based on molecular weight (i.e., above or below the entanglement M_n) to be less rigid systems; however, the degree of crosslinking can become variable as new chemical functionalities and compositions are introduced to the gel matrix. The behavior of self-assembled crosslinked materials falls somewhere between those of chemical and physical crosslinked systems. In self-assembled systems, typically block copolymers are used, which are composed of either amphiphilic domains [34] or domains with a large variation in their T_g behavior [35] (Fig. 6.7).

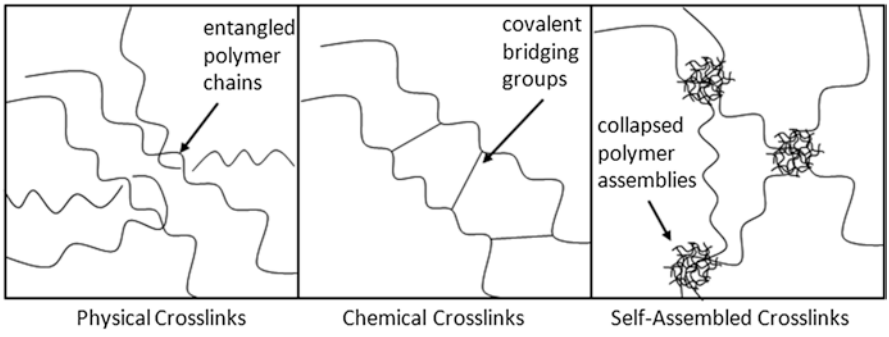

Fig. 6.6 Diagram of the criteria for hydrogel formation within physiological systems

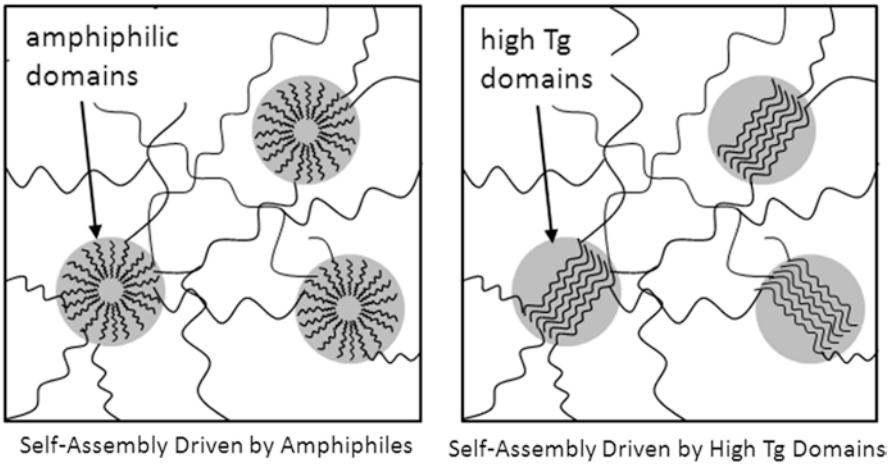

Fig. 6.7 Diagram of the crosslinking behavior for hydrogel systems

As we discussed in Chap. 4, the aggregation of the hydrophobic domains of amphiphilic polymers can form a number of self-assembled shapes (i.e., sphere, toroid, cylinder, plane). At a critical concentration, these domains begin to form a gel phase, which becomes networked three-dimensionally [34] (i.e., gel point). Block copolymers with a different T_g behavior in each of their block domains follows a similar behavior. In these cases, the high-T_g blocks tend to aggregate together [35], similarly to how the hydrophobic domains aggregate in the amphiphilic system, leaving the low-T_g block to occupy the remaining volume.

The strain of the system is also propagated from the rigidity or elasticity of the polymer chains between the crosslink points. This elasticity can be due to several properties of the polymer, including hydrophilicity and flexibility [36]. The hydrophilicity is a measure of the polymer's solubility or hydrogen bonding with water, while flexibility refers to the number of bond rotations within a fixed volume. As one would expect, the polymers with a higher degree of solubility should swell to their maximum volume rapidly, and vice versa. This solubility can be tied to either nonionic or ionic functional groups, whose behavior is discussed in more depth in Chap. 7. The flexibility of the polymer chain can dictate the rate of swelling of the gel, the maximum volume, and its malleability [37] (i.e., ability to be fit into tight corners of the body) (Fig. 6.8).

One critical factor that remains unaddressed is the size of the hydrogel particles. For the answer to this question, we can turn to a number of different fabrication techniques to provide a wide range of particle sizes [38]. What we can begin to see from this discussion is that there are a number of knobs that the engineer can use to design and build a system to comply with the physical and chemical requirements of a physiological system for an implantable treatment.

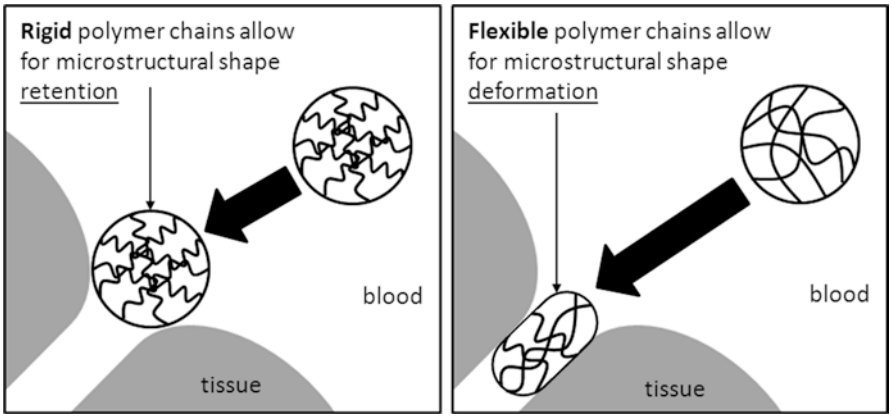

Fig. 6.8 Diagram of polymer chain flexibility and solubility

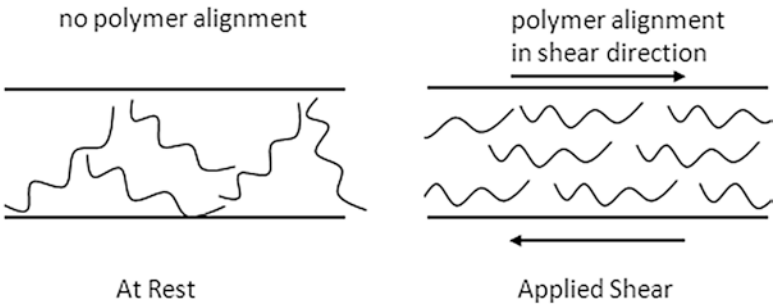

Fig. 6.9 Diagram of directionality and applied shear in polymer systems

6.2.1.2 Injectable Systems

While in the case of implantable systems we looked at retaining the gel integrity enough to allow for controlled release but remain flexible, for injectable systems we are looking at materials that need to have no gel integrity for a portion of their application. As we discussed in Sect. 6.1, these materials need to be shear thinning, with a shear recovery within a matter of seconds to minutes [39]. In order for this to occur, the system must be designed with a few unique characteristics. If a material needs to have a response to shear stress, a component having a degree of orientation is required. This component can align in the direction of the applied shear, causing more fluidic behavior [40]. For example, think of this as tree branches flowing down a river. At points where the current is strong, the branches appear more directional than when you reach calmer river beds, where they appear more random in their orientation (Fig. 6.9).

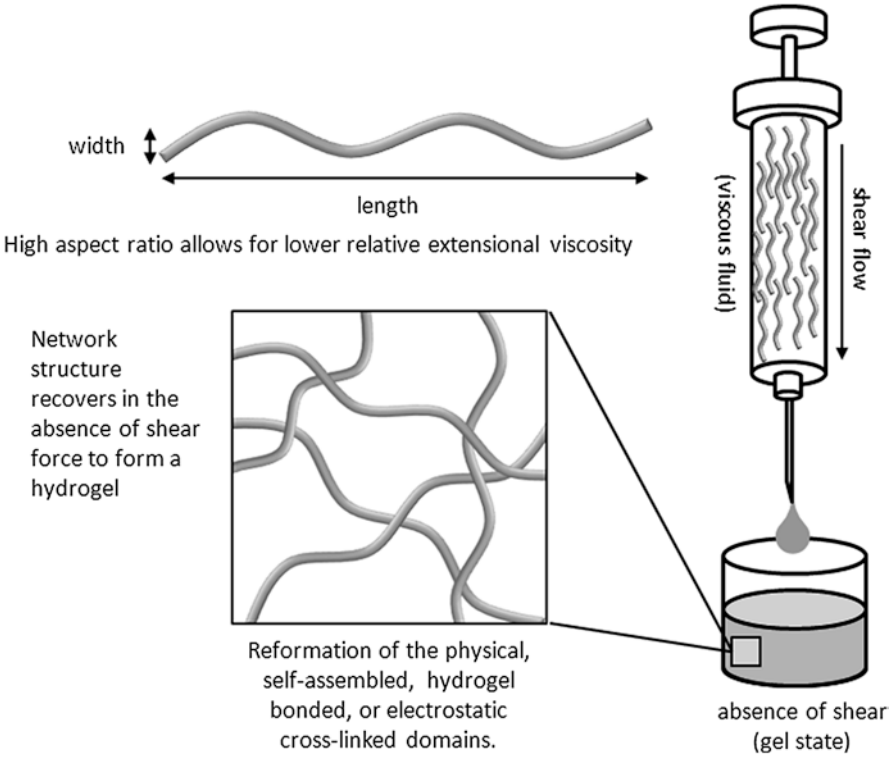

Fig. 6.10 Diagram of viscoelastic materials with high aspect ratio for injection applications

When the shear force is removed from the system, the hydrogel needs to return to its native gel state at a rapid rate. This once again is tied to the component with orientation, known as its *aspect ratio* [40] (i.e., length to width), and to the *viscoelasticity* of the polymer. The viscoelasticity [41] describes a behavior where the polymer exhibits both viscous liquid and elastic solid properties of materials. These materials exhibit a time-dependent strain, where rapid strain rates show more elastic properties, while slower strain rates show viscous fluid behavior (Fig. 6.10). These viscoelastic polymers with the appropriate aspect ratio additives can provide the ideal injectable materials for drug delivery applications.

It is important to remember that upon the removal of shear, these injectable systems must not only recover to a gel state, but also both fill the volume into which they are injected and retain adequate rheological properties for the intended therapeutic application [42]. For this reason, these systems (Table 6.1) are typically designed on an application-by-application basis since the requirements for filling the injection site and retaining the appropriate rheological properties will differ depending on whether the injectable system is a site for cartilage repair, bone repair, or spinal treatment.

Table 6.1 Common injectable and implantable hydrogels for drug delivery applications

Polymer	Structure	Application	Biocompatible or bioinert
Poly(ethylene glycol-b-lactic acid) (PEG-PLA PLA-PEG-PLA PCLA-PEG-PCLA)	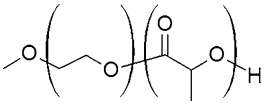	Injectable	Bioinert
Poly(hydroxy-ethyl methacrylate) (PHEMA)	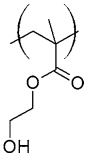	Implantable	Bioinert
Poly(*N*-vinyl-2-pyrrolidone) (PNVP)	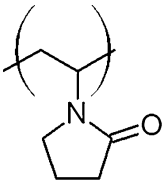	Implantable	Bioinert
Hyaluronic acid (HLA)	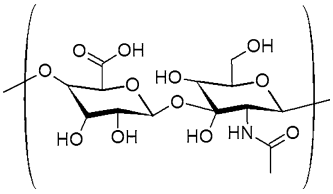	Injectable	Biocompatible
Chitosan	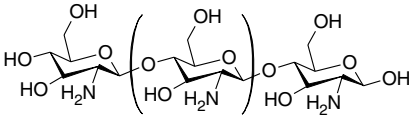	Injectable	Biocompatible
Chondroitin sulfate (A,C,D,E)	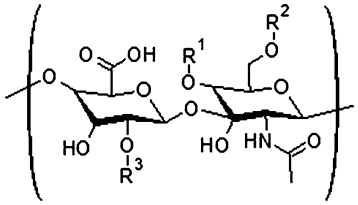 **A:** $R^1 = SO_3^-$; $R^2 = H$; $R^3 = H$ **C:** $R^1 = H$; $R^2 = SO_3^-$; $R^3 = H$ **D:** $R^1 = H$; $R^2 = SO_3^-$; $R^3 = SO_3^-$ **E:** $R^1 = SO_3^-$; $R^2 = SO_3^-$; $R^3 = H$	Injectable	Biocompatible

In this section, we discussed the basic design parameters for hydrogel systems involved in implantable and injectable drug delivery applications. In Sect. 6.3, we focus on an implantable hydrogel system for diabetes treatment and an injectable hydrogel system for cartilage repair. These systems will provide an extension of the fundamental properties outlined in this chapter while providing insight into the future of therapeutic approaches with hydrogel materials.

6.3 Implementation

6.3.1 Implantable Microgels and Injectable Hydrogels

Throughout this chapter we have discussed the fundamental material properties and design strategies of hydrogels as they pertain to drug delivery. This discussion has focused on two primary systems that have garnered significant interest in the field of drug delivery, implantable materials and injectable materials. In Sect. 6.2, we discussed the basic physical requirements to sustain a functional drug delivery system, while in Chap. 2, we discussed the release kinetics as they apply to both swellable and erodible systems. We will now focus our discussion on specific applications of implantable and injectable hydrogels for use in drug delivery.

6.3.1.1 Implantable Hydrogels for Biosensors and Drug Delivery

The current for implantable sensing and responsive devices in medicine has been gaining interest over the last three decades [43]. In diseases such as diabetes, patients require the consistent monitoring and correction of insulin levels within the blood. Common monitoring has shifted in the last several years to more noninvasive sampling. Yet there still remains a desire to reduce potential errors associated with insulin correction using the least invasive method. For this reason, "smart" biosensors have gained traction as an attractive method for the correction of insulin levels in diabetes mellitus patients. Currently, these sensors suffer from issues concerning the fouling and biocompatibility of the surface of the implantable device.

The use of hydrogel films has been proposed by Brahim et al. [44] as a means for both mitigating the biocompatibility, due to their high water levels, and modulating the insulin release through the use of pH-responsive component polymers. Sensors typically encounter complications in their amperometric response due to interfering agents, such as ascorbic acid, uric acid, and acetaminophen. The system of our focus [44] involves three components: (1) the base hydrophilic hydrogel matrix [i.e., crosslinked p(HEMA)], (2) the polyeletrolyte [i.e., polypyrrole (p(Pyr)], and (3) the glucose oxidase (i.e., Ox) (Fig. 6.11). The system's three components have different functional objectives in terms of their structural design. The crosslinked p(HEMA) functions as a barrier to the sensor surface and is equivalent to a fairly rigid, nonionic, chemically crosslinked hydrogel with swelling characteristics that are predicted by

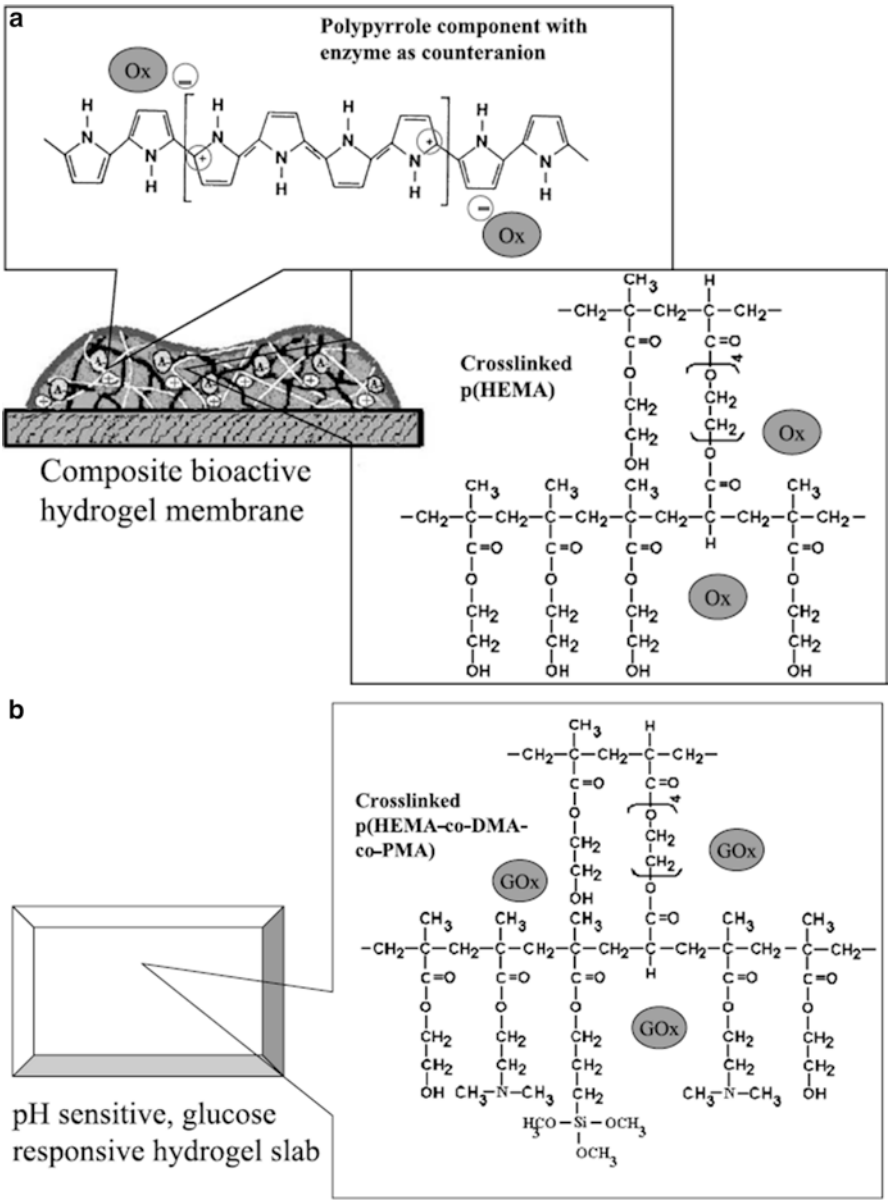

Fig. 6.11 (**a**) Schematic representation of the three components of the novel hydrogel composite matrix, the cross-linked hydrophilic hydrogel, the positively charged electroactive PPy component, and the negatively charged (net) oxidase enzyme. (**b**) Partial structure of the hydrogel network used for the fabrication of engineered devices for the controlled release of insulin [44]

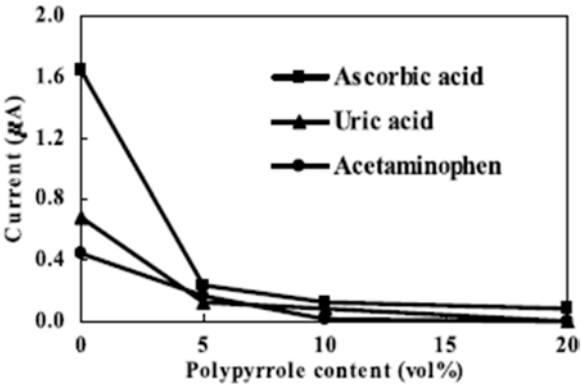

Fig. 6.12 Effect of varying the composition of PPy content (vol.%) of the composite hydrogel membrane on the amperometric current generated by oxidation of interferent at the electrode surface [44]

Eqs. (6.6) and (6.7). The p(HEMA) is crosslinked by the presence of an amine-containing methacrylate monomer (DMA). The p(Pyr) functions as an electroactive conducting polymer to provide physical crosslinks, structural rigidity, and electrostatic interactions with the Ox enzyme within the hydrogel matrix. The Ox serves to provide the functional "drug" of the system, which in this case is a glucose-responsive enzyme that enhances the magnitude of the insulin release from the matrix.

In order to effectively create an interface that is shielded from confounding interactions, the hydrogel must suppress the interference by creating a barrier to diffusion of common electroactive compounds, such as ascorbic acid, uric acid, and acetaminophen. This suppression can be measured through a reduction in the current by increasing the content of the p(Pyr) component of the p(HEMA) crosslinked hydrogel (Fig. 6.12).

Here we can see a significant (i.e., <87 %) reduction in the current with 5 % added p(Pyr) content to the p(HEMA) hydrogel network. Since it appears that these systems have been effectively passivated to interfering compounds, we can also look at the controlled release of insulin stimulated by glucose levels. The authors monitored the release of insulin with three different levels of glucose (0, 12, and 500 mg/dl) at several different levels of the glucose oxidase enzyme (0, 3,800, 7,600, 15,200, and 30,400 mg) (Table 6.2).

We can see that the diffusion coefficient associated with the insulin release is increasing with increasing levels of the glucose oxidase enzyme. The authors suggest that the similar behavior of the diffusion coefficients, which are irrespective of the glucose or enzyme amount, may be due to the plasticization of the hydrogel network by the influx of either compound, resulting in a swelling or burst release kinetic behavior. This does not appear to be the case with high levels of glucose (i.e., 500 mg), where the diffusion coefficients for insulin release appear to be significantly different than in the cases of 12 or 0 mg/dl.

Finally, the authors monitored the degree of swelling of the network with changes to the pH of the hydrogel system (Fig. 6.13).

Table 6.2 Variation of insulin diffusion coefficient (Dip) from glucose-responsive hydrogels immersed in aqueous glucose solutions when insulin is loaded by equilibrium partitioning

[Glucose] (mg/dl)	GO_x loading (enzyme units)	Diffusion coefficient, D_{ip} ($cm^2/s \times 10^{-7}$)
0	0	2.9
	7,600	3.2
	30,400	3.9
12	0	3.9
	3,800	7.1
	7,600	7.4
	15,200	8.5
	30,400	3.3
500	0	4.1
	3,800	7.2
	7,600	7.1
	15,200	8.5
	30,400	7.6

Diffusion coefficient (D_{ip}) calculated using the formula $M_t/M_\infty 4/p1/2(D_{ipt}/L^2)^{1/2}$, where M_t and M_∞ are the [insulin] released at time "t" and at equilibrium, respectively; L is the device thickness. Dimensions of hydrogel slab used: $3 \times 2.5 \times 0.05$ cm) [44]

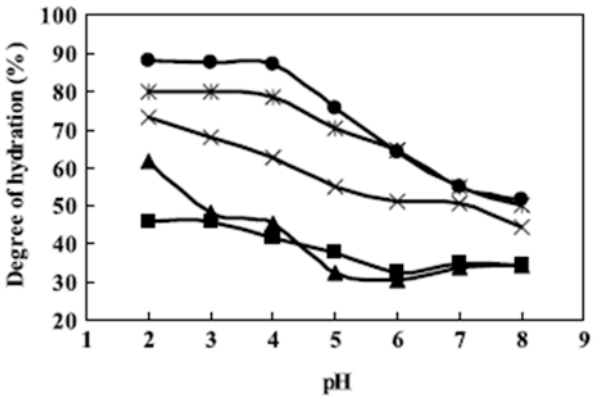

Fig. 6.13 Effect of pH on the degree of hydration of hydrogel slabs of varying DMA monomer compositions. All slabs were immersed in the respective buffered solutions for 24 h before measurements of wet and dry weights. *Square*, 0 mol% DMAEMA; *triangle*, 5 mol% DMA; *Cross*, 10 mol% DMA; *asterisk*, 15 mol% DMA; *circle*, 20 mol% DMA [44]

It is important to note that during the enzymatic reaction, the crosslinker (DMA) is effectively protonated by the gluconic acid being generated. This added charge introduces electrostatic repulsion within the hydrogel network, which results in a net swelling in the system. The authors monitored this effect in Fig. 6.13, where they clearly see an increase in the swelling behavior [i.e., degree of hydration (%)] as a function of a decrease in pH for cases involving a range of percentage of DMA crosslinking agent.

This biomaterial system offers a unique hybrid of sensor technology with biocompatibility and drug delivery to effectively monitor and deliver insulin based on glucose levels in a controlled and safe manner. This work represents a continuing focus of the biomedical community toward combining material design at the biointerface to enhance the compatibility, utility, and control of drug delivery systems.

6.3.1.2 Injectable Hydrogels for Cartilage Repair

Diseases that involve the degeneration of cartilage tissue, such as osteoarthritis, affect a wide age range, with symptoms such as pain, immobility, and joint destruction. These diseases are challenging to treat since the affected regions are both difficult to reach and imprudent to perform surgery on due to their location and progression. For this reason, approaches known in tissue engineering have recently been co-opted in the form of injectable hydrogels, in an effort to develop minimally invasive treatments to promote cellular growth in affected regions. These treatments typically involve the preculturing of chondrocytes within the hydrogel matrix, followed by their injection via a syringe into the affected area. Upon injection, the gel must regain its preinjection modulus in order for chondrocyte proliferation to occur.

As we discussed in Sects. 6.1 and 6.2, in order for hydrogels to be good candidates for injectable treatments, they must have a high storage modulus (G') and have shear-thinning viscosity behavior in response to changing shear rate. In this type of system, the "drug" is actually seeded chondrocyte cells, whereby their proliferation is analogous to drug release, as previously discussed. Park et al. [45] have developed a thermoresponsive shear-thinning hydrogel system for application as an injectable biomedical material. The system is a composite of a poly(ethylene oxide-propylene oxide-ethylene oxide) amphiphilic triblock copolymer, known as a Pluronic (F127) and chitosan (referred to as CP) (Fig. 6.14).

Typically, natural materials are used to develop matrices for regenerative tissues such as cartilage since they are easily shaped and retain a degree of modulus. These materials also can have difficulty with cell seeding and proliferation due in part to the porosity and flexibility of the matrix, which translates into what is known as poor self-healing. The authors developed a Pluronic-chitosan (CP) system that can take advantage of the improved flexibility of the polymer component to allow for better injectability, while the chitosan can help with retaining some of the gel modulus for the system to recover. This specific system has the additional benefit of thermoresponsive behavior, which we discuss in more detail in Chap. 7. For the purposes of our current discussion, the system is one where the gel structure swells, or breaks up, in response to decreasing temperature through a critical transition point, known as the LCST (Fig. 6.15).

There are four basic design requirements that the injectable hydrogel system must satisfy in order to be a candidate for cartilage therapy: The system must (1) maintain an adequate swelling ratio for a long enough duration to allow for chondrocyte proliferation to occur, (2) maintain a high storage modulus (G') at elevated temperatures, (3) maintain a high level of glycosaminoglycan (GAG) as an indicator for cartilage tissue formation, and (4) promote cartilage proliferation.

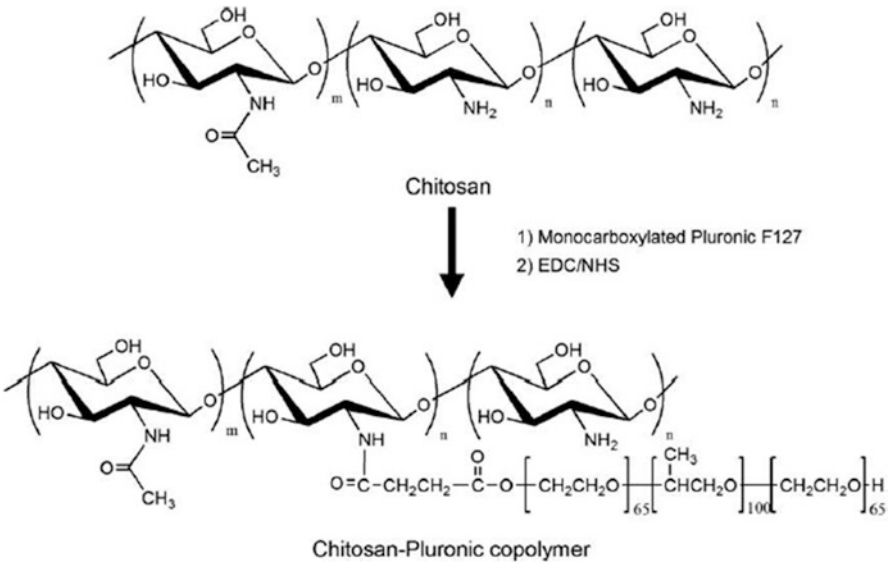

Fig. 6.14 Synthesis of the CP copolymer by grafting monocarboxylated Pluronic F127 onto chitosan using EDC/NHS in 0.1 M MES [44]

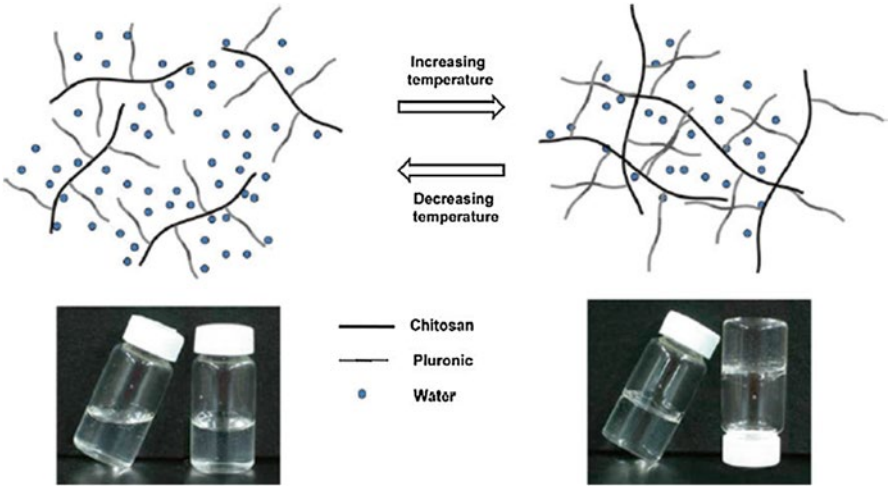

Fig. 6.15 The hydrogel formation of the thermosensitive CP hydrogel in aqueous solution via the hydrophobic interaction of a PPO group in Pluronic and the dehydrated chitosan chain [45]

If we look at the swelling ratio of the CP complex, we can clearly see a high degree of swelling (>1.2) retained for up to 10 days, followed by a steep drop-off. An increasing CP concentration appeared to improve the magnitude of the swelling but not prevent the impending drop-off after 10 days (Fig. 6.16).

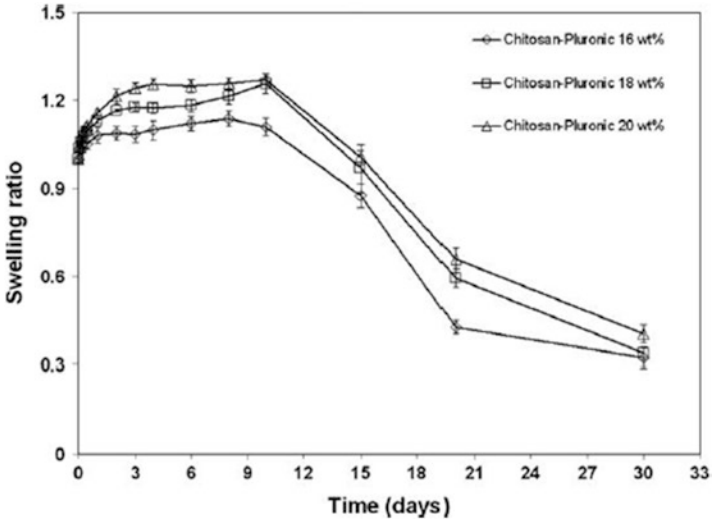

Fig. 6.16 The swelling ratio and degradation behavior of the CP hydrogel in PBS buffer (0.01 M and pH 7.4) at 37 °C with different polymer concentration (-◇-, 16 wt.%; -□-, 18 wt.%; -Δ-, 20 wt.%) [45]

The relative drop-off, however, appeared to decrease with increasing the concentration of CP, which may indicate an effect of crosslink density on the swelling ratio. The storage modulus (G') appears to reach a discrete transition with increasing temperature through the 28 °C range, which is consistent with the sol-gel transition of Pluronic copolymer materials (Fig. 6.17).

The transition in modulus supports that this material would be a good candidate for injection at a reduced temperature, followed by setting at elevated physiological temperature. This method is analogous to our previous discussion surrounding shear-thinning materials. In this system, the LCST transition is used as a means for maintaining the seeded gel in a fluid state (i.e., analogous to shear-thinned), whereby introduction of the fluid gel into a warmer (i.e., >28 °C) environment would trigger the gelation and recovery of the matrix integrity. This appears to be the case, where a 10,000-Pa modulus is attained with the stated temperature increase.

If we now turn our attention to cell viability, we can see that the CP system affords a greater than 1×10^5 increase in viable chondrocyte cells over the traditional alginate seeding methods (Fig. 6.18), with an increase of 1 mg of GAG after 14–28 days. This supports the rationale that the addition of the amphiphilic polymer allows for the increase in viable chondrocyte culturing over the traditional natural porous matrix materials.

The work of Park et al. illustrates a system designed from readily available biologically inert components that allows for injection and gel-setting behavior. The gel state of this system is naturally triggered by the physiological temperature within the human body into a state that promotes chondrocyte cell proliferation to

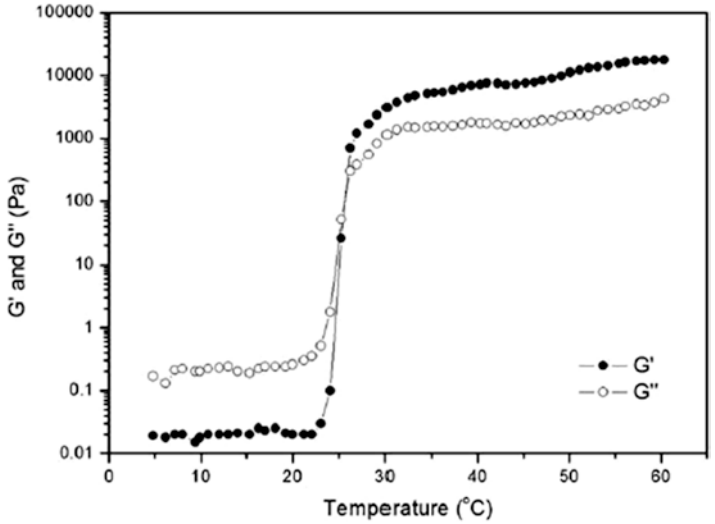

Fig. 6.17 The storage modulus (G') and loss modulus (G'') of the 16 wt.% and 20 wt.%. A frequency of 0.1 Hz and a strain of 0.1 % were applied (adapted from Park KM, Lee SY, Joung YK, et al. Thermosensitive chitosan–Pluronic hydrogel as an injectable cell delivery carrier for cartilage regeneration. *Acta Biomaterialia*, *5*(6), 1956–1965, 2009) [45]

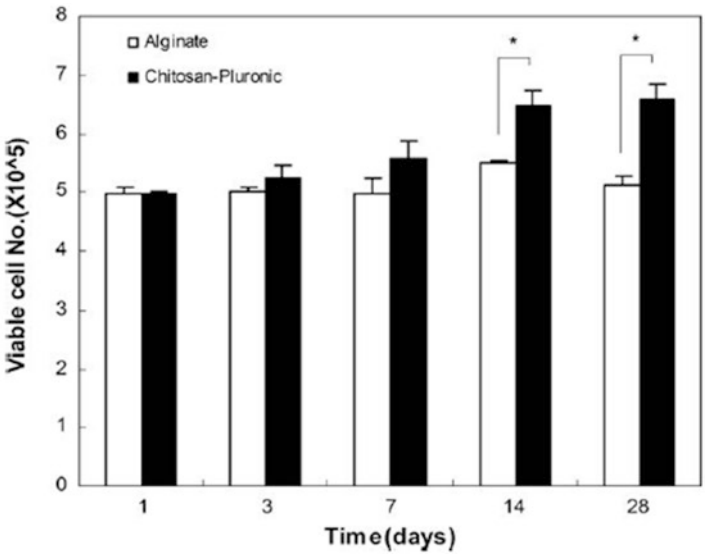

Fig. 6.18 The chondrocyte proliferation MTS assay: alginate hydrogel (*white bar*) and the CP hydrogel (*black bar*), $*P<0.05$ [45]

improved levels relative to typical cell seed technologies, such as alginate. In Chap. 7, we discuss other implications and advantages to this thermoresponsive design method for other drug delivery applications.

6.3.2 Summary

The extension of controlled-release materials into the domain of hydrogels allows for dynamic approaches to current challenges encountered in drug delivery. In Sect. 6.1, we discussed *diffusion*, *swelling*, and *shear recovery* as an extension of the principles of Chap. 2. We proceeded to extend those principles into Sect. 6.2, where we designed systems based on the *self-assembly* and *crosslinking* of polymer and matrix materials. We applied these design principles to implantable and injectable hydrogel systems and focused on two specific cases in Sect. 6.3, those of biosensors and cartilage repair. Currently, hydrogel systems represent a promising and facile mode for combining controlled-release drug delivery methodologies to maintain systems that are more compliant to the physiological demands of the patient (Table 6.3).

Table 6.3 Common scientific disciplines tied to critical fundamentals in hydrogel drug delivery systems

Fundamental	Disciplines
Diffusion	• Chemistry • Chemical engineering • Materials engineering • Physics
Shear recovery	• Chemical engineering • Materials engineering • Rheology • Polymer physics
Self-assembly	• Chemical engineering • Chemistry • Materials engineering • Biochemistry
Degradation	• Materials engineering • Chemical engineering • Chemistry
Swelling	• Chemistry • Biomedical engineering • Materials engineering
Cell seeding	• Cell biology • Biochemistry • Biomedical engineering

6.4 Clinical Applications

6.4.1 Hydrogels for Wound Dressings and Wound Closure

Wound closure and wound healing represent major clinical challenges worldwide. Wounds resulting from traumatic injuries are a leading cause of death, particularly in developing countries. In addition to traumatic wounds, surgical wounds can be a significant source of morbidity and mortality. Surgical wounds often suffer from leakage, both between sutures and staples and through the holes created by sutures and staples. Improved methods for wound closure are urgently needed to prevent complications such as blood loss, infection, sepsis, and death. Hydrogels are ideal for this purpose. Like human tissues, hydrogels are flexible, soft, and fluid; hydrogels are also water-absorbent, making these materials suitable for dressing an actively bleeding or seeping wound. Adhesive hydrogels can simultaneously protect wounds and deliver antiinflammatory therapeutics, antimicrobial drugs, and tissue-promoting growth factors.

New tissue adhesives based on polyethylene glycol (PEG) have been developed to provide highly biocompatible, bioresorbable, synthetic hydrogels for wound closure. Polyethylene glycol hydrogel-based tissue adhesives are advantageous relative to other synthetically derived sealants, including cyanoacrylates, GRF glues, and albumin-glutaraldehyde glues, because PEG is much more compatible with biological tissues, and PEG hydrogels are readily degraded by hydrolysis. In addition, synthetic PEG-based adhesives avoid the risks associated with biological fibrin glues, including viral transmission and sensitization; moreover, PEG-based sealants circumvent the potential immunogenicity of bovine albumin-glutaraldehyde glues. Polyethylene glycol polymers have a long history of clinical use as drug delivery agents for therapeutic proteins [46]. Polyethylene glycol conjugation reduces the immunogenicity of proteins and imparts “stealth” properties; PEG-modified proteins are nonimmunogenic, even with repeated infusions [47, 48]. Polyethylene glycol polymers are thus well known in clinical medicine as biocompatible materials. Three major PEG-based tissue adhesives that have been designed for clinical medicine are photopolymerizable PEG sealants, PEG-PEG sealants, and PEG-trilysine sealants; all three of these adhesive platforms are reviewed in this section. In general, PEG-based sealants are characterized by excellent biocompatibility but are high-swelling with very fast degradation profiles that limit their functionality in wound reinforcement.

Hydrogel adhesives based on water-soluble, photopolymerizable macromers were developed in the early 1990s; these bioresorbable hydrogels are formed by the photopolymerization of poly(ethylene glycol)-co-poly(α-hydroxy acid) diacrylate macromers [49]. In 1994, photopolymerized PEG sealants were reported to prevent postsurgical adhesion formation and allow intraabdominal healing in experimental models [50, 51]. In 1995, photopolymerizable PEG adhesives were demonstrated to seal human blood vessel anastomoses without inducing thrombogenicity [52]. By 1997, the photopolymerized hydrogel adhesives were found to be effective for

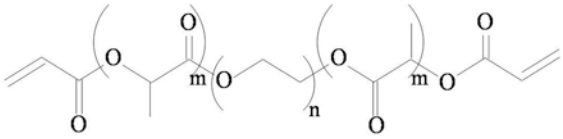

AA-$(LA)_m$-(PEG)-$(LA)_m$-AA

Primer Macromer

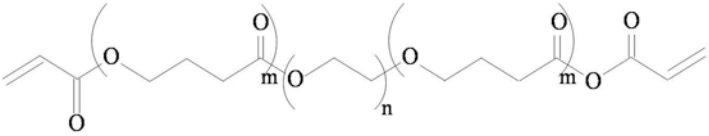

AA-$(TMC)_m$-(PEG)-$(TMC)_m$-AA

Sealant Macromer

Fig. 6.19 Chemical structures of primer and sealant macromers used in photopolymerizable PEG tissue adhesives. In each macromer, polyethylene glycol (PEG) is linked on each end to either trimethylene carbonate (TMC) or lactate (LA) hydolyzable segments, and end-capped with polymerizable acrylate groups (AA)

sealing bronchial and parenchymal air leaks in experimental lung surgery [53]. On May 26, 2000, the FDA approved the commercial sealant FocalSeal®-L (Focal Incorporated, Lexington, Massachusetts) for sealing air leaks on the lungs following surgical removal of cancerous lung tumors. The photopolymerizable tissue adhesive also received CE Mark approval for sealing air leaks following lung surgery.

Each macromer of the commercial photopolymerizable adhesive consists of PEG modified with biodegradable and photoreactive elements. In each macromer, polyethylene glycol is linked on both ends to hydrolyzable trimethylene carbonate or lactate oligomeric segments, and then end-capped with polymerizable acrylate groups (Fig. 6.19). The macromers are amphiphilic in nature, with hydrophobic end regions on the central PEG chain, and form micellar structures in aqueous solution. The formation of such preorganized configurations in aqueous solutions enables the macromers to undergo rapid photopolymerization and gelation. During clinical use, the macromers are applied to the target tissue in two parts: a primer solution to provide tissue bonding, and a sealant solution to provide desired mechanical properties. Both components are introduced as aqueous solutions to the target site. The primer layer is first brushed onto the tissue surface to allow the low-viscosity solution to flow into tissue interstices. The sealant solution is then mixed with the primer solution using a brush to provide a transition layer. The thicker sealant layer is then flowed in a continuous manner over the application area, and the macromers are photopolymerized.

To enable photopolymerization, the macromers are formulated in buffered saline solutions containing triethanolamine and eosin Y as the photoinitiator [54]. The polymerization is initiated using visible blue-green light illumination from a xenon

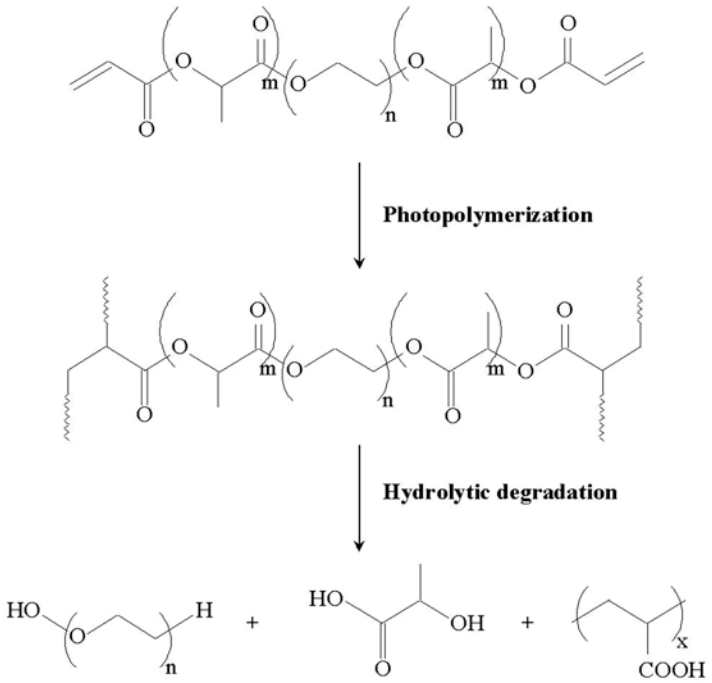

Fig. 6.20 Photopolymerization and biodegradation reactions of poly(ethylene glycol)-co-poly(L-LACTIDE) diacrylate monomer. The degradation products are soluble and biocompatible

arc lamp (470–520 nm) for 40 s at an intensity of 100 mW/cm. The macromers crosslink to form a clear, flexible, and adherent hydrogel network. Because the sealant is polymerized in situ, the polymer conforms to the tissue surface. The hydrogel expands upon contact with body fluids and reaches its equilibrium swell volume within 24 h; the hydrogel contains 95 % water at equilibrium. Following implantation, the poly(L-lactide) and poly(trimethylene carbonate) segments of the hydrogel degrade by hydrolysis (Fig. 6.20); the sealant thus degrades by dissolution rather than fragmentation. The biodegradation products are water-soluble and biocompatible; the components are sufficiently low in molecular weight to be cleared through the kidneys or locally metabolized.

Photopolymerizable PEG tissue adhesives have been utilized clinically in their approved application for sealing air leaks following pulmonary resection [55, 56]; the adhesives have also been used to treat air leaks in patients suffering lung injury at cardiac reoperation [57]. In addition, there is a clinical report of the successful use of photopolymerized PEG adhesives for repairing ventricular wall rupture following mitral valve replacement [58]. In experimental models, the sealants have demonstrated efficacy for repairing acute aortic dissection [59], coronary artery anastomoses [60], inguinal hernia [61], pancreatic-jejunal anastomoses [62], and intestinal anastomoses [63], as well as for prevention of peritendinous adhesions following flexor tendon repair surgery [64]. However, despite desirable characteristics

Fig. 6.21 CoSeal® PEG-PEG tissue sealant. The sealant is a two-component system, comprising two functionalized star-branched PEGs. Upon mixing, the PEGs react to form a covalently bonded three-dimensional matrix. The sealant can be delivered as a sprayed barrier, as shown (Food and Drug Administration)

of biocompatibility, biodegradability, and potential versatility in surgical applications, the photopolymerizable PEG adhesives have failed to achieve widespread clinical use. The requirement for additional equipment (a blue-green visible light lamp) in the operating room may limit the ease-of-use and ultimately reduce the clinical acceptability of photopolymerizable sealants.

A second PEG-based sealant system is the PEG-PEG platform. A rapidly gelling synthetic PEG-PEG tissue sealant, formed by reacting two multifunctional four-arm star-branched PEG molecules was first reported in 2001. The sealant, composed of tetra-succinimidyl-derivatized polyethylene glycol and tetra-thiol-derivatized polyethylene glycol, demonstrated adhesion to carotid arteries, collagen membranes, and PTFE grafts in vitro [65]. In subsequent clinical studies, the PEG-PEG tissue adhesive was successful in sealing suture lines of the aorta and coronary artery bypass grafts [66], as well as prosthetic vascular grafts [67]. On December 14, 2001, the commercial sealant CoSeal® (Cohesion Technologies, Palo Alto, CA) received FDA approval as a hemostatic adjunct during vascular reconstruction surgery (Fig. 6.21). The PEG-PEG sealant also received CE Mark approval for adjunctive hemostasis in vascular reconstructions.

The commercial PEG-PEG system is comprised of two PEG powder components: powdered pentaerythritol poly(ethylene glycol) ether tetra-succinimidyl glutarate, and powdered pentaerythritol poly(ethylene glycol) ether tetra-thiol (Fig. 6.22). The molecular weight of each four-arm star-branched PEG is approximately 10,000. Immediately prior to clinical use, the powder components are dissolved in an aqueous buffer; the two components are then mixed as they are delivered to the tissue site. Upon mixing, the functional groups on multiple arms of the PEGs react to form a covalently bonded three-dimensional matrix. The sulfur group of the multiarm PEG thiol nucleophilically attacks the carbonyl group attached to *N*-hydroxysuccinimide in the multiarm PEG succinimidyl ester. The hydrogel is formed by the release of *N*-hydroxysuccinimide and concurrent formation of a thioester bond between the two substituted multiarm PEGs (Fig. 6.23).

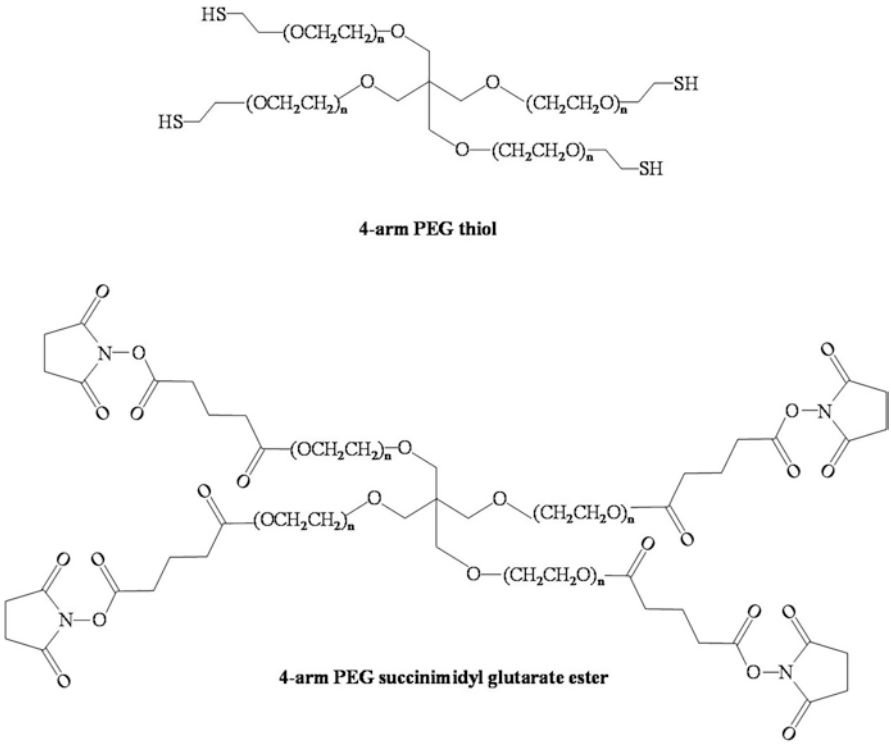

Fig. 6.22 Chemical structures of multifunctional star-branched four-arm PEG polymers used in PEG-PEG tissue adhesives. The two components of the PEG-PEG system are pentaerythritol poly(ethylene glycol) ether tetra-thiol, and pentaerythritol poly(ethylene glycol) ether tetra-succinimidyl glutarate

There is a small amount of disulfide bond formation between thiol groups. The functionalized PEG end groups additionally react with functional groups (particularly amine groups) in the tissue matrix to form covalent bonds, providing a chemical linkage between the PEG-PEG hydrogel and the surrounding tissue. When applied to prosthetic vascular grafts, the PEG-PEG hydrogel partially penetrates the irregular graft surface and creates a mechanical bond.

The PEG-PEG tissue sealant provides sealing within 60 s; the mean time to complete anastomotic sealing during placement of prosthetic vascular grafts is 16.5 s. Following implantation, the PEG-PEG hydrogel absorbs water and swells to up to four times its original volume within 24 h; application of the sealant should therefore be avoided near anatomic structures that are sensitive to compression. The hydrogel is biodegradable and contains two hydrolyzable bonds: the thioester between the two multiarm PEGs and an O-ester that is within one of the PEGs and glutarate. The sealant is fully resorbed within 4 weeks.

Beyond its indicated use for adjunctive hemostasis of peripheral vascular anastomoses, the PEG-PEG system has demonstrated efficacy for minimizing anastomotic

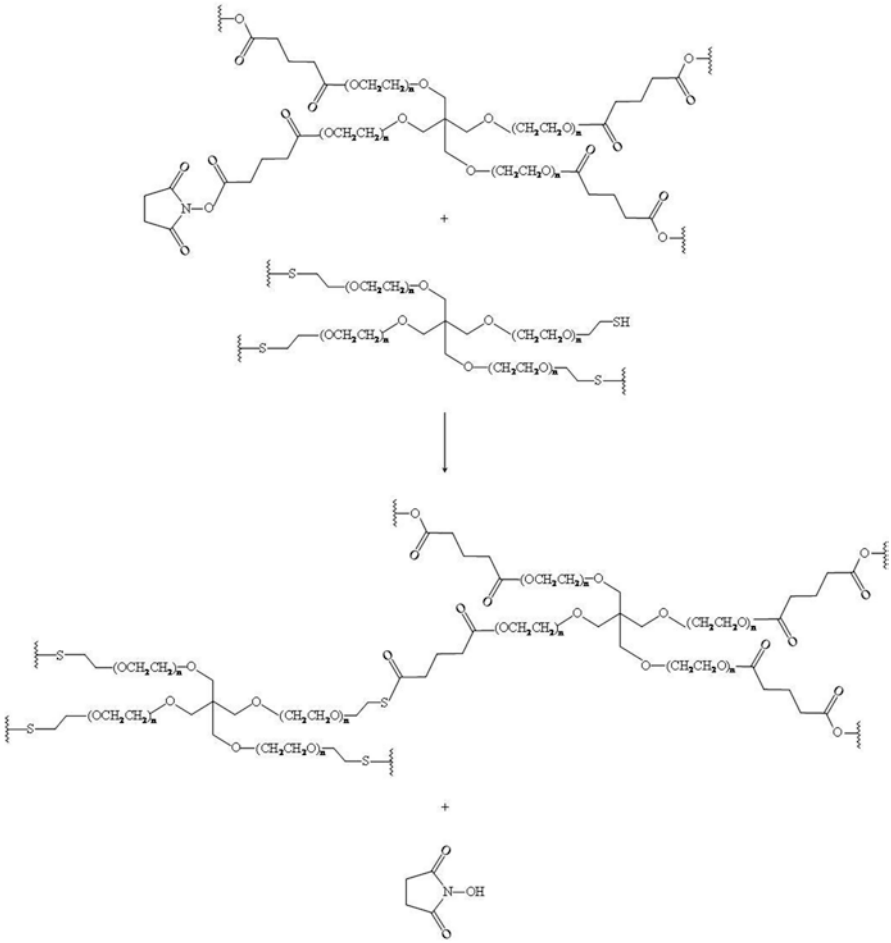

Fig. 6.23 Reaction of multifunctional star-branched four-arm PEG polymers to form PEG-PEG tissue adhesives. The sulfur group of the multiarm PEG thiol nucleophilically attacks the carbonyl group attached to *N*-hydroxysuccinimide in the multiarm PEG succinimidyl ester. The hydrogel is formed by the release of *N*-hydroxysuccinimide and concurrent formation of a thioester bond between the two substituted multiarm PEGs

bleeding during aortic reconstruction [68]. In addition, PEG-PEG hydrogels have been successfully applied as sprayed barriers to reduce postoperative adhesion formation following uterine surgery [69] as well as adult and pediatric cardiac surgery [70, 71]. The major limitations of the PEG-PEG sealant are its high degree of swell and its relatively weak adhesion to tissue. On anastomotic closures, both cyanoacrylate glue and albumin-glutaraldehyde glue demonstrate greater mechanical integrity than the PEG-PEG sealant and are capable of resisting higher loads before failure [72]. On the cut tissue surface of the kidney, fibrin sealant adheres more

Fig. 6.24 DuraSeal® PEG-trilysine tissue adhesive. The sealant is a two-component system, comprising a PEG ester and a trilysine amine. The two solutions mix as they are sprayed onto dural tissue, and the components crosslink to form a watertight seal. The system also contains blue dye to allow visualization of hydrogel coverage on the tissue surface (Food and Drug Administration)

effectively than PEG-PEG sealant [73]. A practical limitation of the PEG-PEG system is the requirement for preparation and dissolution of the powdered PEGs into aqueous buffer prior to use; this may limit the convenient use of the sealant in the operating room.

A third PEG-based adhesive biomaterial is the PEG-trilysine system. A novel hydrogel sealant, composed of a PEG ester and a trilysine amine, was described in 2003 as an effective agent for dural closure to prevent cerebrospinal fluid leakage following neurosurgery [74]. In a preliminary clinical study conducted in 2005, the PEG-trilysine tissue adhesive demonstrated 100 % closure of intraoperative cerebrospinal fluid leaks [75]. The commercial PEG-trilysine sealant DuraSeal® (Confluent Surgical, Waltham, Massachusetts) was granted FDA approval on April 7, 2005, as an adjunct to sutured dural repair during cranial surgery to provide watertight closure (Fig. 6.24).

The commercial sealant is supplied as a two-component system comprised of a PEG ester powder and a trilysine amine solution. The PEG component is dissolved in an aqueous solution immediately prior to clinical use. The two solutions mix as they are sprayed onto the dural tissue, and the components crosslink to form a watertight hydrogel seal. The sealant system also contains FD&C blue dye #1 to allow visualization of hydrogel coverage and thickness. The hydrogel absorbs water following implantation and swells by approximately 50 % in volume; the sealant therefore should not be applied to confined bony structures where nerves are present, since neural compression can result due to hydrogel swelling. The tissue adhesive degrades hydrolytically within four to eight weeks, and the degradation products are readily cleared by the kidneys. The PEG-trilysine system has continued to demonstrate 100 % efficacy in stopping cerebrospinal fluid leakage in patients undergoing neurosurgical procedures [76].

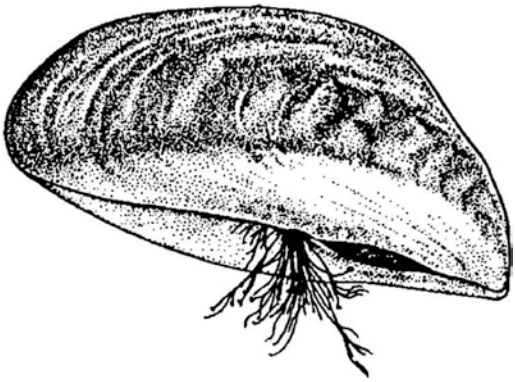

Fig. 6.25 Adhesive byssal threads of the mussel (National Oceanic and Atmospheric Administration). The tough byssal threads are coated with mussel adhesive proteins to enable attachment to natural and manmade surfaces

6.4.1.1 Naturally Inspired Hydrogels for Wound Closure

A number of original adhesive platforms are currently being pursued for soft tissue repair and regeneration. Several of these innovative sealant technologies have demonstrated promise in experimental models of wound closure, but they have not yet reached clinical use. Three families of novel tissue adhesives are described here: naturally inspired tissue adhesives, polysaccharide-based tissue adhesives, and dendrimeric tissue adhesives. These emerging sealants are directed toward a variety of clinical applications, including external skin closure, gastrointestinal surgery, orthopedic surgery, and ophthalmic surgery.

Naturally occurring adhesive structures, such as frog glues, mussel proteins, and sticky gecko feet, have provided the inspiration for unique new tissue sealants. For instance, the Australian frog *Notaden benetti* secretes an exudate that rapidly forms a tacky elastic solid. This protein-based material acts as a pressure-sensitive adhesive that functions in wet conditions, and covalent crosslinking does not seem to be necessary for the glue to set [77]. The frog glue demonstrated efficacy in repairing torn meniscal tissue of the knee in an ex vivo model and showed superior mechanical strength to both gelatin and fibrin glues [78]. This recently discovered biological glue may be considered for meniscal repairs in the future.

Marine and freshwater mussels also secrete specialized protein adhesives for rapid and durable attachment to wet surfaces. Mussels exude tough byssal threads (Fig. 6.25) and coat these threads with adhesive proteins to attach to natural and manmade structures. Glues based on mussel adhesive proteins may thus be ideal for achieving adhesion to wet tissue substrates. Adhesive proteins extracted from *Mytilus edulis* mussel have demonstrated success in vitro for bonding porcine skin [79] and porcine small intestinal submucosa [80]; however, the mussel protein extracts required excessively long cure times.

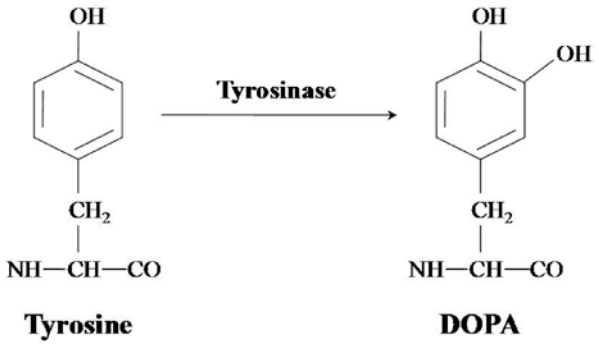

Fig. 6.26 Posttranslational modification of tyrosine residues in the *Mytilus edulis* mussel adhesive protein. Hydroxylation of tyrosine residues creates L-3,4-dihydroxylphenylalanine (DOPA) residues, which are essential for adhesive protein crosslinking

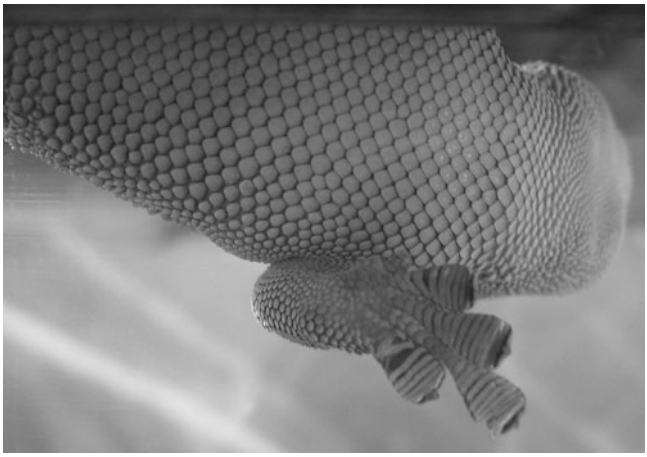

Fig. 6.27 Adhesive footpads of the Madagascar gecko lizard (Montreal Biodome)

Synthetic polymers containing mussel protein functionality have been designed as a strategy for creating effective adhesives. The amino acid L-3,4-dihydroxylphenylalanine (DOPA) contributes to mussel protein solidification through oxidation and crosslinking reactions [81]; DOPA is formed in mussel proteins by posttranslational hydroxylation of the amino acid tyrosine (Fig. 6.26). Biomimetic DOPA-functionalized PEG polymers have been shown to crosslink upon exposure to oxidizing reagents, and they successfully bond porcine skin in vitro [82].

While frog glues and mussel adhesive proteins have inspired novel sealants based on their chemical compositions, the sticky footpad of the gecko lizard (Fig. 6.27) has inspired new tissue adhesives based on its nanostructure. The gecko footpad is covered with a dense array of fibrils (setae), which maximize interfacial adhesion to surfaces [83]. Individual setae operate by van der Waals forces; the intermolecular attraction allows geckos to adhere to vertical and inverted surfaces.

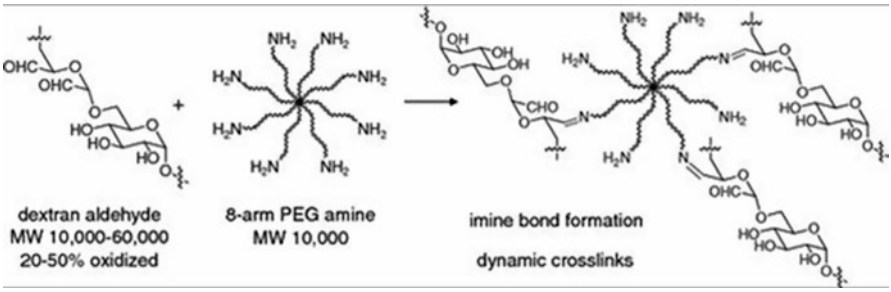

Fig. 6.28 Foundation chemistry for dextran-based tissue adhesives. The oxidized polysaccharide dextran aldehyde reacts with an eight-arm star PEG amine to form a crosslinked hydrogel network

A biodegradable and biocompatible tissue adhesive has been designed to mimic the nanotopography of the gecko foot [84]. The gecko-inspired tissue adhesive is manufactured from a poly(glycerol-co-sebacate acrylate) (PGSA) elastomeric surface. The PGSA surface is etched into an array of nanoscale pillars to mimic the nanopatterns of the gecko foot, and the etched polymer is subsequently coated with oxidized dextran to allow tissue bonding. Applied as a tissue tape, the gecko-inspired adhesive has demonstrated efficacy in binding porcine intestinal tissue in vitro and rat abdominal tissue in vivo. The geckolike tissue adhesive may provide the basis for an entirely new family of nanopatterned surgical adhesives.

Surgical glues composed of functionalized natural polysaccharides, including chondroitin and dextran, are showing early success as biocompatible sealants. The biopolymer chondroitin sulfate is a major component of cartilage extracellular matrix, and may provide an ideal foundation for designing biomaterials for cartilage repair. A photopolymerizable hydrogel composed of chondroitin sulfate functionalized with methacrylate and aldehyde groups has shown success in binding articular cartilage defects in vivo [85]. The chondroitin sulfate-methacrylate-aldehyde hydrogel is noncytotoxic and noninflammatory and is able to encapsulate cartilage cells, making it a promising platform for cartilage reconstruction. In addition, a photopolymerizable polysaccharide-based sealant composed of hyaluronic acid functionalized with methacrylate groups has shown efficacy in sealing experimental corneal incisions [86].

Finally, a polysaccharide-based sealant composed of dextran aldehyde and multiarm PEG amine has been developed for wound closure (Fig. 6.28). The two components undergo a Schiff base reaction to form a crosslinked hydrogel. This two-component tissue adhesive system crosslinks in water, cures rapidly (<1 min) at room temperature, adheres to moist tissue, and degrades hydrolytically. The dextran-based tissue adhesive is noncytotoxic to fibroblasts cell lines and noninflammatory to macrophage cell lines [87]. In addition, the dextran-based sealant requires no external photoinitiator or other extra equipment and has demonstrated efficacy in an ex vivo model of corneal closure [88]. The polysaccharide-based tissue adhesive successfully seals corneal incisions to pressures of >10 psi (500 mmHg) and is noncytotoxic to bovine corneal endothelial cells. Another advantage of this sealant, in terms of clinical acceptance, is that dextran has a long history of clinical use as a plasma expander.

Highly branched dendritic macromers have provided the basis for a new class of hydrogel sealants with unique physical and mechanical properties [89]. Dendrimers possess three main structural components: a central core, internal branching layers, and peripheral functional groups. Unlike linear polymers, in which growth is accomplished by adding a single monomer, dendritic polymers grow by branching each monomer, leading to multiple additions. When used to construct hydrogel scaffolds, dendritic macromers allow increased crosslink density of the scaffold without significantly increasing the polymer concentration, as compared to linear polymer analogs; this approach leads to improved mechanical properties and minimal swelling of the hydrogel.

Biodendrimeric tissue adhesives, based on peptide dendrons functionalized with terminal cysteine residues, have been developed for ophthalmic applications. When the cysteine-terminated peptide dendrons are mixed with PEG dialdehyde, a hydrogel forms as a consequence of thiazolidene linkages between the two macromers [90]. These biodendrimeric sealants have been successful in sealing ex vivo corneal incisions and securing ex vivo corneal transplants [91]. A photocrosslinkable biodendrimeric tissue adhesive has also been created from triblock copolymers; these hybrid dendritic-linear copolymers consist of a PEG core and methacrylated poly(glycerol succinic acid) dendrimer terminal blocks. The photopolymerized dendrimeric sealant is effective in sealing experimental full-thickness corneal lacerations [92] and in securing ex vivo laser in situ keratomileusis (LASIK) flaps [93]. In addition, the photocrosslinkable dendrimer adhesive attaches to experimental cartilage defects [94] and encapsulates chondrocyte cells [95]. Dendrimer-based sealants may thus be a promising new technology for cartilage repair.

6.4.2 Summary

Adhesive hydrogels can be constructed from synthetic polymers such as PEG, naturally derived polymers such as polysaccharides, and naturally inspired polymers such as nanopatterned PGSA. These hydrogels exhibit biocompatibility, biodegradability, tunable mechanical properties and degradation rates, and adherence to moist tissues. As described earlier in this chapter, hydrogels can be a valuable strategy for drug delivery. Adhesive hydrogels that deliver therapeutics hold a great deal of promise for wound healing, tissue repair, and tissue regeneration.

6.5 Problems

6.1 A physician would like to treat a pancreatic cancer patient with an implantable, covalently crosslinked, polymer hydrogel loaded with paclitaxel capable of swelling to the dimensions of a volume adjacent to the malignant interface (shown ahead). If the unswelled drug-loaded hydrogel is spherical in shape

with a radius of 100 μm, with your knowledge of hydrogel materials for drug delivery, answer the following questions.

(i) What degree of swelling is necessary to fill the void volume adjacent to the malignancy?
(ii) What are the key characteristics of the paclitaxel release profile?
(iii) How long would it take for the drug to reach its cumulative release plateau?
(iv) How would you expect the release rate to change if you decreased the molecular weight of the polymer chains between the crosslink points?

6.2 A medical research lab is screening potential injectable hydrogel candidates for use as cartilage repair agents by facilitating chondrocyte growth within void spaces within the tissue matrix. Using your knowledge of hydrogel materials for drug delivery, answer the following questions.

(i) With the following rheology data, plot the storage modulus versus time for each of the hydrogel polymers.
(ii) Given the rheology data, which candidate(s) would be ideal for treatment in cartilage tissue repair? Why?
(iii) If not, what can be done to the system in order to shift the rheology plot to an acceptable domain?

6.3 A first-year graduate student in materials engineering is interested in designing a basic hydrogel system with ultimate control of release kinetics and degradation. Using the components here and your knowledge of hydrogels in drug delivery, answer the following questions.

(i) Label the polymer and crosslinks.
(ii) Which components are rigid and which are flexible? Why?
(iii) Construct a gel structure from these components. What would you expect its properties to be?
(iv) How would you select your hydrogel components for use in an injectable cartilage repair treatment? Would these components change for a bone graft replacement? Why?
(v) How could you control the release profile of this system?

6.4 A research lab in biomedical engineering would like to design a hydrogel system consisting of polyethylene glycol (PEG) as the arms between crosslink points to release a 10-nm nanoparticle upon swelling. If we assume that the PEG polymer chains are in their fully extended state (i.e., rigid linear chains) upon swelling, use your knowledge of hydrogel systems to answer the following questions.

(i) If we assume that the geometry of the void space within the gel is consistent with the following diagram of a tetrafunctional crosslinked hydrogel system, and $\upsilon_{2m} = 0.1$, $\chi_1 = 0.52$, $V_1 = 1$, $\upsilon = 1.5$ cm/g [3], calculate the molecular weight of the polymer arms between crosslink points.
(ii) What is the largest-diameter nanoparticle that could be released from the void space of this swelled hydrogel system?
(iii) How would the void space change if the crosslinking group was changed from a tetrafunctional group to a trifunctional group?

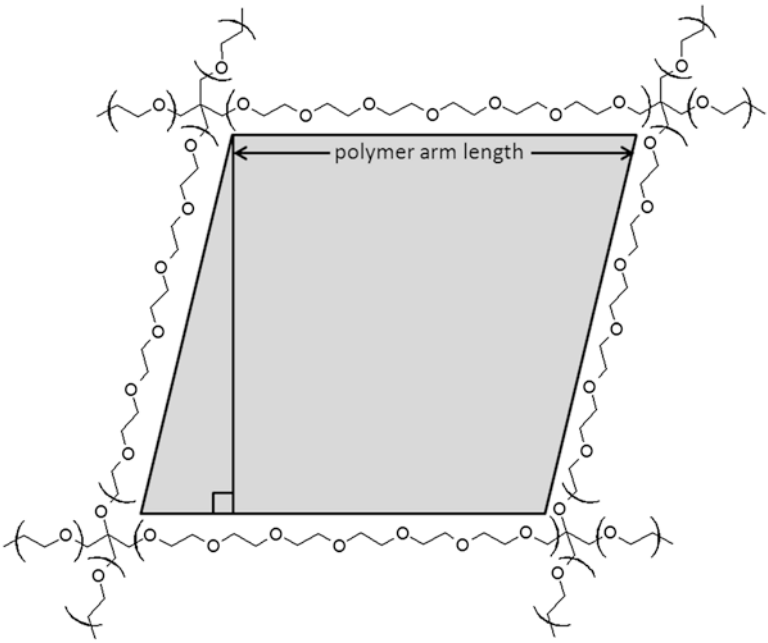

6.5 A medical research group is interested in using hydrogels to facilitate the controlled delivery of neurological drugs within the corpus callosum of the brain. With your knowledge of hydrogel systems in drug delivery, answer the following questions.

(i) Based on the nature of the delivery required and the physiological environment, what method of application would be preferred for a hydrogel system: injection or implantation? Why?
(ii) What method of application would be preferred for a hydrogel system if the target area is the lower spinal cord (i.e., pelvis area)? Why?
(iii) Some neurological drugs function by disrupting the sodium-potassium pump within neuronal cells. If a researcher is using a hydrogel with polyelectrolyte arms between crosslinks, discuss what effects may be felt by the hydrogel in the presence of an environment of changing ionic potential.

References

1. Hoare, T. R., & Kohane, D. S. (2008). Hydrogels in drug delivery: Progress and challenges. *Polymer, 49*(8), 1993–2007.
2. Vijayasekaran, S., Fitton, J. H., Hicks, C. R., Chirila, T. V., Crawford, G. J., & Constable, I. J. (1998). Cell viability and inflammatory response in hydrogel sponges implanted in the rabbit cornea. *Biomaterials, 19*(24), 2255–2267.
3. Maleux, G., Deroose, C., Fieuws, S., Van Cutsem, E., Heye, S., Bosmans, H., et al. (2013). Prospective comparison of hydrogel-coated microcoils versus fibered platinum microcoils in

the prophylactic embolization of the gastroduodenal artery before yttrium-90 radioembolization. *Journal of Vascular and Interventional Radiology: JVIR, 24*(6), 797–803.
4. Elisseeff, J. (2008). Hydrogels: Structure starts to gel. *Nature Materials, 7*(4), 271–273.
5. (a) Battig, M. R., Soontornworajit, B., & Wang, Y. (2012). Programmable release of multiple protein drugs from aptamer-functionalized hydrogels via nucleic acid hybridization. *Journal of the American Chemical Society, 134*(30), 12410–12413. (b) Misra, G. P., Singh, R. S. J., Aleman, T. S., Jacobson, S. G., Gardner, T. W., & Lowe, T. L. (2009). Subconjunctivally implantable hydrogels with degradable and thermoresponsive properties for sustained release of insulin to the retina. *Biomaterials, 30*(33), 6541–6547. (c) Lee, K. Y., Peters, M. C., Anderson, K. W., & Mooney, D. J. (2000). Controlled growth factor release from synthetic extracellular matrices. *Nature, 408*(6815), 998–1000.
6. (a) Huynh, D. P., Nguyen, M. K., Pi, B. S., Kim, M. S., Chae, S. Y., Lee, K. C., et al. (2008). Functionalized injectable hydrogels for controlled insulin delivery. *Biomaterials, 29*(16), 2527–2534. (b) Ifkovits, J. L., Tous, E., Minakawa, M., Morita, M., Robb, J. D., Koomalsingh, K. J., et al. (2010). Injectable hydrogel properties influence infarct expansion and extent of postinfarction left ventricular remodeling in an ovine model. *Proceedings of the National Academy of Sciences of the United States of America, 107*(25), 11507–11512.
7. Drury, J. L., & Mooney, D. J. (2003). Hydrogels for tissue engineering: Scaffold design variables and applications. *Biomaterials, 24*(24), 4337–4351.
8. (a) Kappel, R. M., & Pruijn, G. J. M. (2012). The Monobloc hydrogel breast implant, experiences and ideas. *European Journal of Plastic Surgery, 35*(3), 229–233. (b) Arion, H. (2001). [Carboxymethylcellulose hydrogel-filled breast implants. Our experience in 15 years]. *Annales de Chirurgie Plastique et Esthétique, 46*(1), 55–59.
9. (a) Hyon, S.-H., Cha, W.-I., Ikada, Y., Kita, M., Ogura, Y., & Honda, Y. (1994). Poly(vinyl alcohol) hydrogels as soft contact lens material. *Journal of Biomaterials Science, Polymer Edition, 5*(5), 397–406. (b) Karlgard, C. C. S., Wong, N. S., Jones, L. W., & Moresoli, C. (2003). In vitro uptake and release studies of ocular pharmaceutical agents by silicon-containing and p-HEMA hydrogel contact lens materials. *International Journal of Pharmaceutics, 257*(1), 141–151.
10. Heller, A. (1999). Implanted electrochemical glucose sensors for the management of diabetes. *Annual Review of Biomedical Engineering, 1*, 153–175.
11. Saim, A. B., Cao, Y., Weng, Y., Chang, C. N., Vacanti, M. A., Vacanti, C. A., et al. (2000). Engineering autogenous cartilage in the shape of a helix using an injectable hydrogel scaffold. *The Laryngoscope, 110*(10 Pt 1), 1694–1697.
12. (a) Xing, B., Yu, C.-W., Chow, K.-H., Ho, P.-L., Fu, D., & Xu, B. (2002). Hydrophobic interaction and hydrogen bonding cooperatively confer a vancomycin hydrogel: A potential candidate for biomaterials. *Journal of the American Chemical Society, 124*(50), 14846–14847. (b) Paramonov, S. E., Jun, H.-W., & Hartgerink, J. D. (2006). Self-assembly of peptide-amphiphile nanofibers: The roles of hydrogen bonding and amphiphilic packing. *Journal of the American Chemical Society, 128*(22), 7291–7298.
13. (a) Ostroha, J., Pong, M., Lowman, A., & Dan, N. (2004). Controlling the collapse/swelling transition in charged hydrogels. *Biomaterials, 25*(18), 4345–4353. (b) Mann, B. A., Kremer, K., & Holm, C. (2006). The swelling behavior of charged hydrogels. *Macromolecular Symposia, 237*(1), 90–107.
14. Kim, W. K., & Sung, W. (2011). Charge density and bending rigidity of a rodlike polyelectrolyte: Effects of multivalent counterions. *Physical Review. E, Statistical, Nonlinear, and Soft Matter Physics, 83*(5 Pt 1), 051926.
15. Schmaljohann, D., Oswald, J., Jørgensen, B., Nitschke, M., Beyerlein, D., & Werner, C. (2003). Thermo-responsive PNiPAAm-g-PEG films for controlled cell detachment. *Biomacromolecules, 4*(6), 1733–1739.
16. (a) Brannon-Peppas, L., & Peppas, N. A. (1991). Equilibrium swelling behavior of dilute ionic hydrogels in electrolytic solutions. *Journal of Controlled Release, 16*(3), 319–329. (b) Elliott, J. E., Macdonald, M., Nie, J., & Bowman, C. N. (2004). Structure and swelling of poly(acrylic acid) hydrogels: Effect of pH, ionic strength, and dilution on the crosslinked polymer structure. *Polymer, 45*(5), 1503–1510.
17. Katchalsky, A., Lifson, S., & Exsenberg, H. (1951). Equation of swelling for polyelectrolyte gels. *Journal of Polymer Science, 7*(5), 571–574.

18. Lai, F., Li, H., & Luo, R. (2010). Chemo-electro-mechanical modeling of ionic-strength-sensitive hydrogel: Influence of Young's modulus. *International Journal of Solids and Structures, 47*(22–23), 3141–3149.
19. Flory, P. J., & Rehner, J., Jr. (1943). Statistical mechanics of crosslinked polymer networks II. Swelling statistical mechanics of cross-linked polymer networks. *Journal of Chemical Physics, 11*, 521.
20. Peppas, N. A., & Merrill, E. W. (1976). Poly(vinyl alcohol) hydrogels: Reinforcement of radiation-crosslinked networks by crystallization. *Journal of Polymer Science: Polymer Chemistry Edition, 14*, 441–457.
21. Zhu, J., & Marchant, R. E. (2011). Design properties of hydrogel tissue-engineering scaffolds. *Expert Review of Medical Devices, 8*(5), 607–626.
22. Zustiak, S. P., & Leach, J. B. (2010). Hydrolytically degradable poly(ethylene glycol) hydrogel scaffolds with tunable degradation and mechanical properties. *Biomacromolecules, 11*(5), 1348–1357.
23. Kim, S. W., Bae, Y. H., & Okano, T. (1992). Hydrogels: Swelling, drug loading, and release. *Pharmaceutical Research, 9*(3), 283–290.
24. Haines-Butterick, L., Rajagopal, K., Branco, M., Salick, D., Rughani, R., Pilarz, M., et al. (2007). Controlling hydrogelation kinetics by peptide design for three-dimensional encapsulation and injectable delivery of cells. *Proceedings of the National Academy of Sciences of the United States of America, 104*(19), 7791–7796.
25. Yan, C., Altunbas, A., Yucel, T., Nagarkar, R. P., Schneider, J. P., & Pochan, D. J. (2010). Injectable solid hydrogel: Mechanism of shear-thinning and immediate recovery of injectable β-hairpin peptide hydrogels. *Soft Matter, 6*(20), 5143–5156.
26. Daniels, C. A. (1989). *Polymers: Structure and properties* (Vol. 1989, p. 120). Boca Raton, FL: CRC Press.
27. (a) Zhang, S. (2003). Fabrication of novel biomaterials through molecular self-assembly. *Nature Biotechnology, 21*(10), 1171–1178. (b) Schneider, J. P., Pochan, D. J., Ozbas, B., Rajagopal, K., Pakstis, L., & Kretsinger, J. (2002). Responsive hydrogels from the intramolecular folding and self-assembly of a designed peptide. *Journal of the American Chemical Society, 124*(50), 15030–15037.
28. Hennink, W. E., & van Nostrum, C. F. (2002). Novel crosslinking methods to design hydrogels. *Advanced Drug Delivery Reviews, 54*(1), 13–36.
29. Bhattacharya, S., & Acharya, S. N. G. (1999). Pronounced hydrogel formation by the self-assembled aggregates of N-alkyl disaccharide amphiphiles. *Chemistry of Materials, 11*(12), 3504–3511.
30. Huang, Y., Yu, H., & Xiao, C. (2007). pH-Sensitive cationic guar gum/poly (acrylic acid) polyelectrolyte hydrogels: Swelling and in vitro drug release. *Carbohydrate Polymers, 69*(4), 774–783.
31. Zhang, Y., Gu, H., Yang, Z., & Xu, B. (2003). Supramolecular hydrogels respond to ligand-receptor interaction. *Journal of the American Chemical Society, 125*(45), 13680–13681.
32. (a) Berger, J., Reist, M., Mayer, J. M., Felt, O., Peppas, N. A., & Gurny, R. (2004). Structure and interactions in covalently and ionically crosslinked chitosan hydrogels for biomedical applications. *European Journal of Pharmaceutics and Biopharmaceutics, 57*(1), 19–34. (b) Hennink, W. E., & van Nostrum, C. F. (2012). Novel crosslinking methods to design hydrogels. *Advanced Drug Delivery Reviews, 64*(Suppl), 223–236.
33. (a) Molina, I., Li, S., Martinez, M. B., & Vert, M. (2001). Protein release from physically crosslinked hydrogels of the PLA/PEO/PLA triblock copolymer-type. *Biomaterials, 22*(4), 363–369. (b) Wu, J., Gong, X., Fan, Y., & Xia, H. (2011). Physically crosslinked poly(vinyl alcohol) hydrogels with magnetic field controlled modulus. *Soft Matter, 7*(13), 6205. (c) Liu, Y., Vrana, N. E., Cahill, P. A., & McGuinness, G. B. (2009). Physically crosslinked composite hydrogels of PVA with natural macromolecules: Structure, mechanical properties, and endothelial cell compatibility. *Journal of Biomedical Materials Research. Part B, Applied biomaterials, 90*(2), 492–502.
34. Petka, W. A. (1998). Reversible hydrogels from self-assembling artificial proteins. *Science, 281*(5375), 389–392.

35. Wright, E. R., McMillan, R. A., Cooper, A., Apkarian, R. P., & Conticello, V. P. (2002). Thermoplastic elastomer hydrogels via self-assembly of an elastin-mimetic triblock polypeptide. *Advanced Functional Materials, 12*(2), 149–154.
36. Peppas, N. A., & Merrill, E. W. (1977). Crosslinked poly(vinyl alcohol) hydrogels as swollen elastic networks. *Journal of Applied Polymer Science, 21*(7), 1763–1770.
37. Gong, J. P., Katsuyama, Y., Kurokawa, T., & Osada, Y. (2003). Double-network hydrogels with extremely high mechanical strength. *Advanced Materials, 15*(14), 1155–1158.
38. Caldorera-Moore, M., Kang, M. K., Moore, Z., Singh, V., Sreenivasan, S. V., Shi, L., et al. (2011). Swelling behavior of nanoscale, shape- and size-specific, hydrogel particles fabricated using imprint lithography. *Soft Matter, 7*(6), 2879.
39. Glassman, M. J., Chan, J., & Olsen, B. D. (2013). Reinforcement of shear thinning protein hydrogels by responsive block copolymer self-assembly. *Advanced Functional Materials, 23*(9), 1182–1193.
40. Beebe, D., Moore, J., Bauer, J., Yu, Q., Liu, R., Devadoss, C., et al. (2000). Functional hydrogel structures for autonomous flow control inside microfluidic channels. *Nature, 404*(6778), 588–590.
41. (a) Sarvestani, A. S., He, X., & Jabbari, E. (2007). Viscoelastic characterization and modeling of gelation kinetics of injectable in situ cross-linkable poly(lactide-co-ethylene oxide-co-fumarate) hydrogels. *Biomacromolecules, 8*(2), 406–415. (b) McCrum, N. G., Buckley, C. P., & Bucknall, C. B. (1997). *Principles of polymer engineering* (p. 447). Oxford, UK: Oxford University Press.
42. Yu, L., & Ding, J. (2008). Injectable hydrogels as unique biomedical materials. *Chemical Society Reviews, 37*(8), 1473–1481.
43. Bazaka, K., & Jacob, M. (2012). Implantable devices: Issues and challenges. *Electronics, 2*, 1–34.
44. Brahim, S., Narinesingh, D., & Guiseppi-Elie, A. (2002). Bio-smart hydrogels: Co-joined molecular recognition and signal transduction in biosensor fabrication and drug delivery. *Biosensors and Bioelectronics, 17*, 973–981.
45. Park, K. M., Lee, S. Y., Joung, Y. K., Na, J. S., Lee, M. C., & Park, K. D. (2009). Thermosensitive chitosan-Pluronic hydrogel as an injectable cell delivery carrier for cartilage regeneration. *Acta Biomaterialia, 5*(6), 1956–1965.
46. Caliceti, P., & Veronese, F. M. (2000). Pharmacokinetic and biodistribution properties of poly(ethylene glycol)-protein conjugates. *Advanced Drug Delivery Reviews, 55*, 1261.
47. Abuchowski, A., van Es, T., Palczuk, N. C., & Davis, F. F. (1977). Alteration of immunological properties of bovine serum albumin by covalent attachment of polyethylene glycol. *Journal of Biological Chemistry, 252*, 3578.
48. Abuchowski, A., McCoy, J. R., Palczuk, N. C., van Es, T. T., & Davis, F. F. (1977). Effect of covalent attachment of polyethylene glycol on immunogenicity and circulating life of bovine liver catalase. *Journal of Biological Chemistry, 252*, 3582.
49. Sawhney, A. S., Pathak, C. P., & Hubbell, J. A. (1993). Bioerodible hydrogels based on photopolymerized poly(ethylene glycol)-co-poly(α-hydroxy acid) diacrylate macromers. *Macromolecules, 26*, 581.
50. Sawhney, A. S., Pathak, C. P., van Rensburg, J. J., Dunn, R. C., & Hubbell, J. A. (1994). Optimization of photopolymerized bio-erodible hydrogel properties for adhesion prevention. *Journal of Biomedial Materials Research, 28*, 831.
51. Hill-West, J. L., Chowdhury, S. M., Sawhney, A. S., Pathak, C. P., Dunn, R. C., & Hubbell, J. A. (1994). Prevention of postoperative adhesions in the rat by in situ photopolymerization of bioresorbable hydrogel barriers. *Obstetrics & Gynecology, 83*, 59.
52. Dumanian, G. A., Dascombe, W., Hong, C., Labadie, K., Garrett, K., Sawhney, A. S., et al. (1995). A new photopolymerizable blood vessel glue that seals human vessel anastomoses without augmenting thrombogenicity. *Plastic and Reconstructive Surgery, 95*, 901.
53. Ranger, W. R., Halpin, D., Sawhney, A. S., Lyman, M., & Locicero, J. (1997). Pneumostasis of experimental air leaks with a new photopolymerized synthetic tissue sealant. *American Surgeon, 63*, 788.
54. Sawhney, A. S., & Hubbell, J. A. (1999). In situ photopolymerized hydrogels for vascular and peritoneal wound healing. In J. R. Morgan & M. L. Yarmush (Eds.), *Tissue engineering methods and protocols*. Totowa, NJ: Humana Press.

55. Wain, J. C., Kaiser, L. R., & Johnstone, D. W. (2001). Trial of a novel synthetic sealant in preventing air leaks after lung resection. *Annals of Thoracic Surgery, 71*, 1623.
56. Macchiarini, P., Wain, J., Almy, S., & Dartevelle, P. (1999). Experimental and clinical evaluation of a new synthetic, absorbable sealant to reduce air leaks in thoracic operations. *Journal of Thoracic and Cardiovascular Surgery, 117*, 751.
57. Gillinov, A. M., & Lytle, B. W. (2001). A novel synthetic sealant to treat air leaks at cardiac reoperation. *Journal of Cardiac Surgery, 16*, 255.
58. Fasol, R., Wild, T., & El Dsoki, S. (2004). Left ventricular rupture after mitral surgery: Repair by patch and sealing. *Annals of Thoracic Surgery, 77*, 1070.
59. Tanaka, K., Takamoto, S., Ohtsuka, T., Kotsuka, Y., & Kawauchi, M. (1999). Application of AdvaSeal for acute aortic dissection: Experimental study. *Annals of Thoracic Surgery, 68*, 1308.
60. White, J. K., Titus, J. S., Tanabe, H., Aretz, H. T., & Torchiana, D. F. (2000). The use of a novel tissue sealant as a hemostatic adjunct in cardiac surgery. *The Heart Surgery Forum, 3*, 56.
61. Kato, Y., Yamataka, A., Miyano, G., Tei, E., Koga, H., Lane, G. J., et al. (2005). Tissue adhesives for repairing inguinal hernia: A preliminary study. *Journal of Laparoendoscopic & Advanced Surgical Techniques. Part A, 15*, 424.
62. Argyra, E., Polymeneas, G., Karvouni, E., Kontorravdis, N., Theodosopoulos, T., & Arkadopoulos, N. (2009). Sutureless pancreatojejunal anastomosis using an absorbable sealant: Evaluation in a pig model. *Journal of Surgical Research, 153*, 282.
63. Sweeney, T., Rayan, S., & Warren, H. (2002). Intestinal anastomoses detected with a photopolymerized hydrogel. *Surgery, 131*, 185.
64. Ferguson, R. E., & Rinker, B. (2006). The use of a hydrogel sealant on flexor tendon repairs to prevent adhesion formation. *Annals of Plastic Surgery, 56*, 54.
65. Wallace, D. G., Cruise, G. M., Rhee, W. M., Schroeder, J. A., Prior, J. J., Ju, J., et al. (2001). A tissue sealant based on reactive multifunctional polyethylene glycol. *Journal of Biomedial Materials Research, 58*, 545.
66. Marc Hendrikx, M., Mees, U., Hill, A. C., Egbert, B., Coker, G. T., & Estridge, T. D. (2001). Evaluation of a novel synthetic sealant for inhibition of cardiac adhesions and clinical experience in cardiac surgery procedures. *The Heart Surgery Forum, 4*, 204.
67. Glickman, M., Gheissari, A., Money, S., Martin, J., Ballard, J. L., & CoSeal Multicenter Vascular Surgery Study Group. (2002). A polymeric sealant inhibits anastomotic suture hole bleeding more rapidly than gelfoam/thrombin: Results of a randomized controlled trial. *Archives of Surgery, 137*, 326.
68. Hagberg, R. C., Safi, H. J., Sabik, J., Conte, J., & Block, J. E. (2004). Improved intraoperative management of anastomotic bleeding during aortic reconstruction: Results of a randomized controlled trial. *American Surgeon, 70*, 307.
69. Mettler, L., Hucke, J., Bojahr, B., Tinneberg, H. R., Leyland, N., & Avelar, R. (2008). A safety and efficacy study of a resorbable hydrogel for reduction of post-operative adhesions following myomectomy. *Human Reproduction, 23*, 1093.
70. Konertz, W. F., Kostelka, M., Mohr, F. W., Hetzer, R., Hübler, M., Ritter, J., et al. (2003). Reducing the incidence and severity of pericardial adhesions with a sprayable polymeric matrix. *Annals of Thoracic Surgery, 76*, 1270.
71. Napoleone, C. P., Oppido, G., Angeli, E., & Gargiulo, G. (2007). Resternotomy in pediatric cardiac surgery: Co-Seal initial experience. *Interactive Cardiovascular and Thoracic Surgery, 6*, 21.
72. Saunders, M. M., Baxter, Z. C., Abou-Elella, A., Kunselman, A. R., & Trussell, J. C. (2009). BioGlue and Dermabond save time, leak less, and are not mechanically inferior to two-layer and modified one-layer vasovasostomy. *Fertility and Sterility, 91*, 560.
73. Bernie, J. E., Ng, J., Bargman, V., Gardner, T., Cheng, L., & Sundaram, C. P. (2005). Evaluation of hydrogel tissue sealant in porcine laparoscopic partial-nephrectomy model. *Journal of Endourology, 19*, 1122.
74. Preul, M. C., Bichard, W. D., & Spetzler, R. F. (2003). Toward optimal tissue sealants for neurosurgery: Use of a novel hydrogel sealant in a canine durotomy repair model. *Neurosurgery, 53*, 1189.

75. Boogaarts, J. D., Grotenhuis, J. A., Bartels, R. H., & Beems, T. (2005). Use of a novel absorbable hydrogel for augmentation of dural repair: Results of a preliminary clinical study. *Neurosurgery, 57*(1 Suppl), 146.
76. Cosgrove, G. R., Delashaw, J. B., Grotenhuis, J. A., Tew, J. M., Van Loveren, H., Spetzler, R. F., et al. (2007). Safety and efficacy of a novel polyethylene glycol hydrogel sealant for watertight dural repair. *Journal of Neurosurgery, 106*, 52.
77. Graham, L. D., Glattauer, V., Huson, M. G., Maxwell, J. M., Knott, R. B., White, J. W., et al. (2005). Characterization of a protein-based adhesive elastomer secreted by the Australian frog *Notaden bennetti. Biomacromolecules, 6*, 3300.
78. Szomor, Z. L., Murrell, G. A. C., Appleyard, R. C., & Tyler, M. J. (2008). Meniscal repair with a new biological glue: An ex vivo study. *Tech Knee Surg, 7*, 261.
79. Ninan, L., Monahan, J., Stroshine, R. L., Wilker, J. J., & Shi, R. (2003). Adhesive strength of marine mussel extracts on porcine skin. *Biomaterials, 24*, 4091.
80. Ninan, L., Stroshine, R. L., Wilker, J. J., & Shi, R. (2007). Adhesive strength and curing rate of marine mussel protein extracts on porcine small intestinal submucosa. *Acta Biomaterialia, 3*, 687.
81. Strausberg, R. L., & Link, R. (1990). Protein-based medical adhesives. *Trends in Biotechnology, 8*, 53.
82. Burke, S. A., Ritter-Jones, M., & Lee, B. P. (2007). Thermal gelation and tissue adhesion of biomimetic hydrogels. *Biomedical Materials, 2*, 203.
83. Autumn, K., Liang, Y. A., Hsieh, S. T., Zesch, W., Chan, W. P., Kenny, T. W., et al. (2000). Adhesive force of a single gecko foot-hair. *Nature, 405*, 681.
84. Mahdavi, A., Ferreira, L., Sundback, C., Nichol, J. W., Chan, E. P., Carter, D. J. D., et al. (2008). A biodegradable and biocompatible gecko-inspired tissue adhesive. *Proceedings of the National academy of Sciences of the United States of America, 105*, 2307.
85. Wang, D. A., Varghese, S., Sharma, B., Strehin, I., Fermanian, S., Gorham, J., et al. (2007). Multifunctional chondroitin sulphate for cartilage tissue-biomaterial integration. *Nature Materials, 6*, 385.
86. Miki, D., Dastgheib, K., Kim, T., Pfister-Serres, A., Smeds, K. A., Inoue, M., et al. (2002). A photopolymerized sealant for corneal lacerations. *Cornea, 21*, 393.
87. Bhatia, S. K., Arthur, S. D., Chenault, H. K., & Kodokian, G. K. (2007). Interactions of polysaccharide-based tissue adhesives with clinically relevant fibroblast and macrophage cell lines. *Biotechnological Letters, 29*, 1645.
88. Bhatia, S. K., Arthur, S. D., Chenault, H. K., Figuly, G. D., & Kodokian, G. K. (2007). Polysaccharide-based tissue adhesives for sealing corneal incisions. *Current Eye Research, 32*, 1045.
89. Grinstaff, M. W. (2008). Dendritic macromers for hydrogel formation: Tailored materials for ophthalmic, orthopedic, and biotech applications. *Journal of Polymer Science Part A: Polymer Chemistry, 46*, 383.
90. Wathier, M., Jung, P. J., Carnahan, M. A., Kim, T., & Grinstaff, M. W. (2004). Dendritic macromers as in situ polymerizing biomaterials for securing cataract incisions. *Journal of the American Chemical Society, 126*, 12744.
91. Wathier, M., Johnson, C. S., Kim, T., & Grinstaff, M. W. (2006). Hydrogels formed by multiple peptide ligation reactions to fasten corneal transplants. *Bioconjugate Chemistry, 17*, 873.
92. Degoricija, L., Johnson, C. S., Wathier, M., Kim, T., & Grinstaff, M. W. (2007). Photo crosslinkable biodendrimers as ophthalmic adhesives for central lacerations and penetrating keratoplasties. *Investigative Ophthalmology & Visual Science, 48*, 2037.
93. Kang, P. C., Carnahan, M. A., Wathier, M., Grinstaff, M. W., & Kim, T. (2005). Novel tissue adhesives to secure laser in situ keratomileusis flaps. *Journal of Cataract and Refractive Surgery, 31*, 1208.
94. Degoricija, L., Bansal, P. N., Söntjens, S. H., Joshi, N. S., Takahashi, M., Snyder, B., et al. (2008). Hydrogels for osteochondral repair based on photocrosslinkable carbamate dendrimers. *Biomacromolecules, 9*, 2863.
95. Söntjens, S. H., Nettles, D. L., Carnahan, M. A., Setton, L. A., & Grinstaff, M. W. (2006). Biodendrimer-based hydrogel scaffolds for cartilage tissue repair. *Biomacromolecules, 7*, 310.

Chapter 7
Smart Drug Delivery Systems

7.1 Engineering Concepts

7.1.1 Energetic Transitions of Materials

In previous chapters, we identified the nature of the pharmacokinetic profile for a series of controlled-release systems. The zero-order release represented a simple, idealized, gradual release response, which allowed for a predicted dosage to be delivered over a predictable time regime. As we shifted our discussion to encapsulated and targeted systems, it became apparent that the zero-order release would be less relevant since the design strategy for these systems is to prevent interaction between the drug and physiological environment until the drug reaches the tissue target. Upon reaching the target, the system is either consumed or degraded in order to release the drug dosage form into the cellular environment. An important question that arises at this point in the discussion is

What facilitates the release of drug into the cellular environment?

In Chap. 5, we identified the targeting groups on the surface of self-emulsifying systems that contribute to their adhesion and consumption by cellular species through *receptor-mediated endocytosis* or *macropinocytosis*. In our previous discussion, we assumed that the vesicle or micelle was being either destabilized or degraded within the cell lysosomes to release the drug into the intracellular environment. This approach has some functional limitations since it consists of several factors that are dependent on cellular function and response. The analogy would be when you fly on a plane and arrive at a destination, one surefire way to know that you have arrived, aside from the landing, is that the doors open and people leave. Can you imagine an airline where the plane would have to erode completely, or worse crash, before you were permitted to leave? For this precise reason, it is often

E.P. Holowka, S.K. Bhatia, *Drug Delivery: Materials Design and Clinical Perspective*, DOI 10.1007/978-1-4939-1998-7_7

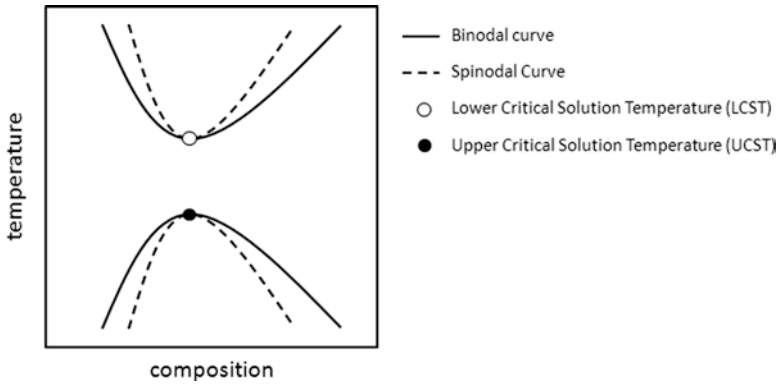

Fig. 7.1 Plot of the binodal and spinodal curves for a polymer solution

desirable to have what is known as a stimuli-responsive group incorporated within your system in order to facilitate this release upon reaching a target environment. A **stimuli-responsive** group is a functionality that undergoes an energetic transition in response to temperature, pH, magnetism, sound, or light [1]. Throughout this section we will discuss several stimuli and their corresponding energetic transitions, which we later use as a foundation for building a responsive drug delivery system.

7.1.1.1 Temperature

For the discussion of temperature-responsive material behavior, we begin by looking at the effects of a polymer in aqueous solution. The combination of a polymer with a solvent in a binary mixture involves a series of phases of varying degrees of stability primarily in relation to its composition and temperature. Within some compositional range, a material can reach a minimum energy equilibrium state, known as the *binodal curve*. The binodal curve describes a critical limit at which two phases can be either stable on one side or unstable on the other side, representing the limits of solvent interaction between two phases [2]. If we move within the area of the binodal curve, another limit will be reached; it describes the transition between metastable mixtures outside and absolute instability inside. This curve, known as the *spinodal curve*, describes the limit of absolute instability between phases. Within the spinodal curve, changes to composition result in complete decomposition of the system [3]; the mechanism for this decomposition into multiple phases is referred to as the *spinodal decomposition*. If these two behaviors are overlayed on the same plot, we can gain some important insight into the behavior of different polymers in solution (Fig. 7.1).

The area inside the spinodal curve represents a zone where it is impossible to create a single-phase system regardless of the process. Outside the spinodal curve, where the mixture is in a metastable state consisting of two phases, it is possible to create a single-phase system. The point at which the spinodal and binodal curves

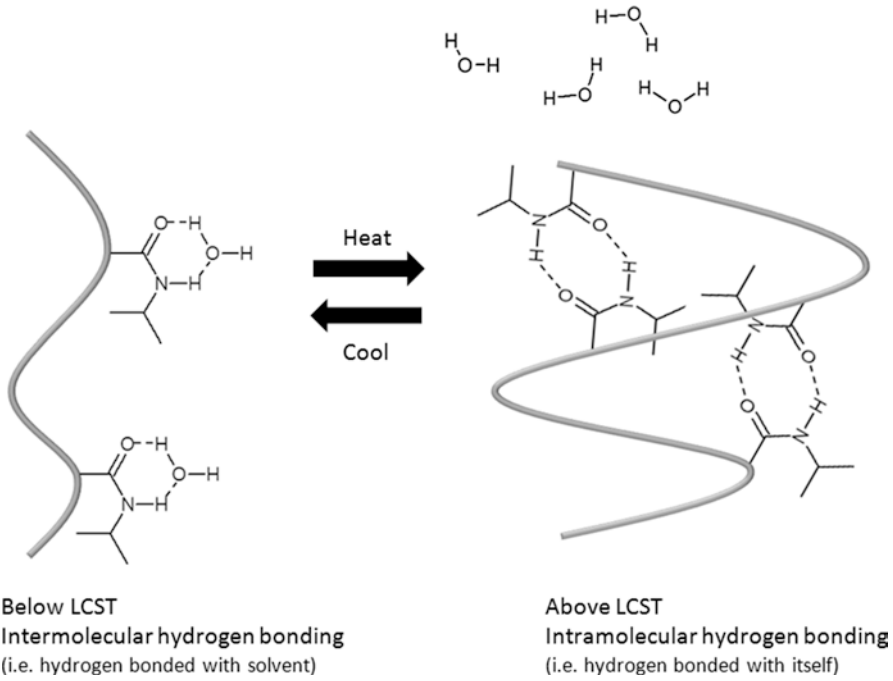

Fig. 7.2 Diagram of the intramolecular versus intermolecular hydrogen bonding through the LCST transition

meet is known as the *lower critical solution temperature* (LCST) [4]. The LCST represents a point below which the material becomes miscible, where the Gibbs free energy of mixing is negative (–ΔG) and above which it is completely immiscible, where the Gibbs free energy of mixing is positive (+ΔG) due to poor entropy of mixing [5]. The degree of polymerization and the polydispersity of the polymer chains can be a strong influence on the energetics of mixing and therefore can shift the values for the LCST. Typically, polymer chains with higher degrees of polymerization lead to higher values for the LCST. Similarly, polymers with increasing polydispersities will exhibit broader thermal transition ranges.

The entropically disfavored state can be explained through the presence of chemical functionalities capable of intermolecular hydrogen bonding with solvent molecules (i.e., water) and not intramolecular hydrogen bonding with themselves [6]. The energetic transition represents the energy above which this hydrogen bonding with polymer molecules is unfavorable and below which it is favorable. The perception of miscibility is simply the formation of hydrogen-bonded species between the solvent and the polymer functionality (Fig. 7.2).

For this reason, polymers that exhibit an LCST behavior can have their solubility tuned based on temperature change.

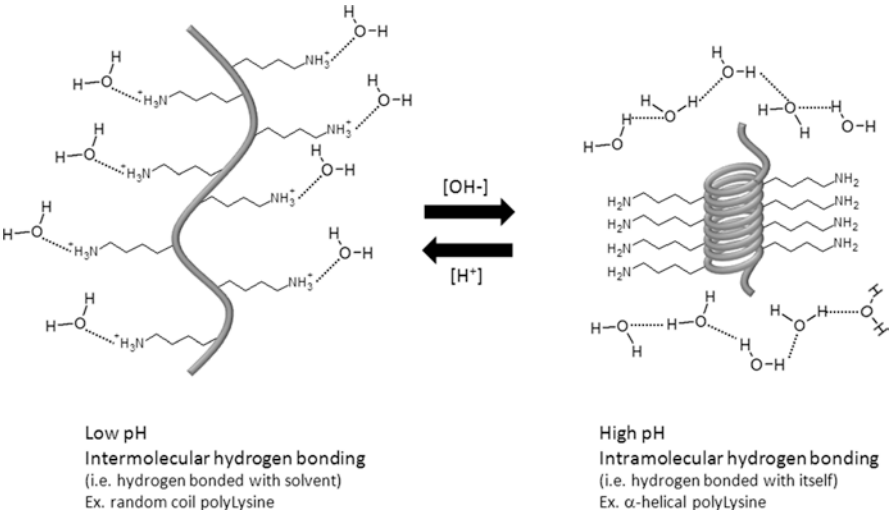

Fig. 7.3 Diagram of the intramolecular versus intermolecular hydrogen bonding through the protonation–deprotonation of the pendant groups on the polymer chain

7.1.1.2 pH

The sensitivity of a material system to pH typically involves an ionizable functionality within the polymer structure. These functionalities become ionized at a specific pH, where they acquire a ± charge [7]. In aqueous solvent, this ionization will result in the transition of the functional group from one of water insolubility to one of water solubility. These water-soluble polymer species are referred to as *polyelectrolytes*, due to the presence of electrostatic charges repeated throughout the structure.

Polymeric charged functionalities have a markedly different behavior than their uncharged counterparts in terms of their intermolecular effects on the surrounding environment and intramolecular effects within their own polymer molecules. We can segregate this behavior into two types of interactions: those between a *polyelectrolyte and a solvent* [8], and those between a *polyelectrolyte and a surface* [9]. In the case of the interaction between a polyelectrolyte and a solvent, similarly to the LCST case discussed previously, there is a point where the Gibbs free energy of mixing shifts from negative ($-\Delta G$), where it is soluble, to positive ($+\Delta G$), where it is insoluble, due to poor entropy of mixing caused by the transition from an intermolecular hydrogen-bonded species to an intramolecular hydrogen-bonded species. This effect is easily seen in the change in the secondary structure [10] of polypeptides or proteins that consist of lysine (Lys), glutamate (Glu), aspartate (Asp), and arginine (Arg). In these polypeptides, there is a transition from an α-helical to a random coil secondary structure as a result of deprotonation (i.e., Glu, Asp) or protonation (i.e., Lys, Arg), generating a negatively or positively charged polyelectrolyte of the respective amino acid residues (Fig. 7.3).

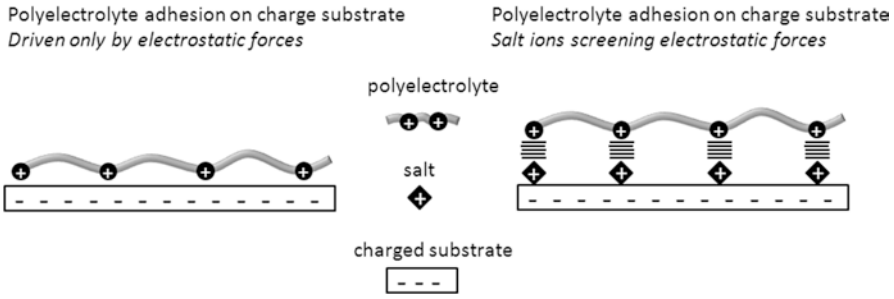

Fig. 7.4 Diagram of the basic polyelectrolyte interactions with a charged surface in the presence and absence of salt ions

Typical nonbiological polyelectrolytes exhibit a similar transition of solubility properties with changes to pH, however in a less ordered charge-neutral state. These polyelectrolytes condense to form an irregularly aggregated structure due to poor entropy of mixing [11]. Aligned intramolecular hydrogen-bonded species can be formed using physical changes such as pressure and temperature to stabilize order within the condensed phase.

If we look more closely at the intermolecular interactions between the polyelectrolyte and a surface, we can see several characteristic interactions. If presented with an oppositely charged surface, the polyelectrolyte has been proposed to interact in a number of different ways. If there is a long-range electrostatic interaction (i.e., adsorption), it would likely be due to the rearrangement of the polyelectrolyte chain to express charged functionalities at the surface [12]. This rearrangement would change based on the length and distribution of charges along the polymer chain, the charge density, the composition and distribution of charges along the polymer chain, the affinity of the polymer to the surface and the solvent, the pH, and the ionic strength of the solvent. For the purposes of our discussion in this section, we focus on *ionic strength*, *pH*, and *charge density*.

The primary driving force for the adsorption of the polyelectrolyte chain on a charged surface is the entropic gain from the release of counterions from that surface [13]. We know that the introduction of salts will screen the electrostatic forces between the polyelectrolyte and the surface as well as reduce both the intermolecular and intramolecular electrostatic repulsions. In the present case of interactions between polyelectrolytes and charged surfaces, there can also be a nonelectrostatic affinity under certain conditions [14]. When the adsorption of polyelectrolyte on a charged surface is driven by only electrostatic forces, any increase in the ionic strength through the presence of salts would decrease the electrostatic affinity of the polyelectrolyte to the charged surface since the salt ions would more favorably displace the polyelectrolyte in what is referred to as *screening-reduced adsorption*. If the nonelectrostatic affinity is high enough, the adsorption increases to an upper limit (Fig. 7.4).

The polyelectrolyte charge density is a determining factor for the strength and thickness of the polyelectrolyte–surface layer. This interaction can vary in two

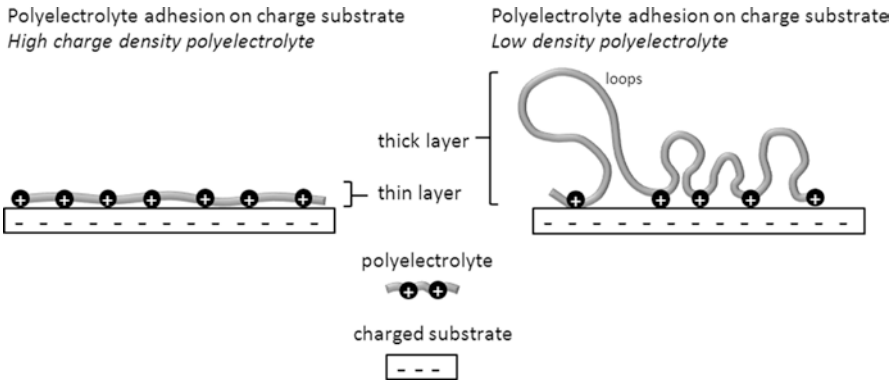

Fig. 7.5 Diagram of the basic interactions between a charged surface and a polyelectrolyte with a high or low charge density

notable cases when under low-ionic-strength solutions [15]. In the first case, a polyelectrolyte with a high charge density will result in a flat adsorbed layer of the charged surface. In the second case, a polyelectrolyte with a low charge density will result in a thicker adsorbed layer. This somewhat counterintuitive behavior is tied to the charge density, or space between charges on the polymer chain. In the case where the charge density is low, the polymer chain has less interchain electrostatic repulsion, allowing for a more flexible chain. Since the polyelectrolytes trend toward the full passivation of the surface charge, uncharged sections of polymer chain will begin to loop away from the surface, creating a thick polyelectrolyte layer on the surface [16] (Fig. 7.5).

From our discussion it becomes clear that the behavior of pH-dependent stimuli-responsive materials is that of a collapse of intramolecular interactions or a disassociation from a surface in response to a change in pH or charge. We can mathematically determine the effects of the charge distribution on the distance that the electrostatic effects extend into solution, known as the *Debye–Hückel length (DL)* [17]. When the DL reaches a critical length, intermolecular electrostatic interactions either cease via dissociation or initiate via adsorption. We can begin determining this approximation by looking at the *Poisson–Boltzman equation* [18], which approximates the effects of solvents with different ionic strengths on charged species such as polyelectrolytes, proteins, and DNA:

$$\vec{\nabla}\left[-\left(\vec{r}\right)\vec{\nabla}\psi\left(\vec{r}\right)\right]=-4\pi\rho^{f}\left(\vec{r}\right)-4\pi\sum_{i}c_{i}^{\infty}z_{i}q\lambda\left(\vec{r}\right)e^{\left[\frac{z_{i}q\Psi\left(\vec{r}\right)}{k_{B}T}\right]}, \tag{7.1}$$

where $\vec{\nabla}$ is the divergence operator (or measure of a vector field's source), $-\left(\vec{r}\right)$ is the position-dependent dielectric constant, $\vec{\nabla}\Psi\left(\vec{r}\right)$ is the gradient of electrostatic potential, $\rho^{f}\left(\vec{r}\right)$ is the charge density embedded in the molecule, $c_i\infty$ is the concentration of ion i at an infinite distance from the molecule, z_i is the charge number, q is the proton charge, $\lambda\left(\vec{r}\right)$ is a factor for the location-dependent accessibility to

ions in solution, T is temperature, and k_B is Boltzmann's constant. Another way to look at it is that $\rho^f(\vec{r})$ is the charge distribution due to the macromolecule and $\sum_i c_i^{\infty} z_i q \lambda(\vec{r}) e^{\left[\frac{z_i q \Psi(\vec{r})}{k_B T}\right]}$ is the implicit charge distribution due to counterions. We can simplify the *Poisson–Boltzman equation* to the following form [19]:

$$\nabla\left[\varepsilon(\vec{r})\nabla\psi(\vec{r})\right] - K'^2 \sinh\left\{\psi(\vec{r})\right\} = -4\pi\rho^f(\vec{r}), \tag{7.2}$$

where K' is related to the Debye–Hückel length (K), which can be written as the following:

$$K^2 = \frac{K'^2}{\varepsilon} = \frac{8\pi N_A e^2 I}{1{,}000\varepsilon kT}, \tag{7.3}$$

where e is the electronic charge, I is the ionic strength of the solution, and N_A is Avogadro's number. Here we have the term e approximating the electric charge in terms of its charge density for a polyelectrolyte. We now know that the electric charge and the ionic strength of solution describe the critical length associated with electrostatic interactions.

The stimuli-responsive behavior of pH-sensitive materials can then be described as those having a change in the electronic charge density of the material, such that they move either within or outside the DL. In Sect. 7.2, we discuss design parameters such as chemical functionalities, composition, and valency as a means of adjusting the pH where the stimuli-responsive behavior occurs.

7.1.1.3 Magnetism

In the first two cases of temperature and pH, the stimuli-responsive behavior is dependent on the local physiological environment for which the drug delivery system is targeted. Instead of having the stimuli-responsive behavior depending on a localized environment, we can also direct the stimuli toward the targeted area of delivery. If there is fine control over sources capable of inducing a directed movement, such as with a magnetic field, or by activation when reaching a specific region, as with light and sound, then we can adjust the chemical functionality to allow for a relevant response. In the case of magnetic materials, the response is an attractive or repulsive force relative to the field direction. The material selection will dictate whether you have a freely rotating magnetic dipole or a fixed dipole [20]. Both the material chemical functionality [21] and the viscosity [22] properties of the particle within a physiological system are critical in determining the extent of the response to a magnetic field (Fig. 7.6).

The basis for the magnetic field–induced separation of particles during flow involves the magnetic force applied to the drug delivery system. We can see that

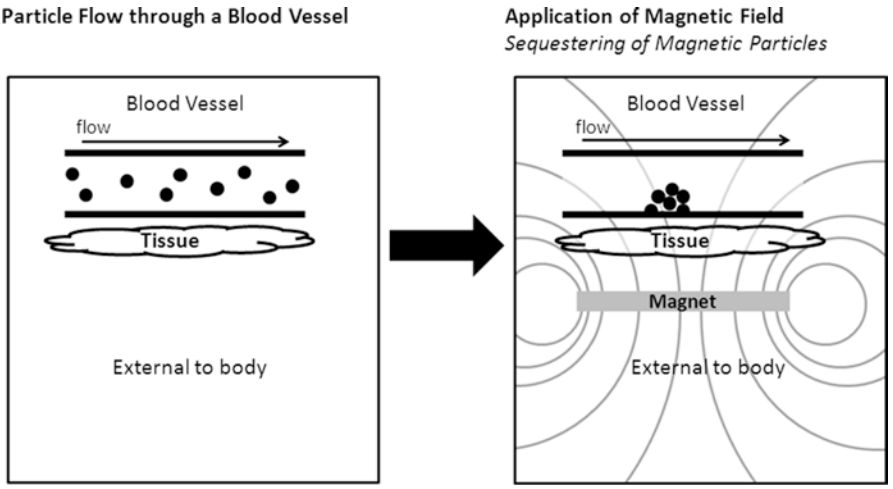

Fig. 7.6 Diagram of the basic forces involved in the sequestration of magnetic nanoparticles in the bloodstream

the magnetic force (F_m) [23] is a function of the magnetostatic field energy density (1/2 BH):

$$F_m = V_m \quad \chi \nabla \left(\frac{1}{2} BH \right), \tag{7.4}$$

where V_m is the magnetic potential, $\Delta\chi$ is the change in the magnetic susceptibility, B is the vector magnetic flux, and H is the vector magnetic field. The gradient felt from the magnetic field causes the immobilization of magnetic particles. We recall from Chap. 5 that particles under flow experience a drag force (F_d) associated with their motion in a tube. The magnetic force must overcome the drag force felt by the particles in order to immobilize the particle and be in a target zone for drug release [24]:

$$F_d = 6\pi\eta R_m \Delta v, \tag{7.5}$$

where η is the viscosity, R_m is the radius of the particle, and Δv is the velocity of the particle relative to its solvent (i.e., blood), which is also referred to as its *carrier fluid*. If we combine Eqs. (7.4) and (7.5), we can see the velocity of the separation of magnetic particles from their carrier fluid relative to the applied magnetic field and the intrinsic properties of the particle [24]:

$$v = \frac{\xi}{\mu_0} \nabla B^2 \quad \text{where} \quad \xi = \frac{R_m^2 \chi}{9\eta}, \tag{7.6}$$

where ξ is the *magnetophoretic* ability (i.e., ability to manipulate) of the magnetic particle, and μ_0 is the permeability of free space. Therefore, if a magnetic particle

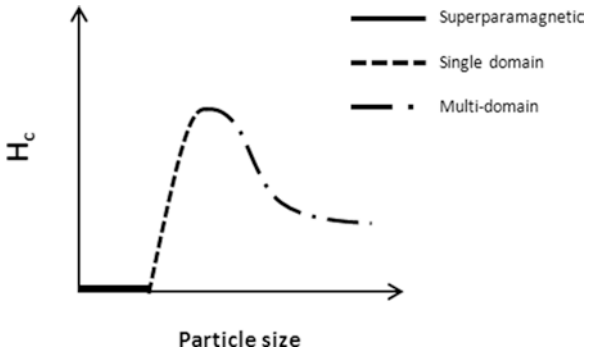

Fig. 7.7 Plot of the responses of superparamagnetic, single-domain, and multidomain magnetic particles under a magnetic field

has a high Δv, then it would indicate that there is rapid separation from the carrier fluid with exposure to a magnetic field. We can also see that the magnetophoretic ability is directly related to the radius of the magnetic particle by a squared term. This indicates that the radius is a strong indication of a particle's ability to be manipulated by a magnetic field, where larger particles appear to separate rapidly from their carrier fluid.

It is important to keep in mind that this is only a portion of a larger discussion. Magnetic particles are typically divided based on size into *single-domain* and *multidomain* particles [25]. The single-domain particles fall in a small size regime, where decreases in size correspond to an increase in *coercivity* (i.e., ability of a ferromagnetic material to be affected by a magnetic field) to a peak level before dropping to zero. The zero point identifies a *superparamagnetic* material [26], which is one whose magnetic moment is induced in the direction of the applied magnetic field and in the absence of a magnetic field returns to an unaligned state (Fig. 7.7).

There is no hysteresis effect in superparamagnetic materials; therefore, there is no compounded effect on the particle due to repeatedly applied magnetic fields. These superparamagnetic materials associated with the drug delivery systems we discussed involve the immobilization of magnetic particle species. As the size of the particle increases, the energy of formation begins to favor the segregation of magnetic moments into domains. The multidomain particles typically consist of domain walls, which exist if their energy of formation is less than a single-domain site [27].

The magnetic field can also be used as a means of increasing the local temperature through the use of a high-frequency, high-amplitude magnetic field for multidomain ferromagnetic particles. In addition to particle size, this heating effect or energy dissipation (P_{MDP}) is correlated with the domain properties (ξ, V_{m}, χ) of the magnetic particle [27]:

$$P_{\mathrm{MDP}} = \frac{\left(\mu_0 \chi_{\mathrm{o}} H^2 \omega^2 \tau\right)}{2\tau\left(1+\omega^2\tau^2\right)} \quad \text{where} \quad \frac{1}{\tau} = \frac{1}{\tau_{\mathrm{B}}} + \frac{1}{\tau_{\mathrm{N}}}, \tag{7.7}$$

where τ is the relaxation time, τ_N is the Néel relaxation, τ_B is the Brownian relaxation, ω is the magnetic field frequency with $\omega = 2\pi f$, whereby f is the cyclic frequency, and χ_o is the equilibrium magnetic susceptibility of the particle. We can also simplify this relationship by solving for the magnetic susceptibility in terms of the domain magnetization (M_d) of the particle to show the following [27]:

$$\chi_o = \frac{\phi M_d}{H}\left(\coth\xi - \frac{1}{\xi}\right) \quad \text{where} \quad \xi = \frac{\mu_o M_d H V_m}{k_B T}, \tag{7.8}$$

where ϕ is the volume fraction of solids. The heating phenomenon in magnetic particles is due to the heat losses during the hysteresis cycles referred to as *magnetic hyperthermia* [28]. If each magnetic particle consists of multiple subdomains (represented as a triangle within the square) with associated directionality (represented by the arrows), then as the particle is exposed to a magnetic field, the subdomains in alignment with the field will expand while the other domains contract. The effect is not reversible, which leads to magnetization curves that do not overlap with increasing or decreasing the magnitude of the magnetic field. The resulting heat generated by the magnetic particle is attributed to this hysteresis effect [28]. We discuss this method in more detail in Sect. 7.2, where we couple magnetic hypothermia to thermoresponsive behavior to generate a tandem stimuli-responsive system, which can be used to alter the pore structure of hydrogel systems (Fig. 7.8).

7.1.1.4 Light

In magnetic systems the particle species is influenced by the direction of the magnetic field, whereas in light-responsive systems, the material species is influenced by the presence of a specific energy wavelength of light. If visible, ultraviolet (UV), or infrared (IR) light is directed at a desired target region, the chemical structure of the drug delivery system destabilizes or changes conformation in response to the absorbed energy input. For the purposes of our discussion, we focus on the photoisomerization of labile double bonds [29] and the photodegradation of labile linkages [30].

The process of photoisomerization functions by the excitation of a molecule to a higher-energy state stimulated by the introduction of light energy. This is commonly seen in photoexcitable double-bond species, where the introduction of light energy causes the breaking of a double bond, which allows for free bond rotation. This free bond rotation occurs until the double bond reforms into either a *cis* or *trans* species [31]. As the chemical species returns to a lower-energy transition state, it has some propensity to form either *cis* species (A) or *trans* species (B), which differ depending on the chemical functionality of the photoisomerizable species. This phenomenon has a number of potential applications [32]. For our discussion of drug delivery systems, we focus on the stabilization or destabilization of packed species such as bilayers or liquid crystals [29], which we discuss in detail in Sect. 7.2 (Fig. 7.9).

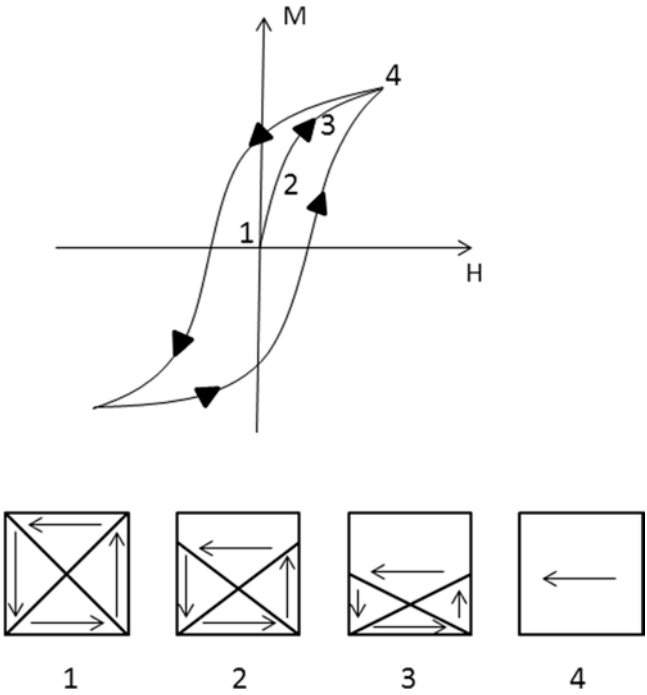

Fig. 7.8 Plot of the hysteresis effect of a multidomain magnetic particle under an alternating magnetic field (AMD)

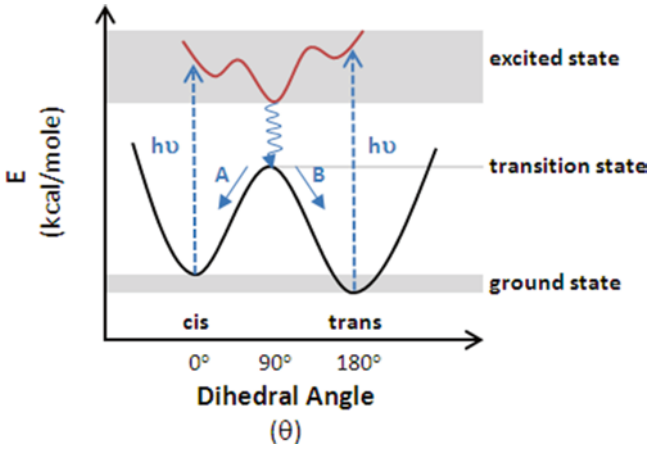

Fig. 7.9 Plot of the excitation and emission of energy of a photoresponsive molecule

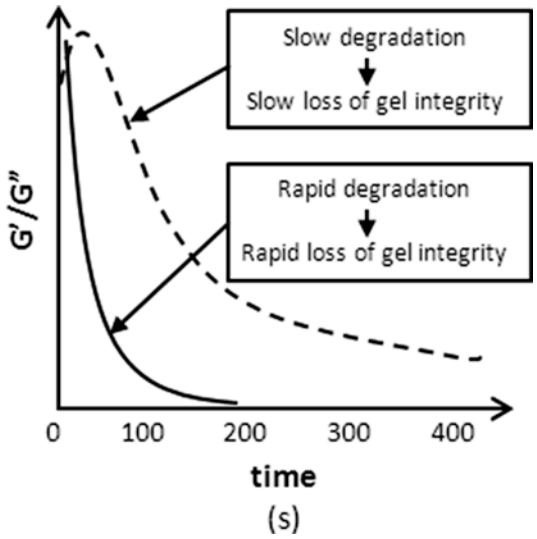

Fig. 7.10 Plot of the loss of modulus with the degradation of a photodegradable network over time

The photodegradation of labile linker species follows a number of the principles that were discussed in Chaps. 2 and 3 with regard to biodegradation and hydrolysis (i.e., chemical, enzymatic). The relevant labile linkers should have degradation rate kinetics within a relevant physiological time window. We can determine the degradation kinetics (k_{app}) through the following relationship [33]:

$$k_{app} = \frac{\phi \varepsilon \lambda I_0 \left(2.303 \times 10^{-6}\right)}{N_A hc}, \tag{7.9}$$

where ϕ is the quantum yield, ε is the molar absorptivity, I_0 is the light intensity, λ is the wavelength, N_A is Avogadro's number, h is Planck's constant, and c is the speed of light. The degradation kinetics are critical to the design elements of the material. Typically, researchers associate the degradation rates to the decay or collapse of a physical species in a type of tandem effect [34]. For example, a gel may have a reduction in its elasticity and consequently an increase in its pore size at a rate proportional to the degradation of a labile linker species, which was tasked with holding the native gel structure together. If we begin to combine concepts from earlier chapters, we can see that the collapse of a linker-supported matrix will result in the release of its chemical constituents provided they are within a relevant size regime [35]. This release would follow a first-order pharmacokinetic profile or burst release. We discuss this principle in more detail in Sect. 7.2, where we focus on the structure property design elements that can be exploited using a photodegradable linker group as a support (Fig. 7.10).

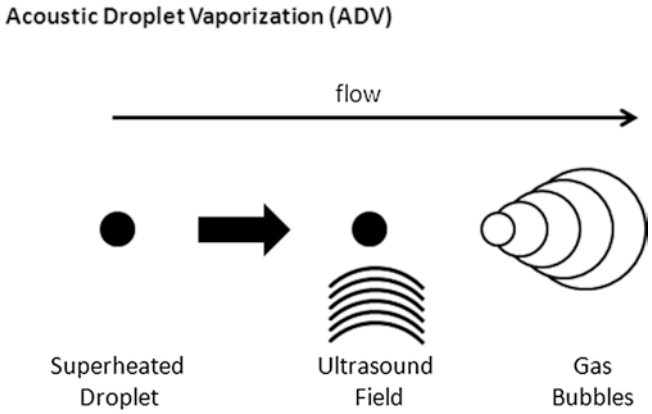

Fig. 7.11 Diagram of the acoustic input and response of a drug solution droplet to an ultrasonic device

7.1.1.5 Sound

The use of ultrasound technology can induce a self-assembled species to act as a nucleation site for pore formation in a membrane barrier to enhance delivery [36]. The induction of pore formation can occur through a process known as *acoustic droplet vaporization* (ADV) [37], which pushes a superheated droplet through a phase transition, yielding gas microbubbles. These gas microbubbles lead to membrane pore formation by a process known as *sonoporation* [38], where the acoustic cavitation creates spaces in the membrane from the displaced volume of the gas. In order to stabilize the newly generated phase interface between gas and liquid, surfactants are introduced to form what are known as *phase-shift nanoemulsions* (PSNEs) [39] (Fig. 7.11).

The ultrasonic power entering the droplet system can be determined by measuring the temperature at several points in time during the process and extrapolating the relationship to a zero point through the following relationship [40]:

$$\text{power} = \frac{dTC_{\text{p}}M}{dt}, \tag{7.10}$$

where T is the temperature, C_{p} is the specific heat, M is the mass of the solvent, and t is time. The surfactant materials are added as a means of effectively stabilizing the microbubbles in physiological media. These stabilized microbubbles, or encapsulated microbubbles (EMBs), have high compliance relative to the surrounding solution, which allows for a wide range of microbubble sizes (1–5 μm). This is in part due to the balance of the co-oscillation of a liquid layer on the outer surface of the microbubble and the elasticity of the interface of the microbubble referred to as the *shell elasticity*. We can form a relationship among the acceleration forces of the

co-oscillation liquid and the pressure contributions from the gas, surfactant-stabilized shell interface, and drive pressure [41]:

$$\rho\left(R\ddot{R}+\frac{3}{2}R^2\right)=-B\left(R,\dot{R}\right)-p_{\mathrm{i}}\left(t\right), \tag{7.11}$$

where ρ is the solution density, R is the instantaneous microbubble radius, B is the microbubble pressure generated by the gas and shell, $\dot{R}$ is the velocity of the microbubble wall, $\ddot{R}$ is the acceleration of the microbubble wall, and p_{i} is the incident drive pressure. We can rewrite this expression in terms of the bubble pressure in the form of the following relationship [41]:

$$B\left(R,\dot{R}\right)=\left(p_0+\frac{2\sigma}{R_0}\right)\left(\frac{R_0}{R}\right)^{3\kappa}-S\left(R_0,R\right)+p_0+\frac{2\sigma}{R}+\mu\frac{\dot{R}}{R}, \tag{7.12}$$

where p_0 is the atmospheric pressure, σ is the surface tension, R_0 is the equilibrium microbubble radius, and κ is the polytropic exponent. If we look more carefully at Eq. (7.9), we can see that $\left(p_0+\frac{2\sigma}{R_0}\right)\left(\frac{R_0}{R}\right)^{3\kappa}$ represents the gas pressure, $S(R_0,R)$ represents the pressure contribution from the encapsulating shell, p_0 represents the ambient hydrostatic pressure, $\frac{2\sigma}{R}$ represents the surface tension of the gas–liquid interface, and $\mu\frac{\dot{R}}{R}$ represents the damping effects. From this relationship it becomes clear that the microbubble radius and pressure can be determined through acoustic frequency inputs and surfactant materials to stabilize the gas–liquid interface. We discuss the surfactants in greater detail in Sect. 7.2, where we focus on both the stabilization of gas microbubbles as well as their interaction with physiological tissue.

7.2 Material Design

7.2.1 Temperature, pH, Magnetism, Sound, and Light

We can now begin to look at the chemical functionalities or domains that are necessary to exhibit the stimuli-responsive behavior discussed in Sect. 7.1. These triggering stimuli in some cases are within the proximity of the internal physiological environment of the drug delivery system, and in other cases they are imposed in an ex vivo environment directed at an internal location of targeted interest [1]. We can also imagine a drug delivery system that is designed with multiple stimuli-responsive systems operating in tandem [42]. For example, a magnetic system may induce a temperature change in a thermoresponsive system, leading to drug release. In the following subsections, we discuss the components of each stimuli-responsive system described in Sect. 7.1.

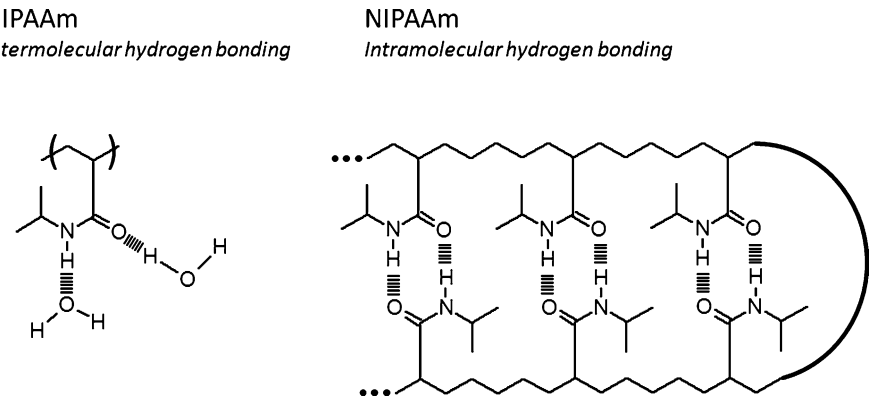

Fig. 7.12 Diagram of the intramolecular versus intermolecular hydrogen bonding of poly(NIPAAm)

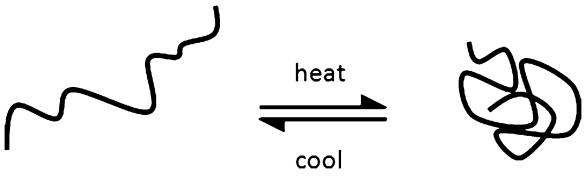

Fig. 7.13 Diagram of the response of thermoresponsive polymer chains to changes in heat through the LCST thermal transition

7.2.1.1 Thermoresponsive Systems

As we discussed earlier in this chapter, the thermoresponsive nature of a chemical functionality is predicated on the temperature change through the spinodal decomposition phase where the Gibbs free energy of mixing is positive ($+\Delta G$) due to poor entropy of mixing. In these systems the intramolecular hydrogen bonding is favored over hydrogen bonding with the water in solution upon heating. A common polymer system that exhibits these properties consists of the monomer *N*-isopropylacrylamide (NIPAAm) [43] (Fig. 7.12).

Polymers consisting of NIPAAm repeat units exhibit an LCST at 37 °C, meaning that when heating through the transition temperature, the polymer chain changes from an expanded coil to a compact globule conformation (Fig. 7.13).

The question that we can begin to ask ourselves in terms of the design strategy is

How can this physical behavior aid in drug delivery?

We will discuss two basic design strategies with thermoresponsive systems that involve (1) the destabilization of a self-assembled structure [44] and (2) the swelling or contraction [45] of a hydrogel system.

We have discussed that the self-assembly of vesicle and micellar species is driven by several factors, which include shape, charge, chemical functionality, and chemical composition. These factors allow for the assembly of species with specific size,

shape, bilayer thickness, stability, and delivery efficiency. A rapid change in any of these factors would destabilize the self-assembled structure [46]. For example, imagine if the shape of a bilayer-forming lipid with positive bilayer curvature ($C^{\circ} > 0$) were to spontaneously change to one with a negative curvature ($C^{\circ} < 0$). This change would place an immediate strain on the bending elasticity of the bilayer membrane, which would need to be dissipated in order for the self-assembled species to remain stable. If the dissipation is not possible, then the integrity of the membrane will be disrupted and the structure will be compromised [46]. Let's look more closely at the chemical functionality and composition aspects of self-assembly. For a vesicle species comprised of amphiphilic copolymers, there are a few primary areas of focus in terms of their design. The chemical functionality will tell us how hydrophobic or hydrophilic the respective chains are as well as whether a charged species is present. The functionality will also tell us the rigidity of the system [47]. We know from our previous discussion that the more rigid systems typically require higher molecular weights in order to reach the entanglement regime. This is in part due to the limitations in the modes of bending due to bond rotations of rigid species (i.e., PET), where it requires a higher number of polymer repeats before the chains begin to bend at an appreciable angle, as opposed to those of flexible systems (i.e., PEG), which bend readily after only a few polymer repeats. The chemical composition will tell us the ratio of the hydrophilic and hydrophobic components as well as the degree of polymerization of the collapsed hydrophobic domain. The closer (or greater than) the molecular weight is to the entanglement molecular weight, the more stable the assembled species [48].

Thermoresponsive polymers, such as NIPAAm, offer a unique variation to these relationships. On the chemical functionality side, the NIPAAm allows a localized change in the hydrophobicity–hydrophilicity of the collapsed self-assembled structure. If the driving force for self-assembly is the collapse from the aggregation of hydrophobic domains, then this domain can be changed to one of hydrophilic functionality with a change in temperature. The change in the chemical functionality destabilizes an aqueous self-assembled species predicated on hydrophobic collapse [49] (Fig. 7.14).

This destabilization is also largely dependent on the composition of the polymer chain. The number of NIPAAm repeat groups within the hydrophobic domain provides a gauge of the degree to which the hydrophobicity has changed through the temperature transition. One way the cosmetics industry uses to gauge the changes made to the compositional ratio of hydrophobic and hydrophilic domains in amphiphilic species is the hydrophilic–lipophilic balance (HLB) [50]. The HLB is an approximate estimate of the relative hydrophobicity of the amphiphiles, which vary in their self-assembly behavior relative to compositional analogs within the same functional domains. For example, if a copolymer of methyl methacrylate and methacrylic acid has a composition that gives an HLB of 15, then the same composition for a copolymer of methyl methacrylate and ethylene glycol may give a significantly different HLB value. The functional domains of the methyl methacrylate and methacrylic acid are easily comparable to one another with respect to the HLB and

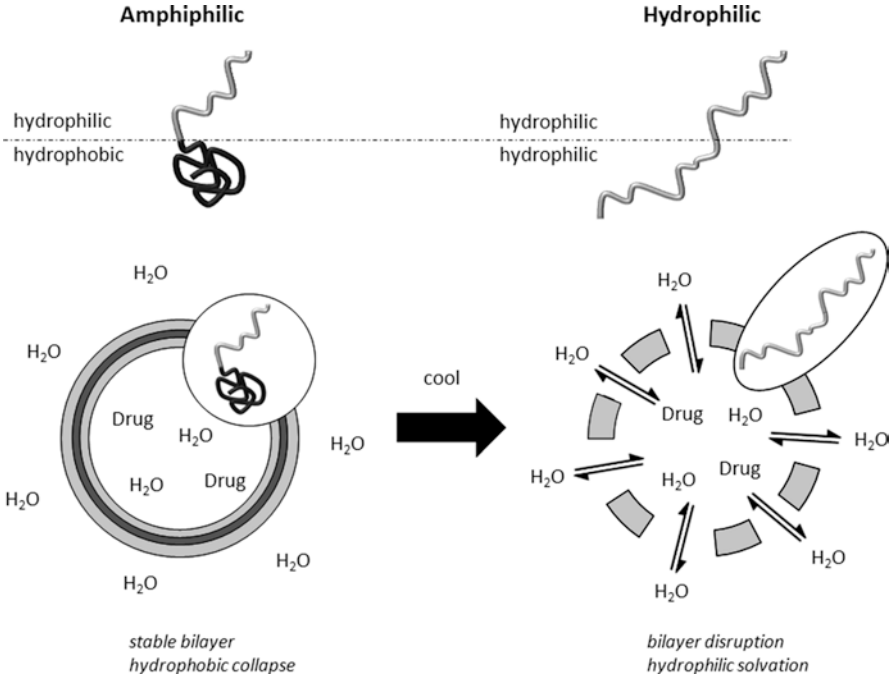

Fig. 7.14 Diagram of the effect of cooling on thermoresponsive vesicle assemblies

self-assembly, while the functional domains of methyl methacrylate and ethylene glycol are intercomparable within their HLB and self-assembly behaviors [50]:

$$\mathrm{HLB} = 7 + m\mathrm{H}h - n\mathrm{H}\ell, \tag{7.13}$$

where m is the degree of polymerization of the hydrophilic domain, Hh is the value of the hydrophilic functional groups, n is the degree of polymerization of the hydrophobic domain, and Hl is the value of the hydrophobic functional groups. If we look at aqueous drug cargo encapsulated within a vesicle species, the pharmacokinetic profile may have indications of a shift from zero order to first order upon stimulation through the LCST transition (Fig. 7.15).

Keep in mind that the release profile and strategy depend on the relative hydrophilicity or hydrophobicity of the drug molecule as well. The polarity of the drug molecule dictates whether it sequesters within the hydrophobic domains of vesicles or micellar cores, or within the internal vesicle aqueous environment, or sequesters on hydrophilic surfaces on the faces of vesicles and micelles. For each system, the solvation of the hydrophobic domain drives the destabilization of the self-assembled region surrounding the drug, facilitating its release into solution.

The controlled release of drug molecules from a hydrogel system based on swelling was the central discussion of Chap. 6. Much of this effect was tied to a controlled rate of swelling due to crosslink density and polymer chain flexibility imparted by

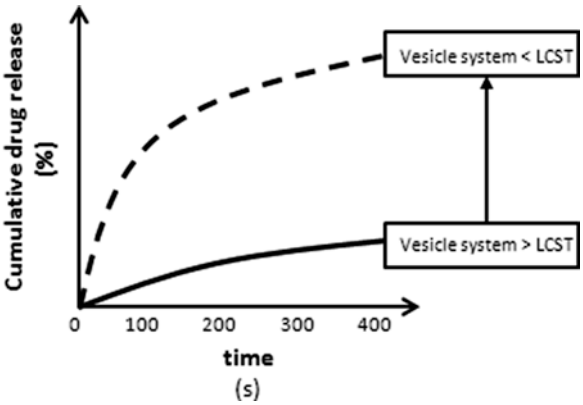

Fig. 7.15 Plot of the differences in drug release between stable vesicle systems and thermally (i.e., LCST) destabilized vesicle systems

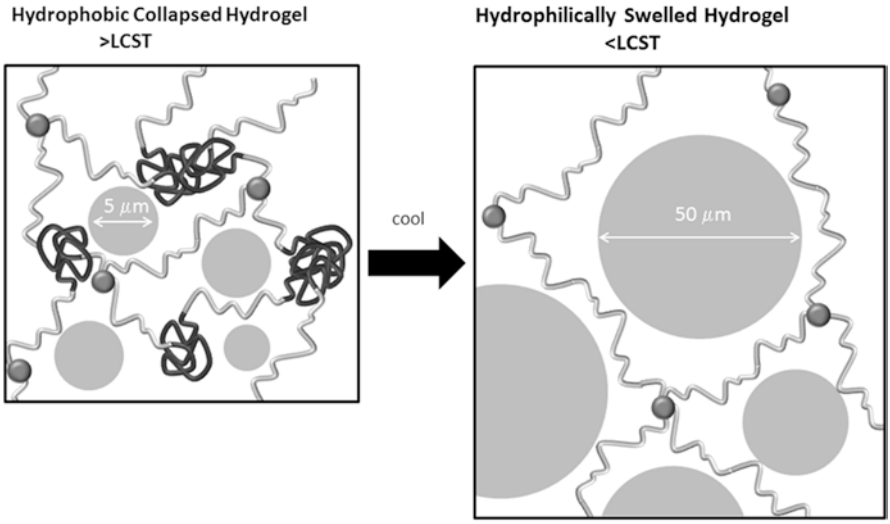

Fig. 7.16 Diagram of the effect of cooling on thermoresponsive hydrogel assemblies

chemical functionality, which corresponded to changes in the porosity of the system [51]. By adjusting the porosity, we see that the rate kinetics of drug release change. If we now incorporate thermoresponsive groups within the hydrogel structure, these changes in porosity can be induced by stimuli instead of requiring a system redesign. The strategy involved in this approach is one where all crosslink points or a subdomain of the crosslink points are driven by the hydrophobic collapse of thermoresponsive groups such as NIPAAm within a polymer species. When the temperature drops below the LCST, the crosslink point is lost due to preferential hydrogen bonding to surrounding water molecules and the gel swells. As with the previously discussed hydrogel systems, the crosslink density can be tuned to allow for a desired pore size both before and after introduction of the temperature stimulus (Fig. 7.16).

The adjustment of pore size can be estimated by starting with the number of covalent crosslinking groups and assuming the polymer above the LCST is in a collapsed state and will therefore contribute to the net number of crosslink points in the hydrogel [52]. Upon transitioning the system to temperatures below the LCST, the polymer is now in a freely extended chain conformation and the number of crosslink points is equal to the covalent crosslinks within the network. The pharmacokinetics of drug release from this matrix hydrogel system would be similar to that of a vesicle discussed earlier in this section, where a decrease in temperature would increase the porosity of the system and allow for a transition from a zero-order release system to one of first-order release kinetics [53].

In addition to NIPAAm, there are several other widely studied thermoresponsive functionalities that can be incorporated within the polymer domain in order to stimulate porosity or swelling of a system. Each system will have a different LCST or in some cases a tunable LCST [54]. Appropriate selection of the thermoreponsive functionality for the application region is critical to elicit the desired behavior. It is also important to keep in mind that the selection of the responsive functionality should reflect the rationalization that the system should be at the very least bioinert in order to be a candidate for a drug delivery system (Table 7.1).

7.2.1.2 pH-Responsive Systems

The responsiveness of a molecule to pH presents an intriguing target for stimulated drug delivery. When a cell proceeds to internalize an encapsulated drug species by receptor-mediated endocytosis, it will enter the lysosome at some point within the process. The pH typically found within the lysosome of cells is 4.5–5 [55], which is exclusively different from other intracellular vesicle species. Therefore, the pH will trigger a collapse or dissociation of the self-assembled species, resulting in the release of the encapsulant. Based on our discussion in Chap. 5, if the species undergoes endocytosis, we would expect it to (**I**) bind to the cell surface, induce a clathrin-mediated membrane concavity (**II & III**), which is internalized in the form of a lysosome, at which point (**IV**) the internalized self-assembled structure is destabilized by the pH to release its drug cargo and (**V**) the membrane material is recycled to the cell surface [56] (Fig. 7.17).

Similar to rational design using thermoresponsive components, there are a number of approaches that can be taken to effectively exploit this phenomenon. For the purposes of our discussion, we focus on two systems: (1) the destabilization of the hydrophobic domain [57], and (2) the swelling of a gel particle system [58].

In Chap. 5, we discussed that the role of the hydrophobic domain in the self-assembly of vesicle and micellar systems was to minimize the interfacial free energy between incompatible phases (i.e., hydrophobe and water). The hydrophobe could be tuned by increasing the molecular weight into the entanglement regime, which more effectively stabilizes both the hydrophobic domain and the self-assembled species, as evidenced by a decrease in the CMC. If we begin to change the composition of the hydrophobic domain by introducing water-soluble functionalities, it will begin to destabilize the condensed, self-assembled structure [57] (Fig. 7.18).

Table 7.1 Commonly used thermoresponsive chemical functionalities for drug delivery

Polymer	Structure	LCST (°C)	Biocompatible or bioinert
Poly(*N*-isopropylacrylamide) pNIPAAm	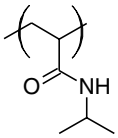	37	Bioinert
Poly(hydroxypropylcellulose) pHPC	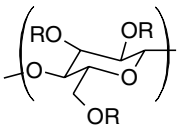	45	Biocompatible
Poly(vinylcaprolactam) pVCL	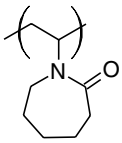	31	Biocompatible
Poly(methyl vinyl ether) pMVE		37	Bioinert
Poly(*N*-vinyl propylacetamide) pVPA	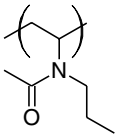	40	Bioinert
Poly(oligoethylene glycol methacrylates)	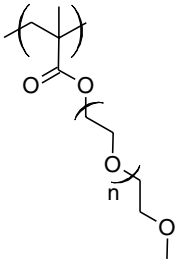		Bioinert
pMEMA		23	
$pMEO_2MA$		26	
$pMEO_3MA$		52	
$pOEGMA_{300}$		64	
$pOEGMA_{475}$		90	
Polyethylene glycol (PEG)	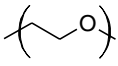	85	Bioinert

At some point within the compositional ratios, the CMC will increase to a point where the self-assembled system dissociates. This dissociation or dissolution corresponds to the release of the encapsulated drug species with a first-order pharmacokinetic profile [57]. In the case of the reduced pH, there would be a rapid breakdown of the vesicle bilayer in the lysosome of the cell, which corresponds to the first-order burst release kinetics seen at early time points within the drug release profile.

What remains interesting is that, consistent with thermoresponsive systems, there is a nearly discrete release behavior relative to the exposure to stimuli, where the

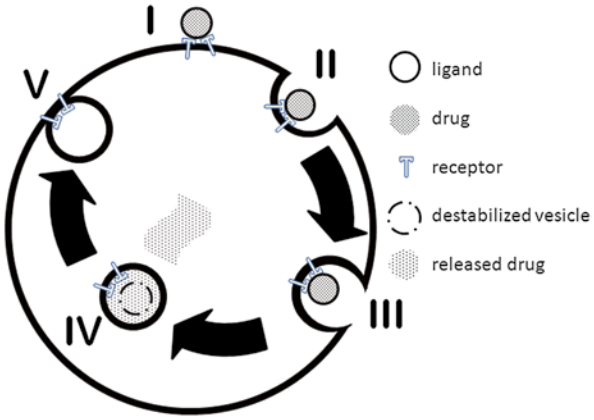

Fig. 7.17 Diagram of degradation of pH-responsive systems within the lysosome of a cell during RME

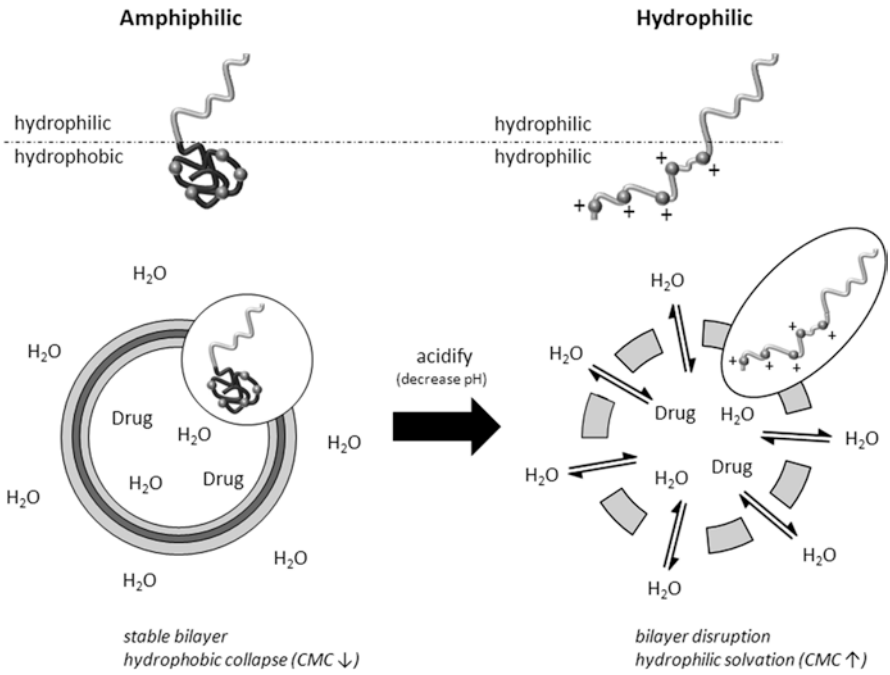

Fig. 7.18 Diagram of the effect of acidification on pH-responsive vesicle assemblies

destabilization leads to an immediate release of drug encapsulant. This implies that interim pH values or temperatures (in the case of thermoresponsive systems) retain the encapsulated cargo within the self-assembled structure [59]. This provides a safeguard for exposure to nonideal dissociation conditions for drug release. The drug contents will only be released when the pH or temperature falls within the

Table 7.2 Measure of pH in different physiological regions of the human body

Physiological region	pH
Stomach	1–3
Blood	7.35–7.45
Colon	7–7.5
Duodenum	4.8–8.2
Early endosome	6–6.5
Late endosome	5–6
Lysosome	4.5–5
Golgi	6.4

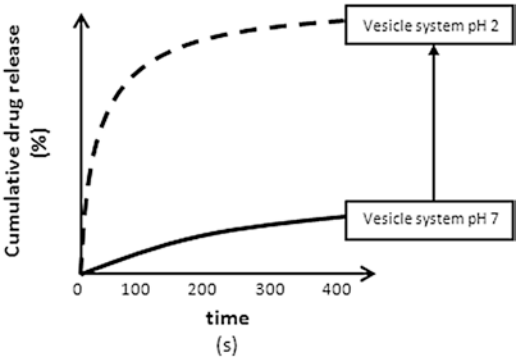

Fig. 7.19 Plot of the differences in drug release between stable vesicle systems and pH-destabilized vesicle systems

defined range. Unlike the thermoresponsive system, which is relevant for oral or intravenous (IV) drug delivery, the pH-responsive vesicle or micellar systems would not be orally relevant if the stimuli range is ~5 since premature release of drug cargo would occur in the acidic environment of the stomach (pH 1–3) (Table 7.2) [59].

Stimuli-responsive swelling behavior can be used in a similar way to release drug contents suspended in a hydrogel matrix. These systems function similarly to those of the thermoresponsive hydrogel in terms of their design [60] (Fig. 7.19).

The hydrogel particles are designed such that the crosslinked domains are a combination of covalent bonds and the collapse of multiple hydrophobic domains. In these cases, a change in the pH of the environment surrounding the base material leads to the conversion of an otherwise nonpolar collapsed hydrophobic species to turn into a charged species. The change to a charged species increases the ability of the system to take up water, leading to the propensity to swell. The change to charged groups also leads to the electrostatic repulsion of polyelectrolyte chains within close proximity to one another, which further drives the expansion of the gel network pore structure [61]. This design is typically used in drug applications where the drug needs to be delivered within the immediate proximity of a desired cell and does not require the system to facilitate the cellular internalization response (i.e., embolics). In either of these cases, systems can be designed with negative charges as well,

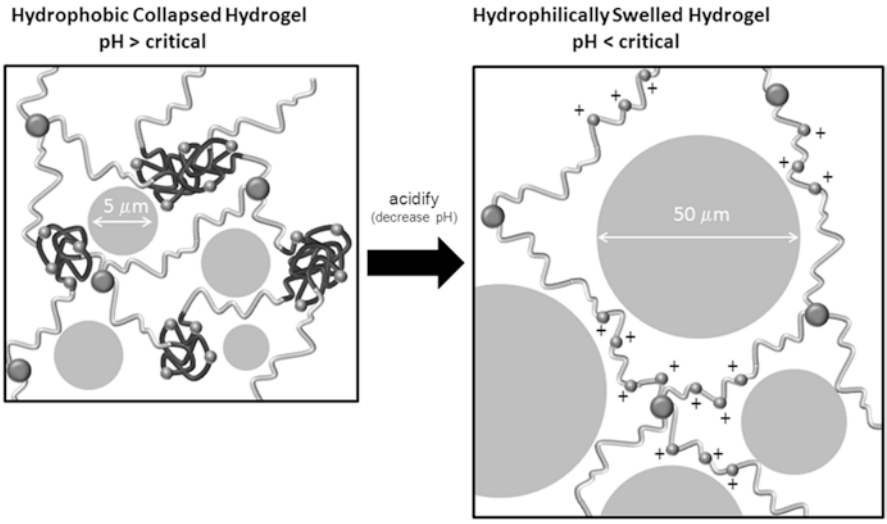

Fig. 7.20 Diagram of the effect of acidification (or basification) on pH-responsive hydrogel assemblies

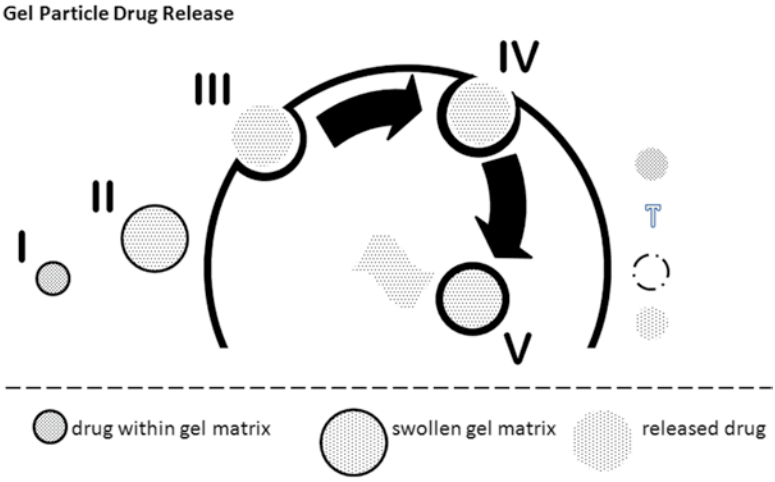

Fig. 7.21 Diagram of pH-responsive swelling of hydrogel and uptake within the lysosome of a cell during RME

which shifts the operable pH range to more basic stimuli. One can envision tuning their respective systems by compositionally shifting their ratios of cationic to anionic stimuli-responsive groups to allow for a specific release window (Fig. 7.20).

These swellable gel particle systems [61] (**I**) function by swelling in the presence of a designated pH range (**II**), which results in the first-order pharmacokinetic release of drug cargo, followed by (**III**) the internalization of drug by (**IV** and **V**) endocytosis or pinocytosis (Fig. 7.21).

One aspect of these particular types of systems that will become repetitive in our discussion is the presence of charge in the drug delivery system. Charged functionalities become a challenge in terms of avoidance of physiological response within the body [62]. As we discussed earlier, complexation occurs with especially cationic charge groups on the surface of our systems, which contributes to their recognition by opsonins. For this reason, uncharged systems are often used for drug delivery systems for their so-called stealth capabilities. It is worth noting, however, that recent work has identified another possible strategy. The use of zwitterionic polyelectrolyte species [63] has shown the potential for avoiding physiological response provided the molecular weight and composition fall within a specific range. These new strategies, combining our knowledge of the chemical, biological, and engineering constraints of stimuli-responsive drug delivery, can allow for more robust materials to be developed for drug delivery (Table 7.3).

7.2.1.3 Magnetoresponsive Systems

As we discussed in Sect. 7.1, magnetoresponsive materials represent systems that interact with an *applied* stimulus as opposed to an *encountered* stimulus, as was the case with temperature- and pH-responsive systems. Light and sound also fall within this subcategory of responsive materials to an applied stimulus [64]. In the case of magnetic materials, the stimulus is an externally applied magnetic field that can either immobilize a particle under flow [65] or generate localized heat in the environment surrounding the particle [66] (i.e., magnetic hypothermia). The design of the magnetic material involves several criteria, which include *atomic identity*, *particle size*, *physiological interaction*, and *stabilizing material* [67]. The *atomic identity* refers to the metal atoms used in the particle composition (i.e., iron, nickel, cobalt). The *particle size* refers to the size of the magnetic particle, keeping in mind that the larger the multidomain particle size, the more susceptible it will be toward manipulation by a magnetic field. The *physiological interaction* simply refers to the propensity for the body to interfere with the responsive behavior in its intended target location (i.e., pharmacodynamics). The *stabilizing functionality* is the chemical functionality at the particle surface that is necessary to allow for the particle to effectively function as a physiological system.

We focus first on a single-domain magnetic particle strategy [68] for the immobilization of drug species through the application of a magnetic field. This system relies on a small ferromagnetic nanoparticle system (i.e., 5–10-nm diameter) in order to fall within the superparamagnetic regime. Typically, systems such as iron oxide (i.e., Fe_3O_4) are used, where drug candidates are conjugated to the surface. Since the iron oxides are not themselves bioinert, these ferromagnetic particles are then suspended in a larger silica particle system as its matrix, which is then surface-functionalized with chemically inert groups (i.e., PEG, dextran, aminosilanes) [68] (Fig. 7.22).

It is important to keep in mind that with the introduction of surface-modifying groups for biocompatibility, the magnitude of the magnetic moment at the surface of the particle becomes reduced or passivated, which may limit its physiological

Table 7.3 Commonly used pH-responsive chemical functionalities for drug delivery

Polymer	Structure	pH	Biocompatible or bioinert
Poly(L-Lysine) K	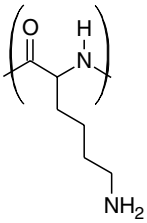	<9	Biocompatible
Poly (L-Glutamate) E	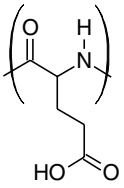	>6 <11	Biocompatible
Polyacrylic acid (PAA)	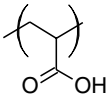	<5.5	Bioinert
Chitosan	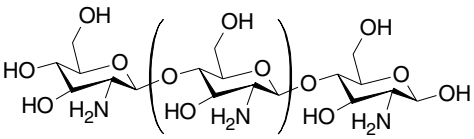	>6	Biocompatible
Polyethylene glycol (PEG)	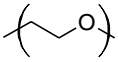	<5.5	Bioinert
Cellulose	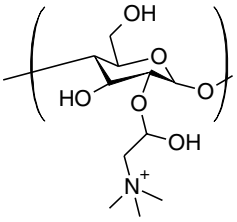	8	Biocompatible
Polyethylene imine (PEI)	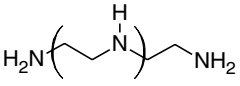	4	Bioinert

application. The design of these immobilized magnetic systems therefore involves three basic criteria: particle size (<10 nm), bioinert surface functionalities (limited passivation of magnetic moment), and mode of drug incorporation (conjugated or dispersed within matrix) [69]. Magnetic drug delivery systems formed using this design strategy have shown promise for clinical evaluation and treatment of brain tumor patients using a tandem approach involving acoustic and magnetic targeting of tissue across the blood–brain barrier.

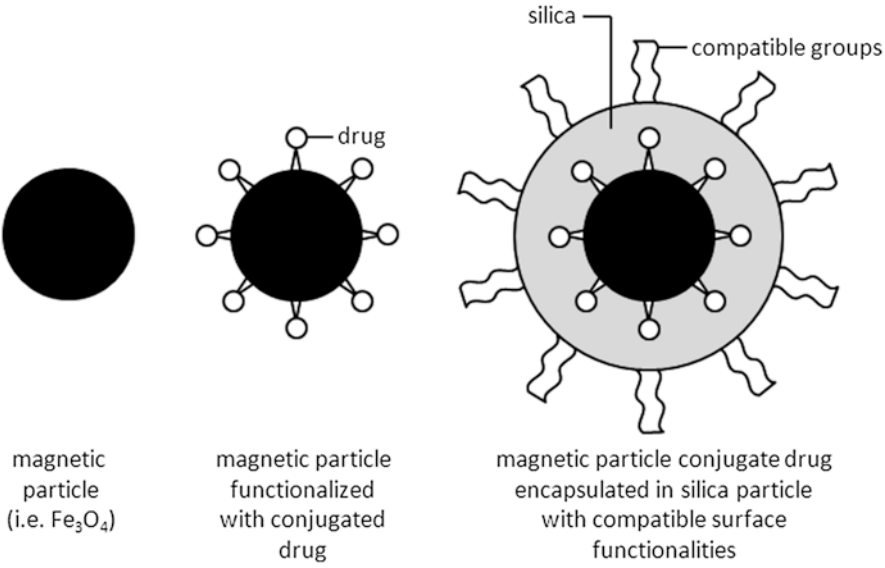

Fig. 7.22 Schematic for the design of bioinert, magnetoresponsive drug delivery systems

The second strategy we focus on is a multidomain ferromagnetic (FM) particle system [70] for the induction of localized heat through magnetic hypothermia. As discussed previously, the multidomain structure allows for the generation of heat energy in response to an alternating magnetic field. The heat energy can be approximated by a hysteresis curve by the following relationship [71]:

$$P_{\mathrm{FM}} = \mu_0 f \oint H\, dM, \tag{7.14}$$

where μ_0 is the magnetic permeability, f is the frequency of the alternating magnetic field, H is the magnetic field strength, and dM is the change in the magnetization. In our earlier discussion surrounding multidomain particles, we determined that the particle size was critical for the system's response to an applied alternating magnetic field. In this case, the larger the particle size is, the larger the influence of the applied magnetic field. If we look at the behavior of this system within physiological media, it is evident that the heat generated (100 mW/cm^3) by the hypothermic particle would affect its surrounding environment, with only <25 % affecting the tissue environment. The localized temperature change may require cooling by dilution, which involves increased blood flow to the affected area [72]. Another factor that can complicate this strategy is the effective dosage of particles. Since there is no targeting mechanism, unlike the single-domain species, the dosage will vary depending on the mode of application. Intravenous (IV) holds the advantage of requiring the least material since it's a direct injection into the bloodstream. It has been observed that 5–10 mg/cm^3 is an effective amount of localized magnetic

Table 7.4 Commonly used magnetoresponsive chemical functionalities for drug delivery

Component	Magnetic, matrix, or surface	Single-domain or multidomain	Biocompatible or bioinert
Fe_3O_4	Magnetic	Single-domain (15–55 nm)	Biocompatible
		Multidomain (>55 nm)	
Fe_2O_3	Magnetic	Single-domain (20–60 nm)	Biocompatible
		Multidomain (>60 nm)	
FePt	Magnetic	Single-domain (5–50 nm)	Neither
		Multidomain (>50 nm)	
Ni	Magnetic	Single-domain (30–70 nm)	Neither
		Multidomain (>70 nm)	
Fe	Magnetic	Single-domain (15–50 nm)	Biocompatible
		Multidomain (>50 nm)	
Co	Magnetic	Single-domain (6–27 nm)	Neither
		Multidomain (>27 nm)	
Polyethylene glycol (PEG)	Surface	Single-domain	Bioinert
SiO_2	Matrix	Single-domain	Neither
Dextran	Surface	Single-domain	Biocompatible

material at the target site with a particle size <10 μm for an effective treatment using magnetic hypothermia [73].

The generation of localized heat using magnetic materials is not exclusive to multidomain species. Single-domain superparamagnetic species (SPM) can also generate heat energy in the form of a ferri-fluid [74], where the effective heat absorption is on the order of greater than three times that of the multidomain analogs. In these systems, there are an in-phase component and an out-of-phase component of the magnetization relative to the magnetic field strength. This out-of-phase component is what contributes to the heat generated from the single-domain particles [71]:

$$P_{\mathrm{SPM}} = \mu_0 f \pi \chi'' H^2, \tag{7.15}$$

where χ'' is the out-of-phase component. Here we see that the dependence of the heat generated on the magnetic field in single-domain SPM systems is exponentially greater than in the case of a multidomain ferromagnetic system.

The domain choices allow tunable size and magnetic susceptibility for the drug delivery system. This degree of versatility allows for a multitude of surface functionalizations in order to present a drug delivery system that is physiologically bioinert (Table 7.4).

7.2.1.4 Photoresponsive Systems

As with magnetoresponsive materials, photoresponsive materials represent systems that interact with *applied* stimuli, which in this case is light. For photoresponsive

Table 7.5 Common scientific disciplines tied to critical fundamentals in stimuli-responsive drug delivery systems

Fundamental	Disciplines
Thermal phase behavior	• Chemistry • Chemical engineering • Materials engineering • Physics
Electrostatics	• Electrical engineering • Chemistry • Materials engineering • Biochemistry
Magnetophoresis	• Mechanical engineering • Electrical engineering • Materials engineering • Metallurgy • Medicine
Light excitation	• Chemistry • Optics • Physics • Materials engineering
Acoustic cavitation	• Physics • Medicine

materials, light can either allow for the formation of an isomer [75] (i.e., photoisomerization) or degrade a self-assembled component [76]. We will discuss these as separate design strategies for the remainder of this section. The photoisomerization strategy relies on the effective destabilization of a liquid crystal phase within the hydrophobic domain of a micelle or vesicle species. From our previous discussion in Chap. 4, we know that vesicles and micelles are formed from amphiphilic molecules or macromolecules, which minimize interfacial free energy in aqueous solution by the aggregation of hydrophobic domains. If the hydrophobic domain now consists of mesogenic liquid crystal groups, this aggregated region will be highly rigid and densely packed in the *trans* state [77]. If UV light is then applied to a system, such as azobenzene [78], the mesogens will change from a *trans* to a *cis* state and greatly disrupt the dense packing within the monolayer or bilayer (Fig. 7.23).

There have been some examples of the reversibility of the destabilized self-assembly in photoisomerization-induced systems, where visible light or heat is used to return the structure to its native initial state [79]. These systems typically involve highly stable vesicle or micellar self-assembled systems that rapidly reform their densely packed domains.

The function of the degradation of a self-assembled component is to force the molecule into a state where it acts to rapidly destabilize the self-assembled species. This can be done through decreasing the hydrophobicity [80], domain packing [80], or changing the curvature of subdomains [80] within the structure. The last strategy

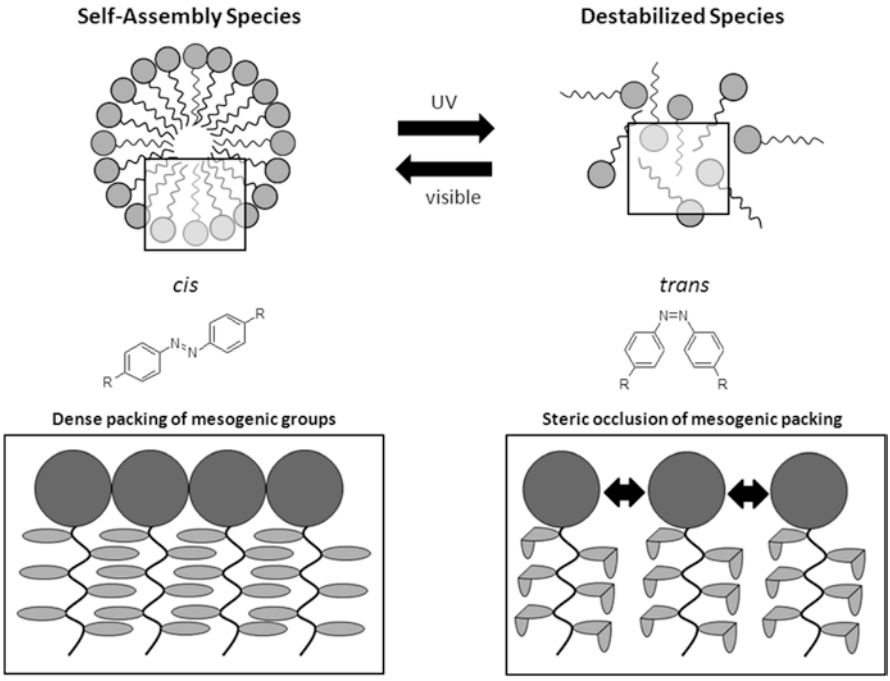

Fig. 7.23 Diagram of photoresponsive changes to the packing of mesogenic groups in a self-assembled species

is of particular interest to our current discussion. The change in the curvature of a bilayer species can lead to the formation of membrane pores at random intervals throughout the bilayer. This increase in porosity corresponds to a change in osmotic potential, which may release encapsulated cargo at a specific time. The photooxidation of plasmalogen is a common degradation mode for destabilizing lipid vesicles [81]. This approach involves the photooxidation of the plasmalogen vinyl ether linkage within the dual-chain plasmenylcholine lipid to form a single-chain species. The formation of a single-chain species increases the curvature of the lipid membrane at the affected areas, which stabilizes the pore formation (Fig. 7.24).

The key advantage in this strategy is that the release kinetics can be modulated by the use of different sensitizing agents to absorb light ($\leq$300 mW/cm^2) to allow the wavelength (630–820 nm) to reach greater membrane penetration depths at rapid rates [81]. These two strategies permit both the modulation of release kinetics and encapsulation based on exposure to a range of wavelengths of light under different time durations to achieve targeted drug delivery.

7.2.1.5 Acoustic Responsive Systems

In the case of acoustic responsive systems, gas bubbles generated from acoustic *cavitation* (i.e., oscillation, growth, and collapse) require both stabilization of their

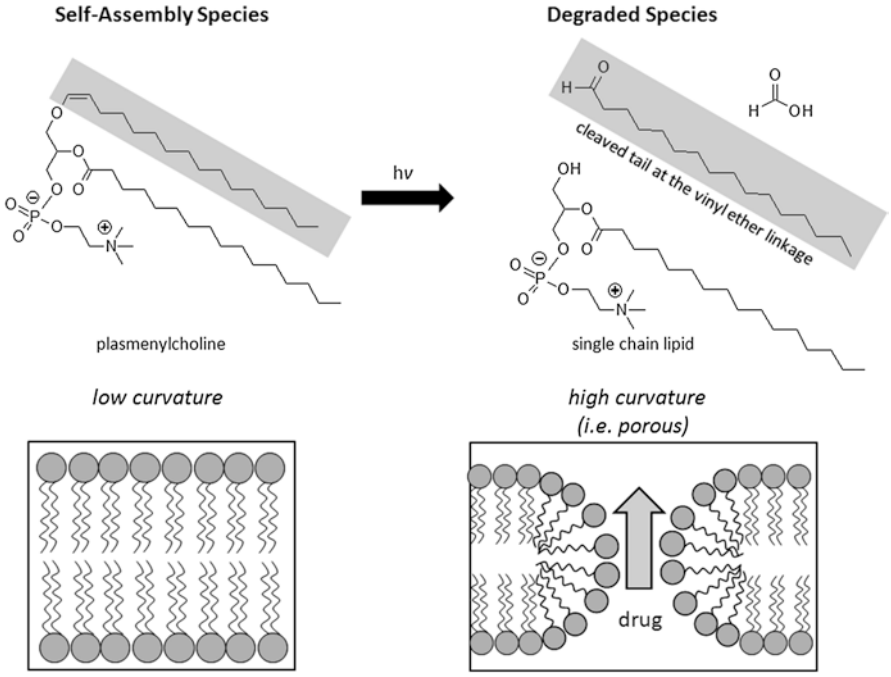

Fig. 7.24 Diagram of photoinduced pore formation within lipid bilayers

gas–liquid interface and the compatibilization with lipid interfaces. The primary requirements of the *stabilized system* are the *extended circulation lifetime*, the *effective size range*, and the *efficient stimulated release* of encapsulated drug via the application of ultrasound [62, 82].

We can address each of these requirements sequentially, beginning with the stabilization of the gas–liquid interface. The generation of this interface involves the mismatch of *acoustic impedances*, or molecular vibration due to sound stimuli, of two components [i.e., water and perfluoropentane (PFP)] [83]. The material that stabilizes the interface is typically an amphiphilic copolymer species with a non-ionic hydrophilic component (i.e., PEG) and a range of hydrophobic components (i.e., PLA, PCL) [83]. This amphiphilic species is prepared as a prebubble in the form of a nanodroplet, consisting of the (**I**) encapsulated drug housed within an amphiphilic copolymer stabilized droplet. With the (**II**) introduction of acoustic stimuli, the amphiphilic copolymer (**III**) stabilizes the gas–liquid interface, with the internal environment being the gas, the external environment being the liquid, and the drug positioning at the interface (i.e., shell). As the microbubbles flow, they can recombine to a larger size, with the ideal size being ~750 nm, until reaching a desired bilayer where the system (**IV**) occupies an interstitial space in the membrane and releases the drug [84].

The *circulation lifetime* of the gas microbubbles is associated with the amphiphilic component that stabilizes the interface. Based on our previous discussion in

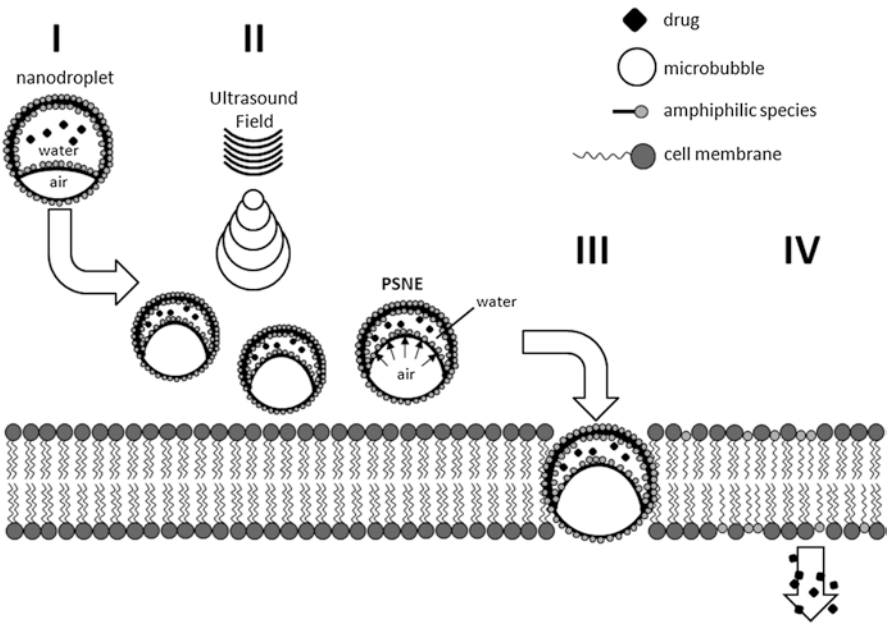

Fig. 7.25 Diagram of the cavitation of PSNE nanodroplets from ultrasound

Chap. 4, we know that lipid bilayer systems have a significantly short thickness, which, in the case of gas–liquid interfaces, offers little stability of microbubbles in vivo. Amphiphilic copolymer systems offer a significant improvement to the interfacial membrane stability, while maintaining tunability to drive membrane curvature [85].

We know that the targeted *size regime* is <750 nm to allow for tumor membrane permeability and gas microbubble stabilization. Recent work [86] has suggested that curvature can be further tuned to form *nanobubbles* as a preform to merge into microbubble systems at the cell membrane interface. This approach is an example of improving the stability of the microbubble with no discernible effect to the biological delivery. These size regimes can be effectively tuned by the energy of the applied ultrasound stimulus and the amphiphilic copolymer composition to effectively stabilize the desired interfacial curvature [86] (Fig. 7.25).

The effective delivery of the adhered drug is correlated to the *echogenicity*, or the ability to bounce a signal based on oscillation, growth, and collapse of the microbubble system [87]. The echogenicity is affected by the choice of component mixtures (i.e., water and PFP), the surfactant, and the size of the microbubble system. The trend appears to be that the maximization of the impedance between components and the stabilization (i.e., thick interfaces) of high-curvature (i.e., small) systems can improve drug release profiles in vivo [87].

In this section we have discussed a series of design elements that are critical to the exploitation of stimuli by materials for application in drug delivery. We can

envision that combinations of these strategies may present a novel approach for improving pharmacokinetic profiles and permitting more robust therapeutic methods. In Sect. 7.3, we discuss two systems that combine elements from both internal and externally applied stimuli separately and in tandem to effectively deliver a targeted drug species.

7.3 Implementation

7.3.1 Stimuli-Responsive Material Systems

7.3.1.1 Photoresponsive Vesicle Drug Release

In this chapter we have focused on two drug delivery strategies involving the stimulation of drug release through the introduction of light. These approaches have focused on either altering the chirality of the molecule or influencing the degradation properties of the material. An extension of the latter strategy involves the use of encapsulated agents to destabilize an intracellular component upon exposure to an external stimulus in order to enhance drug release within the cell itself. This method holds potential advantage for targeting specific intracellular pathways that may otherwise be inaccessible.

Febvay et al. [88] designed a system based on this strategy, which involved the use of a mesoporous silica nanoparticle to house the drug system, whose surface is decorated with both PEG and antibodies for cell surface targeting. The drug in this case is a model compound, or an Alexa546 membrane impermeable dye to ensure that all fluorescence is attributed to internalized species from the nanoparticle drug delivery system (Fig. 7.26).

The Febvay's group propose that upon internalization into an endosomal vesicle, the nanoparticle system will release Alexa546 with a light stimulus, which initiates ROS-mediated membrane degradation, as discussed in Sect. 7.2, to facilitate delivery of dye into the cytosol.

The authors began the fabrication of their system by controlling the size of silica particles through the introduction of multiple silica sources, which included both orthosilicate (TEOS) and mercaptopropyltrimethoxysilane (MPTMS) in combination with a PEG, PEG-imine, and PEO-PPO-PEO triblock copolymer (Pluronic® F127). The resulting nanoparticle sizes could be controlled by varying the amount of F127 polymer, reaching the sub-50-nm size regime. In vitro testing of nanoparticle (NP) systems functionalized with streptavidin ligands was performed, demonstrating the effective internalization of the NP species into endosomal compartments. The internalized NPs were confirmed to reside within lysosomal compartments by the colocalization of the Alexa546 encapsulated NP species with a LAMP-GFP species that exclusively resides within lysosomal compartments.

The NP system was evaluated for its ability to release Alexa546 species upon stimulation by light. Light stimulation for 120 s showed a noticeable increase in

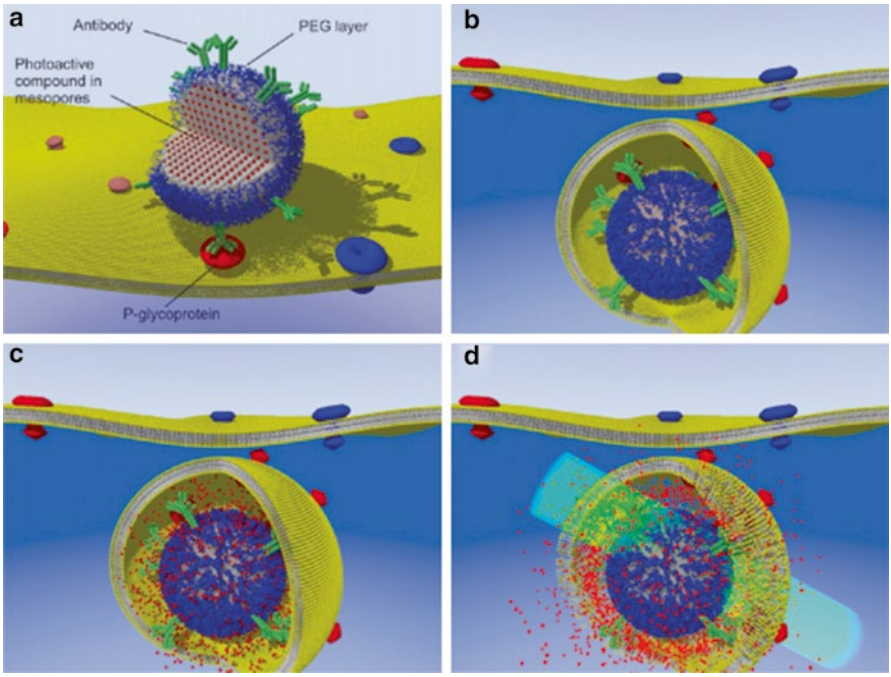

Fig. 7.26 Schematic of light-activated and targeted cytosolic delivery of membrane-impermeable compounds. (**a**) Antibody-functionalized nanoparticles are loaded with a model compound (the fluorescent dye Alexa546 in our experiments) and targeted to cells expressing P-gp-GFP (GFP bound to the P-glycoprotein transporter). After nanoparticle endocytosis (**b**), the cargo is released in the endosome (**c**). Exposure to light at the dye's excitation wavelength (546 nm) promotes ROS-mediated membrane damage (**d**) with cytosolic delivery of Alexa546 exclusively in the P-gp expressing cells [88]

fluorescent species in both confocal microscopy images and fluorescence quantification measurements (Fig. 7.27).

In order to further probe the extent of the Alexa546 release from the internalized vesicles, the authors elected to coencapsulate another species (Alexa 633), one that is incapable of release from the internalized vesicles as a contrast. The additional encapsulant showed no evidence of release upon internalization, as shown through both confocal cellular imaging and fluorescence quantification measurements. The NP species also showed visual evidence of intracellular lysosome disruption through differential interference contrast (DIC) imaging. Each of the cellular assays appeared to support the authors' strategy for the selective release of internalized drug encapsulant by destabilizing the vesicle membrane by ROS upon stimulation by light (Fig. 7.28).

The strategy of light-stimulated drug delivery through the disruption of internalized lysosomal species shows a novel tactical progression in the design of effective stimuli-responsive drug delivery species. This system allows for a more finite

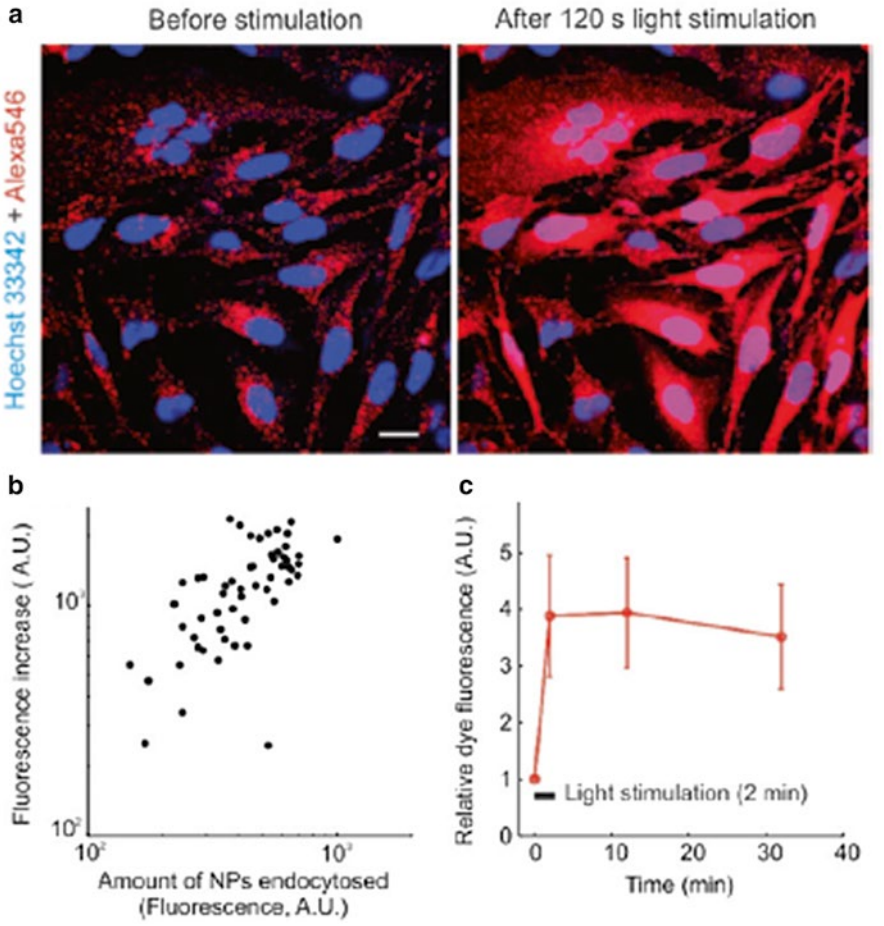

Fig. 7.27 Light-induced cytosolic release of Alexa546 loaded into mesoporous silica nanoparticles. (**a**) Confocal micrographs of live LN-229 cells after surface biotinylation-mediated uptake of streptavidin-functionalized particles loaded with Alexa546 (60× water-immersion objective). Images were acquired before (left panels) and immediately after (right panels) exposure to light from a TRITC-filtered mercury lamp. (**b**) Relationship between the amount of cytosol-released Alexa546 and the amount of endocytosed NPs. Each data point in the scatter plot represents one cell. (**c**) Time evolution of Alexa546 fluorescence following stimulation. Fluorescence is normalized for each cell to its initial value preceding light exposure. The *bars* represent SD ($n = 57$ cells). *Scale bars* are 20 **μ**m in all images [88]

control over the route of drug delivery and begins to address another critically important question that lies largely unanswered. What can be done to effectively promote the intracellular activity of an internalized drug?

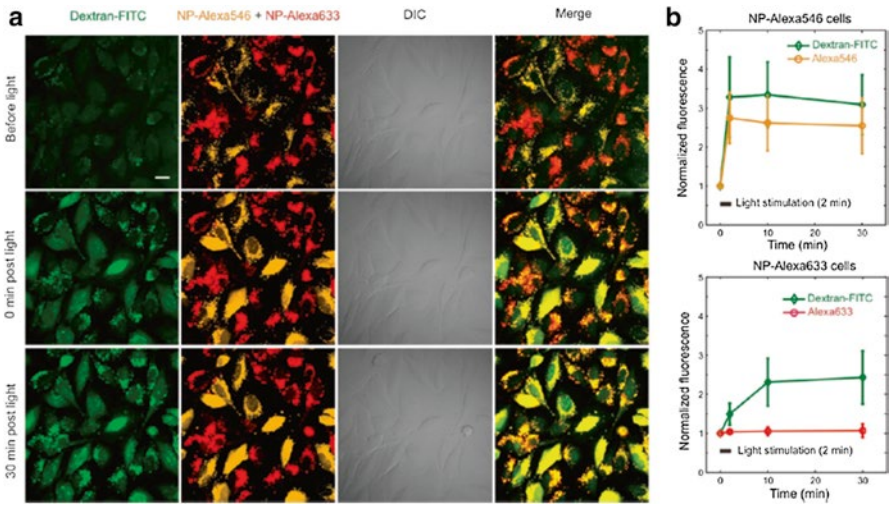

Fig. 7.28 (**a**) Confocal micrographs of LN-229 cells after NP and dextran-FITC coendocytosis (60× water-immersion objective). Orange NPs were loaded with Alexa546 after synthesis, while red NPs contain covalently bound Alexa633, which cannot be released. The two types of NPs were endocytosed separately and the two populations subsequently mixed and incubated with dextran. Images were acquired before (*top row*) and at various time points following 2 min of light stimulation of the NPs (*following rows*). Dextran-FITC cytosolic release is observed with both NP types with different kinetics. *Scale bars* are 20 μm. (**b**) Time evolution of NP and dextran-FITC average cell fluorescence (normalized to initial fluorescence) following light stimulation, for both Alexa546-NPs loaded cells (*left*, $n = 14$ cells) and Alexa633-NPs loaded cells (*right*, $n = 20$ cells). The *bars* represent SD [88]

7.3.1.2 Multifunctional Magnetic-Thermoresponsive Drug Release Systems

Up to this point, we have discussed the exclusive use of a single stimulus to trigger drug release or targeting to a specific physiological region. These single stimuli were separated into domains defined by whether the system responded to localized effects such as temperature or pH or induced effects such as magnetic field, light, or sound. We have discussed in this chapter how differently each of these systems responds to its respective stimulus. In specific cases, it is desirable to have a system be induced by one stimulus and respond in a manner consistent with another. For example, the application of a magnetic field is desirable due to its ease of application; however, due to biocompatibility concerns [89], it is limited from specific modes of interaction (i.e., within membranes). Thermoresponsive materials such as NIPAAm can be readily incorporated into self-assembled species that can be taken up by cells [90]. For these reasons, an opportunity exists to design a tandem system where a magnetoresponsive material is coupled to a thermoresponsive material.

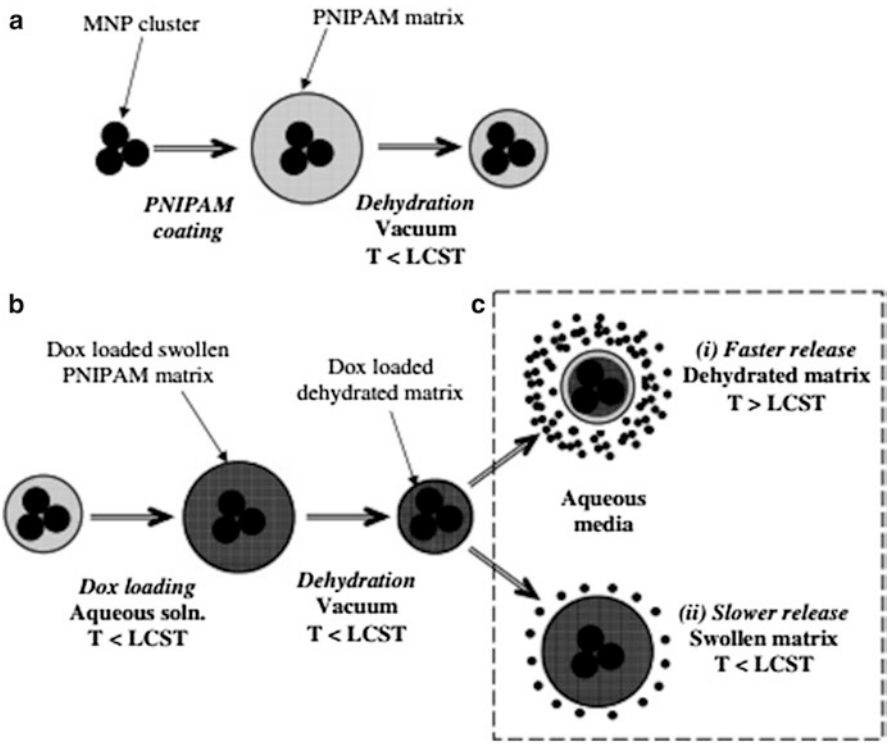

Fig. 7.29 Schematic overview of (**a**) the composite magnetic nanoparticle preparation, (**b**) drug loading, and (**c**) drug release processes [91]

In this system, under alternating magnetic field, the magnetic particles would generate enough heat to shift the thermoresponsive material through its LCST and destabilize the self-assembled species to release the encapsulated drug.

Purushotham et al. [91] have designed and validated a cooperative stimuli-responsive system based on a core–shell morphology. The core of the system is the magnetic nanoparticle (i.e., γ-Fe_2O_3), and the shell of the system is a thermoresponsive polymer [i.e., poly(*N*-isopropylacrylamide (pNIPAAm)]. The drug molecule in this case, doxorubicin (DOX), was embedded in the polymer shell layer. The strategy with Purushotham et al.'s. system is to apply an alternating magnetic field, whereby the superparamagnetic Fe_2O_3 nanoparticle cores will begin to generate heat through magnetic hyperthermia (i.e., Neél relaxation). This heat generated will push the NIPAAm shell through its helix to globule transition at the LCST. The motion of the polymer chain as it collapses through that transition will therefore release the entrapped drug (Fig. 7.29).

The additional caveat of this strategy is that the magnetic nanoparticle system can be guided to the desired location through an externally applied magnetic field as well. The cooperative system was shown to have a nanoparticle diameter in the

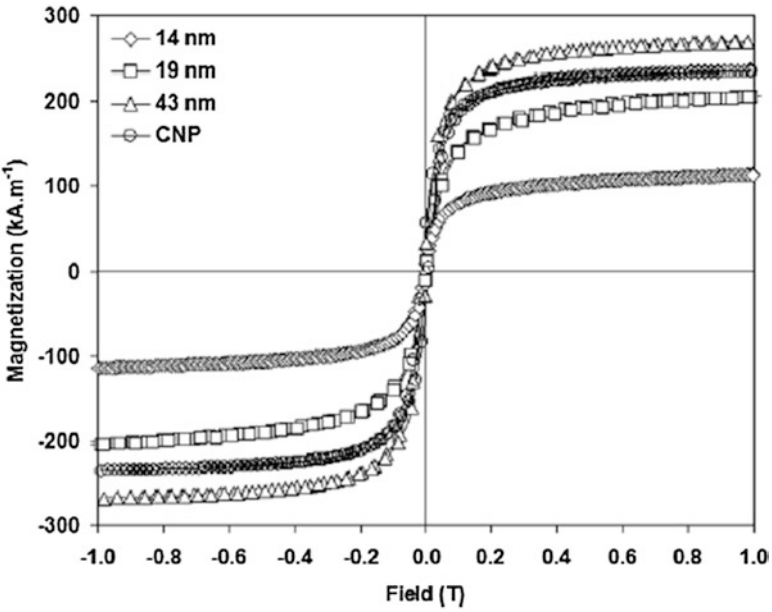

Fig. 7.30 Room-temperature magnetization curves of 14-, 19-, and 43-nm uncoated iron oxide nanoparticles as well as PNIPAAM-encapsulated 43-nm composite nanoparticles (CNP). M_S increases with increasing size for the bare particles [91]

14–43-nm size regime, where the DOX drug was loaded through swelling and dehydration of the nanoparticle shell by changes to temperature above and below the LCST. In order to select the most effective nanoparticle size, the authors evaluated the magnetization and temperature of the system with an alternating magnetic field (AMF). The magnetization curves appeared to show a clear advantage for increased sizes of nanoparticles in response to a magnetic field, with 43 nm being optimal within the designated range (Fig. 7.30).

The temperature release of the systems was also measured with exposure to a 375-kHz, 1.7-kA/m AMF, which showed a temperature increase within the hyperthermia range (i.e., 2–4 min). The rate of the temperature increase correlated with increases in particle size (Fig. 7.31).

The DOX release was then measured as a function of temperature change in the absence of magnetic field in order to confirm the activity of the pNIPAAm thermoresponsive domain and its corresponding release kinetics. The cumulative release kinetics appeared to show the expected increase in release rate with increase in temperature through the LCST of 37 °C. When the system was tested in vitro, it was determined that the temperature change of the nanoparticle system reached the hyperthermia range within the expected 2 min in the presence of AMF and subsequently dropped with the removal of the AMF (Fig. 7.32).

This thermal response to the AMF appears to confirm the performance requirement of this system to generate enough heat to push the system through its LCST,

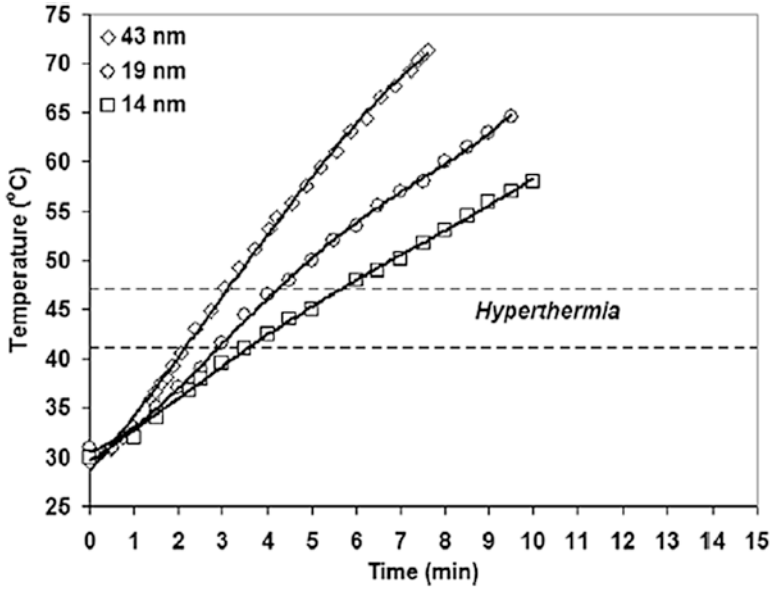

Fig. 7.31 Heating characteristics of the iron oxide nanoparticles dispersed in water and subjected to a 375-kHz, 1.7-kA/m alternating magnetic field. Ambient temperature = 30 °C. Ferrofluid concentration = 10 mg/ml, volume = 5 ml. Dashed horizontal lines indicate the hyperthermia range of 41–48 °C [91]

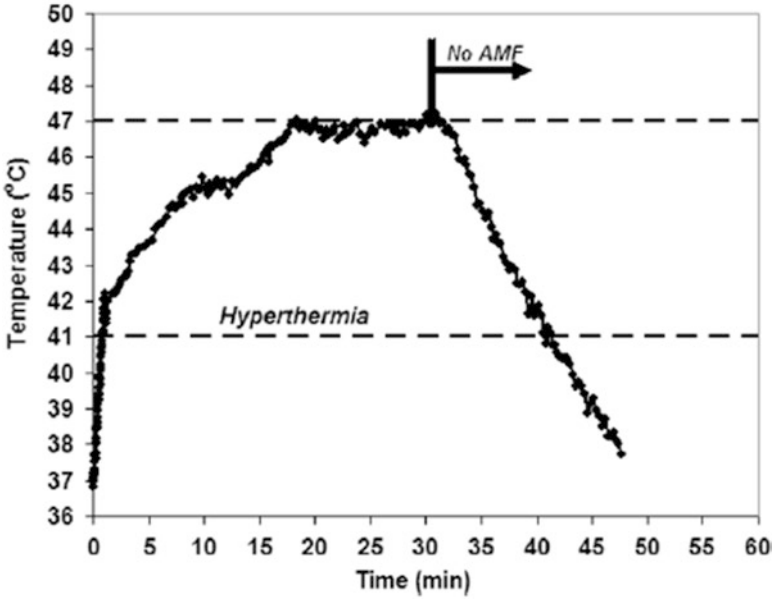

Fig. 7.32 Temperature plot from the in vitro simultaneous drug release and hyperthermia test of DOX-loaded composite magnetic nanoparticles in a 375-kHz, variable-strength, alternating magnetic field. Field was switched off after 30 min of hyperthermia exposure. Ferrofluid conc. = 2.5 mg/ml, vol = 5 ml. DOX release = 14.7 % (48 **μ**g) of loaded DOX [91]

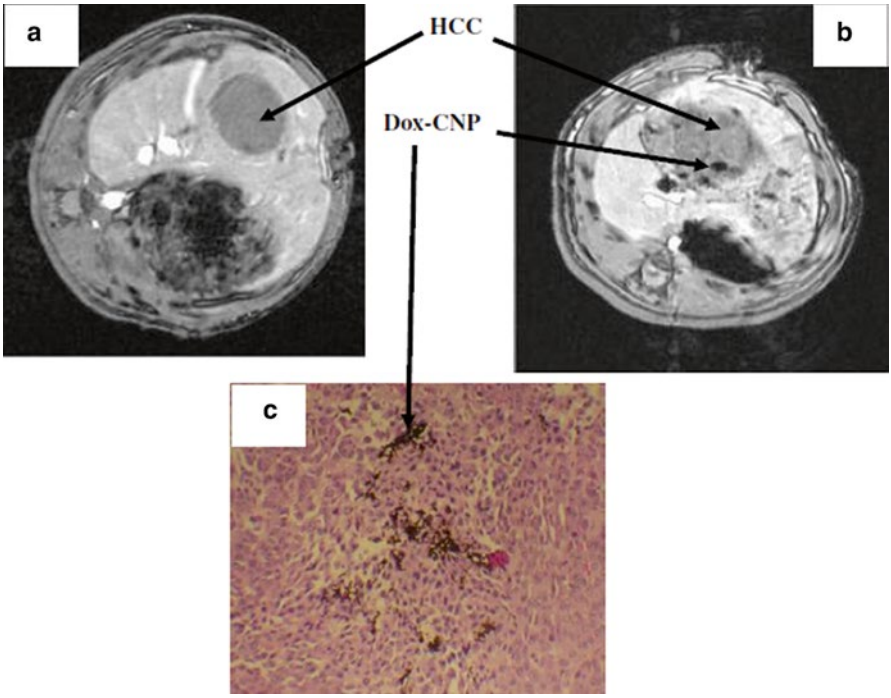

Fig. 7.33 MRI scan of the buffalo Rat implanted with HCC: (**a**) baseline before injection of the DOX-CNP and (**b**) 30 min after injection. Particles are seen as new dark regions in the HCC. (**c**) Histology slide of the HCC showing particles as dark deposits [91]

and the LCST data independently confirm the necessary release kinetics for DOX delivery. The added benefit of magnetic nanoparticle systems exploited by this work was the localization of this system to a tumor site in response to an externally applied magnetic field. The authors demonstrated this behavior with an implanted system within a buffalo rat. They showed that approximately 30 min after injection and application of the magnetic field within the tumor area, the nanoparticles were noticeably sequestering, as evidenced by the black domains in the imaging (Fig. 7.33).

The work of Purushotham et al. [91] demonstrates a cooperative stimuli-responsive drug delivery system based on a combination of magnetic and thermally triggered chemical species. The combination of these behaviors and triggers allows the engineer to devise more versatile drug delivery systems in response to physiological stimuli.

7.3.1.3 Summary

The use of smart materials to tailor the release response of a drug delivery system to a specific physiological environment is a highly desirable approach for effective therapeutic treatment. So far in this chapter, we have discussed the fundamental

behavior and materials design associated with five stimuli-responsive systems based on *temperature*, *pH*, *magnetism*, *light*, and *sound*. These are commonly classified in the scientific literature as "smart" materials. The material design section outlined two key strategies for each system. These strategies drew upon our previous knowledge of *swelling*, *degradation*, *release*, and *self-assembly*, while introducing new concepts of *excitation*, *cavitation*, and *magnetophoresis*. Selected concept strategies of light excitation and a cooperative strategy of magnetophoresis and thermal phase change were illustrated with current literature systems successfully implemented in the academic environment. A number of smart material systems are currently in various stages of clinical development, such as ultrasound and magnetic hyperthermia systems for treating cancer.

7.4 Clinical Applications

7.4.1 Smart Micelles for Cancer

This chapter has discussed smart, environmentally responsive drug delivery vehicles for the treatment of specific cells and tissues. Chapter 4 discussed self-assembled materials for drug delivery, and Chap. 5 discussed actively targeted self-assembled materials for drug delivery. In this clinical applications section, we go beyond these two concepts and discuss smart, self-assembled micelles for cancer treatment. We will see that smart micelles can often provide unique treatment options, particularly for cancer.

Micelles can be passively targeted to cancerous tumors by leveraging the enhanced permeability and retention effect. Micelles can be actively targeted to cancerous tumors by leveraging ligand attachment and specific receptor–ligand attachment. Beyond ligand attachment, micelles can also be functionalized to enable site-specific drug release to tumor tissues. When micelles reach the tumor site, efficient drug release from micelle carriers is essential for drug bioavailability and the desired cytotoxic effect. Micelle structures may be designed as environmentally responsive systems, so that drug release is triggered specifically at the tumor site. Such functionality is typically incorporated into micelles by introducing pH-sensitive, temperature-sensitive, or ultrasound-activated polymers. Micelles that dynamically change their physical properties in response to environmental triggers such as pH, temperature, and chemical species are also known as "smart micelles." Table 7.6 provides a summary of reported "smart micelle" formulations that allow site-specific drug release.

The second strategy for imparting pH sensitivity to micelles is a noncovalent method. In this technique, the micelle copolymer incorporates an ionizable component, which alters its conformation upon protonation. The resulting micelle has a pH-dependent stability. When the micelle encounters an acidic environment, it destabilizes and releases its drug payload. For example, pH-sensitive micelles have been created from poly(β amino esters), a class of polymers with pH-dependent stability. These biodegradable polymers are hydrophobic at neutral pH but can

Table 7.6 Environmentally responsive micelle formulations for site-specific drug release to tumors

Polymer composition	Release mechanism	Micelle size (nm)	Therapeutic drug
pH sensitivity			
Acid-labile bonds (covalent)			
PEG-PLA-DOX	Acid-labile bond	89	Doxorubicin
PEG-p(Asp-Hyd-DOX)	Acid-labile bond	65	Doxorubicin
PEG-acetal linked dendritic polyester/ polylysine	Acid-labile bond	35	Doxorubicin
Noncovalent pH sensitivity			
Hydrophobic core			
PLA-PEG PHis-PEG	Histidine protonation	50–114	Doxorubicin
Pluronic–β amino ester	β Amino ester protonation	130	Paclitaxel
pNIPAM copolymer	Undecanoate protonation	160	Doxorubicin
Hydrophilic core			
PEG-PMA	Nanogel swelling	130	Cisplatin
Temperature sensitivity			
pNIPAM	LCST transition	12–31	Doxorubicin
pNIPAM-PLA	LCST transition	40–65	Doxorubicin
pNIPAM-copol-PLGA	LCST transition	85–120	Paclitaxel
Ultrasound activation			
Pluronic, PEG-lipid	Ultrasound	13	Doxorubicin
NNDEA Pluronic	Ultrasound	50–100	Doxorubicin

Sutton D, Nasongkla N, Blanco E, et al., Functionalized micellar systems for cancer targeted drug delivery. *Pharm Res,* 24:1029, 2007

become fully soluble at pH below 6.1. Micelles have been constructed by surrounding a hydrophobic poly(β amino ester) core with a PEG corona from the Pluronic copolymer F108; the resulting micellar particles were loaded with Paclitaxel [92]. In animal models, the pH-sensitive micelles demonstrated the long residence time and improved half-life typical of micellar nanoparticles. Moreover, the pH-responsive β-amino ester micelles achieved a 23-fold improvement in Paclitaxel deposition within tumors compared to free Paclitaxel administration. The pH-sensitive micelles also achieved a threefold improvement in Paclitaxel deposition in tumors compared to non-pH-sensitive micelles [93]. This case reveals the potential of pH-sensitive micelles to increase drug delivery to cancerous tumors.

An alternative method for constructing environmentally responsive micelles is to build temperature sensitivity into the micelle structure. Local temperatures inside the body can be readily raised, making temperature-triggered drug release a viable strategy for site-specific drug delivery. In addition, localized hyperthermia is sometimes used clinically to treat tumors, since the chaotic vasculature of tumors is more vulnerable to hyperthermia than normal tissue [94]. Temperature-sensitive micelles could therefore be part of a synergistic treatment regimen, in which the elevated temperature not only induces local drug release, but also directly destroys tumor cells. The most common technique for designing temperature-responsive micelles

is to utilize a thermosensitive coronal polymer with LCST behavior. The LCST is the critical temperature below which a mixture is miscible. The resulting micelles are stable below the LCST, but a temperature increase above the LCST induces the entire system to be hydrophobic and precipitate out of solution.

The most extensively used polymer for temperature-responsive biomaterials is poly(*N*-isopropylacrylamide), or pNIPAM. Pure pNIPAM homopolymer has an LCST of 32 °C, which can be adjusted by random copolymerization with monomers such as dimethylacrylamide to obtain LCST values within a desired range. For instance, temperature-responsive micelles have been created using pNIPAM as the corona and poly(butyl methacrylate) (PBMA) as the core-forming segment [95]. The pNIPAM-PBMA micelles were loaded with doxorubicin and exhibited significant sensitivity to temperature: The micelles released only 15 % of the loaded drug after 15 h at 30 °C but released 90 % of the loaded drug after 15 h at 37 °C. Drug release could also be switched on and off using temperature cycling. Importantly, the micelles showed temperature-sensitive cytotoxicity: At a 0.1-μg/ml dose, the micelles destroyed less than 5 % of cells at 29 °C but killed 65 % of cells when the temperature was increased to 37 °C. Another temperature-sensitive micelle system has been constructed from pNIPAM-PLGA copolymers [96]. In this case, pNIPAM was copolymerized with dimethylacrylamide (DMMAAm) to develop materials with a desirable LCST of 39 °C. The micelles were loaded with Paclitaxel, and showed temperature sensitivity over a very tight range, with a fourfold increase in Paclitaxel release at 39.5 °C versus 37 °C, and an eightfold increase in cytotoxicity toward tumor cells at 39.5 °C versus 37 °C. Temperature can thus serve as a tunable trigger for chemotherapeutic delivery to tumors.

A final major strategy for site-specific drug release from smart micelles is ultrasound activation. Ultrasound facilitates drug delivery through numerous mechanisms, including a local temperature increase in exposed tissues; cavitation, which increases the permeability of cell membranes; and the production of highly reactive free radical species, which can accelerate polymer degradation [97]. The most frequently used polymer in ultrasound-triggered micelles is Pluronic® copolymer (PEG-PPO-PEG). This polymer also appears to have a synergistic effect with some chemotherapeutic agents and has been proposed to inhibit the p-glycoprotein that causes multidrug resistance in many cancer cells [98]. Ultrasound-sensitive Pluronic micelles have been designed that incorporate PEG-phospholipids (PEG-DSPE) for micellar stabilization [99]. These micelles were loaded with doxorubicin and evaluated in vivo. Ultrasound was able to improve the antitumor efficacy of both free doxorubicin and micelle-encapsulated doxorubicin; in the latter case, micelles with ultrasound delayed tumor growth an additional 2.6 days over micelles without ultrasound. Biodistribution studies revealed that ultrasound not only increased the level of drug accumulation in the tumor, but also lowered the level of drug accumulation in the kidneys and heart. This last result is particularly relevant, as cardiotoxicity is a major side effect of traditional doxorubicin administration. Overall, ultrasound-sensitive micelles may have the capacity to both increase chemotherapeutic effectiveness and decrease adverse effects during tumor treatment.

While passively targeted micelles are already entering clinical trials, smart micelles have not yet reached the clinic. Micelles can be triggered by modulating

temperature, pH, and ultrasound application. Well-designed micellar biomaterials for drug delivery could decrease mortality not only from lung cancer, but from other cancers as well.

7.4.1.1 Ultrasound-Sensitive Drug Delivery for Theranostics

Micelles are but one of the possible designs for an ultrasound-triggered drug delivery system. Ultrasound is a highly useful modality for smart therapies, as ultrasound is already in wide clinical use and is readily integrated into clinical practices in a variety of specialties. Moreover, ultrasound-triggered drug delivery vehicles can be combined with ultrasound contrast agents, or microbubbles, to create "theranostic" vehicles; such theranostics incorporate both therapy via drug delivery and diagnostics via imaging [100]. Structurally, microbubbles consist of two components: an encapsulating polymer shell and an inner gas core. Drugs or genes can be loaded into or onto the polymer shell. The microbubbles oscillate in an acoustic field, leading to substantial improvements in imaging signal-to-noise ratio [101]. Upon sufficient application of ultrasound, the microbubbles cavitate to release the drug payload. Ultrasound-activated theranostics can dramatically improve the detection and treatment of cancerous tumors, inflammatory lesions, ischemic regions, and cardiovascular pathologies such as atherosclerotic plaque.

For instance, ultrasound-triggered carrier microbubbles have been developed for the delivery of plasmid DNA encoding vascular endothelial growth factor (VEGF), a pro-angiogenic growth factor [102]. The microbubbles are created with a cationic lipid shell, by sonicating an aqueous solution of polyethyleneglycol-40-stearate, distearoyl phosphatidylcholine, and 1,2-distearoyl 3-trimethyl-ammoniumpropane with decafluorobutane gas [103]. Plasmid DNA was then charge-coupled to the microbubbles. The DNA-containing microbubbles are 3.9–5.4 μm in diameter. The microbubbles were introduced intravascularly into a rat model of chronic hindlimb ischemia (representing severe peripheral arterial disease), and ultrasound was applied to trigger cavitation of the microbubbles. Delivery of the DNA resulted in significant improvement in tissue perfusion, arteriogenesis, and microvascular blood flow [102]. The ability of ultrasound-triggered microbubbles to induce therapeutic angiogenesis has clinical relevance not only for peripheral artery disease, but also for coronary artery disease, stroke, and any other ischemic organ that can be visualized and accessed via ultrasound.

Ultrasound-triggered theranostics have also been demonstrated for cancer treatment. The chemotherapeutic doxorubicin has been incorporated into micelles composed of biodegradable diblock copolymers (polyethylene glycol/poly-L-lactic acid and polyethyleneglycol/polycaprolactone) along with perfluoropentane-based nanobubbles and microbubbles stabilized by the same biodegradable block copolymers [104]. The mixtures of doxorubicin-loaded micelles with doxorubicin-loaded nano-/microbubbles were injected intravenously into mice bearing breast cancer tumors. The agents were visualized at the tumor target site using ultrasound and were then degraded via ultrasound to release the doxorubicin at the tumor site. Ultrasound enhanced the intracellular uptake of doxorubicin by tumor cells, and

administration of the ultrasound-triggered agents resulted in breast tumor regression in the mouse model. These results could have broad impact for the treatment of any cancerous tumor via ultrasound-mediated visualization and drug delivery.

Ultrasound-triggered microbubbles thus represent the ultimate in smart materials; these vehicles are able to simultaneously detect areas requiring therapy and target drug delivery to these areas upon the introduction of an ultrasound stimulus. These smartest of smart materials are in the early stages of development but hold potential for enabling rational treatment of diseases, improving clinical outcomes, and promoting a better quality of life for patients with complex chronic diseases.

7.5 Problems

7.1 An oncologist has an interest in evaluating the use of iron oxide (Fe_2O_3) magnetic nanoparticles in the form of a single-domain ferrifluid, for localized treatment of metastasized tumors with an alternative magnetic field frequency of 150 kHz at a magnetic field strength of 500 Oe. If the particle diameter is 30 nm, and the magnetic permeability is 1.2566×10^{-6} Wb/Am, answer the following questions with your knowledge of stimuli-responsive magnetic materials for drug delivery.

(i) What is the heat generated by the magnetic nanoparticle system if the out-of-phase component of the magnetic field is 1.5 emu/g?
(ii) If a tumor required 42 °C of heat generated for 30 min to destroy a 10-mm diameter spherical tumor, would your answer to (i) be an effective treatment? If not, what could you change to improve its effectiveness in destroying tumor cells?
(iii) What is the minimum level that the magnetic force needs to be in order to avoid the physiological drag force felt within blood vessels of the body if the velocity of the system is 50 mm/s in blood plasma with a viscosity of 4 cP?
(iv) If the magnetic nanoparticle system has become immobilized, what is one variable in the design of the material that can improve the magnetic force?

7.2 A medical research lab would like to design a micellar drug delivery system to interact with a tissue surface to illicit macropinocytosis in blood plasma with an ionic strength of 0.1 at 37 °C. If the particle diameter is 50 nm, answer the following questions with your knowledge of pH-responsive materials for drug delivery.

(i) What is the critical distance, in terms of proximity to the tissue interface, that the micelle needs to be if $\varepsilon = 10$?
(ii) What is one design method the research lab could use to increase the Debye length of the micelle system?
(iii) What would the effective Debye length change to in the presence of multiple ion channels on the tissue surface, changing the ε to 2?

7.3 A biomedical consulting firm has been hired to design a transdermal, thermoresponsive, drug delivery thin film hydrogel for use in temperatures exceeding 40 °C to deliver protein bioactives. If the firm is restricted in the selection of its system components to the customers' base technologies in the table below, answer the following questions with your knowledge of thermoresponsive materials for drug delivery.

Chemical Name	Structure
poly(N-isopropylacrylamide) p(NIPAAm)	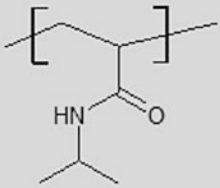
poly(N-isopropylacrylamide)-co-(hydroxyethyl methacrylate) p(NIPAAm-co-HEMA)	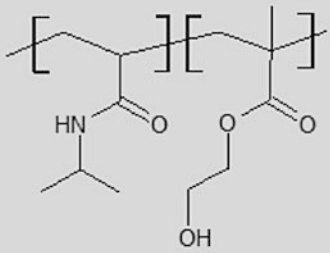
p(hydroxyethyl methacrylate) p(HEMA)	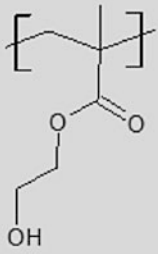
poly(N-isopropylacrylamide)-co-(methyl methacrylate) p(NIPAAm-co-MMA)	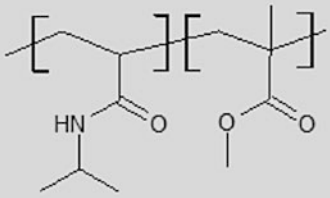
poly(vinyl pyrrolidone) PVPy	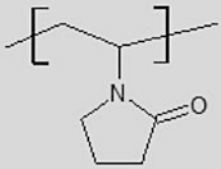

(i) Identify the thermoresponsive components from the table and describe the changes to the free energy of mixing when they are prepared in water.
(ii) Describe the thermoresponsive hydrogel system (i.e., structures, reactions, schematics) in the states before and after exposure to temperatures >40 °C.
(iii) Another consulting firm proposed a similar system, only they focused on light-responsive materials as a mechanism to facilitate drug delivery. Discuss two advantages for using a thermoresponsive hydrogel thin film for drug delivery over the photoinduced method.

7.4 A research lab in biomedical engineering is testing a photoresponsive hydrogel contact lens as a matrix for the controlled release of a prostaglandin analog prodrug to treat glaucoma patients. If the contact lens material has a molar absorptivity of 30,000 M^{-1} cm^{-1}, answer the following questions using your knowledge of photoresponsive drug delivery systems.

(i) What is the degradation kinetics if the applied light intensity is 7 mW/cm^2 with a quantum yield of 0.05 and a wavelength of 370 nm?
(ii) As the contact lens degrades over time, would you expect the molar absorptivity to change? Why?
(iii) How might you change the hydrogel contact lens structure to allow for a more Fickian pharmacokinetic release profile?

7.5 A patient suffering from pancreatic cancer has been deemed an appropriate candidate for a therapeutic treatment involving ultrasound-mediated ablation by the vaporization of phase-shift nanoemulsions (PSNE). If the solution density is 1 g/ml and $\ddot{R}$ is 2 nm/s^2, $\dot{R}$ is 10 nm/s and p_i is 2,000 Pa after 5 s, answer the following questions with your knowledge of acoustic responsive drug delivery systems.

(i) What would be the expected instantaneous radius of the microbubble if cancer cells require a microbubble pressure of 1,200 Pa to initiate ablation?
(ii) Using your approach to (i), how large of a radius microbubble would be required if 12,000 Pa was the pressure necessary to initiate ablation?
(iii) What would happen to the pressure of the microbubble if the radius doubled? Do you think it would be more or less effective at ablation? Why?

References

1. (a) Shimizu, K., Fujita, H., & Nagamori, E. (2010). Oxygen plasma-treated thermoresponsive polymer surfaces for cell sheet engineering. *Biotechnology and Bioengineering, 106*(2), 303–310. (b) Twaites, B. R., de Las Heras Alarcón, C., Lavigne, M., Saulnier, A., Pennadam, S. S., Cunliffe, D., & Alexander, C. (2005). Thermoresponsive polymers as gene delivery vectors: Cell viability, DNA transport and transfection studies. *Journal of Controlled Release: Official Journal of the Controlled Release Society, 108*(2–3), 472–483.

2. Kaul, R. H. (Ed.). (2000). *Aqueous two-phase systems: Methods and protocols* (p. 440). New York: Humana Press.
3. Cahn, J. W. (1961). On spinodal decomposition. *Acta Metallurgica, 9*(9), 795–801.
4. Charlet, G., & Delmas, G. (1981). Thermodynamic properties of polyolefin solutions at high temperature: 1. Lower critical solubility temperatures of polyethylene, polypropylene and ethylene-propylene copolymers in hydrocarbon solvents. *Polymer, 22*(9), 1181–1189.
5. Southall, N. T., Dill, K. A., & Haymet, A. D. J. (2002). A view of the hydrophobic effect. *The Journal of Physical Chemistry B, 106*(3), 521–533.
6. Kwei, T. K., Pearce, E. M., & Min, B. Y. (1985). The effect of hydrogen bonding on the lower critical solution temperature of a polymer mixture. *Macromolecules, 18*(11), 2326–2327.
7. Samal, S. K., Dash, M., Van Vlierberghe, S., Kaplan, D. L., Chiellini, E., van Blitterswijk, C., et al. (2012). Cationic polymers and their therapeutic potential. *Chemical Society Reviews, 41*(21), 7147–7194.
8. Joanny, J. F., & Leibler, L. (1990). Weakly charged polyelectrolytes in a poor solvent. *Journal de Physique, 51*(6), 545–557.
9. Andelman, D., & Joanny, J.-F. (2000). Polyelectrolyte adsorption. *Comptes Rendus de l'Académie des Sciences—Series IV—Physics, 1*(9), 1153–1162.
10. Goto, Y., Calciano, L. J., & Fink, A. L. (1990). Acid-induced folding of proteins. *Proceedings of the National Academy of Sciences, 87*(2), 573–577.
11. Somasundaran, P. (Ed.). (2006). *Encyclopedia of surface and colloid science* (p. 6675). Taylor & Francis: New York.
12. Schmidt, M. (Ed.). (2004). *Polyelectrolytes with defined molecular architecture II (Google eBook)* (p. 231). Springer: Heidelberg.
13. Stuart, M. A. C., Huck, W. T. S., Genzer, J., Müller, M., Ober, C., Stamm, M., et al. (2010). Emerging applications of stimuli-responsive polymer materials. *Nature Materials, 9*(2), 101–113.
14. Bohmer, M. R., Evers, O. A., & Scheutjens, J. M. H. M. (1990). Weak polyelectrolytes between two surfaces: Adsorption and stabilization. *Macromolecules, 23*(8), 2288–2301. doi:10.1021/ma00210a027.
15. Lyklema, J. (2005). *Fundamentals of interface and colloid science: Particulate colloids (Google eBook)* (Vol. 4, p. 692). Burlington, MA: Morgan Kaufmann.
16. Rojas, O. (2002). *Adsorption of polyelectrolytes on mica. Encyclopedia of surface and colloid science*. New York: Marcel Dekker.
17. Châtellier, X., & Joanny, J.-F. (1996). Adsorption of polyelectrolyte solutions on surfaces: A Debye-Huckel theory. *Journal de Physique II, 6*(12), 1669–1686.
18. Dobrynin, A. V., Deshkovski, A., & Rubinstein, M. (2001). Adsorption of polyelectrolytes at oppositely charged surfaces. *Macromolecules, 34*(10), 3421–3436.
19. Coolidge, A. S., & Juda, W. (1946). The Poisson–Baltzmann equation derived from the transfer of momentum. *Journal of the American Chemical Society, 68*(3), 608–611.
20. Pankhurst, Q. A., Connolly, J., Jones, S. K., & Dobson, J. (2003). Applications of magnetic nanoparticles in biomedicine. *Journal of Physics D: Applied Physics, 36*(13), R167–R181.
21. Zhang, Y., Kohler, N., & Zhang, M. (2002). Surface modification of superparamagnetic magnetite nanoparticles and their intracellular uptake. *Biomaterials, 23*(7), 1553–1561.
22. Voltairas, P. A., Fotiadis, D. I., & Michalis, L. K. (2002). Hydrodynamics of magnetic drug targeting. *Journal of Biomechanics, 35*(6), 813–821.
23. Shevkoplyas, S. S., Siegel, A. C., Westervelt, R. M., Prentiss, M. G., & Whitesides, G. M. (2007). The force acting on a superparamagnetic bead due to an applied magnetic field. *Lab on a Chip, 7*(10), 1294–1302.
24. Arruebo, M., Fernández-Pacheco, R., Ibarra, M. R., & Santamaría, J. (2007). Magnetic nanoparticles for drug delivery. *Nanotoday, 2*(3), 22–32.
25. Gittleman, J., Abeles, B., & Bozowski, S. (1974). Superparamagnetism and relaxation effects in granular Ni-SiO_2 and Ni-Al_2O_3 films. *Physical Review B, 9*(9), 3891–3897.
26. Aharoni, A. (2000). *Introduction to the theory of ferromagnetism* (p. 319). Oxford: Oxford University Press.

27. (a) Okabe, F., Park, H. S., Shindo, D., Park, Y., Ohashi, K., & Tawara, Y. (2006). Microstructures and Magnetic Domain Structures Studied by Transmission Electron Microscopy. *Materials Transactions, 47*(1), 218–223. (b) Zhang, C., Johnson, D. T., & Brazel, C. S. (2008). Numerical study on the multi-region bio-heat equation to model magnetic fluid hyperthermia (MFH) using low Curie temperature nanoparticles. *IEEE Transactions on Nanobioscience, 7*(4), 267–275.
28. Vallejo-Fernandez, G., Whear, O., Roca, A. G., Hussain, S., Timmis, J., Patel, V., et al. (2013). Mechanisms of hyperthermia in magnetic nanoparticles. *Journal of Physics D: Applied Physics, 46*(31), 312001.
29. Mueller, A., Bondurant, B., & O'Brien, D. F. (2000). Visible-light-stimulated destabilization of PEG-liposomes. *Macromolecules, 33*(13), 4799–4804.
30. Vasdekis, A. E., Scott, E. A., Roke, S., Hubbell, J. A., & Psaltis, D. (2013). Vesicle photonics. *Annual Review of Materials Research, 43*(1), 283–305.
31. Anzai, J., Ueno, A., & Osa, T. (1987). Photo-excitable membranes. Photoinduced membrane potential changes across poly(vinyl chloride) membranes doped with azobenzene-modified crown ethers. *Journal of the Chemical Society, Perkin Transactions, 2*(1), 67.
32. Dugave, C., & Demange, L. (2003). Cis-trans isomerization of organic molecules and biomolecules: Implications and applications. *Chemical Reviews, 103*(7), 2475–2532.
33. Rabek, J. F. (1995). *Polymer photodegradation: Mechanisms and experimental methods (Google eBook)* (p. 664). Heidelberg: Springer.
34. Muratov, A., & Baulin, V. A. (2012). Degradation versus self-assembly of block copolymer micelles. *Langmuir, 28*, 3071–3076.
35. Duncan, R. (2006). Polymer conjugates as anticancer nanomedicines. *Nature Reviews Cancer, 6*(9), 688–701.
36. Deng, C. X., Sieling, F., Pan, H., & Cui, J. (2004). Ultrasound-induced cell membrane porosity. *Ultrasound in Medicine & Biology, 30*(4), 519–526.
37. Kripfgans, O. D., Fowlkes, J. B., Miller, D. L., Eldevik, O. P., & Carson, P. L. (2000). Acoustic droplet vaporization for therapeutic and diagnostic applications. *Ultrasound in Medicine & Biology, 26*(7), 1177–1189.
38. Pan, H., Zhou, Y., Sieling, F., Shi, J., Cui, J., & Deng, C. (2004). *Sonoporation of cells for drug and gene delivery*. In *Proceedings of the* Annual International Conference of the IEEE Engineering in Medicine and Biology Society. *IEEE Engineering in Medicine and Biology Society Conference, 5*, 3531–3534.
39. Zhang, P., & Porter, T. (2010). An in vitro study of a phase-shift nanoemulsion: A potential nucleation agent for bubble-enhanced HIFU tumor ablation. *Ultrasound in Medicine & Biology, 36*(11), 1856–1866.
40. Pitt, W. G., Husseini, G. A., & Staples, B. J. (2004). Ultrasonic drug delivery—A general review. *Expert Opinion on Drug Delivery, 1*(1), 37–56.
41. Lindseth, F., Langø, T., Selbekk, T., Hansen, R., Reinertsen, I., Askeland, C., et al. (2013). Ultrasound-based guidance and therapy. *INTECH*.
42. Mano, J. F. (2008). Stimuli-responsive polymeric systems for biomedical applications. *Advanced Engineering Materials, 10*(6), 515–527.
43. Ono, Y., & Shikata, T. (2006). Hydration and dynamic behavior of poly(N-isopropylacrylamide) s in aqueous solution: A sharp phase transition at the lower critical solution temperature. *Journal of the American Chemical Society, 128*(31), 10030–10031.
44. (a) Guillet, J. E., Dhanraj, J., Golemba, F. J., & Hartley, G. H. (1968). Stabilization of polymers and stabilizer processes. In Platzer N. A. J. (Ed.) *Advances in chemistry* (Vol. 85, pp. 272–286). Washington, DC: American Chemical Society. (b) Kang Derwent, J. J., & Mieler, W. F. (2008). Thermoresponsive hydrogels as a new ocular drug delivery platform to the posterior segment of the eye. *Transactions of the American Ophthalmological Society, 106*, 206–213; discussion 213–214.
45. Doorty, K. B., Golubeva, T. A., Gorelov, A. V., Rochev, Y. A., Allen, L. T., Dawson, K. A., et al (n.d.). Poly(N-isopropylacrylamide) co-polymer films as potential vehicles for delivery of an antimitotic agent to vascular smooth muscle cells. *Cardiovascular Pathology*, *12*(2), 105–110.

46. Kita-Tokarczyk, K., Grumelard, J., Haefele, T., & Meier, W. (2005). Block copolymer vesicles—Using concepts from polymer chemistry to mimic biomembranes. *Polymer, 46*(11), 3540–3563.
47. Shavit, A., & Riggleman, R. A. (2013). Influence of backbone rigidity on nanoscale confinement effects in model glass-forming polymers. *Macromolecules, 46*(12), 5044–5052.
48. Aranda-Espinoza, H., Bermudez, H., Bates, F., & Discher, D. (2001). Electromechanical limits of polymersomes. *Physical Review Letters, 87*(20), 208301.
49. Yin, X., Hoffman, A. S., & Stayton, P. S. (2006). Poly(N-isopropylacrylamide-co-propylacrylic acid) copolymers that respond sharply to temperature and pH. *Biomacromolecules, 7*(5), 1381–1385.
50. (a) Griffin, W. C. (1954). HLB values of non-ionic surfactants. *Journal of the Society of Cosmetic Chemists*, Presented at the May Meeting, New York City. (b) Company, P. (1949). Classification of surface-active agents by HLB (pp. 311–326). *Journal of the Society of Cosmetic Chemists,* Presented at the October Meeting.
51. Zhu, Z., & Sukhishvili, S. A. (2009). Temperature-induced swelling and small molecule release with hydrogen-bonded multilayers of block copolymer micelles. *ACS Nano, 3*(11), 3595–3605.
52. Stile, R. A., & Healy, K. E. (2001). Thermo-responsive peptide-modified hydrogels for tissue regeneration. *Biomacromolecules, 2*(1), 185–194.
53. Zhang, X.-Z., Wu, D.-Q., & Chu, C.-C. (2004). Synthesis, characterization and controlled drug release of thermosensitive IPN–PNIPAAm hydrogels. *Biomaterials, 25*(17), 3793–3805.
54. Ward, M. A., & Georgiou, T. K. (2011). Thermoresponsive polymers for biomedical applications. *Polymers, 3*(4), 1215–1242.
55. Cooper, G. M. (2000). *The cell: A molecular approach* (2nd ed.). Sunderland, MA: Sinauer Associates.
56. Wileman, T., Harding, C., & Stahl, P. (1985). Receptor-mediated endocytosis. *The Biochemical Journal, 232*(1), 1–14.
57. (a) Guo, X., MacKay, J. A., & Szoka, F. C. (2003). Mechanism of pH-triggered collapse of phosphatidylethanolamine liposomes stabilized by an ortho ester polyethyleneglycol lipid. *Biophysical Journal, 84*(3), 1784–1795. (b) Bellomo, E. G., Wyrsta, M. D., Pakstis, L., Pochan, D. J., & Deming, T. J. (2004). Stimuli-responsive polypeptide vesicles by conformation-specific assembly. *Nature Materials, 3*(4), 244–248.
58. (a) Yao, K. D., Peng, T., Feng, H. B., & He, Y. Y. (1994). Swelling kinetics and release characteristic of crosslinked chitosan: Polyether polymer network (semi-IPN) hydrogels. *Journal of Polymer Science Part A: Polymer Chemistry, 32*(7), 1213–1223. (b) Pillay, V., & Fassihi, R. (1999). In vitro release modulation from crosslinked pellets for site-specific drug delivery to the gastrointestinal tract. *Journal of Controlled Release, 59*(2), 229–242.
59. De, S. K., Aluru, N. R., Johnson, B., Crone, W. C., Beebe, D. J., & Moore, J. (2002). Equilibrium swelling and kinetics of pH-responsive hydrogels: Models, experiments, and simulations. *Journal of Microelectromechanical Systems, 11*(5), 544–555.
60. Gao, X., Cao, Y., Song, X., Zhang, Z., Xiao, C., He, C., et al. (2013). pH- and thermo-responsive poly(N-isopropylacrylamide-co-acrylic acid derivative) copolymers and hydrogels with LCST dependent on pH and alkyl side groups. *Journal of Materials Chemistry B, 1*(41), 5578.
61. Itano, K., Choi, J., & Rubner, M. F. (2005). Mechanism of the pH-induced discontinuous swelling/deswelling transitions of poly(allylamine hydrochloride)-containing polyelectrolyte multilayer films. *Macromolecules, 38*(8), 3450–3460.
62. Du, J., & O'Reilly, R. K. (2009). Advances and challenges in smart and functional polymer vesicles. *Soft Matter, 5*(19), 3544.
63. Keefe, A. J., & Jiang, S. (2012). Poly(zwitterionic)protein conjugates offer increased stability without sacrificing binding affinity or bioactivity. *Nature Chemistry, 4*(1), 59–63.
64. Kataoka, K., Scholz, C., & Rapoport, N. (2007). Physical stimuli-responsive polymeric micelles for anti-cancer drug delivery. *Progress in Polymer Science, 32*(8), 962–990.

65. Senyei, A., Widder, K., & Czerlinski, G. (1978). Magnetic guidance of drug-carrying microspheres. *Journal of Applied Physics, 49*(6), 3578.
66. Gordon, R. T., Hines, J. R., & Gordon, D. (1979). Intracellular hyperthermia. A biophysical approach to cancer treatment via intracellular temperature and biophysical alterations. *Medical Hypotheses, 5*(1), 83–102.
67. Hatch, G. P., & Stelter, R. E. (2001). Magnetic design considerations for devices and particles used for biological high-gradient magnetic separation (HGMS) systems. *Journal of Magnetism and Magnetic Materials, 225*(1), 262–276.
68. Gómez-Lopera, S., Plaza, R., & Delgado, A. (2001). Synthesis and characterization of spherical magnetite/biodegradable polymer composite particles. *Journal of Colloid and Interface Science, 240*(1), 40–47.
69. Mitsumori, M., Hiraoka, M., Shibata, T., Okuno, Y., Nagata, Y., Nishimura, Y., et al. (1996). Targeted hyperthermia using dextran magnetite complex: A new treatment modality for liver tumors. *Hepato-gastroenterology, 43*(12), 1431–1437.
70. Motoyama, J., Hakata, T., Kato, R., Yamashita, N., Morino, T., Kobayashi, T., et al. (2008). Size dependent heat generation of magnetite nanoparticles under AC magnetic field for cancer therapy. *Biomagnetic Research and Technology, 6*, 4.
71. Muxworthy, A. R., & Williams, W. (2009). Critical superparamagnetic/single-domain grain sizes in interacting magnetite particles: Implications for magnetosome crystals. *Journal of the Royal Society, Interface/The Royal Society, 6*(41), 1207–1212.
72. Hergt, R., Dutz, S., Müller, R., & Zeisberger, M. (2006). Magnetic particle hyperthermia: Nanoparticle magnetism and materials development for cancer therapy. *Journal of Physics: Condensed Matter, 18*(38), S2919–S2934.
73. Martinez-Boubeta, C., Simeonidis, K., Makridis, A., Angelakeris, M., Iglesias, O., Guardia, P., et al. (2013). Learning from nature to improve the heat generation of iron-oxide nanoparticles for magnetic hyperthermia applications. *Scientific Reports, 3*, 1652.
74. Moroz, P., Jones, S. K., & Gray, B. N. (n.d.). Magnetically mediated hyperthermia: Current status and future directions. *International Journal of Hyperthermia*, *18*(4), 267–284.
75. Brown, W. (1963). Thermal fluctuations of a single-domain particle. *Physical Review, 130*(5), 1677–1686.
76. Shum, P., Kim, J.-M., & Thompson, D. H. (2001). Phototriggering of liposomal drug delivery systems. *Advanced Drug Delivery Reviews, 53*(3), 273–284.
77. Musa, K. A. K., & Eriksson, L. A. (2009). Photodegradation mechanism of the common non-steroid anti-inflammatory drug diclofenac and its carbazole photoproduct. *Physical Chemistry Chemical Physics: PCCP, 11*(22), 4601–4610.
78. Kyu, T. (2012). Photoisomerization *induced mesophase transitions in mixtures of crystalline liquid crystalline azobenzene with photocurable mesogenic monomers*. 57th Annual report on research under sponsorship of The American Chemical Society Petroleum Research Fund, Petroleum Research Fund.
79. Wagner, S., Leyssner, F., Kördel, C., Zarwell, S., Schmidt, R., Weinelt, M., et al. (2009). Reversible photoisomerization of an azobenzene-functionalized self-assembled monolayer probed by sum-frequency generation vibrational spectroscopy. *Physical Chemistry Chemical Physics: PCCP, 11*(29), 6242–6248.
80. Peppas, N. A., Rösler, A., Vandermeulen, G. W. M., & Klok, H.-A. (2012). Advanced drug delivery devices via self-assembly of amphiphilic block copolymers. *Advanced Drug Delivery Reviews, 64*, 270–279.
81. Thompson, D. H., Gerasimov, O. V., Wheeler, J. J., Rui, Y., & Anderson, V. C. (1996). Triggerable plasmalogen liposomes: Improvement of system efficiency. *Biochimica et Biophysica Acta (BBA)—Biomembranes, 1279*(1), 25–34.
82. Bajic, G., Yatime, L., Sim, R. B., Vorup-Jensen, T., & Andersen, G. R. (2013). Structural insight on the recognition of surface-bound opsonins by the integrin I domain of complement receptor 3. *Proceedings of the National Academy of Sciences of the United States of America, 110*(41), 16426–16431.

83. Rapoport, N. Y., Efros, A. L., Christensen, D. A., Kennedy, A. M., & Nam, K.-H. (2009). Microbubble generation in phase-shift nanoemulsions used as anticancer drug carriers. *Bubble Science Engineering and Technology, 1*(1–2), 31–39. doi:10.1179/175889709X446516.
84. Song, Y., Hahn, T., Thompson, I. P., Mason, T. J., Preston, G. M., Li, G., et al. (2007). Ultrasound-mediated DNA transfer for bacteria. *Nucleic Acids Research, 35*(19), e129.
85. Sirsi, S., & Borden, M. (2009). Microbubble compositions, properties and biomedical applications. *Bubble Science Engineering and Technology, 1*(1–2), 3–17.
86. Lukianova-Hleb, E. Y., Ren, X., Zasadzinski, J. A., Wu, X., & Lapotko, D. O. (2012). Plasmonic nanobubbles enhance efficacy and selectivity of chemotherapy against drug-resistant cancer cells. *Advanced Materials (Deerfield Beach, Fla.), 24*(28), 3831–3837.
87. Tiukinhoy-Laing, S. D., Huang, S., Klegerman, M., Holland, C. K., & McPherson, D. D. (2007). Ultrasound-facilitated thrombolysis using tissue-plasminogen activator-loaded echogenic liposomes. *Thrombosis Research, 119*(6), 777–784.
88. Febvay, S., Marini, D. M., Belcher, A. M., & Clapham, D. E. (2010). Targeted cytosolic delivery of cell-impermeable compounds by nanoparticle-mediated, light-triggered endosome disruption. *Nano Letters, 10*(6), 2211–2219.
89. Lübbe, A. S., Bergemann, C., Brock, J., & McClure, D. G. (1999). Physiological aspects in magnetic drug-targeting. *Journal of Magnetism and Magnetic Materials, 194*(1), 149–155.
90. Cui, Z., Lee, B. H., Pauken, C., & Vernon, B. L. (2011). Degradation, cytotoxicity, and biocompatibility of NIPAAm-based thermosensitive, injectable, and bioresorbable polymer hydrogels. *Journal of Biomedical Materials Research, Part A, 98*(2), 159–166.
91. Purushotham, S., Chang, P. E. J., Rumpel, H., Kee, I. H. C., Ng, R. T. H., Chow, P. K. H., et al. (2009). Thermoresponsive core-shell magnetic nanoparticles for combined modalities of cancer therapy. *Nanotechnology, 20*(30), 305101.
92. Potineni, A., Lynn, D. M., Langer, R., et al. (2003). Poly(ethylene oxide)-modified poly(beta-amino ester) nanoparticles as a pH-sensitive biodegradable system for paclitaxel delivery. *Journal of Controlled Release, 86*, 223.
93. Shenoy, D., Little, S., Langer, R., et al. (2005). Poly(ethylene oxide)-modified poly(beta-amino ester) nanoparticles as a pH-sensitive system for tumor-targeted delivery of hydrophobic drugs: Part 2. In vivo distribution and tumor localization studies. *Pharmaceutical Research, 22*, 2107.
94. van der Zee, J. (2002). Heating the patient: A promising approach? *Annals of Oncology, 13*, 1173.
95. Chung, J. E., Yokoyama, M., Yamato, M., et al. (1999). Thermo-responsive drug delivery from poly-meric micelles constructed using block copolymers of poly(N-isopropylacrylamide) and poly(butylmethacrylate). *Journal of Controlled Release, 62*, 115.
96. Liu, S. Q., Tong, Y. W., & Yang, Y. Y. (2005). Thermally sensitive micelles self-assembled from poly(N-isopropylacrylamide-co-N, N-dimethylacrylamide)-b-poly(D, L-lactide-co-glycolide) for controlled delivery of paclitaxel. *Molecular BioSystems, 1*, 158.
97. Mitragotri, S. (2005). Healing sound: The use of ultrasound in drug delivery and other therapeutic applications. *Nature Reviews Drug Discovery, 4*, 255.
98. Kabanov, A. V., Batrakova, E. V., & Alakhov, V. Y. (2002). Pluronic block copolymers for overcoming drug resistance in cancer. *Advanced Drug Delivery Reviews, 54*, 759.
99. Gao, Z. G., Fain, H. D., & Rapoport, N. (2005). Controlled and targeted tumor chemotherapy by micellar-encapsulated drug and ultrasound. *Journal of Controlled Release, 102*, 203.
100. Nguyen, A. T., & Wrenn, S. P. (2014). Acoustically active liposome-nanobubble complexes for enhanced ultrasonic imaging and ultrasound-triggered drug delivery. *Wiley Interdisciplinary Reviews in Nanomedicine and Nanobiotechnology, 6*(3), 316–325.
101. Martin, K. H., & Dayton, P. A. (2013). Current status and prospects for microbubbles in ultrasound theranostics. *Wiley Interdisciplinary Reviews in Nanomedicine and Nanobiotechnology., 5*, 329–343.

102. Leong-Poi, H., Kuliszewski, M. A., Lekas, M., et al. (2007). Therapeutic arteriogenesis by ultrasound-mediated VEGF165 plasmid gene delivery to chronically ischemic skeletal muscle. *Circulation Research, 101*, 295–303.
103. Christiansen, J. P., French, B. A., Klibanov, A. L., et al. (2003). Targeted tissue transfection with ultrasound destruction of plasmid-bearing cationic microbubbles. *Ultrasound in Medicine and Biology, 29*, 1759–1767.
104. Rapoport, N., Gao, Z., & Kennedy, A. (2007). Multifunctional nanoparticles for combining ultrasonic tumor imaging and targeted chemotherapy. *Journal of the National Cancer Institute, 99*, 1095–1106.

Chapter 8
Conclusion

8.1 Future Challenges

8.1.1 Uniting Form with Function

This textbook has described innovative technologies for achieving the controlled release of therapeutic agents; such drug delivery platforms rely on advances in multiple fields, including polymer science, molecular biology, nanotechnology, and chemical engineering. Novel structures for drug delivery incorporate hydrogels, micelles, liposomes, and thin films with unique mechanical and biological properties. These structures can be designed for responsiveness to internal or external stimuli, creating "smart" environmentally triggered systems. These structures can also be modified with immunomodulating polymers, creating "stealth" systems that can circulate through the body for extended periods of time. The kinetics of drug release can be tailored to achieve zero-order, first-order, diffusion-controlled, or erosion-controlled delivery, or a combination of these mechanisms. Virtually every clinical discipline can benefit from new drug delivery strategies.

Both opportunities and challenges exist for drug delivery technologies. One of the most compelling future opportunities for drug delivery lies in drug–device combinations. Implantable medical devices such as stents, grafts, and joint replacements are crucial to the treatment of numerous chronic diseases, including coronary artery disease, stroke, diabetes, arthritis, neurodegeneration, and cancer. In the developed world, chronic noncommunicable diseases have long been the most prominent contributor to morbidity and mortality; aging populations will further raise the incidence of such diseases. In the developing world, chronic noncommunicable diseases are on a rapid rise, so that low- and middle-income countries are now facing a dual burden of infectious diseases and chronic diseases. Such diseases are complex and multifactorial, requiring creative medical device solutions. Yet most implanted devices have limited compatibility with surrounding tissues and consequently suffer from limited device lifetimes and adverse host responses and poor healing due to

E.P. Holowka, S.K. Bhatia, *Drug Delivery: Materials Design and Clinical Perspective*, DOI 10.1007/978-1-4939-1998-7_8

inflammation. Further, traditional medical devices are not biologically active; the implants do not actively modify the surrounding biological environment and do not respond to changes in the environment. For instance, a traditional knee replacement implant does nothing to modify inflammation in adjacent tissues. Drug–device combinations aim to address such limitations and are the newest generation of implantable medical devices. Such bioactive devices are comprised of a mechanical or electromechanical device along with one or more therapeutic agents.

Devices and drugs often have synergistic roles in treating disease. Drugs and biologics enable control of cellular survival, proliferation, differentiation, and adhesion responses to implanted devices, while implanted devices facilitate controlled release and targeted delivery of biologic agents. Drugs and biologics have the potential to increase the biocompatibility, stability, and efficacy of devices. In turn, site-directed delivery of potent drugs and biologics from devices can enable optimized therapy and preclude complications associated with systemic therapy. Innovative drug–device combinations are increasingly being developed. The most commercially successful drug–device combination has been the drug-eluting stent, described in detail in the clinical applications section of Chap. 3. Bioactive stents in cardiology have demonstrated the promise of controlled drug delivery from devices.

Yet drug–device combinations in other clinical fields have revealed the challenges of controlled drug release from devices. In particular, orthopedics offers several examples of growth factor–device combinations, which show both the potential and the difficulties of incorporating bioactive agents into devices. Specifically, implantable bone grafts have been embedded with growth factors to induce bone repair. The case of BMP-2-eluting bone grafts is especially illustrative. Bone morphogenetic protein-2 (BMP-2) is known as an osteoinductive growth factor because this protein promotes bone regeneration. Delivery of BMP-2 from collagen scaffolds induces healing of human bone fractures [1]. The INFUSE® bone graft system (Medtronic, Minneapolis, MN, USA) combines BMP-2 with an absorbable collagen matrix. The system, in combination with a metallic cage, is FDA-approved for spinal fusion surgery to treat degenerative disc disease. The system is also utilized for open fractures of the tibia (the long bone of the lower leg) as well as dental bone grafting procedures. However, the incorporation of BMP-2 into bone grafts has been fraught with difficulties. It is estimated that the risk of adverse events associated with BMP-2 use in spine fusion ranges from 10–50% [2]. The bioactive implants have resulted in complications including ectopic bone formation, pain, and malignancies. Because BMP-2 increases the cell division rate of bone-forming cells [3], such complications may be the result of excessive BMP-2 release from the implants. While growth factors may have benefits for promoting tissue healing, the diverse biological effects of these factors must be well understood, and the dosing and delivery of biologics must be finely tuned prior to clinical introduction of bioactive devices.

Drug–device combinations thus unite the biological functionality of drugs and biologics with the mechanical structures of implantable medical devices; these combinations represent the next frontier for drug delivery. Such combinations have the potential to improve patient outcomes by enabling targeted treatment of complex

medical conditions. Novel drug–device combinations are being created in virtually every clinical discipline. Medical devices containing small molecules, peptides, enzymes, antibodies, and growth factors have already been created, and it is conceivable that devices could incorporate nucleic acids, polysaccharides, and live cells as well. Yet, as illustrated by BMP-2-releasing implants, there are considerable engineering challenges to the successful clinical implementation of drug delivery from devices. Materials scientists, chemists, biologists, and engineers must develop an increased understanding of intricate cellular signaling pathways, as well as of robust mathematical models for signaling cascades, so that the proper bioactive agents can be chosen for each disease state. Scientists and engineers should also create analytical models that allow selection of the proper dose and delivery strategy for a given bioactive agent. Further, process engineers must continue to develop manufacturing processes that ensure safe, reliable, and consistent production of biologic agents. Finally, chemical engineers must implement cost-effective, scalable manufacturing methods for the incorporation of biologics into implantable electromechanical devices. In both the analysis and the manufacturing of drug–device combinations, engineering advances will provide physicians and surgeons with innovative therapeutic options for enhanced patient care. As always, engineers and scientists, working on innovative designs for drug delivery, should consider themselves not only part of the research team or the manufacturing team, but also part of the patient care team.

References

1. Swiontkowski, M. F., Aro, H. T., Donell, S., Esterhai, J. L., Goulet, J., Jones, A., et al. (2006). Recombinant human bone morphogenetic protein-2 in open tibial fractures. A subgroup analysis of data combined from two prospective randomized studies. *Journal of Bone and Joint Surgery (American), 88*(6), 1258–1265.
2. Carragee, E. J., Hurwitz, E. L., & Weiner, B. K. (2011). A critical review of recombinant human bone morphogenetic protein-2 trials in spinal surgery: Emerging safety concerns and lessons learned. *Spine Journal, 11*, 471–491.
3. de Luca, F., Barnes, K. M., Uyeda, J. A., De-Levi, S., Abad, V., Palese, T., et al. (2001). Regulation of growth plate chondrogenesis by bone morphogenetic protein-2. *Endocrinology, 142*, 430–436.

Chapter 2 Problems—Answers

2.2 Draw *one example* for the chemical reaction for each of the following:

(i) Chemical degradation of a polypeptide

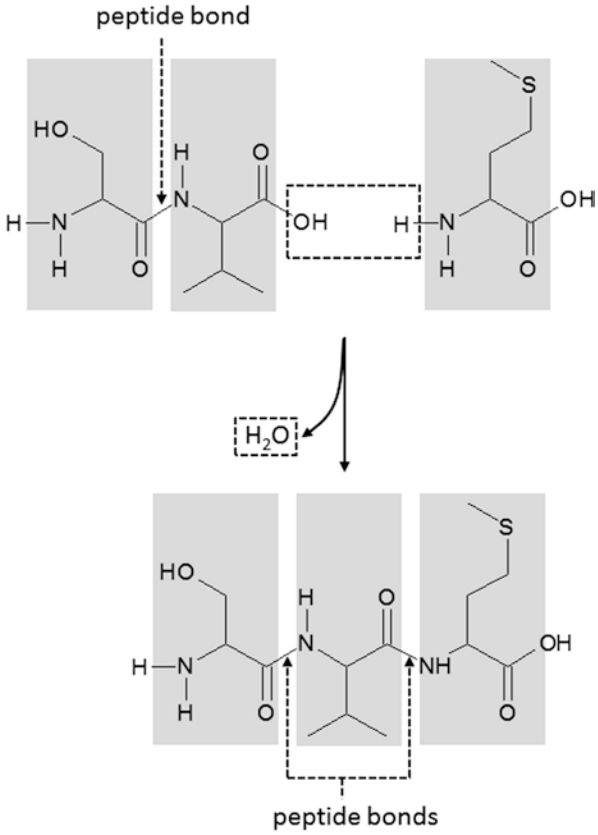

E.P. Holowka, S.K. Bhatia, *Drug Delivery: Materials Design and Clinical Perspective*, DOI 10.1007/978-1-4939-1998-7

(ii) Enzymatic degradation of a polypeptide

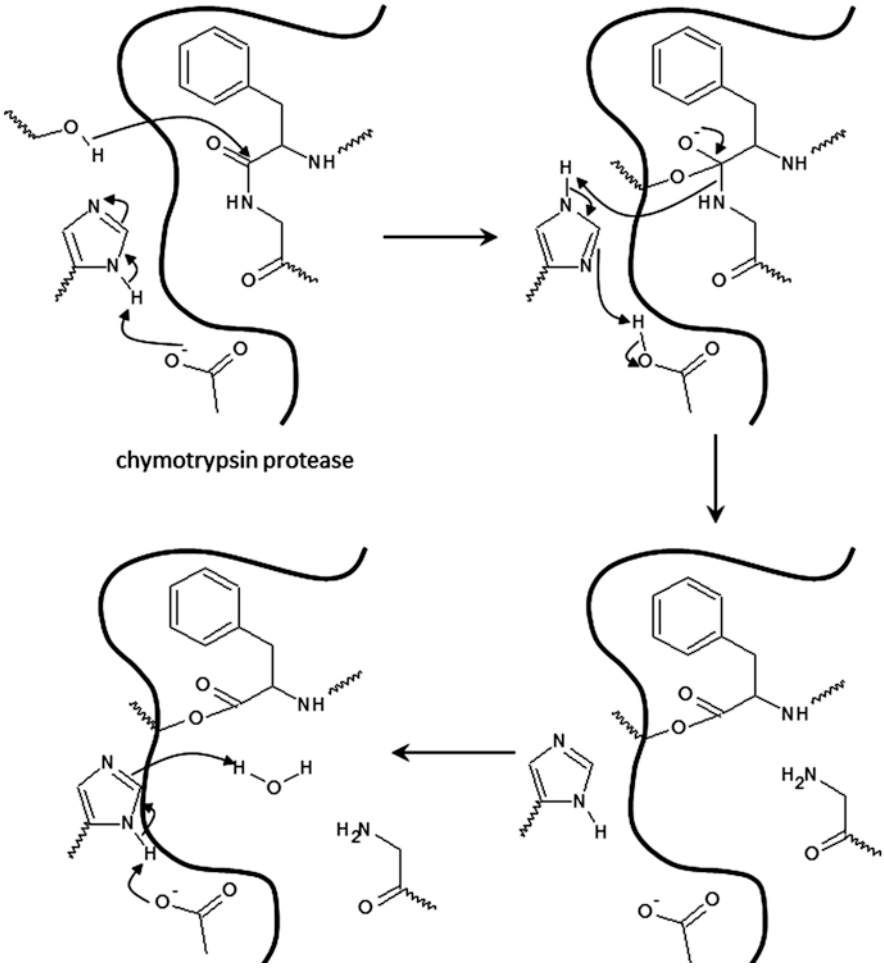

2.4 A biomaterials scientist is trying to design a system that has a high amplitude burst release pharmacokinetic drug release profile. In order to fabricate a relevant system, several factors are necessary. Look at the following polymer structures and answer the following questions:

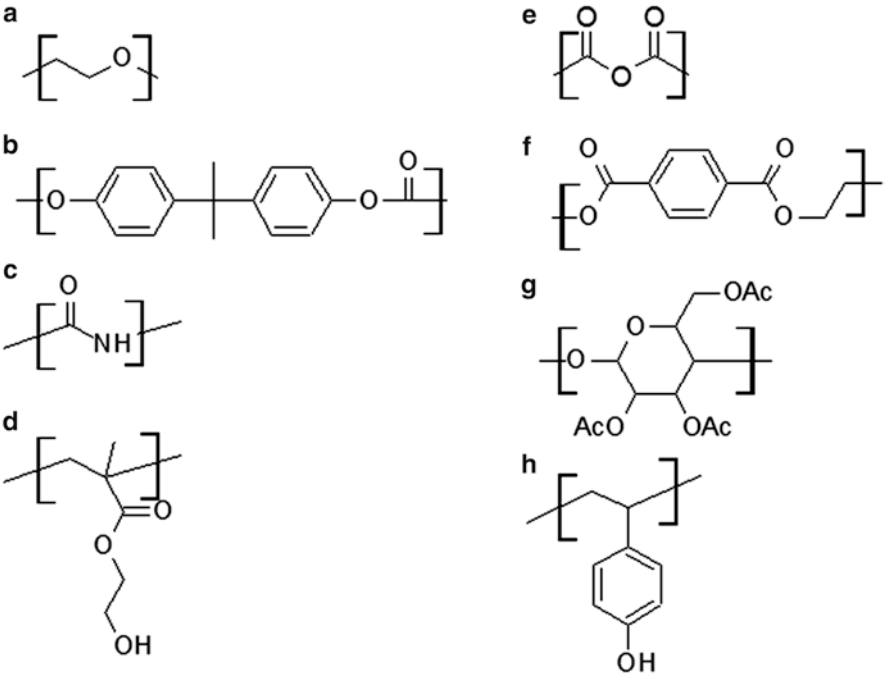

(i) What do the structural characteristics of a crosslinked material typically contribute to high burst release behavior?

Burst release is typically associated with a rapid change in the internal volume of the system that is occupied by water. One example of this behavior is the swelling of a matrix or hydrogel system, which is dependent on the flexibility of the solvated polymer chains. Therefore, polymer chains that are conformationally or rotationally restricted will have difficulty swelling rapidly, leading to release kinetics resembling Fickian diffusion and not zero-order.

(ii) Which of the polymers above exhibit these characteristics from (i)? Why?

Polymers (a), (c), (d), and (h) would not be considered rotationally or conformationally restricted, which would allow them to have high flexibility upon being solvated. This would translate into a higher degree of swelling.

(iii) From the components above, how might a biomaterials scientist change the pharmacokinetic release profile for a crosslinked system from a burst release to Fickian release kinetics?

As stated in (i), if the scientist began to mix or substitute in rigid polymer components such as (b), (e), (f), and (g) in for (a), (c), (d), and (h), the system would begin to resemble a more Fickian pharmacokinetic release profile.

2.6 A group has invented a novel drug release technology (listed below as Composition 1) and is comparing it to a currently marketed product. The group compared release of the drug metoprolol from the new composition with that from the existing marketed product. (These data are from US Patent Application US20090053310 A1.) From your knowledge of controlled-release drug delivery systems, answer the following questions:

Time (hours)	Composition 1 % Cumulative Drug Release	A Marketed product % Cumulative Drug Release
0	0	0
1	15.5	11.87
2	21.2	14.34
4	33.2	25.43
6	42.3	35.50
8	53.7	45.75
12	65.4	64.46
16	76.6	77.44
20	84.9	91.5

(i) Prepare a plot of drug release versus time for each of these technologies (the new composition and the existing marketed product).

The following plot shows the drug released as a function of time.

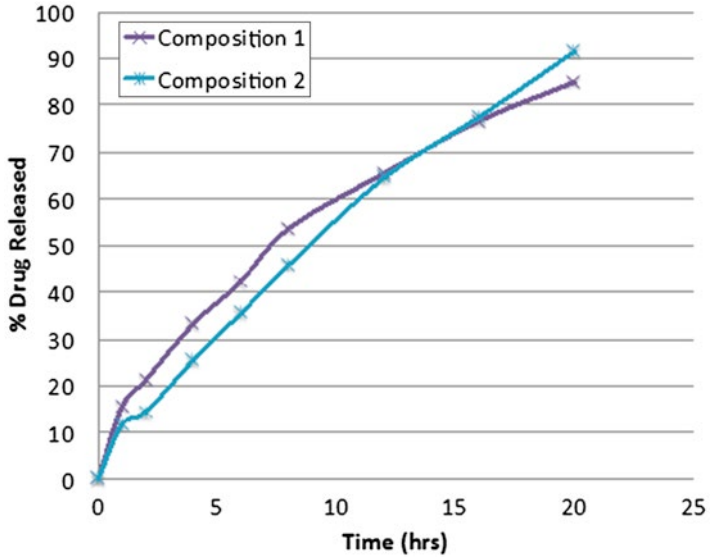

(ii) Then conduct an analysis to determine the mechanism of drug release from each of these technologies.

In order to figure out what mechanism is at play here for each of the compositions, the Korsmeyer–Peppas analysis can be employed:

$\log (M_t/M_\infty) = \log k + n \log t.$

The value of n is determined from a plot of log (percent drug released) versus *log t. A plot of log* (M_t/M_∞) versus *log t will result in a straight line with slope n, which tells us the mechanism of drug release.*

The values of the diffusion exponent were defined in this chapter as the following:

$n = 0.5$ *indicates Fickian diffusion: drug release is diffusion-controlled, as in Higuchi matrix;*

$0.5 < n < 1$ *indicates "anomalous" diffusion: drug release is both diffusion-controlled and erosion-controlled;*

$n = 1$ *indicates "case II transport": drug release is zero-order; release rate is constant and controlled by polymer relaxation;*

$n > 1$ *indicates "super case II transport": drug release is erosion-controlled.*

The following plot was generated using the Korsmeyer–Peppas equation.

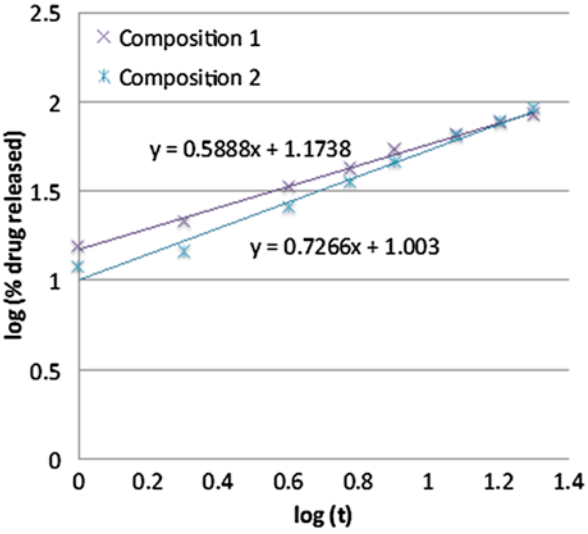

The slope gives us the value of n.
Composition 1: $n = 0.5888$.
Composition 2 (a marketed product): $n = 0.7266$.
Because $0.5 < n < 1$ *for both compositions, the drug release is both diffusion-controlled and erosion-controlled.*

(iii) Calculate rate constants where necessary, and be sure to use correct units.

The kinetic constant is given by the y-intercept of the plot. The y-intercept = log K and the units of K are s^{-n} *or* h^{-n}.
Therefore, for composition 1, K is $14.92h^{-0.5888}$ *and for the marketed product* $10.07h^{-0.7266}$.

Chapter 3 Problems—Answers

3.2 An ophthalmology research assistant is trying to determine if a particular ocular drug will reach the endothelium of the eye as its target. He has estimates regarding the thickness and pore structure of several layers of ocular tissue and knows that the drug is capable of diffusing through the gap junctions within the epithelial layer. From your knowledge of the physiology of the eye and drug delivery answer the following questions.

Ocular tissue layer	N	L (μm)	S_i (μm)	L_i (μm)
Epithelium	7	10	35	500
Bowman's layer	1	7	1	12
Stroma	10	500	250	500
Descemet's membrane	1	5	1	10
Endothelium	2	2	10	80

(i) What is the tortuosity of each tissue layer of the eye?

Using the equation for tortuosity, we can calculate from the columns provided:

$$\tau = \frac{N-1}{L}\sum_{i=1}^{N}\left(\frac{L_i}{S_i}-1\right).$$

Ocular tissue layer	N	L (μm)	S_i (μm)	L_i (μm)	τ
Epithelium	7	10	35	500	7.97
Bowman's layer	1	7	1	12	0
Stroma	10	500	250	500	0.018
Descemet's membrane	1	5	1	10	0
Endothelium	2	2	10	80	3.5

E.P. Holowka, S.K. Bhatia, *Drug Delivery: Materials Design and Clinical Perspective*, DOI 10.1007/978-1-4939-1998-7

(ii) Which tissue layer of the eye would have the highest diffusion of drug?

*Either Bowman's layer or Descemet's membrane since they both have zero tortuosity (*i.e.*, no impedance to diffusion).*

(iii) Would this drug be capable of being effectively delivered to its target tissue? Why?

*The ophthalmology research assistant knows that the drug will diffuse through the gap junctions in the epithelial layer, which has the highest level of tortuosity (*500*) in the entire multilayered system. Since all the other layers are* $\ll$500*, then the drug should be capable of effectively being delivered to the base layer, in this case the endothelium.*

(iv) How would tortuosity change with decreasing particle size? Why?

*The tortuosity would increase since the particle would have access to a higher degree of internal surface area within the membranes (*i.e.*, more internal distances and changes in direction).*

3.4 A graduate student in biomedical engineering decides to explore the use penetration enhancers in order to more effectively deliver a drug sublingually. The researcher decides to monitor the potential activity of the delivery mode using the contact angle and estimating the surface wetting of the drug solution on a membrane of sublingual tissue. From the data collected and your knowledge of oral drug delivery, answer the following questions.

Time (min)	θ*(°)	r_f	r	f
0	85	0.1	0.5	0.20
1	85	0.2	0.5	0.30
2	85	0.3	0.5	0.50
5	85	0.5	0.5	0.95
10	85	0.5	0.5	0.98
20	85	0.5	0.5	1.00

(i) What model does the droplet appear to follow at the zero point of the experiment? Why?

Time (min)	θ (o)	r_f	r	f	Wenzel ($\cos\theta^*$)	Cassie–Baxter ($\cos\theta^*$)
0	**85**	**0.1**	**0.5**	**0.20**	**−0.49**	**−0.82**
1	85	0.2	0.5	0.30	−0.49	−0.76
2	85	0.3	0.5	0.50	−0.49	−0.65
5	85	0.5	0.5	0.95	−0.49	−0.52
10	85	0.5	0.5	0.98	−0.49	−0.50
20	85	0.5	0.5	1.00	−0.49	−0.49

It appears that the Cassie–Baxter model is followed at the zero point due to the lower negative number (−0.82) when compared to the Wenzel calculation (−0.49). This would indicate that the droplet appears to favor a state where it is resting on the tissue surface, with little penetration into the void spaces of the cell gaps.

(ii) What happens to the surface of the sublingual tissue throughout the course of the 20-min experiment?

Time (min)	θ (o)	r_f	r	f	Wenzel ($\cos\theta^*$)	Cassie–Baxter ($\cos\theta^*$)
0	85	0.1	0.5	0.20	−0.49	−0.82
1	85	0.2	0.5	0.30	−0.49	−0.76
2	85	0.3	0.5	0.50	−0.49	−0.65
5	85	0.5	0.5	0.95	−0.49	−0.52
10	85	0.5	0.5	0.98	−0.49	−0.50
20	**85**	**0.5**	**0.5**	**1.00**	**−0.49**	**−0.49**

After 20 min, the values for Cassie–Baxter approach that of the Wenzel model (−0.49). This suggests that the droplet is beginning to ingress into the tissue layer in the area between the cell gaps. One could speculate that this could be due to the increase in the distance of the cell gaps over time due to internal or external stimulus.

(iii) Based on your answers to (i) and (ii), would you expect the sublingual surface to be more or less susceptible to the delivery of the drug at the zero point than after 20 min? Why?

One would suspect that the sublingual surface is less susceptible to the drug at time zero since it follows the Cassie–Baxter model, where the droplet lies on the surface of a tissue layer, whereas after 20 min, the measurements indicate that the droplet follows a Wenzel model, where the droplet wets in the volume between cells, which is more desirable for the delivery of drugs across the tissue membrane.

Chapter 4 Problems—Answers

4.2 A medical research lab is interested in testing a biomedical engineering student's liposomal drug delivery system for use with their new developmental drug as a candidate for oral drug delivery at dosages from 100 to 200 mg and intravenous at dosages from 1 to 2 mg. From your knowledge of self-assembled drug delivery systems, answer the following questions.

(i) If we know that the ratio of the area under the curve for oral and intravenous administration is 0.6, determine the absolute bioavailability of the new developmental drug.

$$\begin{aligned}\text{Absolute bioavailability} &= \frac{\text{AUC}_{\text{oral}}}{\text{AUC}_{\text{IV}}} \times \frac{\text{Dose}_{\text{IV}}}{\text{Dose}_{\text{oral}}}, \\ &= (0.6) \times \frac{2\ \text{mg}}{200\ \text{mg}}, \\ &= 0.6\ \%.\end{aligned}$$

Vesicle size (nm)	Encapsulation efficiency (EE) (%)	Drug loading (DL) (%)
50	**10**	**2.80**
100	**20**	**3.50**
150	30	8.00
200	35	12.00
300	50	16.00
400	52	24.00

E.P. Holowka, S.K. Bhatia, *Drug Delivery: Materials Design and Clinical Perspective*, DOI 10.1007/978-1-4939-1998-7

(ii) Given the data above, would this lipid vesicle system be a good candidate for the new developmental drug as an oral therapy? Why?

The absolute bioavailability of 0.6 % from (i) assumes that roughly 0.6 mg of the original oral dosage is available for physiological absorption. In order to pass through the filtration system of the liver, a 50–100-nm vesicle system would be appropriate, which correlates to a ratio of drug to vesicle of 2.80 %. In order to achieve a 200-mg dosage requirement, then 7.1 g of drug is required. Since 7.1 g is significantly high in terms of dosages, this method would not be desirable for oral delivery of the new developmental drug.

(iii) Would it be effective as an intravenous therapy? Explain.

The absolute bioavailability of 0.6 % from (i) assumes that roughly 0.6 mg of the original oral dosage is available for physiological absorption. In order to pass through the filtration system of the liver, a 50–100-nm vesicle system would be appropriate, which correlates to a ratio of drug to vesicle of 10 %. In order to achieve a 2-mg dosage requirement, then 20 mg of drug is required. Since 20 mg is within a reasonable dosage range, this method would be relevant for IV delivery of the new developmental drug.

4.4 A research lab in biomedical engineering is looking to design a vesicle-based treatment method for the transdermal delivery of a new experimental drug. They are exploring both inverse micellar and vesicle self-assembled structures to determine the most suitable candidate system. Use the components in the table below and your knowledge of self-assembly to answer the following questions.

Lipid	Chemical Structure
DOPC	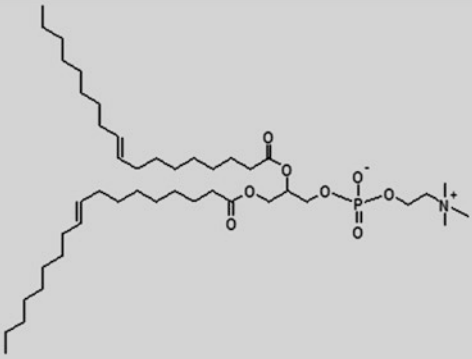
GM1	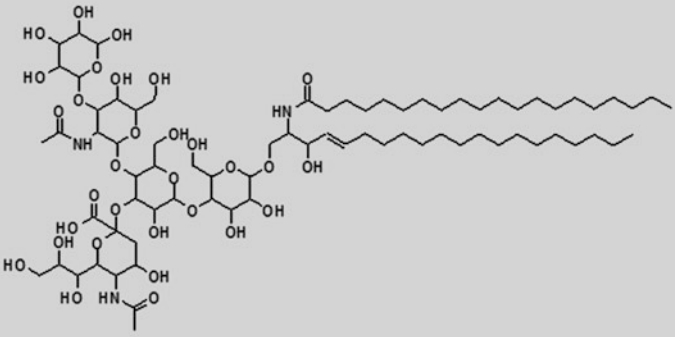
PC	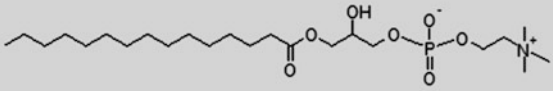
DPPC	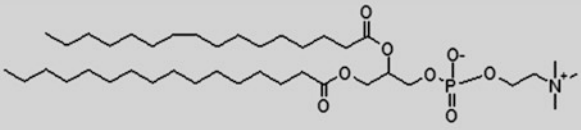

(i) Which lipid(s) would you expect to readily self-assemble into an inverse micellar system? Why?

One would expect the DOPC lipid or any mixture of lipids with a majority of the composition DOPC would assemble into an inverse micelle due to the degree of unsaturation in the lipid tail. The presence of a double

bond within the lipid tail disrupts the packing parameter of the hydrophobic domain in favor of an inverse curvature ($C^o < 0$), which, in the appropriate solvent, forms inverse micellar assemblies.

(ii) Which lipid(s) would you expect to readily self-assemble into a vesicle system? Why?

One would expect that DPPC and PC could each form vesicle species when in a mixed species due to the presence of two hydrocarbon tails that are fully saturated. This favors a high packing parameter with a lower degree of curvature, which is commonly seen to induce bilayer formation indicative of vesicle assemblies.

(iii) What would you expect to be the challenges for the self-assembly of a GM1 vesicle system?

The GM1 lipid system has a significantly large polar head group that can act to sterically occlude the hydrophobic packing of the lipid tail groups if it is assembled homogeneously. The large head group may act to destabilize bilayer formation since the packing parameter of the head group is low relative to that of the tail groups.

(iv) How could you design a vesicle system from the components in the table that would have the GM1 head groups on the surface?

The mismatch between the packing of the GM1 head group relative to its tail group can be alleviated by the addition of other groups such as PC, which has a single lipid tail and small head group to provide some space between the GM1 head groups.

4.6 Liposomes are drug delivery vehicles that mimic the lipid bilayer of the cell. In a typical liposome for drug delivery, a phospholipid bilayer surrounds an aqueous core that contains the drug of interest. If the pH and charge of the bilayer are adjusted appropriately, then a drug in the aqueous core can be released via diffusion through the lipid bilayer.

Liposome for Drug Delivery

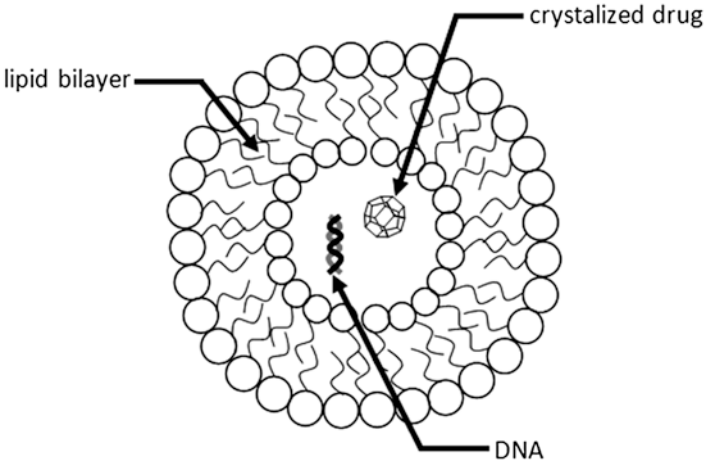

(i) Assuming that the drug is contained in the aqueous core and is released by diffusion through the lipid bilayer, what type of drug delivery kinetics might you expect? Assume that the lipid bilayer does not degrade.

This is a reservoir drug delivery system: The liposomal barrier surrounds a reservoir of aqueous drug solution. You would expect zero-order kinetics for drug release.

(ii) A pharmacy research group in Europe has designed liposomes that encapsulate the chemotherapeutic drug 5-fluorouracil (Glavas-Dodov et al., *Bulletin of the Chemists and Technologists of Macedonia*, 23:13–18, 2004). The group synthesized liposomes with three different compositions in the aqueous phase:

- 1:100 mass ratio of drug/aqueous phase (formulation C1)
- 1:60 mass ratio of drug/aqueous phase (formulation C2)
- 1:40 mass ratio of drug/aqueous phase (formulation C3)

A linear relationship between cumulative drug release and time indicates zero-order kinetics. Your prediction from part (i) is correct.

The researchers measured the release of 5-fluorouracil from each of these liposomal formulations. In each case, a plot of drug concentration versus time was approximately linear:

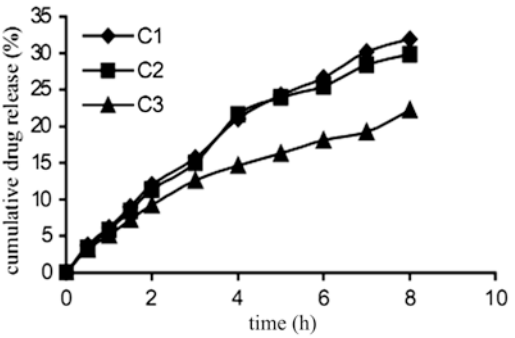

What does this indicate about the kinetics of drug release from the liposomes? Is your prediction for drug delivery kinetics from part (i) correct?

(iii) From the plot above, estimate the rate constant for drug release in each of the three formulations.

Formulation C1 has an approximate zero-order rate constant for drug release of 4 h^{-1}. Formulation C2 has an approximate zero-order rate constant of 3.75 h^{-1}. Formulation C3 has an approximate zero-order rate constant of 2.75 h^{-1}.

(iv) What is the effect of aqueous phase composition (i.e., going from a 1:100 drug/water ratio to a 1:40 drug/water ratio) on the rate constant for drug release in this particular system?

Interestingly, as the aqueous phase composition goes from a 1:100 drug/water ratio to a 1:40 drug/water ratio, the rate constant for drug release actually decreases.

Chapter 5 Problems—Answers

5.2 The allergic response involves the aggregation of IgE receptor molecules within glycosphingolipid-cholesterol microdomains, known as lipid RAFTs, at the surface of mast cells to facilitate a process known as degranulation. If each RAFT domain consists of an average surface area of 0.031 μm^2 relative and the mast cell is 20 μm in diameter with a cell membrane thickness of 5 nm and a Young's modulus of 1.2×10^7 Pa, answer the following questions with your knowledge of the interaction *surface area* between elastic and hard materials.

(i) Calculate the elastic modulus of the mast cell membrane assuming that E^* is approximately equal to the bending energy (e_{bend}) within a contact surface area of 0.01 μm^2.

The bending energy can be calculated based on Eq. (4.-?) from Chap. 4, where

$$\begin{aligned} e_{\text{bend}} &= \frac{E_{\text{bend}}}{L^2} = \frac{1}{24} Y \frac{h^3}{R^2}, \\ &= \frac{1}{24}\left(1.2\times10^7\,\text{Pa}\right)\frac{\left(5\times10^{-9}\,\text{nm}\right)^3}{\left(10\times10^{-6}\,\text{m}\right)^2\left(0.01\times10^{-6}\,\text{m}\right)^2}, \\ &= 6.25\times10^6\,\text{Pa}/\text{m}^2. \end{aligned}$$

(ii) A medical researcher would like to design a functionalized gold nanoparticle system to target a single RAFT domain on a mast cell. What would be the ideal particle radius if the pressure of the interaction between the nanoparticle and cell membrane is 1×10^{-10} Pa?

The radius can be determined by the combination of Eqs. (5.8) and (5.9):

$$F = \frac{4}{3} E^* R^{\frac{1}{2}} d^{\frac{3}{2}} \text{ and } a = \sqrt{Rd}.$$

E.P. Holowka, S.K. Bhatia, *Drug Delivery: Materials Design and Clinical Perspective*, DOI 10.1007/978-1-4939-1998-7

Note: The R-term in the force and surface area equation above is different than the R-term in the bending energy equation from (i). The R-term in (i) is actually equivalent to the a-term in the equation above.

solve for d:

$$d = \left[\left(\frac{3}{4}\right)\frac{F}{E^* R^{1/2}}\right]^{2/3}, \quad d = \frac{a^2}{R};$$

set the d terms equal to one another:

$$\frac{a^2}{R} = \left[\left(\frac{3}{4}\right)\frac{F}{E^* R^{1/2}}\right]^{2/3};$$

solve for R:

$$R = \left(\frac{4}{3}\right)\frac{E^* a^3}{F};$$

substitute values for E, a, and F:*

$$R = \left(\frac{4}{3}\right)\frac{\left(6.25\times10^{6}\,\text{Pa/m}^2\right)\left(0.01\times10^{-6}\,\text{m}\right)^3}{\left(1\times10^{-10}\,\text{Pa}\right)},$$
$$= 83\ \text{nm}.$$

(iii) What would the ideal nanoparticle radius be if the surface area of the RAFT domain doubled?

*In order to answer this question, we start by multiplying the bending energy R-term (*i.e.*, surface area) by 2:*

$$e_{\text{bend}} = \frac{1}{24}\left(1.2\times10^{7}\,\text{Pa}\right)\frac{\left(5\times10^{-9}\,\text{nm}\right)^3}{\left(10\times10^{-6}\,\text{m}\right)^2\left(2\times\left(0.01\times10^{-6}\,\text{m}\right)\right)^2},$$
$$= 1.56\times10^{6}\,\text{Pa/m}^2.$$

*We can then substitute the bending energy into the equation for radius, while multiplying the a-term (*i.e.*, surface area) by 2 in this equation:*

$$R = \left(\frac{4}{3}\right)\frac{\left(1.56\times10^{6}\,\text{Pa/m}^2\right)\left(2\times\left(0.01\times10^{-6}\,\text{m}\right)\right)^3}{\left(1\times10^{-10}\,\text{Pa}\right)},$$
$$= 667\ \text{nm}.$$

Realize that an eightfold increase in the micelle size results in a twofold increase in the cell binding domain for this example of a cubed relationship (i.e., 23 = 8).

5.4 A research lab in biomedical engineering wishes to design a micellar oral drug delivery system that effectively targets the heart. If the micellar system is 20 nm in diameter and charge-neutral, answer the following questions with your knowledge of self-assembled and targeted systems.

(i) Discuss the sequence of physiological constraints in order as the oral drug passes from the mouth to the small intestine.

*The oral drug delivery system begins in the mouth, where it needs to remain stable in the presence of starch and avoid premature adsorption to buccal or sublingual tissue. The drug then passes though the esophagus, where it is exposed to a pulsatile flow, causing a propensity for the drug to adhere to the inner tissue walls. The drug then finds itself in the stomach, where it needs to remain stable in a pH 2 environment. Before being absorbed into the bloodstream, the drug must pass through the liver, which filters anything >150 nm in size. Once in the bloodstream, the drug must avoid electrostatic Van der Waals complexation with biomolecules. The drug will also be in a more diluted state in a system with mixed "colloids" (*i.e.*, cells and polymers), which it must not interact with so that it avoids flocculating the system and creating blood clots.*

(ii) Would changing the diameter of the nanoparticle from 20 to 200 nm affect the constraints of the oral delivery system? Why?

Yes. The increase in the diameter of the micelle to 200 nm would cause it to be trapped within the liver filtration system (>150 nm).

(iii) Would changing the surface charge of the nanoparticle to one that is highly cationic affect the constraints of the oral delivery system? Why?

*Yes. Changing to a highly cationic surface charge would lead to electrostatic complexation with opsonins within the human bloodstream, which act to effectively tag foreign contaminants for phagocytosis my immune cells (*i.e.*, T-cells) and macrophages.*

Chapter 6 Problems—Answers

6.2 A medical research lab is screening potential injectable hydrogel candidates for use as cartilage repair agents by facilitation of chondrocyte growth within void spaces within the tissue matrix. Using your knowledge of hydrogel materials for drug delivery, answer the following questions.

(i) With the rheology data below, plot the storage modulus versus time for each of the hydrogel polymers.

Sample	time (min)	G' (Pa)
Hydrogel 1	0	2
	1	250
	2	500
	3	750
	4	1000
	5	1250
	6	1500
	7	1750
	10	1800
	15	1800

Sample	time (min)	G' (Pa)
Hydrogel 2	0	1
	1	2
	2	2
	3	3
	4	10
	5	100
	6	150
	7	250
	10	500
	15	510

Sample	time (min)	G' (Pa)
Hydrogel 2	0	1
	1	2
	2	3
	3	3
	4	4
	5	4
	6	5
	7	5
	10	5
	15	7

E.P. Holowka, S.K. Bhatia, *Drug Delivery: Materials Design and Clinical Perspective*, DOI 10.1007/978-1-4939-1998-7

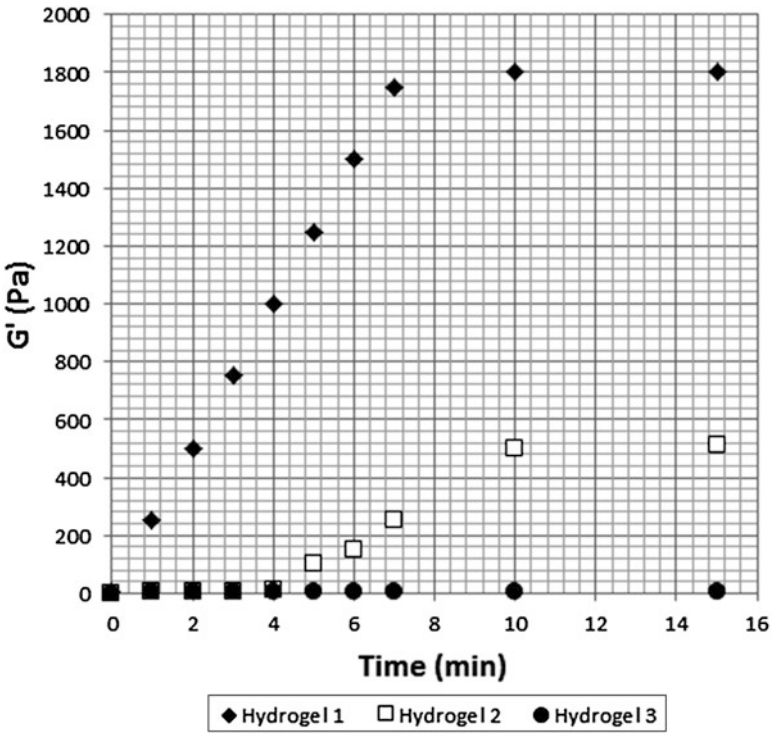

(ii) Given the rheology data, which candidate(s) would be ideal for treatment in cartilage tissue repair? Why?

The increase in storage modulus (G′) indicates the onset of gelation. In cartilage repair, the onset of gelation must be quick upon removal of the shear stress of injection in order to serve its function. Since the Hydrogel 1 begins to increase earlier than the other two samples and has a significantly greater magnitude with respect to G′, it would hold as the most desirable candidate for injectable hydrogels in cartilage repair.

(iii) If not, what can be done to the system in order to shift the rheology plot to an acceptable domain?

In the cases of Hydrogels 2 and 3, the systems more closely resemble a viscous fluid that a networked gel structure. In order to shift the G′ plot, one could form a mixture of Hydrogels 1 and 2 at different relative amounts in order to dial in strength. One could also look at this combination as a means of shifting the time for the onset of gelation for applications requiring strong gel formation that may not require immediate setting in the gel state.

6.4 A research lab in biomedical engineering would like to design a hydrogel system consisting of polyethylene glycol (PEG) as the arms between crosslink points to release a 10-nm nanoparticle upon swelling. If we assume that the PEG polymer chains are in their fully extended state (i.e., rigid linear chains) upon swelling, use your knowledge of hydrogel systems to answer the following questions.

(i) If we assume that the geometry of the void space within the gel is consistent with the diagram below of a tetrafunctional crosslinked hydrogel system, and that υ_{2m} is 0.1, χ_1 is 0.52, V_1 is 1, υ is 1.5 cm^3/g, calculate the molecular weight of the polymer arms between crosslink points.

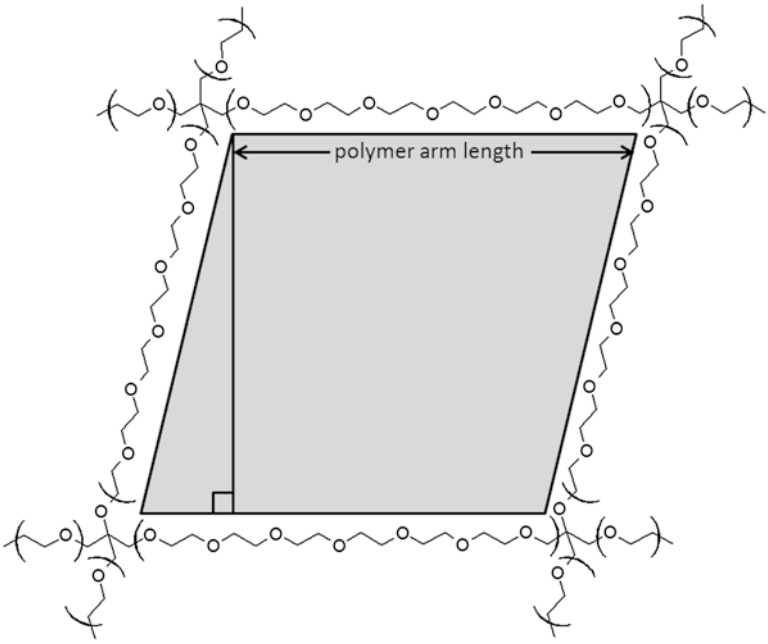

Begin by using Flory's estimate of molecular weight between crosslink points:

$$\frac{1}{M_c} = -\frac{\left(\frac{\upsilon}{V_1}\right)\left[\ln\left(1-\upsilon_{2m}\right)+\upsilon_{2m}+\chi_1\upsilon_{2m}^2\right]}{\left[\upsilon_{2m}^{1/3}-\frac{\upsilon_{2m}}{2}\right]},$$

$$= -\frac{(1.5)\left[\ln(1-0.1)+(0.1)+(0.52)(0.1)^2\right]}{\left[(0.1)^{1/3}-(0.05)\right]}.$$

$$M_c = 1,720.12\,\text{Da},$$

where M_c is the molecular weight of the polymer arms between crosslinks.

(ii) What is the largest-diameter nanoparticle that could be released from the void space of this swelled hydrogel system?

If we know that the linear distance between the β-carbon and oxygen atoms in a PEG repeat unit is 3.5 Å, then the largest diameter of a particle to fit into the hydrogel void space would be equivalent to the length of the fully extended PEG polymer arm between crosslink points:

$$d = \frac{(1{,}720.12\ \text{Da})}{(44\ \text{Da})} \times (0.35\ \text{nm}) = 13.65\ \text{nm}.$$

(iii) How would the void space change if the crosslinking group was changed from a tetrafunctional group to a trifunctional group?

The void space would decrease if the crosslinking group was changed from a tetrafunctional group to a trifunctional group since the density of crosslinking points within the networked gel would decrease. As you decrease the density of crosslinking points within a network structure, the system shifts from a gel state to that of a viscous polymer solution.

Chapter 7 Problems—Answers

7.2 A medical research lab would like to design a micellar drug delivery system to interact with a tissue surface to elicit macropinocytosis in blood plasma with an ionic strength of 0.1 at 37 °C. If the particle diameter is 50 nm, answer the following questions with your knowledge of pH-responsive materials for drug delivery:

(i) What is the critical distance, in terms of proximity to the tissue interface, that the micelle needs to be if ε is 10?

$$K^2 = \frac{8\pi N_A e^2 I}{1{,}000\varepsilon kT},$$

$$= \frac{8\pi\left(6.02\times10^{23}\right)\left(1.602\times10^{-19}\,\mathrm{C}\right)^2(0.1)}{1{,}000(10)\left(1.38\times10^{-23}\,\mathrm{m^2kgs^2K^{-1}}\right)(310\ \mathrm{K})},$$

$$K = 30.13\frac{\mathrm{C}^2}{\mathrm{m^2kgs^2}}.$$

(ii) What is one design method the research lab could use to increase the Debye length of the micelle system?

The research lab could increase the Debye length of the micellar system by altering the ionic strength of its surface.

E.P. Holowka, S.K. Bhatia, *Drug Delivery: Materials Design and Clinical Perspective*, DOI 10.1007/978-1-4939-1998-7

(iii) What would the effective Debye length change to in the presence of multiple ion channels on the tissue surface changing the ε to 2?

If e = 2:

$$K^2 = \frac{8\pi\left(6.02\times10^{23}\right)\left(1.602\times10^{-19}\,\mathrm{C}\right)^2\left(0.1\right)}{1{,}000\left(2\right)\left(1.38\times10^{-23}\,\mathrm{m^2kgs^2K^{-1}}\right)\left(310\mathrm{K}\right)},$$

$$K = 67.38\frac{\mathrm{C}^2}{\mathrm{m^2kgs^2}}.$$

The Debye length would increase by a factor >2, which indicates that the micelle has a stronger association with the membrane.

7.4 A research lab in biomedical engineering is testing a photoresponsive hydrogel contact lens as a matrix for the controlled release of a prostaglandin analog prodrug to treat glaucoma patients. If the contact lens has a molar absorptivity of 30,000 $\mathrm{M^{-1}\,cm^{-1}}$, answer the following questions using your knowledge of photoresponsive drug delivery systems.

(i) What is the degradation kinetics if the applied light intensity is 7 $\mathrm{mW/cm^2}$ with a quantum yield of 0.05 at a wavelength of 370 nm?

$$k_{\mathrm{app}} = \frac{\phi\varepsilon\lambda I_0\left(2.303\times10^{-6}\right)}{N_{\mathrm{A}}hc},$$

$$= \frac{\left(0.05\right)\left(30{,}000\mathrm{M^{-1}cm^{-1}}\right)\left(370\mathrm{nm}\right)\left(7\mathrm{mW/cm^2}\right)\left(2.303\times10^{-6}\right)}{\left(6.02\times10^{23}\right)\left(6.626\times10^{-34}\,\mathrm{m^2kg/s}\right)\left(3\times10^{9}\,\mathrm{m/s}\right)},$$

$$= 7.5\times10^{-6}\,\mathrm{M^{-1}m^{-3}s^{-1}}.$$

(ii) As the contact lens degrades over time, would you expect the molar absorptivity to change? Why?

Yes, you would expect it to reduce. This is true since the molar absorptivity is directly proportional to concentration and path length through the Beer–Lambert law:

$$A = \varepsilon cl\ \left(\mathrm{Beer}\quad\mathrm{Lambert\,law}\right),$$

*where A is the absorbance of the sample, c is the concentration, and l is the path length (*i.e.*, thickness of the film or lens). As the contact lens degrades, both the concentration on a macroscale and path length on a nanoscale, are reducing, which changes the molar absorptivity of the contact lens material.*

(iii) How might you change the hydrogel contact lens structure to allow for a more Fickian pharmacokinetic release profile?

To create a more Fickian release profile, one may avoid using materials that highly swell. More rigid polymeric materials with high T_g values that approximate glass in their structure would also provide a hard matrix structure that could be tuned to provide a first-order release profile.

Index

E.P. Holowka, S.K. Bhatia, *Drug Delivery: Materials Design and Clinical Perspective*, DOI 10.1007/978-1-4939-1998-7